Combining ATR inhibition with topoisomerase I inhibitors for the treatment of colorectal cancer

Avigayil Chalk

A thesis submitted to University College London

for the Degree of

Doctor of Philosophy

August 2021

CRUK Drug-DNA Interactions Research Group

Department of Oncology

Cancer Institute

University College London

72 Huntley Street, London, WC1E 6BT, UK

Declaration

I, Avigayil Chalk, confirm that the work presented in this thesis is my own.

Where information has been derived from other sources, I confirm that this has been indicated in the thesis.

Abstract

Metastatic colorectal cancers are commonly treated with irinotecan, a topoisomerase 1 (TOP1) inhibitor. TOP1 inhibition results in the formation of TOP1-DNA cleavage complexes, which induce replication stress, and lead to activation of the Ataxia Telangiectasia and Rad-3 related (ATR) signalling pathway. Activation of ATR leads to cell cycle arrest and DNA repair, reducing the cytotoxicity of TOP1 inhibition.

Using a panel of colorectal cancer (CRC) cell lines and patient derived organoids (PDOs), a synergistic interaction was identified between SN38 (active irinotecan metabolite) and VX-970 (ATR inhibitor). Treating CRC cell lines and PDOs with a combination of TOP1 and ATR inhibition resulted in increased γH2AX accumulation and the activation of double strand break (DSB) repair kinases, DNA-PK and ATM. Increased DNA DSBs and the formation of micronuclei in combination treated cells, further demonstrated the elevated levels of DNA damage. Colocalisation of cGAS with micronuclei was detected in combination treated cells, suggesting increased DNA damage may result in immune activation.

Trastuzumab deruxtecan (DS-8201a) is a novel HER2 targeting antibody drug conjugate (ADC), carrying a potent TOP1 inhibitor (Dxd) warhead. Previous studies have reported minimal sensitivity of HER2-low expressing CRCs to DS-8201a therapy. In this study, several HER2-low CRC cell lines and PDOs were sensitised to DS-8201a by ATR inhibition (VX-970 and AZD6738). Loss of replication arrest and increased DNA-damage were identified as the mechanisms for the synergy observed.

ATR inhibition was also explored as a possible mechanism to overcome irinotecan resistance. However, neither ATR inhibition combined with SN38, or ATR inhibition combined with DS-8201a was effective at reducing survival in two SN38 resistant cell lines. Understanding the interaction between TOP1 and ATR inhibition will better inform the treatment of CRC.

Impact statement

Cancer is the leading cause of death worldwide, with nearly 10 million cancer related deaths reported in 2020. Colorectal cancer is the third most common cancer, with 1.93 million new cases diagnosed in 2020 (WHO 2021). The incidence rate of CRC has been rising globally since the early 1990s, with the prevalence highest in developed countries (Siegel et al. 2019; Arnold et al. 2017). Approximately 20% of CRC patients present with metastatic disease (Argilés et al. 2020). The prognosis for these patients is poor, with 44% of patients surviving 1 year, and just 10% surviving 5 years in the UK (CRUK 2020). New therapeutic options are required for metastatic CRC (mCRC), to increase patient response rates and prolong survival.

Improved therapeutic outcomes can be achieved by either optimising the use of currently approved drugs or by the development of novel agents. Irinotecan, a TOP1 inhibitor is widely used for the treatment of mCRC, however responses are often short lived and disease progression or recurrence is common (Douillard et al. 2000). In this thesis, it has been demonstrated that inhibiting the DNA damage response kinase, ATR, alongside irinotecan-based therapy, reduces the survival of CRC models. Efficacy of this therapeutic combination is due to be explored by AstraZeneca in an upcoming mCRC clinical trial.

Trastuzumab deruxtecan (DS-8201a), a novel ADC has shown efficacy in HER2+ mCRC patients in a phase I clinical trial (Siena et al. 2021). However, no efficacy has been reported in CRCs with low HER2 expression, which makes this an unlikely therapeutic for more than 95% of mCRC patients (Siena et al. 2018). In this thesis, it has been demonstrated for the first time that ATR inhibition can sensitise HER2-low expressing CRC models to DS-8201a, with a very dramatic loss in cancer viability. This project was carried out in collaboration with Daiichi Sankyo and AstraZeneca. The findings in this study have contributed to the preclinical evidence for the combined

use of ATR inhibition and DS-8201a. A phase I clinical trial is now exploring the tolerability and potential efficacy of this novel combination in cancer patients. If the findings of this trial are positive, efficacy in the mCRC setting will then be investigated.

Acknowledgements

Firstly, I would like to thank my supervisor Prof. Daniel Hochhauser for giving me the opportunity to do a PhD in such a stimulating environment. Thank you for all the support and guidance over the past few years, but also for the scientific independence to explore my own ideas. Thank you to my secondary supervisor, Dr Tim Witney for the scientific advice and encouragement, I received throughout this project. I must also thank Prof. John Hartley and Prof. Tony Ng for their scientific input in the oncology lab meetings.

I must express my tremendous gratitude to The Constance Travis Charitable Trust and the Rosetrees Foundation for funding this PhD project.

Thank you to Maria Ramos from the Tape lab for running the CyTOF organoid experiments, and for always being so happy to assist with the analysis. Thank you to all the members of the Tape lab, including Petra Vlckova, Jahangir Sufi, Dr Xiao Qin and Ferran Cardoso Rodriguez for the optimisation and setting up of the CyTOF protocol. Petra, I have really appreciated the continued guidance and support while establishing the use of organoids in the lab.

I must also acknowledge members of UCL departments that supported my work. Dr Heli Vaikkinen from the genomics facility and Dr Stephen Henderson from the Bill Lyons Informatics Centre who ran the RNAseq experiment and analysis. Thank you to the members of the UCL pathology team who processed and stained IHC samples. Thank you to Dr Paul Barber from the Imaging and Computational Oncology Group for performing the synergy analysis.

Thank you to all my lab colleagues for their friendship and support over the last few years. A special thank you to Dr Juan Jose Garcia Gomez for always being so helpful in every way. Thank you for guiding me through new experimental techniques and for

the many weekends spent proofreading my thesis. Thank you to my fellow PhD student Jo Clancy for being there throughout my PhD journey, providing support through the ups and downs of PhD life. Thank you Kenrick, Fei, Arman, Simon, Arola, Sylwia, Valenti, Jose and Shiran for making the lab such a great place to work.

Thank you to the love of my life, Ephraim. I could never have completed this PhD journey without you by my side. The practical and emotional support you have given me over these years has been immense. Thank you for always believing in me, encouraging me and loving me.

To my precious children, Ariel and Sarah, thank you for lighting up every day of my life.

Thank you to my parents for their unconditional love, for their belief in me, their encouragement and support. Thank you to my brothers and sisters, Yitzchok, Aryeh, Chananyoh, Akiva, Sarah, Elisheva, Azaryoh and Yehudis for being my best friends.

Table of Contents

Table of Figures

Table of Tables

Abbreviations

5-DFCR	5’deoxy-5-fluorocytadine
5-DFUR	5’deoxy-5-fluorouradine
9-1-1	RAD9-RAD1-HUS1
AAD	ATR activation domain
ABC	ATP binding cassette
ADC	Antibody drug conjugate
ADCC	Antibody dependent cytotoxicity
AML	Acute myeloid leukaemia
ATM	A-T mutated kinase
ATR	Ataxia Telangiectasia and Rad-3 related kinase
B-ALL	B-cell acute lymphoblastic leukaemia
BER	Base excision repair
BLM	Bloom syndrome protein
BRD4	Bromodomain-containing protein 4
BSA	Bovine serum albumin
BSC	Best supportive care
CAPOX	Capecitabine and oxaliplatin

CDC	Complement dependent cytotoxicity
Cdk1	Cyclin dependent kinase 1
Cdk2	Cyclin-dependent kinase-2
CES	Carboxylesterase
cGAMP	Cyclic-GMP-AMP
cGAS	cGAMP synthase
Chk1	Checkpoint kinase 1
Chk2	Checkpoint kinase 2
cHL	Classical Hodgkin’s lymphoma
CIMP	CpG island methylator phenotype
CIN	Chromosomal instability
CKBD	Chk1 binding domain
CLL	Chronic lymphocytic leukaemia
CMG	Cdc45-MCM-GINS
CPT	Camptothecin
CR	Complete response
CRC	Colorectal cancer
CTG	CellTitre-GLO

CYP	Cytochrome P450
DACH	1,2-diaminocyclohexane
DAR	Drug to antibody ratio
DC	Dendritic cell
dCK	Deoxycytidine kinase
DDR	DNA-damage response
dH_2O	Distilled H_2O
DHFU	Dihydrofluorouracil
DLBCL	Diffuse large B-cell lymphoma
DLT	Dose limiting toxicity
DMSO	Dimethyl sulfoxide
DNA-PK	DNA-dependent protein kinase
DNMT	DNA methyltransferase
dNTP	Deoxynucleotide
DPD	Dihydropyrimidine dehydrogenase
DREMI	Density Resampled 1133 Estimation of Mutual Information
DSB	Double strand break
dsDNA	Double stranded DNA

Dxd	Deruxtecan
E1	Ubiquitin-activating enzyme
E3	CUL-3-based ubiquitin ligase
ECACC	European Collection of Authenticated Cell Cultures
EGF	Epidermal growth factor receptor
EMD	Earth Mover’s Distance
EP-SCNC	Extra-pulmonary small cell neuroendocrine cancers
ETAA1	Ewing tumour-associated antigen 1
FA	Fanconi anaemia
FACT	Facilitates chromatin transcription
FAP	Familial adenomatous polyposis
FAT	FRAP-ATM-TRAAP
FAT-C	FAT C-terminal
FBS	Fetal bovine serum
FdUMP	Fluorodeoxyuridine monophosphate
FdUTP	Fluorodeoxyuridine triphosphate
FEN1	Flap endonuclease 1
FGF-19	Fibroblast growth factor 19

FISH	Fluorescence *in situ* hybridisation
FOLFIRI	Folinic acid, fluorouracil and irinotecan
FOLFOX	Folinic acid, fluorouracil and oxaliplatin
FOLFOXIRI	Folinic acid, fluorouracil, oxaliplatin and irinotecan
FUDR	Fluorodeoxyuridine
FUTP	Fluorouridine triphosphate
GO	Gemtuzumab ozogamicin
GSH	Reduced glutathione
H&E	Haematoxylin and eosin
HEAT	Huntingtin, elongation factor 3, A subunit protein phosphatase 2A, TOR1 (HEAT) repeat domain
HER	Human epidermal growth factor receptor
HGSOC	High grade serous ovarian cancer
HNSCC	Head and neck squamous cell carcinoma
HR	Homologous recombination
HRP	Horseradish peroxidase
ICI	Immune checkpoint inhibitors
ICL	Interstrand cross link
IdU	Idoxuridine

IHC	Immunohistochemistry
mAb	Monoclonal antibody
mCRC	Metastatic colorectal cancer
Mec1	Mitosis entry checkpoint protein
MF	Mycosis fungoides
MHC-1	Major histocompatibility complex class I
MM	Multiple myeloma
MMAE	Monomethyl auristatin E
MMEJ	Microhomology-mediated end joining
MMR	Mismatch repair
MMRd	Mismatch repair deficient
MRN	MRE11-RAD50-NBS1
MSI	Microsatellite instability
NER	Nucleotide excision repair
NHEJ	Non-homologous end joining
NHL	Non-Hodgkin’s lymphoma
NSCLC	Non small cell lung cancer
OPRT	Ortate phosphoribosylytransferase

OS	Overall survival
PARP1	Poly ADP ribose polymerase 1
PBD	Pyrrolo[2,1-c][1,4]benzodiazepines
PBMCs	Peripheral blood mononuclear cells
PBS	Phosphate-buffered saline
pcALCL	Primary cutaneous anaplastic large cell lymphoma
PCNA	Proliferating cell nuclear antigen F
PD-1	Programmed cell death protein 1
PDAC	Pancreatic ductal adenocarcinoma
PD-L1	Programmed death-ligand 1
PDO	Patient derived organoid
PDX	Patient derived xenograft
PFA	paraformaldehyde
PFS	Progression free survival
PI	Propidium iodide
PIKK	Phosphoinositide 3-kinase related kinase
PLK	Polo-like kinase 1
PLL	Prolymphocytic leukaemia

PNKP	Polynucleotide kinase-phosphatase
PR	Partial response
pRb	Retinoblastoma protein
PRD	PIKK regulatory domain
PRPP	Phosporibosyl pyrophosphate
PTCL	Peripheral T-cell lymphoma
PTM	Post-translational modification
RNR	Ribonucleotide reductase
ROS	Reactive oxygen species
RPA	Replication protein A
Rrm1	Ribonucleotide reductase family member 1
Rrm2	Ribonucleotide reductase family member 2
RSR	Replication stress response
RT	Room temperature
RTK	Receptor tyrosine kinase
sALCL	Systemic anaplastic large cell lymphoma
SCF	Skp1, Cul1 and F-box
SCLC	Small cell lung cancer

SD	Stable disease
SLC	Solute carrier protein
SRB	Sulforhodamine B
SSB	Single strand break
ssDNA	Single stranded DNA
STR	Short tandem repeat
SWI/SNF	Switch/sucrose non-fermentable
TBST	Tris buffered saline with tween
TCRT	Treslin C-terminal domain
T-DM1	Ado-trastuzumab emtansine
TDP1	Tyrosyl DNA phosphodiesterase 1
TEAE	Treatment emergent adverse events
TI	Therapeutic index
TK	Thymidine kinase
TNBC	Triple negative breast cancer
TOP1	Topoisomerase I
TOP1cc	Topoisomerase I DNA cleavage complex
TOP1mt	Mitochondrial topoisomerase I

TOP2α	Topoisomerase 2α
TOP2β	Topoisomerase 2β
TOP3α	Topoisomerase 3α
TOP3β	Topoisomerase 3β
TopBP1	Topoisomerase II binding protein 1
TS	Thymidylate synthase
UGT1	UDP glucuronosyltransferase isoforms
UK	Uridine kinase
UMAP	Uniform Manifold Projection
UP	Uridine phosphorylase
VEGF	Vascular endothelial growth factor
WRN	Werner syndrome ATP dependent helicase
XPA	Xeroderma pigmentosum group A
ZIP	Zero interaction potency model

1 Introduction

1.1 Colorectal cancer

1.1.1 Colorectal cancer epidemiology

Colorectal cancer (CRC) is the third most common cancer worldwide, with 1.93 million new cases diagnosed in 2020 (WHO 2021). CRC accounts for 11.4% of male cancer cases, and 9.7% of female cancer cases worldwide (WCRF 2018). The incidence rate of CRC has been rising globally since the early 1990s. The prevalence of CRC is highest in developed countries, such as the UK (Siegel et al. 2019; Arnold et al. 2017). In the UK alone, more than 42,000 new cases of CRC were diagnosed in 2018, making up 12% of all cancer diagnoses. The lifetime risk for developing CRC in the UK is approximately 6% for females and 7% for males (CRUK 2020).

It is approximated that 54% of CRC cases are preventable, with several lifestyle factors playing a role including, lack of dietary fibre (28%), excessive consumption of red meat (13%), obesity (11%), smoking (7%), alcohol (6%) and lack of physical activity (5%) (Bagnardi et al. 2015; Brown et al. 2018; CRUK 2020; Huxley et al. 2009; Kyrgiou et al. 2017). The overall 5-year survival rate for CRC is approximately 64%. However, the 5 year survival rate is largely dependent on disease stage at diagnosis, for early stage CRC it is approximately 90%, however this falls to 70% for locally advanced cases and 14% for metastatic cases (NIH 2020). The majority of CRC cases are caused by sequential somatic mutations, with only 5% of cases being as a result of heritable germ-line mutations (Burn, Mathers, and Bishop 2013).

1.1.2 Molecular pathogenesis of CRC and molecular subtypes

CRC develops from the mucosa of the colon or rectum, with growth into the bowel lumen and wall (Argilés et al. 2020). The classical model for CRC development is through an accumulation of genetic and epigenetic aberrations, with loss of tumour

suppressors and increased oncogene activity resulting in the sequential transformation of normal colon mucosa to adenoma, then to carcinoma (Figure 1.1) (Vogelstein et al. 2013). However, in recent years genomic studies have identified that tumour development is not a linear pathway, but a highly heterogenous process, with cancers evolving from multiple tumour sub-colonies, each with a unique mutational profile (Bailey et al. 2021). A small number (3.6%) of CRC patients present with multiple or synchronous lesions, with tumours sometime displaying unique histological profiles (Lam et al. 2011). Genomic instability in CRC occurs via three molecular processes, including chromosomal instability (CIN), microsatellite instability (MSI) and CpG island methylator phenotype (CIMP). The genomic instability may occur via a single molecular process, or a combination of processes at different stages of disease progression (Manne et al. 2010).

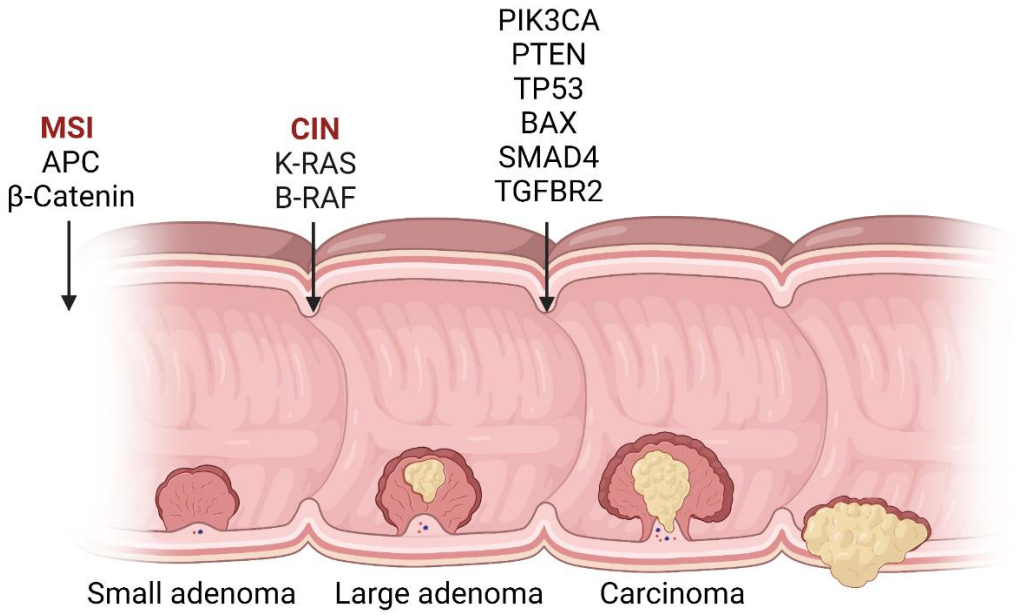

Figure 1.1. **Classical model of genetic mutations driving CRC progression.**
Schematic representation of CRC progression from a small adenoma to carcinoma. This process is highly heterogenous, and genetic alterations driving the progression (shown above image) vary within patients and between patients. Mutations may occur at different stages than indicated. Redrawn from (Markowitz and Bertagnolli 2009). Created with Biorender.

CIN is the most frequent cause of genomic instability in CRC, occurring in 80-85% of sporadic cases. CIN alters both chromosome number and structure, with tumour suppressor inactivation resulting from aneuploidy and loss of heterozygosity. Frequently lost tumour suppressors in sporadic cancers include APC, PTEN p53, BAX, SMAD4 and TGFBR2. Oncogenes activated in CIN sporadic tumours typically include K-Ras, B-Raf, PIK3CA and β-Catenin (Markowitz and Bertagnolli 2009; Smith et al. 2002). CIN tumours also occur in Familial Adenomatous Polyposis (FAP) cases, which arise as a result of loss of function APC germline mutations (Fearon 2011).

1.2 CRC treatment

1.2.1 CRC treatment overview

As with all forms of malignancy, the treatment of CRC depends on disease stage at diagnosis. On CRC diagnosis, pathological staging is performed using the TNM classification system. The T stage includes the tumour size and site, the occurrence of macroscopic tumour invasion, the histological grade, and the extent of invasion into the bowel wall and adjacent organs. The N stage describes the extent of regional lymph node involvement. The M stage classifies the metastatic status of the disease. The TNM system is then used to give an overall cancer anatomic stage (Labianca et al. 2013). Approximately 20% of CRC patients present with metastatic disease, with the liver being the most frequently involved organ (van der Geest et al. 2015).

Surgical resection of the tumour and surrounding lymph nodes is the main therapeutic option for patients with early stage or locally advanced cancer (stages I-III). Patients with stage 0-I or low risk stage II disease, do not routinely receive any adjuvant therapy. Treatment for stage II disease is dependent on risk classification, with some patients with intermediate risk (high grade tumours with lymphatic, vascular or perineural invasion) receiving adjuvant fluorouracil (5-FU) or capecitabine treatment. For stage III or high-risk stage II disease (high grade tumours and lymphatic, vascular

or perineural invasion or T4 disease), patients will typically receive adjuvant chemotherapy to eliminate microscopic disease and reduce the risk of reoccurrence. Chemotherapy is usually a combination of folinic acid, 5-FU, and oxaliplatin (FOLFOX) or capecitabine and oxaliplatin (CAPOX) (Argilés et al. 2020; NICE 2020).

For stage IV disease, surgery may be curative in a small proportion of patients with resectable metastases. Unresectable liver lesions may be managed using transarterial chemo-embolisation or radiofrequency ablation. Additionally, if chemotherapy results in significant tumour regression, curative surgery should be considered if the primary tumour and metastasis become resectable. For the majority of stage IV patients, surgery is palliative, to prevent bowel obstruction. Patients with metastatic disease are generally treated with combination therapy, including chemotherapies and vascular endothelial growth factor (VEGF) or epidermal growth factor receptor (EGFR) targeted agents (Table 1.1). Chemotherapy regimens include one of the following drug combinations, FOLFOX, CAPOX or FOLFIRI (folinic acid (Leucovorin), 5-FU, and irinotecan) (NICE 2020; Van Cutsem et al. 2014). Recent clinical trial results have also shown pembrolizumab (anti-programmed cell death protein 1 (PD-1) antibody therapy) to dramatically enhance progression free survival (PFS) for approximately 60% of patients with MSI(H)/mismatch repair deficient (MMRd) cancers, and therefore should be the preferred therapy over combination chemotherapy for this subset of patients (Andre et al. 2020).

Table 1.1. Therapeutic agents used in the treatment of CRC

Chemotherapy	**EGFR targeted therapies**	**VEGF targeted therapies**	**Immunotherapies MSI(H) / MMRd patients**
Fluoropyrimidines (5-FU, Capecitabine)	Cetuximab	Bevacizumab	Pembrolizumab
Oxaliplatin	Panitumumab	Aflibercept	
Irinotecan		Regorafenib	
TAS-102 (Trifluridine/Tipiracil)		Ramucirumab	

1.2.2 Chemotherapy backbone

First line treatment for advanced CRC typically includes a fluoropyrimidine (5-FU or capecitabine) in combination with either irinotecan or oxaliplatin. FOLFIRI and FOLFOX have been shown to have comparable clinical outcomes in the GERCOR and GOIM trials, but different toxicity profiles and interactions with biologicals (Colucci et al. 2005; Tournigand et al. 2004). The initial choice of chemotherapy is dependent on the preferred toxicity profile, with alopecia and diarrhoea being more severe with irinotecan and, neuropathy occurring with oxaliplatin (Grothey et al. 2004; Tournigand et al. 2004; Van Cutsem et al. 2014). CAPOX can be used as an alternative to FOLFOX, with very similar mechanisms and toxicity profiles (Van Cutsem et al. 2014). The efficacy of a triple combination chemotherapy regimen, including 5-FU, oxaliplatin and irinotecan (FOLFOXIRI) is disputed, with superior efficacy to FOLFIRI demonstrated in an Italian study, but not in a Greek study (Falcone et al. 2007; Souglakos et al. 2006).

Second-line chemotherapy is an option for patients with good performance status and organ function at the time of disease progression. Data suggests that exposure to 5-FU, oxaliplatin and irinotecan over the course of treatment, results in an increase in overall survival (OS) by 3.5 months (Grothey et al. 2004). Therefore, patients who progress on an oxaliplatin-based regimen should be treated with second line irinotecan-based therapy, and vice versa.

1.2.2.1 Fluoropyrimidines

Antimetabolites work by inhibiting key biosynthetic processes, or via incorporation into cellular macromolecules such as DNA and RNA. The mechanism of action of 5-FU involves inhibition of a key nucleotide synthase enzyme, thymidylate synthase (TS) and incorporation into RNA. 5-FU is a uracil analogue, with the hydrogen atom at the C5 position of uracil replaced with a fluorine atom (Figure 1.2). 5-FU is converted into

three active metabolites, fluorodeoxyuridine monophosphate (FdUMP), fluorodeoxyuridine triphosphate (FdUTP) and fluorouridine triphosphate (FUTP) (Longley, Harkin, and Johnston 2003). FdUMP binds to the dUMP binding site of TS, and thereby inhibits the reduction of dUMP to dTMP. TS activity is the only *de novo* source of thymidylate, which is essential for DNA replication and repair. Depletion in dTTP levels results in a reduction in other deoxynucleotide (dNTP) levels, due to generalised disruption of feedback pathways (Longley, Harkin, and Johnston 2003; Santi, McHenry, and Sommer 1974; Sommer and Santi 1974). Altered dNTP levels and relative abundances have also been found to disrupt DNA synthesis and repair (Houghton, Tillman, and Harwood 1995; Yoshioka et al. 1987). FUTP is extensively incorporated into RNA, widely disrupting RNA processing and function, including that of mRNA, rRNA, tRNA and snRNA (Longley, Harkin, and Johnston 2003) .

High levels of intracellular folate are required for binding of FdUMP to TS. 5-FU is given in combination with folinic acid (Leucovorin), to increase intracellular folate levels, maximising FdUMP binding to TS and the stability of the FdUMP-TS complex. The addition of folinic acid to 5-FU improves patient outcome (Longley, Harkin, and Johnston 2003; Thirion et al. 2004).

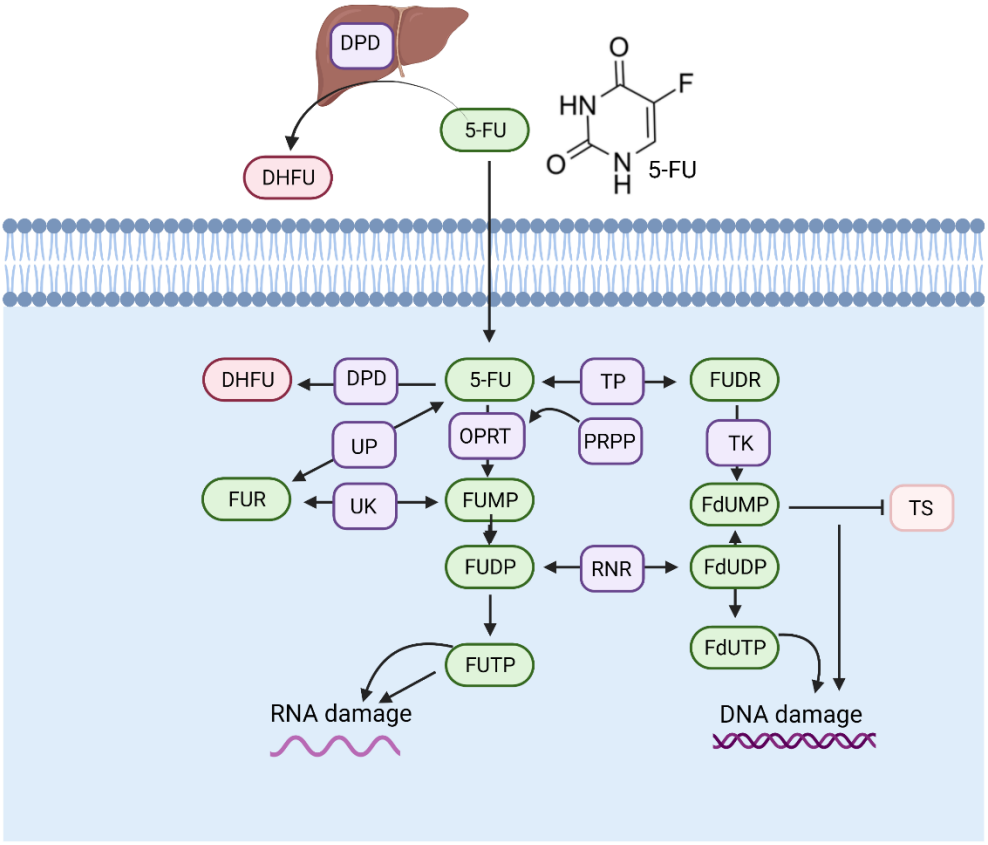

Figure 1.2. **5-FU chemical structure and mechanism of action.**
5-FU (chemical structure shown) is converted into 3 active metabolites FdUMP, FUTP and FdUTP. Ortate phosphoribosylytransferase (OPRT) together with cofactor phosporibosyl pyrosphosphate (PRPP) converts 5-FU into FUMP. Uridine phosphorylase (UP) together with uridine kinase (UK) also convert 5-FU into FUMP. Ribonucleotide reductase (RNR) converts FUDP to FdUDP. 5-FU can also be converted into fluorodeoxyuridine (FUDR), which is then converted into FdUMP via thymidine kinase (TK). Dihydropyrimidine dehydrogenase (DPD) catabolises 5-FU into dihydrofluorouracil (DHFU). Redrawn from (Longley, Harkin, and Johnston 2003). Created with Biorender.

Capecitabine is absorbed through the intestinal mucosa and is sequentially metabolised to 5'-deoxy-5-fluorocytidine (5'-DFCR), 5'-deoxy-5-fluorouridine (5'-DFUR) and 5-FU by the liver and tumour tissues (Pentheroudakis and Twelves 2002). The advantage of Capecitabine is its oral bioavailability, however as many patients require a IV infusion of oxaliplatin or irinotecan this often has very little impact (Pentheroudakis and Twelves 2002).

1.2.2.2 Irinotecan

Irinotecan is a topoisomerase I (TOP1) inhibitor widely used in the treatment of metastatic CRC (mCRC) as part of the FOLFIRI regimen. The addition of irinotecan to 5-FU chemotherapy, increases OS by approximately 3 months (Douillard et al. 2000; Saltz et al. 2001). Dose limiting toxicities include myelosuppression and diarrhoea (Van Cutsem et al. 2014). The mechanism of action of irinotecan is covered in depth in section 1.3.

1.2.2.3 Oxaliplatin

Oxaliplatin is a platinum derivative containing a 1,2-diaminocyclohexane (DACH) carrier. On entry into the cell, oxaliplatin becomes aquated, loosing oxalate ions, and gaining two water molecules (Rabik and Dolan 2007). Once aquated, the oxaliplatin metabolite has a positive charge and therefore interacts with nucleophilic molecules within the cell, including DNA, RNA, and proteins. The N7 atoms of the imidazole rings of guanosine and adenosine in DNA is the most preferred and most frequent cytotoxic target of aquated oxaliplatin. Binding of oxaliplatin to purines can result in the formation of intrastrand crosslinks, interstrand crosslinks (ICLs) and DNA-protein crosslinks (Figure 1.3) (Misset et al. 2000; Rabik and Dolan 2007; Raymond et al. 2002).

Intrastrand crosslinks are the most abundant DNA adducts formed following platinum therapy, with crosslinks forming between two adjacent guanine bases d(GpG) or two adjacent guanine–adenine bases d(GpA) (Misset et al. 2000). The DACH-platinum DNA adducts are highly bulky and hydrophobic, causing greater distortion of the DNA than other platinum agents, thereby inhibiting both DNA and RNA polymerases (Misset et al. 2000; Rabik and Dolan 2007; Raymond et al. 2002). Additionally, the steric interference caused by DACH-platinum DNA adducts prevents the binding of DNA repair complexes, such as the mismatch repair (MMR) machinery, preventing

resolution of the DNA lesions (Chaney et al. 2005; Misset et al. 2000). Both primary and secondary DNA lesions following oxaliplatin treatment contribute to genomic instability and apoptosis (Misset et al. 2000).

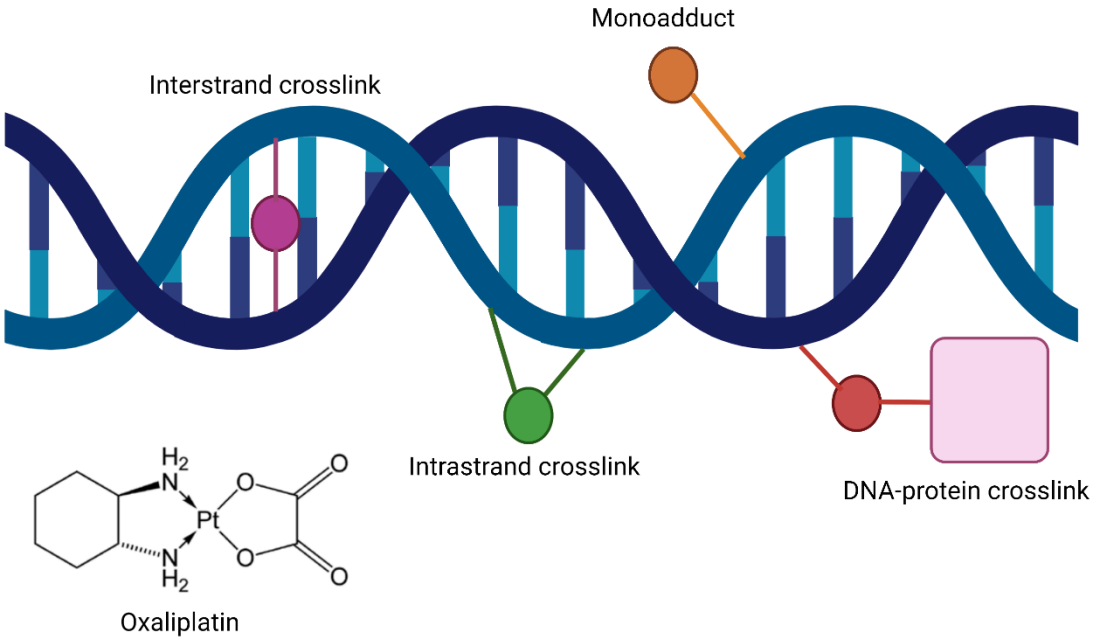

Figure 1.3. **Oxaliplatin is a DNA crosslinking agent.**
Oxaliplatin (chemical structure shown) is metabolised to form a positively charged derivative which interacts with the DNA. DNA adducts include interstrand crosslinks, intrastrand crosslinks, DNA-protein crosslinks and monoadducts. Created with Biorender.

For the treatment of CRC, oxaliplatin treatment is combined with a fluoropyrimidine (5-FU or capecitabine). The combination of oxaliplatin with a fluoropyrimidine is highly synergistic, with oxaliplatin induced downregulation of TS expression believed to contribute to the observed synergy (Fischel et al. 2002; Raymond et al. 2002). Oxaliplatin monotherapy has shown minimal efficacy, but the addition of oxaliplatin to 5-FU increases PFS and best response rates in patients (de Gramont et al. 2000).

1.2.3 Biological targeted therapeutics

Monoclonal antibodies (mAbs) (cetuximab and panitumumab) against EGFR, and mAbs (bevacizumab) or proteins (aflibercept) against VEGF when combined with chemotherapy improve the outcome for mCRC patients. Median OS of >24 months is only consistently achieved in patients who receive a combination of cytotoxic and biological therapeutics (Van Cutsem et al. 2014).

Recent evidence from meta-analyses suggested mCRC patients with left sided, RAS wildtype tumours may experience improved survival outcomes when chemotherapy is combined with anti-EGFR (cetuximab) compared to anti-VEGF (bevacizumab) in the first-line setting (Arnold et al. 2017; Holch et al. 2017). Patients with right sided, RAS wildtype tumours have a poorer prognosis than those with left sided tumours, and may have an improved response when chemotherapy is combined with anti-VEGF (bevacizumab) in the first line setting (Holch et al. 2017).

1.2.3.1 Anti-VEGF biological therapeutics

Antiangiogenic therapies have become standard of care for the treatment of mCRC. Interruption of VEGF and VEGF receptor interaction blocks a key angiogenesis pathway, and has been found to restrict tumour growth and increase patient survival (Tabernero et al. 2015).

Bevacizumab is an anti-VEGF-A mAb, which binds to VEGF-A, and prevents binding of the ligand to VEGF receptors. When combined with cytotoxic agents, bevacizumab has been found to significantly improve patient outcome. The addition of bevacizumab to fluoropyrimidine treatment in patients who are not suitable candidates for oxaliplatin or irinotecan-based therapies, has been shown to increase median OS and PFS (Cunningham et al. 2013; Kabbinavar et al. 2008; Tebbutt et al. 2010). Combining bevacizumab with FOLFIRI, was found to increase OS by approximately 5 months (Hurwitz et al. 2004; Kabbinavar et al. 2008). As both a first line and second

line treatment, the combination of bevacizumab and FOLFOX has been found to increase median OS and PFS compared to FOLFOX alone (Giantonio et al. 2007; Saltz et al. 2008). Continuation of bevacizumab while changing the chemotherapy backbone following disease progression with first-line treatment, has been shown to increase OS and PFS (Bennouna et al. 2013).

1.2.3.2 Anti-EGFR biological therapies

EGFR was the first receptor tyrosine kinase (RTK) linked to human cancers, and has been found to be an important oncogene in CRC (Hynes and Lane 2005). EGFR signalling drives cell cycle progression, cell growth, proliferation, protein synthesis, endothelial to mesenchymal transition and survival. EGFR has become a therapeutic target for some cancer types including CRC (Yarden and Sliwkowski 2001). Anti-EGFR antibody therapy has been shown to improve patient outcome as a monotherapy and in combination therapy, in all lines of treatment. The efficacy of anti-EGFR therapy is limited to patients with RAS-wildtype tumours, and therefore patients with RAS mutant tumours should not receive anti-EGFR therapy at any treatment stage (Amado et al. 2008; Ciardiello et al. 2014; Karapetis et al. 2008; Price et al. 2014; Tejpar et al. 2014; Van Cutsem et al. 2009; Van Cutsem et al. 2011).

Cetuximab is a human-mouse chimeric mAb that binds to the extracellular domain of EGFR, blocking ligand binding and causing down regulation of EGFR (Li et al. 2005; Vincenzi et al. 2008; Wong 2005). Cetuximab has also shown anti-tumour activity *in vivo*, by modulating the anti-tumour immune response via antibody dependent cellular cytotoxicity (ADCC) and complement dependent cytotoxicity (CDC) (Correale et al. 2010).

Cetuximab monotherapy has been shown to increase OS and PFS in patients who have exhausted oxaliplatin, irinotecan and fluoropyrimidine therapies (Jonker et al. 2007; Karapetis et al. 2008). The addition of cetuximab to FOLFIRI in first line and

second line treatment increases PFS and OS in RAS wildtype patients (Ciardiello et al. 2014; Van Cutsem et al. 2014; Van Cutsem et al. 2009; Van Cutsem et al. 2011). There have been conflicting reports as to whether there is any clinical benefit in the addition of cetuximab to oxaliplatin based regimens. In the OPUS study, the addition of cetuximab to FOLFOX, for first line treatment improved PFS and OS (Tejpar et al. 2014). However, Bokemeyer et al., found no statistical change in the PFS with the addition of cetuximab to FOLFOX (Bokemeyer et al. 2009). The COIN study and the NORDIC VII study found there to be no clinical benefit to the addition of cetuximab to FLOX (oxaliplatin and bolus 5-FU / folinic acid) regimens in first line therapy for mCRC (Maughan et al. 2011; Tveit et al. 2012).

Panitumumab is a fully humanized mAb to EGFR. Panitumumab binds to EGFR, causing receptor internalisation thus inhibiting ligand binding in a competitive manner. Binding of panitumumab to EGFR has been shown to inhibit EGF induced proliferation, pro-inflammatory cytokine release and VEGF secretion, as well as increasing autophagy (Keating 2010).

Like cetuximab, panitumumab monotherapy increases PFS in patients with chemo refractory mCRC compared to best supportive care (BSC) (Amado et al. 2008; Van Cutsem et al. 2007). A head-to-head study evaluating cetuximab and panitumumab monotherapies for the treatment of chemo refractory mCRC, found the two anti-EGFR antibodies to have comparable clinical activity (Price et al. 2014). As a second line treatment for mCRC, panitumumab in combination with irinotecan results in a longer PFS than irinotecan alone (Peeters et al. 2010; Seymour et al. 2013). In first line treatment, the addition of panitumumab to oxaliplatin based regimens has been found to extend PFS and OS (Douillard et al. 2013; Douillard et al. 2010).

1.3 Topoisomerase I

1.3.1 Topoisomerase enzymes resolve DNA torsional stress

DNA is highly coiled and supercoiled to enable compaction of the ~2m long polynucleotide in a cell nucleus with a diameter of ~6µm. Furthermore, the genome is organised in loops, which play a role in both DNA compaction and transcriptional regulation. DNA topoisomerases are vital enzymes that resolve DNA torsional stress arising from strand separation during DNA replication and transcription (Pommier et al. 2016; Wang 2002; Watson and Crick 1953). Topoisomerases release topological stress by introducing transient DNA breaks using a transesterification mechanism, minimising the genomic instability that would result from topologically induced strand breaks (Vos et al. 2011).

The human genome encodes six topoisomerases, TOP1, TOP1mt (mitochondrial), topoisomerase IIα (TOP2α), topoisomerase IIβ (TOP2β), topoisomerase IIIα (TOP3α) and topoisomerase IIIβ (TOP3β), with each topoisomerase having both specialised and shared roles (Table 1.2) (Pommier et al. 2016). TOP1 (nuclear) and TOP1mt relax negative and positive DNA supercoils, nicking one DNA strand and facilitating rotation of the broken strand around the intact strand (Stewart et al. 1998). TOP2α and TOP2β enzymes relax negative and positive DNA supercoils, and resolve DNA catenanes and DNA knots, making TOP2 enzymes essential for cell division. TOP2 enzymes cleave both DNA strands, facilitating the passage of one DNA duplex through another duplex (Nitiss 2009b, 2009a). TOP3α relaxes and resolves negatively supercoiled DNA, DNA hemicatenanes, DNA double holiday junctions and DNA loops. TOP3β relaxes hyper negative supercoiling, as well as resolving RNA knots and loops (Pommier et al. 2016; Vos et al. 2011).

Table 1.2. Overview of eukaryotic topoisomerases

	TOP1 + TOP1mt	**TOP2α + TOP2β**	**TOP3α + TOP3β**
Substrates	DNA Sc^- DNA Sc^+	DNA Sc^- DNA Sc^+ DNA knots DNA catenanes	TOP3α: DNA Sc^- Hemicatenanes Double holiday junctions D-loops TOP3β: DNA HSc^- RNA knots R loops
Cofactors	None	$Mg2^+$ and ATP	$Mg2^+$
Mouse knockout phenotype	TOP1: embryonic lethal TOP1mt: viable	TOP2α: embryonic lethal TOP2β: death at birth	TOP3α: embryonic lethal TOP3β: death at birth
Classification	Type 1B	Type 2A	Type 1A

Sc^-, negative supercoiling; Sc^+, positive supercoiling; HSc^-, hypernegative supercoiling (Pommier et al. 2016)

1.3.2 TOP1 relieves torsional stress during replication and transcription

The two strands of the DNA complex must be separated for them to act as templates for replication, recombination, repair, and transcription. There is very limited free rotation of DNA regions flanking transcription and replication complexes, causing supercoiling ahead of replication and transcription forks. TOP1 relaxes the DNA supercoiling, by binding to the DNA duplex and nicking a single DNA strand (Figure 1.4) (Gilbert, Chalmers, and El-Khamisy 2012; Koster et al. 2005; Stewart et al. 1998). Knockdown of TOP1 leads to genomic instability, with an accumulation of stalled replication forks and DNA double strand breaks (DSBs) (Tuduri et al. 2009). Loss of TOP1 activity in transcription leads to the accumulation of R-loops, (tracts of DNA-RNA hybrids), preventing the progression of the elongation polymerase and resulting in the formation of DNA DSBs.

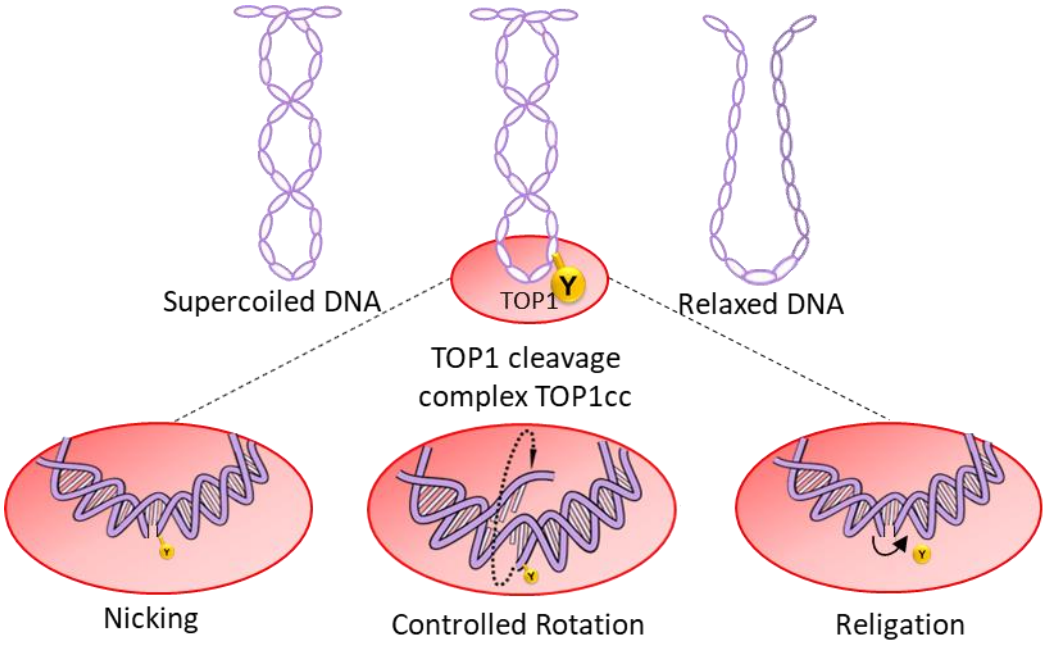

Figure 1.4. **Relaxation of supercoiling by TOP1-mediated DNA cleavage complexes.** The introduction of DNA single-strand breaks by TOP1 enables rotation of the intact DNA strand around the nicked strand, facilitating DNA relaxation. The first step (left) is when the catalytic tyrosine (Y) becomes linked to the 3′ DNA end, nicking DNA. In the second step (middle), the torsional strain drives the rotation of the 5′ end of the nicked DNA strand around the intact strand. In the last step, the 5′ end of the nicked DNA is realigned with the 3′ end, enabling DNA religation. Redrawn from (Pommier 2006).

TOP1 binds to the DNA by the formation of a covalent bond between the catalytic tyrosine (723) residue and 3’ DNA terminus created by the cleavage. This facilitates the rotation of the cleaved strand around the TOP1 bound DNA. Once the supercoiled DNA has been relaxed, TOP1 religates the DNA by aligning the tyrosile-DNA phosphodiester bond with the 5’ end of the cleaved DNA. Reversal of the covalent linkage between the TOP1 tyrosine and 3’ end of cleaved DNA results in the reformation of the phosphodiester bond between the exposed DNA ends. The TOP1-DNA cleavage complex (TOP1cc) is transient, and religation of the DNA is favoured over cleavage (Koster et al. 2005; Pommier 2006; Stewart et al. 1998).

1.3.3 TOP1 recruitment to chromatin is tightly regulated

The interaction of TOP1 with the chromatin is highly dynamic and is controlled by several mechanisms, of which some are discussed in this section. Nucleosomes have been found to shield DNA from TOP1 activity, and restrict TOP1-indcued DNA cleavage (Salceda, Fernández, and Roca 2006). The switch/sucrose non-fermentable (SWI/SNF) complexes are nucleosome remodellers that control nucleosome deposition and histone methylation via recruitment of histone methyltransferases (Hohmann and Vakoc 2014). Apart from modulating access of TOP1 to the DNA, the SMARCA4 component of the SWI/SNF complex directly interacts with TOP1, recruiting TOP1 to the DNA (Husain et al. 2016).

TOP1 is also recruited to transcriptionally active chromatin (marked by H3k4me3), by binding to the facilitates chromatin transcription (FACT) complex, which is a histone chaperone and elongation factor (Husain et al. 2016). Nucleolin, a large T-antigen replication helicase and Werner syndrome ATP-dependent helicase (WRN) also bind and recruit TOP1 to the chromatin (Laine et al. 2003; Seinsoth, Uhlmann-Schiffler, and Stahl 2003). The androgen specific transcription factor NKX3.1, binds directly to TOP1 and increases its catalytic activity (Bowen et al. 2007). Basal transcription factors have also been implicated in the recruitment and modulation of TOP1 in the context of transcription initiation and elongation (Kretzschmar, Meisterernst, and Roeder 1993; Merino et al. 1993; Shykind et al. 1997). One study has demonstrated that TOP1 is kept inactive at transcription initiation start sites to maintain the negative supercoiling required for the promotion of duplex melting, with activation of TOP1 on transcription initiation requiring the Pol II mediated activity of bromodomain-containing protein 4 (BRD4) (Baranello et al. 2016).

1.3.4 TOP1 inhibitors trap DNA in TOP1ccs

Camptothecin (CPT), the first TOP1 inhibitor, was isolated from the bark of a Chinese tree, *Camptotheca acuminata*. Camptothecin carboxylate was tested as an anticancer agent in the 1970s, but was discontinued because of toxicity, despite clinical efficacy. The target of CPT was later identified to be TOP1, leading to the successful development of the water-soluble CPT derivatives, topotecan and irinotecan (Figure 1.5).

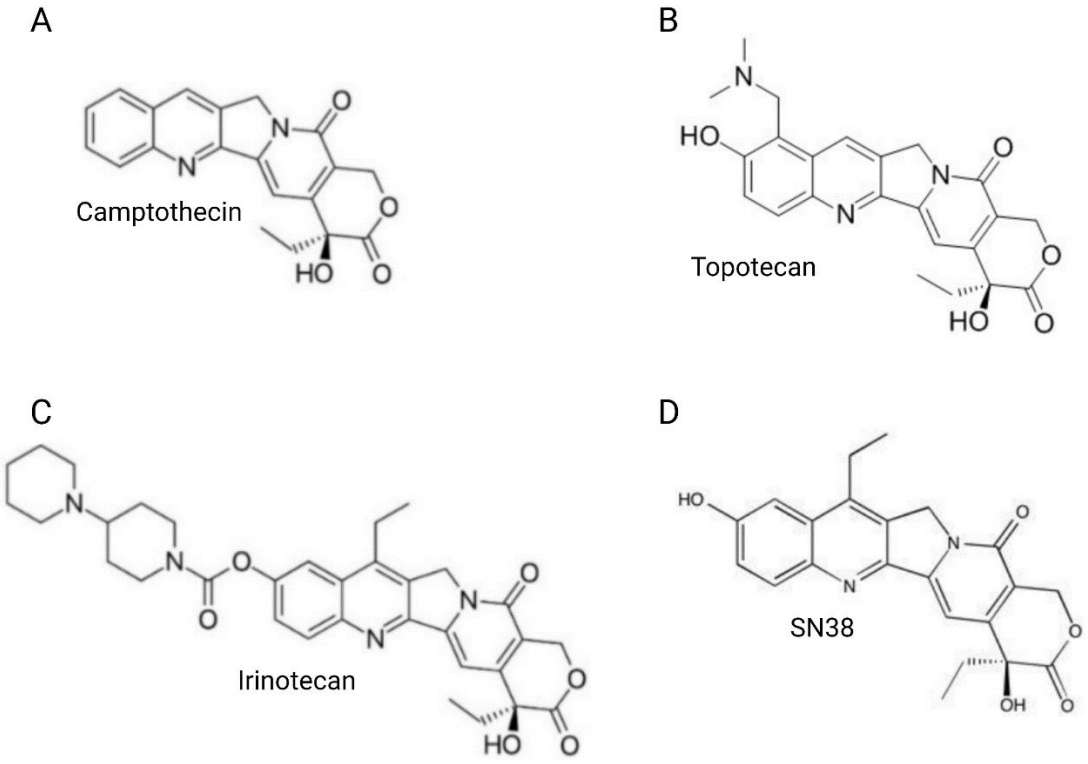

Figure 1.5. **Molecular structure of TOP1 inhibitors.**
A. Camptothecin **B.** Topotecan **C.** Irinotecan **D.** SN38, the active metabolite of irinotecan.

Irinotecan, which is used to treat CRC, is a pro-drug and is converted into its active metabolite SN38 by carboxylesterases (CES) (Hsiang et al. 1985; Wall and Wani 1995). The metabolic pathway of irinotecan is shown in Figure 1.6.

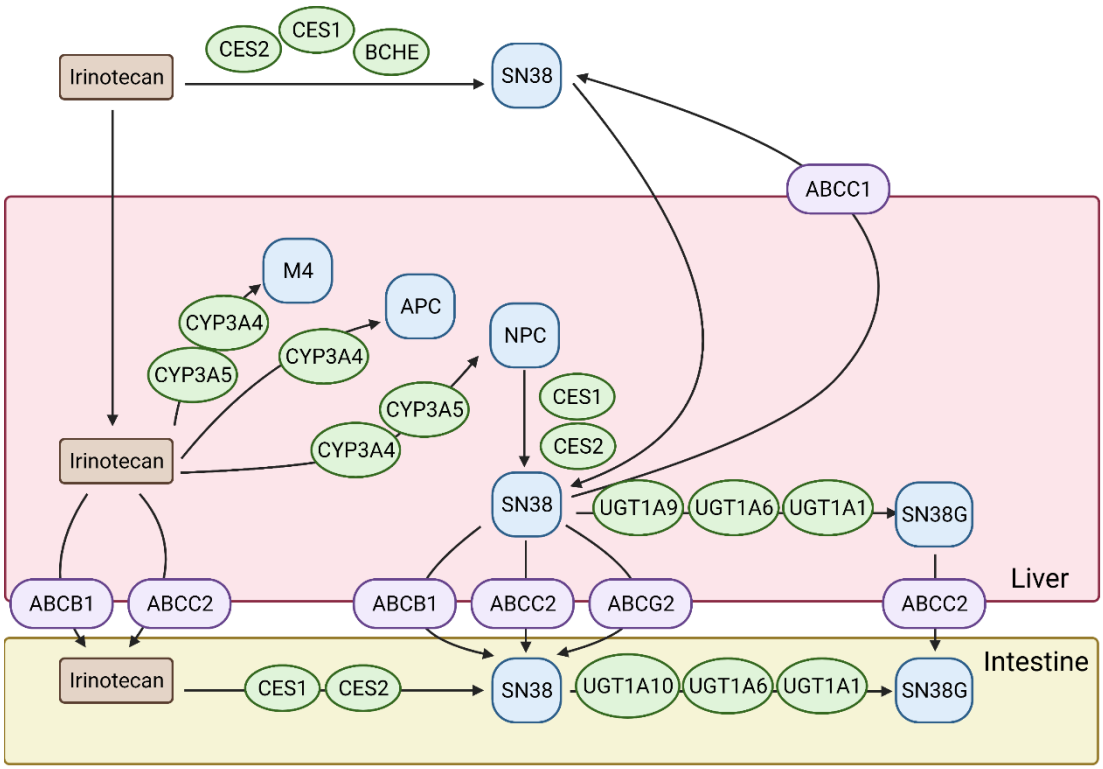

Figure 1.6. **Metabolism of irinotecan.**
Irinotecan is metabolized by cytochrome P450 (CYP) isoforms, human UDP glucuronosyltransferase isoforms (UGT1) and carboxylesterases (CES). Irinotecan and its metabolites are pumped across cell membranes by members of the ABC-binding cassette transporter family. SN38, SN38G, M4, APC and NPC are all irinotecan metabolites. Redrawn from (Scripture and Figg 2006). Created with Biorender.

CPT and its derivatives bind to the TOP1cc, trapping the DNA in the cleavage complex, thereby preventing DNA religation. Binding of CPT occurs via a network of H-bonds forming between the drug and residues Asn722, Arg364 and Asp533 of TOP1 (Thomas and Pommier 2019). Furthermore the polycyclic ring of CPT and its derivative can stack with the base pairs flanking the cleavage site (Jaxel et al. 1991). CPT rapidly penetrates cells and binds to TOP1 within a few minutes of exposure. The binding of CPT to TOP1ccs is reversible, and religation of the DNA occurs within minutes of CPT removal (Pommier 2006). Importantly, TOP1 is the only target of CPT and its derivatives, with loss of TOP1 in yeast cells, causing complete CPT resistance (Eng et al. 1988; Nitiss and Wang 1988).

The trapping of TOP1ccs alone is not toxic to cells, but rather the collision between TOP1ccs and the replication fork, which leads to replication run off, and the formation of irreversible TOP1-DNA complexes and DNA DSBs. As such, quiescent cells are resistant to TOP1 inhibitors, while highly replicative cells are the most sensitive (Horwitz and Horwitz 1973; Hsiang, Lihou, and Liu 1989). The formation of DSBs in response to TOP1 inhibition leads to rapid phosphorylation of histone variant H2AX to form γH2AX. The DNA repair factors involved in the repair of DNA DSBs are covered in section 1.4.

1.3.5 TOP1ccs are resolved by proteasomal degradation and DNA-repair factors

Several cellular mechanisms exist to resolve trapped TOP1ccs prior to replication fork collision. Trapped TOP1ccs are rapidly SUMOylated, ubiquitylated and digested by the 26s proteosome (Desai et al. 1997; Desai et al. 2003; Mao et al. 2000). Transcription and replication fork stalling in response to TOP1ccs has been shown to trigger TOP1cc ubiquitin dependant proteasomal degradation of TOP1ccs (Desai et al. 2003; Lin et al. 2009). The ubiquitination is mediated by the ubiquitin-activating enzyme (E1) and a CUL-3-based ubiquitin ligase (E3), which form Lys-48-linked polyubiquitin chains on TOP1 (Lin et al. 2009). Recently, the activity of SPRTN, a specialised DNA-dependent and DNA replication-coupled metalloprotease has been identified as a proteasomal independent pathway for TOP1cc degradation (Maskey et al. 2017; Vaz et al. 2016). Proteolytic digestions of TOP1 by either SPRTN or the proteosome is unable to fully resolve the TOP1cc due to the unproteolysable nature of the protein-DNA phosphortyrosyl bond (Sun, Saha, et al. 2020). A successive nuclease pathway is required to resolve the TOP1-DNA interaction and generate free single stranded DNA (ssDNA) for DNA repair. The large size of TOP1 and the positioning of the TOP1-DNA crosslink prevents access to DNA repair factors, making

this TOP1cc debulking an essential first stage in the resolution of TOP1ccs (Sun, Saha, et al. 2020).

Tyrosyl DNA phosphodiesterase 1 (TDP1) was the first eukaryotic enzyme discovered to catalyse the removal of TOP1 from TOP1ccs. TDP1 hydrolyses the tyrosyl-DNA phosphodiester bond by forming an intermediary TDP1cc, releasing TOP1 from the cleavage complex. TDP1 is recruited to the TOP1cc in a poly (ADP ribose) polymerase 1 (PARP1) dependent manner. PARP binds to single stranded DNA and catalyses poly ADP ribosylation of itself and other effector proteins including TDP1, stimulating TDP1 activity (Das et al. 2014; Dexheimer et al. 2008). Phosphorylation of TDP1 on residue Ser81 by DNA-dependent protein kinase (DNA-PK) or A-T mutated (ATM) kinase has been found to increase recruitment of TDP1 to CPT-induced TOP1ccs (Das et al. 2009). Additionally, SUMOylation of Lys111 has been implicated in the recruitment of TDP1, with SUMOylation deficient mutant cells displaying impaired resolution of TOP1ccs (Hudson et al. 2012). Methylation of Arg361 and Arg586 by methyltransferase PRMT5 has been found to enhance the repair of TOP1cc, with loss of methylation reducing DNA repair and survival (Rehman et al. 2018). Arginine methylation and poly ADP ribosylation of TDP1 facilitate the recruitment of XRCC1, a key scaffold protein in DNA single strand break (SSB) repair (Das et al. 2014; Rehman et al. 2018).

TOP1ccs can also be resolved by nucleases which cleave and resect the DNA around the TOP1-DNA linkage. The MRE11 endonuclease has been shown to cleave the covalent 3'-phosphotyrosyl-DNA bonds that attach TOP1 to the DNA (Sacho and Maizels 2011). It has also been found that the XPF–ERCC1 nuclease is able to cleave DNA and resolve TOP1ccs, with one study finding the recruitment of XPF–ERCC1 to be PARP and TDP1 dependent (Das et al. 2014; Zhang et al. 2011). Nuclease complexes, MUS81-SLX4 and SLX1-SLX4 have also been implicated in the repair of TOP1ccs (Kim et al. 2013). Once DNA ends have been freed by nuclease activity,

polynucleotide kinase-phosphatase (PNKP) phosphorylates the 5' hydroxyl end, and hydrolyses the 3' phosphate end, readying the DNA ends for polymerase mediated repair (Mei et al. 2020).

Repair of the DNA SSBs can occur via short patch or long patch DNA repair. Short patch repair involves the insertion of a single nucleotide by DNA polymerase β, with religation catalysed by DNA ligase III. Long patch repair which involves the insertion of 2-10 nucleotides can be mediated by polymerases β, ε or δ. Flap endonuclease 1 (FEN1) removes the extraneous DNA flap, and religation is catalysed by proliferating cell nuclear antigen (PCNA) bound DNA ligase I (Caldecott 2008; Mei et al. 2020).

ssDNA generated at trapped TOP1ccs is rapidly bound by replication protein A (RPA) leading to activation of the Ataxia Telangiectasia and Rad-3 related (ATR) signalling. Activation of ATR leads to replication fork arrest, limiting collisions between replication machinery and TOP1ccs (Josse et al. 2014; Thomas et al. 2021). The role of ATR signalling in replication arrest and DNA damage is covered in depth in section 1.5. In the absence of ATR signalling, replication run off occurs, forming DSBs which trigger ATM and DNA-PK mediated repair via homologous recombination (HR) or non-homologous end joining (NHEJ) (section 1.4).

1.4 DNA Damage repair

1.4.1 DNA damage is a continuous process in cells

Endogenous and exogenous factors result in continued damage of nuclear DNA. Spontaneous DNA alterations arise from introduction of base mismatches during replication, interconversion between DNA bases as a result of deamination, loss of DNA bases by depurination, and the modification of bases by alkylation and methylation. Reactive oxygen species (ROS) produced during cellular metabolism cause base oxidation and the induction of DNA strand breaks. SSBs and DSBs can

also occur as a result of abortive topoisomerase activity (Blackford and Jackson 2017; Ciccia and Elledge 2010; Roos, Thomas, and Kaina 2016). It is estimated that each human cell could accumulate as many as 10^5 spontaneous mutations a day (Hoeijmakers 2009). In addition, chemical reactions, exposure to UV, ionizing radiation and exogenous chemicals can cause the formation of DNA base adducts, DNA cross-links, SSBs and DSBs (Roos, Thomas, and Kaina 2016).

1.4.2 Phosphoinositide 3-kinase related kinases (PIKKs) drive DNA damage repair pathways

As maintenance of the genome is essential at the cellular and organismal level, all organisms have evolved DNA-damage response (DDR) pathways. The cellular DDR involves lesion recognition, stalling of the cell cycle and DNA repair. The DDR may result in apoptosis or cellular senescence for unrepairable lesions, preventing the propagation of mutant cells (Blackford and Jackson 2017). Like many other cellular processes, the DDR is mediated by intracellular signalling cascades driven by protein phosphorylation. The human genome encodes a protein Ser/Thr kinases family known as the phosphoinositide 3-kinase related kinases (PIKKs) which master regulate the DDR. The 3 key DDR PIKKs are, DNA-PK, ATM and ATR (Ciccia and Elledge 2010). DNA-PK, ATM and ATR are all very large polypeptides (4128, 3056 and 2644 amino acids respectively) with similar domain and structural features (Figure 1.7) (Bosotti, Isacchi, and Sonnhammer 2000; Mordes et al. 2008; Perry and Kleckner 2003). ATR and ATR signalling are covered in depth in section 1.5.

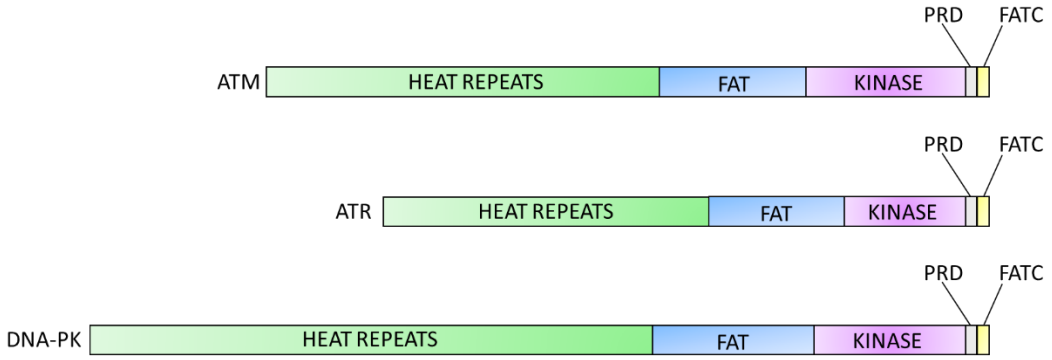

Figure 1.7. **Shared domain features of the 3 DDR PIKKs.**
All 3 proteins have a huntingtin, elongation factor 3, A subunit protein phosphatase 2A, TOR1 (HEAT) repeat domain, a FRAP-ATM-TRAAP (FAT) domain, a kinase domain, a PIKK regulatory (PRD) domain, and a FAT-C terminal (FATC) domain. Redrawn from (Blackford and Jackson 2017).

1.4.3 DNA-PK promotes NHEJ repair of DNA DSBs

The catalytic subunit of DNA-PK, known as DNA-PKcs is recruited specifically to DSBs, where it promotes DNA repair via the NHEJ pathway (Jette and Lees-Miller 2015). The majority of DSBs in mammalian cells are repaired via the NHEJ pathway, with HR preferentially occurring only when the DSB is detected at a replication fork (Beucher et al. 2009; Karanam et al. 2012). NHEJ, involves the religation of the two broken DNA ends without the need for a DNA template, and involves only minimal end resection (3-5bp). In contrast, HR involves significant end resection of the DNA ends, and invasion of the single stranded DNA into another DNA molecule, which is used as a template for DNA repair. Although more error prone than HR, NHEJ is highly efficient and mostly accurate (Bétermier, Bertrand, and Lopez 2014).

Recruitment and activation of DNA-PKcs in response to DSBs requires binding of the Ku heterodimer, comprised of Ku70 and Ku80 (Gell and Jackson 1999; Singleton et al. 1999). There are multiple autophosphorylation sites on DNA-PKcs, with Ser2056 and Thr2609 marking DNA-PK activation (Chan et al. 2002; Chen et al. 2005). Binding

of DNA-PK to the site of DSBs leads to the recruitment of further NHEJ factors including XRCC4, XLF, DNA ligase IV, which align and ligate the DNA (Ahnesorg, Smith, and Jackson 2006; Grawunder et al. 1997; Li et al. 1995). The endonuclease Artemis is also recruited in a DNA-PKcs dependent manner and plays an important role in DNA-end processing (Moshous et al. 2001). The NHEJ machinery and DNA-PKcs are stabilised on the damaged chromatin by PAXX (Ochi et al. 2015). Following DNA-end ligation, disassembly of DNA-PK and the NHEJ machinery occurs (Figure 1.8).

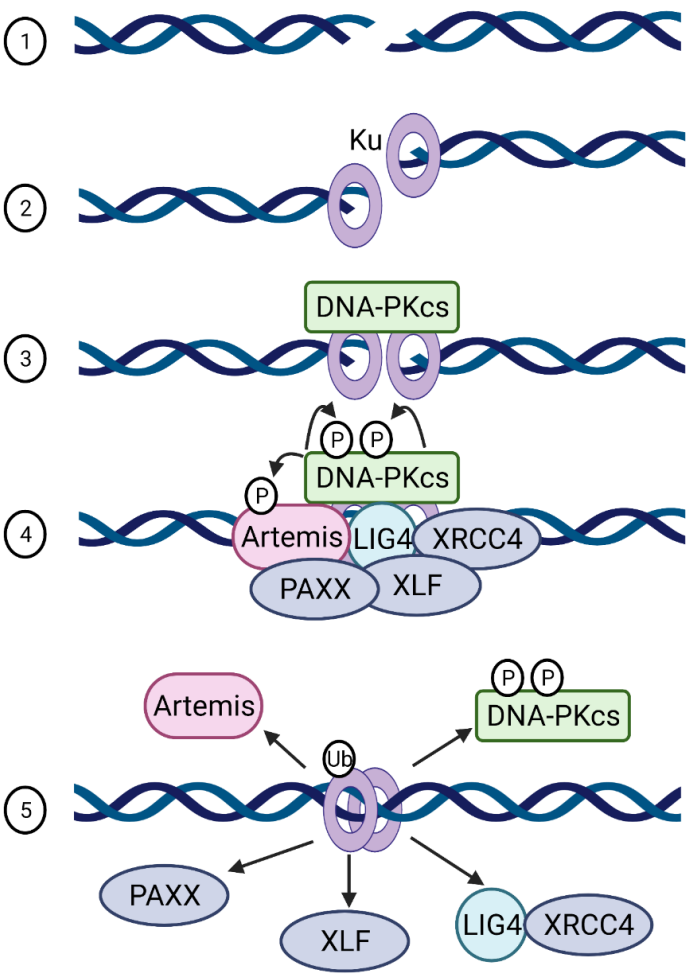

Figure 1.8. **The role of DNA-PK in NHEJ.**

1. DNA DSB formation. 2. The Ku heterodimer binds to the DNA ends. 3. DNA-PKcs is recruited to the DSB. 4. Recruitment of the NHEJ core factors. 5. DNA end ligation and NHEJ complex disassembly. Redrawn from (Blackford and Jackson 2017). Created with Biorender.

1.4.4 ATM orchestrates the cellular response to DNA DSBs

ATM is described as the apical kinase responsible for an orchestrated cellular response to DSBs. ATM and downstream kinases phosphorylate hundreds of substrates in response to DNA damage, influencing a wide range of cellular processes including, checkpoint activation, DNA repair, senescence, apoptosis, chromatin remodelling and transcription (Figure 1.9) (Phan and Rezaeian 2021). A few of the key elements of ATM signalling are discussed in this section.

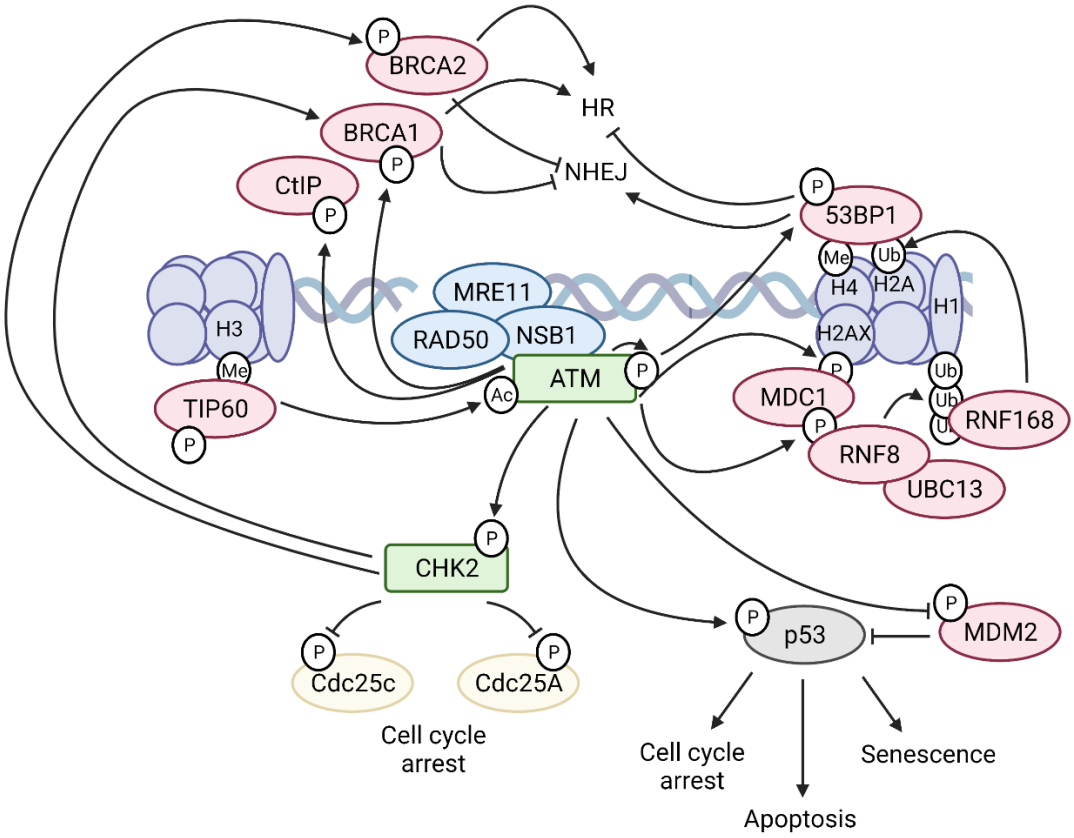

Figure 1.9. **ATM signalling in response to DNA DSBs.**
ATM cell signalling leads to cell cycle arrest, DNA repair, senescence, and apoptosis. Some of the key proteins involved in ATM signalling are shown. Redrawn from (Blackford and Jackson 2017). Created with Biorender.

ATM recruitment and activation in response to DSBs requires the MRE11-RAD50-NBS1 (MRN) complex, with ATM binding to the C-terminus of NBS1 (Chaney et al. 2005; Falck, Coates, and Jackson 2005). Following DSBs, exposed nucleosomes with the H3K9me3 histone mark are recognised by the TIP60 acetyltransferase, which acetylates residue Lys3016 of ATM, stimulating ATM activity (Barlow et al. 1996; Sun et al. 2005; Sun et al. 2009; Sun et al. 2007). On activation, ATM goes from a resting heterodimer to an active monomer (Bakkenist and Kastan 2003). Following activation, ATM auto-phosphorylates on residue Ser1981, however this phosphorylation is not required for kinase activity, with its exact function not currently understood (Blackford and Jackson 2017; Daniel et al. 2008; Pellegrini et al. 2006).

DSBs trigger rapid phosphorylation of Ser139 in the C-terminal histone variant H2AX, a modification termed ɣH2AX (Rogakou et al. 1998). This histone modification is largely mediated via ATM (Burma et al. 2001). MDC1 specifically binds to ɣH2AX at DSB sites, and is phosphorylated by ATM, leading to MDC1 dimerization (Jungmichel et al. 2012; Liu et al. 2012). pMDC1 interacts with NBS1 of the MRN complex, leading to further recruitment of ATM and phosphorylation of H2AX, thereby amplifying the DNA damage signal (Chapman and Jackson 2008). Furthermore, phosphorylation of MDC1 by ATM leads to the recruitment and retention of RNF8 (a ubiquitin ligase), which together with UBC13 (a ubiquitin conjugating enzyme) stimulates the ubiquitination of linker H1 (Thorslund et al. 2015). This ubiquitin modification in turn leads to the recruitment of an additional ubiquitin ligase, RNF168, which ubiquitylates Lys15 of H2A histones (Mattiroli et al. 2012). 53BP1, a major scaffold protein in the NHEJ pathway is recruited to the ubiquitylated H2A histones, and is phosphorylated by ATM, leading to the recruitment of NHEJ factors (Fradet-Turcotte et al. 2013). Importantly, ATM signalling at DSBs renders the site transcriptionally inactive, preventing any collision between the DNA-repair and transcription machinery (Shanbhag et al. 2010) .

ATM can also promote HR by phosphorylating CtIP, which is a key factor required for DNA end resection. DNA end resection produces tracts of ssDNA that can be bound by the RAD51 recombinase, which enables strand invasion of another DNA molecule (Sartori et al. 2007; Wang et al. 2013). ATM also phosphorylates BRCA1 on multiple residues in response to DSBs, with BRCA1 activity required for the unloading of 53BP1 and the recruitment of RAD51 (Ahlskog et al. 2016; Cortez et al. 1999).

One of the most well studied targets of ATM signalling is checkpoint kinase 2 (Chk2). Following DNA damage Chk2 is phosphorylated on residue Thr68 by ATM, resulting in Chk2 activation (Ahn et al. 2002; Xu, Tsvetkov, and Stern 2002). Chk2 kinase activity regulates cell cycle arrest, DNA damage repair, senescence and apoptosis. Multiple phosphorylation targets are common to both Chk2 and ATM (Zannini, Delia, and Buscemi 2014). Chk2 stalls the cell cycle in response to DNA damage, one mechanism involves the phosphorylation of the CDC25A phosphatase, leading to its proteasomal degradation. This prevents the dephosphorylation and activation of cyclin-dependent kinase-2 (Cdk2) required for G1/S transition and S-phase progression (Falck et al. 2001). In addition, Chk2 phosphorylation of CDC25C prevents dephosphorylation of the cyclinB1/cyclin dependent kinase 1 (Cdk1) complex and prevents G2/M transition (Matsuoka, Huang, and Elledge 1998; Takizawa and Morgan 2000). Like ATM, pChk2 can also promote HR following DSB formation. Chk2 phosphorylates BRCA1 and BRCA2, leading to RAD51 recruitment and stabilisation at DSBs, favouring repair via HR over NHEJ (Bahassi et al. 2008; Lee et al. 2000).

Another well studied target of ATM is p53. The tumour suppressor p53 is activated in response to DNA damage, leading to the transcription of genes involved in cell cycle arrest, senescence, or apoptosis (Shiloh and Ziv 2013). ATM phosphorylates p53 on multiple sites, with phosphorylation of residue Ser15 essential for p53 stabilization (Banin et al. 1998; Canman et al. 1998). Ser15 phosphorylation of p53 disrupts the

interaction between p53 and the ubiquitin ligase MDM2, preventing ubiquitin mediated degradation of p53 (Shieh et al. 1997). ATM-dependent phosphorylation of MDM2, further inhibits p53 degradation (Cheng and Chen 2010).

1.5 ATR

1.5.1 Discovery and structure of ATR

ATR was first identified in 1996 as the mammalian orthologue of the budding yeast protein, mitosis entry checkpoint protein (Mec1) and the fission yeast protein, Rad3 (Cimprich et al. 1996; Bentley et al. 1996). The Mec1/Rad3 kinase acts as the master regulator of DNA damage checkpoints in yeast (Cimprich et al. 1996; Bentley et al. 1996).

ATR is a very large polypeptide of ~300kDa, and shares much of its domain organisation with the other members of the PIKK family. The kinase domain is close to the C-terminus of the protein, with the FAT domain directly upstream, followed by a helical solenoid HEAT repeat region and the ATRIP binding domain, which is at the N-terminus. The PRD and FAT C-terminal motif are downstream of the kinase domain (Figure 1.10) (Mordes et al. 2008).

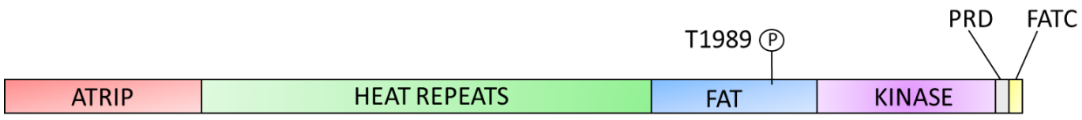

Figure 1.10. **Protein domains of ATR.**
ATR contains a HEAT repeat domain, a FRAP-FAT domain, a PRD domain, a FATC domain and an ATRIP binding domain.

The HEAT repeat domain of the protein is believed to be important in ATR protein-protein interactions. The C-terminus of HEAT repeats, contains an ATRIP binding domain, and loss of this domain prevents ATRIP binding and inhibits ATR function

(Blackford and Jackson 2017; Chen et al. 2007; Perry and Kleckner 2003). The PRD domain has been demonstrated to play an important role in regulating the kinase activity of ATR, although loss of this domain does not impair kinase function. It has been shown that the PRD domain is critical for the activation of ATR via topoisomerase II binding protein 1 (TopBP1) (Mordes et al. 2008). While the FATC domains in ATM and DNA-PKcs are essential for the binding of Tip60 and the subsequent activation of the kinases, this is not thought to be the case for ATR, which is not known to interact with Tip60 (Jiang et al. 2006). However, the FATC region of ATR is essential to the kinase function of ATR, with all kinase activity lost on mutation of the FATC domain. It is proposed that the FATC domain is essential for the correct folding of the kinase domain in ATR (Mordes et al. 2008). The function of the FAT domain is poorly understood, but like the FATC domain, it is believed to be important for kinase regulation (Weber and Ryan 2015).

1.5.2 Activation of ATR is a multistep process

The recruitment and activation of ATR is a multi-stage process (Figure 1.11). ATR is activated by extended tracts of ssDNA (minimum 50-75 nucleotides), coated with RPA. Activation of ATR primarily occurs at junctions between double stranded DNA (dsDNA) and ssDNA (Zou and Elledge 2003). ssDNA and dsDNA junctions largely occur due to uncoupling of the helicase-polymerase complex at the site of stalled replication forks. The presence of ssDNA and dsDNA junctions can also occur due to nucleolytic processing of a wide range of DNA aberrations, such as during nucleotide excision repair (NER), base excision repair (BER) and DNA end resection following DSBs (Bradbury et al. 2020). Coating of ssDNA with RPA prevents nucleolytic degradation of damaged DNA, and marks DNA aberrations, initiating the repair process (Maréchal and Zou 2015).

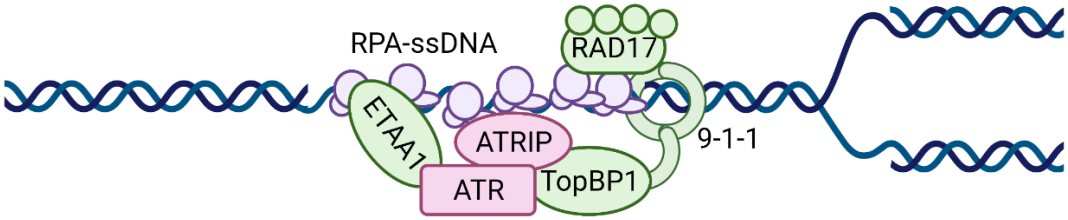

Figure 1.11 **ATR activation.**
Recruitment of ATR to RPA-coated ssDNA requires either TopBP1 or ETAA1. Created with Biorender.

In mammalian cells, ATR is constitutively bound to ATRIP, via an ATRIP binding site at the N-terminus of ATR. ATRIP contains an ATR binding site at its C-terminus, and an RPA binding site at its N-terminus (Ball et al. 2007; Ball, Myers, and Cortez 2005; Cortez et al. 2001; Zou and Elledge 2003). Binding to ATRIP is essential for the function of ATR, with loss of ATRIP being phenotypically identical to loss of ATR, resulting in embryonic lethality and loss of cell viability. Recruitment of ATR to RPA-coated ssDNA occurs via its binding partner ATRIP (Ball et al. 2007; Cortez et al. 2001; Zou and Elledge 2003).

Binding of the ATR-ATRIP complex to RPA-coated ssDNA is insufficient to activate ATR. Kinase activity of ATR requires the presence of an activator protein, of which two have been identified, TopBP1 and Ewing tumour-associated antigen 1 (ETAA1) (Bass et al. 2016; Feng et al. 2016; Haahr et al. 2016; Kumagai et al. 2006; Lee et al. 2016; Mordes et al. 2008). TopBP1 binds and activates ATR in an ATRIP dependant manner, with binding surfaces on both ATR and ATRIP required (Kumagai et al. 2006; Mordes et al. 2008). TopBP1 is believed to cause a conformational change in the ATR-ATRIP complex, which enables ATR kinase activity (Kumagai et al. 2006). Loss of the PRD domain on ATR, which abolishes binding of TopBP1 to ATR, results in complete loss of ATR function (Mordes et al. 2008). As is the case with ATR and ATRIP, loss of TopBP1 is embryonic lethal in mice (Jeon et al. 2011). The embryonic

lethality of TopBP1 loss is due to loss of ATR function, as mutation of the ATR activation domain (AAD) of TopBP1 is phenotypically the same as total loss of TopBP1 (Zhou et al. 2013).

The recruitment of TopBP1 to the site of DNA damage occurs via the RAD9-RAD1-HUS1 (9-1-1) complex, which has a heterotrimeric ring structure, and the RAD17-RFC complex (Delacroix et al. 2007; Ellison and Stillman 2003; Lee, Kumagai, and Dunphy 2007; Zou, Cortez, and Elledge 2002; Zou, Liu, and Elledge 2003). The RAD17-RFC complex, which is comprised of RAD17, Rfc2, Rfc3, Rfc4 and Rfc5 is constitutively bound to DNA (Ellison and Stillman 2003). When the DNA adopts a conformation that is associated with DNA damage, such as ssDNA-dsDNA junctions or DNA gaps, the RAD17-RFC complex, which binds strongly to RPA coated DNA, recruits the 9-1-1 complex (Zou, Liu, and Elledge 2003). The N-terminus of TopBP1 binds with c-terminal tail of the RAD9 component of the 9-1-1 complex, facilitating ATR activation (Delacroix et al. 2007; Lee, Kumagai, and Dunphy 2007). The MRN complex has also been implicated in the recruitment of TopBP1 to RPA-coated DNA, with MRE11, being the critical subunit for TopBP1 interaction (Duursma et al. 2013; Lee and Dunphy 2013). The RHINO protein has also been identified to play a role in the recruitment and activity of TopBP1, although the mechanism by which this occurs remains unknown (Cotta-Ramusino et al. 2011; Lindsey-Boltz et al. 2015).

A second ATR kinase activator, ETAA1 was identified in 2016. ETAA1 contains two RPA binding sites (one at the C-terminus and another at the centre of the polypeptide), and binds directly to RPA-coated ssDNA. ETAA1 contains an ATR activating domain, and binding of ETAA1 to ATR, stimulates ATR kinase activity (Bass et al. 2016; Feng et al. 2016; Haahr et al. 2016; Lee et al. 2016). ETAA1 and TopBP1 work in parallel, and the activity of each ATR activator is independent of the other, with TopBP1 being fully functional with loss of ETAA1 and vice versa (Haahr et al. 2016). While TopBP1 and ETAA1 are both activators of ATR, they appear to play

differential roles, with ETAA1 being the principal activator of ATR during mitosis of unperturbed cells and TopBP1 being the primary activator in response to replication stress (Bass and Cortez 2019; Saldivar et al. 2018). Indeed, the phosphorylation targets of ATR are dependent on the associated ATR activator. TopBP1 activation of ATR results in phosphorylation of targets involved in the replication stress response, while ETAA1 activation results in ATR phosphorylating effectors in mitosis (Bass and Cortez 2019). Unlike TopBP1, loss of ETAA1 in mice is part embryonic lethal, with a reduced number of embryos surviving. Adult mice with loss of ETAA1 appear healthy but display deficient T-cell expansion (Saldivar et al. 2018).

Phosphorylation analysis of activated ATR, identified a phospho-site on residue Thr1989, located within the FAT domain of ATR. Phosphorylation of threonine 1989, has been identified as autophosphorylation, with ATR kinase activity required for the protein modification (Liu et al. 2011; Nam et al. 2011). Consensus has not been achieved on the role of this phospho-site, with conflicting data reported. Liu et al., have reported autophosphorylation to occur on recruitment of the ATR-ATRIP complex to RPA, with phosphorylation being important for the binding of TopBP1 (Liu et al. 2011). Nam et al., have published that loss of the PRD domain on ATR, which prevents binding of TopBP1, results in loss of Thr1989 autophosphorylation. In addition, they found loss of Thr1989 to have no impact on TopBP1 recruitment (Nam et al. 2011). Thr1989 phosphorylation has been identified by some as non-essential for ATR kinase activity, with mutant ATR-T1989A, having very little impact on kinase activity or cell viability, while others report a reduction in ATR signalling (Liu et al. 2011; Nam et al. 2011).

1.5.3 ATR arrests the cell cycle in response to replication stress

The central role of ATR is in initiating the replication stress response (RSR), which prevents breakage and collapse of stalled replication forks. Much of ATR signalling in response to replication stress, occurs via the downstream kinase, checkpoint kinase 1 (Chk1). Indeed, loss of Chk1 results in pre-implantation embryonic lethality in mice, with cells being phenotypically similar to those with ATR loss (Liu et al. 2000). Chk1 is constitutively associated with chromatin, and on ATR activation is recruited to sites of DNA damage via the adapter protein Claspin (Chini and Chen 2006; Jeong et al. 2003; Kumagai and Dunphy 2003; Smits, Reaper, and Jackson 2006). In the presence of DNA damage, residues Ser864 and Ser895 in the Chk1 binding domain (CKBD) of claspin become phosphorylated, and enable binding to the N-terminal kinase domain of Chk1 (Jeong et al. 2003; Kumagai and Dunphy 2003). On recruitment to the DNA-damage complex, Chk1 is phosphorylated on residues Ser317 and Ser345 by ATR (Guo et al. 2000; Hekmat-Nejad et al. 2000; Liu et al. 2000; Zhao and Piwnica-Worms 2001). Chk1 phosphorylation results in Chk1 kinase activation and causes dissociation from claspin, facilitating the interaction of Chk1 with downstream targets (Jeong et al. 2003; Smits, Reaper, and Jackson 2006).

Once activated, Chk1 phosphorylates a multitude of downstream targets inducing S phase and G2 cell cycle checkpoints, facilitating DNA repair and preventing cell cycle progression (Figure 1.12). Chk1 phosphorylates the phosphatase CDC25A on residues Ser123, Ser178, Ser278 and Ser292, which results in CDC25A ubiquitination by the multi-subunit E3 ligase, Skp1, Cul1 and F-box (SCF) complex. Once ubiquitinated CDC25A undergoes proteasomal degradation (Dai and Grant 2010; Sørensen et al. 2003; Zhao and Piwnica-Worms 2001). CDC25A removes an inhibitory phosphate from Tyr15 of Cdk2. In the absence of active Cdk2-cyclin E/A complexes, the cell cannot progress into S phase. Loss of Cdk2 activity also prevents S phase progression with replication fork firing inhibited and the intra-S phase DNA

damage checkpoint activated (Dai and Grant 2010; Smits and Gillespie 2015). Chk1 also phosphorylates CDC25C on residue Ser216, this results in binding of CDC25C to the 14-3-3 protein, which promotes nuclear export of CDC25C (Peng et al. 1997; Sanchez et al. 1997; Zeng et al. 1998). CDC25C removes the inhibitory phosphate from Tyr15 of Cdk1. Loss of nuclear CDC25C, results in high levels of phosphorylated Cdk1. Without active Cdk1/Cyclin B complexes, cells cannot progress from G2 into mitosis (Dai and Grant 2010; Smits and Gillespie 2015). It has also been reported that Chk1 phosphorylates Wee1 on Ser549, leading to binding of Wee1 to 14-3-3. Binding of Wee1 to 14-3-3 results in nuclear retention of Wee1 and increased kinase activity. Wee1 phosphorylates Cdk1/2 on residue Tyr15, resulting in inhibition of Cdk/cyclin complexes and stalling of the cell cycle (Lee, Kumagai, and Dunphy 2001).

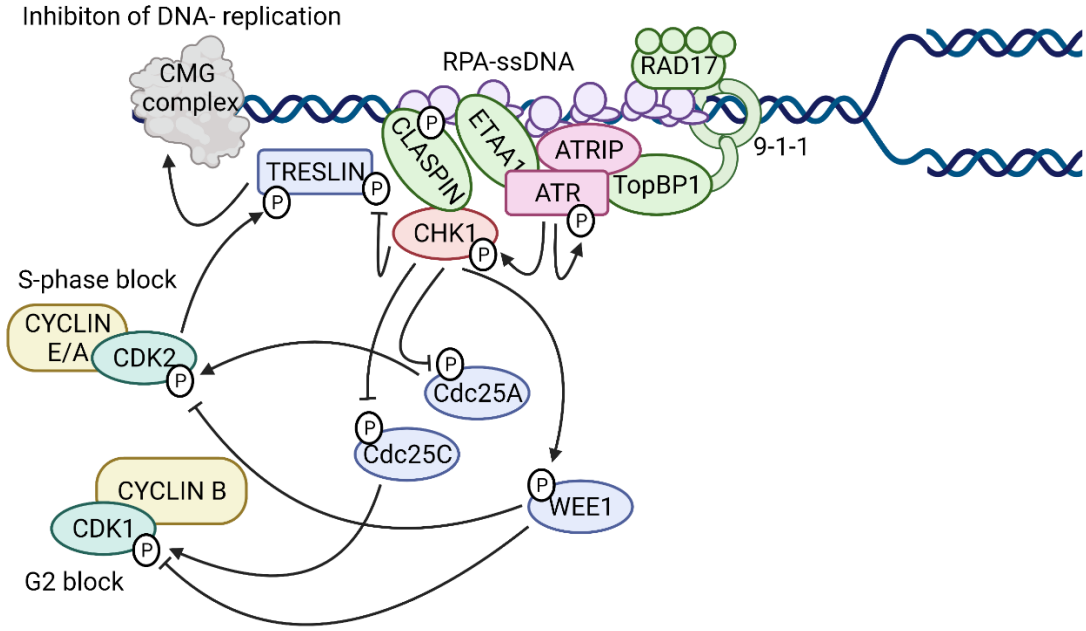

Figure 1.12. **ATR activation causes cell cycle arrest.**
Upon activation, ATR phosphorylates downstream kinase Chk1, which leads to cell cycle arrest. Created with Biorender.

For DNA replication to occur during S-phase, loading of Cdc45 and GINS onto the chromatin must occur. Cdc45 and GINS, complex with minichromosome maintenance (MCM) to from the Cdc45-MCM-GINS (CMG) complex, which is the fully functional helicase required for replication origin firing (Tanaka and Araki 2013). Loading of Cdc45 and GINS is mediated by the TopBP1-Treslin complex (Kumagai et al. 2010; Sansam et al. 2010). The S-phase Cdk2 phosphorylates Treslin on residues T969 and S1001 and this causes binding of TopBP1 to the N-terminus of Treslin (Kumagai et al. 2011). Activation of Chk1 due to replication stress results in reduced Cdk2 activity and therefore inhibits the binding of TopBP1 to Treslin, preventing replication origin firing (Boos et al. 2011). Furthermore, Chk1 binds directly to the C-terminus of Treslin and phosphorylates residues Ser1893 and Thr1897 in the Treslin C-terminal domain (TCRT). Phosphorylation of the TCRT domain inhibits Treslin activity and thereby inhibits the initiation of DNA replication (Guo, Kumagai, et al. 2015).

1.5.4 ATR prevents replication fork collapse

ATR signalling acts to stabilize stalled DNA replication forks, promote DNA repair and stimulate replication initiation (Figure 1.13). Replication fork collapse can result in incomplete DNA replication. While collapsed replication forks can be restored through DNA recombination and activation of DNA damage repair pathways, this increases genetic instability due to nucleotide deletion, chromosomal translocations, and low fidelity replication. Replication fork collapse can occur as a result of RPA exhaustion, replisome disassembly or aberrant activity of fork processing enzymes such as nucleases (Cortez 2015).

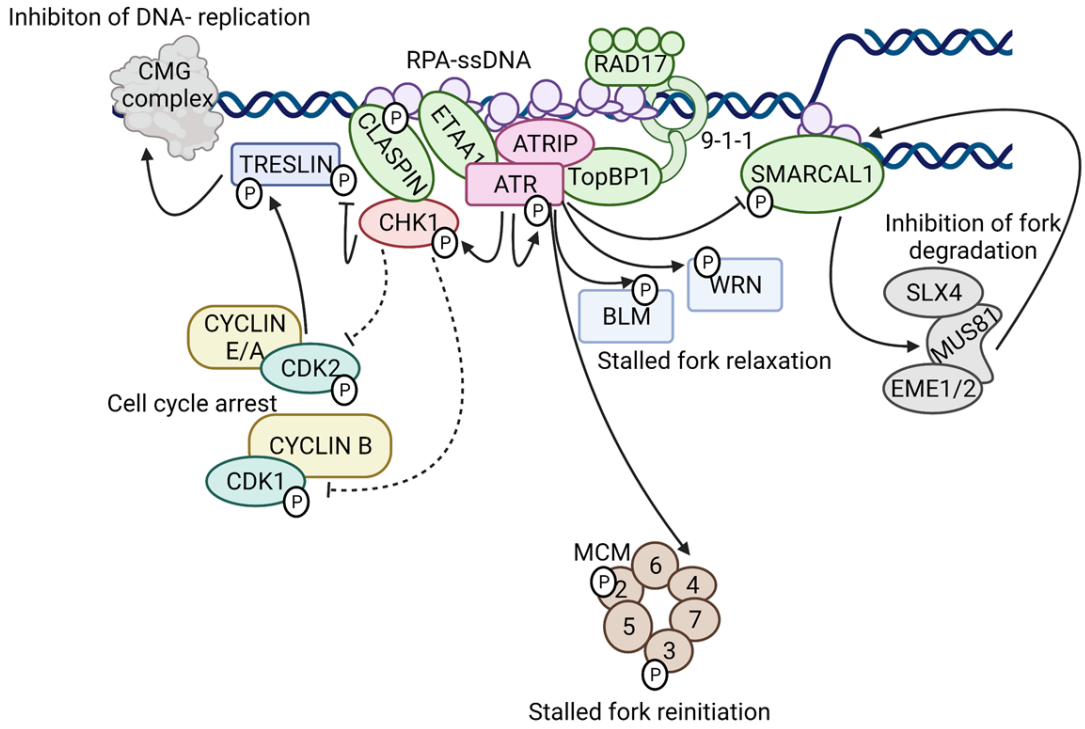

Figure 1.13. **ATR signalling prevents replication fork collapse.**
ATR activation leads to cell cycle arrest, inhibition of origin firing, stalled fork relaxation and reinitiation, and inhibition of fork degradation. Created with Biorender.

RPA exhaustion occurs when origins of replication are initiated, despite the presence of other stalled replication forks and DNA damage. ssDNA which occurs at stalled replication forks cannot be bound by RPA if the cell is in an RPA exhausted state, leaving the ssDNA exposed. Without RPA, the ssDNA is rapidly degraded, and signalling to the ATR pathway is not initiated. With lack of ATR signalling, the replication fork undergoes a permanent replication block and cannot be reinitiated, even when RPA supplies are replenished (Toledo et al. 2013). ATR signalling acts to protect cells from RPA depletion by inhibiting firing of new replication forks, while the cell is undergoing replication stress. ATR inhibits origin firing via Chk1 phosphorylation of CDC25A and WEE1, which results in Cdk2 inhibition and inactivation of Treslin. In addition, Chk1 directly inhibits Treslin, all which has been

described in section 1.5.3 (Boos et al. 2011; Guo, Kumagai, et al. 2015; Kumagai et al. 2011).

There is much debate as to whether ATR influences replisome unloading at stalled replication forks in mammalian cells (Cortez 2015). Early reports showed a reduction in replisome components associated with chromatin in the presence of stalled replication forks (Dimitrova and Gilbert 2000). Ragland et al., identified this unloading to be ATR dependant. In the presence of ATR, the E3 Ubiquitin ligase RNF4 and the PLK1-AURKA complex were inhibited and this prevented replisome disassembly, allowing for replication fork recovery (Ragland et al. 2013). However, more recent reports using more sophisticated techniques have argued against replisome unloading being the cause of replication fork collapse in human cells (Cortez 2015; De Piccoli et al. 2012; Dungrawala et al. 2015; Sirbu et al. 2011).

SMARCAL1 is a DNA translocase that can anneal to RPA-coated DNA at stalled replication forks via its N-terminus. Among other enzymatic activities, SMARCAL1 catalyses replication fork regression. Controlled SMARCAL1 activity promotes efficient DNA replication, with fork regression putting the replisome back at dsDNA, where excision repair can act to remove DNA lesions. Fork regression also facilitates lesion bypass via template switching and replication fork restart (Bansbach et al. 2009; Bétous et al. 2012; Cortez 2015; Couch et al. 2013). However, in the absence of tight regulation, SMARCAL1 catalyses excessive fork regression, which results in DNA degradation by nucleases and replication fork collapse. ATR phosphorylates SMARCAL1 on residue Ser652, this reduces SMARCAL1's catalytic activity and fork regression. In the absence of ATR, the DNA products of SMARCAL1 activity are recognised by SLX4 dependant nucleases, leading to DNA degradation, preventing fork restoration (Couch et al. 2013). SLX4 is a scaffold protein for the XPF-ERCC1, MUS81-EME1 and SLX1 nucleases (Fekairi et al. 2009; Svendsen et al. 2009).

Indeed, in the absence of ATR, MUS81 activity is increased, resulting in collapsed replication forks and DSBs (Forment et al. 2011).

ATR has been found to colocalise with the Bloom syndrome protein (BLM) helicase at the sites of replication stress, with ATR phosphorylating BLM on residues Thr99 and Thr122 (Davies et al. 2004; Davies, North, and Hickson 2007; Franchitto and Pichierri 2002; Tripathi, Kaur, and Sengupta 2008; Wang et al. 2018). Phosphorylation of BLM results in successful unwinding of complex DNA secondary structures at stalled forks, enabling fork restart (Wang et al. 2018). It has also been reported that BLM activity facilitates efficient HR dependant fork restart (Davies et al. 2004). Phosphorylation of BLM also prevents firing of new replication forks, prioritising repair and restart of stalled forks (Davies, North, and Hickson 2007). BLM also recruits the MRN complex to abnormal DNA structures (Franchitto and Pichierri 2002; Trenz et al. 2006; Tripathi, Kaur, and Sengupta 2008). MRE11 shows exonuclease and endonuclease activity when recruited to stalled forks by BLM, playing a role in stalled fork restart (Franchitto and Pichierri 2002).

ATR has also been shown to modulate the activity of the WRN helicase, enabling increased fork stability and stalled fork restart (Ammazzalorso et al. 2010; Pichierri, Rosselli, and Franchitto 2003). In response to replication stress, ATR phosphorylates the C-terminal fragment of WRN on residues Ser991, Thr1152 and Ser1256. Phosphorylation of WRN increases efficiency of WRN recruitment to stalled replication forks and maintains the helicase at the site of replication fork damage. Mutation of the phosphorylation sites on WRN results in deficient replication fork restart, DSB formation and reduced ability to re-enter the cell cycle after S-phase arrest (Ammazzalorso et al. 2010).

The MCM complex is the catalytic core of the DNA replication helicase, with its activity being critical for replication fork initiation and elongation. The MCM complex is

hexameric, with the subunits being MCM 2-7 (Labib, Tercero, and Diffley 2000). Due to the central nature of the MCM complex to DNA replication, interaction between the ATR complex and the MCM subunits has been explored. ATR has been identified to phosphorylate MCM2 on Ser108, and MCM3 on Ser535 (Cortez, Glick, and Elledge 2004; Yoo et al. 2004). In addition, ATRIP binds to the C-terminus of MCM7 (Cortez, Glick, and Elledge 2004). While the function of these phosphorylation sites / interactions remains unclear, it is apparent that the MCM complex is a target of ATR signalling. Constitutive inhibitory phosphorylation of MCM3 by Chk1 in the absence of replication stress has also been reported. As a result of DNA damage, Chk1 is released from the chromatin, resulting in a reduction in MCM3 inhibitory phosphorylation, and increased helicase activity to allow fork reinitiation (Han et al. 2015).

1.5.5 ATR promotes deoxynucleotide synthesis and salvage preventing further replication stress

ATR activation also reduces the impact of replication stress on genomic stability by ensuring sufficient dNTP availability for replication fork restart, global DNA replication and DNA repair. *De novo* nucleotide synthesis involves the ribonucleotide reductase (RNR) enzyme complex, which catalysis the reduction of newly formed ribonucleoside diphosphates to deoxyribonucleoside diphosphates.

The RNR complex is a heterodimeric tetramer, with the large subunit comprised of two ribonucleotide reductase family member 1 (Rrm1) proteins, and the small subunit comprised of two ribonucleotide reductase family member 2 (Rrm2) proteins (Zhang et al. 2009). Increased expression of Rrm1 and Rrm2 was identified to occur in an ATR dependant manner following treatment with CPT (Zhang et al. 2009). Increasing cellular dNTP levels was found to reduce replication stress in cells with reduced ATR function. Indeed, overexpression of the RRM2 gene protects against replication stress

and chromosomal breakage in the presence of ATR inhibition or DNA damaging agents. Mice deficient in ATR (ATR-Seckel Mice) have a two-fold increase in lifespan on overexpression of the RRM2 gene (Lopez-Contreras et al. 2015).

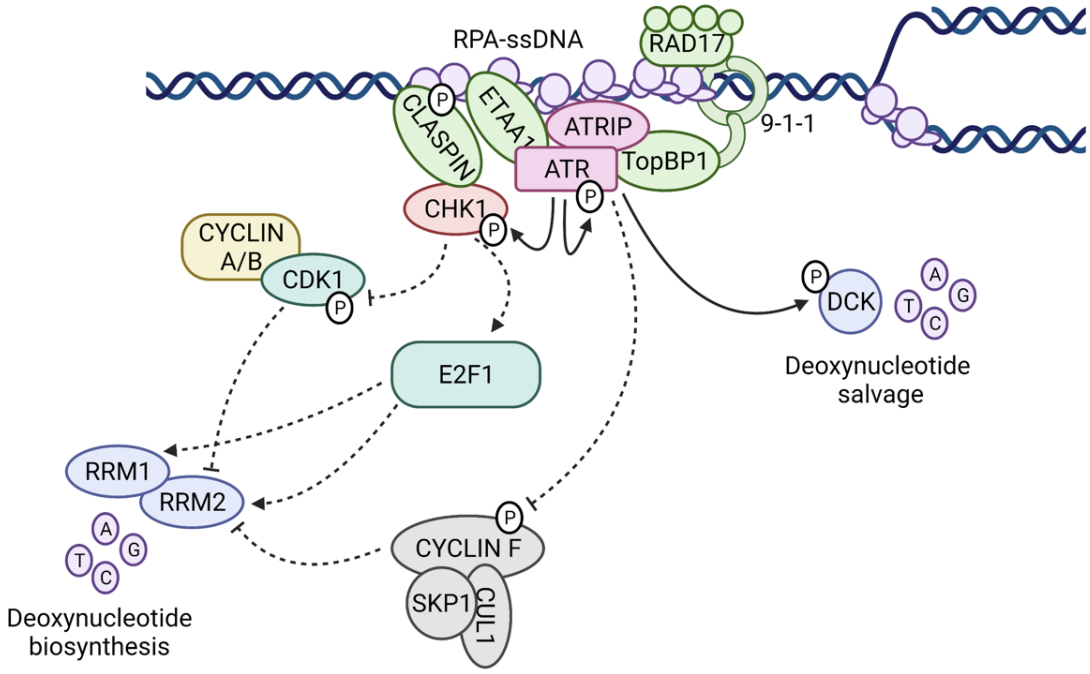

Figure 1.14. **ATR signalling promotes deoxynucleotide salvage and biosynthesis.** ATR signalling stabilises and increases the expression of the RNR complex leading to deoxynucleotide biosynthesis. Phosphorylation of deoxycytidine kinase (dCK) increases deoxynucleotide salvage. Created with Biorender.

The RRM1 and RRM2 genes are both transcriptional targets of the replication and stress associated transcription factor E2F1. Inhibition of Chk1 results in reduced E2F1 expression and a reduction in Rrm2 levels. Indeed, E2F1 deletion prevents DNA-damage dependant upregulation of Rrm2 (Zhang et al. 2009). In addition to modulating RNR activity at the transcription level, ATR signalling also prevents degradation of Rrm2. The cellular level of the RNR complex is dependent on Rrm2 expression and stability, as Rrm1 expression is always in excess of Rrm2.

Degradation of Rrm2 is mediated by the multi subunit E3 ubiquitin ligase, SCF. The F-box subunit of the SCF complex targets different substrates for ubiquitination. Cyclin F is a member of the F-box protein family, and binds Rrm2, resulting in Rrm2 ubiquitination and proteasomal degradation.

Phosphorylation of Rrm2 on residue Thr33 by the Cdk1/Cyclin B complex is required for binding of Cyclin F (D'Angiolella et al. 2012). Chk1 kinase activity results in a reduction of Cdk1 activity, via inhibition of CDC25C and activation of Wee1. A reduction in Cdk1 activity prevents Cyclin F dependant degradation of Rrm2 (Ammazzalorso et al. 2010; Buisson et al. 2015; D'Angiolella et al. 2012; Pfister et al. 2015). Furthermore, Cyclin F is directly regulated by ATR. Cyclin F contains a consensus sequence for ATR kinase activity, which becomes phosphorylated in response to replication stress. Phosphorylation of Cyclin F, results in Cyclin F degradation and increased RNR activity (D'Angiolella et al. 2012).

In addition to upregulating *de novo* synthesis of dNTPs, ATR also upregulates the nucleotide salvage pathway (Le et al. 2017). The nucleotide salvage pathway uses salvage kinases and phosphoribosyltransferases to convert preformed nucleobases, ribonucleosides, and deoxyribonucleosides into nucleotides. Among the nucleoside salvage kinases, deoxycytidine kinase (dCK) has the broadest kinase activity and is able to salvage both purines and pyrimidines (Sabini et al. 2008). ATR directly phosphorylates dCK on residue Ser74, which enhances dCK kinase activity. ATR inhibition results in a loss of dCK phosphorylation, and an approximately 30% reduction in dNTP pools (Le et al. 2017).

1.5.6 ATR plays a central role in the repair of DNA ICLs

DNA ICLs involve a covalent bond between the two strands of the DNA helix. ICLs are highly toxic DNA lesions as they prevent separation of the DNA strands, a requirement for both transcription and replication. Persistent ICLs result in DNA

breakage and chromosomal rearrangements. Repair of ICLs, requires activation of the Fanconi Anaemia (FA) pathway, which coordinates the involvement of the NER, HR proteins and translesion DNA synthesis polymerases. ATR plays a central role in the repair of ICLs by activating key components of the FA pathway, as well as other DNA repair effectors (Figure 1.15) (Blackford and Jackson 2017; Ceccaldi, Sarangi, and D'Andrea 2016).

Recognition of ICLs by the FA pathway occurs via binding of FANCM complex (FANCM-FAAP24-MHF1-MHF2) to the DNA lesion. Phosphorylation of FANCM on residue Ser1045, is required for recruitment of the FANCM complex to the ICL site. The phosphorylation of FANCM, is ATR dependant, and loss of ATR prevents recognition of ICLs by the FA pathways (Singh et al. 2013). Once bound to the DNA, FANCM acts as a landing platform for the ubiquitin ligase FA core complex, which is comprised of FANCA, FANCB, FANCC, FANCE, FANCF, FANCG, FANCL, FANCM, FANCT, FAAP100, MHF1, MHF2, FAAP20 and FAAP24 (Ceccaldi, Sarangi, and D'Andrea 2016). FA core complex Ubiquitin ligase activity has been shown to be ATR dependant, in the presence of DNA damage (Collins et al. 2009; Wilson et al. 2008). In response to ICLs, FANCA, is phosphorylated in an ATR (but not Chk1) dependant manner on residue Ser1449. ATR is suspected to directly phosphorylate FANCA, with FANCA phosphorylation by ATR occurring *in vitro* (Collins et al. 2009). Another component of the FA core complex, FANCG becomes phosphorylated on residue Ser7 in an ATR dependant manner in the presence of ICLs (Wilson et al. 2008).

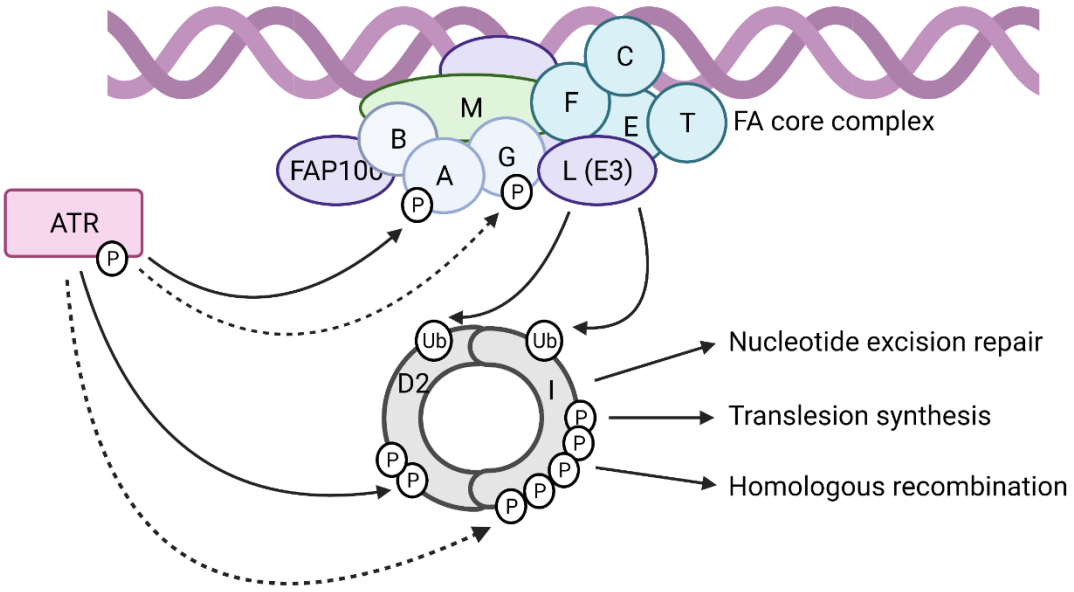

Figure 1.15. **ATR activates the Fanconi Anaemia pathway in response to ICLs.**
ATR activity is critical for the phosphorylation and activation of multiple components of the FA pathway, leading to ICL repair. Created with Biorender.

The FA core complex acts as a ubiquitin ligase for FANCD2 and FANCI, which bind together to form the ID complex (Andreassen, D'Andrea, and Taniguchi 2004; Ishiai et al. 2008; Shigechi et al. 2012). Activity of the ID complex is dependent on multiple post-translational modifications, FANCD2 and FANCI phosphorylation and monoubiquitylation. Phosphorylation of FANCD2 and FANCI is required for monoubiquitinating of the ID complex (Chen et al. 2015; Ho et al. 2006; Ishiai et al. 2008). ATR and ATM can both catalyse the phosphorylation of FANCD2 on residues Thr691 and Ser717 (Ho et al. 2006). FANCI phosphorylation on Ser556, Ser559, Ser565, Ser596 and Ser617 occurs in ATR dependant manner, although it has not been demonstrated to date whether this phosphorylation is catalysed directly by ATR, or a kinase downstream of ATR (Chen et al. 2015; Ishiai et al. 2008). Following ID complex phosphorylation, the FA complex monoubiquitinates FANCD2 on Lys561, and FANCI on Lys523 (Andreassen, D'Andrea, and Taniguchi 2004; Ishiai et al. 2008; Shigechi et al. 2012; Smogorzewska et al. 2007). Monoubiquitylation of the ID

complex acts a chromatin localisation tag and is required for binding to the ICL site (Ishiai et al. 2008). Once bound, the ID complex mediates the recruitment of NER factors, translesion synthesis polymerases and the homologous repair proteins to repair the ICL (Ceccaldi, Sarangi, and D'Andrea 2016; Shigechi et al. 2012).

1.5.7 ATR can activate the NER pathway

ATR also plays a key role in the NER pathway, facilitating the removal of helix distorting DNA adducts following UV exposure. Following UV exposure, ATR was found to colocalise with Xeroderma pigmentosum group A (XPA), an indispensable component of the NER machinery (Lee et al. 2014; Wu et al. 2006). XPA binds to DNA lesions and facilitates recruitment and loading of NER machinery on to the chromatin (Ammazzalorso et al. 2010; Lee et al. 2014). In response to UV exposure, ATR directly phosphorylates XPA on residue Ser196 (Ammazzalorso et al. 2010; Wu et al. 2006). Nuclear translocation of XPA in response to UV exposure was also identified to be ATR dependant, although the exact mechanism of this translocation is not understood (Wu et al. 2007). XPA is targeted for proteasomal degradation by the HERC2 E3 ubiquitin ligase. Phosphorylation of XPA by ATR causes dissociation of HERC2 from XPA, protecting XPA from ubiquitination and subsequent degradation (Lee et al. 2016).

1.5.8 ATR plays a key role in homologous recombination

The initial stage of HR involves DNA end resection, catalysed by helicases such as BLM, and nucleases such as MRE11. ATR regulates the activity of BLM and MRE11 in the context of replication stress (section 1.5.4) (Bradbury et al. 2020; Davies et al. 2004; Franchitto and Pichierri 2002). Following DNA end resection, RPA-coating of ssDNA must be replaced with RAD51, to form a RAD51 nucleofilament. RAD51 loading mediates the homology search and strand invasion of the sister chromatid, that is required for HR (Ahlskog et al. 2016). Exchange of RPA for RAD51 is

performed by the BRCA2-PALB2 complex, which in turn is recruited to the DNA lesion by BRCA1 (Ahlskog et al. 2016; Buisson, Niraj, et al. 2017; Guo, Feng, et al. 2015). BRCA1, BRCA2, PALB2 and RAD51 are all phosphorylated in an ATR dependant manner, with each posttranslational modification being essential for efficient HR.

Following replication stress, ATR colocalises with BRCA1, and phosphorylates BRCA1 on residue Ser143 (Tibbetts et al. 2000). The N-terminus of PALB2 interacts with BRCA1, with this interaction requiring direct phosphorylation of PALB2 on Ser59 by ATR (Ahlskog et al. 2016; Buisson et al. 2015; Guo, Feng, et al. 2015). Optimal recruitment of PALB2 to BRCA1 foci at the site of DNA damage, requires phosphorylation of Ser59 and hypophosphorylation of Ser64. While phosphorylation of Ser59 is directly catalysed by ATR, the phosphorylation of Ser64 is catalysed by Cdks. In response to ATR activation, Cdks undergo inhibitory phosphorylation on Tyr15 (section 1.5.3). As such, activation of ATR causes phosphorylation of Ser59 and hypophosphorylation of Ser64, facilitating efficient recruitment of PALB2 to the site of DNA damage (Buisson, Niraj, et al. 2017). Phosphorylation of PALB2 has also been found to be essential for binding of RAD51 to the PALB2-BRCA2 complex (Ahlskog et al. 2016). Phosphorylation of Ser3291 on BRCA2 blocks the interaction between BRCA2 and RAD51, and prevents RAD51 loading. Phosphorylation of BRCA2 is catalysed by Cdks, and therefore inhibition of Cdks via ATR signalling promotes interaction between BRCA2 and RAD51 (Esashi et al. 2005). Phosphorylation of RAD51 is required for the formation of RAD51 foci. On activation, Chk1 binds to RAD51 and RAD51 becomes phosphorylated in a Chk1 dependant manner (Sørensen et al. 2005).

1.5.9 Genetic models show ATR signalling to be essential for tumour development

ATM and Chk2 have been identified as tumour suppressor genes, with loss of expression or loss of function mutations driving tumourigenesis (Barlow et al. 1996; Cremona and Behrens 2014; Lecona and Fernandez-Capetillo 2018; Stolz, Ertych, and Bastians 2011; Halazonetis, Gorgoulis, and Bartek 2008). Due to the homology between ATR / Chk1 and ATM / Chk2, it was speculated that ATR and Chk1 would also play tumour suppressive roles, however, this is not the case (Lecona and Fernandez-Capetillo 2018). Complete loss of ATR and Chk1 is embryonic lethal, and as such this phenotype cannot be studied in a complete organism. In mice, embryonic lethality occurs before E6.5, in both ATR-/- and Chk1-/- genotypes (Brown and Baltimore 2000; de Klein et al. 2000; Liu et al. 2000; Takai et al. 2000). Cells from ATR-/- and Chk1-/- early blastocysts display defective cell cycle checkpoints, defective cell cycle arrest, fragmented chromatin and abundant micronuclei (Brown and Baltimore 2000; Liu et al. 2000; Takai et al. 2000).

Seckel syndrome is a rare human disorder, in which a hypomorphic ATR mutation arises due to incorrect splicing of the ATR transcript. Impaired ATR function results in intrauterine growth retardation, dwarfism, microcephaly, and cognitive impairment of affected individuals. There is no increase in cancer incidence for individuals with Seckel syndrome, indicative of ATR not having a tumour suppressive role (O'Driscoll et al. 2003). Mouse models of Seckel syndrome display similar characteristics including severe dwarfism, micrognathia, microcephaly, ageing and death. On the cellular level, cells display pan-ɣH2AX staining, chromosomal breakage, p53 phosphorylation and pan-caspase 3 activation. Seckel mice do not display increased tumour incidence, even with co-deletion of p53 (Murga et al. 2009). In ATR-Seckel mice, MYC driven lymphomas and pancreatic tumours fail to develop. In addition, Ras driven tumours, which are deficient in p53 also fail to develop in Seckel mice. Addition

of a Chk1 allele to Seckel mice promotes malignant transformation, further demonstrating the dependence of tumourigenesis on ATR-Chk1 signalling (López-Contreras et al. 2012).

Data from many genetic studies show that some ATR-Chk1 signalling is required for tumour formation. Chk1 deficiency has been shown to prevent mammary tumour formation in p53 null mice and mice carrying a heterozygous deletion of p53 (Fishler et al. 2010). Deletion of Chk1 in the epidermis, supresses papilloma formation and is incompatible with epithelial tumourigenesis in mouse models (Tho et al. 2012). In addition, deletion of ATR in skin cells also prevents tumour formation on exposure to UV irradiation in mice (Kawasumi et al. 2011). Furthermore ATR-Chk1 signalling is often upregulated to support malignant transformation and to sustain tumour development. In mouse models, MYC driven B-cell lymphomas display increased Chk1 expression, with reduction to basal levels slowing tumour progression (Höglund et al. 2011). In addition, overexpression of Chk1 in osteocytes causes malignant transformation (Schulze et al. 2014). Tumour samples from patients with triple negative breast cancer (TNBC) display very high levels of Chk1 expression (Verlinden et al. 2007). More than 50% of diffuse large B-cell lymphoma (DLBCL) patient samples display increased Chk1 expression and phosphorylation (Derenzini et al. 2015). Chk1 is also overexpressed and hyperactivated in human T-cell lymphoblastic leukaemia (Sarmento et al. 2015).

While a significant loss of ATR / Chk1 signalling prevents tumour formation, a modest loss in function has been demonstrated to marginally enhance tumourigenesis. Mice with heterozygous loss of ATR show a small increase in tumour incidence (Brown and Baltimore 2000). There is a modest increase in tumour formation with Chk1 heterozygous deletion in WNT-1 transgenic mouse (Liu et al. 2000). Ras induced tumourigenesis is also promoted by haploinsufficient ATR expression (Gilad et al.

2010). Partial loss of Chk1 expression has also been found to accelerate epidermal benign-malignant progression in mouse models (Tho et al. 2012).

Due to reliance of tumours on ATR and Chk1, complete loss of these kinases has never been reported in cancers. Loss of function ATR mutations have only been reported in a small proportion (6%) of human melanomas, with this accelerating tumour progression (Chen et al. 2017). An extremally rare familial disorder in which individuals have a heterozygous loss of function ATR mutation, has been shown to increase the incidence of oropharyngeal cancer formation (Tanaka et al. 2012).

While genomic instability can be source of mutations that drive tumourigenesis, catastrophic DNA damage is intrinsically toxic and not compatible with cell viability. Tumour cells require an efficient replication stress recovery pathway to support growth and development, making the ATR-Chk1 signalling pathway an attractive target in cancer therapy.

1.6 ATR Inhibition

1.6.1 ATR is a promising therapeutic target for cancer treatment

The overarching principle behind ATR inhibition for the treatment of cancer is to exacerbate replication stress and genomic instability, resulting in catastrophic DNA damage that is not compatible with cell viability. Genomic instability was recognised as one of the hallmarks of cancer by Hanahan and Weinberg. It is often deregulation of DDR genes that contribute to this genomic instability (Bradbury et al. 2020; Hanahan and Weinberg 2011). An increased replication rate, a further cancer hallmark leads to amplification of DNA damage and an increase in replication errors (Sundar et al. 2017; Hanahan and Weinberg 2011; Macheret and Halazonetis 2015). Up to 70% of cancers display high levels of replication stress due to loss of tumour suppressor ATM or its downstream target p53. While loss of ATM or p53 drives

tumourigenesis due to loss of cell cycle checkpoints and accelerated mutagenesis, it also results in heavy reliance on ATR to resolve replication stress (Bolt et al. 2005; Ding et al. 2008; Gurpinar and Vousden 2015; Reaper et al. 2011; Jin and Oh 2019). Dysregulation of cell signalling pathways by oncogenes such as Ras, MYC and cyclin E, have been shown to cause loss of cell cycle checkpoints and increased replication stress, with increased reliance on ATR signalling (Gilad et al. 2010; Höglund et al. 2011; Karnitz and Zou 2015; Murga et al. 2011; Toledo et al. 2011).

Many studies have identified tumour dependence on ATR signalling, making ATR inhibition an attractive therapeutic option. In a study of 1650 human breast cancers with loss of tumour suppressor PTEN, upregulation of ATR was linked to higher grade malignancies, larger tumour size and poor survival, demonstrating reliance of tumours on ATR (Al-Subhi et al. 2018). High ATR expression and phosphorylation has also been associated with poor prognosis in bladder cancers, demonstrating the role of a functional replication stress response in tumour progression (Li et al. 2016). A link between patient survival following cisplatin therapy for the treatment of oesophageal cancer and ATR expression has been identified, with higher ATR expression driving tumour survival (Shi et al. 2018). In addition, tumour samples from TNBC patients show very high levels of Chk1 expression (Verlinden et al. 2007). More than 50% of DLBCL patient samples display increased Chk1 expression and phosphorylation (Derenzini et al. 2015). Chk1 is also overexpressed and hyperactivated in human T-cell lymphoblastic leukaemia (Sarmento et al. 2015). As shown in section 1.5.9, genetic models have demonstrated a loss in ATR activity to prevent tumour formation across multiple cancer types (Fishler et al. 2010; Höglund et al. 2011; Kawasumi et al. 2011; Tho et al. 2012). Unlike ATM, which is frequently mutated or lost in cancers, loss or mutation of ATR is extremely rare. This makes ATR an attractive drug target, as primary resistance is unlikely (Blackford and Jackson 2017; Bolt et al. 2005; Ding et al. 2008; Jin and Oh 2019; Reaper et al. 2011).

Many current cancer therapeutics are highly genotoxic and potent inducers of replication stress. However, successful cell cycle arrest and checkpoint activation enable DNA repair or cell senescence, with cells evading death. As such, there is strong rationale for combining ATR inhibition with many established cancer therapeutics, with loss of ATR sensitising cells to treatment (Blackford and Jackson 2017; Lecona and Fernandez-Capetillo 2018).

1.6.2 Development of ATR inhibitors

Despite genetic studies providing evidence for potential efficacy of ATR inhibitors in cancer treatment, development of drugs specifically targeting ATR has been slow. The large size of ATR, and high homology between the active site of ATR and other members of the PIKK family has posed a significant challenge (Lecona and Fernandez-Capetillo 2018). The first molecule identified to inhibit ATR was caffeine. However, with an IC_{50} of 1.1mM, the dose required for any cellular effect also inhibits other PIKKs, including ATM (Sarkaria et al. 1999). Next, schisandrin B, an active compound from *Fructus schisandrae* was found to inhibit ATR. As a monotherapy, schisandrin B had no impact on the survival of lung cancer cells *in vitro*. However, treatment with schisandrin B did reduce cell survival in combination with UV irradiation, by abolishing the G2/M checkpoint. With an IC_{50} of 7.5μM, schisandrin B was not found to have sufficient potency for clinical use (Nishida et al. 2009).

NU6027, which was originally developed as a CDK2 inhibitor, was identified to inhibit ATR, with an IC_{50} of 6.7 μM. Treatment with NU6027 sensitized breast and ovarian cancer cell lines to cisplatin, with impaired G2/M arrest and HR following DNA damage (Peasland et al. 2011). Using a high throughput screen approach with ɣH2AX as a readout for ATR activity, ETP-46464 was identified as a potent ATR inhibitor (IC_{50} 25nM). ETP-46464 did not display any action against the kinase activity of ATM or DNA-PKcs, however, it did inhibit other kinases including PI3K and mTOR. Due to

poor pharmacokinetic properties ETP-46464 could not enter clinical trials (Toledo et al. 2011).

Vertex pharmaceuticals developed a high throughput screening approach, utilising an ATR specific kinase assay, to identify compounds which selectively inhibit ATR. This led to the discovery of a series of amino pyrazines which inhibit ATR (but not other PIKKs), of which VE-821 was found to be the most potent (IC_{50} 26nM). VE-821 was found to markedly enhance the cytotoxicity of DNA damaging agents in cancer cells but not normal cells (Charrier et al. 2011). Many preclinical studies showed efficacy of VE-821 as a monotherapy and in combination therapy (sections 1.6.3-1.6.7). The potency and pharmacological properties of VE-821 were optimised by Vertex to develop VX-970 (VE-822) (Table 1.3). VX-970 was sold to the Merck group and was renamed M6620 (Berzosertib). VX-970 has shown efficacy in pre-clinical experiments and clinical trials (sections 1.6.3-1.6.7 and 1.6.9). Another highly potent ATR inhibitor, VX-803 was also developed by Vertex. VX-803 displays oral bioavailability, and has an IC_{50} of 8nM (Table 1.3). VX-803 was similarly sold to Merck and is now known as M4344. Pre-clinical data shows synergy between VX-803 and DNA damaging agents in cancer models (Jo, Senatorov, et al. 2021). A dose escalation phase 1 trial, with M4344 as a monotherapy and in combination with cisplatin is ongoing for patients with advanced solid tumours NCT02278250 (Zenke et al. 2019).

AstraZeneca used a similar high throughput approach to Vertex to identify AZ20, which has an IC_{50} of 5nM (Foote et al. 2013). Due to low aqueous solubility and off target inhibition of cytochrome CYP3A4, AZ20 did not progress into clinical studies. However, AstraZeneca went on to develop the AZD6738 (Ceralasertib), an orally bioavailable ATR inhibitor with an IC_{50} of 74nM (Table 1.3) (Foote et al. 2018). AZ6738 has shown efficacy in pre-clinical experiments and is currently in clinical trials (sections 1.6.3-1.6.7 and 1.6.10).

Bayer developed an ATR inhibitor, with an IC_{50} of 78nM, named as BAY-937. Despite *in vitro* efficacy, BAY-937 was not taken to clinical trials due to poor aqueous solubility and bioavailability (Luecking et al. 2017). BAY-937 was optimised to form BAY1895344 (Table 1.3), which has an IC_{50} of 7nM. BAY1895344 has shown preclinical efficacy as a monotherapy in DDR defective xenograft models, and in combination with DNA damage inducing therapies and radiotherapy in a range of cancer models. Complete remission in mantle cell lymphoma models has been observed. Synergy has also been observed with anti-androgen therapy in hormone dependant prostate cancer models (Luecking et al. 2017; Wengner et al. 2020; Wengner et al. 2017; Wengner et al. 2018). Several phase I trials are ongoing to evaluate the safety, tolerability, pharmacokinetics, pharmacodynamics, and maximum tolerated dose of BAY1895344 as a monotherapy and in combination with chemotherapies, a PARP inhibitor and pembrolizumab (NCT03188965, NCT04095273 and NCT04267939, NCT04576091, NCT04491942, NCT04616534).

Table 1.3. Summary of the ATR inhibitors currently in clinical trials, with their structure, inhibition and specificity data (Bradbury et al. 2020).

Name	Structure	IC_{50}	Specificity
VX-970 **(VE-822)** **(M6620)** **(Berzosertib)**	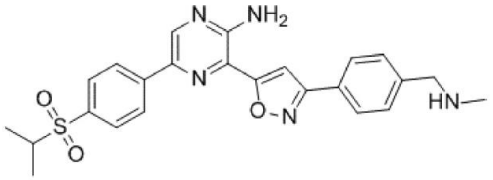	19nM	>100-fold ATR vs ATM/DNAPK
VX-803 **(M4344)**	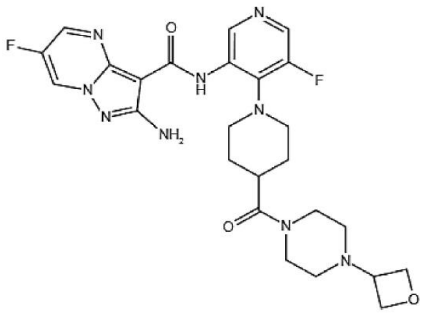	8nM	>100 fold selectivity against 308 of a panel of 312 kinases
AZ6738 **Ceralasertib**	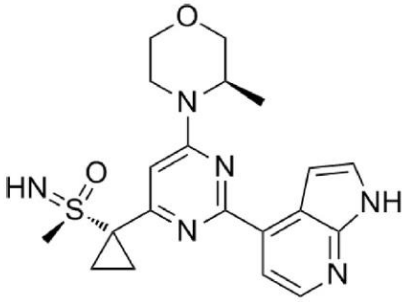	74nM	
BAY1895344	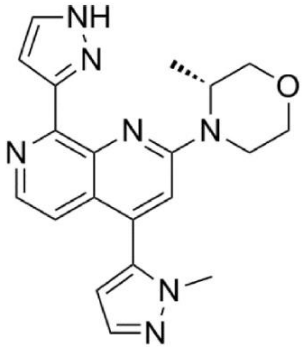	7nM	>60 fold selectivity to ATR compared to PI3K/AKT /mTOR pathway

1.6.3 ATR inhibitors synergise with platinum therapy

Platinum-based chemotherapy remains the primary therapeutic for many solid tumours. Platinum drugs and their derivatives form bulky DNA adducts via covalent interaction between the platinum compounds and nucleotide bases. The bulky platinum adducts, which include intra and interstrand crosslinks, distort the DNA

structure, leading to replication fork stalling and high levels of replication stress. Activation of ATR and subsequent G2/M cell cycle arrest is one of the earliest cellular responses to platinum treatment. Loss of ATR, with subsequent lack of cell cycle arrest and genomic instability could result in catastrophic DNA damage following platinum treatment, incompatible with cell viability (Bradbury et al. 2020; Galluzzi et al. 2012; Gorecki et al. 2020).

Multiple preclinical studies have demonstrated a synergistic interaction between platinum-based therapies and ATR inhibition. The combination of ATR inhibitors and cisplatin or oxaliplatin has led to dramatically reduced cell survival in a very broad range of cancer cell lines including, ovarian, lung, oesophageal, head and neck, osteosarcoma and colorectal (Combès et al. 2019; Hall et al. 2014; Huntoon et al. 2013; Leonard et al. 2019; Leszczynska et al. 2016; Mohni et al. 2015; Nagel et al. 2019; Reaper et al. 2011; Vendetti et al. 2015). This synergy has also been observed *in vivo* in primary human none small cell lung cancer (NSCLC) xenograft models, oesophageal squamous cell carcinoma models, paediatric solid tumour models and head and neck squamous cell carcinoma (HNSCC) models (Combès et al. 2019; Hall et al. 2014; Kurmasheva et al. 2018; Leonard et al. 2019; Nagel et al. 2019; Shi et al. 2018; Vendetti et al. 2015).

1.6.4 ATR inhibitors synergise with gemcitabine and cytarabine

The mechanism of action of antimetabolites such as gemcitabine and cytarabine, would suggest efficacious combination with ATR inhibition for cancer treatment. Metabolites of gemcitabine inhibit nucleotide synthesis / salvage as well becoming incorporated into DNA. dFdUMP, which is the active metabolite of gemcitabine is structurally similar to the thymidylate synthase substrate (dUMP), acting as a competitive inhibitor and preventing synthesis of dTMP (Honeywell et al. 2015; Mini et al. 2006). Gemcitabine metabolites have also been shown to inhibit the

ribonucleotide reductase complex and inhibit the *de novo* synthesis of nucleotides (Liu, Ge, et al. 2017). dFdUMP also competes with deoxycytidine for binding to the nucleoside salvage enzyme dCK (Honeywell et al. 2015). As well as reducing the pool of nucleotides available for DNA replication and repair, gemcitabine metabolites become incorporated into the DNA in place of cytidine, inhibiting DNA polymerases causing replication fork stalling, thereby further elevating replication stress (Fordham et al. 2018; Honeywell et al. 2015).

Resistance to gemcitabine occurs via upregulation of the ribonucleotide reductase subunits, Rrm1 and Rrm2, increasing the cellular pool of nucleotides (Liu, Ge, et al. 2017). Cytarabine, a deoxycytosine analogue commonly used in the treatment of acute myeloid leukaemia (AML), also becomes incorporated into DNA, resulting in inhibition of DNA and RNA polymerases. Cytarabine also inhibits the ribonucleotide reductase complex, with resistance involving upregulation of Rrm1 and Rrm2 via increased ATR expression and signalling (Ma et al. 2017). ATR inhibition results in reduced expression and catalytic activity of the RRM subunits, and loss of the nucleotide salvage pathway, and as such could greatly synergise with gemcitabine and cytarabine (Ammazzalorso et al. 2010; D'Angiolella et al. 2012; Sabini et al. 2008; Zhang et al. 2009). Loss of ATR could also result in altered cell cycle arrest and poor resolution of replication stress induced by gemcitabine and cytarabine (Fordham et al. 2018).

The addition of an ATR inhibitor to gemcitabine treatment has been shown to reduce cell survival in ovarian, colorectal, osteosarcoma, breast, lung, AML and pancreatic cancer cell lines, with cell cycle disruption and increased DNA damage observed (Fokas et al. 2012; Fordham et al. 2018; Hall et al. 2014; Huntoon et al. 2013; Middleton, Pollard, and Curtin 2018; Prevo et al. 2012). Synergy has also been observed *in vivo* in pancreatic ductal adenocarcinoma (PDAC) and AML mouse models (Fokas et al. 2012; Fordham et al. 2018). The combination of ATR inhibition

and cytarabine has been found to reduce the survival of AML and pancreatic cancer cell lines, and increases survival in pancreatic cancer mouse models (Liu, Ge, et al. 2017; Ma et al. 2017).

1.6.5 ATR inhibition in combination with PARP inhibitors

PARP enzymes play a central role in the initiation of DNA repair and genome integrity. There are 18 members of the PARP family, with PARP1 playing the dominant role in DNA repair. PARP1 catalyses the addition of ADP-ribose to multiple DNA repair enzymes, and is crucial for the recruitment of DNA repair factors to the sites of DNA damage (Zheng et al. 2020). It is long established that PARP is required for the recruitment of factors for SSB repair and BER, however more recent findings have also identified PARP involvement in both HR, NHEJ and MMEJ (microhomology-mediated end-joining) (Ceccaldi et al. 2015; Chou et al. 2010; Haince et al. 2008; Hegan et al. 2010; Zheng et al. 2020). PARP inhibitors are currently approved for the treatment of BRCA1/2 mutant breast and ovarian cancers, with synthetic lethality observed (Ledermann 2019). Loss of PARP activity results in severe replication fork stress and activation of ATR signalling. Furthermore, upregulation of ATR signalling has been identified as a primary and acquired mechanism of resistance to olaparib in BRCA1 deficient cells (Yazinski et al. 2017). Combining PARP inhibition, which drives replication stress with ATR inhibition, would result in unresolved DNA damage, with a lethal effect on tumour cells (Gorecki et al. 2020).

Increased sensitivity to PARP inhibition with the addition of ATR inhibition has been shown across several cancer types. ATR inhibition in combination with PARP inhibition, reduces survival compared to PARP inhibition alone in ovarian, osteosarcoma, colorectal, prostrate, leukemic and Ewing sarcoma cancer cell lines (Abu-Sanad et al. 2015; Huntoon et al. 2013; Jette et al. 2019; Mohni et al. 2015; Murai et al. 2016; Yazinski et al. 2017). The synergistic relationship between ATR and

PARP inhibition has also been demonstrated in patient derived xenograft (PDX) models of NSCLC, HNSCC, ovarian cancer and TNBC (Kim et al. 2017; Lau et al. 2017).

1.6.6 ATR inhibition increases efficacy of anti PD-L1 therapy

Anti programmed death-ligand 1 (PD-L1) therapy has shown efficacy in a small subset of patients, suffering from cancers with high mutational burdens. However, for many patients PD-L1 therapy does not result in disease control, even when combined with other therapeutics. Drugs combined with anti PD-L1 therapy often aim at increasing the mutational burden of the cancer, so that the cancer is more readily targeted by T-cells. As many chemotherapeutic agents are highly genotoxic and therefore increase cancer mutational burden, it was proposed that combining anti PD-L1 treatment with chemotherapy would result in clinical benefit. Even in combination with chemotherapeutics, many patients do not benefit from anti PD-L1 therapy and as such new combinations are required (Demaria et al. 2019). The addition of ATR inhibitors to standard cancer therapy has been shown to increase DNA damage and mutational burden in preclinical studies (Combès et al. 2019; Josse et al. 2014). Combining an ATR inhibitor with anti PD-L1 monotherapy or combination therapy could result in increased cancer mutational burden, due to an impaired replication stress response and compromised DNA damage repair machinery (Alimzhanov et al. 2019).

Anti-tumour efficacy of platinum-based chemotherapy in combination with avelumab (anti PD-L1) and VX-970 was explored in the MC38 murine colorectal tumour model. The triple combination regimens resulted in reduced tumour growth, increased tumour regression and increased OS compared to the dual combination of platinum and avelumab. Mice which displayed a complete response (CR) were found to be refractory to subsequent tumour inoculations, suggestive of the development of anti-tumour immunity (Alimzhanov et al. 2019).

1.6.7 ATR inhibitors act as radiosensitisers

ATR inhibition will exacerbate any replication stress and DNA damage occurring in tumour cells. Irradiating mammalian cells with 1Gy, causes approximately 800-1,600 damaged deoxyribose bases, 200-300 alkaline labile sites, 500-1,000 SSBs, 20-40 DSBs, 30 DNA-DNA covalent bonds and 150 DNA-protein covalent bonds (Gorecki et al. 2020). Loss of ATR will prevent resolution of the DNA aberrations induced by radiation and therefore will reduce cell viability. Radioresistance prevents patient responses and results in disease relapse, as such successful radiosensitisation via ATR inhibition would fill an unmet medical need (Fokas et al. 2012; Pires et al. 2012; Prevo et al. 2012; Vendetti et al. 2015)

There have been multiple studies demonstrating a synergistic relationship between radiation and ATR inhibition. Radiosensitisation of colorectal, osteosarcoma, glioblastoma, breast, bladder, cervical, melanoma, head and neck, pancreatic, leukaemia, oesophageal cancer cell lines have been reported. ATR inhibition was found to exacerbate radiation induced DNA damage, with increased γH2AX and 53BP1 foci, persistent DSBs and increased micronuclei observed (Fokas et al. 2012; Middleton, Pollard, and Curtin 2018; Pires et al. 2012; Prevo et al. 2012; Vávrová et al. 2013; Dillon et al. 2017; Leszczynska et al. 2016; Tu et al. 2018). *In vivo*, treatment with an ATR inhibitor has been shown to radiosensitise PDAC, oesophageal, TNBC, glioma and CRC mouse models (Chen et al. 2018; Dillon et al. 2017; Fokas et al. 2012; Leszczynska et al. 2016; Tu et al. 2018; Vendetti et al. 2015).

1.6.8 ATR inhibition in combination with DNA damage therapy could produce an anti-tumour immune response

In vitro and *in vivo* models, have shown increased DNA damage in response to the combined use of TOP1 and ATR inhibition (Huntoon et al. 2013; Hur et al. 2021; Josse et al. 2014; Thomas et al. 2018; Thomas et al. 2021). In recent years, the cGAS-

STING pathway has been identified as a link between DNA damage in tumour cells and an anti-tumour immune response (Figure 1.16) (Vanpouille-Box et al. 2018). This is suggestive of an immunomodulatory advantage of therapeutics that increase DNA damage, with anti-tumour immunity likely to give a more durable response. To date, activation of the cGAS-STING pathway in response to TOP1 and ATR inhibition remains unexplored.

Unrepaired DNA lesions (including DNA DSBs), as well as impaired segregation of chromosomes during mitosis results in endogenous cytosolic DNA (Vanpouille-Box et al. 2018). Furthermore, when cells with extensive DNA damage pass through mitosis, fragmented DNA can end up being enclosed in a micronuclear envelope, creating small nuclear bodies, known as micronuclei. The fragile nature of micronuclei membranes, results in lack of membrane integrity and the leakage of DNA into the cytosol (Harding et al. 2017; Mackenzie et al. 2017). DNA damage-induced cytosolic DNA triggers cellular responses common to those observed upon viral or bacterial infections. In mammalian cells, cytosolic DNA is detecting by multiple enzymes and factors leading to activation of an immune response (Vanpouille-Box et al. 2018).

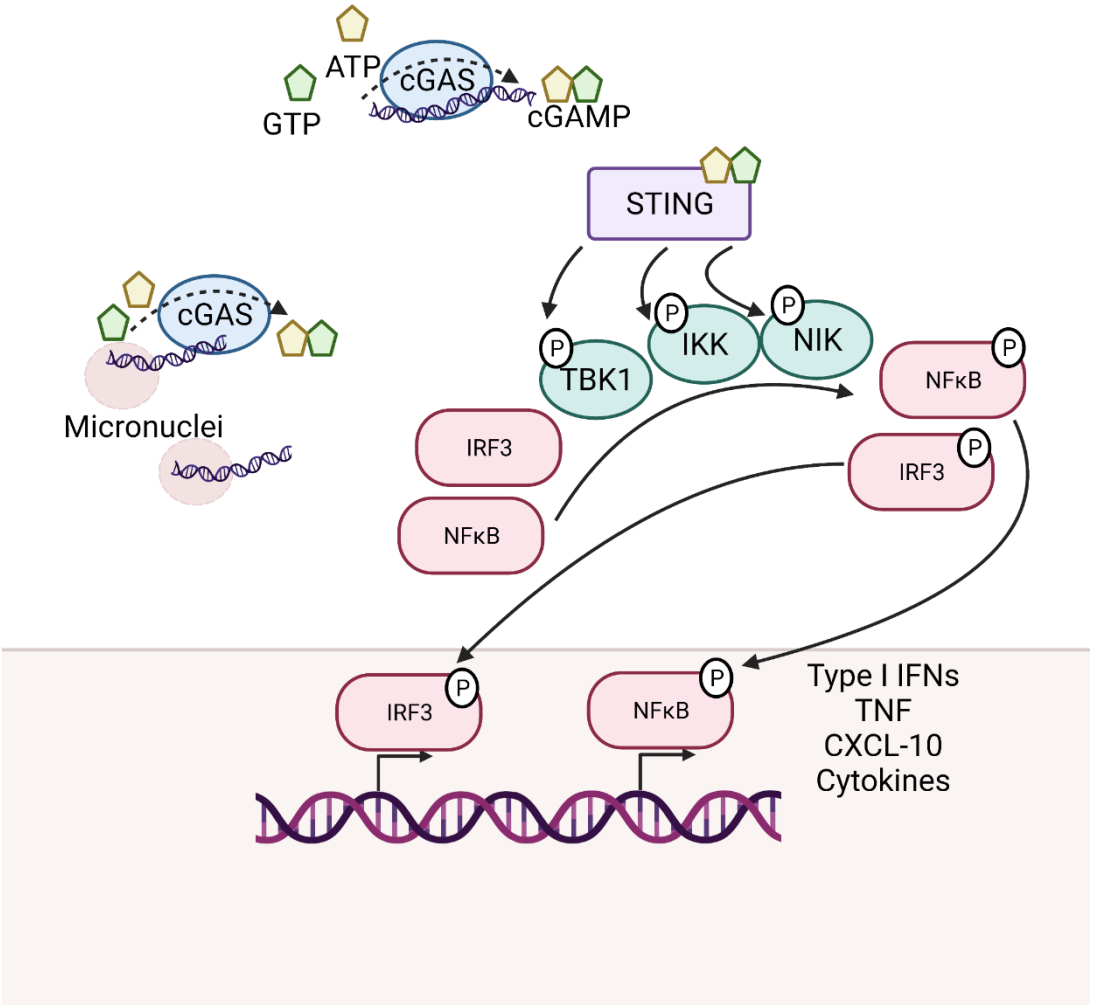

Figure 1.16. **Cytosolic DNA activates the cGAS-STING pathway.**
Cytosolic DNA is bound by cGAS which generates the secondary messenger cGAMP, leading to STING activation. STING in turn activates TBK1, IKK and NIK kinases. Nuclear translocation of NFκB and IRF3 lead to the transcription of proinflammatory genes. Created using Biorender.

cGAMP synthase (cGAS) is a cytosolic nucleotidyltransferase that binds to dsDNA in a sequence non-specific manner (Civril et al. 2013). On binding to DNA, cGAS catalyses the synthesis of cyclic-GMP-AMP (cGAMP) from ATP and GTP. cGAMP acts a secondary messenger, activating the adapter protein STING (Ablasser et al. 2013; Sun et al. 2013; Wu et al. 2013). Upon cGAMP binding, STING undergoes a structural transformation and translocates from the ER to the Golgi apparatus via the ER–Golgi intermediate compartment (Burdette and Vance 2013; Ishikawa and Barber

2008). On translocation, STING activates kinases TBK1, IKK, and NIK, which in turn phosphorylate IRF3 and IκBα. Phosphorylation of IκBα results in its proteasomal degradation, releasing the inhibition of NFκB transcription factors (Fitzgerald et al. 2003; Ishikawa and Barber 2008; Ishikawa, Ma, and Barber 2009; Tanaka and Chen 2012).

Once activated, IRF3 and NFκB translocate to the nucleus and drive transcriptional programmes, which stimulate the synthesis of immunomodulatory factors, including type I IFNs, TNF (drives helper T-cells toward a pro-inflammatory profile), CXCL-10 (a chemoattractant for T-helper cells and cytotoxic T-lymphocytes), and several cytokines (IL1β, IL-2, IL12 and IL10) involved in the expansion and activation of immune effector cells (Vanpouille-Box et al. 2018) (Figure 1.16). Type I IFN secretion by tumour cells supports a tumour targeting immune response in multiple ways, including driving the maturation of dendritic DCs, increasing the effector functions of cytotoxic T-lymphocytes, increasing the persistence and reactivation of memory cytotoxic T-lymphocytes, inactivation of immunosuppressive T_{REG} cells, and promoting a switch in tumour associated macrophages form an immunosuppressive subtype (M2) to an antitumour subtype (M1) (Parker, Rautela, and Hertzog 2016; Zitvogel et al. 2015).

1.6.9 VX-970 shows efficacy in early clinical trials

VX-970 was the first ATR inhibitor to enter clinical trials in 2012, for a summary of all active and recruiting trials see Table 1.4. Results have been reported from several phase I trials and phase II trials.

A large multi-arm phase I trial (NCT02157792) explores the use of VX-970 as a monotherapy and in combination with chemotherapies in patients with advanced solid tumours. In the VX-970 monotherapy cohort, 17 patients were treated with escalating VX-970 doses, with no dose-limiting toxicities (DLTs) reported. Adverse events were

mild and included only grade 1-2 nausea, flushing, headaches and pruritus. One patient with advanced CRC with 100% ATM loss, loss of MLH1 and PMS2 (mismatch repair deficient), and truncating mutations in ARID1A, Chk1, FANCM, RAD50, POLD1 and SLX4 achieved a *RECIST* CR that was ongoing at two years. Five further patients had a best response of stable disease (SD) (Yap et al. 2020). In the VX-970 + carboplatin cohort, 15/23 patients achieved SD, with one partial response (PR) (>6 months) reported in a patient with BRCA1 and TP53 mutant, heavily pre-treated high-grade serous ovarian cancer (Yap et al. 2020).

In the VX-970 + cisplatin cohort, 4/26 patients achieved a PR, with one response lasting ~14 months. A further 15/26 achieved SD. Patients achieving a PR included a patient with BRCA2 mutant high grade serous ovarian cancer (HGSOC), a patient with TP53 mutant, RB1 null TNBC, and a patient with BRCA2 mutant prostate cancer bearing a duplication of exons 1-3 of ATR (Shapiro et al. 2021). In the VX-970 + gemcitabine arm, 4/48 patients (including a BRCA2 mutant BC patient) achieved a PR (71-211 days) and 29/48 had SD (Middleton et al. 2021).

In the VX-970 + gemcitabine + cisplatin cohort, 1/7 patients achieved a PR (94 days), with 4/7 achieving SD (Middleton et al. 2021). In a cohort expansion, patients with NSCLC were treated with VX-970 + gemcitabine, 3/24 patients achieved a PR, and 18/24 achieved SD, with 4 patients having a response duration >6 months (Plummer et al. 2018). In a further cohort expansion, 35 patients with TNBC (BRCA wild-type) were treated with VX-970 + cisplatin / carboplatin. PFS of ≥ 6 months was observed in 2 patients, and PFS of ≥3 months was observed in 8 patients. A response was ongoing in 4 patients at the time of reporting (Telli et al. 2018). While VX-970 monotherapy was well tolerated, combination of VX-970 with chemotherapies resulted in a high number of treatment emergent adverse events (TEAEs), leading to dose reductions and delays in treatment. The cytotoxicity profiles of the combination treatments, matched those commonly seen with the chemotherapies alone.

Preliminary results from a trial combining VX-970, veliparib (PARP inhibitor) and cisplatin in patients with advanced solid tumours have been reported (NCT02723864). 3/22 patients achieved a PR (lasting >4 treatment cycles), including 1 patient with ATM-mutant NSCLC and 1 patient with oesophageal cancer with biallelic loss of ATM. 12/22 patients had SD (median response duration 105 days). Haematological grade 3-4 TEAEs were reported in several patients (O'Sullivan Coyne et al. 2018).

In a further phase I trial (NCT02487095), 21 patients with advanced solid malignancies were treated with VX-970 + topotecan (TOP1 inhibitor). 2/19 evaluable patients had ongoing PR at the time of reporting (>18 months and > 7 months) and 8/19 achieved SD (median duration 9 months). The combination treatment was generally well tolerated by patients, with the toxicity profile matching that already known for topotecan treatment. One patient with a PR and two with SD were found to harbour mutations in the DDR pathway - ARID1A, Chk2 and BRCA1 respectively. Peripheral blood mononuclear cells (PBMCs) were collected from the patients at several stages during the trial and immune cell subsets analysed. A significant redistribution of monocyte subsets was observed. Prior to treatment, the major population was classic immunosuppressive monocytes, with immunostimulatory intermediate and non-classical monocytes being in the minority. Following the combination treatment, the more immunostimulatory subsets of monocytes were found to be in the majority. No change in the distribution of T-cell subsets was observed (Thomas et al. 2018).

Following promising outcomes in the phase I trial combining VX-970 and topotecan, a phase II trial was set up to evaluate efficacy of VX-970 in combination with topotecan in patients with small cell lung cancer (SCLC) and extra-pulmonary small cell neuroendocrine cancers (EP-SCNC). 9/25 patients with SCLC had a confirmed PR, and 17/25 had tumour regression, with a median PFS of 4.8 months. The OS at 12 months was 32%, with 2 patients having ongoing responses (13 and 24 months).

Despite being a single arm study, this data strongly supports efficacy, as typically platinum-resistant SCLC is fatal within weeks of relapse. 3/10 patients with EP-SCNC achieved a PR, and 2/10 achieved SD. 2/5 responders had progressed on previous TOP1 treatments, showing the combination treatment to be effective even with TOP1-inhibition resistant cancers (Thomas et al. 2021).

Data from a further phase II trial has been reported, in which the combination of VX-970 + gemcitabine was compared to gemcitabine treatment alone in patients with platinum resistant HGSOC. Large scale genomic studies of tumours from HGSOC patients show near universal loss of the G1/S checkpoint and have very high frequency of mutations in the DNA damage repair pathways, potentially increasing dependence on ATR signalling (Konstantinopoulos et al. 2020). 36 patients were treated with gemcitabine alone, while 34 patients received gemcitabine + VX-970. Median PFS was 22.9 weeks in the gemcitabine + VX-970 group compared to 14.7 weeks in the gemcitabine alone group. Median OS was 59.4 weeks vs 43 weeks. Sub-group analysis showed increased efficacy in patients who had a platinum-free period of <3 months, PFS 27.7 weeks vs 9 weeks and OS 84.4 weeks vs 40.4 weeks. It is proposed that tumours recently treated with platinum are likely to be enriched for biomarkers of replication stress and likely to have a higher ATR dependence. The addition of VX-970 to gemcitabine was well tolerated with the similar adverse events for both groups reported, indicating that toxicity was gemcitabine related (Konstantinopoulos et al. 2020).

Many of the ongoing studies focused on combining VX-970 with chemotherapies. Two studies are exploring the combination of VX-970 with radiation (NCT02589522 and NCT04052555). Several studies are combining VX-970 with an anti-PD-L1 antibody (Avelumab) (NCT03704467, NCT04216316 and NCT04266912). VX-970 is also being trailed as a monotherapy in the context of specific genetic backgrounds

including ATM, BRCA1, BRCA2 and ARID1A loss, and MYC and Cyclin E1 amplification (NCT03718091).

Table 1.4. Summary of active / recruiting VX-970 clinical trials as reported on ClinicalTrials.Gov database

Clinical Trial Identifier	Phase	Year of posting	Combination agent	Cancer type / characteristics
NCT02627443	I/II	2015	Carboplatin or gemcitabine	Recurrent and metastatic ovarian, primary peritoneal or fallopian tube
NCT02589522	I	2015	Whole brain radiation	Brain metastasis from NSCLC, SCLC or neuroendocrine tumours
NCT02567409	II	2015	Cisplatin and gemcitabine	Metastatic urothelial cancer
NCT02595892	II	2015	Gemcitabine	Recurrent ovarian, primary peritoneal, or fallopian tube cancer
NCT02567422	I	2015	Cisplatin and radiation	Locally advanced HNSCC
NCT02595931	I	2015	Irinotecan	Solid tumours which are metastatic or cannot be surgically resected
NCT02487095	I/II	2015	Topotecan	SCLC and extrapulmonary small cell cancer
NCT02723864	I	2016	Veliparib and cisplatin	Advanced / refractory solid tumours
NCT03309150	I	2017	Monotherapy or carboplatin and paclitaxel	Advanced solid tumours
NCT03718091	II	2018	Monotherapy	Solid tumours
NCT03641547	I	2018	Radiotherapy + cisplatin + capecitabine	Oesophageal cancer
NCT03641313	II	2018	Irinotecan	Progressive, metastatic, or unresectable TP53 mutant gastric or gastroesophageal junction cancer
NCT03704467	I/II	2018	Avelumab, carboplatin + paclitaxel, gemcitabine, doxorubicin + bevacizumab	PARP inhibitor resistant, recurrent ovarian cancer
NCT03517969	II	2018	Carboplatin, carboplatin + docetaxel	Metastatic castration-resistant prostate cancer

NCT04052555	I	2019	Radiation	Breast cancer
NCT03896503	II	2019	Topotecan	SCLC and extrapulmonary small cell cancer
NCT04216316	I/II	2020	Carboplatin + gemcitabine + avelumab	NSCLC
NCT04266912	I/II	2020	Avelumab	DDR deficient metastatic or unresectable solid tumours
NCT04768296	II	2021	Topotecan	Relapsed platinum resistant NSCLC
NCT04802174	I/II	2021	Lurbinectedin	NSCLC and High grade neuroendocrine cancers

1.6.10 AZD6738 is in early phase clinical trials

AZD6738 was the first orally bioavailable ATR inhibitor to enter clinical trials, a list of active / recruiting clinical trials can be seen in Table 1.5. The results of a multiple arm phase I/II trial have been reported in abstract form (NCT02264678). In the initial phase of the trial, 11 patients received AZD6738 monotherapy, to monitor for any drug toxicities. No DLTs or >grade 2 drug related toxicities were observed. A CR occurred in an advanced CRC patient with complete ATM loss, with the response ongoing at 59 weeks. 4/11 patients achieved SD (median duration 11 weeks). In the phase II expansion, patients with advanced solid tumours received either AZD6738 + carboplatin, AZD67368 + olaparib or AZD6738 + durvalumab. In the AZD6738 + carboplatin arm of the study, 3/36 patients achieved a PR (1 patient with ATM loss and 1 patient harbouring an ATM mutation). Haematological toxicities limited both the dosing and scheduling in the AZD6738-carboplatin arm of the study. The combination of AZD6738 with olaparib (45 patients) was well tolerated with short treatment cycles, however longer treatment cycles resulted in TEAEs. 1/ 39 evaluable patients had a CR, and 6/39 had a PR. In the durvalumab and AZD6738 arm of the study, 1/21 achieved a CR and 3/21 achieved a PR, with one haematological DLT observed (Krebs et al. 2018; Yap et al. 2016; Yap et al. 2015). The results from NCT02264678, demonstrated potential efficacy and manageable toxicity of AZD6738 in combination

with PARP inhibition or anti-PD-L1 therapy, and has led to an eruption of clinical trials involving these combination treatments in multiple cancer types.

Outcomes of a further phase I trial (NCT02630199) evaluating the combination of AZD6738 and paclitaxel have also been reported. 57 patients with advanced solid cancers (33 melanoma, progressed with anti PD-1/L1 therapy) were treated with paclitaxel and AZD6738, with 1/57 achieving an ongoing CR, 12/57 (2 ongoing) achieving a PR and 18/57 achieving SD. The main toxicities for grade 3 and higher were haematological (neutropenia 30%, anaemia 23% and thrombocytopenia 9%) (Lee et al. 2020).

Table 1.5. Summary of AZD6738 active clinical trials as reported on ClinicalTrials.Gov database

Clinical Trial Identifier	Phase	Year of posting	Combination agent	Cancer type / characteristics
NCT01955668	I	2013	Monotherapy	Relapsed / refractory chronic lymphocytic lukaemia (CLL), Prolymphocytic leukaemia (PLL) or B cell lymphoma
NCT02223923	I	2014	Monotherapy or radiotherapy	Refractory solid tumour
NCT02264678	I/II	2014	Carboplatin / olaparib / durvalumab	Advanced solid cancers
NCT02630199	I	2015	Paclitaxel	Refractory metastatic cancers
NCT02576444	II	2015	Olaparib	Advanced solid tumours
NCT02664935	II	2016	Durvalumab	NSCLC
NCT02937818	II	2016	Olaparib	Platinum refractory SCLC
NCT03330847	II	2017	Olaparib	TNBC
NCT03182634	II	2017	Olaparib	Advanced breast cancer
NCT03334617	II	2017	Durvalumab	Metastatic NSCLC with progression on an anti-PD-1/PD-L1 containing therapy
NCT03022409	I	2017	Monotherapy	HNCC
NCT03328273	I/II	2017	Monotherapy or acalabrutinib	Relapsed / refractory high-risk chronic lymphocytic leukaemia
NCT03527147	I	2018	Acalabrutinib	Relapsed / refractory aggressive non-Hodgkin's lymphoma (NHL)
NCT03780608	II	2018	Durvalumab	Refractory gastric adenocarcinoma or malignant melanoma
NCT03462342	II	2018	Olaparib	Recurrent ovarian cancer
NCT03428607	II	2018	Olaparib	Relapsed SCLC
NCT03682289	II	2018	Monotherapy or olaparib	Renal cell carcinoma, urothelial carcinoma, pancreatic cancers and all advanced solid tumours
NCT03787680	II	2018	Olaparib	Metastatic castration-resistant prostate cancer
NCT03669601	I	2018	Gemcitabine	Advanced solid tumours
NCT03740893	II	2018	Monotherapy	Post neoadjuvant chemotherapy resistant residual disease in patients with TNBC
NCT03770429	I	2018	Monotherapy	Myelodysplastic syndrome or chronic myelomonocytic leukaemia

NCT04090567	II	2019	Olaparib	Germline BRCA mutated breast cancer
NCT03833440	II	2019	Durvalumab	Advanced NSCLC with progression on an anti-PD-1/PD-L1 containing therapy
NCT04065269	II	2019	Olaparib	Gynaecological cancers
NCT03878095	II	2019	Olaparib	IDH mutant cholangiocarcinoma or solid tumours
NCT04361825	II	2020	Durvalumab	Relapsed SCLC
NCT04298008	II	2020	Durvalumab	Advanced biliary tract cancer
NCT04239014	II	2020	Olaparib	Platinum-sensitivity relapsed epithelial ovarian cancer, patients have previously responded to PARPi maintenance therapy
NCT04298021	II	2020	Durvalumab or olaparib	Advanced biliary tract cancer
NCT04417062	II	2020	Olaparib	Recurrent osteosarcoma
NCT04564027	II	2020	Monotherapy	Advanced solid tumours and metastatic castration resistant prostrate cancer

1.6.11 Biomarkers and patient selection for ATR inhibition

Successful clinical use of ATR inhibitors requires identification of patients who are most likely to respond to the therapy. Predictive biomarkers must be utilised to ensure patients receiving ATR inhibitors are likely to derive clinical benefit.

Deficiencies in several genes have been linked to increased sensitivity to ATR inhibition. ATR loss in the context of p53 deletion was initially identified as deleterious in ATR-Seckel mice. p53 loss results in abrogation of the G1 cell cycle checkpoint, increasing dependence on ATR induction of S-phase and G2/M checkpoints. Loss of p53 also creates general deficiencies in DDR, enabling proliferation of cells containing severe DNA lesions. Loss of p53 in Seckel mice results in a 4-fold increase in γH2AX staining, increased replication stress, loss of G1, S-phase and G2/M checkpoints and increased apoptosis. In addition, p53 loss typically leads to spontaneous formation

of tumours, however in the presence of hypomorphic ATR in Seckel mice, tumours fail to develop (Murga et al. 2009). In a further adult mouse model, the combination of ATR and p53 loss resulted in tissue regeneration, defective hair follicles, intestinal epithelial degeneration, and severe inflammatory disease, and was not compatible with long term survival (Ruzankina et al. 2009). Many *in vivo* and *in vitro* studies have demonstrated p53 loss to sensitise cancer cells and cancer mouse models to ATR inhibition. Multiple p53 null models have displayed reduced viability, increased ɣH2AX and increased loss of cell cycle checkpoints in response to ATR inhibition in comparison to p53 proficient models (Kwok et al. 2016; Middleton, Pollard, and Curtin 2018; Reaper et al. 2011; Toledo et al. 2011). Not all studies have found p53 status to be a promising predictive biomarker, with matched p53 null and proficient models showing similar sensitivity to ATR inhibition (Dillon et al. 2017; Hall et al. 2014). Data emerging from clinical trials will demonstrate whether p53 status acts as a predictive biomarker in patients.

There has also been a strong clinical focus on the use of ATM status as a predictive biomarker for ATR inhibition. How ATM deficiency might increase sensitivity to ATR inhibitors is not fully understood, however it is proposed that ATM-dependant DDR is required for repair of DSBs which arise as a result of unresolved replication forks in the absence of ATR (Lecona and Fernandez-Capetillo 2018). As there is much crosstalk between the ATR and ATM signalling pathways, with many downstream targets the same, it is hypothesised that a synthetic lethal relationship occurs between ATR and ATM. Indeed, in the absence of ATR, ATM becomes activated in response to replication stress (Reaper et al. 2011). Multiple *in vitro* and *in vivo* studies have identified ATM deletion or an ATM loss of function mutation, to be predictive of ATR inhibition sensitivity. ATM deficient cancer models have shown increased sensitivity, increased DNA damage and increased loss of cell cycle checkpoints on ATR inhibition in comparison with ATM proficient models (Kwok et al. 2016; Menezes et al. 2015;

Min et al. 2017; Reaper et al. 2011; Schmitt et al. 2017). Several patients with loss of ATM have responded well to ATR inhibition in early phase clinical trials (Krebs et al. 2018; O'Sullivan Coyne et al. 2018; Yap et al. 2020). Multiple active clinical trials now have expansion cohorts for patients with ATM deficient cancers (NCT03718091, NCT02264678, NCT01955668, NCT03896503), with trial data required for validation that ATM acts as a suitable biomarker for ATR inhibition therapy.

An RNAi screen identified a synthetic lethal relationship between ARID1A, a component of the SWI/SNF complex and ATR, with several studies supporting this finding (Jo, Murai, et al. 2021; Thomas et al. 2021; Williamson et al. 2016). The SWI/SNF complex remodels chromatin structure by removing nucleosomes from DNA, thereby modulating DNA replication, transcription, and repair (Hohmann and Vakoc 2014). Loss of ARID1A expression results in a reduction of Top2α binding to chromatin, leading to increased topological stress and subsequent dependence on ATR. Both *in vitro* and *in vivo* loss of ARID1A has been shown to increase sensitivity to ATR inhibition (Williamson et al. 2016). ARID1A mutant cohorts are currently being studied in 3 clinical trials of ATR inhibitors (NCT03718091, NCT03682289, NCT04062569).

SLFN11 expression protects against genomic instability, with cell death occurring in response to DNA damage. Overexpression of SLFN11 leads to increased sensitivity to a wide range of chemotherapeutics. SLFN11 mRNA expression is suppressed in ~50% of cancer cell lines, with cell lines having increased genomic instability and replication stress. A genome wide siRNA screen identified ATR as a therapeutic target for SLFN11 deficient cells. Indeed, ATR inhibition sensitised SLFN11 deficient cells to a range of therapeutics including irinotecan, etoposide, talazoparib and cisplatin (Jo, Murai, et al. 2021).

ATR and Chk1 amplification frequently occur in genomically unstable cancers, with dependence on ATR signalling for resolution of replication stress and DNA damage. It is therefore unsurprising that deficiencies in the DDR pathways have been identified as biomarkers for ATR inhibition (Krajewska et al. 2015). XRCC1 is a scaffold protein with a critical role in BER and SSB repair, with loss of XRCC1 leading to accumulation of SSBs. Inhibition of ATR in XRCC1 deficient but not XRCC1 proficient ovarian cancer cell lines, results in increased SSBs, increased γH2AX accumulation and increased apoptosis (Sultana et al. 2013). ATR inhibition of BRCA1 deficient ovarian cancer cell lines has been shown to cause dramatic sensitisation to a range of therapies including cisplatin, topotecan and olaparib. While ATR inhibition did sensitise BRCA1 proficient cell lines to several therapies, this was to a lesser extent than seen in BRCA1 deficient cells (Huntoon et al. 2013). These findings are further supported by Krajewska et al., who found ovarian cancer cells with HR deficiencies to be sensitive to ATR inhibition (Krajewska et al. 2015). Loss of the ERCC1-XPF complex which functions to remove bulky DNA adducts, ICLs and DSBs was also found to be a predictive biomarker for ATR inhibition. Cells deficient in ERCC1 display increased dependence on ATR for DNA repair, with loss of ATR resulting in significantly reduced viability (Mohni et al. 2015).

Overexpression of replication stress inducing oncogenes can increase ATR dependency, thereby acting as a biomarker for ATR inhibition. Overexpression of cyclin E, the regulatory subunit of Cdk2, results in premature entry into S-phase leading to genomic instability, replication stress and increased dependence on S-phase and G2/M checkpoints (Spruck, Won, and Reed 1999). Cells overexpressing cyclin E display increased sensitivity to ATR inhibition with increased γH2AX accumulation and apoptosis (Toledo et al. 2011). Patients with amplification of cyclin E are being assessed for sensitivity to VX-970 monotherapy in an ongoing clinical trial (NCT03718091). Overexpression of other replication stress inducing oncogenes

including hRAS and MYC also increases sensitivity to ATR inhibition with increased DNA damage and apoptosis observed (Schoppy et al. 2012). Indeed, MYC driven tumours fail to develop in ATR-Seckel mice, with MYC overexpression creating ATR dependency (Murga et al. 2011). An ongoing clinical trial is exploring sensitivity of patients with MYC overexpressing tumours to VX-970 monotherapy (NCT03718091).

Overexpression of CDC25A, leads to accelerated S-phase entry, driving genomic instability. ATR activation results in proteasomal degradation of CDC25A, resulting in cell cycle arrest. The level of CDC25A has been identified as a predictive biomarker for ATR inhibition, with cells expressing very low levels of CDC25A being resistant to ATR inhibition and those expressing very high levels displaying greatest sensitivity (Ruiz et al. 2016). APOBEC enzymes are not normally expressed in unstressed proliferating cells, with their DNA mutator function part of the cellular response to viral RNA/DNA. APOBEC3A and APOBEC3B enzymes are expressed in a wide range of cancers and cause replication stress by inducing abasic sites at replication forks, leading to replication fork arrest and ATR activation. APOBEC expressing cancer display very marked sensitivity to ATR inhibition, with failure to overcome replication stress leading to loss of cell viability (Buisson, Lawrence, et al. 2017; Nikkilä et al. 2017). Sensitivity of APOBEC expressing cancers to ATR inhibition (AZD6738) is currently being explored in a clinical trial (NCT02576444).

1.7 Antibody drug conjugates (ADCs)

1.7.1 The development of ADCs

ADCs are a novel class of anticancer agents, which harness the specificity of mAbs and the cytotoxic potency of small molecules. An ADC is comprised of three components, a highly cytotoxic drug, a synthetic linker and a mAb which has been raised against a tumour surface antigen (Figure 1.17). ADCs enable targeted drug delivery to tumour cells through the antibody–antigen interaction, while sparing

healthy cells from chemotherapeutic damage (Abdollahpour-Alitappeh et al. 2019; Sievers and Senter 2013).

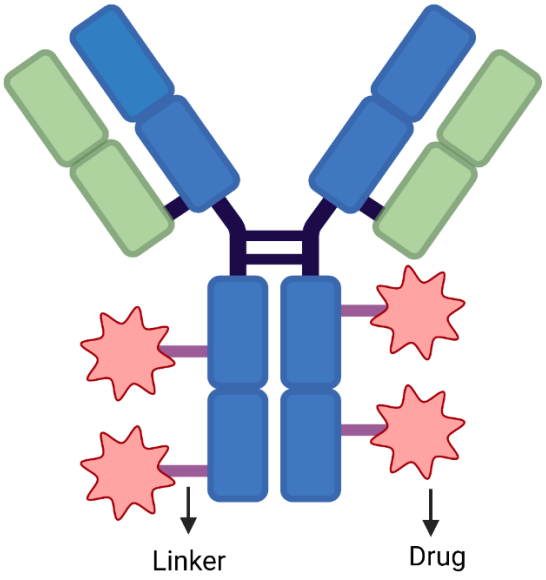

Figure 1.17. **General structure of an antibody-drug conjugate.**
Basic ADC structure illustrating a full length IgG1 antibody (heavy chain: blue; light chain: green), drug molecule (pink) and linker (purple). Created with Biorender.

The concept of targeted drug delivery to tumours was first proposed by Paul Ehrlich, who believed that drugs could be specifically delivered to cancer cells using a “magic bullet” approach (Strebhardt and Ullrich 2008). It was almost half a century after the idea of targeted drug delivery was conceived, that the first *in vitro* investigations involving a cytotoxic agent bound to an antibody began (Mathe, Tran Ba, and Bernard 1958). At that time, it was clear that the chemotherapeutic agents used, including methotrexate, taxanes, anthracyclines, nitrogen mustards, vinca alkaloids and folate analogues were affecting both the cancer cells and healthy dividing cells (Abdollahpour-Alitappeh et al. 2019; DeVita and Chu 2008). The therapeutic index (TI = maximum tolerated dose/minimum efficacious dose) of these drugs was low resulting in a very narrow therapeutic window. ADCs were seen as a promising way

of widening the therapeutic window of cancer treatment, by selectively delivering cytotoxic agents to cancer cells (Figure 1.18) (Panowski et al. 2014; Peters and Brown 2015).

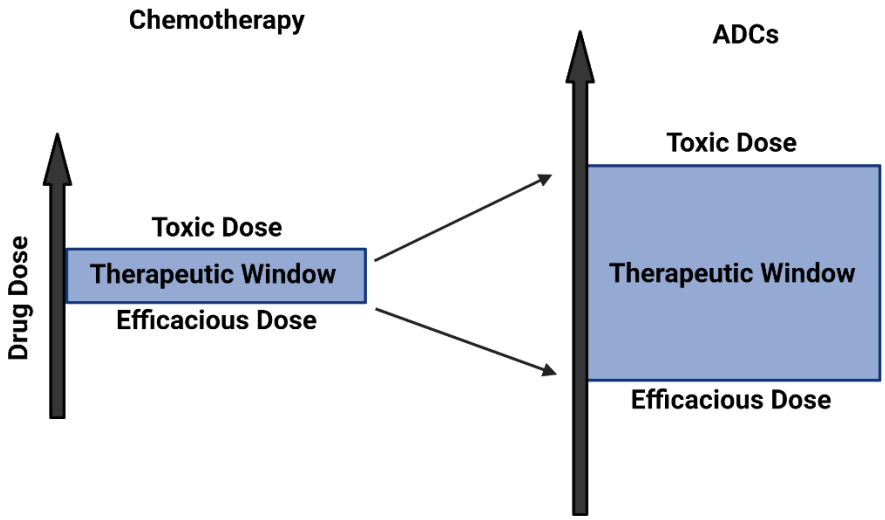

Figure 1.18. **ADCs have a wider therapeutic window than classic chemotherapy drugs.** ADCs have a lower efficacious drug dose and a higher toxic dose than classical chemotherapies, widening the therapeutic window. Created with Biorender.

First generation ADCs were comprised of classic chemotherapeutic agents such as mitomycin C, N-acetyl melphalan, doxorubicin, vinca alkaloids and methotrexate, coupled via non cleavable linker to murine mAbs (Chou et al. 2010; Endo et al. 1987; Kato et al. 1983; Pimm et al. 1988; Rowland, Pietersz, and McKenzie 1993; Smyth, Pietersz, and McKenzie 1987; Spearman et al. 1987). Early clinical trials using first generation ADCs yielded poor results, with the conjugates often being less efficacious than the parent drugs (Chari 1998). There were multiple contributing factors in the failure of first generation ADCs, these included; lack of drug potency, as the circulating serum concentrations in patients were below the therapeutic range; target-antigen expression, with the number of antigen molecules expressed on tumour cells resulting in delivery of sub-therapeutic doses of drug; ADC internalisation, the number of ADCs internalised is often lower than the number of ADCs bound at the cell surface; tumour

localisation, poor accumulation of ADC at the tumour site; linker stability, the linkers used were either too stable leading to reduced potency, or to labile leading to systemic toxicity; immunogenicity, mAbs used were either murine or chimeric, with patients producing an anti-mouse immune response preventing repeated treatment cycles (Abdollahpour-Alitappeh et al. 2019).

Using lessons learned from the 1st generation of ADCs, gemtuzumab ozogamicin (GO) was the first ADC to achieve FDA approval in 2000. GO was comprised of an anti-CD33 humanised mAb linked to a highly potent calicheamicin derivative (Sievers and Linenberger 2001). GO was voluntarily withdrawn from the market in 2010, when a phase III clinical trial showed poor clinical benefit and excess mortality (Petersdorf et al. 2013). GO was reapproved for the treatment of AML in 2017, with an optimised dosing schedule (Castaigne et al. 2012).

Advancements in mAb technology, biochemical drug synthesis and linker chemistry led to the development of second-generation ADCs. Three second-generation ADCs achieved FDA approval, brentuximab vedotin in 2011, ado-trastuzumab emtansine (TDM-1) in 2014, and inotuzumab ozogamicin in 2017 (Beck et al. 2017). The optimisation of the ADC technology has led to an explosion of novel ADCs in clinical development and on the market, with two ADCs approved in 2019 and three approved in 2020, and one approved in 2021 so far (Drago, Modi, and Chandarlapaty 2021).

1.7.2 Key aspects of ADC design

Selection of the correct target antigen is considered the most crucial element of ADC design. For an ADC to have a high TI, the tumour cells should have high expression of the target antigen, while healthy cells should ideally have little or no antigen expression (Lambert and Berkenblit 2018). Unfortunately, tumour specific antigens are rare, and the target antigen is more commonly a tumour associated antigen. Apart from increasing toxicity, expression of the target antigen on healthy tissue results in

reduction of ADC dose available to the tumour (Peters and Brown 2015). The level of antigen expression on tumour cells required for the uptake of a lethal quantity of ADC is dependent on the properties of the ADC, particularly the drug to antibody ratio (DAR) (Drago, Modi, and Chandarlapaty 2021). The rate and mechanism of antigen internalisation, as well the route for intracellular trafficking are also important, with more rapid internalisation and processing increasing the efficiency of drug delivery (de Goeij et al. 2015).

The antibody should bind selectively and with high affinity to the target antigen, as off target binding increases toxicity and can result in accelerated clearance (Abdollahpour-Alitappeh et al. 2019). IgG remains the predominant antibody backbone in ADCs, with high target avidity and a long circulatory half-life, leading to accumulation at the tumour site (Schuurman and Parren 2016). ADCs have IgG1, IgG2 or IgG4 mAbs, IgG3 isotypes are not used due to the comparatively fast rate of clearance. IgG1 is the most commonly used isotype, due to its ability to induce a strong ADCC and CDC response (Yu, Song, and Tian 2020).

The cytotoxic payload is typically more toxic than standard chemotherapeutics, and many are highly potent in sub-nanomolar concentrations (Drago, Modi, and Chandarlapaty 2021). In addition to potency, the physiochemical properties of the payload are also of importance. Hydrophobic agents are unsuitable payloads as they have low aqueous solubility and cause ADC aggregation, immunogenicity and accelerated clearance (Beck et al. 2017). Payloads of ADCs currently licensed or in development, inhibit tubulin, interact with DNA or inhibit cellular enzymes (Figure 1.19). Auristatins, which are microtubule inhibitors, are the payloads carried by four of the ten ADCs which have currently received FDA approval (Waight et al. 2016). A maytansinoid, which is also a microtubule inhibitor is the payload on one approved ADC (Oroudjev et al. 2010). Calicheamicins, which bind to DNA and induce DSBs are the payload for two of the licensed ADCs (Ricart 2011). Camptothecin derivatives,

which are TOP1 inhibitors are the payload for two licenced ADCs (Abdollahpour-Alitappeh et al. 2019; Goldenberg et al. 2015; Ogitani, Aida, et al. 2016). SG3199, a pyrrolo[2,1-c][1,4]benzodiazepines (PBD) dimer is the warhead for the most recently FDA approved ADC, loncastuximab tesirine-lpyl (Lee 2021). PBD dimers bind to the minor groove of DNA forming ICLs, inhibiting transcription and replication (Zammarchi et al. 2018).

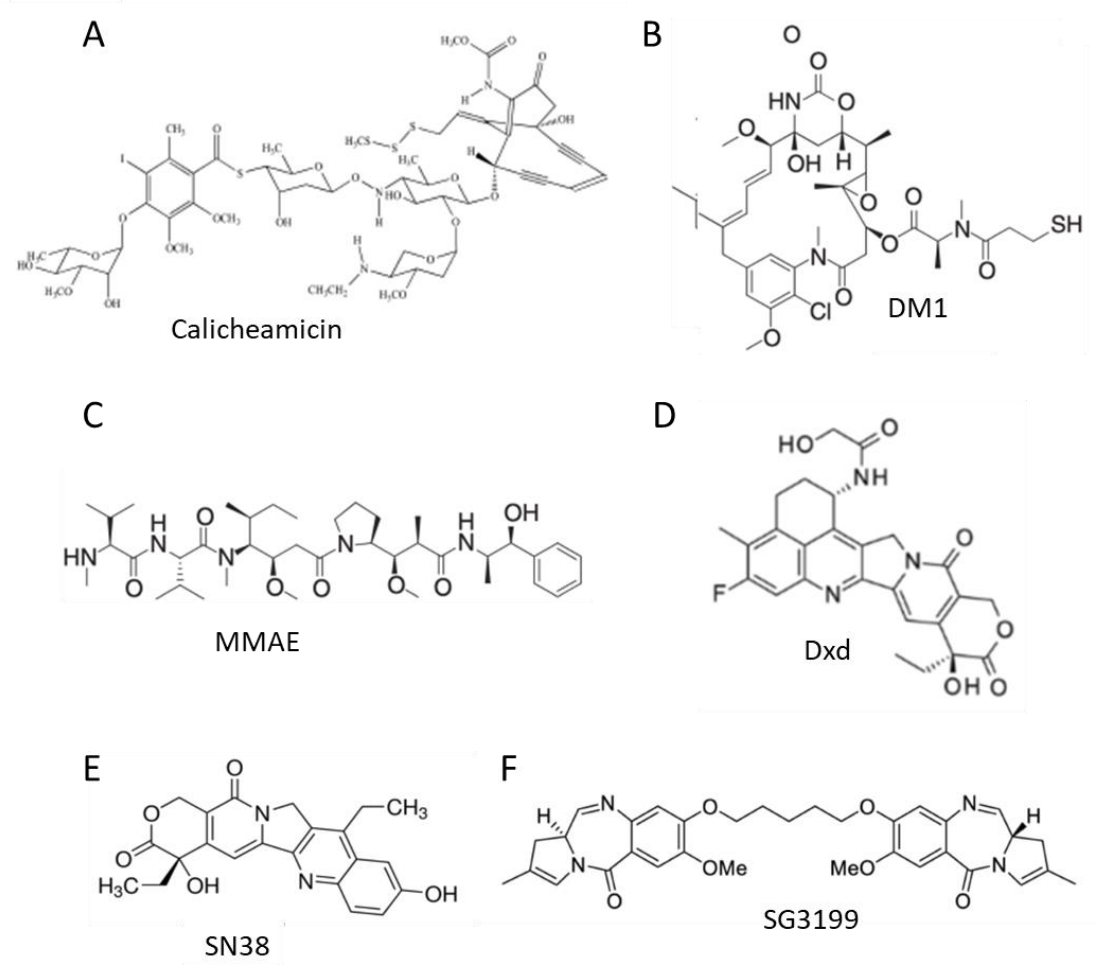

Figure 1.19. **Molecular structure of FDA approved ADC payloads.**
A. Calicheamicin, a DNA damage inducing drug. **B.** DM1, a microtubule formation inhibiting maytansinoid derivative. **C.** Monomethyl auristatin E (MMAE), a microtubule formation inhibiting auristatin derivative. **D.** Deruxtecan (Dxd), Exatecan derivative TOP1 inhibitor. **E.** SN38, camptothecin derivative TOP1 inhibitor. **F**. SG3199, a PBD dimer.

The purpose of the linker, which attaches the payload to the antibody is two-fold. The first role of the linker is to maintain the attachment of the payload to the antibody whilst the ADC is circulating in the plasma. An unstable linker results in premature release of the payload, resulting in systemic toxicity and reduced payload delivery to the tumour site (Jain et al. 2015). The second role of the linker is to release the payload from the antibody once ADC internalisation has occurred (Drake and Rabuka 2015).

Linkers fall into two categories, cleavable and non-cleavable. Cleavable linkers are designed to break down and release their cytotoxic payload inside cells and are cleaved as a result of acidic conditions, reducing conditions, or the abundance of proteolytic enzymes, such as cathepsins (Tsuchikama and An 2018). Non-cleavable linkers are more stable than cleavable linkers but require lysosomal degradation of the entire antibody to release the payload. Payloads released by antibody degradation often retain amino acid components, which can affect their potency and membrane permeability (Jain et al. 2015). Details of the currently FDA approved ADCs are outlined in Table 1.6.

Table 1.6. Current FDA approved ADCs for the treatment of cancer

ADC	Target antigen	mAb isotype	Linker type	Payload (payload class)	Drug antibody ratio (DAR)	Indication (Year of 1st approval)
Gemtuzumab ozogamicin	CD33	IgG4	Cleavable	Ozogamicin (Calicheamicin) DNA cleavage	2-3	AML (2000)
Brentuximab vedotin	CD30	IgG1	Cleavable	MMAE (Auristatin) Microtubule inhibitor	4	sALCL, cHL, pcALCL, MF PTCL, (2011)
Ado-trastuzumab emtansine (T-DM1)	HER2	IgG1	Non-cleavable	DM1 (Maytansinoid) Microtubule inhibitor	3.5 (mean)	Breast cancer (2013)
Inotuzumab ozogamicin	CD22	IgG4	Cleavable	Ozogamicin (Calicheamicin) DNA cleavage	5-7	B-ALL (2017)
Trastuzumab deruxtecan (DS-8201a)	HER2	IgG1	Cleavable	Dxd (Camptothecin) TOP1 inhibitor	8	Breast cancer (2019)
Polatuzumab vedotin-piiq	CD79b	IgG1	Cleavable	MMAE (Auristatin) Microtubule inhibitor	3.5 (mean)	DLBCL (2019)
Sacituzumab govitecan-hziy	TROP2	IgG1	Cleavable	SN38 (Camptothecin) TOP1 inhibitor	8	TNBC (2020)
Enfortumab vedotin-ejfv	Nectin 4	IgG1	Cleavable	MMAE (Auristatin) Microtubule inhibitor	4	Urothelial carcinoma (2020)
Belantamab mafodotin-blmf	BCMA	IgG1	Non-cleavable	MMAF (Auristatin) Microtubule inhibitor	Unknown	MM (2020)
loncastuximab tesirine-lpyl	CD19	IgG1	Cleavable	SG3199 (PBD dimer)	2.3	DLBCL (2021)

AML, acute myeloid leukaemia; B-ALL, B-cell acute lymphoblastic leukaemia; cHL, classical Hodgkin lymphoma; DLBCL, diffuse large B-cell lymphoma; MF, mycosis fungoides; pcALCL, primary cutaneous anaplastic large cell lymphoma; PTCL, peripheral T-cell lymphoma; sALCL, systemic anaplastic large cell lymphoma; TNBC, triple negative breast cancer; MM, multiple myeloma

1.7.3 ADC internalisation

Following antigen binding, internalisation of the antibody-antigen complex is crucial for payload delivery. Receptor mediated endocytosis can occur through clathrin-mediated, caveolin-mediated, or clathrin and caveolin independent mechanisms, such as micropinocytosis which can be triggered by receptor clustering (Ritchie, Tchistiakova, and Scott 2013). Antigen independent uptake of ADCs via pinocytosis can also occur. Clathrin-mediated endocytosis is the predominant mechanism of ADC uptake. The clathrin-mediated pathway involves clustering of the ADC-antigen (receptor) complex into pits, where clathrin proteins form multimeric lattices which induce membrane internalisation (Le Roy and Wrana 2005). Dynamin, a GTPase self-assembles around the neck of the clathrin-coated vesicle and triggers the release of the vesicle from the plasma membrane (Ferguson and De Camilli 2012).

The clathrin is subsequently lost from the vesicles, which fuse together to form early endosomes. Following the formation of early endosomes, receptor complexes can be recycled back to the cell surface via either a fast or slow route. Endosomes that express the GTPase Rab4 are rapidly recycled back to the cell surface membrane, while those that express Rab8 or Rab11 are slowly recycled (Stenmark 2009). Ideally for ADC metabolism, the early endosomes mature into acidic late endosomes, which fuse with lysosomes through the action of Rab7 (Ritchie, Tchistiakova, and Scott 2013). Payloads that are attached using acid-cleavable linkers are released in the early or late endosomes, while those that require enzymatic cleavage or proteolytic degradation are typically released in the late endosomes or lysosomes (Erickson et al. 2006; Kovtun and Goldmacher 2007; Sutherland et al. 2006). Once released some payloads can passively cross the endosomal / lysosomal membrane, this includes Dxd which is lipophilic (Ogitani, Hagihara, et al. 2016). Other payloads such as maytansinoids require lysosomal membrane transporters for effective release into the cytosol (Kinneer et al. 2018).

1.7.4 ADCs mechanism of action

ADCs are complex cancer therapeutics, integrating antibody and cytotoxic therapies as one treatment. The canonical model of ADC action involves the antigen binding, ADC internalisation, payload release and cytotoxic impact (Drago, Modi, and Chandarlapaty 2021). The reality is a much more complex picture and varies between different ADCs (Figure 1.20). Upon antigen engagement, ADCs retain their mAb function, and can therefore begin exerting anti-tumour effects prior to payload release. ADCs can block target function by disrupting receptor-ligand binding, preventing dimerization, or inducing degradation of the target antigen (Junttila et al. 2011; Ogitani, Aida, et al. 2016; Redman et al. 2015). This suggests that ADCs with a functional target are likely to have greater anti-tumour activity.

There is also growing evidence that ADCs act as immunotherapies. The Fc region of the mAb on binding to the target antigen can trigger ADCC, CDC and antibody dependant phagocytosis. (Abdollahpour-Alitappeh et al. 2019; Junttila et al. 2011; Ogitani, Aida, et al. 2016; Ogitani, Hagihara, et al. 2016; Redman et al. 2015). Treatment with ADCs has been found to lead to increase in cytotoxic T-cells and antigen presenting cells in the tumour microenvironment (Abdollahpour-Alitappeh et al. 2019; Müller et al. 2015; Rios-Doria et al. 2017). Patient data is also emerging, with infiltrating tumour cells present in biopsy samples of individuals treated with T-DM1 (Müller et al. 2015).

Antigen expression on tumour cells is very heterogenous, with some tumour cells being antigen negative. There are also many non-tumour antigen negative cells, which form an essential part of the tumour, such as cells of the vasculature, cells in the extracellular matrix and tumour promoting immune cells. For effective tumour eradication, cells with low levels of target antigen or lacking the target antigen completely must also be targeted. The bystander effect is the cytotoxic impact of the

payload on cells, that have not internalised the ADC (Kovtun et al. 2006). For ADCs that carry a lipophilic payload, the bystander effect is achieved by diffusion of the payload across the plasma membrane to neighbouring cells (Modi, Park, et al. 2020; Ogitani, Hagihara, et al. 2016). Many ADCs with cleavable linkers will also begin to release their payload into the tumour microenvironment prior to internalisation, as a result of excreted proteases. While the bystander effect increases ADC efficacy, it can also result in off target toxicities and narrow the therapeutic window (Pondé, Aftimos, and Piccart 2019).

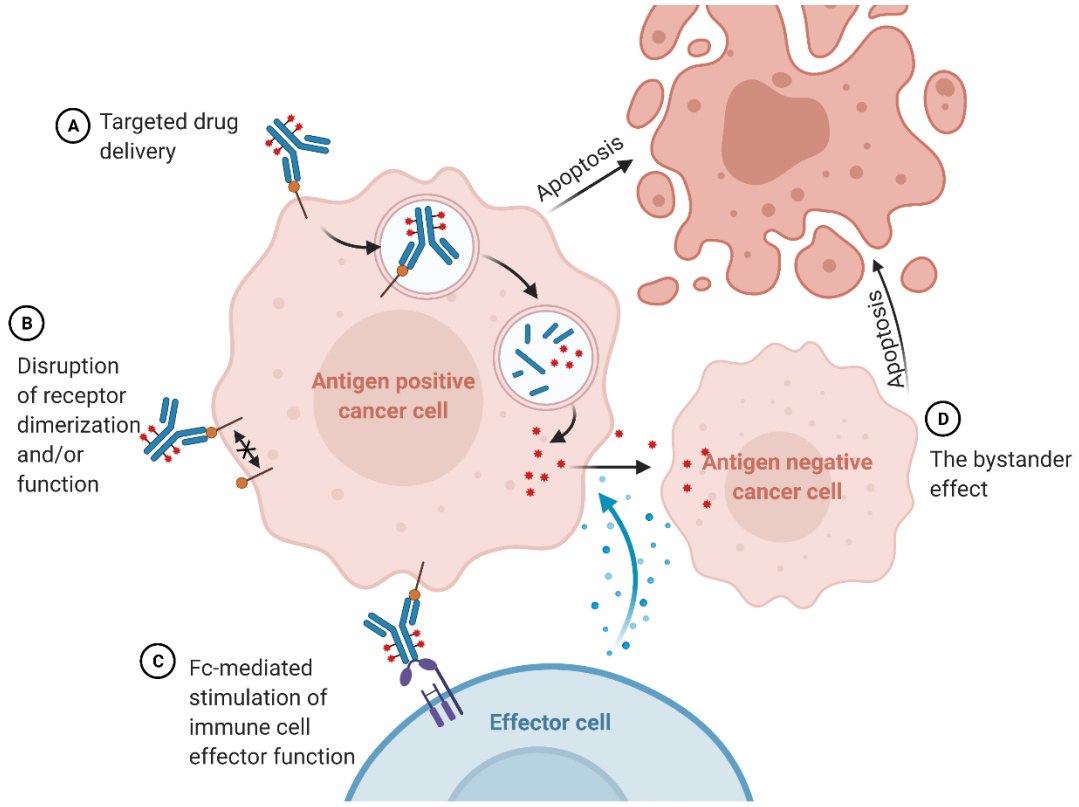

Figure 1.20. **Mechanisms of action of ADCs.**
A. Following receptor binding, the ADC is internalised and passes through the endosomal-lysosomal pathway, releasing the cytotoxic payload. **B.** Binding of the ADC to a receptor can disrupt receptor dimerization and/or function and lead to a loss of downstream signalling. **C.** The mAb can trigger Fc-mediated ADCC, CDC and antibody dependent phagocytosis. **D.** The bystander killing effect, released payload can pass into neighbouring antigen negative cells. Created with Biorender.

1.8 Trastuzumab Deruxtecan (DS-8201a)

1.8.1 Structure of DS-8201a

DS-8201a is a HER2 targeting ADC composed of an anti-HER2 antibody, a TOP1 inhibitor (Dxd) payload and an enzymatically cleavable peptide linker (Figure 1.21) (Ogitani, Aida, et al. 2016). The antibody is a humanised IgG1 mAb, produced using the same amino acid sequence as trastuzumab, giving it the same binding and stability as the mAb widely used for the treatment of HER2+ cancers (Nakada et al. 2019). The CPT analogue Dxd is a novel exatecan derivative, with a TOP1 inhibitory potency 10-fold higher than SN38 (Nakada et al. 2019). The high potency of Dxd make it a suitable ADC payload, with potency many magnitudes greater than its chemotherapeutic counterpart, irinotecan. The payload is attached to the antibody via an enzymatically cleavable peptide (GGFG)-based linker and a self-immolative amino methylene spacer.

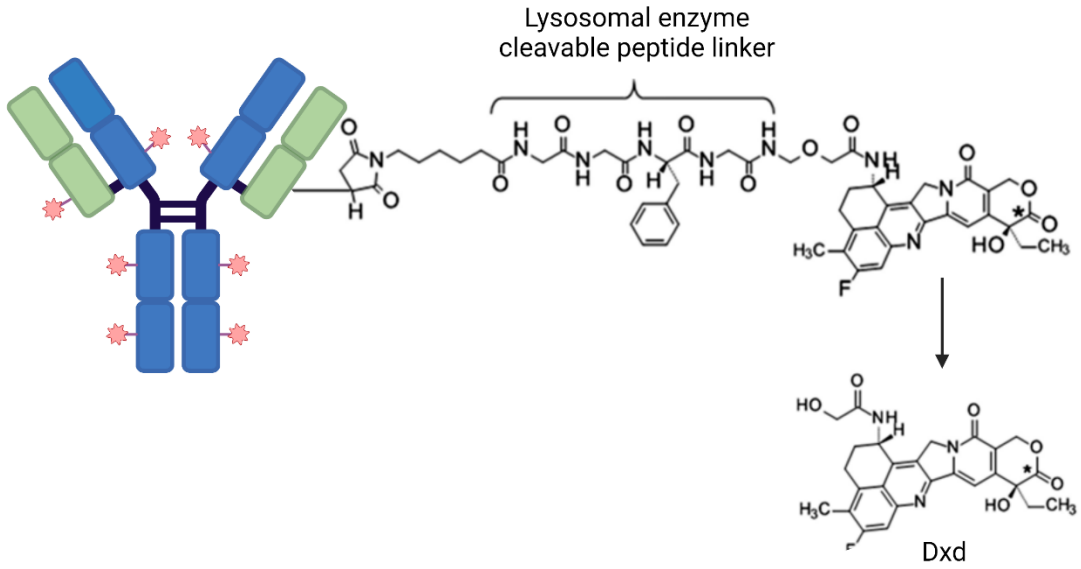

Figure 1.21. **Chemical structure of DS-8201a.**
Dxd is attached to the HER2-targeting antibody via a an enzymatically cleavable peptide (GGFG)-based linker and a self-immolative amino methylene spacer. Cleavage of the linker releases the Dxd payload. Each antibody carries ~8 payload molecules (pink stars). The asterisk indicates the position of ^{14}C. Created with Biorender.

The GGFG linker is cleaved by cathepsins B and L, which are abundant in the lysosomal compartment of tumour cells, allowing rapid payload release. The linker has reduced hydrophobicity compared to the conventional *p*-amino benzyl spacer and is highly stable in systemic circulation (Nakada et al. 2019; Ogitani, Aida, et al. 2016; Ogitani, Hagihara, et al. 2016). The release rate of the payload in human plasma is incredibly low, with only 2.1% release with 21 days incubation, in contrast to payload release from T-DM1 which is 18.4% after just four days (BLA. 2013; Ogitani, Aida, et al. 2016). The linker-payload is conjugated via cysteine residues to the antibody, following the reduction of interchain disulphide bonds. There are four internal disulphide bonds, which can be used for interchain cysteine conjugation, with DS-8201a having the highest possible DAR, with eight Dxd molecules conjugated to each antibody. The potency of Dxd and the high DAR make DS-8201a highly cytotoxic, requiring lower expression of antigen target than other ADCs (Nakada et al. 2019; Ogitani, Aida, et al. 2016).

1.8.2 HER2 as a target antigen

HER2 is a member of the human epidermal growth factor receptor (HER) family, which includes four tyrosine kinases, EGFR (HER1, erbB1) HER2 (erbB2, HER2/*neu*), HER3 (erbB3) and HER4 (erbB4) (Ghosh, Marrocco, and Yarden 2020). The HER receptors all share a common structure including an extracellular ligand biding domain, a transmembrane domain, and an intracellular protein tyrosine kinase domain (Lemmon, Schlessinger, and Ferguson 2014). There are multiple ligands of the HER family receptors including EGF, TGF-a, HB-EGF, AREG, BTC, EPG, EPR and NRG1–4 (Ghosh, Marrocco, and Yarden 2020). Ligand binding leads to receptor dimerization, which is critical for activation of the HER family receptors. HER2 lacks the capacity to bind with extracellular ligand, but is able to form heterodimers with other members of the HER family and is able to generate potent cell signalling (Citri and Yarden 2006). In HER2 overexpressing cells, HER2 can be activated by

homodimerization. HER2 is the only HER family receptor that has a permanently exposed dimerization arm, enabling ligand independent dimerization (Yarden and Sliwkowski 2001). HER family receptor activation initiates signalling cascades via many networks, including the MAPK, PI3K/Akt and JAK/STAT pathways, impacting upon cell growth, proliferation, survival, differentiation and angiogenesis (Ghosh, Marrocco, and Yarden 2020).

HER2 was initially identified as an oncology drug target when it was discovered that 25-30% of breast cancers display HER2 amplification or overexpression, leading an aggressive phenotype and poor patient outcome (Slamon et al. 2001). It has since been identified that HER2 overexpression occurs in a broad range of cancers including bladder, cervical, cholangial, colorectal, endometrial, oesophageal, gastric, head and neck, liver, lung, ovarian, and salivary gland (Yan et al. 2014; Yan et al. 2015). Trastuzumab, lapatinib, pertuzumab and T-DM1 are all HER2 targeting therapeutics, which have been approved for the treatment of HER2 expressing tumours (Bang et al. 2010; Baselga et al. 2012; Geyer et al. 2006; Slamon et al. 2001).

Besides DS-8201a, T-DM1 is the only other HER2-targeting ADC approved for use. In the EMILIA study, T-DM1 was shown to prolong survival and improve quality of life in patients with metastatic HER2+ breast cancer (Verma et al. 2012). The success of the KATHERINE trial, led to the approval of T-DM1 for early stage HER2+ breast cancer, with residual disease following neoadjuvant chemotherapy (von Minckwitz et al. 2019). Currently, only patients with tumours expressing high levels of HER2, either immunohistochemistry (IHC)3+ or IHC2+/ fluorescence *in situ* hybridisation (FISH)+ derive benefit from HER2 targeting treatment. There is no HER2 targeting therapeutic currently approved for the treatment of HER2-low expressing tumours, those IHC2+/FISH- or IHC1+ (Ogitani, Hagihara, et al. 2016; von Minckwitz et al. 2019). With a DAR of 8, a highly potent payload and properties that enable the bystander effect, DS-8201a was designed to have efficacy in tumours with low expression of

HER2, as well as those expressing high levels of HER2 (Ogitani, Hagihara, et al. 2016).

HER2 is ubiquitously expressed at low levels on normal epithelial tissues, with expression detected in multiple healthy organs including the lungs, liver and heart (Brown et al. 2021; Morgan et al. 2010; Press, Cordon-Cardo, and Slamon 1990). The expression of HER2 on healthy tissues poses a challenge for HER2-targeted therapies, with the potential of on-target toxicity, particularly in the treatment of HER2-low expressing tumours. Indeed, CAR-T cells engineered to target HER2 expressing solid tumours have demonstrated severe toxicity, due to CAR-T cells binding in a HER2-dependent manner to healthy tissue (Morgan et al. 2010). For a HER2-targeting ADC to have a manageable toxicity profile, the tumour associated antigen should be expressed at higher levels on tumour cells than healthy cells, enabling increased payload accumulation in the tumour cells, relative to healthy cells. Furthermore, differential sensitivity of healthy tissue and the tumour to the payload must exist, thereby widening the therapeutic index. T-DM1 carries a microtubule inhibitor payload, while DS-8201a carries a topoisomerase I inhibitor payload. As cancer cells have greater sensitivity to these chemotherapeutic payloads than healthy tissue, this limits the toxicity of these agents when minimal uptake by healthy HER2 expressing cells occurs.

1.8.3 DS-8201a shows efficacy *in vivo* and *in vitro*

A dramatic growth inhibitory effect was observed when HER2+ breast and gastric cancer cell lines were treated with DS-8201a (IC_{50} values ranging from 6.7- 204.2 ng/mL). The IC_{50} value was found to strongly correlate with HER2 expression, with higher HER2 expression resulting in a lower IC_{50} value. Treatment with an anti-HER2 mAb had either no effect, or a minimal effect on the viability of cell lines. No impact on viability was observed in any of the cell lines following treatment with a non-

targeting IgG control ADC. Treatment with DS-8201a or Dxd, but not an anti-HER2 mAb led to phosphorylation of Chk1 and H2AX, and the cleavage of PARP. These results indicate that DS-8201a induces DNA damage and apoptosis following the release of the Dxd payload. The anti-HER2 mAb remains functional post payload conjugation, with DS-8201a treatment leading to a 70% reduction in Akt phosphorylation in a HER2 overexpressing cell line. *In vivo*, 4mg/kg DS-8201a was found to cause 99% tumour growth inhibition in a HER2 positive gastric cancer xenograft model. In contrast, treatment with the unconjugated anti-HER2 antibody only resulted in 31% tumour growth inhibition (Ogitani, Aida, et al. 2016).

DS-8201a may also provide an effective therapeutic option for patients who have developed resistance to T-DM1 therapy. A gastric cancer cell line and a gastric cancer xenograft model resistant to T-DM1, due to upregulation of ABCC2 and ABCG2 were found to be sensitive to DS-8201a. The T-DM1 resistant cells were also found to be resistant to the T-DM1 payload, but not Dxd. The HER2 expression level of T-DM1 resistant cells and xenografts was unchanged compared to parental models. This suggested that DS-8201a may be used following T-DM1 treatment failure, in cases where resistance is not due to a change in HER2 expression levels (Takegawa et al. 2017).

1.8.4 DS-8201a shows immunomodulatory properties *in vivo*

Several chemotherapeutic agents have been found to induce an anti-tumour immune response. A major limitation of chemotherapeutic agents as stimulators of an immune response, is their tendency to induce lymphopenia. ADCs which are designed to selectively target cancer cells, while sparing normal tissue, are possibly ideal candidates to act as immunomodulators as monotherapies and with immune checkpoint inhibitors (ICIs) (Gerber et al. 2016).

Studies using immunocompetent mice, showed that mice bearing HER2+ positive tumours cured by DS-8201a treatment, failed to develop tumours when rechallenged with the same tumour type. Furthermore, mice also failed to develop tumours when challenged with the same tumour lacking HER2 expression, demonstrating that DS-8201a can induce an anti-tumour response with target antigens being independent of HER2 expression. The splenocytes of rechallenged mice also showed increased IFNɣ secretion, signifying immune activation. Eight days following DS-8201a treatment, a substantial increase in tumour infiltrating CD8+ T-cells was detected. Furthermore, a greater percentage of CD8+ T-cells were found to be Granzyme B+ following DS-8201a treatment compared to vehicle treatment. In addition to increased activation of the adaptive immune response, DS-8201a increased the ratio of DCs to lymphocytes in tumours. DS-8201a was also found to increase the expression of PD-L1 and major histocompatibility complex class I (MHC-CI) on tumour cells. Increased MHC-CI expression would promote increased recognition of tumour cell by infiltrating T-cells. An increase in PD-L1, provides the rational for combining DS-8201a treatment with anti-PD-L1/PD-1 blocking agents. Indeed, combining DS-8201a with an anti-PD-1 antibody increase the survival of tumour bearing mice on day 38 from 20% with each monotherapy to 80% with the combination therapy (Iwata et al. 2018).

The combination of DS-8201a with a further ICI, CTLA-4 has also been explored *in vivo* with 80% survival of tumour bearing mice at 70 days. The survival of vehicle, DS-8201a and anti-CTLA-4 treated mice was 0%, 10% and 20% respectively. Mice cured following DS-8201a and anti-CTLA-4 treatment failed to develop tumours when rechallenged the same tumour type, both with and without HER2 expression. Splenocytes from rechallenged mice exhibited very high levels of IFNɣ secretion (Iwata et al. 2019).

1.8.5 DS-8201a approved for the treatment of breast cancer

DS-8201a was FDA approved in 2019 for the treatment of HER2+ metastatic breast cancer based on findings in the phase II DESTINY-Breast01 trial (NCT03248492) and two dose expansion cohorts in a phase I trial (NCT02564900) (Narayan et al. 2021). In 2021, DS-8201a was approved by NICE for the same indication in the UK (NICE 2021). In a cohort expansion phase I study, 115 patients who had progressed on T-DM1 treatment received DS-8201a. Patients were heavily pre-treated, with 82% having received ≥5 lines of therapy. 66% of the patients acheived a CR and 93.7% achieved disease control. The median duration of response was 20.7 months and PFS was 22.2% (Tamura et al. 2019). In a second arm of the cohort expansion, 54 heavily pre-treated patients with low HER2+ breast cancer (IHC1+ or IHC2+/ FISH-) received DS-8201a. The confirmed response rate was 37%, with a median response duration of 10.4 months. The PFS was 11.1 months and median OS was 29.4 months. The current standard of care for these patients is single line chemotherapies, which typically only give a PFS of 3-5 months (Modi, Park, et al. 2020).

The phase II DESTINY-Breast01 trial evaluated the efficacy of DS-8201a in 184 patients with HER2+ (IHC3+ or FISH+) breast cancer. All patients were heavily pre-treated, with 100% of patients receiving prior trastuzumab and T-DM1 therapy. 97.3% of patients achieved disease control and the confirmed response rate was 60.9%, with 6% of patients having a complete response. The median duration of response was 14.8 months and the median PFS 16.4 months (Modi, Saura, et al. 2020). These finding suggest superiority of DS-8201a over T-DM1, with a response rate of 43.6% and PFS of 9.6 in the EMILIA trial (Verma et al. 2012).

Trial data shows a durable response in a very high percentage of breast cancer patients treated with DS-8201a. Of note, is the confirmed response rate of ~60% in patients who have been previously treated with T-DM1, demonstrating the value of an

additional HER2 targeting ADC. Of additional importance is the response rate observed in patients with HER2-low expressing tumours, for whom all current anti-HER2 treatments are not recommended due to lack of efficacy (Cardoso et al. 2018; Fehrenbacher et al. 2020). Approximately, 40-50% of breast cancer patients have HER2-low expressing tumours, making this an area of high unmet need (Giuliani et al. 2016; Lal et al. 2004; Schalper et al. 2014). The high DAR and ability to elicit the bystander effect, make DS-8201a the first anti-HER2 therapy to show any clinical benefit in this cohort of patients. The limitation of DS-8201a is the toxicity observed in patients (section 1.8.7).

1.8.6 DS-8201a approved for the treatment of gastric cancer

In 2021, the FDA approved the use of DS-8201a for the treatment of metastatic or locally advanced HER2+ gastric cancers based on data from the DESTINY-Gastric01 phase II clinical trial (NCT03329690). 125 patients on the trial were treated with DS-8201a, while 62 received physician's choice of therapy (irinotecan / paclitaxel). The confirmed response rate was 43% in the DS-8201a treatment group and 12% in the irinotecan / paclitaxel group. 8% of patients achieved a CR following DS-8201a treatment, no CRs were observed in the control treatment group. The median duration of response was 8 months longer in patients treated with DS-8201a compared to patients in the control arm. DS-8201a was found to extend median OS by 4 months (Shitara et al. 2020). In contrast to these findings, T-DM1 was not found to improve OS when compared to taxane therapy in the phase III GATSBY study (Thuss-Patience et al. 2017). Results from a dose expansion cohort phase I trial (NCT02564900) reported a 41% objective response rate in HER2+ gastric cancer patients who had been previously treated with irinotecan, suggesting DS-8201a treatment as a potential therapeutic for irinotecan resistant cancers (Shitara et al. 2019).

1.8.7 DS-8201a induced adverse events

Pooled analysis form phase I and II trials showed the most common adverse reactions following DS-8201a to be nausea, fatigue, vomiting, alopecia, constipation, decreased appetite, anaemia, neutropenia, diarrhoea, leukopenia, cough, and thrombocytopenia. The most common grade 3/4 adverse reactions were neutropenia (16%), anaemia (7%), nausea (7%), fatigue (6%) and leukopenia (6%). Severe adverse reactions occurred in 20% of patients, and included interstitial lung disease, pneumonia, vomiting, nausea, cellulitis, hypokalaemia, and intestinal obstruction. Adverse events leading to death occurred in 4.3% of patients, with interstitial lung disease being the most reported cause (Keam 2020).

1.8.8 Ongoing DS-8201a clinical trials

There are many ongoing clinical trials assessing the efficacy of DS-8201a in solid tumours, currently active trials are summarised in Table 1.7.

Table 1.7. Summary of active / recruiting DS-8201a clinical trials as reported on ClinicalTrials.Gov database

Clinical Trial Identifier	Phase	Year of posting	Combination agent	Cancer type / characteristics
NCT03334617	II	2017	Durvalumab	Metastatic NSCLC with previous anti PD-1 / PD-L1 therapy
NCT03742102	Ib	2018	Durvalumab	First line metastatic TNBC
NCT03505710	II	2018	Monotherapy	HER2 mutant / HER2 overexpressing NSCLC
NCT03529110	III	2018	Monotherapy (Head to head comparison with T-DM1 arm)	HER2+ metastatic or unresectable breast cancer
NCT03734029	III	2018	Monotherapy	HER2-low metastatic or unresectable breast cancer
NCT03523585	III	2018	Monotherapy	Previously treated HER2+ metastatic or unresectable breast cancer
NCT04014075	II	2019	Monotherapy	HER2+ metastatic or unresectable gastric cancer
NCT04644237	II	2020	Monotherapy	HER2 mutant NSCLC
NCT03523572	I	2018	Nivolumab	HER2+ breast cancer or urothelial carcinoma
NCT04622319	III	2020	Monotherapy (Head to head comparison with T-DM1 arm)	HER2+ primary breast cancer with residual disease following neoadjuvant therapy
NCT04553770	II	2020	Monotherapy or anastrozole	HER2-low, hormone receptor positive tumours
NCT04494425	III	2020	Monotherapy	HER2-low, hormone receptor positive tumours
NCT04616560	II	2020	Monotherapy	HER2+ osteosarcoma
NCT04539938	II	2020	Tucatinib (HER2 inhibitor)	Unresectable or metastatic HER2+ breast cancer
NCT04482309	II	2020	Monotherapy	HER2+ bladder cancer, biliary tract cancer, cervical cancer, endometrial cancer, ovarian cancer, pancreatic cancer or rare tumours
NCT04420598	II	2020	Monotherapy	Previously treated metastatic or unresectable breast cancer with or without brain or leptomeningeal metastasis
NCT04639219	II	2020	Monotherapy	Metastatic or unresectable HER2 mutant solid tumours
NCT04538742	Ib/II	2020	Monotherapy or tucatinib or	HER2+ metastatic breast cancer

			durvalumab or pertuzumab or paclitaxel or durvalumab + paclitaxel	
NCT04294628	I	2020	Monotherapy	HER2+ advanced solid tumours
NCT04585958	I	2020	Olaparib	HER2+ advanced tumours and endometrial cancers
NCT04042701	I	2020	Pembrolizumab	Locally advanced or metastatic HER2+ (high and low) breast cancer, HER2 expressing NSCLC and HER2 mutant NSCLC
NCT04379596	II	2020	Monotherapy or tucatinib or paclitaxel or durvalumab or pertuzumab or 5-FU or capecitabine or durvalumab + paclitaxel or 5-FU + oxaliplatin or capecitabine + oxaliplatin or 5-FU + durvalumab or capecitabine + durvalumab or 5-FU / capecitabine + cisplatin / oxaliplatin or 5-FU / capecitabine and durvalumab	Gastric cancer
NCT04556773	I	2020	Capecitabine or durvalumab + paclitaxel or capivasertib (Akt inhibitor) or anastrozole or fulvestrant	HER2-low advanced or metastatic breast cancer
NCT04752059	II	2021	Monotherapy	HER2+ breast cancer with brain metastasis
NCT04744831	II	2021	Monotherapy	HER2 overexpressing metastatic CRC
NCT04784715	II	2021	Monotherapy or pertuzumab	HER2+ metastatic breast cancer without prior anti-HER2 targeted therapy

1.9 Research aims

Although many mCRC patients initially respond well to current treatments, the majority of patients progress or relapse with the current therapeutics, making mCRC an area of unmet clinical need. Early clinical trials have shown efficacy of TOP1 and ATR inhibition for the treatment of NSCLC and EP-SCNC, but this combination has not been extensively researched in the CRC setting. Furthermore, targeted TOP1 treatment, using ADC DS-8201a in the context of CRC has only shown efficacy in the context of high HER2 expression, making this a non-viable treatment for many CRC cancer patients. The aim of this thesis was to investigate whether ATR inhibition could increase the efficacy of targeted (DS-8201a) and non-targeted (SN38) TOP1 inhibition in CRC models.

Research aims are addressed as follows:

1. Chapter 3 evaluates the efficacy of SN38 and VX-970 combination treatment in CRC cell lines and patient derived organoids, by looking at survival and the induction of DNA damage. The potential link between DNA damage and an anti-tumour immune response is also investigated.

2. Chapter 4 investigates the sensitivity of HER2-low expressing CRC cell lines and patient derived organoids to DS-8201a as a monotherapy and in combination with ATR inhibition. The induction of DNA damage signalling with DS-8201a monotherapy and combination therapy is also investigated.

2. Chapter 5 explores the use of SN38 and VX-970 combination treatment to overcome SN38 resistance in CRC cell lines. The efficacy of DS-8201a as a monotherapy and in combination with ATR inhibition in a SN38 resistant cell line is also assessed.

2 Materials and methods

2.1 Materials

2.1.1 Cancer cell lines and organoids

CACO2 cells were purchased from the European Collection of Authenticated Cell Cultures (ECACC). HCT116 cells were provided by Prof. Bert Vogelstein. LS174T cells were provided by Prof. Kerry Chester's lab. SW48 cells were obtained from Merck Serono (Darmstadt). HT29, MDA-MB-231 and HCC1954 cells were obtained from Prof. Tony Ng's lab. L-WRN mouse fibroblasts for preparing conditioned media for organoid maintenance, were kindly provided by Dr Chris Tape's lab. Cell lines were authenticated using short tandem repeat (STR) profiling by Eurofins genomics at the start of the study. CRC organoids were kindly provided by the Welcome Sanger institute.

2.1.2 Therapeutic agents

SN38 was purchased from Sigma-Aldrich and prepared as a 5mM stock in dimethyl sulfoxide (DMSO), and stored at -20°C. DS-8201a was provided by Daiichi Sankyo, long-term storage was at -80°C, and short-term storage (1 week) was at 5°C. VX-970 was purchased from Stratech and prepared as a 10mM stock in DMSO, and stored at -20°C. AZD6738 was purchased from Cambridge bioscience and prepared as a 5mM stock in DMSO, and stored at -20°C. Working stocks were freshly prepared for each experiment, and diluted to the required final concentrations in cell culture media.

2.2 Methods

2.2.1 Cell line maintenance

Cells were cultured in T75 tissue culture flasks at 37°C in a humidified atmosphere of 5% CO_2. The media used for each cell line is shown in Table 2.1. All cell procedures

requiring a sterile environment were carried out in a Class II biological safety cabinet. Cells were routinely passaged (3 times a week) by removing the media and gently washing once with sterile phosphate-buffered saline (PBS) (Gibco). Following PBS removal, cells were detached by incubation with 2-5ml of Trypsin-EDTA (Sigma-Aldrich) for 3-5min at 37°C. After detachment of cells, trypsin was inactivated by the addition of complete media in a 3:1 ratio. Cells were then reseeded into culture dishes at 1:10 ratio in fresh media. Cells were passaged for a maximum of two months, before being discarded and replaced with a new batch of cells from liquid nitrogen storage.

Table 2.1. Cell culture medium for cancer cell lines.

Cell line	**Culture Medium**
CACO2	DMEM (Sigma-Aldrich), 10% fetal bovine serum (FBS) (Gibco), 2mM L-glutamine (Sigma-Aldrich)
HCT116	McCoys 5-A (Sigma-Aldrich), 10% FBS (Gibco), 2mM L-glutamine (Sigma-Aldrich)
HT29	McCoys 5-A (Sigma-Aldrich), 10% FBS (Gibco), 2mM L-glutamine (Sigma-Aldrich)
LS174T	DMEM (Sigma-Aldrich), 10% FBS (Gibco), 2mM L-glutamine (Sigma-Aldrich)
SW48	McCoys 5-A (Sigma-Aldrich), 10% FBS (Gibco), 2mM L-glutamine (Sigma-Aldrich)
MDA-MB-231	RPMI (Sigma-Aldrich), 10% FBS (Gibco), 2mM L-glutamine (Sigma-Aldrich)
HCC1954	RPMI (Sigma-Aldrich), 10% FBS (Gibco), 2mM L-glutamine (Sigma-Aldrich)
L-WRN Fibroblasts	DMEM (Sigma-Aldrich), 10% FBS (Gibco), 2mM L-glutamine (Sigma-Aldrich), 1% penicillin-streptomycin (Sigma-Aldrich)

2.2.2 Cell line storage and retrieval from liquid nitrogen

Cells were kept frozen in liquid nitrogen for long-term storage. Cells plated in T75 tissue cultured flasks, were trypsinised and collected in complete media. A cell pellet was obtained by centrifugation at 1200rpm for 3 minutes. The cell pellet was then resuspended in 2mL of freezing media (90% FBS and 10% DMSO (Sigma-Aldrich)) and aliquoted in 2 crytotubes (Thermo scientific). Cells were stored at -80°C for 24-

72 hours prior to long-term storage in liquid nitrogen tanks. Cells were retrieved from frozen stocks by thawing in a 37°C water bath, after which the cells were transferred into 9mL complete media. Cells were centrifuged for 3 minutes at 1200rpm to remove the DMSO. The resulting pellet was then gently resuspended in fresh media, and cells seeded in a T75 tissue culture flask.

2.2.3 Statistical analysis

Unless otherwise stated in the experimental protocol or individual experiment, statistical analysis was performed using the GraphPad Prism software. The ANOVA test for multiple comparisons, was the most commonly used statistical test and the T-test was used if comparison was only between two experimental groups.

2.2.4 Generation of SN38 resistant cell lines

HT29 and SW48 cells seeded at 50% confluence were exposed to multiple, increasing SN38 treatment cycles (1nM, 2nM, 5nM, 10nM, 20nM, 50nM and 100nM). Each treatment cycle was 72 hours, followed by a 2-week recovery period, during which cells were passaged as required. After each recovery period, the dose was escalated until a concentration of 100nM SN38 was reached. The clonogenic assay was used to assess the sensitivity of the resultant resistant cell lines to SN38.

2.2.5 Cell proliferation – Sulforhodamine B (SRB) assay

Cells were seeded in 96 well plates (at a density of 2,500 cells per well for 3-day assays, and 1,250 cells per well for 6-day assays unless otherwise stated) and left to adhere overnight. Each experimental group contained 6 intraexperimental technical repeat wells. The following day, a plate of cells was fixed to act as a baseline when calculating proliferation, the other cells were treated with the required drugs. Cells in 96-well plates were fixed with 50µL Carnoy's fixative (Methanol to acetic acid ratio 3:1) at appropriate time-points and stored at 4°C for up to 2 weeks. Plates were then

washed 5 times with distilled H_2O (dH_2O) and allowed to dry overnight, before staining with 100µL 0.4% SRB (Sigma-Aldrich) dissolved in 1% acetic acid (v/v) for 30 min. Unbound stain in wells was then washed off by washing the plate 5 times in 1% acetic acid. A fresh batch of 1% acetic acid was used for each plate, to reduce the background SRB signal. Bound SRB was then solubilised in 100µl/well of 10mM Tris-HCL (pH10.5), and optical density measured at 570nm using a Varioskan LUX plate reader. Growth inhibition was calculated as a percentage of absorbance compared to an untreated control, and where applicable GI_{50} values were calculated in GraphPad Prism (log (inhibitor) vs normalized response slope).

2.2.6 Clonogenic assay

Cell were seeded in duplicate for each experimental condition, at 100, 500 and 1,000 cells/well of a 6-well pate. Cells were left to adhere to tissue culture plates for 24 hours prior to drug treatment. Two different treatment protocols were used in this thesis. In the first treatment schedule, cells were exposed to drug treatment for 72 hours, after which the drug-containing media was removed, and cells were washed with PBS. Media was then replaced, and plates returned to the incubator for 14 days, to allow for colony formation. In the second treatment schedule, cells were treated with drug containing media, and left to form colonies for 14 days without drug removal.

After 14 days for colony formation, media was aspirated and the colonies fixed with Carnoy's fixative. Subsequently, they were stained with 0.4% (w/v) crystal violet (Sigma-Aldrich) dissolved in dH_2O for 5 min, washed with slow running cold water and allowed to dry over-night. Visible colonies (>50 cells) were counted, and cloning efficiency in control samples was calculated using the following formula: (Counted colonies/colonies seeded) × 100. Percentage survival at each data-point was derived by normalising the colony counts to the estimated expected number of surviving colonies based on the cloning efficiency of that cell line. Where possible the same

seeding density was used to compare between treatment groups, however due to the toxicities of some therapeutics, higher seeding densities were required for some treatment groups.

2.2.7 Synergy analysis

Synergy scores were calculated using the zero interaction potency (ZIP) model from the SynergyFinder R package (Zheng 2021) (synergyfinder: Calculate and Visualize Synergy Scores for Drug Combinations. R package version 2.4.16, http://synergyfinder.org/). Synergy scores for each biological replicate were individually calculated and used to produce a mean and SEM for each condition. The synergy score reported is an average over the 2D dose matrix. A ZIP synergy score below -10 indicates antagonism, a score between -10 and +10 indicates an additive relationship and a score greater than +10 demonstrates synergy (Yadav et al. 2015).

2.2.8 Western blotting – cell lines

2.5-5.0 x 10^5 cells were seeded in 6-well plates in growth media, and left to adhere for 24 hours. Cells were then treated with drugs as described in individual experiments, with all drug incubations at 37°C. At the designated timepoints, plates were transferred onto ice, and media aspirated. Cells were then washed twice with ice-cold PBS and lysates collected by adding 50 µL lysis buffer (0.0625M Tris-HCL, 2 % SDS, 10% glycerol) and scraping the cells. Lysates were then boiled at 95 ºC for 10 minutes. Lysates were then homogenised by sonication (amplitude 40%, 10 pulses of 1 seconds, (QSonica sonicator)).

Protein quantification was done using the colorimetric RC-DC protein assay from Bio-Rad laboratories. A 1 in 10 dilution of each protein sample was prepared, and 10µL of each sample was added to the wells of a round bottom 96-well plate in triplicate. A Bovine Serum Albumin (BSA) (Sigma-Aldrich) standard curve was used to calculate the protein concentration of samples. 10µl of each of the BSA standards (100µg/ml,

200µg/ml, 400µg/ml, 600µg/ml, 800µg/ml, 1000µg/ml) were also added to the plate in triplicate. Reagents S and A were mixed at 1:50 ratio and 25µl of this mix was added per well. 200µl of reagent B was then added to each well, and the content of the plate was mixed on a shaking platform for 10min at room temperature (RT). Absorbance was measured at 750nm with the Varioskan LUX plate reader. The average absorbance measurement of a blank sample was subtracted from all the measurements of both standard and unknown samples. A standard curve was prepared by plotting the average absorbance value of each BSA standard against its concentration. The standard curve generated was used to calculate the concentration of each unknown sample.

For the immunoblotting, 50µg of protein from each sample was boiled for 5 minutes at 95°C with sample buffer (Invitrogen). Samples were loaded into a 4-15% Criterion TGX gel (Bio-Rad Laboratories), together with the Dual colour MW ladder (Bio-Rad Laboratories) in a Criterion electrophoresis tank (Bio-Rad Laboratories). A Tris/Glycine running buffer (Bio-Rad Laboratories) was used. For high MW proteins, samples were electrophoresed at 100V for 3 hours, and for other proteins at 80V for 10 minutes and 120V for 75 minutes. Proteins were transferred onto a 0.2µm nitrocellulose membrane (Bio-Rad Laboratories) using the Trans-Blot Turbo Transfer System (Bio-Rad Laboratories). For the transfer of proteins with a MW >200kDa, the high MW transfer programme was selected. Membranes were subsequently blocked for 1 hour at RT, with 2.5% milk in tris buffered saline with tween (TBST, 20mM Tris-base (Sigma-Aldrich), 150mM NaCl (Sigma-Aldrich), 0.1% Tween 20 (Sigma-Aldrich) in dH_20).

All primary antibodies (Table 2.2) were incubated overnight at 4°C. The antibody dilutions were prepared in 2.5% BSA (in TBST supplemented with 0.01% Sodium Azide (Severn Biotech)). Anti-rabbit or mouse IgG, horseradish peroxidase (HRP)-linked antibodies (Cell Signalling Technologies) were used to detect the primary

antibodies, with a 1/5000 dilution in 2.5% milk (in TBST). Membranes were washed three times in TBST for 5 minutes following incubation with primary and secondary antibodies. The antibody binding to the protein of interest was detected by enhanced chemiluminescence (ECL system, Amersham) on autoradiography film (Kodak X-Omat).

Table 2.2. List of the primary antibodies for Western blotting

Primary antibody	Dilution	Supplier
pThr1989 ATR	1:1000	Cell signaling, 58014
ATR	1:500	Cell signaling, 2790
pSer345 Chk1	1:500	Cell signaling, 2341
Chk1	1:1000	Cell signaling, 2360
pSer1981 ATM	1:1000	Cell signaling, 4526
ATM	1:1000	Cell signaling, 2873
pSer2056 DNA-PK	1:1000	Abcam, 124918
DNA-PK	1:1000	Abcam, 32566
pThr68 Chk2	1:1000	Cell signaling, 2661
Chk2	1:1000	Cell signaling, 2662
pSer15 p53	1:1000	Cell signaling, 9284
p53	1:1000	Abcam, 80644
pSer139 H2AX	1:1000	Millipore, 05-636
HER 2	1:1000	Cell signaling, 2165
Cleaved PARP	1:1000	Cell signaling, 9546
cGAS	1:1000	Cell signaling, 15102
STING	1:1000	Cell signaling, 13647
Calnexin (loading control)	1:1000	Cell signaling, 2679

2.2.9 Immunofluorescence

For immunofluorescence, cells were grown on glass coverslips (VWR). One coverslip was placed in each well of a 24-well dish, and 500µL of 0.1% porcine gelatin (Sigma-Aldrich) in PBS was added to each well to increase cell adherence. After 20 minutes at RT, the gelatin was aspirated, and the culture plate put at 37°C for 4 hours. The wells were washed once with PBS, prior to cell seeding. The cell seeding and

attachment protocol differed between cell lines, with HT29 seeded at 25,000 cells/well 24 hours before drug treatment, and SW48 seeded at 10,000 cells/well, 72 hours before drug treatment. Cells were treated as indicated in individual experiments.

Culture media was aspirated, and coverslips were washed twice with PBS (5 minutes at RT). Cells were fixed with 4% paraformaldehyde (PFA) (Thermo Fisher Scientific) in PBS at RT for 10 minutes. PFA was aspirated, and coverslips washed twice (5 minutes at RT) with PBS. Cells were permeabilized by incubation with 0.5% Triton X-100 (Sigma-Aldrich) in PBS at RT for 10 minutes. Coverslips were then washed twice (5 minutes at RT) with PBS. For blocking, cells were incubated in 5% BSA / 10% FBS in PBS for 40 minutes at RT. Cells were incubated with the cGAS primary antibody (cell signaling, 15102) 1:200 dilution in 1% FBS in PBS, for 40 minutes in a wet chamber at RT. A non-stained control sample was included, and this was incubated with 1% FBS in PBS. Coverslips were then washed 3 times for 5 minutes with PBS at RT. Cells were incubated for 20 mins in a dark wet chamber with a Goat anti-rabbit, Alexa fluor-488 secondary antibody (Thermo Fisher Scientific) at a 1:320 dilution in 1% FBS in PBS. Coverslips were then washed three times (5 minutes at RT) with PBS. Cells were then incubated with Hoechst (Thermo Fisher Scientific) (5µg/mL in PBS) for 20 minutes in the dark at RT. Coverslips were mounted on slides using 5µL of mounting media (Prolong® Gold Antifade, Thermo Fisher Scientific). The mounting media was left to dry for approximately 16 hours, and coverslips were sealed onto slides using clear nail varnish. Slide were stored in the dark at 4°C for a maximum of 2 weeks prior to microscopy.

Cells were imaged using a confocal microscope. The Zeiss LSM 880 confocal microscope with AiryScan was used for confocal microscopy. The microscope is maintained by the staff of the Imaging and Microscopy Translational Technology Platform in the Cancer Institute. The range of optimal emission detection was manually adjusted based on fully stained samples with the highest signal, and

maintained for all images captured in that experiment. Images were exported as .czi files and exposure normalised across all images using Imaris image analysis software. Micronuclei analysis was also performed using the Imaris image analysis software tool.

2.2.10 Alkaline single cell gel electrophoresis (Comet) assay

The alkaline comet assay is a sensitive technique used to measure the presence of DNA SSBs and DSBs in single cells (Fairbairn, Olive, and O'Neill 1995). 3.0 x 10^5 cells were seeded in each well of a 6-well dish and left to adhere for 24 hours. Cells were then treated as indicated in individual experiments. At the required time, cells were washed twice with ice cold PBS, and detached by adding 500µL trypsin to each well (5 minutes, 37°C). Cells were collected with ice cold complete media, and spun down (1,200rpm, 3 minutes, 4°C). The cells were resuspended in freezing media (10% DMSO in FBS) at a density of 50,000 cells/mL. Cells were stored at -80°C in cryovials for up to 1 month.

Cells were thawed on ice, and where indicated were irradiated using the A.G.O. HS 321 kV X-ray system. 500µL of cell suspension was mixed with 1mL of 1% agarose type VII (Sigma-Aldrich). 1mL of this mixture was then pipetted onto a 1% type 1A agarose (Sigma-Aldrich) pre-coated glass slide, covered with a coverslip and left to set on ice. Two slides per sample were prepared. Once the agarose embedded cells had set, the coverslip was removed, and the slides were placed on a tray (on ice). Cells were then covered with ice cold lysis buffer (100nM disodium EDTA (Sigma-Aldrich), 2.5M NaCl, 10mM Tris HCL, 1% Triton X-100, pH 10.5), and incubated in the dark for 1 hour on ice. The cells were washed 4 times (15 minutes) with ice cold dH_2O, and transferred into an electrophoresis tank. The slides were covered with ice cold alkali electrophoresis buffer (50mM NaOH, 1mM disodium EDTA, pH 12.5) in the dark for 45 minutes prior to electrophoresis. Electrophoresis was carried out in the

same buffer, for 25 minutes at 18V. After electrophoresis, the slides were placed in a tray, rinsed with neutralizing buffer (0.5M Tris-HCl, pH 7.5) for 10 minutes and washed with PBS (10 minutes). PBS was gently drained from the slides, which were then left to dry overnight. The next day, the slides were rehydrated for 20 minutes with dH_2O, and DNA was stained using 2.5µg/mL propidium iodide (Sigma-Aldrich) for 30 minutes at RT in the dark. The slides were washed with dH_2O, and left to dry in an oven at 40°C. Once completely dry, slides were stored in the dark at RT until data analysis.

Acquisition of images was performed with a NIKON inverted microscope with a high-pressure mercury light source, a 510-560nm excitation filter and a 590nm barrier filter at 20x magnification. Images were acquired using an on-line charge-couple device (CCD) camera and analysis was carried out with the Komet Analysis software (Kinetic Imaging, Liverpool). For each sample, 50 cells were analysed per duplicate slide. The tail moment is used as a measure of DNA damage and is defined as the product of the percentage DNA in the comet tail and the distance between the means of the head and tail distributions, based on the definition of Olive et al., (Olive 2002).

2.2.11 Neutral single cell gel electrophoresis (Comet) assay

The neutral comet assay was performed as described for the alkaline comet assay (section 2.2.10), with modifications to the lysis and electrophoresis protocol. Cells were lysed in the dark on ice, for one hour in ice cold lysis buffer (100mM EDTA, 2.5M NaCl, 10 mM Tris-HCl pH 8.0) containing 0.5% Triton X-100 (Sigma-Aldrich, UK), 1% N-lauroylsarcosine (Sigma-Aldrich, UK), 3% DMSO (Sigma-Aldrich, UK) added fresh and pH adjusted to 9.5. Slides were then washed twice in ice cold dH_2O for 10 minutes. 400µL of proteinase K solution 1mg/mL (Sigma-Aldrich) was pipetted onto each slide, and slides were incubated for two hours at 37°C in the dark. Slides were then washed twice with ice cold electrophoresis buffer (300 mM sodium acetate, 100

mM Tris-HCL, pH 8.3, containing 1% DMSO added freshly) for 10 minutes. Slides were covered with neutral electrophoresis buffer, incubated in the dark on ice for one hour, then placed in an electrophoresis tank, and covered in fresh electrophoresis buffer and electrophoresed for 60 minutes at 30V.

2.2.12 Cytokine Array

Cells were seeded at a density of 0.5-2.0 x 10^5 (depending on treatment cytotoxicity) in each well of 12 well plate, and incubated at 37°C for 24 hours to allow cell attachment. Cells were then treated according to individual experiment protocols in 1mL of media. At the indicated time, media was collected and transferred into an ice-cold Eppendorf. The media was spun down 2,000rpm for 10 minutes at 4°C, to remove cells. The supernatant was then transferred to a new Eppendorf on ice. The media was transferred to the cytokine arrays and processed as per the manufacturer's instructions (R and D Systems, Human XL Cytokine array kit, ARY022B). A full list of the cytokines detected by the arrays can be seen in Table 2.13.

The intensity of signal was determined using ImageQuant software. The intensity of signal in each array was normalised using the reference control spots, to allow comparison between arrays. Once a signal intensity was determined for each target, this was then normalised according to the signal intensity of that protein in the untreated control.

Table 2.3. Proteins detected by cytokine array

Adiponectin	Apolipoprotein A-I	Angiogenin	Angiopoietin-1
Angiopoietin-2	BAFF	BDNF	C5/C5a
CD14	CD30	CD40 ligand	Chitnase 3-like 1
CFD	CRP	Cripto-1	Cystatin C
Dkk-1	DPPIV	EGF	Emprin
ENA-78	Endoglin	Fas ligand	FGF basic
FGF-7	FGF-19	Flt-3 ligand	G-CSF
GDF-15	GM-CSF	GROα	Growth hormone
HGF	ICAM-1	IFNɣ	IGFBP-2
IGFBP-3	IL-1α	IL-1β	IL-1ra
IL-2	IL-3	IL-4	IL-5
IL-6	IL-8	IL-10	IL-11
IL-12p70	IL-13	IL-15	IL-16
IL-17A	IL-18 Bpa	IL-19	IL-22
IL-23	IL-24	IL-27	IL-31
IL-32	IL-33	IL-34	IP-10
I-TAC	Kallikrein 3	Leptin	LIF
Lipocalin-2	MCP-1	MCP-3	M-CSF
MIF	MIG	MIP-1α/1β	MIP-3α
MIP-3β	MMP-9	Myeloperoxidase	Osteopontin
PDGF-AA	PDGF-AB/BB	Pentraxin 3	PF4
RAGE	RANTES	RBP-4	Relaxin-2
Resistin	SDF-1α	Serpin E1	SHBG
ST2	TARC	TFF3	TfR
TGF-α	Thrombospondin-1	TNF-α	uPAR
VEGF	Vitamin D BP	CD31	TIM-3
VCAM-1			

2.2.13 Immunohistochemistry (IHC)

Cells were collected by trypsinisation of exponentially growing cells, and resuspended in PBS at a density of 1.0 x 10^6 cells/mL. Organoids were collected from 6 wells of a 6-well plate using 2mL of ice-cold PBS per well. Organoids were then washed twice with ice cold PBS to remove Matrigel (1500rpm, 3 minutes). Organoids were then resuspended in 1mL of ice-cold PBS. The cells/organoids were spun at 1500rpm for

5 minutes and supernatant discarded. Pellets were resuspended in 3mL10% formol saline and were left overnight at RT. 2% agar was melted in a microwave, and cooled to 60ºC in a water bath. 500µL of agarose was pipetted into a 1.5ml Eppendorf tube and was left to set. Cells were spun down to a pellet (2000rpm, 5 minutes) and formalin supernatant discarded. The cell pellet was placed in a water bath at 60ºC to warm for 2 minutes. The cell pellet was resuspended in 750µL of melted agar and transferred to the Eppendorf tube with the set agarose. The tube was spun the at 7000 rpm for 25 minutes, and agar was left to set. The end of the Eppendorf was cut off, and the cell pellet pushed through the top of the tube, out into a histology cassette. Cassettes were embedded in paraffin and slices cut.

Samples were processed and stained with haematoxylin and eosin (H&E), and an anti-HER2 antibody (cell signaling, 2242) by the UCL pathology department using a BOND polymer refine detection kit (Leica) on the BOND Rx machine. The protocol was set as follows, antigen retrieval 20 minutes, primary antibody 15 minutes, and secondary antibody 8 minutes.

2.2.14 RNAseq

Cells were seeded at 1.0 x 10^6 in a 10cm dish and were left for 48 hours. Media was aspirated and cells were washed twice with ice cold PBS. RNA was extracted using the RNeasy kit (Qiagen) as per the manufacturer's instructions. mRNA was quantified by Nanodrop (Nanodrop one, Thermo Fisher Scientific).

Prior to mRNA library preparation each RNA sample was corrected to 100ng/µL in RNase-free milliQ water. A standard Kapa mRNA Hyperprep library preparation kit (Kapa) was used to process each RNA sample. In brief, mRNA capture beads were washed and resuspended in 52.5µL of mRNA bead binding buffer. 50µL of re-suspended mRNA capture beads were mixed and incubated with 50µL of RNA sample. First round mRNA capture was performed in a thermocycler at 65°C for 2

minutes. The samples were placed on a magnet, washed in 200µL of mRNA bead wash buffer and resuspended in 50µL of RNase-free water. The second round mRNA capture was performed in a thermocycler at 70°C for 2 minutes. 50µL of bead binding buffer was added and each sample was incubated at RT for 5 minutes. The samples were placed on a magnet and washed with 200µL of mRNA bead wash buffer. The samples were resuspended with 22µL of fragment, prime and elute Buffer. Fragmentation and priming was performed in a thermocycler, 6 minutes at 94°C. The samples were placed on a magnet and 20µL of the supernatant containing the eluted, fragmented, and primed RNA was pipetted into a separate tube. 10µL of 1st strand synthesis master mix was added to the sample and 1st strand synthesis was performed in a thermocycler using the following program: primer extension at 25°C for 10 minutes, 1st strand synthesis at 42°C for 15 minutes, enzyme inactivation at 70°C for 15 minutes. 30µL of second strand synthesis and A-tailing master mix was added and second round strand synthesis was performed in a thermocycler using the following program: 2nd strand synthesis at 16°C for 30 minutes, A-tailing at 62°C for 10 minutes. 5µL of 1.5µM adapter and 45µL of ligation mix was added and the sample was incubated at 20°C for 15 minutes.

First post-ligation cleanup was performed by resuspending the sample with 70µL of Kapa pure beads, placing the sample on a magnet, washing twice with 200µL of 80% ethanol and resuspending with 50µL of 10 mM Tris-HCl. Second post-ligation clean-up was performed by resuspending the sample with 35µL of PEG/NaCl solution, placing the sample on a magnet, washing twice with 200µL of 80% ethanol and resuspending with 22µL of 10mM Tris-HCl. 20µL of the supernatant containing adapter ligated, cleaned library sample was pipetted into a separate tube. 30µL of library amplification master mix was added.

Library amplification was performed in a thermocycler using the following program: One cycle of initial denaturation at 98°C for 45 seconds. One cycle of denaturation at

98°C for 15 seconds. Twelve cycles of annealing at 60°C for 30 seconds, extension at 72°C for 30 seconds, final extension at 72°C for 1 minute. One cycle of final extension at 72°C for 10 minutes. Library amplification cleanup was performed by resuspending the sample with 50µL of Kapa pure beads, placing the sample on a magnet, washing twice with 200µL of 80% ethanol and resuspending with 22µL of 10mM Tris-HCl. 20µL of the supernatant containing amplified cleaned library sample was pipetted into a separate tube and stored at -20°C.

The concentration of each library was estimated using a Qubit DNA high sensitivity assay (Thermofisher) and the fragment size was estimated using a Bioanalyzer DNA high sensitivity assay (Agilent). The concentration and fragment size of each library were used to estimate their concentration in nanomoles using the following calculation:

$$\frac{(\text{concentration in ng}/\mu\text{l})}{(660\ \text{g/mol} \times \text{average library size in bp})} \times 10^6 = \text{concentration in nM}$$

Each library was corrected to 10nM, and 5µL of each was pooled together to create the final pooled library.

Prior to the pooled library denature and dilution, an Illumina Nextseq 500 mid output 150 cycle reagent cartridge (Illumina) was defrosted in a water bath at RT for 45 minutes. The pooled library was denatured into single stranded DNA using 5µL of freshly prepared 0.2M sodium hydroxide and left to stand at RT for five minutes. The denatured library was diluted to 20pM using 5µL of 0.2M Tris HCL and 985µL of cold HT1 buffer (Illumina). 10µL of the denatured and diluted library was removed and 10µL of a 20pM control library, Phi-X (Illumina) was added. The final 20pM pooled library with Phi-X was diluted further to 1.5pM by taking 97.5µL of library and diluting it with 1202.5µL of water. The final denatured and diluted library was pipetted into the

reagent cartridge and loaded into the Nextseq 500. The sequencing was completed using a paired end 75 cycle run.

RNAseq expression data was quantified using kallisto software (Bray et al. 2016) together with an Ensembl GRCh38 transcript set. Further filtering, normalisations and statistical analyses were then performed using DESeq2 library for the R programming language (Love, Huber, and Anders 2014). Statistical significance where stated uses multiple testing adjustment with the false discovery rate and independent hypothesis weighting (IHW). Gene Set Enrichment Analysis (GSEA) (Subramanian et al. 2005) was performed using the Broad Institute tools together with pathways from their MSigDB site (Liberzon et al. 2011).

2.2.15 Organoid maintenance

Organoids were maintained in culture embedded in growth-factor reduced Matrigel (Corning), covered with complete organoid media. For general maintenance, organoids were embedded in 3 drops (25µL) in 12-well dishes and covered with 1.5mL media and kept at 37°C in a humidified atmosphere of 5% CO_2. The complete organoid media was prepared using a base culture media, supplemented with 25% (R-spondin-1, wnt-3 and Noggin) conditioned media from mouse fibroblasts (section 2.2.16), and several other growth supplements and specific pathway inhibitors (Table 2.4 and Table 2.5). Media was replenished with 50% fresh media every 2-3 days.

Passaging could be done with or without organoid trypsinisation. Without trypsinisation, media was removed from the well, and organoids collected from the plate using of 1mL (12 well dish) ice cold PBS. Organoids were transferred to a chilled Eppendorf tube on ice. To remove Matrigel, organoids were spun down (20 secs, benchtop mini centrifuge) and supernatant removed. Two further PBS washes were done, before resuspension in ice cold Matrigel (all on ice). Drops of Matrigel were then

added to culture dish and left to set for 5 minutes at 37°C. 1.5mL of complete media was then added to each well of dish.

If organoids had reached maximal growth, or were required as single cell for experimentation, organoids were disassociated during passage. After removing Matrigel by washing, organoids were suspended in 200µL of TripLE Express (animal free trypsin, Gibco), and incubated at 37°C for 10 minutes. Trypsin was inactivated with 800µL of 10% FBS (in PBS), and disassociation completed by pipetting the organoids up and down multiple times. Organoids were spun down (20 secs, benchtop mini centrifuge) and the trypsin removed. Two further PBS washes were done, before resuspension in ice cold Matrigel (all on ice). Drops of Matrigel were then added to culture dish and left to set for 5 minutes at 37°C. 1.5mL of warm complete media was then added to each well of dish.

Table 2.4. Base culture media preparation

Base culture media (Sterile filtered with 500mL filter system (Corning))
DMEM F/12 (Gibco)
2mM L-glutamine (Sigma-Aldrich)
1% of 10,000 units penicillin – 10mg/mL streptomycin (Sigma-Aldrich)
1mM N-acetyl-l-cysteine (stock prepared at 500mM in PBS, Wako)
10mM Hepes solution (stock prepared at 1M in PBS, Sigma-Aldrich)

Table 2.5. Complete organoid media preparation

Complete organoid media (Sterile filtered)
Base culture media
25% L-WRN conditioned media from fibroblasts
50ng/mL EGF
10nM Gastrin (stock prepared at 10µM)
500nM TGF β / ALK inhibitor A83-01 (stock prepared in DMSO at 500µM)
10µM p38 inhibitor SB202190 (stock prepared in DMSO at 10mM)
10mM Nicotinamide (stock prepared at 10µM)
RHO inhibitor (Y27632) (only when thawing or trypsinising organoids)

2.2.16 WRN conditioned media preparation

L-WRN mouse fibroblasts were expanded in T150 cell culture flasks in 25mL DMEM (10% FBS (Gibco), 2mM L-glutamine (Sigma-Aldrich), 1% penicillin-streptomycin (Sigma-Aldrich)). Once 80% confluence had been reached, media in each flask was replaced with 25mL fresh media, and cells were left in the incubator at 37°C for 72 hours. Media was then collected from flasks and filtered to remove any cells or debris using a 500mL filter system (Corning). Conditioned media was aliquoted and stored at -80°C until use.

2.2.17 Organoid storage and retrieval from liquid nitrogen

Organoids were kept frozen in liquid nitrogen for long-term storage. To freeze down organoids, media was removed from each well of a 12 well dish, and organoids collected using 1mL of ice-cold PBS per well. Organoids were then transferred into chilled Eppendorfs on ice. To remove Matrigel, organoids were spun down (20 secs, benchtop mini centrifuge) and the supernatant removed. Two further PBS washes were done, before organoid resuspension in 1mL cell recovery freezing media (Gibco) per Eppendorf. Organoids suspended in freezing medium were then transferred into cryotubes. Organoids were stored at -80°C for 24-72 hours prior to long-term storage in liquid nitrogen tanks. Organoids were retrieved from frozen stocks by thawing in a 37°C water bath, after which the organoids were transferred into an Eppendorf. Organoids were spun down (20 secs, benchtop mini centrifuge) and the cell recovery media removed. Two washes in PBS were done, before resuspension in ice cold Matrigel (all on ice). Drops of Matrigel (3 x 25µL) were then added to a well of 12-well culture dish and left to set for 5 minutes at 37°C. 1.5mL of warm complete media (containing the RHO inhibitor) was then added to the culture dish well.

2.2.18 Organoid viability – 3D CellTiter-Glo (CTG) assay and imaging

Organoids were expanded and grown in a well of a 6-well dish (7 drops (40µL) Matrigel). Organoids were seeded and treated in the same experiment for imaging and CTG analysis. Media was removed from the culture plate, and organoids collected in 3mL ice-cold PBS, and transferred to 15mL Falcon tubes on ice. The culture plate was rewashed with ice-cold PBS to collect any remaining organoids, which were also transferred to the Falcon. A further 4mL of ice-cold PBS was then added to the Falcon to ensure Matrigel was full dissolved. To remove Matrigel organoids were spun down at 1200rpm for 5 minutes (4°C), and supernatant removed. Two further washes with 10mL ice-cold PBS were performed to ensure removal of all Matrigel. PBS was removed and 1mL of TripLE Express was added to the organoid pellet. Organoids were incubated at 37°C for 10 minutes with the TripLE Express. Trypsin was inactivated by the addition of 4mL 10% FBS in PBS. The cell suspension was pipetted up and down to ensure full dissociation of organoids into single cells. Cells were spun down at 1200rpm for 5 minutes (4°C), and supernatant removed. Two further washes with 10mL ice-cold PBS were performed to ensure complete removal of trypsin. Organoids were then split across 2 Falcons, with one Falcon used for experiment seeding and the other for further organoid expansion.

For experiment seeding organoids were suspended in 5mL Matrigel (volume dependent on experiment setup) and gently pipetted up and down to ensure even distribution of organoid cells. Note, at all times organoids must be kept on ice to prevent Matrigel setting. 50µL of organoid containing Matrigel were added to each well of a 96-well white flat-bottom pate (Thermo Fisher Scientific) for CTG assay and to a standard 96-well flat-bottom plate (TPP) for imaging. Matrigel was pipetted up and down throughout seeding to ensure an equal distribution of organoids. Each experiment contained 3 technical repeats of each sample group, to enable generation of a reliable mean. Plates were incubated for 10 minutes at 37°C to ensure Matrigel

setting, after which 200µL of media warmed to 37°C was added to each well. Plates were incubated for 2 days at 37°C, for organoids to begin growing.

After 2 days small organoids were visible. Media was gently removed from each well using a pipette, and was replace with drug containing, warm complete organoid media as indicated for individual experiments. Organoids were left with drug containing media for 72 hours. After 72 hours, depending on the individual experimental protocol, drug containing media was either replaced with fresh drug-free warm media, or drug-containing media, with care taken not to disrupt Matrigel when removing or adding media. Media was replaced every 2-3 days for the duration of the treatment protocol.

At the required timepoint, media was removed from wells of the plate for CTG analysis and was replaced with 50µL of 3D-CTG reagent (Promega). The plate was placed on a shaker in the dark at RT for 30 minutes. The bioluminescence of well was measured using the Varioskan LUX plate reader. A mean value was calculated for each treatment group for the three technical repeats. Percentage viability was calculated by normalising each treatment group to the DMSO control. Images were taken of organoids grown in the translucent 96-well plate at the same time using an EVOS microscope.

2.2.19 Organoid Western blot

Organoids were expanded and grown in a well of a 6-well dish (7 drops (40µL) Matrigel). Media was removed from the culture plate, and organoids collected in 3mL ice-cold PBS, and transferred to 15mL Falcon tubes on ice. The culture plate was rewashed with ice-cold PBS to collect any remaining organoids, which were also transferred to the Falcon. A further 4mL of ice-cold PBS was then added to the Falcon to ensure Matrigel was full dissolved. To remove Matrigel organoids were spun down at 1200rpm for 5 minutes (4°C), and supernatant removed. Two further washes with 10mL ice-cold PBS were performed to ensure removal of all Matrigel. PBS was

removed and 1mL of TripLE Express was added to the organoid pellet. Organoids were incubated at 37°C for 10 minutes with the TripLE Express. Trypsin was inactivated by the addition of 4mL 10% FBS in PBS. The cell suspension was pipetted up and down to ensure full dissociation of organoids into single cells. Cells were spun down at 1200rpm for 5 minutes (4°C), and supernatant removed. Two further washes with 10mL ice-cold PBS were performed to ensure complete removal of trypsin. Single organoid cells were resuspended in 2mL Matrigel, and plated by adding 3 x 25µL drops into 8 wells of a 2x12-well plates (2 wells per condition). Matrigel was left to set at 37°C for 10 minutes, after which 1.5mL of warm organoid media was added to each well. Organoids were left to grow for 5 days, with media being replaced every 2-3 days.

On day 5 post-seeding, organoids were treated as indicated in experiments. Prior to organoid collection at the timepoints specified in individual experiment, organoids were incubated with protease and phosphatase inhibitors to preserve cellular signalling. 1 phosSTOP (Roche) tablet was dissolved in 500µL sterile ddH_2O. An inhibitor cocktail was made by combining 350µL phosSTOP, and 140µL 100 x Protease Inhibitor Cocktail (Sigma-Aldrich). 53.5µL of inhibitor cocktail was added to each well (containing 1.5mL media), and organoids incubated for 10 minutes at 37°C. Media was removed from wells and organoids collected with 1mL ice-cold PBS per well. Organoids were spun down for 20 seconds using benchtop mini centrifuge, and supernatant removed. Two further washes in ice-cold PBS were performed to completely remove all Matrigel. PBS was removed from the organoid pellet and 50µL of lysis buffer was added each to Eppendorf. Organoids were briefly vortexed to ensure disruption of organoids and cell lysis. The organoid suspension was then sonicated for 30 minutes on ice using a Fisherbrand sonicator. Following sonication samples were boiled at 95°C for 10 minutes. Lysates were then processed for

Western blotting and procedures were carried out as described for cell lines (section 2.2.8)

2.2.20 CyTOF

The cyTOF technique described was developed by the Tape lab. This multiplexed mass cytometry protocol uses Thiol-reactive Organoid Barcoding *in situ* (TOB*is*) and a CyTOF signalling analysis pipeline (CyGNAL) for 126-plex single cell analysis of cell state, protein expression and post-translational modifications in organoids (Sufi J. et al. In press) (Figure 2.1). This enables in depth single cell analysis of organoids, which is not achievable by other techniques.

Organoids were expanded and grown in a well of a 6-well dish (7 drops (40µL) Matrigel). Media was removed from the culture plate, and organoids collected in 3mL ice-cold PBS, and transferred to 15mL Falcon tubes on ice. The culture plate was rewashed with ice-cold PBS to collect any remaining organoids, which were also transferred to the Falcon. A further 4mL of ice-cold PBS was then added to the Falcon to ensure Matrigel was full dissolved. To remove Matrigel organoids were spun down at 1200rpm for 5 minutes (4°C), and supernatant removed. Two further washes with 10mL ice-cold PBS were performed to ensure removal of all Matrigel. PBS was removed and 1mL of TripLE Express was added to the organoid pellet. Organoids were incubated at 37°C for 10 minutes with the TripLE Express. Trypsin was inactivated by the addition of 4mL 10% FBS in PBS. The cell suspension was pipetted up and down to ensure full dissociation of organoids into single cells. Cells were spun down at 1200rpm for 5 minutes (4°C), and supernatant removed. Two further washes with 10mL ice-cold PBS were performed to ensure complete removal of trypsin. Organoids were then split across 2 Falcons, with one Falcon used for experiment seeding and the other for further organoid expansion.

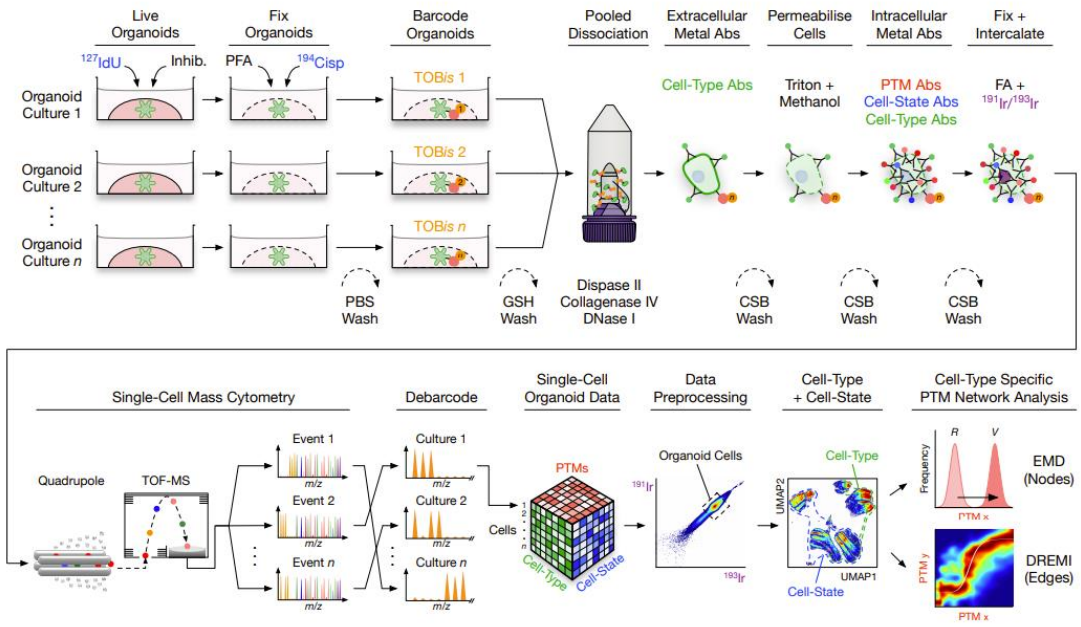

Figure 2.1. **A scheme demonstrating the CyTOF protocol used.**
^{127}IdU (identifying S-phase cells) and phosphatase and phosphatase inhibitors are added. Organoids are fixed in situ with paraformaldehyde (PFA) and stained with ^{194}Cisplatin to identify dead / dying cells. Organoids from different experimental conditions are barcoded with TOBis reagents while still in Matrigel, washed with reduced glutathione (GSH), and pooled. Organoids are dissociated into single cells using Dispase II, Collagenase IV, and DNase I and stained with extracellular cell-1123 type rare-earth metal conjugated antibodies. Cells are then permeabilised with Triton and Methanol, stained with intracellular post-translational modification (PTM), cell-state, and cell-type Abs. Abs are cross-linked to their antigens using formaldehyde (FA) and cells are incubated with 191/193 1126 Iridium (Ir) DNA intercalators. Single cells are analysed using a mass cytometer. Different experimental conditions are debarcoded, pre-processed and single-cell organoid data is visualised using Uniform Manifold Projection (UMAP). Cell-type-specific PTM node intensity is NP-PI200047 Multiplexed Single-Cell Organoid Signalling calculated using Earth Mover's Distance (EMD) between reference and variable populations and PTM-PTM connectivity is calculated using Density Resampled 1133 Estimation of Mutual Information (DREMI) (Sufi J. et al. In press).

For experiment seeding, organoids were suspended in 5mL Matrigel (volume dependent on experiment setup) and gently pipetted up and down to ensure even distribution of organoid cells. Note, at all times organoids must be kept on ice to prevent Matrigel setting. 50µL of Matrigel were added to each well of a 96-well white flat-bottom pate (TPP). Each experiment contained 3 technical repeats of each

sample group. Plates were incubated for 10 minutes at 37°C to ensure Matrigel setting, after which 200µL of complete organoid media (with RHO inhibitor) was added to each well, and the culture plate was returned to 37°C.

After 24 hours, the media was gently removed from the wells, and replaced with complete organoid media without any RHO inhibitor (the RHO inhibitor was found to reduce the proliferation rate). After a further 24 hours, the media was once again removed and replace with organoids media containing recombinant proteins in place of WRN-conditioned media (mEGF 50ng/mL (Thermo Fisher Scientific), mWNT 100ng/mL (Peprotech) and hR-spondin-1 500ng/mL (Peprotech)). Organoids were left for a further 72 hours for growth and development.

On day 5 post seeding, media was removed and replaced with 200µL drug containing organoid media (with recombinant proteins). In the CyTOF experiment with the SN38 combination treatment, media was not replaced before organoid collection. However, organoid media appeared spent so in the subsequent DS-8201a combination experiments, drug containing media was replaced every 24 hours until organoid collection. 30 minutes prior to organoid collection, ^{127}5-Iodo-2'-deoxyuridine (IdU, Fluidigm) was added to the media (25µM final concentration), to mark DNA replication and S-phase progression, and the culture plate was returned to the incubator. 5 minutes prior to organoid collection, 7µL of a protease/phosphatase inhibitor cocktail was added to each well containing 200µL of media, and the plate was returned to the incubator until the experiment endpoint. The inhibitor cocktail was prepared by dissolving 1 phosSTOP (Roche) tablet in 500µL sterile ddH_2O, and combining with 100 x Protease Inhibitor Cocktail (Sigma-Aldrich) at a ratio of 2.5:1. At the experiment endpoint, media was removed from the wells, and replaced with 200µL warmed 4% PFA (Thermo Fisher Scientific). Organoids were kept at 37°C for 1 hour to allow fixation of organoids and Matrigel. After fixation, PFA was removed from the wells, and wells were washed twice for 10 minutes with PBS (plate gently shaking). 200µL

of fresh PBS was added to each well, and plates were sealed and stored at 4°C for up to two weeks.

The remainder of the protocol including barcoding, disassociation, staining, running samples on the Helios mass cytometer, debarcoding and generation of uMAPS and Earth Mover's Distance (EMD) maps was performed by Maria Ramos and other members of the Tape lab according to their protocol which is in press to be published in the Nature Protocols journal (Sufi J. et al. In press). Antibodies used in cyTOF experiments are listed in Table 2.6.

Table 2.6. Antibody panel used for CyTOF experiments

Antibody	Supplier	Channel / Metal
pHistone H3 (S28)	BioLegend	89/Y
CD44	BioLegend	111/Cd
EPHB2	BD Bioscience	112/Cd
CD326	BioLegend	113/In
CK18	Abcam	114/Cd
Pan-CK	BioLegend	115/In
pPDK1 (S241)	BD Bioscience	141/Pr
cCaspase-3	Cell signaling	142/Nd
Geminin	Insight Biotechnology	143/Nd
pMEK 1/2 (S221)	Cell signaling	144/Nd
FABP1	R&D systems	145/Nd
pMKK4 (S257)	Cell signaling	146/Nd
pBTK (Y511)	BD Bioscience	147/Sm
pSRC (Y418)	BD Bioscience	148/Nd
P4E-BP1 (T37/46)	Fluidigm	149/Sm
pRb (S807/811)	Fluidigm	150/Nd
pPKCα (T497)	BD Bioscience	151/Eu
pAKT (T308)	BD Bioscience	152/Sm
pCREB (S133)	Cell signalling	153/Eu
pSMAD1/5 (S463/465) / pSMAD9 (S465/467)	Cell signalling	154/Sm
pAKT (S473)	Cell signaling	155/Gd
pNF-κB p65 (S529)	BD Bioscience	156/Gd
pMKK3/MMK6 (S189/207)	Cell signaling	157/Gd
pP38 (T180/Y182)	Cell signaling	158/Gd

pMAPKAPK2 (T334)	Abcam	159/Tb
pAMPKα (T172)	Cell signaling	160/Gd
pBAD (S112)	Cell signaling	161/Dy
pHistone H2A.X (S139)	Cell signaling	162/Dy
pP90RSK (T359)	Cell signaling	163/Dy
p120-Catenin (T310)	BD Bioscience	164/Dy
Beta-Catenin	Cell signaling	165/Ho
pGSK-3β (S9)	Cell signaling	166/Er
pERK1/2 (T202/Y204)	BD Bioscience	167/Er
pSMAD2 (S465/467) /pSMAD3 (S423/425)	Cell signaling	168/Er
PLK135-206	Thermo Fisher Scientific	169/Tm
CHGA	Insight Biotechnology	170/Er
pDNAPK (S2056)	Abcam	171/Yb
cPARP (D214)	Cell signaling	173/Yb
pCHK1 (S345)	Cell signaling	175/Lu
Cyclin B1	BD Bioscience	176/Yb

Cell signal and cell state analysis was carried out using the Cytobank software and cells were gated using Gaussian parameters (Sufi J. et al. In press) to remove debris, dead cells and doublets (Figure 2.2).

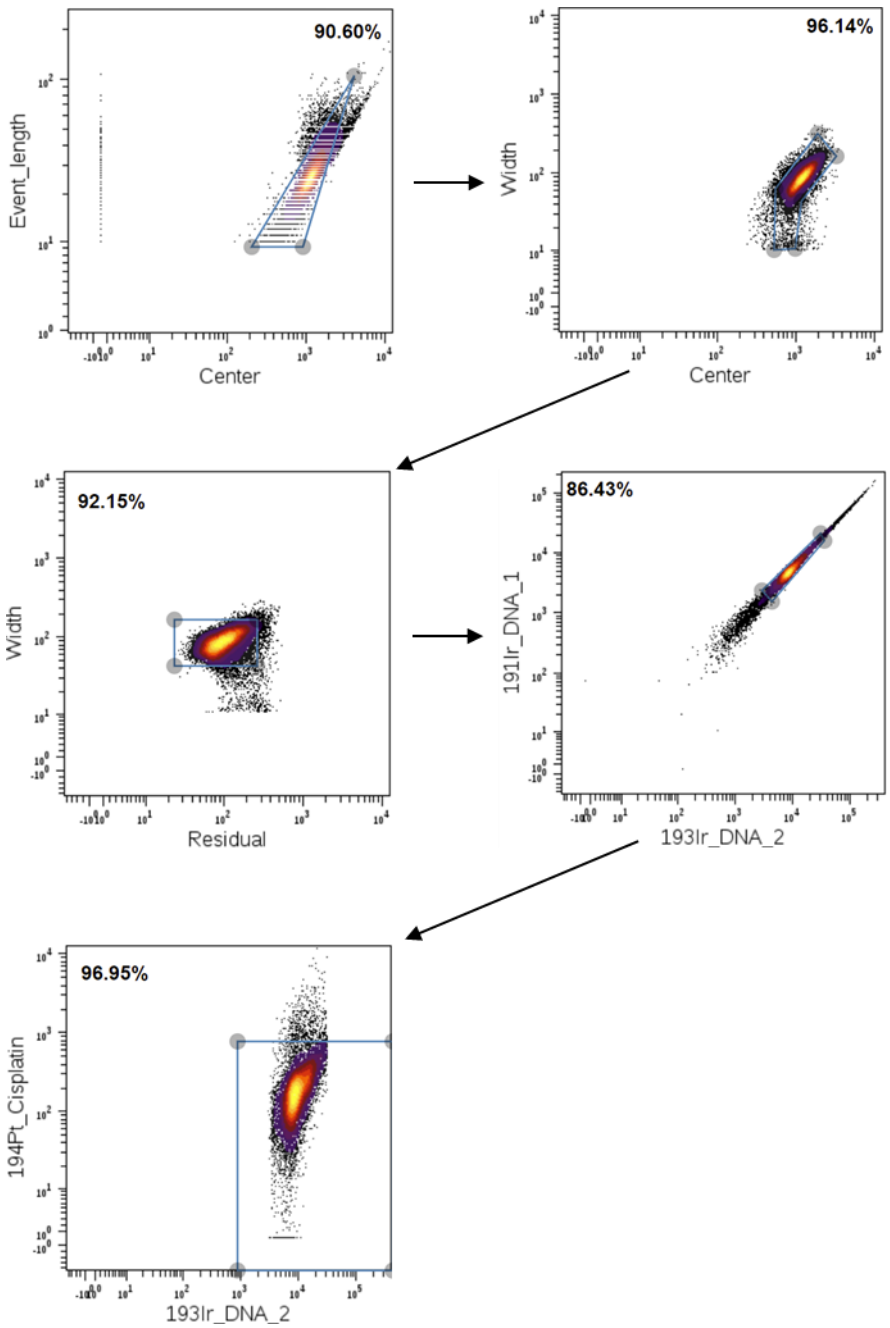

Figure 2.2. **Gaussian parameters were used to remove debris, dead cells and doublets prior to cell signal / cell state analysis.**

3 TOP1 and ATR inhibition synergise to increase DNA damage and reduce survival in CRC models

3.1 Introduction

3.1.1 Irinotecan efficacy in the treatment of CRC is limited by toxicity and DNA damage repair

Approximately 20% of CRC patients present with metastatic disease (Argilés et al. 2020). The prognosis for these patients is poor, with 44% patients surviving 1 year, and just 10% surviving 5 years in the UK (CRUK 2020). As standard of care, patients receive irinotecan as part of the FOLFIRI regimen, however the response rate is below 50% and the response is short lived, with a PFS of 6.7 months (Douillard et al. 2000; Van Cutsem et al. 2014). Additionally, the toxicity profile of irinotecan can be harsh, with 15-20% of patients having dose limiting myelosuppression and diarrhoea (Thomas and Pommier 2019).

The efficacy of irinotecan therapy is limited by the rapid reversal of TOP1ccs within minutes of drug removal. TOP1ccs need to be maintained for a long enough period to cause sustained DNA damage by collisions with replication and transcription machinery (section 1.3.4) (Pommier 2006). The rapid reversal of TOP1ccs combined with DNA-repair activation in response to TOP1cc, limits the DNA damage build up caused by TOP1 inhibitors (section 1.3.5) (Thomas and Pommier 2019).

A possible strategy to increase the efficacy of irinotecan-based therapy, would be to combine TOP1 inhibition with an inhibitor of the DNA damage repair pathway. This would increase the cytotoxicity of TOP1ccs, if they were to persist long enough to collide with the replication machinery.

3.1.2 ATR and TOP1 inhibition as a rational combination

Collision of TOP1ccs with replication machinery, and the presence of TOP1 mediated DNA strand breaks causes replication fork stalling and activation of ATR (Aris and Pommier 2012; Huntoon et al. 2013; Hur et al. 2021; Josse et al. 2014; Thomas et al. 2021). Signalling down the ATR pathway results in cell cycle arrest, DNA damage repair and resolution of replication stress (section 1.5). Combining ATR inhibition with topoisomerase inhibition could prevent induction of cell cycle arrest and replication fork recovery, driving cells into catastrophic genomic instability (Josse et al. 2014; Thomas et al. 2021).

There is preclinical and early clinical evidence to suggest a synergistic relationship between TOP1 and ATR inhibition. Using a siRNA library against 7,000 genes, Josse et al., found loss of ATR to synergise with TOP1 inhibition (CPT and Indotecan (LMP-400)) in a breast adenocarcinoma cell line. *In vitro* short-term cytotoxicity assays showed VE-821 to synergise with CPT and LMP-400 in a breast cancer cell line and two p53 deficient CRC cell lines (Josse et al. 2014). Ovarian cancer cell lines have also been shown to have increased sensitivity to topotecan with the addition of VE-821 (Huntoon et al. 2013). ATR inhibitor, AZD6738 was found to synergise with belotecan (a TOP1 inhibitor) in cell line and mouse models of platinum-resistant ovarian cancer (Hur et al. 2021).

ATR inhibition has also been found to sensitise SCLC tumours to TOP1 inhibition. SCLCs exhibit very high replication stress and responses to combination chemotherapy and PD-L1 typically being brief. SCLC cells exhibit high levels of Chk1, CLSPN and TopBP1, when compared with other solid tumour types, making ATR an attractive therapeutic target. The combination of VX-970 and TOP1 inhibition (including SN-38, irinotecan and topotecan) resulted in a dramatic reduction in survival of SCLC cell lines, and limited tumour growth in an SCLC patient derived

xenograft model (Thomas et al. 2021). Results from a phase II trial of VX-970 in combination with topotecan in SCLC and EP-SCNC patients are promising (section1.6.9) (Thomas et al. 2021).

To date there has not been extensive work on the combination of TOP1 and ATR inhibition in the context of CRC. However, findings from several different cancer models have shown this rational combination to have therapeutic potential. Additionally, phase I and II trials, although not in the context of mCRC, have shown efficacy of this combination.

3.2 Research aim

The aim of this chapter is to explore the cytotoxicity of VX-970 in combination with SN38 in CRC cell lines and patient derived organoids, and to evaluate whether the combination therapy results in increased levels of DNA damage. Additionally, the link between DNA damage induced by the combination therapy and the cGAS-STING pathway will also be investigated.

3.3 Results

3.3.1 SN38 inhibits CRC cell proliferation and induces DNA damage and ATR signalling

The effect of TOP1 inhibitor, SN38 on cell proliferation of cells at 50% confluence was assessed in three CRC cell lines, HCT116, HT29 and SW48. Cells were treated with a range of SN38 drug concentrations for a period of 72 hours and growth inhibition was measured using the SRB assay. The dose required to cause half maximal growth inhibition (GI_{50}) was 170nM (95% CI 144-201), 110nM (95% CI 2.6-3.1) and 2.8nM (95% CI 2.6-3.1) for HCT116, HT29 and SW48 respectively (Figure 3.1).

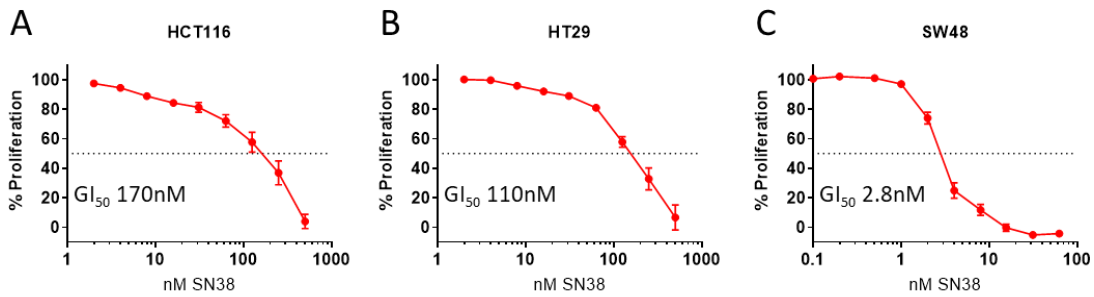

Figure 3.1. **CRC cell lines vary in their sensitivity to SN38 treatment.**
Cell lines were seeded at 15,000 cell per well in a 96-well plate and treated with the indicated doses of SN38 for 72 hours. The SRB assay was used to calculate proliferation rates. **A.** HCT116 cells **B.** HT29 cells **C.** SW48 cells. Each datapoint is the mean of 3 biological repeats. Error bars represent ± SEM.

To confirm induction of DNA damage and activation of ATR signalling following SN38 treatment, HCT116 and HT29 cells were treated with the GI_{50} dose of SN38. Cell lysates were collected over a range of timepoints and analysed by Western blotting. In both cell lines, phosphorylation of ATR (Thr1989) and its downstream kinase Chk1 (Ser345) were observed as early as two hours following SN38 treatment, demonstrating activation of ATR signalling. Phosphorylation of H2AX was observed at 24 hours, marking the presence of DNA damage (Figure 3.2 A-B). Treatment of

SW48 cells with 5nM SN38 (~ 2 x GI_{50}) resulted in delayed phosphorylation of ATR compared to HCT116 and HT29 cells, with the highest level observed at 24 hours. Phosphorylation of Chk1 and H2AX were not observed at this concentration (Figure 3.2 C). On increasing the SN38 treatment dose to 50nM, phosphorylation of ATR, Chk1 and H2AX was observed in SW48 cells (Figure 3.2 D). These findings show SN38 treatment to activate ATR signalling in CRC cell lines.

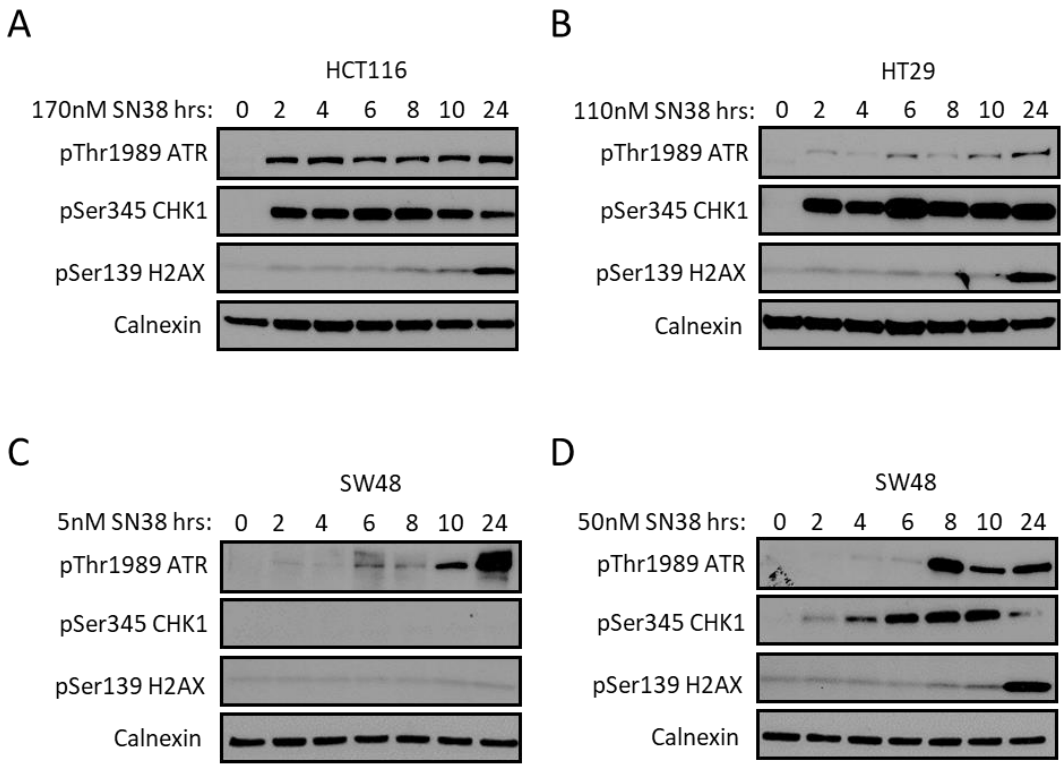

Figure 3.2. **SN38 induces ATR signalling and H2AX phosphorylation.**
Cell lines were treated with SN38 for the indicated time periods and lysates analysed by Western blotting. **A.** HCT116 cells **B.** HT29 cells **C.** and **D.** SW48 cells. Blots are representative images of 3 biological repeats.

3.3.2 Sub-GI_{50} VX-970 treatment abrogates SN38 induced ATR signalling and increases pH2AX levels

The effect of ATR inhibitor VX-970 on the proliferation of HCT116, HT29 and SW48 cell lines at 50% confluence was assessed using the SRB assay. Cells were treated

with a range of VX-970 drug concentrations for a period of 72 hours (Figure 3.3). Concentrations of up to 5µM VX-970 had almost no impact on the proliferation of HCT116 cells. HT29 cells were more sensitive to VX-970 treatment with a GI_{50} of 1.48µM (95% CI 1.41-1.55). SW48 cells were the most sensitive to the ATR inhibitor with a GI_{50} of 0.394µM (95% CI 0.33-0.46).

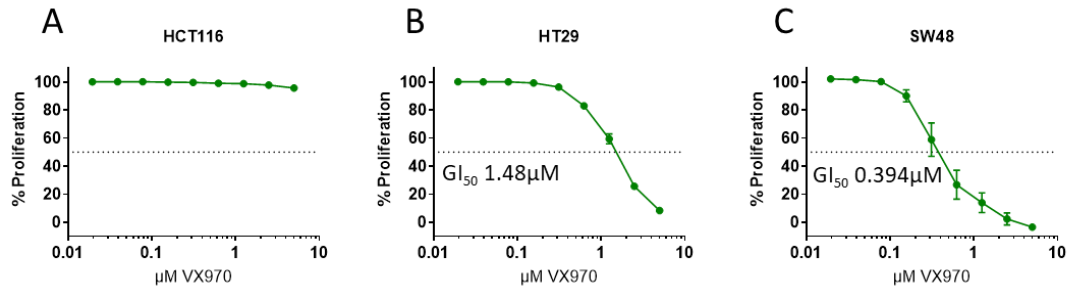

Figure 3.3. **CRC cell lines vary in their sensitivity to VX-970 treatment.**
Cell lines were seeded at 15,000 cell per well in a 96-well plate and treated with the indicated doses of VX-970 for 72 hours. The SRB assay was used to calculate proliferation rates. **A.** HCT116 cells **B.** HT29 cells **C.** SW48 cells. Each datapoint is the mean of 3 biological repeats. Error bars represent ± SEM.

To establish the dose of VX-970 required to inhibit SN38-induced ATR signalling, HCT116, HT29 and SW48 cells were treated with SN38 and a dose range of VX-970. Cell lysates were collected following 24 hours treatment and analysed by Western blotting (Figure 3.4). In HCT116 and SW48 cells, a dose of 0.125µM VX-970 reduced the levels of SN38-induced pATR and pChk1 to the levels observed in untreated cells. In HT29 cells, 0.125µM VX-970 treatment resulted in loss of pChk1, and a band of lower molecular weight for pATR. An increased dose of 0.25µM VX-970, resulted in loss of this lower molecular weight pATR band. A dose of 0.125-0.25µM VX-970 was selected for inhibition of ATR in further assays. In HCT116 and HT29 cells the levels of pH2AX was increased following SN38 and VX-970 combination therapy, in comparison to SN38 monotherapy indicating an increased DNA damage. Of note in all three cell lines, the levels of SN38-induced p53 phosphorylation were reduced with

the addition of VX-970. This data shows VX-970 to be highly effective at inhibiting ATR, with increased pH2AX signal indicative of increased DNA damage with the combination therapy.

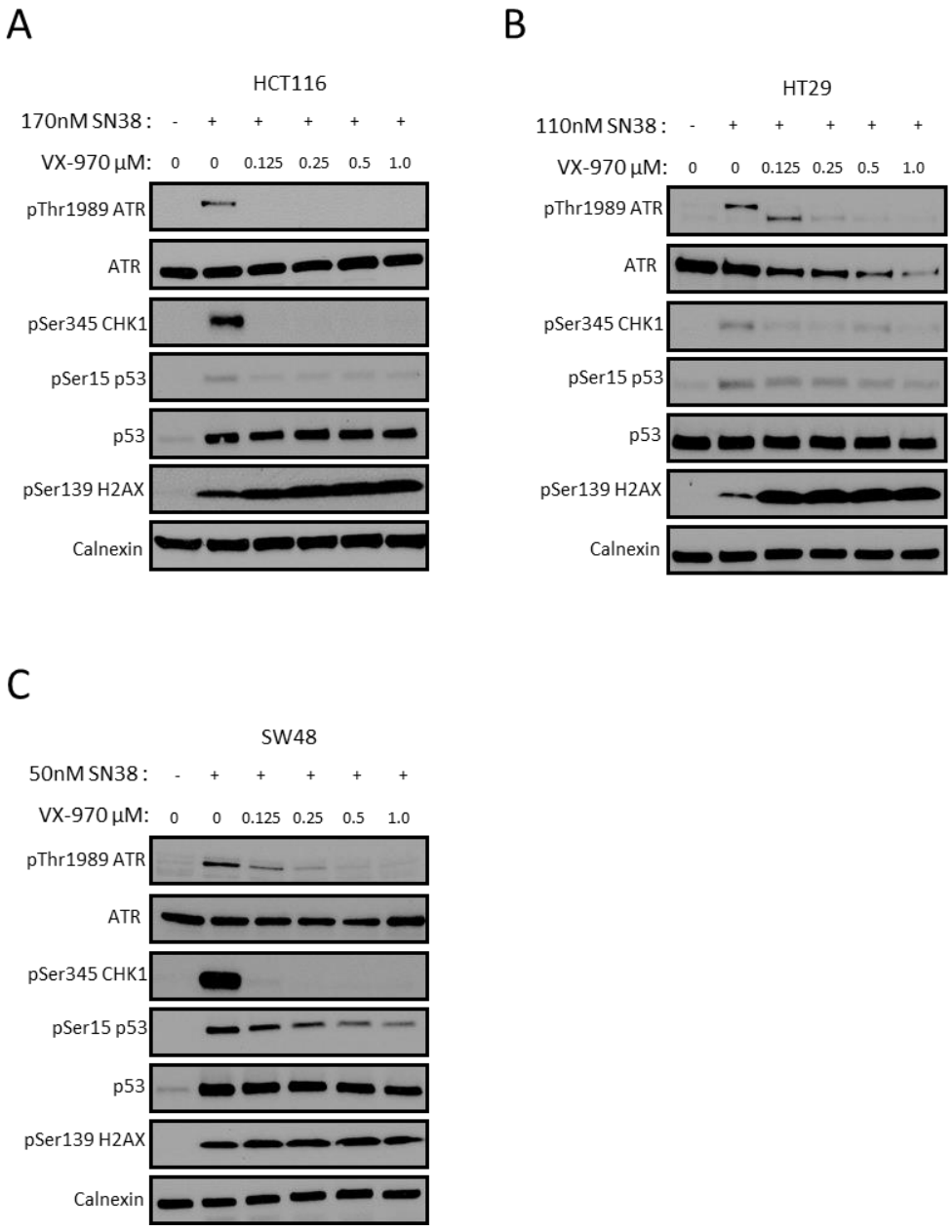

Figure 3.4. **VX-970 abrogates SN38-induced ATR signalling and results in increased H2AX phosphorylation.**

Cell lines were treated with the indicated drugs for 24 hours and lysates analysed by Western Blotting. **A.** HCT116 cells **B.** HT29 cells **C.** SW48 cells. Blots are representative images of 3 biological repeats.

3.3.3 SN38 and VX-970 synergise to reduce proliferation rate and survival in CRC cell lines

The loss of SN38-induced ATR signalling and increase in pH2AX with the addition of VX-970, is indicative of an impaired DDR leading to increased DNA damage. Inhibiting the DDR and increasing the level of DNA damage following SN38 treatment, suggests a potential increase in cytotoxicity of SN38 and VX-970 combination therapy compared to SN38 monotherapy in the CRC cell lines. To assess the impact of SN38 and VX-970 on the proliferation of CRC cell lines, HCT116, HT29 and SW48 cells were seeded at low density and treated with a range of SN38 and VX-970 concentrations as monotherapies and in combination for 72 hours. Reducing the seeding density markedly increased the drug sensitivity of the CRC cell lines.

Using the SRB assay, VX-970 was found to synergise with SN38 and reduce proliferation in all 3 CRC cell lines (Figure 3.5). Synergy was calculated using the zero interaction potency (ZIP) model, a score below -10 indicates antagonism, a score between -10 and +10 indicates an additive relationship and a score greater than +10 demonstrates synergy (Yadav et al. 2015). In HCT116 cells, synergy was observed across a range of drug concentrations, for example 1nM SN38 caused 15.1% (± 5.5) growth inhibition and 0.0625μM VX-970 resulted in 8.53% (± 2.4) growth inhibition, but the combination of 1nM SN38 and 0.0625μM VX-970 caused 74.06% (± 2.04) growth inhibition (Figure 3.5, A-B). The average synergy ZIP score for SN38 and VX-970 treatment in HCT116 cells was 36.8 (± 2.1) (Figure 3.5 C). In HT29 cells, the addition of VX-970 potentiated the growth inhibition induced by SN38, for example 5nM SN38 caused 15.26% (± 7.7) growth inhibition and 0.125μM VX-970 did not inhibit proliferation, and the combination resulted in 82.18% (± 1.95) growth inhibition (Figure 3.5, D-E). The average synergy ZIP score for SN38 and VX-970 treatment in HT29 cells was 17.91 (± 3.5), demonstrating synergy (Figure 3.5 F). In SW48 cells, VX-970 also synergised with SN38, for example 1nM SN38 caused 24.87% (± 4.8)

growth inhibition and 0.125µM VX-970 resulted in 17.91% (± 5.8) growth inhibition, with the combination therapy causing 75.11% (± 6.25) growth inhibition (Figure 3.5 G-H). The average synergy ZIP score for SN38 and VX-970 treatment in SW48 cells was 27.97 (± 4.3) (Figure 3.5 I).

While growth inhibition is a good indicator of cytotoxicity, it is possible for cells to arrest but then re-enter the cell cycle following drug removal. The clonogenic assay can be used to explore longer term survival and colony forming ability following drug treatment. HCT116, HT29 and SW48 cells were treated with 1nM or 5nM SN38 as a monotherapy or in combination with 0.0625µM VX-970 for a period of 72 hours, following which the drugs were removed and the cells were incubated for two weeks to form colonies (Figure 3.6).

HCT116 cells displayed the greatest sensitivity to SN38 and VX-970 monotherapies, with survival reduced to 69.4% (± 1.75) with 1nM SN38 treatment and 23.7% (± 3.44) with 0.0625µM VX-970 treatment. The combination of 1nM SN38 and 0.0625µM VX-970 further reduced survival to 0.35% (± 0.16) (Figure 3.6 B-C). HT29 cells were the least sensitive to SN38 and VX-970 monotherapies, with survival only reduced to 84.0% (± 11.6) with 5nM SN38 treatment and 82.8% (± 5.5) with 0.0625µM VX-970 treatment. However, HT29 cells were highly sensitive to the combination therapy with 5nM SN38 + 0.0625µM VX-970 treatment reducing survival to 1.26% (± 0.14) (Figure 3.6 D-E). A reduction in survival following combination therapy was also observed in SW48 cells, with 1nM SN38 + 0.0625µM VX-970 reducing survival to 6.3% (± 1.718) compared to 91.97% (± 9.96) survival with 1nM SN38 and 59.6% (± 3.36) survival with 0.0625µM VX-970 (Figure 3.6 F-G).

These findings show the combination of SN38 and VX-970 to be synergistic, reducing both the proliferation and survival of CRC cell lines.

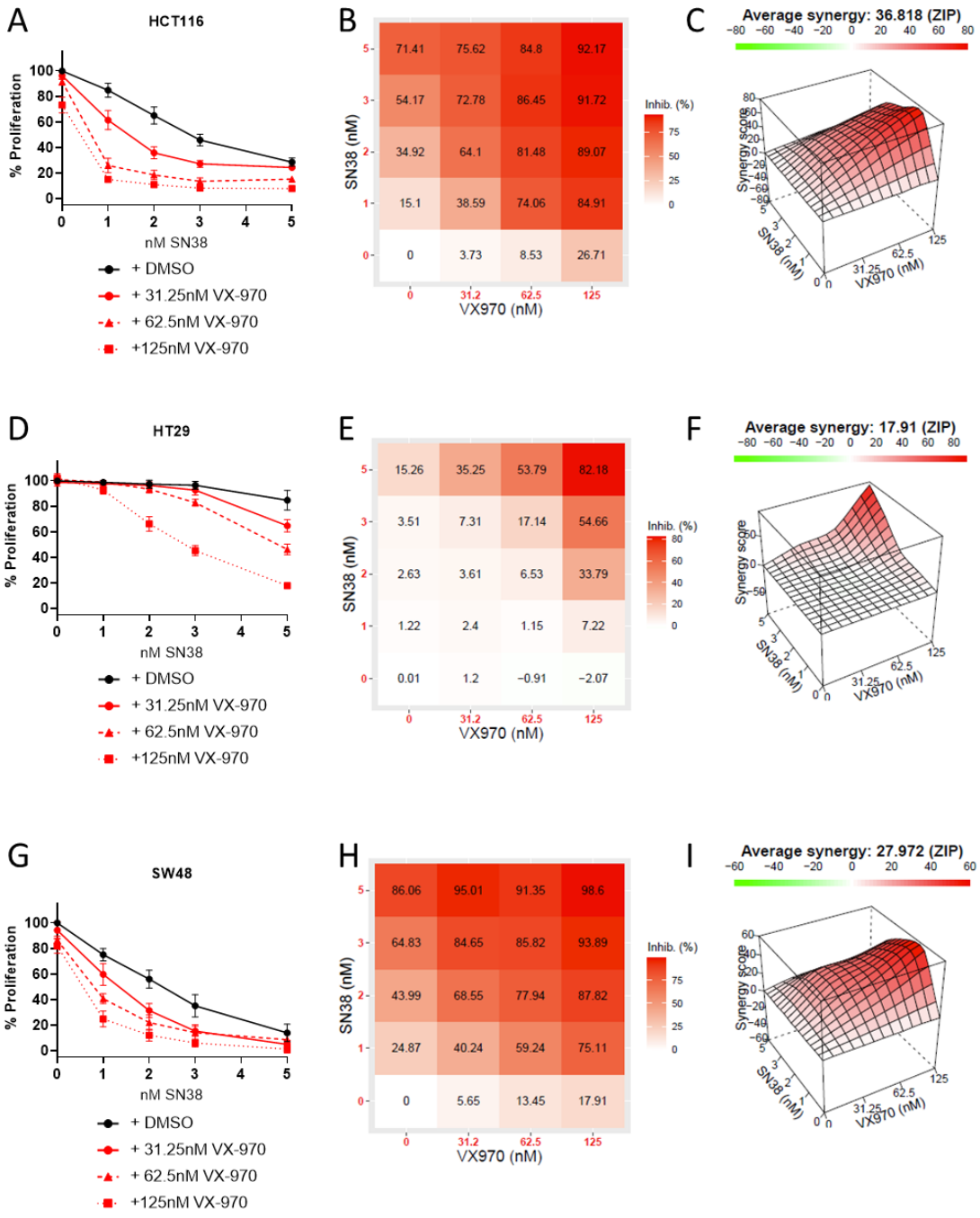

Figure 3.5. **VX-970 synergises with SN38 to reduce proliferation in CRC cell lines.** Cell were seeded at 2,500 cells per well in 96-well plates and treated with the indicated drugs for 72 hours. The SRB assay was used to calculate proliferation rates. **A.** HCT116 cells **D.** HT29 cells **G.** SW48 cells. Each datapoint is the mean of 3 biological repeats. Error bars represent ± SEM. The mean percentage inhibition for each drug combination is shown in a heatmap **B.** HCT116 cells **E.** HT29 cells and **H.** SW48 cells. 3D ZIP models demonstrate the interaction between SN38 and VX-970 in **C.** HCT116 cells **F.** HT29 cells and **I.** SW48 cells.

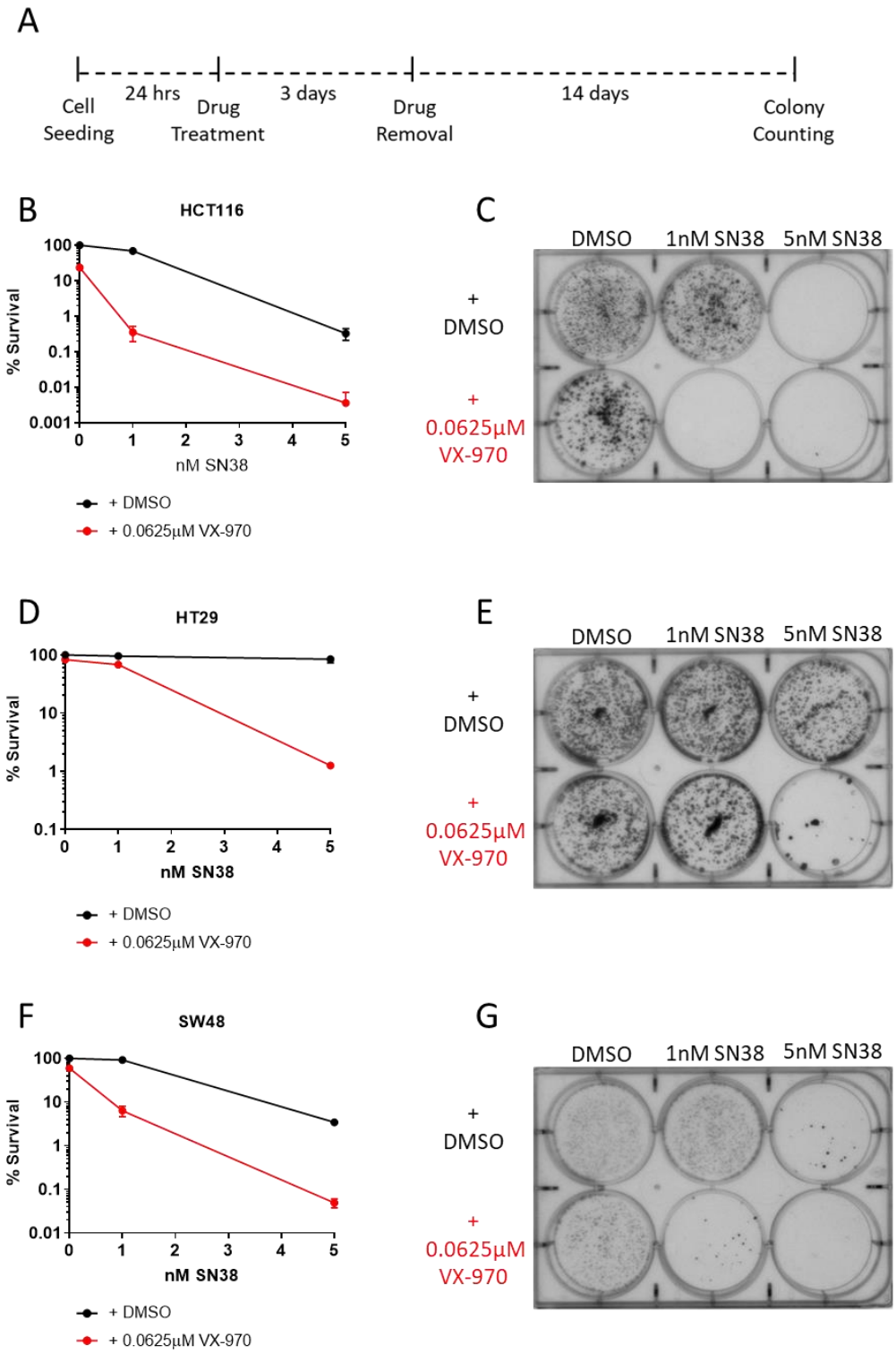

Figure 3.6. **VX-970 + SN38 combination therapy reduces survival in colorectal cancer cell lines.**

A. Scheme demonstrating the treatment and clonogenic assay schedule followed. The percentage survival following combination treatment with SN38 + VX-970 is displayed in **B.** HCT116 cells **D.** HT29 cells and **F.** SW48 cells. Each datapoint is the mean of 3 biological repeats. Error bars represent ± SEM. Representative images of clonogenic plates for **C.** HCT116 cells **E.** HT29 cells and **G.** SW48 cells.

3.3.4 SN38 and VX-970 combination treatment results in activation of DNA-PK and ATM

The abrogation of SN38-induced ATR signalling and increase in cellular pH2AX levels with SN38 and VX-970 combination treatment (Figure 3.4), suggests that the synergy observed between the drugs is at least in part due to increased DNA damage. Loss of ATR function, in the context of SN38-induced TOP1ccs could result in replication fork run off and the formation of DNA DSBs. As DNA-PK and ATM are activated in response to DNA DSBs, a Western blot time course experiment was set up in HCT116, HT29 and SW48 cells to explore the activity of these kinases following SN38 and VX-970 combination treatment (Figure 3.7).

In HCT116 cells, pSer2056 DNA-PK (a marker of DNA-PK activation) could not be detected following 0.125µM VX-970 monotherapy, and a relatively low level could be detected at 24 hours of 170nM SN38 monotherapy. Substantially higher levels of pDNA-PK were detected at 16 and 24 hours of SN38 and VX-970 combination therapy. pSer1981 ATM (a marker of ATM activation) was also detected at 16 and 24 hours following SN38 and VX-970 combination therapy (Figure 3.7 A). In HT29 cells pDNA-PK and pATM were detected at 8, 16 and 24 hours following 110nM SN38 and 0.125µM VX-970 combination therapy, with the highest levels observed at 16 hours. A much lower level of pDNA-PK was observed in HT29 cells at 24 hours following SN38 monotherapy (Figure 3.7 B). In SW48 cells, pDNA-PK was detected following both SN38 monotherapy and SN38 and VX-970 combination therapy at 8, 16, and 24 hours. There was no clear change in the levels of pATM in SW48 cells after SN38 and VX-970 monotherapies or combination therapy (Figure 3.7 C).

In all 3 cell lines, SN38 treatment resulted in p53 phosphorylation as early as 4 hours following SN38 treatment, but this was reduced with the addition of VX-970. In addition, pThr68 Chk2 could be detected in SN38 treated but not untreated cells. In

HT29 and to a lesser extent HCT116 cells, the combination treatment resulted in a reduction of pChk2 at the expected MW ~60kDa, and the appearance of a band at ~40kDa. In HT29 cells, the appearance of a lower MW pChk2 coincided with DNA-PK and ATM phosphorylation, occurring at 8, 16 and 24 hours of SN38 and VX-970 combination treatment.

Synergy between SN38 and VX-970 to reduce cell proliferation and survival was observed at doses between 1nM and 5nM SN38 (Figure 3.5 and Figure 3.6). To assess whether these lower concentrations of SN38 induce ATR signalling, and whether a lower dose combination therapy would result in DNA-PK and ATM activation, a Western blot time course experiment was done in HT29 cells with a range of SN38 concentrations in combination with VX-970 (Figure 3.8).

pATR and pChk1 were only detected in cells treated with 10nM and 100nM SN38, but not 1nM SN38, with the signal being strongest with 100nM SN38. Furthermore, there was no increase in pH2AX signal in cells treated with 1nM SN38 as a monotherapy or in combination with VX-970 compared to untreated cells. There was an increase in p53 phosphorylation with 1nM SN38 monotherapy, at a lower level than observed at 10nM and 100nM SN38. pDNA-PK was only detected with 100nM SN38 and VX-970 combination treatment, and not with the lower SN38 doses of 1nM and 10nM. There was moderate increase in pATM with 10nM SN38 and VX-970 combination treatment at 16 hours compared to 10nM SN38 monotherapy. The level of pChk2 increased with 1nM SN38 and 10nM SN38 in a dose dependent manner, but no further increase was observed with 100nM SN38 treatment compared to 10nM SN38 treatment.

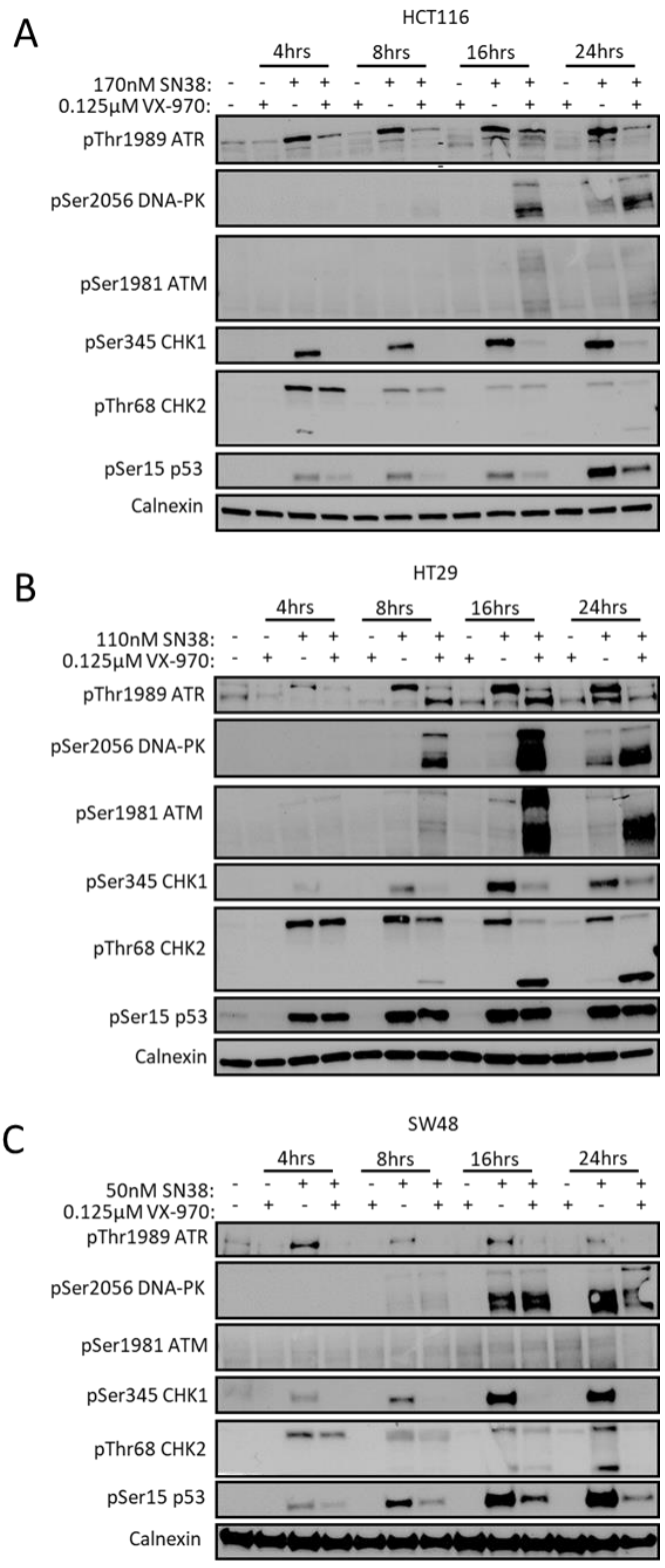

Figure 3.7. **SN38 and VX-970 combination treatment results in the phosphorylation of DNA-PK and ATM.**

Western blots were performed using **A.** HCT116 cells **B.** HT29 cells and **C.** SW48 cells. Blots are representative images of 3 biological repeats.

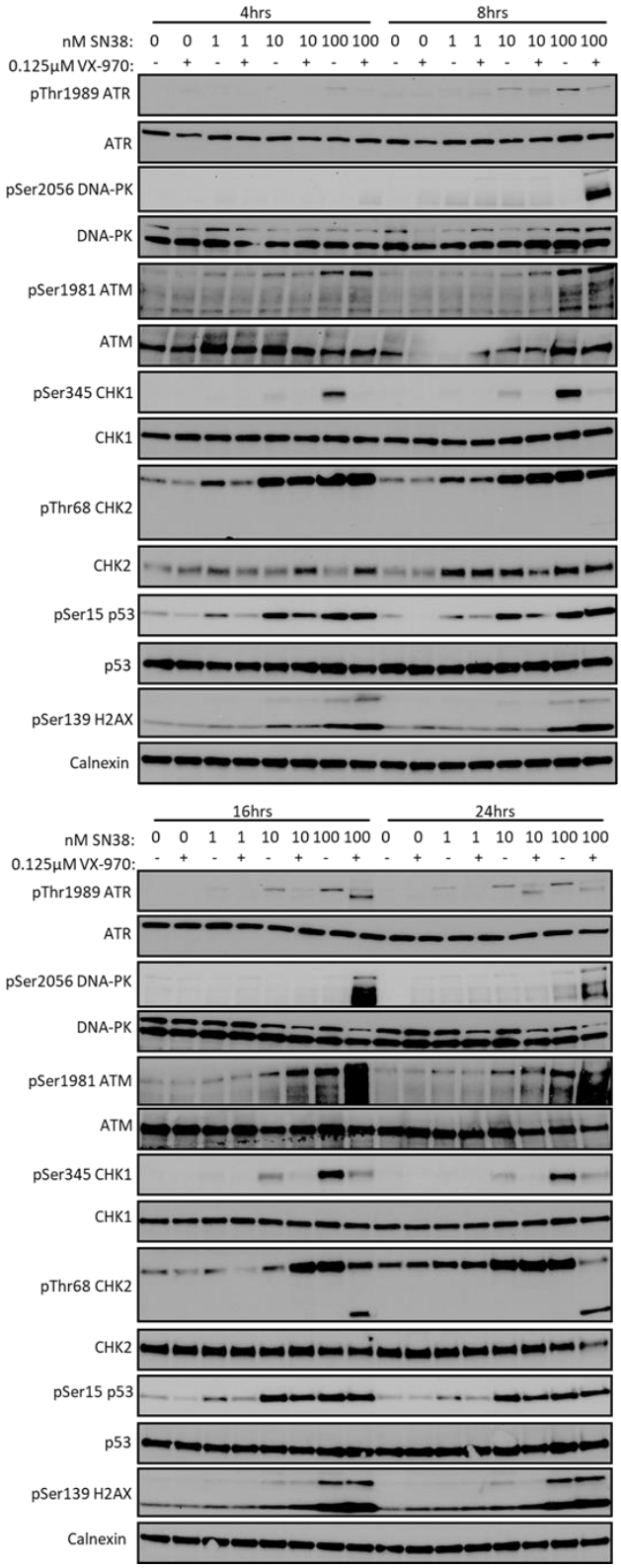

Figure 3.8. **Time course experiment shows increased DNA damage signalling following 100nM SN38 + VX-970 combination treatment in HT29 cells.**

Induction of ATR signalling and phosphorylation of Chk2, p53 and H2AX occur at 10nM SN38.

As no increased activation of DNA-PK and ATM was observed with 50nM SN38 and 0.125µM VX-970 combination therapy in SW48 cells (Figure 3.7), the effect of range of SN38 concentrations and VX-970 combination therapy on DNA damage signalling was explored in a Western blot time course experiment (Figure 3.9). pATR was detectable with 1nM, 10nM and 100nM SN38 treatments, with the signal being lower with 1nM treatments. pChk1 was only clearly detectable with 10nM and 100nM SN38 treatment, with a very faint band representing pChk1 with 1nM SN38 treatment. The time taken for activation of the ATR pathway is also dose dependent. No change in the level of DNA-PK and ATM phosphorylation was observed at any SN38 dose in combination with VX-970 in comparison to SN38 monotherapy. Interestingly, at 16 and 24 hours pChk2 levels increased with 1nM SN38 + VX-970 compared to 1nM SN38 monotherapy. This pattern was also observed with a concentration of 10nM SN38 at 16 hours.

These data show activation of both the DNA-PK and ATM pathways in HT29 and HCT116 cells in response to SN38 and VX-970 combination therapy, which is suggestive of increased DNA DSBs.

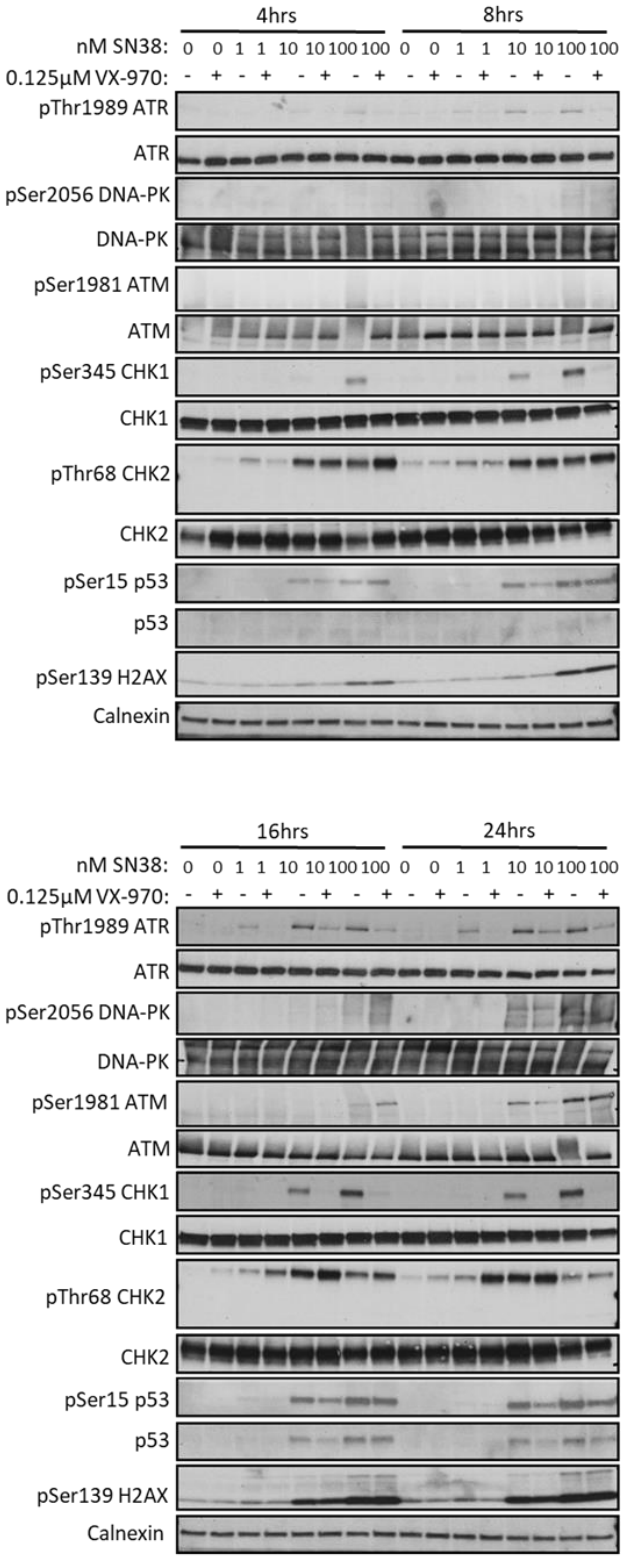

Figure 3.9. **Time course experiment shows induction of ATR signalling at low dose SN38 concentrations in SW48 cells.**

Phosphorylation of ATR can be detected with 1nM, 10nM and 100nM SN38 treatment. Phosphorylation of Chk1 occurs in an SN38 dose dependent manner. ATR signalling is abrogated by VX-970. Blots are representative images of 3 biological repeats.

3.3.5 SN38 and VX-970 combination treatment results in increased DNA SSBs and DSBs

The phosphorylation of H2AX, DNA-PK and ATM strongly indicate the induction of DNA DSBs following SN38 and VX-970 combination therapy. The presence of DNA SSBs and DSBs can be quantified using the single cell gel electrophoresis (comet) assay (Fairbairn, Olive, and O'Neill 1995). In the comet assay, DNA is separated by an electrophoretic current, with fragmented DNA migrating away from the main body of nuclear DNA. The DNA is visualised with propidium iodide (PI) staining and microscopy. Fragmented DNA appears as a smear known as a tail, giving cells with DNA strand breaks a comet like appearance (Figure 3.10-B SN38 and VX-970 combination treatment). The cell lysis in the comet protocol can be varied to enable visualisation of different DNA strand breaks. Using alkaline lysis, the hydrogen bonding holding the DNA duplex is lost, freeing fragments of SSBs. This means that the DNA in the comet tail using the alkaline comet protocol, can arise from both DSBs and SSBs. When a neutral lysis protocol is used, the DNA duplex remains intact, with only fragments produced as a result of DSBs free to migrate and form a comet tail. The Komet software is used to quantify the proportion of DNA in the comet tail generating the mean olive tail moment (OTM).

HCT116, HT29 and SW48 cells were treated with a range of SN38 concentrations as a monotherapy and in combination with VX-970, and harvested at 16 hours for comet assay analysis (Figure 3.10, Figure 3.11 and Figure 3.12). The 16-hour time point was chosen, as this was the time of maximal pDNA-PK and pATM signal in HCT116 and HT29 cells (Figure 3.7).

In HCT116 cells using the alkaline comet, a 9.3-fold (± 1.8, p=0.002) increase in the mean OTM was detected following 100nM SN38 monotherapy compared to untreated cells. This was further increased to 21.5-fold (± 4.4, p=<0.0001) with the addition of

VX-970. There was no increase in the mean OTM of cells treated with VX-970 monotherapy (Figure 3.10 A-B). Using the neutral comet assay, there was no significant fold-change in the mean OTM for either VX-970 or SN38 monotherapies, however the combination therapy resulted in a 6.8-fold increase (± 1.5, p=<0.0001) in the mean OTM compared to untreated cells (Figure 3.10 C-D).

In HT29 cells, a similar pattern was observed, using the alkaline comet a 2.2-fold (± 0.17, p=0.04) increase in the mean OTM was observed with 100nM SN38 monotherapy compared to untreated cells. No increase in OTM was observed with 25nM or 50nM SN38 monotherapies. The addition of VX-970 to 25nM, 50nM and 100nM SN38 treatment resulted in 5.6-fold (± 0.42, p<0.0001), 6.9-fold (± 0.5, p<0.0001) and 6.6-fold (± 0.37, p<0.0001) changes in mean OTM compared to untreated cells, respectively (Figure 3.11 A-B). Using the neutral comet assay, no change in the mean OTM with 1nM, 10nM or 100nM SN38 monotherapy was detected. The combination of VX-970 with 1nM, 10nM or 100nM SN38 resulted in 2.2 (± 0.07, p<0.0001), 2.7 (± 0.31, p<0.0001) and 4.1-fold (± 0.5, p<0.0001) changes in mean OTM compared to untreated cells, respectively (Figure 3.11 C-D).

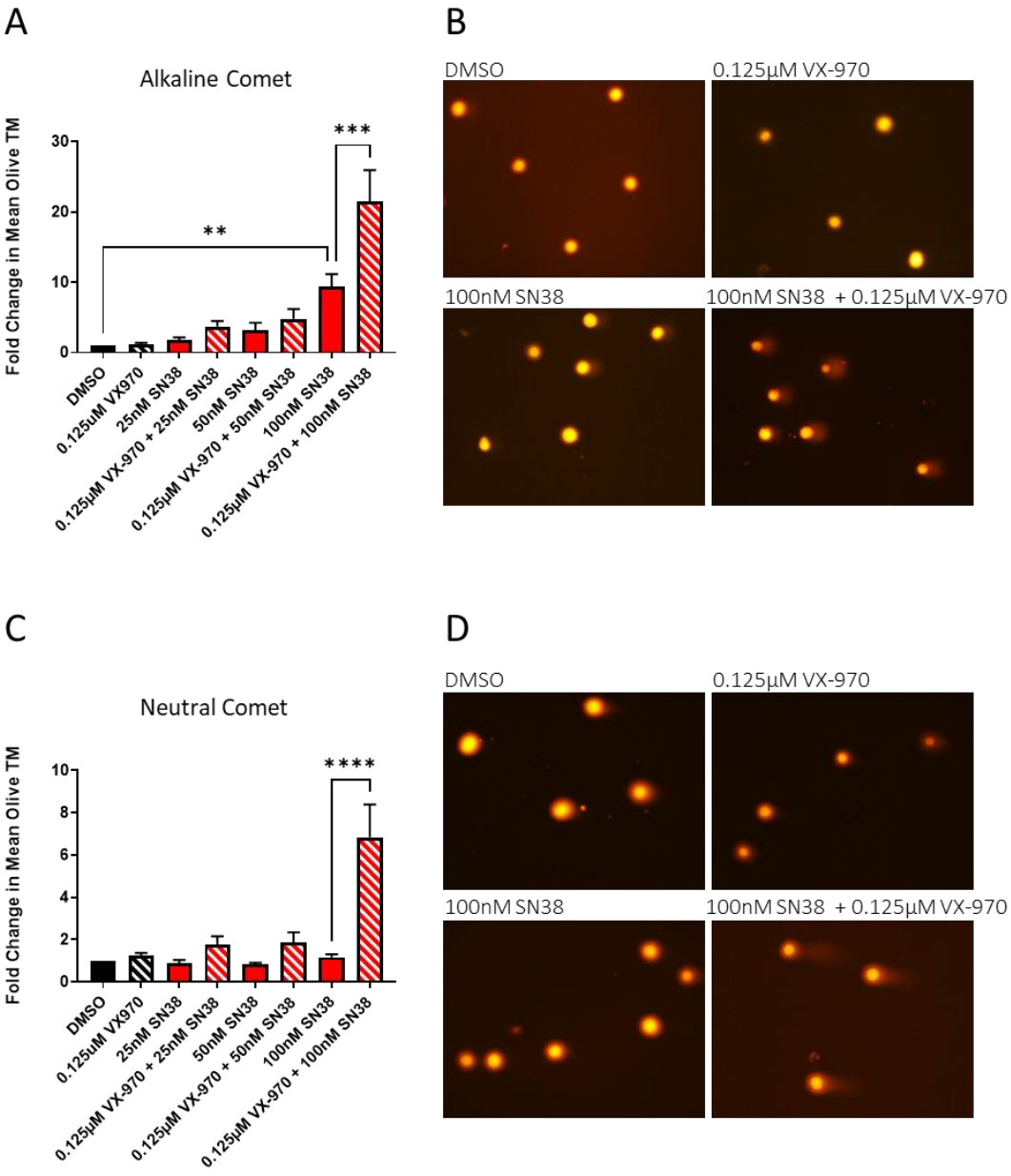

Figure 3.10. **SN38 + VX-970 combination treatment results in increased single and double stranded DNA breaks in HCT116 cells.**

A. and **B.** HCT116 cells were treated with the indicated drugs for 16 hours and analysed using alkaline comet assay. **C.** and **D.** HCT116 cells were treated with the indicated drugs for 16 hours and analysed using Neutral comet assay. Images are representative of 3 biological repeats. Each datapoint is the mean of 3 biological repeats. Error bars represent ± SEM. Statistical significance was calculated using the ANOVA test for multiple comparisons, *p* values ****<0.0001 ***<0.001 **<0.01.

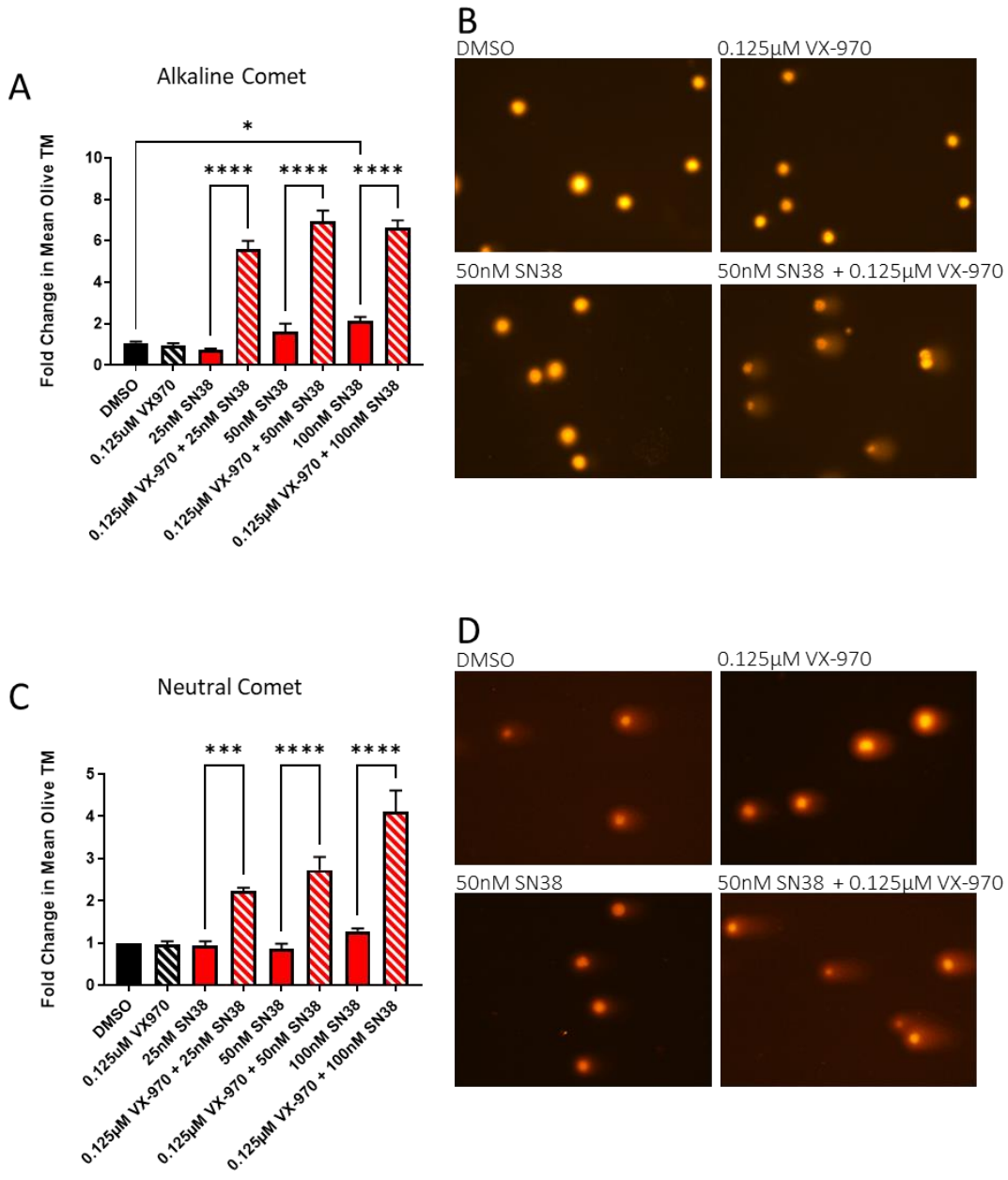

Figure 3.11. **SN38 + VX-970 combination treatment results in increased single and double stranded DNA breaks in HT29 cells.**

A. and **B.** HT29 cells were treated with the indicated drugs for 16 hours and analysed using alkaline comet assay. **C.** and **D.** HT29 cells were treated with the indicated drugs for 16 hours and analysed using Neutral comet assay. Images are representative of 3 biological repeats. Each datapoint is the mean of 3 biological repeats. Error bars represent ± SEM. Statistical significance was calculated using the ANOVA test for multiple comparisons, *p* values ****<0.0001 ***<0.001 **<0.01 *<0.05.

There was no fold change in mean OTM using either the neutral or alkaline comet with 16 hours SN38 and VX-970 combination treatment in SW48 cells (Figure 3.12 A-B). The time taken for accumulation of DNA strand breaks may vary between cell lines. To explore whether there was delayed accumulation in SW48 cells compared to HCT116 and HT29 cells, alkaline comet analysis was performed at 24 and 48 hours of SN38 and VX-970 combination treatment. No change in the mean OTM was detected at either timepoint with 5nM, 25nM or 50nM SN38 monotherapy or in combination with VX-970 (Figure 3.12 C-D). Some cells have very compact chromatin, reducing the separation of fragmented DNA from the main nuclear DNA, reducing suitability of the comet assay to detect DNA breaks. To establish whether fragmented DNA in SW48 cells could be separated from the main DNA body, SW48 cells were irradiated at doses between 15Gy and 25Gy. Irradiation resulted in a mean OTM of 2-3 for all doses of irradiation (Figure 3.13). While irradiation does result in comet tails, the mean OTM is smaller than expected with irradiation.

This data suggests an increase in DNA SSBs following SN38 monotherapy and an increase in both DNA SSBs and DSBs following combination therapy in HCT116 and HT29 cells.

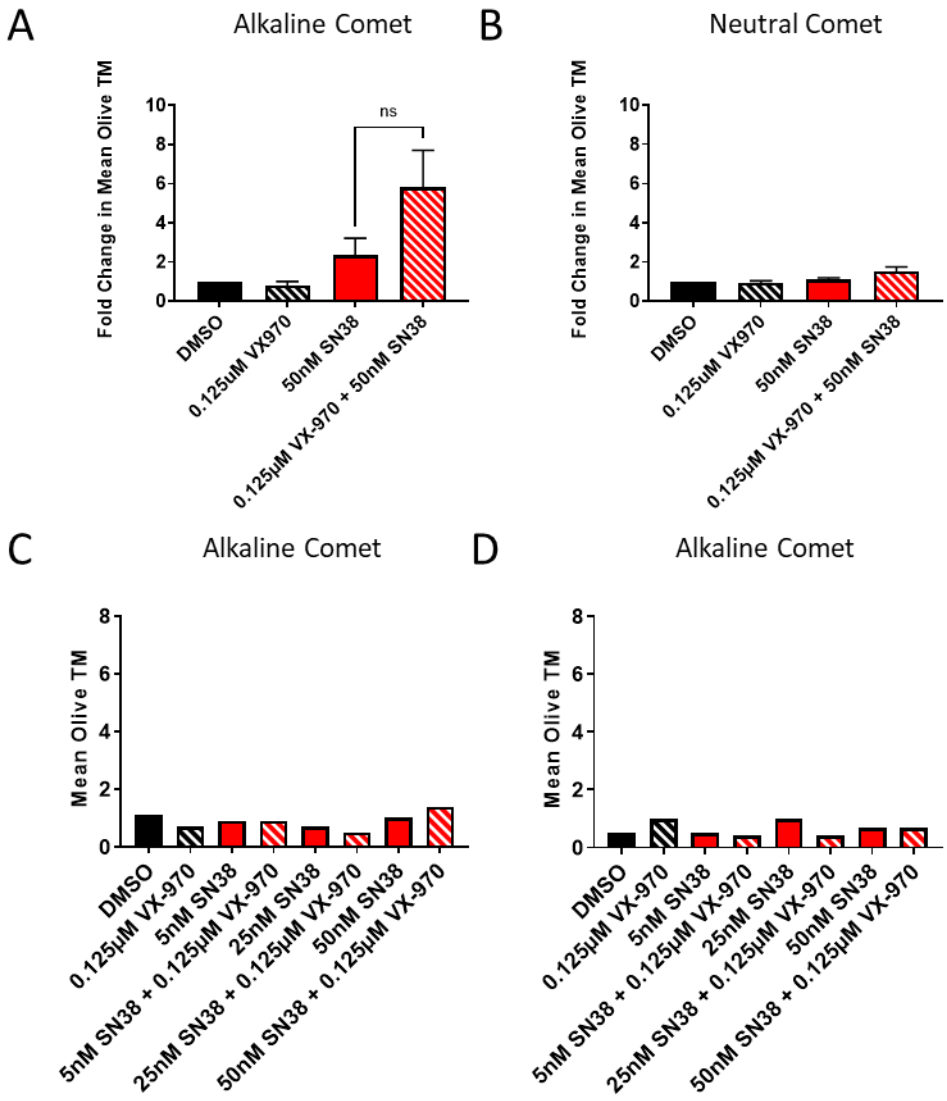

Figure 3.12. **No significant increase in ssDNA or dsDNA breaks in SW48 cells following SN38 + VX-970 treatment.**

A. SW48 cells were treated with the indicated drugs for 16 hours and analysed using alkaline comet assay. **B.** SW48 cells were treated with the indicated drugs for 16 hours and analysed using Neutral comet assay. **C.** SW48 cells were treated with the indicated drugs for 24 hours and analysed using the alkaline comet assay. **D.** SW48 cells were treated with the indicated drugs for 48 hours and analysed using the alkaline comet assay. Each datapoint is the mean of 3 biological repeats. Error bars represent ± SEM. Statistical significance was calculated using the ANOVA test for multiple comparisons.

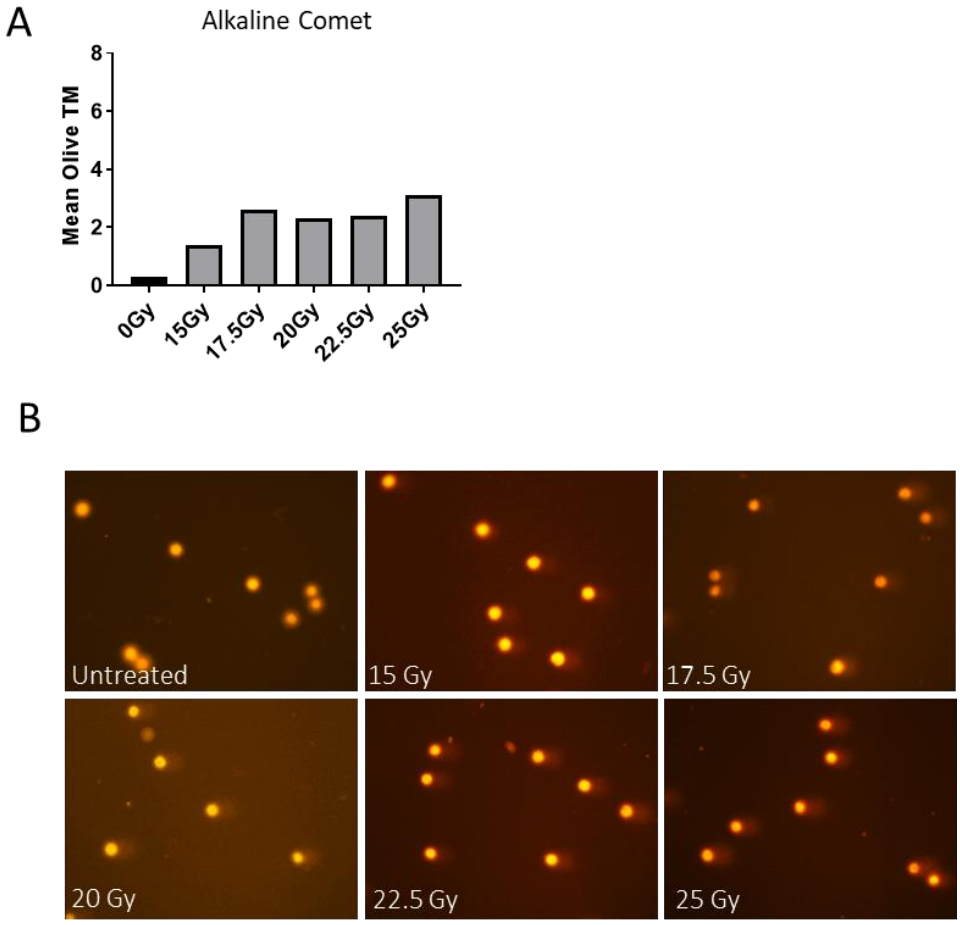

Figure 3.13. **Only small change in Mean Olive Tail Moment of SW48 cells following irradiation.**

A. SW48 cells were irradiated with the indicated doses and immediately analysed using the alkaline comet assay. **B.** Representative comet assay images of irradiated SW48 cells.

3.3.6 SN38 and VX-970 combination treatment results in the formation of cGAS positive micronuclei

If DNA DSBs persist as cells pass through mitosis, fragmented DNA can be encapsulated in a micronuclear envelope, creating small nuclear bodies, known as micronuclei. To establish whether the DNA DSBs induced by SN38 and VX-970 combination therapy leads to the formation of micronuclei, HT29 cells were treated with either SN38 and VX-970 monotherapies or combination therapies for 24 and 48 hours. DNA was stained using Hoechst and cells were visualised with confocal

microscopy (Figure 3.14). At 24 and 48 hours there was no significant change in the ratio of micronuclei to nuclei in cells treated with 1nM or 5nM SN38 monotherapy. However, at 24 hours, the ratio of micronuclei to nuclei in cells treated with 5nM SN38 and 0.25μM VX-970 combination therapy was 0.63 (± 0.06), compared to 0.027 (± 0.04) in untreated cells ($p<0.0001$). At 48 hours, the ratio of micronuclei to nuclei was increased to 0.45 (± 0.1, $p=0.0012$) in cells treated with 1nM SN38 and 0.25μM VX-970, and to 0.804 (± 0.09, $p<0.0001$) in cells treated with 5nM SN38 and 0.25μM VX-970, compared to 0.036 (± 0.007) in untreated cells. The increase in micronuclei following SN38 and VX-970 combination therapy, correlates well with the DNA strand breaks visualised in the comet assay and the increased pDNA-PK and pATM signal observed by Western blotting.

No increase in DNA-PK or ATM phosphorylation, as well as no increase in DNA strand breaks were detected in SW48 cells following SN38 and VX-970 combination therapy. As micronuclei can also be used as an indicator of DNA damage, SW48 cells were treated with SN38 monotherapies and combination therapies and stained for DNA visualisation. Treatment of SW48 cells with 1nM or 10nM SN38 as a monotherapy and in combination with VX-970 did not result in the formation of micronuclei (Figure 3.15).

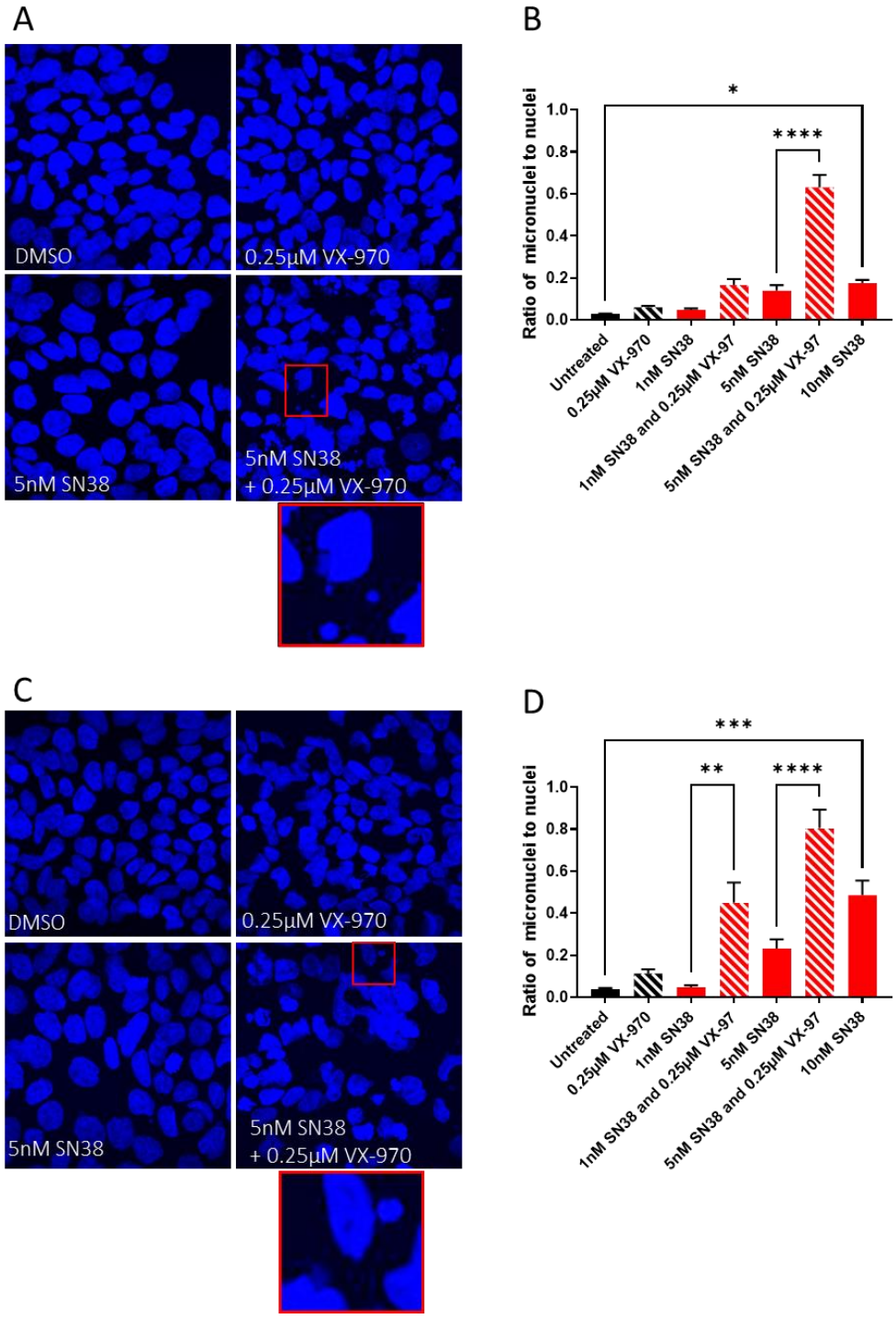

Figure 3.14. **SN38 + VX-970 combination treatment results in the formation of micronuclei in HT29 cells.**

A. and **B.** HT29 cells were treated with the indicated drugs for 24 hours and stained with Hoechst to detect micronuclei. Images were taken with X64 magnification. **C.** and **D.** HT29 cells were treated with the indicated drugs for 48 hours and stained with Hoechst to detect micronuclei. Images are representative of 3 biological repeats. Each datapoint is the mean of 3 biological repeats. Error bars represent ± SEM. Statistical significance was calculated using the ANOVA test for multiple comparisons, *p* values ****<0.0001 ***<0.001 **<0.01 *<0.05.

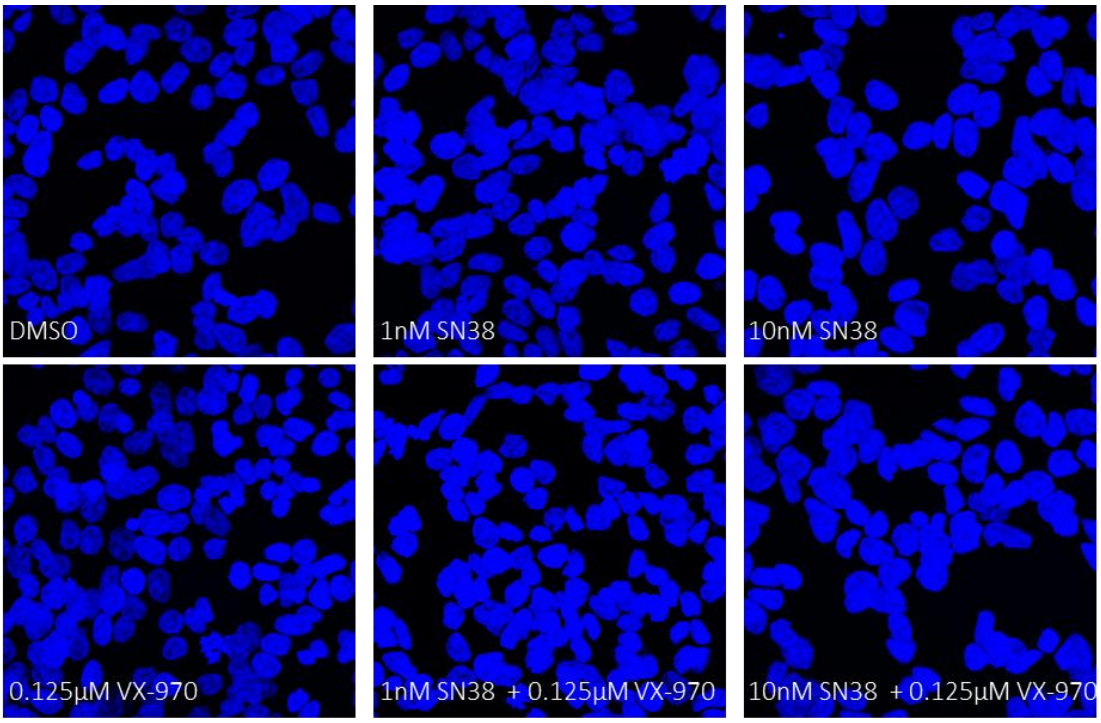

Figure 3.15. **An increase in micronuclei is not detected in SW48 cells following SN38 + VX-970 combination treatment.**

SW48 cells were treated with the indicated drugs for 48 hours and stained with Hoechst to detect micronuclei. Images were taken with X64 magnification. Images are representative of 3 biological repeats.

Cytosolic DNA and DNA in micronuclei can be detected by the cytosolic nucleotidyltransferase cGAS, leading to activation of the cGAS-STING immunostimulatory pathway in response to DNA damage (Chen et al. 2020). To assess whether the DNA damage occurring in HT29 cells following combination therapy could activate cGAS, HT29 cells were stained with an anti-cGAS antibody and Hoechst, to detect colocalization of cGAS with micronuclei using confocal microscopy (Figure 3.16). At 24 hours, the ratio of cGAS positive micronuclei to nuclei was increased in cells treated with 5nM SN38 and VX-970 treatment compared to untreated cells, 0.083 (± 0.02) vs 0.0057 (± 0.003, p=0.005). At 48 hours the ratio of cGAS positive micronuclei to nuclei was increased in cells treated with 1nM and 5nM SN38 in combination with VX-970 compared to untreated cells, 0.12 (± 0.003,

p=0.0015) and 0.19 (± 0.02, p<0.0001) vs 0.007 (± 0.002). There was no significant change in the ratio of cGAS positive micronuclei to nuclei in cells treated with SN38 or VX-970 monotherapies compared to untreated cells.

The finding of cGAS positive micronuclei in HT29 cells following SN38 and VX-970 combination therapy, indicates that increased DNA damage may result in activation of the cGAS-STING pathway. This could potentially result in anti-tumour immune response in SN38 and VX-970 combination treated tumours.

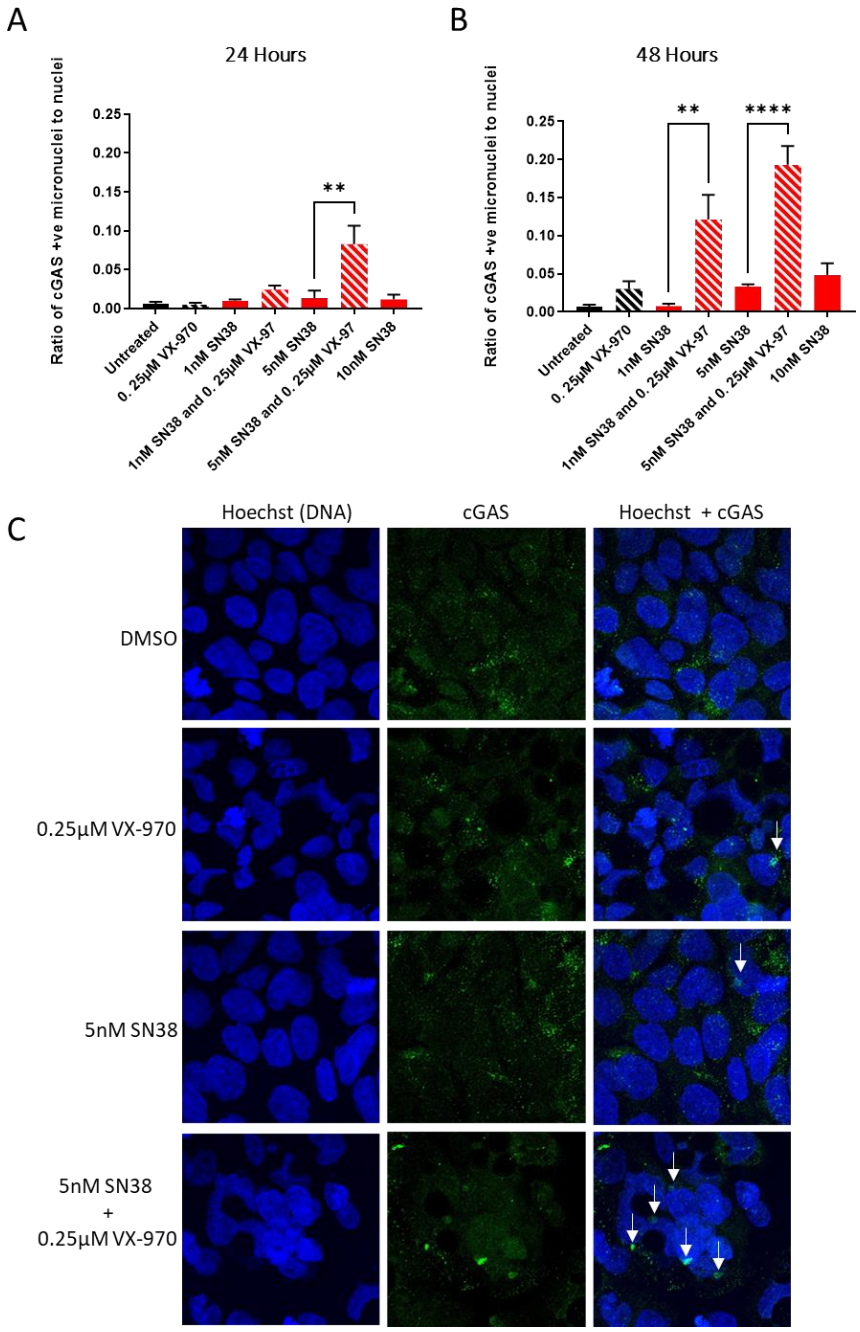

Figure 3.16. **SN38 + VX-970 combination treatment results in the formation of cGAS+ micronuclei in HT29 cells.**

A. HT29 cells were treated with the indicated drugs for 24 hours and stained to detect cGAS+ micronuclei. **B.** and **C.** HT29 cells were treated with the indicated drugs for 48 hours and stained to detect cGAS+ micronuclei. Images were taken with X64 magnification. Images are representative of 3 biological repeats. Each datapoint is the mean of 3 biological repeats. Error bars represent ± SEM. Statistical significance was calculated using the ANOVA test for multiple comparisons, *p* values ****<0.0001 ***<0.001 **<0.01 *<0.05.

3.3.7 Loss of STING expression may be responsible for the lack of cytokine production following SN38 and VX-970 combination therapy

Colocalisation of cGAS with micronuclei in HT29 cells treated with SN38 and VX-970 combination therapy could result in activation of the STING signalling pathway leading to the production of Type 1 IFNs and cytokines. To investigate whether cytokine production occurs following the combination therapy, cells were treated with 5nM SN38 or 0.625µM VX-970 as monotherapy or in combination, and cytokines measured using a protein array. The dose selected was shown to have maximal synergy in reducing proliferation (Figure 3.5) and survival (Figure 3.6).

Following 72-hour 5nM SN38 and VX-970 combination therapy, there was no increase in any of the cytokines measured by the array compared to the SN38 monotherapy. Following VX-970 monotherapy, cystatin C, fibroblast growth factor 19 (FGF-19) and VEGF were altered by ≥2-fold (the cut off for reliable increase), however only VEGF was elevated in the combination therapy, although to a lesser extent than with VX-970 monotherapy (Figure 3.17). Cytokines were also measured following combination treatment with 10nM SN38 and 0.125µM VX-970, as well as 100nM SN38 and 0.25µM VX-970, but no increased cytokine secretion was detected.

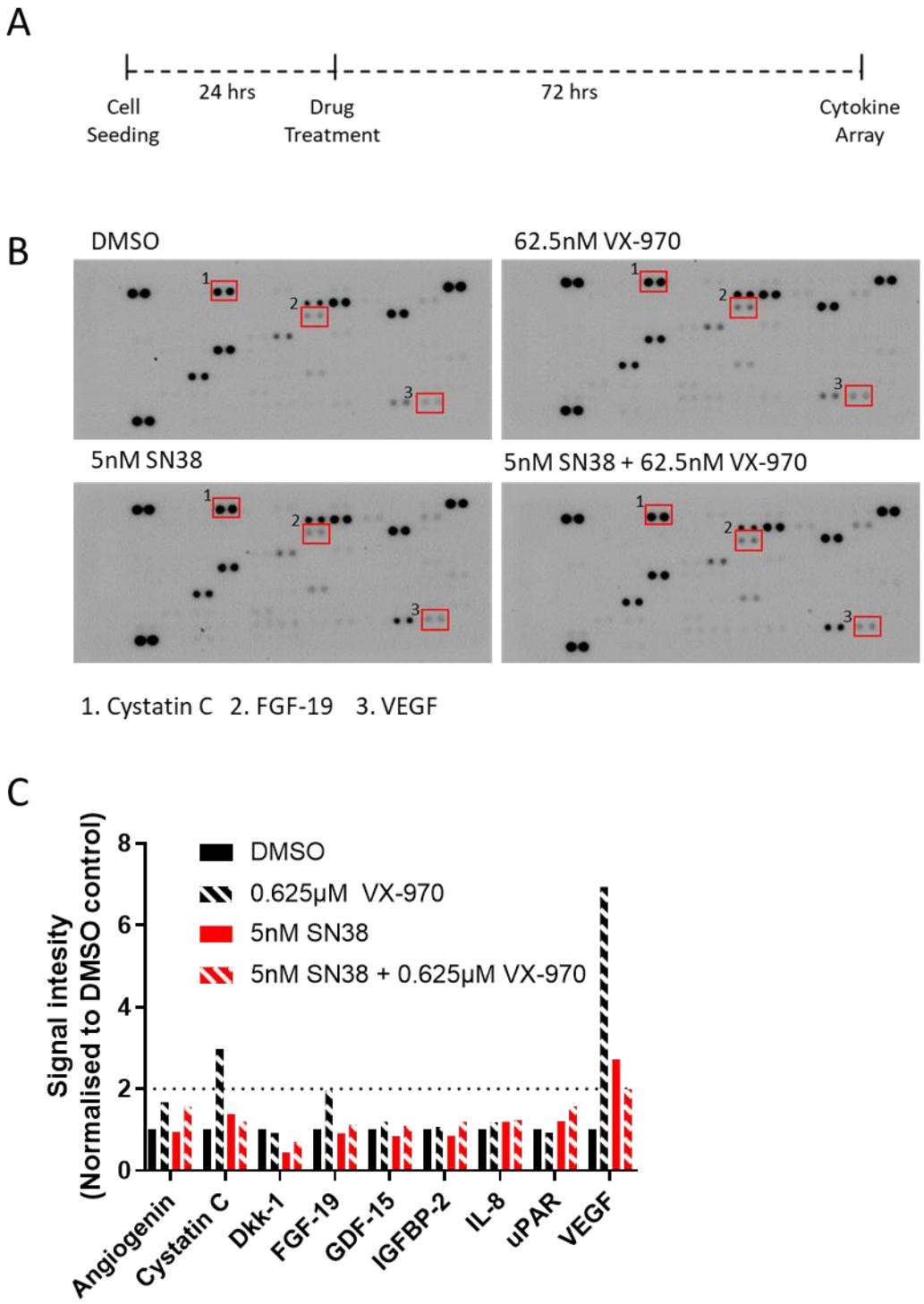

Figure 3.17. **No increase in immunostimulatory cytokines following 5nM SN38 + 0.0625μM VX-970 combination treatment.**

B. Cytokine arrays performed using media collected according to schedule in (**A**). **C.** Quantification of signal density (ImageQuant software) for the spots that were measurable across arrays.

Loss of STING or cGAS expression has been reported to reduce activation of proinflammatory transcription programmes in response to DNA damage (Xia et al. 2016). To explore whether loss of these signalling molecules could prevent immune stimulation in response to SN38 and VX-970 combination treatment, the expression of cGAS and STING in a panel of CRC cell lines was investigated by Western blotting (Figure 3.19). Although HT29 cells express cGAS, STING expression was not detected, providing an explanation for the lack of cytokine secretion in response to elevated DNA damage and cGAS colocalisation with micronuclei. None of the 5 CRC cell lines investigated expressed both cGAS and STING, with CACO2 and HT29 cells expressing cGAS but not STING, and HCT116 and LS174T cells expressing STING but no cGAS. Neither cGAS or STING were detected in SW48 cells. This suggests that a non-compromised cGAS-STING pathway may need to be present in tumours, for the increased DNA damage observed with the combination therapy to cause an anti-tumour immune response.

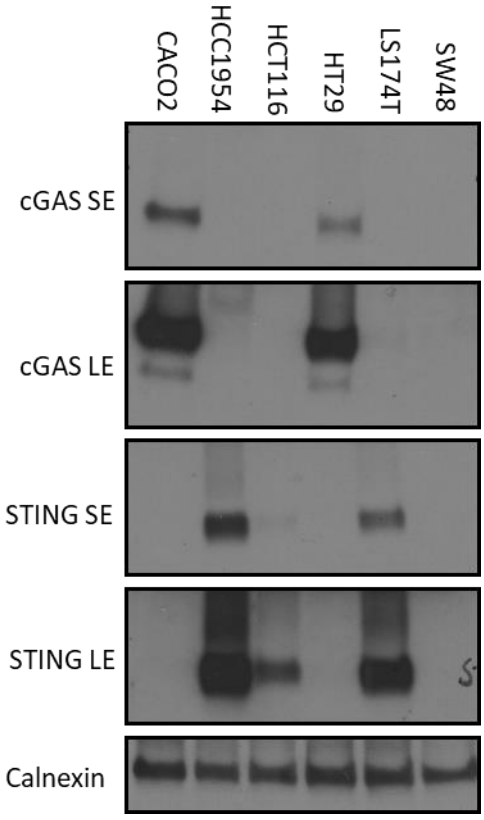

Figure 3.18. **Colorectal cancer cell lines show loss of cGAS or STING expression.** Cell lysates were collected from a panel of colorectal cancer cell lines (and HCC1954 a breast cancer line) and Western blotting was performed. Image shows short exposure (SE) and long exposure (LE) of films. Blots are representative of 2 biological repeats.

3.3.8 The addition of VX-970 to SN38 treatment reduces survival of CRC patient derived organoids

CRC cell lines are simple models for exploring the efficacy of drug treatments, however cell lines are homogenous and not representative of the parental tumours. Patient derived organoids (PDOs), are self-organising 3D tumour models, containing both stem and differentiated cells, making them a superior model for studying the therapeutic potential of anti-cancer agents. Having established that SN38 and VX-970 synergise to reduce proliferation and survival in CRC cell lines, the cytotoxicity of the combination in CRC PDOs was investigated. In this study PDO 021 and PDO 027

were used, both organoids were developed from colon tumours. The mutational profiles of the organoids are displayed in Table 3.1.

Table 3.1. Mutation profile of PDO 021 and 027

Organoid	Source	Mutations
PDO 021	Colon tumour	KRAS, SMAD4, ARID1A, PIK3RI, CTNNB1, NOTCH2
PDO 027	Colon tumour	APC, TP53, B2M, RNF43, ACVR2A, KMT2C, EP300, CEBBP, CCND1, FANCE, FAS, GRIN2A, HDLBP, HNF1A, MSH3, PI3KCB, POLE, SYNE1, TP53BP1, USP9X, ZNF292

PDO 021 and PDO 027 were seeded by trypsinisation of fully developed organoids, and left for 48 hours to allow for the division and differentiation of stem cells. The organoids were then treated with a dose range of SN38 and VX-970 for 72hrs. Following drug removal, organoids were left to grow for a further 7 days. This protocol would show the expansion potential of the organoids following treatment. Following treatment organoids were imaged and viability measured using the 3D CellTiter-Glo assay (Figure 3.19 and Figure 3.20).

In PDO 021, the addition of 0.25µM VX-970 to 1nM SN38 prevented the growth and development of organoids, while organoids treated with 1nM SN38 or 0.25µM VX-970 monotherapies grew fully and resembled untreated organoids (Figure 3.19 B). Viability of PDO 021 was reduced to 37.4% (± 9.3) following 1nM SN38 and 0.25µM VX-970 compared to 100% (± 3.1) with 1nM SN38 monotherapy and 79% (± 4.6) with 0.25µM VX-970 (Figure 3.19 C-D). The average ZIP synergy score for the combination was 8.28 (± 1.7) demonstrating an additive interaction (Figure 3.19 E). However, the ZIP score was reduced due to the complete loss of viability with 10nM and 100nM SN38 monotherapies preventing any drug interaction. The number of PDOs 027 which grew and developed was highly reduced following 1nM SN38 and 0.25µM VX-970 combination therapy compared to either monotherapy (Figure 3.20 B). The viability of the organoids was reduced to 38.9% (± 8) following 1nM SN38 and

0.25µM VX-970 combination therapy versus 95.1% (± 5.8) with 1nM SN38 and 69.8% (± 11.1) with 0.25µM VX-970 (Figure 3.20 C-D). The average ZIP synergy score for the combination of SN38 and VX-970 in PDO 027 was 16.42 (± 1.1) (Figure 3.20 E).

These data show increased cytotoxicity of SN38 and VX-970 combination therapy in CRC PDOs, which are a more representative model of CRC than cell lines. This is predictive of the combination therapy being effective in the treatment of CRC.

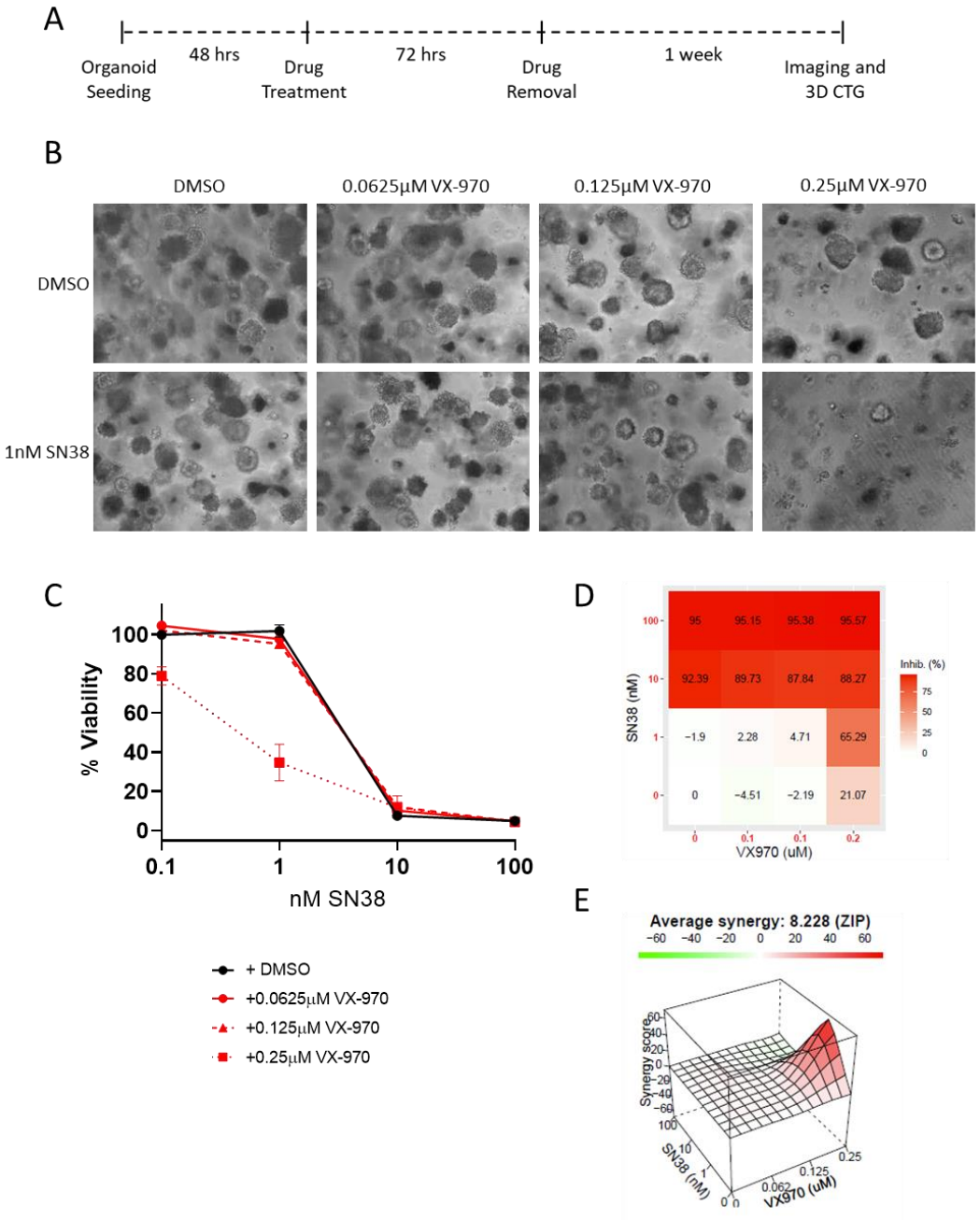

Figure 3.19. **VX-970 synergises with low dose SN38 treatment to reduce viability in PDO 021.**

A. Scheme demonstrating the treatment schedule followed in B, C, D and E. **B.** Representative images of PDO 021 following drug treatment. **C.** Organoids were treated with the indicated drugs and the percentage viability of PDO 021 measured using the 3D CTG assay. Each datapoint is the mean of 3 biological repeats. Error bars represent ± SEM. **D.** The mean percentage inhibition for each drug combination is shown in a heatmap. **E.** 3D ZIP model demonstrates the interaction between VX-970 and SN38 in PDO 021.

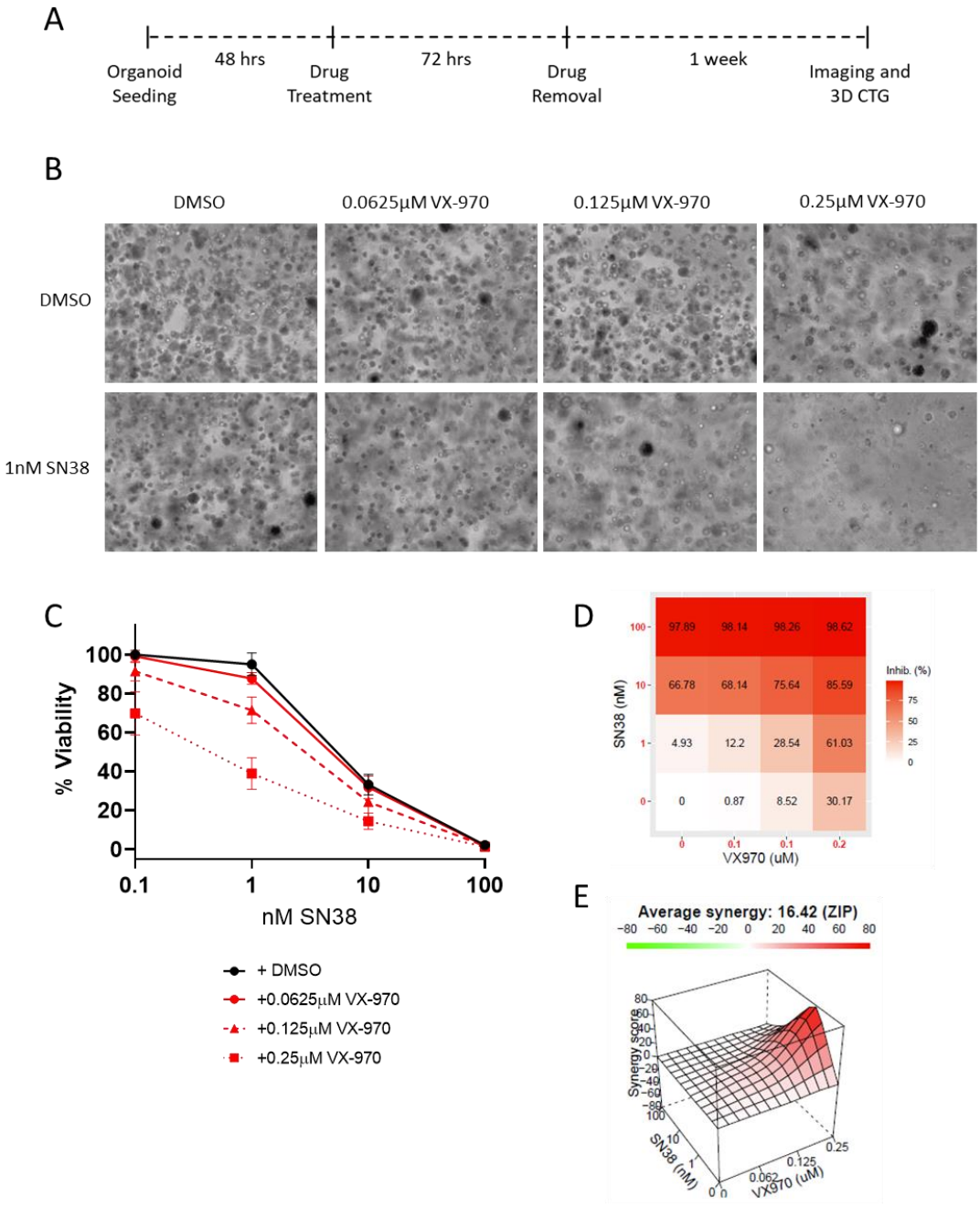

Figure 3.20. **VX-970 synergises with SN38 treatment to reduce viability in PDO 027.** **A.** Scheme demonstrating the treatment schedule followed in B, C, D and E. **B.** Representative images of PDO 027 following drug treatment. **C.** Organoids were treated with the indicated drugs and the percentage viability of PDO 027 measured using the 3D CTG assay. Each datapoint is the mean of 3 biological repeats. Error bars represent +/- SEM. **D.** The mean percentage inhibition for each drug combination is shown in a heatmap. **E.** 3D ZIP model demonstrates the interaction between VX-970 and SN38 in PDO 027.

3.3.9 Phosphorylation of DNA-PK and ATM in CRC PDOs following SN38 and VX-970 combination therapy

To assess whether the combination treatment would cause phosphorylation of DNA-PK and ATM in CRC PDOs, as seen in the CRC cell lines (Figure 3.7), PDO 021 was treated with either 100nM SN38, 0.25µM VX-970 or 100nM SN38 and 0.25µM VX-970 combination therapy. Organoids were treated on day 5 post seeding, harvested 24 and 48 hours later, and lysates were analysed by Western blotting (Figure 3.21). At 48 hours with the combination treatment but not SN38 or VX-970 monotherapy, pDNA-PK and pATM were detected. SN38 treatment led to p53, Chk2 and H2AX phosphorylation by 24 hours. The combination treatment did not lead to an increase in Chk2 or H2AX phosphorylation compared to SN38 monotherapy. As seen in the CRC cell lines, SN38-induced p53 phosphorylation was reduced with VX-970 treatment. Cleavage of PARP was seen with both SN38 monotherapy and in combination with VX-970. This finding indicates an increase in DNA DSBs following the combination treatment, compared to SN38 monotherapy.

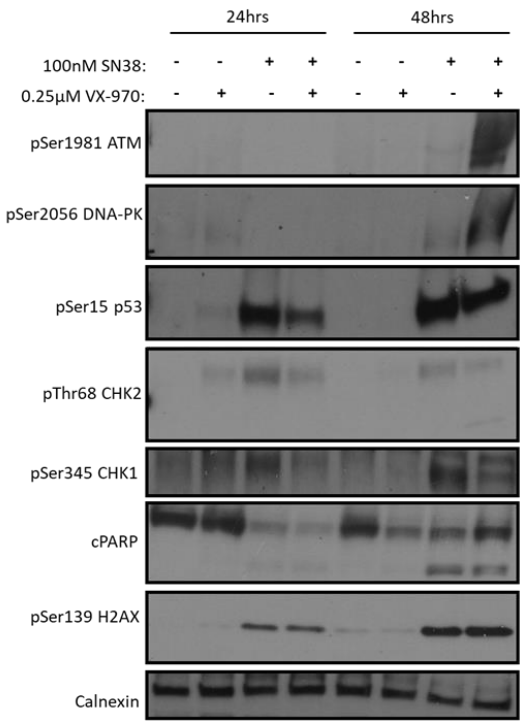

Figure 3.21. **SN38 + VX-970 treatment results in ATM and DNA-PK phosphorylation in PDO 021.**

PDO 021 organoids were treated as indicated and lysates analysed by Western blotting.

3.3.10 Using the CyTOF technique, no increase in cPARP or cCapase-3 was detected in organoids treated with SN38 and VX-970 combination therapy

Using Western blotting to explore cell signalling in organoids, is technically challenging due to the requirement to remove all the Matrigel matrix in which the organoids are imbedded. Furthermore, no information can be gleaned on a single cell level, giving homogenous information for a heterogenous population of cells. The mass cytometry time of flight (CyTOF) technique uses heavy metals conjugated to antibodies to measure protein levels in single cells (Qin et al. 2020). This technique has been adapted for organoid single cell analysis, with organoids fixed in the 3D matrix prior to disassociation and staining, preserving cell signalling and protein expression. Analysis of the antibody signal is done using a Helios mass cytometer,

which detects heavy metal staining in single cells. Prior to organoid staining, samples are barcoded with heavy metals to allow multiplexing of all the samples for staining and analysis (Figure 2.1).

PDO 021 organoids were treated on day 5 post seeding with 1nM, 10nM or 100nM SN38 as a monotherapy or in combination with 0.25µM VX-970. Organoids were fixed at 24, 48 and 72 hours post treatment for CyTOF analysis. Only intact, single cells were included in the analysis (Figure 2.2). cPARP and cCaspase-3 were used as markers for apoptosis, with cells positive for both markers classed as apoptotic. At 24, 48 and 72 hours there was no increase in the percentage of cPARP+/cCaspase-3+ cells with the addition of VX-970 to SN38 monotherapy (Figure 3.22). Failure to detect an increase in apoptotic cells may be due to the timepoint at which the organoids were analysed, with increased DNA damage in the organoids possibly requiring passage through multiple rounds of replication to result in cell death. The lack of dead-cell positive control was a limitation in this experiment. Inclusion of organoids treated with 1µM SN38 would have been a suitable dead cell control.

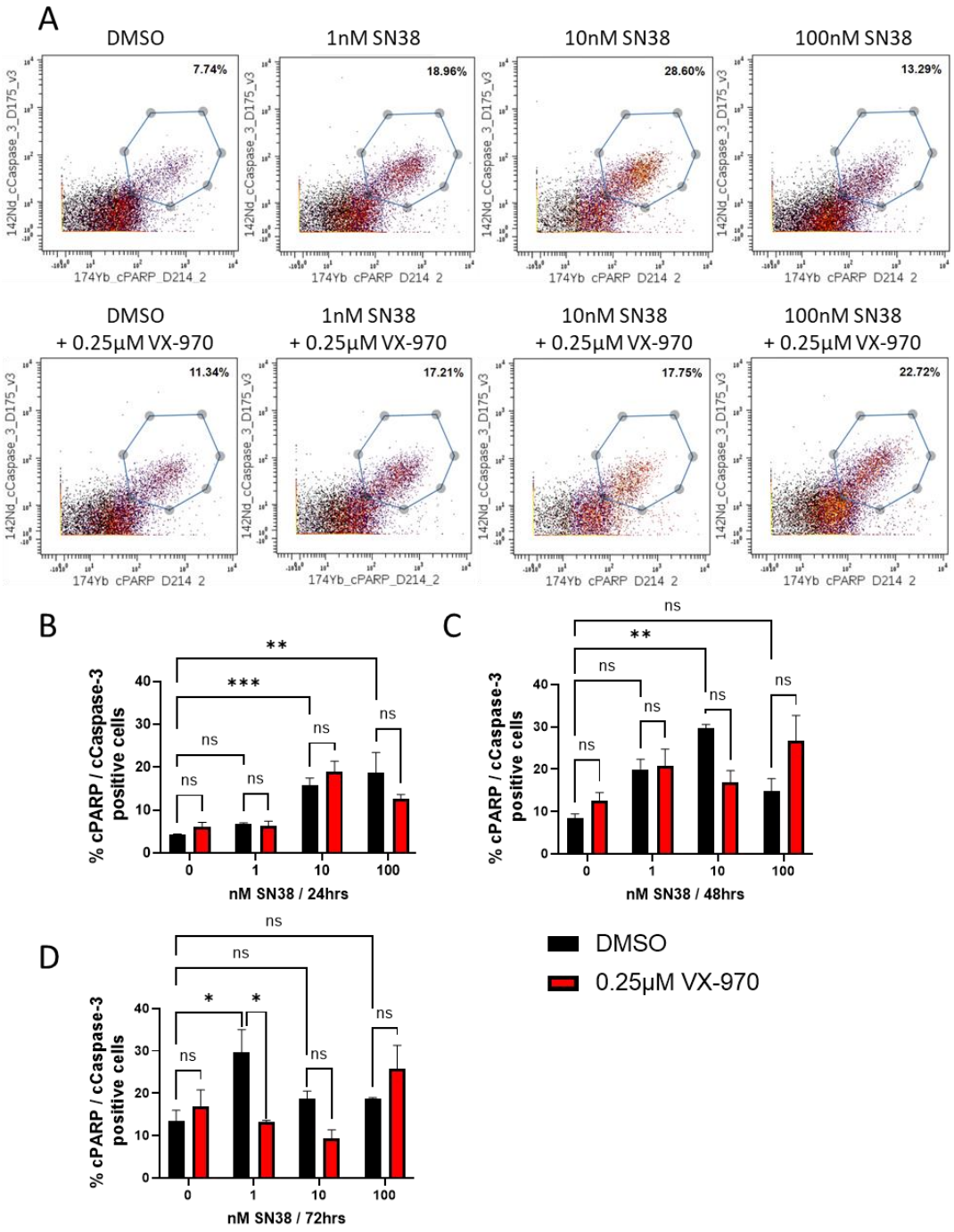

Figure 3.22. **The addition of VX-970 to SN38 treatment of PDO 021 does not lead to increased cleavage of PARP and Caspase-3.**

A. Organoids were treated for 48hrs as indicated and analysed using the CyTOF technique. Cells expressing high level of cPARP and cCaspase-3 are encircled. **B.** The perecentage of cPARP and cCapase-3 positive cells at 24 hours. **C.** The percentage of cPARP and cCapase-3 positive cells at 48 hours. **D.** The percentage of cPARP and cCapase-3 positive cells at 72 hours. Plots are representative of 3 technical repeats. Statistical significance was calculated using the ANOVA test for multiple comparisons, *p* values ****<0.0001 ***<0.001 **<0.01 *<0.05. Error bars represent +/- SEM.

3.3.11 VX-970 reduces SN38-induced replication block

The CyTOF technique can be used to explore the cell cycle distribution of individual organoid cells, by staining with antibodies specific to proteins which fluctuate during the cell cycle. The choice of cell cycle markers is very limited by the availability of antibodies which are suitable for the CyTOF technique. Cell state markers used included retinoblastoma protein (pRb), geminin, polo-like kinase 1 (PLK), cyclin B1 and pSer10 histone 3 (pHH3). Prior to fixation, organoids are pulsed with Idoxuridine (IdU), an iodinated nucleoside analogue to mark cells undergoing DNA replication. The cell cycle distribution of these markers, and the gating strategy used to study cell state is shown in Figure 3.23 A-B. There were no statistically significant changes in the cell state distributions with the addition of VX-970 to SN38 treatment, with the only marked change being an accumulation of cells in G2 with 100nM SN38 treatment at 24 hours, 38.76% (± 4.4) vs 24.77% (± 0.39) in the untreated control ($p<0.0001$). This increase in the G2 population and loss of S-phase population was maintained with the addition of VX-970 (Figure 3.23 C).

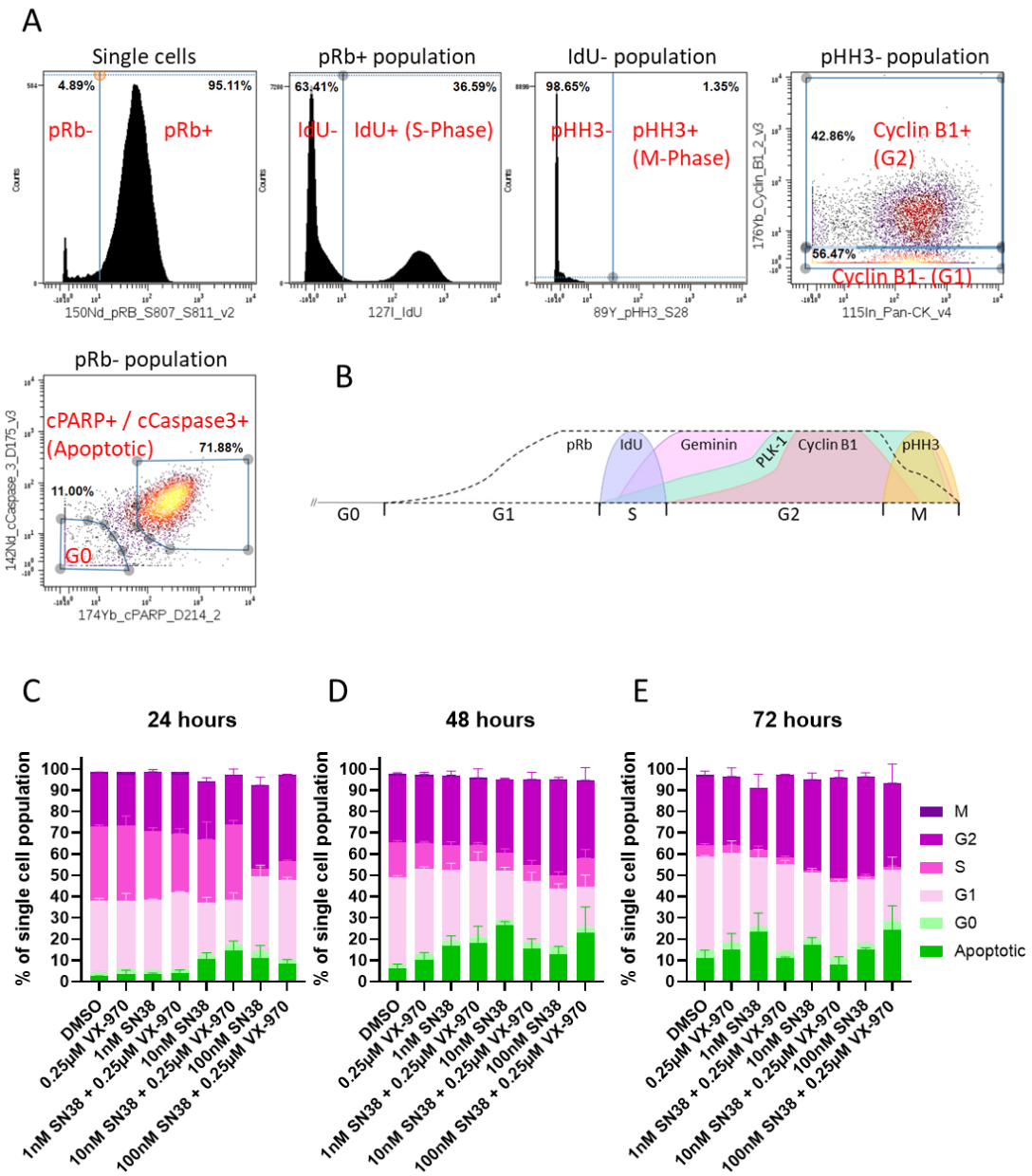

Figure 3.23. **Cell state distribution in PDO 021 treated with SN38 +/- VX-970.**

A. Cell gating strategy for cell cycle distribution analysis using the CyTOF technique. The parent population is indicated above each plot. **B.** Scheme demonstrating the cell cycle distribution of cell state markers used. **C.** The cell state distribution following 24 hours organoid treatment. **D.** The cell state distribution following 48 hours organoid treatment. **E.** The cell state distribution following 72 hours organoid treatment. Each datapoint is the mean of 3 technical repeats. Error bars represent +/- SEM.

Closer analysis of IdU incorporation at 24 hours, showed a difference in S-phase progression in cells treated with SN38 and VX-970 combination treatment compared to SN38 monotherapy. In cells treated with 10nM SN38, a reduced rate of IdU incorporation was observed, with the IdU+ signal being much lower than in untreated cells. The addition of VX-970 to 10nM SN38 returned the IdU signal close to that observed in untreated cells (Figure 3.24 A). A gating strategy to only show cells with high IdU intensity (as observed in untreated cells), revealed a reduction in the percentage of IdU+ cells from 34.32% (± 0.136) in untreated cells, to 9.18% (± 1.57) in cells treated with 10nM SN38 ($p=0.0067$). The addition of VX-970 to 10nM SN38 increased the percentage of IdU+ cells to 29.5% (± 3.0) ($p=0.0008$) (Figure 3.24 B).

Cell state markers can be used to generate uMAPS, with each cell plotted by the signal intensity of a range of cell state markers, each area of the uMAP can then be assigned a cell state. The uMAPS can be coloured by the signal intensity of individual markers. Reduced IdU incorporation with 10nM SN38 could be seen in the uMAPS, as well as the increase of IdU signal with the addition of VX-970 (Figure 3.25).

This finding supports the hypothesis that ATR inhibition results in loss of SN38 induced S-phase arrest, with cells progressing through the cell cycle despite the presence of DNA damage.

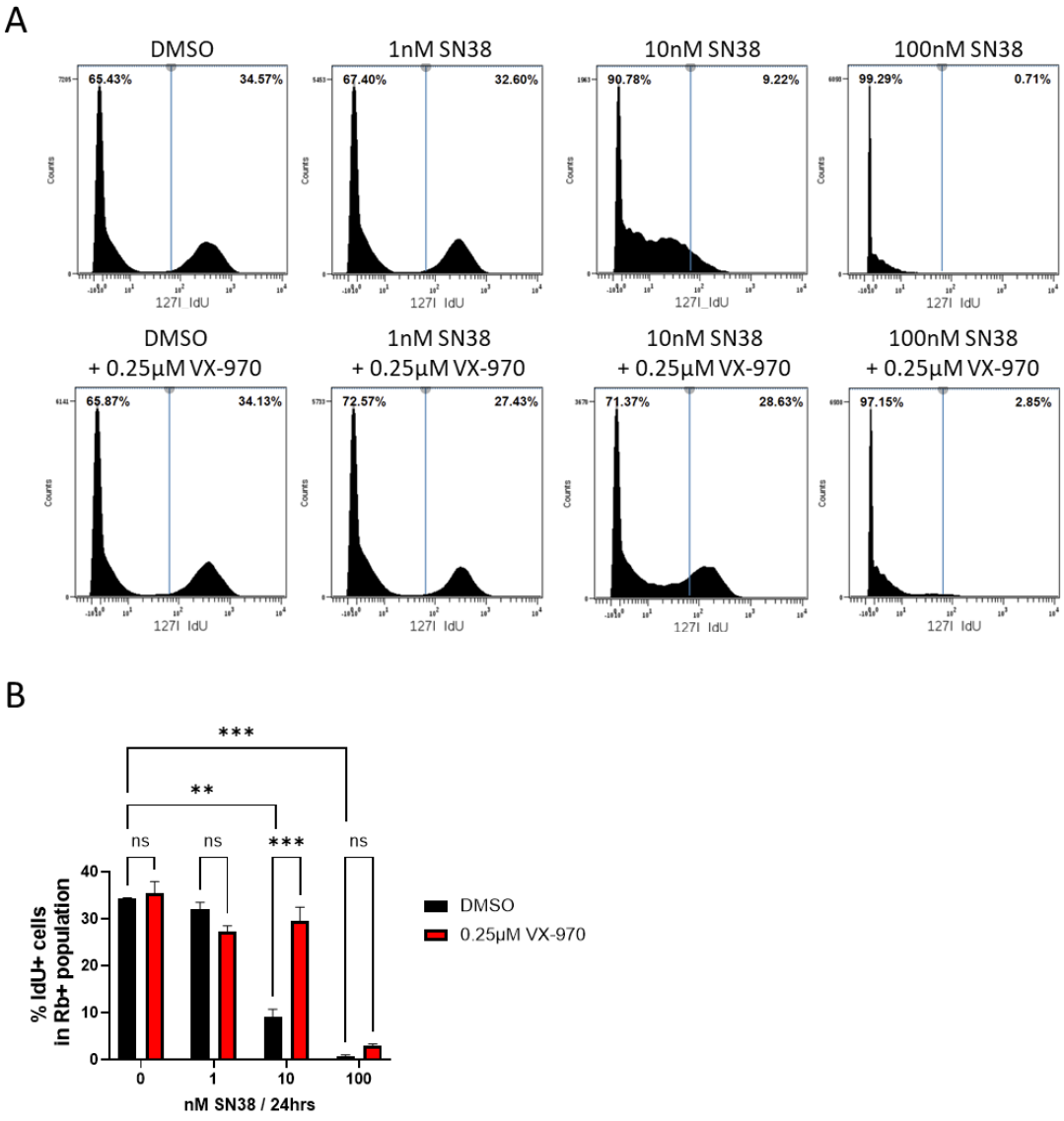

Figure 3.24. **VX-970 reduces SN38 induced S-phase block in PDO 021.**
Organoids were treated for 24hrs with the indicated drugs and IdU incorporation measured using the CyTOF technique. **A.** IdU profiles **B.** The percentage of IdU positive cells gating for only cells with high rates of IdU incorporation at 24 hours following organoid treatment. Plots are representative of 3 technical repeats. Statistical significance was calculated using the ANOVA test for multiple comparisons, *p* values ****<0.0001 ***<0.001 **<0.01 *<0.05. Each datapoint is the mean of 3 technical repeats. Error bars represent +/- SEM.

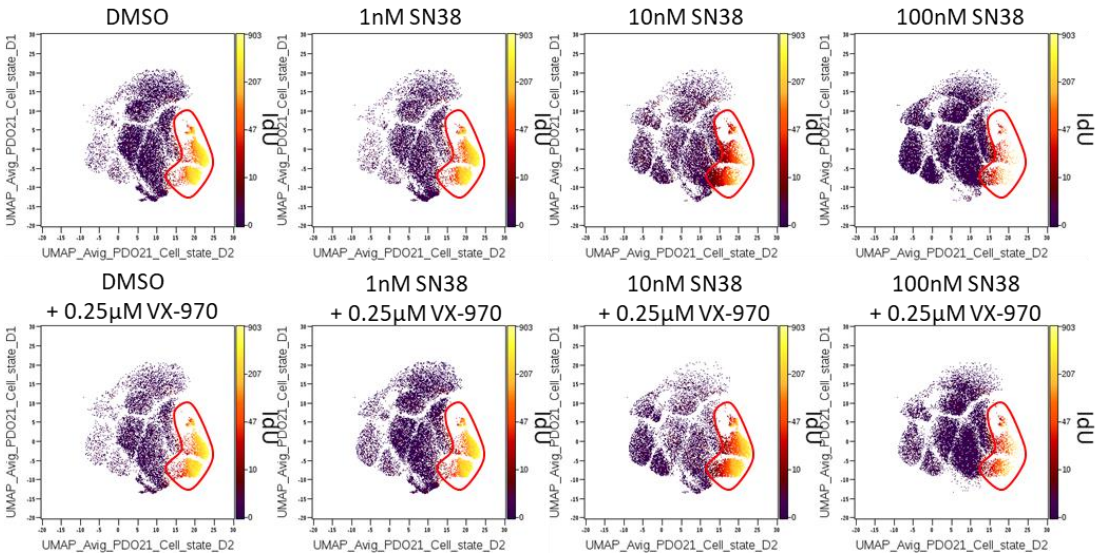

Figure 3.25. **VX-970 reduces SN38 induced S-phase block in PDO 021.**
Organoids were treated for 24 hours with the indicated drugs and IdU incorporation measured using the CyTOF technique. uMAPS were generated to cluster cells according to cell cycle markers and are coloured by the intensity of IdU staining. Cells in S-phase are encircled. Plots are representative of 3 technical repeats.

3.3.12 Increase in DNA-damage signalling detected in CRC PDOs using the CyTOF technique

Having visualised increased pDNA-PK and pATM levels in PDO 021 following SN38 and VX-970 combination therapy using Western blotting (Figure 3.21), markers of DNA damage in organoids were explored using the CyTOF technique. Although a panel of DNA-damage marker antibodies were conjugated with heavy metals for use, only pDNA-PK and pH2AX antibodies gave a reliable signal in a positive control experiment. At 24 hours following treatment, the percentage of pH2AX+ cells increased with SN38 monotherapy from 6.8% (± 0.20) in untreated cells to 19.5% (± 0.62, $p<0.0001$) with 1nM SN38, 59.36% (± 1.77 $p<0.0001$) with 10nM SN38, and 16.58% (± 0.22, $p=0.0006$) with 100nM SN38. VX-970 monotherapy and in combination with SN38 did not increase the percentage of pH2AX+ cells (Figure 3.26

B). The percentage of pH2AX+ cells remained constant at 48 and 72 hours (Figure 3.26 A, C and D).

At 48 hours of 100nM SN38 and VX-970 combination therapy, a population of cells with pH2AX signal several-fold higher than the remaining pH2AX+ cells was detected, this population is termed pH2AX high (Figure 3.26 A). The percentage of pH2AX high cells was much lower with 100nM SN38 monotherapy than with the combination therapy, 6.4% (± 2.0) vs 24.53% (± 2.3, $p<0.0001$). This pH2AX high population was also present in organoids treated with 10nM SN38 and VX-970 combination therapy, although to a lesser extent 5.7% (± 0.65) (Figure 3.26 A and F). The percentage of pH2AX high cells in organoids treated with 100nM SN38 and 0.025μM VX-970 combination therapy was reduced to 15.67% (± 1.6) by 72 hours (Figure 3.26 G).

Using the CyTOF technique, a signal is detected for each antibody target on a single cell level, allowing a relationship between different signals to be established. By looking at both the pH2AX signal and signal from cell state markers, the cell state of pH2AX+ cells could be investigated. Cells pH2AX+ (but not pH2AX high) had slightly higher levels of IdU and much higher levels of Geminin and PLK-1 than pH2AX- cells. The intensity of Cyclin B1 did not differ between pH2AX- and pH2AX+ cells, this indicates that these cells are in late S-phase (Figure 3.27 C-G). Cells positive for pH2AX did not have higher levels of cPARP or cCaspase than pH2AX- cells, suggesting that these cells were not apoptotic (Figure 3.27 A-B). There was no correlation between cells with pH2AX high signal and cell state, with cells not displaying higher signal of cCaspase-3, cPARP, Cyclin B1, IdU, Geminin, PLK or pHH3 than pH2AX+ or pH2AX- cells (Figure 3.28).

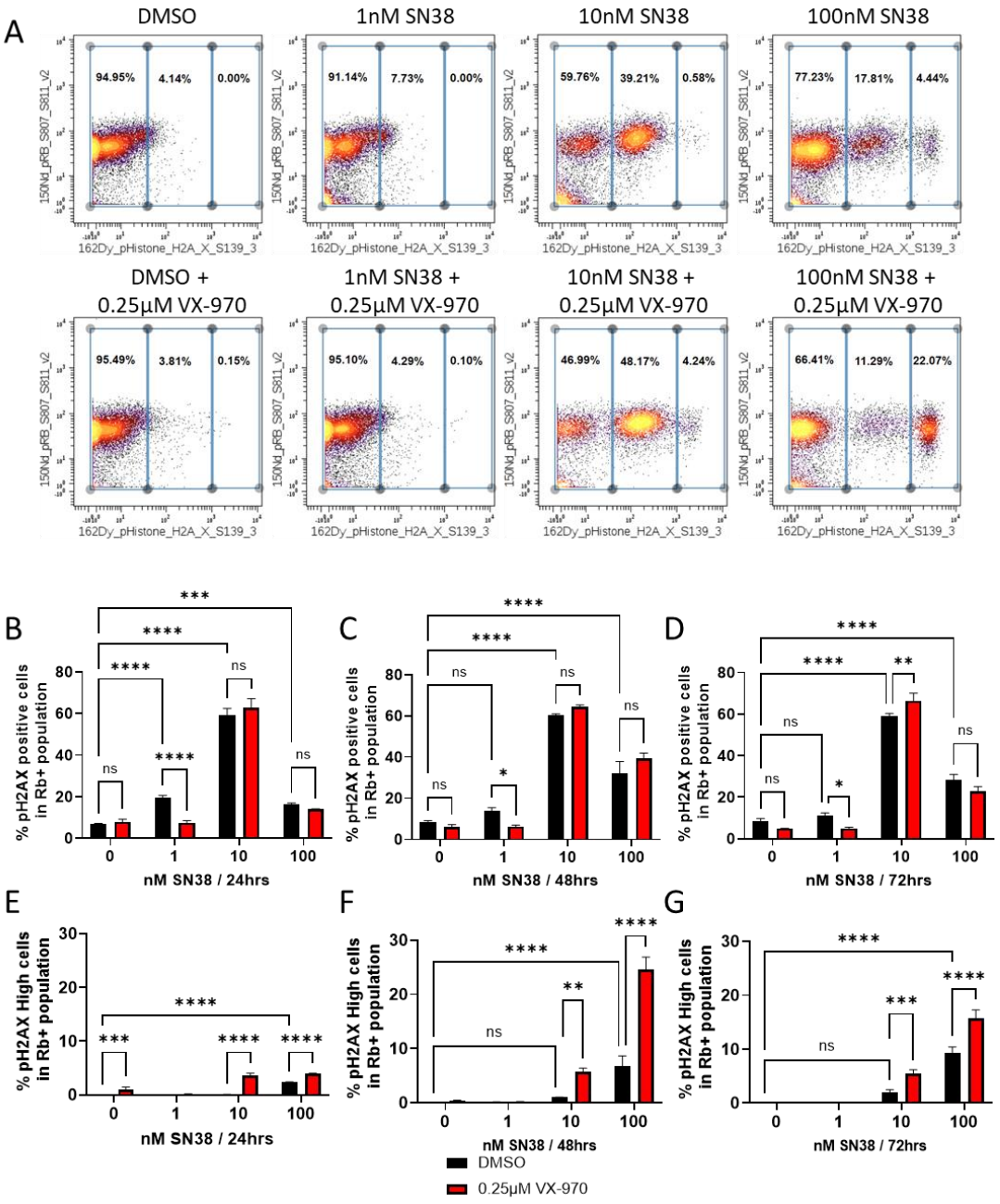

Figure 3.26. **VX-970 + SN38 results in a population of cells with high levels of pH2AX in PDO 021.**

A. Organoids were treated for 48 hours as indicated and analysed using the CyTOF technique. Plots are gated to show the population of cells which are pH2AX+ and those with high pH2AX signal. **B-D.** The percentage pH2AX+ cells at 24-72 hours. **E-G.** The percentage of cells with high pH2AX signal 24-72 hours. Plots are representative of 3 technical repeats. Statistical significance was calculated using the ANOVA test for multiple comparisons, *p* values ****<0.0001 ***<0.001 **<0.01 *<0.05. Each datapoint is the mean of 3 technical repeats. Error bars represent +/- SEM.

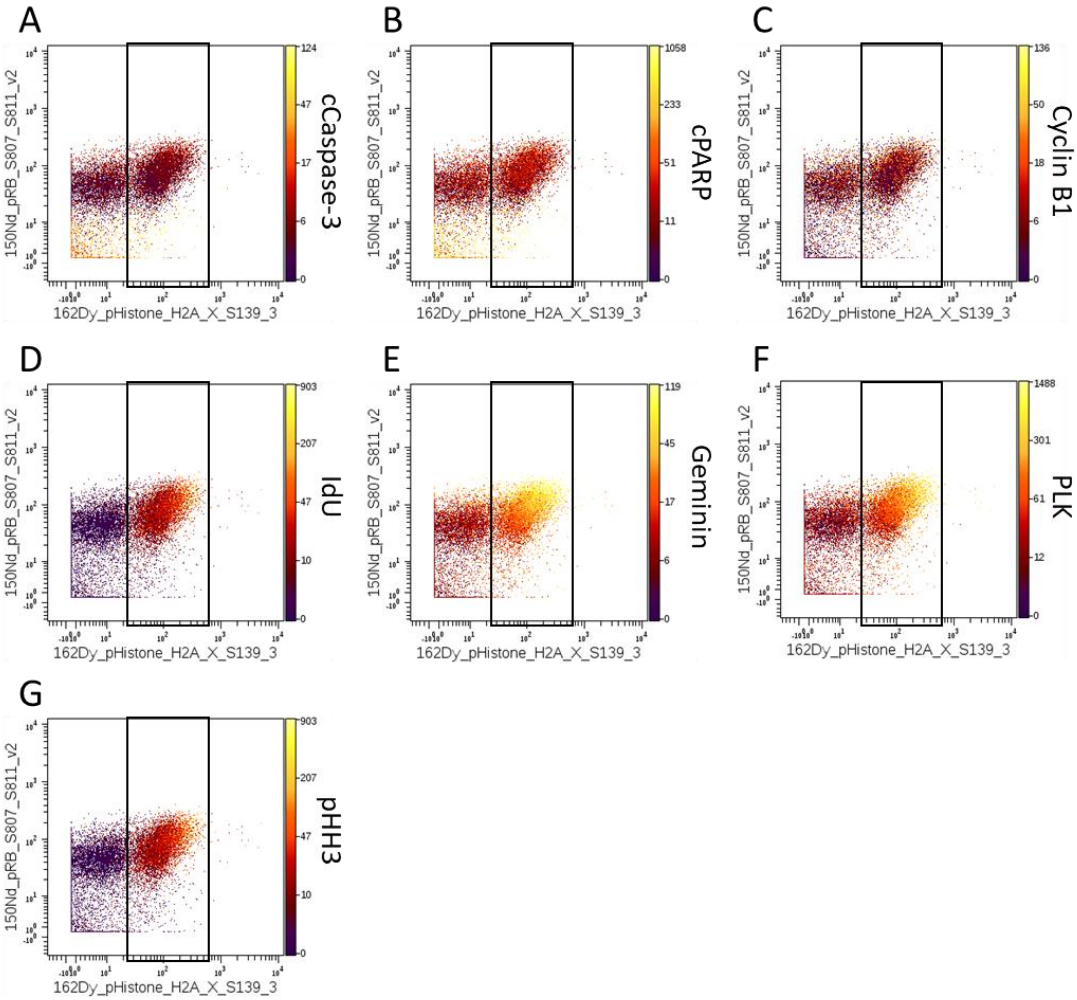

Figure 3.27. **pH2AX+ cells in PDO 021 treated with SN38 are in late S-Phase.**
Organoids were treated for 48 hours with 10nM SN38 and analysed using the CyTOF technique. Plots show pH2AX staining, with pH2AX+ cells shown in the rectangle. Cells in each plot are coloured according to the signal intensity of a cell state marker **A.** cCaspase-3 **B.** cPARP **C.** Cyclin B1 **D.** IdU **E.** Geminin **F.** PLK **G.** pHH3. Plots are representative of 3 technical repeats.

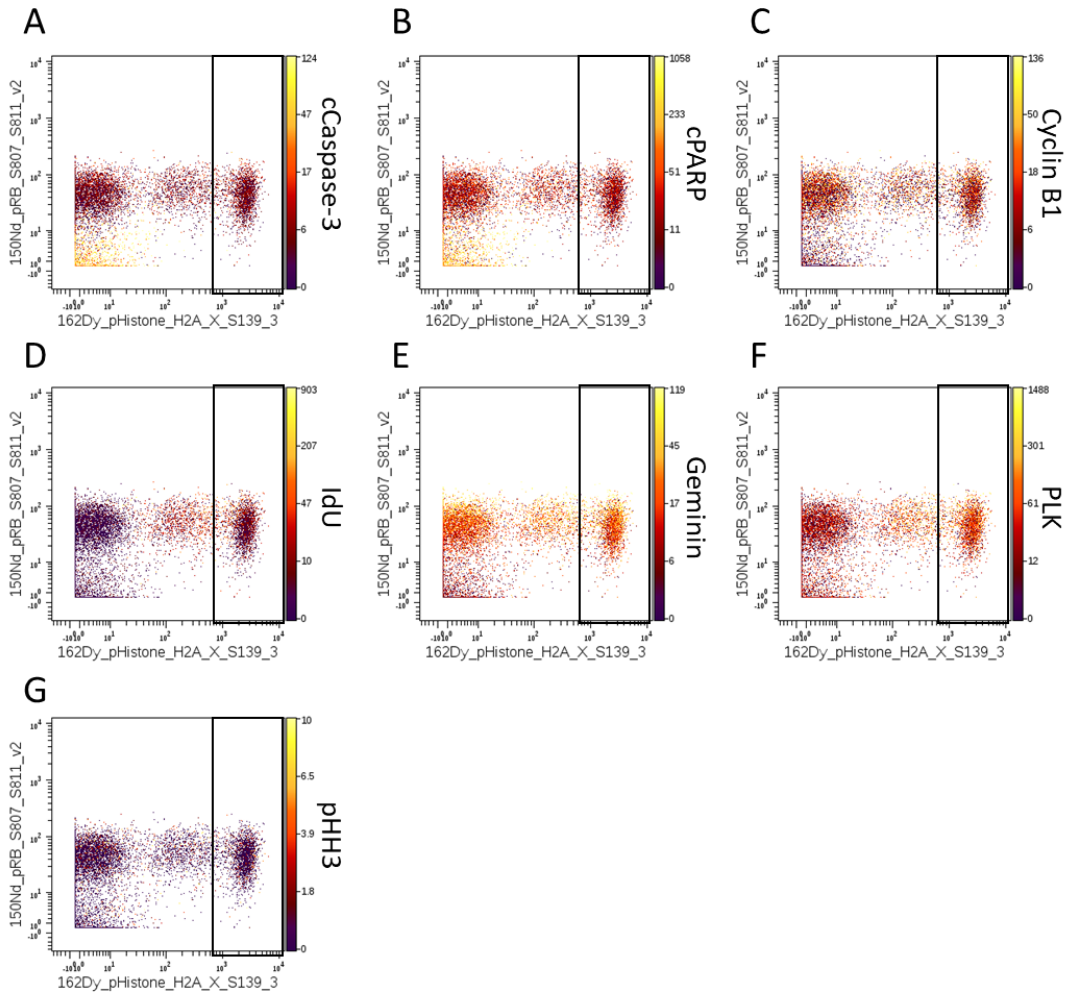

Figure 3.28. **High levels of pH2AX in organoids treated with SN38 + VX-970 does not correlate with cell state.**

Organoids were treated for 48 hours with 100nM SN38 + 0.25µM VX-970 and analysed using the CyTOF technique. Plots show pH2AX staining, with cells with high levels of pH2AX shown in the rectangle. Cells in each plot are coloured according to the signal intensity of a cell state marker **A.** cCaspase-3 **B.** cPARP **C.** Cyclin B1 **D.** IdU **E.** Geminin **F.** PLK **G.** pHH3. Plots are representative of 3 technical repeats.

Activation of DNA-PK was detected at 48 hours following 100nM SN38 and VX-970 combination therapy with 21.79% (± 1.64) cells being pDNA-PK+, compared to 4.93% (± 1.56) of cells treated with 100nM SN38 monotherapy. The percentage of pDNA-PK+ cells had fallen to 7.28% (± 0.57) by 72 hours (Figure 3.29 A-D). Interestingly, cells with high levels of pDNA-PK following SN38 and VX-970 combination treatment, also had very high levels of pH2AX (Figure 3.29 E).

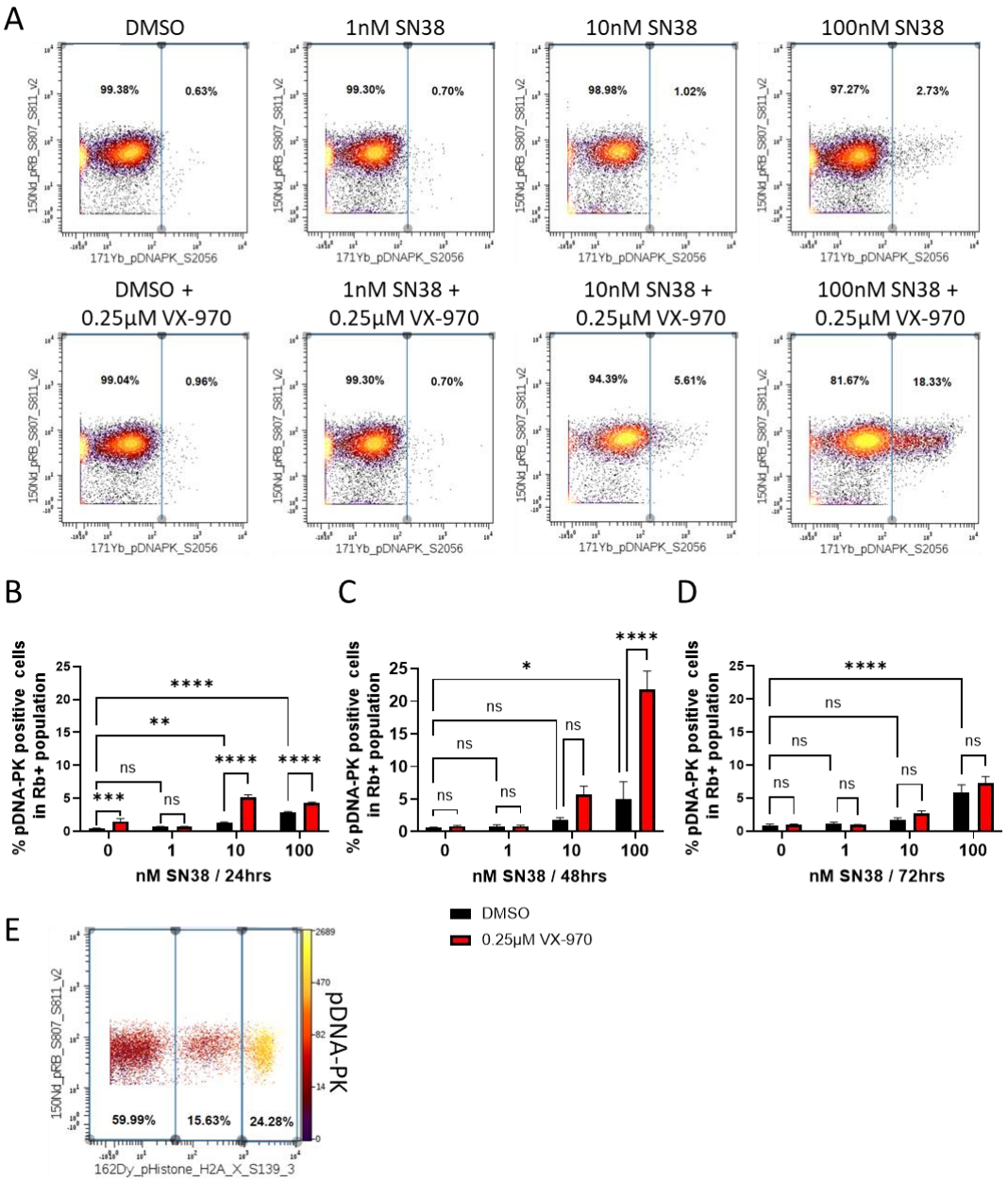

Figure 3.29. **SN38 + VX-970 treatment results in DNA-PK phosphorylation in PDO 021.** **A.** Organoids were treated for 48hrs as indicated and analysed using the CyTOF technique. Plots are gated to show the percentage pDNA-PK positive cells. **B.** The percentage pDNA-PK positive cells at 24 hours. **C.** The percentage pDNA-PK positive cells at 48 hours. **D.** The percentage pDNA-PK positive cells at 72 hours. **E.** Cells with high levels of pH2AX are also DNA-PK positive. Plots are representative of 3 technical repeats. Statistical significance was calculated using the ANOVA test for multiple comparisons, *p* values ****<0.0001 ***<0.001 **<0.01 *<0.05. Each datapoint is the mean of 3 technical repeats. Error bars represent +/- SEM.

In this section, it has been shown that SN38 and VX-970 treatment results in increased DNA damage in PDOs. This is supportive of the proposed mechanism of action of this combination treatment, with lack of ATR-induced S-phase arrest and DNA repair resulting in catastrophic DNA damage.

3.4 Discussion

3.4.1 TOP1 inhibition induces ATR activation

ATR has been proposed as a key modulator of the DNA damage response to TOP1ccs (Aris and Pommier 2012; Huntoon et al. 2013; Hur et al. 2021; Josse et al. 2014; Thomas et al. 2021). Treatment of cancer cell lines with TOP1 inhibitors CPT, LMP-400 and topotecan has been shown to activate the ATR signalling pathway, with pATR and pChk1 being detectable post treatment (Huntoon et al. 2013; Josse et al. 2014). Recently, irinotecan treatment has been shown to induce Chk1 phosphorylation in a TNBC xenograft model (Coussy et al. 2020). In this study, these findings were confirmed with phosphorylation of ATR and downstream kinase Chk1, as early as 2 hours post SN38 treatment in HCT116, HT29 and SW48 cells lines (Figure 3.2). Activation of ATR signalling was also observed in CRC PDO 021 following SN38 treatment, with increased Chk1 phosphorylation compared to untreated organoids (Figure 3.21).

Activation of ATR in response to SN38 treatment, provided a rationale for combination with ATR inhibitor VX-970 for increased cytotoxicity. VX-970 was found to completely abrogate ATR signalling at doses between 0.125µM and 0.25µM, with this being consistent across the CRC cell lines (Figure 3.4). A dose of 0.25µM VX-970 was also found to reduce SN38-induced phosphorylation of Chk1 in PDO 021 (Figure 3.21). The dose of VX-970 required to inhibit SN38-induced ATR signalling is close to the dose reported to inhibit platinum and irradiation induced ATR signalling (Hall et al. 2014; Leszczynska et al. 2016).

3.4.2 TOP1 and ATR inhibition is a highly synergistic combination

In the past few years, there have been multiple studies exploring the combination of TOP1 and ATR inhibition as a cancer therapeutic. Results have been highly promising, with the combination of a range of ATR and TOP1 inhibitors showing

efficacy in multiple cancer models (Coussy et al. 2020; Huntoon et al. 2013; Jo, Murai, et al. 2021; Jo, Senatorov, et al. 2021; Josse et al. 2014; Thomas et al. 2021). In the CRC setting, Josse et al., showed sensitisation of HCT116 and HT29 cell lines to TOP1 inhibitors LMP-400 and CPT with the addition of ATR inhibitor VE-821. The study also showed the combination of irinotecan and VX-970 to reduce tumour growth in a CRC xenograft model (Josse et al. 2014). Further preclinical exploration of the efficacy of SN38 (irinotecan) in combination with VX-970 is required in the CRC models.

In this study, we show the combination of SN38 and VX-970 to synergise to reduce both the proliferation and survival of CRC cells and organoids (Figure 3.5, Figure 3.6, Figure 3.19 and Figure 3.20). The CRC cell lines were selected due to their varied genetic background and subtypes. HCT116 cells are KRAS (G13D) and PIK3CA (H1047R) mutant, HT29 are BRAF (V600E), PIK3CA (P449T) and TP53 (R273H) mutant and SW48 are wild-type KRAS, BRAF, PIK3CA and TP53. HT29 cells are MSS and CIN+, while HCT116 cells are MSI and CIN-. The efficacy of the combination in all 3 cell lines suggest this therapeutic strategy may be efficacious for patients with tumours harbouring a range of genetic aberrations. The reduction in viability and organoid development with the SN38 and ATR combination treatment, suggests the efficacy observed may translate into the clinic for the treatment of CRC. Organoids are an excellent tumour model, with stem cells dividing and differentiating to give a mature tumour organoid containing a heterozygous population of cells (Clevers 2016).

HCT116 cells displayed greater sensitivity to 72-hours VX-970 monotherapy when seeded at low density for proliferation and clonogenic assays, than HT29 and SW48 cells. At low seeding density, HCT116 cells underwent ~4 cycles of cell division, compared to ~3 rounds in SW48 and HT29 cells in a 72-hour time period. A previous study has demonstrated that a reduction of viability in response to ATR loss occurs after approximately 3 cell cycles, providing an explanation for increased loss of

viability in HCT116 cells (Brown and Baltimore 2000). When seeded at a higher density, HCT116 cells only underwent approximately 2 rounds of cell division and demonstrated very little loss of viability (Figure 3.3). These data suggest rapidly dividing cells are likely to be the most sensitive to the TOP1 and ATR inhibitor combination, as it was previously described for irinotecan monotherapy (Horwitz and Horwitz 1973; Hsiang, Lihou, and Liu 1989).

Despite a reduction in viability of PDO 021 and 027 with the addition of VX-970 to SN38 combination treatment, no increase in cPARP or cCaspase 3 was observed in PDO 021 with CyTOF analysis following SN38 and VX-970 combination therapy (Figure 3.22). This does not correlate with the increased cCaspase 3 reported following the treatment of ovarian cancer cell lines with belotecan and AZD6738 combination therapy (Hur et al. 2021). The organoids were treated 5 days post seeding and had developed into established organoids. The drug containing media was left on the organoids over the 72-hour period. The percentage of untreated organoid cells in S-phase was very low at 48 and 72 hours, just 17% and 5% compared to 35% at 24 hours (Figure 3.23). The reduction in S-phase cells, is likely due to the increase in organoid size and media depletion over the course of the experiment. The cytotoxicity of TOP1 and ATR inhibition require S-phase progression (Horwitz and Horwitz 1973; Hsiang, Lihou, and Liu 1989; Josse et al. 2014), with a reduction in cell cycling likely responsible for the lack of synergy observed. To assess SN38 and VX-970 induced cell death using the CyTOF technique, younger organoids should be used and drug containing media should be replaced over the experiment time course.

3.4.3 Loss of ATR results in S-phase progression in the presence of SN38-induced DNA damage

Treatment of cells with TOP1 inhibitors rapidly induces S-phase arrest. Pulse labelling of cells with modified nucleotides has demonstrated lack of replication fork initiation and progression with the TOP1 inhibitor, LMP-400. Inhibition of Chk1, restored both replication and initiation, demonstrating the role of ATR signalling in the activation of cell cycle checkpoints (Seiler et al. 2007). The mechanism by which ATR induces cell cycle arrest is covered in section 1.5.3. Several studies have shown ATR inhibition to force the progression of cells through S-phase and G2-M transition despite high levels of TOP1cc-induced DNA damage (Huntoon et al. 2013; Hur et al. 2021; Josse et al. 2014; Thomas et al. 2021). In one study, the DNA fibre technique demonstrated replication fork stalling in HT29 cells treated with CPT and LMP-400 monotherapy, with very slow nucleotide incorporation. The addition of VE-821 to TOP1 inhibition reversed this effect, with the rate of nucleotide incorporation returning to almost the same rate as untreated cells (Josse et al. 2014). The same effect was also observed with the combination of topotecan and VX-970 in a SCLC cell line (Thomas et al. 2021). Loss of the S-phase and G2/M checkpoint have also been reported with the combined ATR and TOP1 inhibition in ovarian cancer cell lines (Huntoon et al. 2013; Hur et al. 2021). Loss of S-phase and G2/M cell cycle checkpoints has also been reported when combining ATR inhibition with radiotherapy and gemcitabine, cytarabine and platinum-based therapies (Dillon et al. 2017; Fokas et al. 2012; Fordham et al. 2018; Huntoon et al. 2013; Pires et al. 2012; Prevo et al. 2012; Tu et al. 2018).

We have demonstrated the same effect in CRC organoids (Figure 3.24 and Figure 3.25). The rate of IdU incorporation is severely reduced in S-phase organoids treated with SN38, demonstrating the stalling of replication forks. The addition of VX-970 to SN38 treatment, returns the rate of IdU incorporation close to that observed in

untreated organoids. Continued progression through S-phase in the presence of DNA damage, is likely to lead to catastrophic levels of DNA damage.

3.4.4 High levels of DNA damage observed with combined inhibition of TOP1 and ATR

TOP1 inhibition-induced DNA DSBs occur following replication and transcription machinery collision with TOP1ccs. An imaging study by Berniak et al., has shown an accumulation of ɣH2AX at DNA replication sites following TOP1 inhibition, demonstrating the role of replication run off in DSB formation (Berniak et al. 2013). This supports our findings that organoid cells positive for ɣH2AX following SN38 monotherapy, are in late S-phase (Figure 3.27). ATR signalling inhibition in the presence of TOP1ccs, prevents cell cycle arrest and drives replication fork progression (Hur et al. 2021; Josse et al. 2014; Thomas et al. 2021). Continued S-phase progression in the presence of TOP1ccs, would result in increased replication run off and increased DSB accumulation. Furthermore, ATR inhibition has been found to increase the levels of trapped TOP1ccs following TOP1 inhibition, showing ATR to play a role in the early stages of TOP1cc resolution (Thomas et al. 2021). An increase in the number of TOP1ccs, and loss of replication fork arrest, would lead to an increase in replication run off and the subsequent DSBs.

Increased ɣH2AX accumulation has been reported following VE-821 and TOP1 combination therapy in HT29 cells, and AZD7638 and belotecan therapy in ovarian cancer cell lines (Hur et al. 2021; Josse et al. 2014). Furthermore, in a phase I clinical trial of topotecan and VX-970 in patients with advanced solid tumours (NCT02487095), hair samples were collected to measure cellular ɣH2AX levels. Patients who received topotecan and VX-970 had significantly higher levels of ɣH2AX than patients who had received topotecan monotherapy (Thomas et al. 2018).

In this study, we show increased ɣH2AX accumulation in HCT116 and HT29 cells with SN38 and VX-970 combination therapy (Figure 3.4). Combination treatment also resulted in the phosphorylation of DNA-PK and ATM in HT29 and HCT116 cells (Figure 3.7 and Figure 3.8). DNA-PK and ATM are rapidly phosphorylated in response to DNA DSBs (Bakkenist and Kastan 2003; Chan et al. 2002; Chen et al. 2005), further supporting an increase in DSB accumulation with the combination treatment. These findings are supported by a study combining SN38 with VE-821 and PARP inhibition, which showed DNA-PK phosphorylation with the combination of SN38 and VE-821 in HCT116 and HT29 cells (Abu-Sanad et al. 2015). ATR inhibition in combination with DNA-damaging therapeutics, gemcitabine and oxaliplatin has also been shown to induce phosphorylation of DNA-PK and ATM (Combès et al. 2019; Dunlop et al. 2020; Wallez et al. 2018).

In HT29, and to a lesser extent HCT116 cells, as well as in PDO 021 the combination treatment resulted in a reduction of pChk2 at the expected MW ~60kDa, and the appearance of a band at ~40kDa (Figure 3.7 and Figure 3.21). It has been previously reported, that on Chk2 activation, the kinase transiently dimerises, which protects the kinase form proteolytic cleavage. However, following activation, separation of the dimer occurs, with cleavage resulting in a digest with a reduced molecular weight (Cai, Chehab, and Pavletich 2009). Mass spectrometry of cell lysates could be used to identify Chk2 cleavage products.

Despite SN38 and VX-970 combination therapy being highly synergistic in SW48 cells, we were unable to detect increased DNA-PK, ATM or H2AX phosphorylation. Phosphorylation of these DNA damage markers occurred with 10nM and 100nM SN38 monotherapy, but no further increase was observed with the addition of VX-970. However, we did observe an increase in Chk2 phosphorylation with the addition of VX-970 to very low dose 1nM SN38 treatment at 24 hours, suggesting activation of DNA damage repair pathways downstream of ATM, (Figure 3.7 and Figure 3.9)

however it is possible that this is non-canonical Chk2 signalling. The synergy to reduce proliferation and survival was observed with very low doses of SN38 and VX-970 treatment for a period of 72 hours. It is possible that using a longer time course with low dose SN38 would have resulted in increased DNA damage detection with the combination therapy. It is also possible that the ATR inhibition causes off-target toxicity in the SW48 cells, resulting in a mechanism of cell death which differed from that observed in HT29 and HCT116 cells.

Using the CyTOF technique we identified combination treated organoids to have a several fold increase in ɣH2AX accumulation compared to organoids treated with SN38 monotherapy (Figure 3.26). This very high level of ɣH2AX accumulation may be pan-nuclear ɣH2AX, which has been shown to occur with lethal levels of DNA damage and replication stress (Ding et al. 2016; Meyer et al. 2013; Moeglin et al. 2019; Parsels et al. 2018). Loss of ATR function in Myc-driven tumours and cancer models has previously been shown to induce pan-nuclear ɣH2AX (Murga et al. 2011; Toledo et al. 2011). Pan-nuclear ɣH2AX following CPT and VE-821 combination therapy in HT29 cells, and AZD6738 and belotecan combination therapy in ovarian cancer cell lines has also been reported (Hur et al. 2021; Josse et al. 2014). The generation of pan-nuclear ɣH2AX in response to DNA damage is dependent on DNA-PK and ATM activation (Meyer et al. 2013).

Using the CyTOF technique we were able to show DNA-PK phosphorylation in cells with very high levels of ɣH2AX, suggesting that the phosphorylation of H2AX in response to DNA damage is at least in part mediated by DNA-PK (Figure 3.29). In corroboration with this finding, we also identified phosphorylation of ATM and DNA-PK in PDO 021, following SN38 and VX-970 combination treatment by Western blotting (Figure 3.21). Organoid cells with very high levels of ɣH2AX, were not cPARP or cCaspase-3 positive, suggesting that they were not apoptotic (Figure 3.28).

We found VX-970 to reduce SN38-induced p53 phosphorylation in the CRC cell lines and organoids (Figure 3.4, Figure 3.7, Figure 3.8, Figure 3.9 and Figure 3.21). It is well established that p53 is a downstream target of ATM, which would be suggestive of increased p53 phosphorylation with combination treatment (Banin et al. 1998; Canman et al. 1998). While ATM is the main kinase phosphorylating p53 in the context of DNA damage, ATR has been shown to be the principal kinase phosphorylating p53 in response to hypoxia induced replication stress, with ATR kinase dead mutant cells displaying marked loss of hypoxia induced p53 phosphorylation (Hammond et al. 2002). This finding was confirmed by a further study, with ATR inhibitor VE-821 reducing hypoxia induced p53 phosphorylation in CRC cell lines (Pires et al. 2012). Furthermore, p53 levels were found to be reduced with the addition of VE-821 to cisplatin, suggesting increased p53 degradation (Reaper et al. 2011). Overexpression of kinase-dead ATR was shown to reduce p53 phosphorylation and stabilisation in response to UV-induced DNA damage (Tibbetts et al. 1999). ATR inhibition does not lead to a reduction in radiation-induced p53 phosphorylation, suggesting that ATM and ATR may phosphorylate p53 in response to different types of genomic stress or at different stages of the cell cycle (Combès et al. 2019; Hammond et al. 2002).

While phosphorylation of H2AX, DNA-PK and ATM are well established surrogate markers of DNA-DSBs, they do not directly measure the extent of DNA damage. In this study, using the neutral comet assay, we were able to demonstrate high levels of DNA DSBs in HT29 and HCT116 cells following SN38 and VX-970 combination therapy (Figure 3.10 and Figure 3.11). Our findings are supported by a recent study showing increased DNA strand breaks following topotecan and VX-970 combination treatment in a SCLC cell line using the alkaline comet assay (Thomas et al. 2021). While the alkaline comet assay does not enable distinction between DNA DSBs and

SSBs, it does provide evidence of increased strand breaks with the combination therapy.

3.4.5 DNA damage in HT29 cells leads to cGAS activation, but no secretion of immunomodulatory factors

DNA DSBs only progress to form micronuclei if cells pass through the G2/M checkpoint, with inhibition of Cdk1 preventing the formation of radiation-induced micronuclei (Feng et al. 2020). In the presence of ATR, cells are arrested at the G2/M checkpoint and DSBs are repaired, limiting the formation of radiation induced micronuclei (Chen et al. 2020). In this study we show that SN38 and VX-970 combination therapy induced DSBs persist through the cell cycle, leading to the formation of micronuclei (Figure 3.14). Cytosolic DNA and micronuclei have also been reported when ATR inhibition is combined with PARP inhibition and platinum-based therapy (Combès et al. 2019; Schoonen et al. 2019).

Recent studies have shown micronuclei formed in cells treated with ATR inhibition in the context of DNA damage (irradiation and olaparib) leads to activation of the cGAS-STING pathway. cGAS was found to colocalise with the micronuclei and activate the STING signalling pathway, leading to the production of cytokines and interferons (Chen et al. 2020; Feng et al. 2020; Schoonen et al. 2019; Sheng et al. 2020). Approximately 50% of micronuclei have compromised envelope integrity, allowing cGAS to recognize and bind their dsDNA contents (Hatch et al. 2013). In this study, we showed the colocalisation of cGAS with micronuclei following SN38 and VX-970 combination therapy of HT29 cells (Figure 3.16). Although colocalisation of cGAS and micronuclei is indicative of activation of the cGAS-STING pathway, we were unable to detect any change in the secretions of interferons or cytokines (Figure 3.17). Functionality of the cGAS-STING pathway could also be assessed by Western blot

by exploring the phosphorylation of downstream STING targets, such as TBK1 and IRF3 (Vanpouille-Box et al. 2018).

Deregulation of the STING signalling pathway has been reported to prevent DNA damage associated immune responses in CRC cell lines and mouse models. One study found the majority of a large panel of CRC cell lines to have loss of cGAS and / or STING expression. None of the 11 CRC were able to produce IFNs to the same level as a non-tumour colorectal cell lines in response to dsDNA (Xia et al. 2016). Our analysis of CRC cell lines, showed CACO2, HCT116, HT29, LS174T and SW48 cell lines to all have loss of cGAS and / or STING (Figure 3.19). However, while the study of Xia et al., reported only a part loss of STING in HT29 cells, we were unable to detect any STING expression at all by Western blotting. This suggests that loss of STING in the HT29 cells has occurred post-cell line development. Ongoing work in our laboratory is exploring means of re-establish STING expression, to allow for a link between DNA damage and immune activation to be explored.

3.5 Conclusions

The work in this chapter demonstrates a synergistic interaction between SN38 and VX-970 in CRC cell lines and patient derived organoids. We were able to show that the combination therapy results in higher levels of DNA-PK, ATM and H2AX phosphorylation, increased DNA DSBs and increased micronuclei formation than SN38 monotherapy. These findings suggest increased DNA damage as a mechanism for the increased cytotoxicity observed. While the combination therapy resulted in detection of DNA damage by cGAS, we were unable to show any downstream immunostimulatory secretion phenotype. Restoration of cGAS-STING pathway function in CRC models, may enable the increased DNA damage to generate an anti-tumour immune response.

4 ATR inhibition sensitises CRC cell lines and organoids to DS-8201a

4.1 Introduction

4.1.1 Barriers to ADC therapy in colorectal cancer

There are currently no ADCs which have been licensed for use in the treatment of CRC. The development of ADCs for the treatment of solid tumours including CRC, has been hampered by multiple factors including lack of tumour specific antigens, low expression of tumour associated antigens, and heterogeneity of target antigen expression (Abdollahpour-Alitappeh et al. 2019). DS-8201a was developed as a highly potent HER2 targeting ADC, and has been approved for the treatment of metastatic HER2+ breast and gastric cancers (Narayan et al. 2021; Shitara et al. 2020). Only 2-3% of CRC patients have HER2 amplified tumours, which suggests that a very limited number of patients may benefit from a HER2 targeting ADC (Ross et al. 2018; Siena et al. 2018). HER2 targeting ADC, T-DM1 has only shown efficacy in cancers with high levels of HER2 expression, and has only been approved for HER2 IHC3+ or IHC2+/FISH+ tumours, making this an unsuitable therapeutic option for CRC (von Minckwitz et al. 2019). However, there are several properties of DS-8201a which make it more potent than T-DM1, making it a potential therapeutic option for HER2-low expressing or HER2 heterogenous cancers.

4.1.2 DS-8201a shows efficacy in low HER2 expressing cancer models

To compare the HER2 expression level required for treatment with T-DM1 and DS-8201a, Ogitani et al., used four mice xenografts with differing HER2 levels. T-DM1 was found to be only effective against the highest HER2 expressing breast cancer model (KPL-4), while DS-8201a was also effective against the moderately HER2 expressing breast cancer model (JIMT-1) and the comparatively low expressing

HER2 pancreatic cancer model (CAPAN-1). Neither ADC showed efficacy against the HER2- gastric cancer model (GCIY) (Ogitani, Aida, et al. 2016). It must be noted while this demonstrates a lower requirement of HER2 expression for the DS-8201a treatment in comparison to T-DM1 treatment, Capan-1 the lowest expressing HER2 model used, has been described as HER2 amplified (Kimura et al. 2006). The lower HER2 expression requirement of DS-8201a was also demonstrated using patient derived xenograft (PDX) breast cancer models. Both T-DM1 and DS-8201a delayed the growth of HER2+/FISH+ tumours, however only DS-8201a and not T-DM1 treatment led to tumour eradication in 3/5 mice (Ogitani, Aida, et al. 2016). Furthermore, DS-8201a treatment led to marked tumour regression in two HER2 IHC1+/FISH- models, while T-DM1 failed to inhibit tumour growth (Ogitani, Aida, et al. 2016).

To assess whether the high DAR of DS-8201a reduces the threshold of HER2 expression required for sensitivity, a low DAR ADC was developed by Daiichi Sankyo with a mean DAR of 3.4. The low DAR ADC did not completely inhibit the growth of the moderate HER2+ breast xenograft, and caused only very moderate tumour growth inhibition in the CAPAN-1 pancreas model. This demonstrates that the high DAR of DS-8201a enables sufficient payload delivery to induce cytotoxicity even in lower HER2 expressing tumours (Ogitani, Aida, et al. 2016).

The efficacy of DS-8201a in HER2-low expressing tumours was also demonstrated in the phase II DESTINY-Breast01 trial (NCT03248492) which included 54 patients with HER2 IHC2+/FISH- or HER2 IHC1+/FISH- metastatic breast cancers. The trial reported a confirmed response rate of 37% and PFS of 11.1 months (Modi, Park, et al. 2020). This finding suggests that a relatively low HER2 expression level is sufficient for DS-8201a efficacy in some patients.

4.1.3 DS-8201a elicits the bystander effect in HER2 heterogeneous cancers

HER2 expression heterogeneity has been reported in multiple cancer types (Bethune, Mullen, and Chang 2015; Lee et al. 2013). Tumours bearing heterogenous expression of HER2 do not respond well to T-DM1 therapy, with only HER2+ cells being eliminated (Ogitani, Hagihara, et al. 2016). The DS-8201a payload is highly membrane permeable, giving it the potential to cross the plasma membrane and penetrate neighbouring cells (Ogitani, Hagihara, et al. 2016). The ability to induce the bystander effect, could render DS-8201a efficacious in CRC patients with heterogenous HER2 expression.

The bystander effect of DS-8201a has been demonstrated *in vitro* and *in vivo*. DS-8201a treatment of a HER2+ and HER2- breast cancer cell line coculture, resulted in killing of both cell lines. In contrast, treatment with T-DM1 killed only the HER2+ cells. *In vivo*, DS-8201a treatment of a heterogenic mouse model, bearing a mixed tumour of HER2+ and HER2- cells resulted in eradication of both HER2+ and HER2- cells. Treatment with T-DM1 only killed HER2+ cells (Ogitani, Hagihara, et al. 2016). Phosphor-integrated dot imaging analysis of a HER2+/HER2- heterogenous breast cancer xenograft showed accumulation of the HER2 mAb component of DS-8201a only in HER2+ areas of the tumour, however Dxd could be visualised in both HER2+ and HER2- regions of the tumour, showing that the cytotoxic payload was delivered by the bystander effect to HER2- regions of tumours (Suzuki et al. 2021).

4.1.4 Evaluation of DS-8201a as a treatment option for mCRC

A study by Takegawa et al., found CRC cell lines (HCT116, HT29, SW48 and SW480) which all express very low levels of HER2 to be resistant to DS-8201a, but sensitive to Dxd. Ectopic expression of HER2 increased the DS-8201a sensitivity of CRC cells to levels observed in a HER2+ gastric cancer cell line, demonstrating a threshold of HER2 expression for DS-8201a efficacy (Takegawa et al. 2019). This suggests that

DS-8201a is unlikely to be efficacious as a monotherapy in CRC with very low HER2 expression.

The DESTINY-CRC01 (NCT03384940) trial investigated the efficacy of DS-8201a as monotherapy in mCRC patients with both high and low levels of HER2 expression. The trial included three cohorts, categorised based on HER2 expression, cohort A IHC3+/FISH+, Cohort B IHC2+/FISH- and Cohort C IHC1+/FISH-. Of the 78 patients enrolled in cohort A, 45.3% had a confirmed objective response and one patient had a CR. PFS in cohort A was 6.9 months. At the time of publishing, only 7 patients were enrolled in cohort B and 18 in cohort C, of these none had an objective response and PFS was not evaluable (Siena et al. 2021). Due to the promising outcome in patients with HER2-high expressing tumours, a further trial has been set up for patients with HER2 overexpressing mCRC. Although very limited data was reported, DS-8201a did not appear to be efficacious as a monotherapy in HER2-low expressing CRC.

4.1.5 ATR inhibition could sensitise CRC to DS-8201a

As Dxd is a potent TOP1 inhibitor, it would be expected that DS-8201a would induce replication stress and the activation of ATR signalling. Indeed, DS-8201a treatment of a HER2+ breast cancer cell line has been shown to cause Chk1 phosphorylation, demonstrating activation of ATR signalling (Ogitani, Aida, et al. 2016). In this study, we have shown ATR inhibition to synergise with SN38, sensitising CRC cell lines and organoids to very low doses of SN38. The efficacy of DS-8201a in HER2-low expressing cancers is limited by low ADC internalization and payload accumulation. As we have found ATR inhibition to reduce the cytotoxic dose of TOP1 inhibition, ATR inhibitors may sensitise CRC models to DS-8201a.

4.2 Research aim

The aim of this chapter is to investigate the sensitivity of a panel of CRC cell lines and patient derived organoids to DS-8201a as a monotherapy and in combination with ATR inhibitors AZD6738 and VX-970. This will inform as to whether ATR inhibition can be used to sensitise HER2-low expressing CRC to DS-8201a therapy.

4.3 Results

4.3.1 Low HER2 expressing CRC cell lines are resistant to DS-8201a

As DS-8201a is a HER2-targeting ADC, the HER2 status of a panel of 5 CRC cell lines was established prior to drug testing. Using Western blotting the HER2 levels in CACO2, HCT116, HT29, LS174T and SW48 CRC cell lines were compared with the HER2+ breast cancer cell line HCC1954 and the HER2- breast cancer cell line MDA-MB-231 (Figure 4.1 A-B). All 5 CRC cell lines had higher HER2 expression than the HER2- breast cancer cell line, but markedly lower expression than the HER2+ breast cancer cell line. The highest HER2 expression of the CRC cell lines was observed in SW48 cells. IHC was used to score the HER2 expression status of the CRC cell lines, with HCT116 scoring as HER2 IHC-, and the remaining cell lines, HER2 IHC1+ (Figure 4.1 C-D).

To assess the effect DS-8201a had on the proliferation of CRC cell lines, cells were treated with a dose range of DS-8201a for 6 days. Growth inhibition was measured using the SRB assay (Figure 4.2). As expected, the HER2+ breast cancer cell line displayed sensitivity to DS-8201a, with proliferation reduced to 25.03% (± 1.77) with 0.1µg/mL DS-8201a. SW48 cells showed some sensitivity to 10µg/mL, with proliferation reduced to 74.12% (± 5.0). None of the other CRC cell lines had a greater than 10% reduction in proliferation with the highest dose of 10µg/mL.

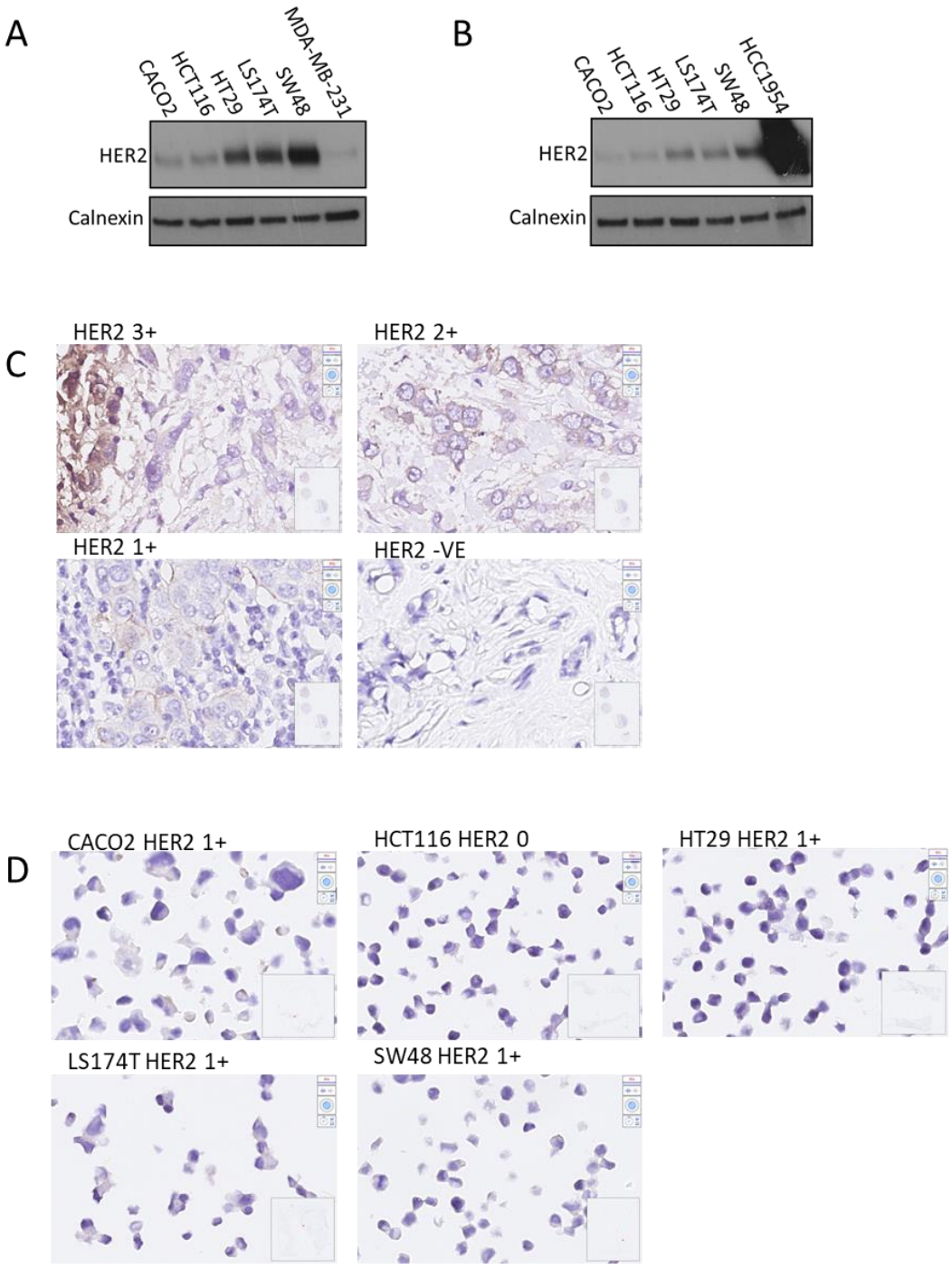

Figure 4.1. **Low levels of HER2 expression in CRC cell lines.**

A. HER2 expression level was analysed by Western blotting in a panel of CRC cells compared with the HER2- breast cancer cell line MDA-MB-231. **B.** HER2 expression level was analysed by Western blotting in a panel of CRC cell lines compared with the HER2+ breast cancer cell line HCC1954. **C.** HER2 (Brown) and H & E (Purple) IHC staining of patient tumours to act as a reference for CRC cell lines**. D.** HER2 (Brown) and H & E (Purple) IHC staining of CRC cell lines.

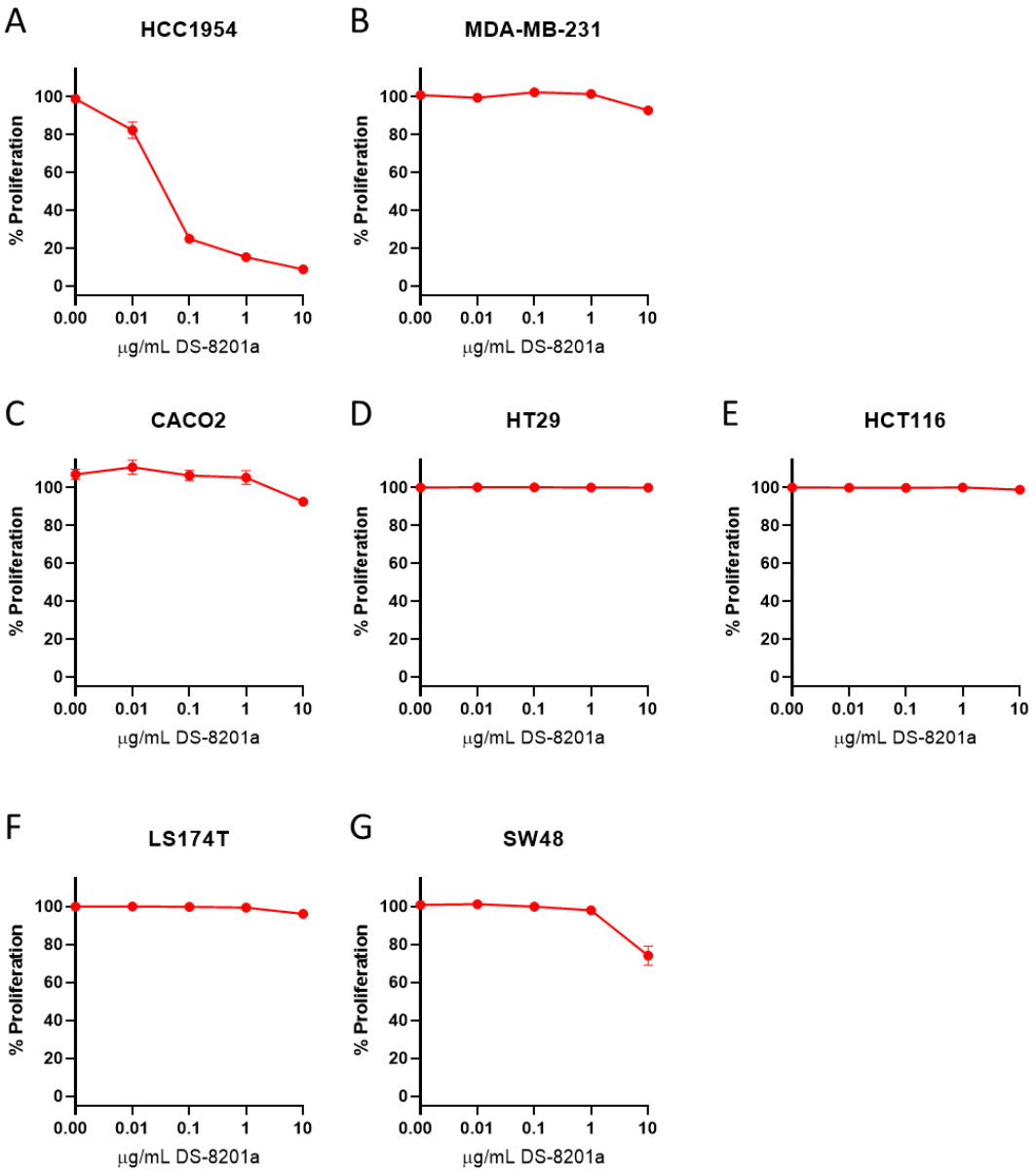

Figure 4.2. **DS-8201a causes almost no growth inhibition in a panel of CRC cell lines.** Cells were treated with the indicated doses of DS-8201a for 6 days. The SRB assay was used to calculate proliferation rates. **A.** HCC1954 cells (HER2+ breast cancer) **B.** MDA-MB-231 cells (HER2- breast cancer) **C.** CACO2 cells. **D.** HCT116 cells **E.** HT29 cells **F.** LS174T cells **G.** SW48 cells. Each datapoint is the mean of 3 biological repeats. Error bars represent +/- SEM.

Having established that DS-8201a had very little effect on the proliferation of CRC cell lines, we investigated the effect of DS-8201a on cell survival using the clonogenic assay. Two different treatment schedules were used, 72 hours treatment followed by drug removal, and 2 weeks continuous drug exposure (Figure 4.3 A and Figure 4.4 A). The survival of HCT116 cells was reduced to 75.49% with 72 hours 10µg/mL DS-8201a treatment, none of the other cell lines had a notable reduction in survival (Figure 4.3). The cell lines showed greater sensitivity to 2-week therapy, with survival reduced to 65.2% (± 3.7) in HCT116 cells, 55.8% (± 9.1) in LS174T cells and 34.4% (± 4.8%) in SW48 cells (Figure 4.4).

These findings show very reduced sensitivity of HER2-low expressing CRC to DS-8201a in comparison to a HER2 overexpressing breast cancer cell line. This suggest that DS-8201a monotherapy is unlikely to be an effective therapy in the treatment of HER2-low expressing CRC.

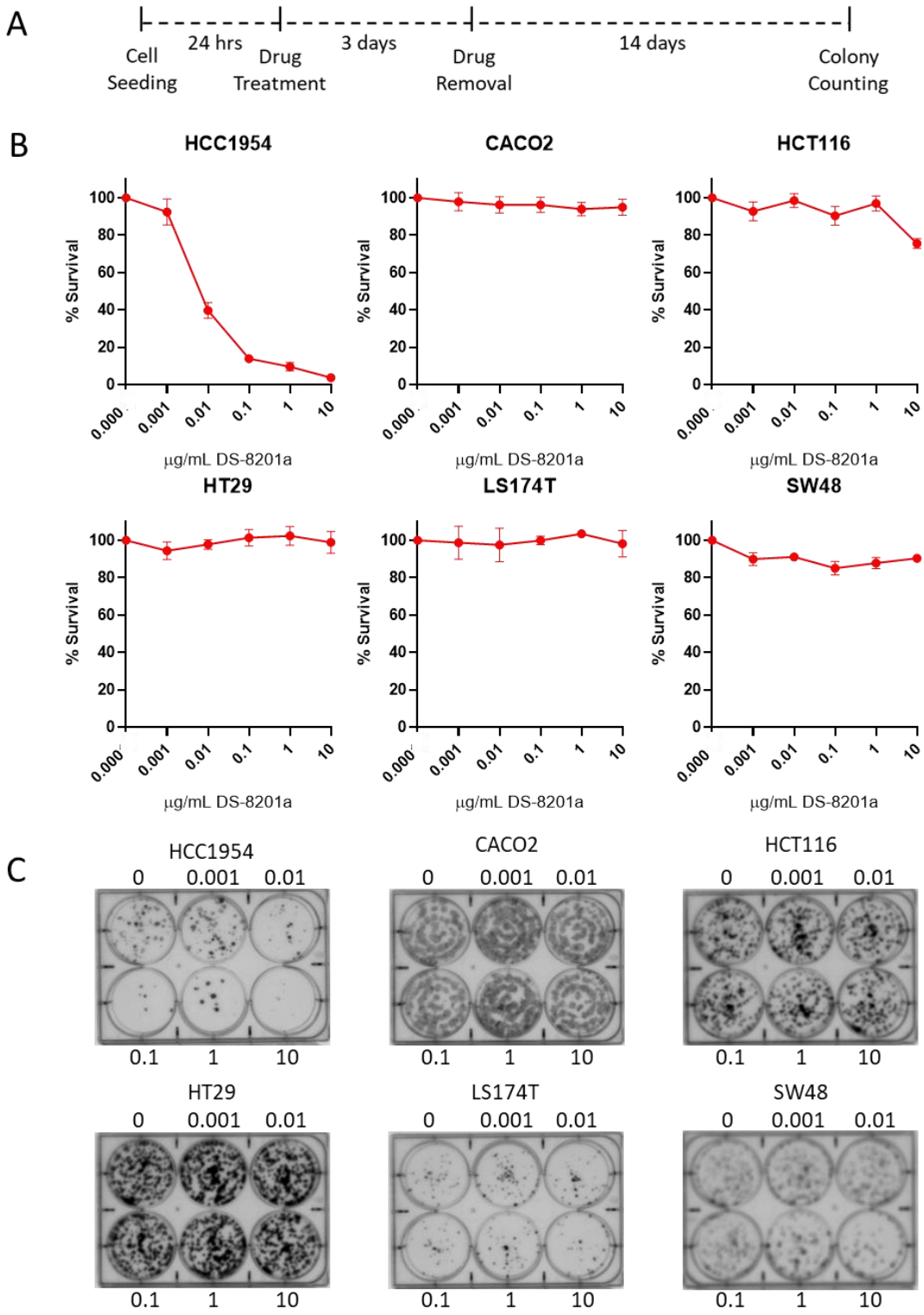

Figure 4.3. **3-day DS-8201a treatment has almost no effect on CRC cell survival.**

A. Scheme demonstrating the treatment and clonogenic assay schedule followed. **B.** The percentage survival following DS-8201a treatment for HCC1954 cells (HER2+ breast cancer) and a panel of CRC cell lines. Each datapoint is the mean of 3 biological repeats. Error bars represent +/- SEM. **C.** Representative images of clonogenic plates for each cell line.

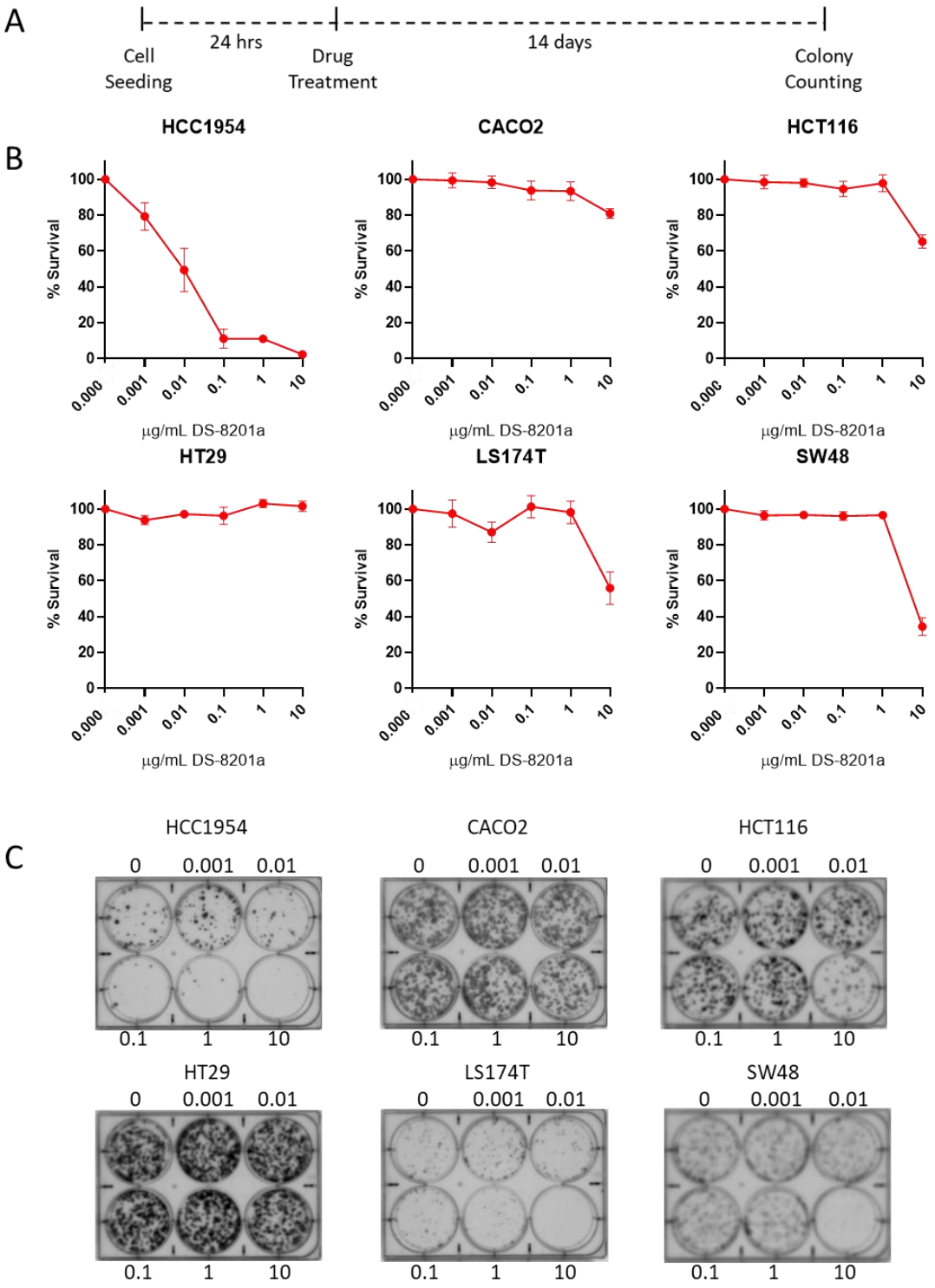

Figure 4.4. **14-day DS-8201a treatment reduces survival in some CRC cell lines.**

A. Scheme demonstrating the treatment and clonogenic assay schedule followed. **B.** The percentage survival following DS-8201a treatment for HCC1954 cells (HER2+ breast cancer) and a panel of CRC cell lines. Each datapoint is the mean of 3 biological repeats. Error bars represent +/- SEM. **C.** Representative images of clonogenic plates for each cell line.

4.3.2 VX-970 sensitises some but not all CRC cell lines to DS-8201a

Having established that the HER2-low expressing CRC cell lines show markedly lower sensitivity to DS-8201a than a HER2+ breast cancer cell lines, we explored whether VX-970 could be used to increase DS-8201a cytotoxicity. The effect of DS-8201a in combination with VX-970 on the proliferation of CRC cell lines was assessed using the SRB assay. Cells were treated with a range of DS-8201a and VX-970 concentrations as monotherapies and in combination for 6 days.

VX-970 synergised with DS-8201a to reduce the proliferation of HCT116, LS174T and SW48 cells, with average ZIP synergy scores of 22.5 (± 1.2), 16.8 (± 0.8) and 46.9 (± 2.8) respectively (Figure 4.5). All 3 cell lines showed an almost complete growth inhibition with addition of VX-970 to 10µg/mL DS-8201a therapy. Sensitisation to lower dose DS-8201a was also observed, particularly in HCT116 cells, with 64.32% (± 4.78) growth inhibition observed with the addition of 0.125uM VX-970 (growth inhibition 5.64% ± 1.96) to 1µg/mL DS-8201a (growth inhibition 0.93% ± 0.098). No synergy was observed in CACO2 and HT29 cell lines, with average ZIP synergy scores of -1.24 (± 1.7) and 0.0 (± 0.02) respectively (Figure 4.6).

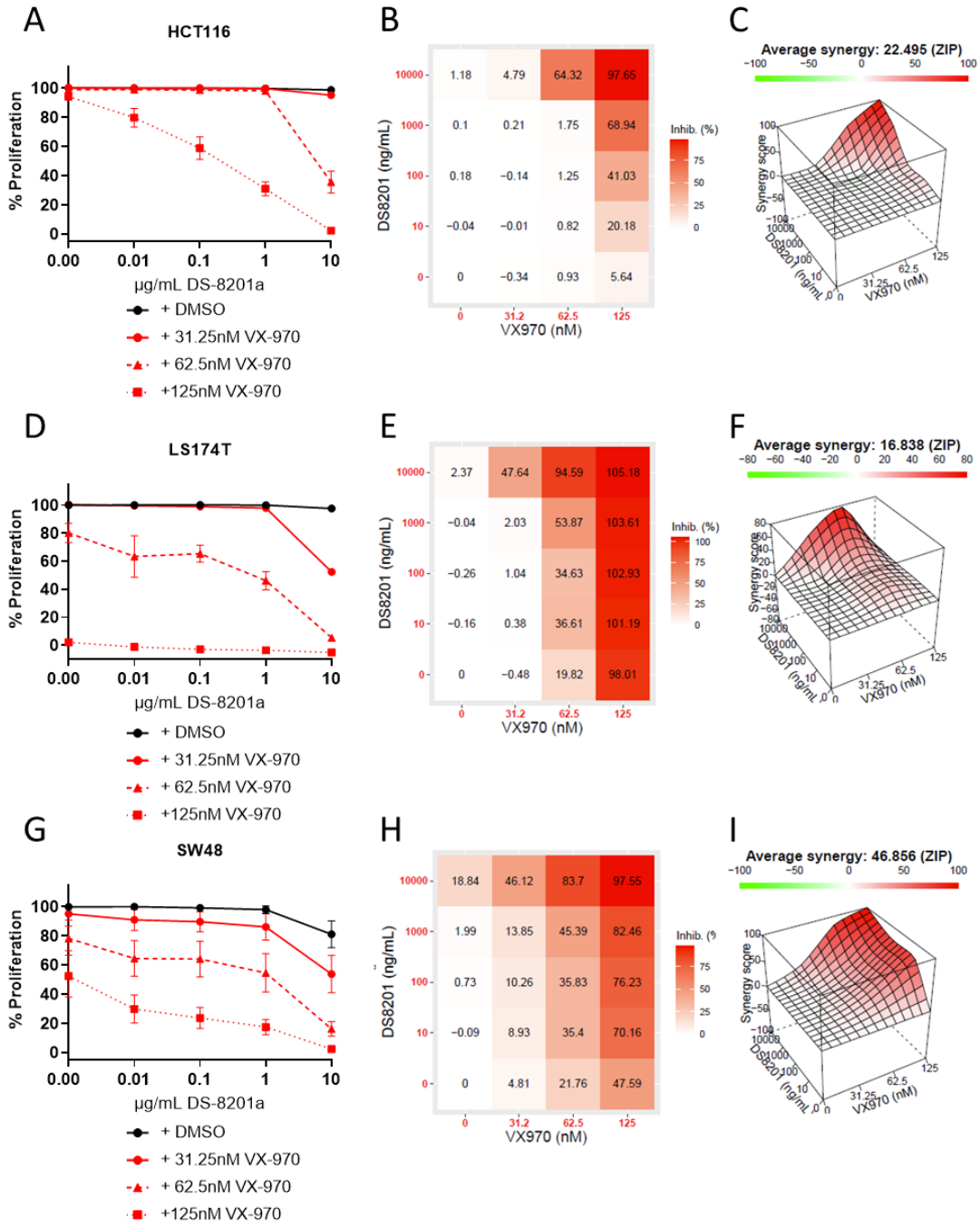

Figure 4.5. **VX-970 synergises with DS-8201a to reduce proliferation in HCT116, LS174T and SW48 CRC cell lines.**

Cells were treated with the indicated drugs for 6 days and the SRB assay was used to calculate proliferation rates. **A.** HCT116 cells **D.** LS174T cells **G.** SW48 cells. Each datapoint is the mean of 3 biological repeats. Error bars represent +/- SEM. The mean percentage inhibition for each drug combination is shown in a heatmap **B.** HCT116 cells **E.** LS174T cells and **H.** SW48 cells. 3D ZIP models demonstrate the interaction between DS-8201a and VX-970 in **C.** HCT116 cells **F.** LS174T cells and **I.** SW48 cells.

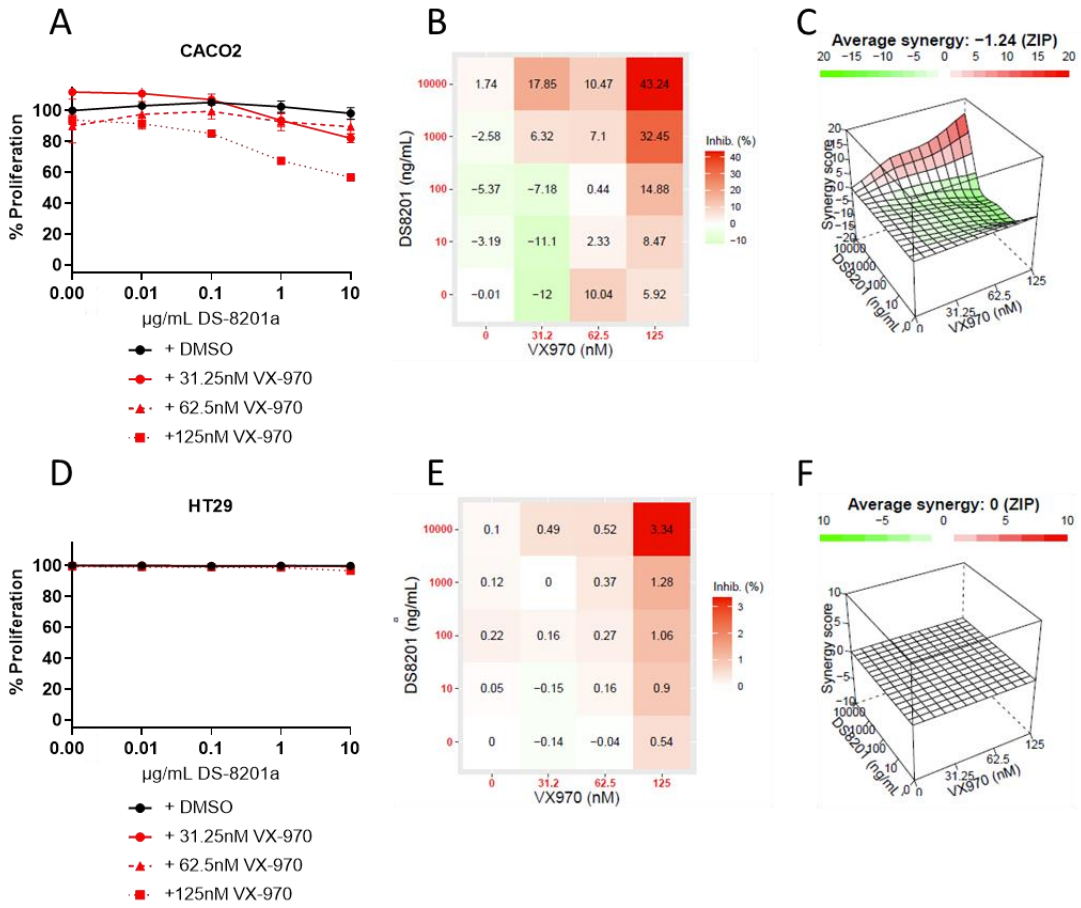

Figure 4.6. **No synergy observed between DS-8201a and VX-970 in CACO2 and HT29 CRC cell lines.**

Cells were treated with the indicated drugs for 6 days and the SRB assay was used to calculate proliferation rates. **A.** CACO2 cells and **D.** HT29 cells. Each datapoint is the mean of 3 biological repeats. Error bars represent +/- SEM. The mean percentage inhibition for each drug combination is shown in a heatmap **B.** CACO2 cells and **E.** HT29 cells. 3D ZIP models demonstrate the interaction between DS-8201a and VX-970 in **C.** CACO2 cells and **F.** HT29 cells.

To investigate the effect of VX-970 and DS-8201a combination therapy on the survival of CRC cell lines, the clonogenic assay was used. HCT116, HT29, SW48 and CACO2 cells were treated with a dose range of DS-8201a as a monotherapy and in combination with 0.0625µM VX-970. As with the DS-8201a monotherapy clonogenic experiment, two different treatment schedules were assessed, 72 hours treatment

followed by drug removal, and 2 weeks continuous drug exposure (Figure 4.7 A and Figure 4.8 A).

With 72-hour treatment, the addition of VX-970 to DS-8201a reduced the survival of HCT116 and SW48, but not HT29 and CACO2 cells (Figure 4.7). In HCT116 cells, the combination of 10µg/mL DS-8201a and 0.0625µM VX-970 reduced survival to 2.32% (± 1.09), compared with 73.25% (± 4.1) with 10µg/mL DS-8201a monotherapy and 33.49% (± 6.8) with 0.0625µM VX-970 monotherapy (Figure 4.7 B-C). In SW48 cells, the combination of 10µg/mL DS-8201a and 0.0625µg/mL VX-970 reduced survival to 11.3% (± 2.0), compared with 89.6% (± 2.4) with 10µg/mL DS-8201a monotherapy and 56.65% (± 1.52) with 0.0625µM VX-970 monotherapy (Figure 4.7 D-E).

A similar effect was seen with 2-week continuous drug exposure, with almost no survival and colony formation in HCT116 (0.02 ± 0.02) and SW48 (0.34% ± 0.34) cells treated with 10µg/mL DS-8201a and 0.0625µM VX-970 combination (Figure 4.8 B-E). HT29 cells showed some sensitivity to the combination treatment, with 10µg/mL DS-8201a and 0.0625µM VX-970 combination treatment reducing survival to 61.3% (± 4.18), compared to 100% (± 4.18) with 10µg/mL DS8201a monotherapy and 93.2% (± 2.05) with 0.0625µM VX-970 monotherapy (Figure 4.8 F-G).

These data show VX-970 has the potential to sensitise HER2-low expressing CRC to DS-8201a. This suggests that the addition of VX-970 to DS-8201a therapy, may increase the number of patients who benefit from the HER2 targeted therapy.

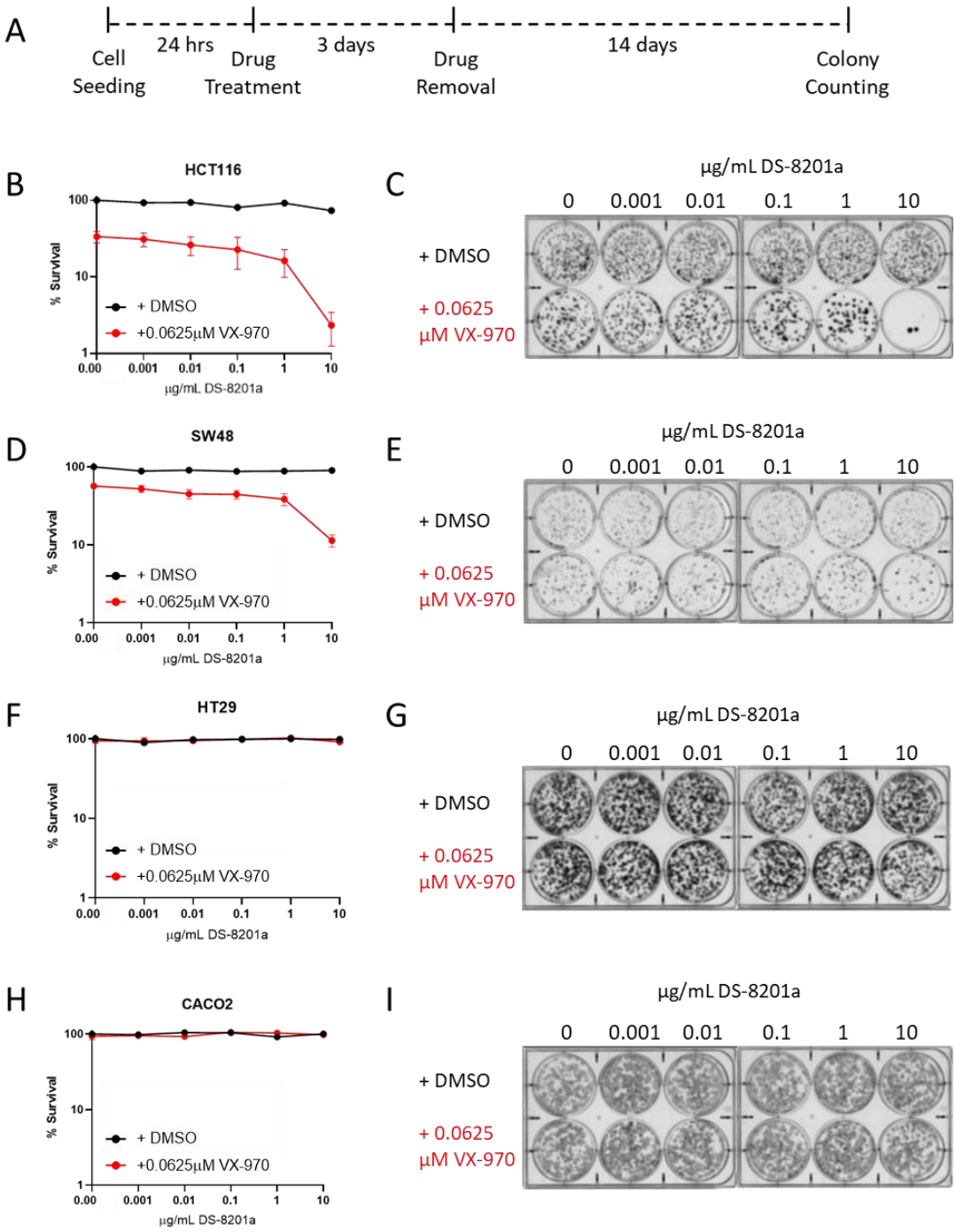

Figure 4.7. **3-day VX-970 + DS-8201a reduces survival in HCT116 and SW48 CRC cell lines.**

A. Scheme demonstrating the treatment and clonogenic assay schedule followed. The percentage survival following combination treatment with DS-8201a + VX-970 is displayed in **B.** HCT116 cells **D.** SW48 cells **F.** HT29 cells and **H**. CACO2 cells. Each datapoint is the mean of 3 biological repeats. Error bars represent +/- SEM. Representative images of clonogenic plates for **C.** HCT116 cells **E.** SW48 cells **G.** HT29 cells and **I.** CACO2 cells.

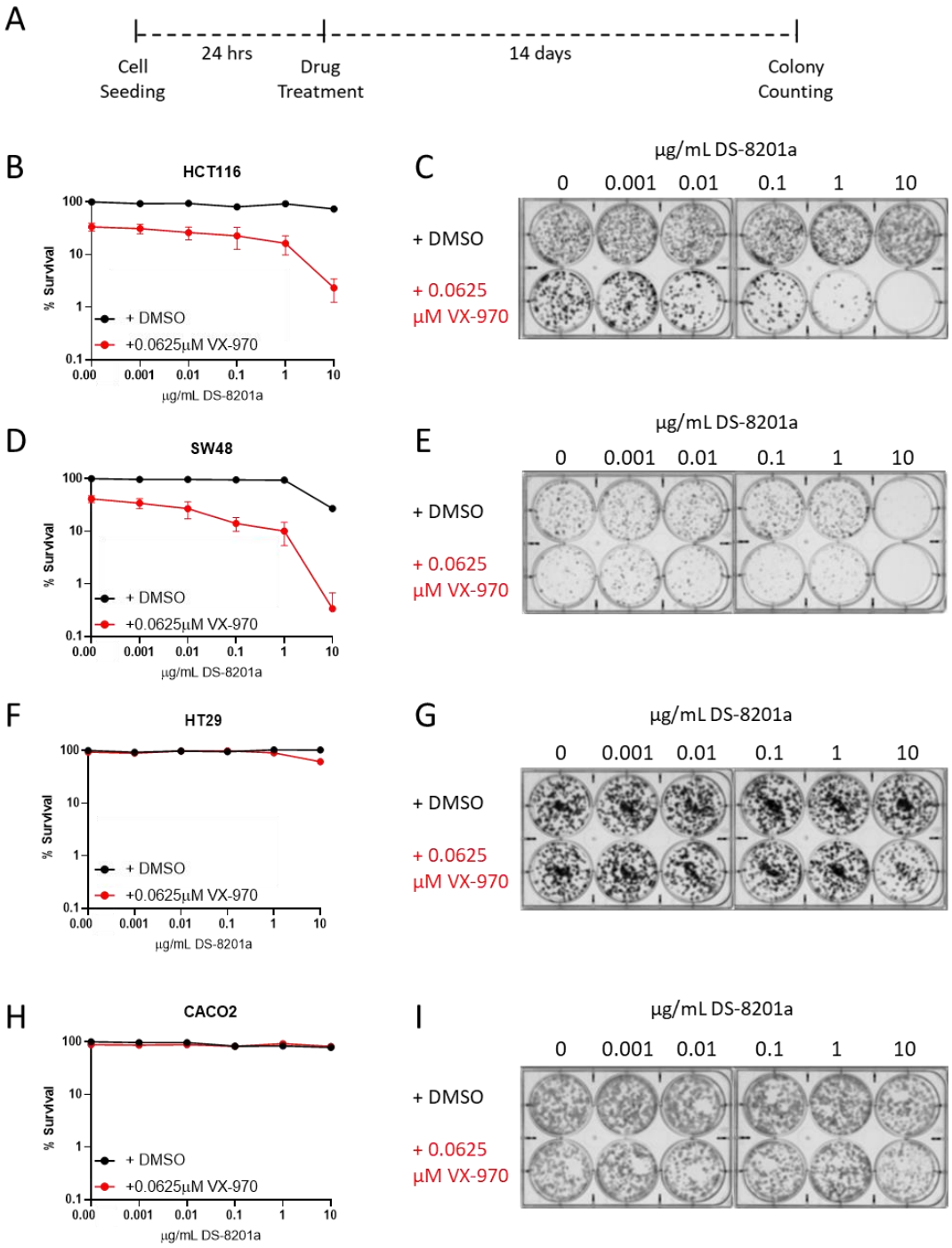

Figure 4.8. **14-day VX-970 + DS-8201a reduces survival in HCT116 and SW48 CRC cell lines.**

A. Scheme demonstrating the treatment and clonogenic assay schedule followed. The percentage survival following combination treatment with DS-8201a + VX-970 is displayed in **B.** HCT116 cells **D.** SW48 cells **F.** HT29 cells and **H**. CACO2 cells. Each datapoint is the mean of 3 biological repeats. Error bars represent +/- SEM. Representative images of clonogenic plates for **C.** HCT116 cells **E.** SW48 cells **G.** HT29 cells and **I.** CACO2 cells.

4.3.3 ATR inhibitor AZD6738 also synergises with DS-8201a to reduce CRC cell line survival and proliferation

In 2019, a collaboration was established between Daiichi Sankyo and AstraZeneca for the further development and commercialization of DS-8201a. As AstraZeneca have developed ATR inhibitor AZD6738, trials exploring the combination of ATR inhibition and DS-8201a, would use AZD6738, over the Merck-owned VX-970. To confirm that a AZD6738 would synergise with DS-8201a, in a manner similar to that observed with VX-970, we investigated the effect of DS-8201a and AZD6738 combination therapy on CRC cell line proliferation and survival.

HCT116, LS174T and SW48 cells were treated with a range of DS-8201a and AZD6738 concentrations as monotherapies and in combination for 6 days, and proliferation measured using the SRB assay (Figure 4.9). As was observed with VX-970, AZD6738 and DS-8201a synergised to reduce proliferation in HCT116, LS174T and SW48 cell lines, with respective average synergy ZIP scores of 16.7 (± 1.02), 19.1 (± 0.25) and 29.2 (± 1.4) (Figure 4.9 C, F and I).

In HCT116 cells, the highest dose of 0.5µM AZD6738 caused only 2.8% (± 0.78) growth inhibition, however 91.97% (± 0.74) growth inhibition was seen in combination with 10µg/mL DS-8201a (Figure 4.9 A-B). LS174T cells, displayed greater sensitivity to AZD6738 monotherapy, with 88.5% (± 4.3) growth inhibition observed with 0.5µM treatment. When a lower dose of 0.25µM AZD6738 was combined with 10µg/mL DS-8201a, growth inhibition was increased to 93.7% (± 1.03), compared to 7.6% (± 3.2) with 0.25µM AZD638 and 5.5% (± 0.77) with 10µg/mL DS8201a monotherapies (Figure 4.9 D-E). In SW48 cells, a 92.9% (± 0.9) growth inhibition was observed with combined 0.25µM AZD6738 and 10µg/mL DS-8201a therapy, compared to 37.74% (± 3.9) with 0.25µM AZD6738 and 23.0% (± 8.1) with 10µg/mL DS8201a monotherapies (Figure 4.9 G-H).

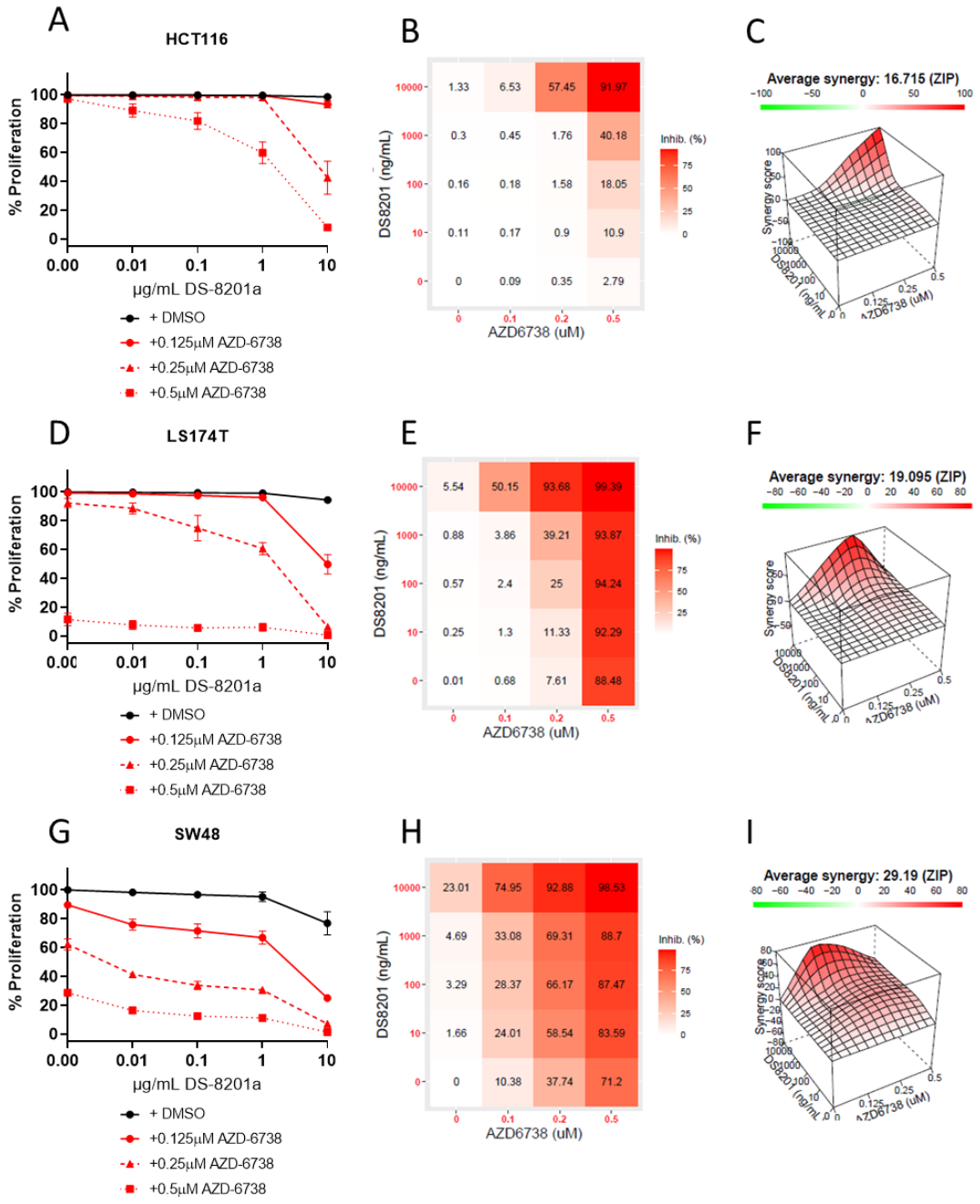

Figure 4.9. **AZD-6738 synergises with DS-8201a to reduce proliferation in CRC cell lines.** Cells were treated with the indicated drugs for 6 days and the SRB assay was used to calculate proliferation rates. **A.** HCT116 cells **D.** LS174T cells and **G.** SW48 cells. Each datapoint is the mean of 3 biological repeats. Error bars represent +/- SEM. The mean percentage inhibition for each drug combination is shown in a heatmap **B.** HCT116 cells **E.** LS174T cells and **H.** SW48 cells. 3D ZIP models demonstrate the interaction between DS-8201a and AZD-6738 in **C.** HCT116 cells **F.** LS174T cells and **I.** SW48 cells.

The effect of DS-8201a and AZD6738 combination therapy on CRC cell survival was investigated using the clonogenic assay. HCT116, LS174T and SW48 cells were treated with multiple doses of DS-8201a and AZD6738, as monotherapy and in combination. Synergy was observed in all 3 cell lines with a 72-hour dosing schedule, with average ZIP synergy scores of 27.6 (± 1.1) in HCTT16 cells, 26.3 (± 3.4) in LS174T cells and 14.4 (± 1.5) in SW48 cells (Figure 4.10 D, G and J). With 72 hours treatment, the survival of HCT116 cells was reduced to 4.6% (± 0.5) with a combination of 0.25μM AZD6738 and 10μg/mL DS-8201a, compared to 90.0% (± 8.2) with 10μg/mL DS-8201a and 63.97% (± 6.7) with 0.25μM AZD6738 monotherapies (Figure 4.10 B-C). A similar effect was observed in LS174T cells, with survival reduced to 1.3% (± 0.43) with a combination of 0.25μM AZD6738 and 10μg/mL DS-8201a, compared to 98.1% (± 7) with 10μg/mL DS-8201a and 45.9% (± 7.7) with 0.25μM AZD6738 monotherapies (Figure 4.10 E-F). In SW48 cells, survival with the combination of 0.25μM AZD6738 and 10μg/mL DS-8201a was reduced (29.06% ± 2.6) compared to 10μg/mL DS-8201a (90.6% ±3.9) and 0.25μM AZD6738 (62.6% ± 3.3) monotherapies, however a much higher percentage of SW48 cells survived than HCT116 and LS174T cells (Figure 4.10 H-I).

Synergy between DS-8201a and AZD6738 in all 3 CRC cell lines was also observed with a 2-week clonogenic dosing schedule, however a lower dose range of AZD6738 was used to reduce toxicity as a monotherapy (Figure 4.11). The average ZIP synergy scores were 28.8 (± 1.1) in HCT116 cells, 36.1 (± 3.7) in LS174T cells and 28.4 (± 3.2) in SW48 cells (Figure 4.11 D, G and J). In HCT116 and LS174T cells, the percentage survival with the addition of 0.125μM AZD6738 to 10μg/mL DS-8201a was close to that observed with a higher dose of 0.25μM AZD6738 with 72-hour drug exposure. However, with 2-week therapy the colonies were much smaller, with many just visible by naked eye (Figure 4.11 B-C and E-F). Greater synergy was observed with 2-week than 72-hour treatment in SW48 cells, with survival reduced to 1.2% (±

0.63) with 0.125μM AZD6738 and 10μg/mL DS-8201a combination therapy, compared to 44.4% (± 7.9) with 10μg/mL DS-8201a and 76.6% (± 2.6) with 0.125μM AZD6738 monotherapies (Figure 4.11 H-I).

These data show AZD6738 to sensitise HER2-low expressing CRC to DS-8201a, as was observed with VX-970. This suggests that the addition of VX-970 or AZD6738 to DS-8201a therapy, may increase the number of patients who may derive benefit the HER2 targeted therapy.

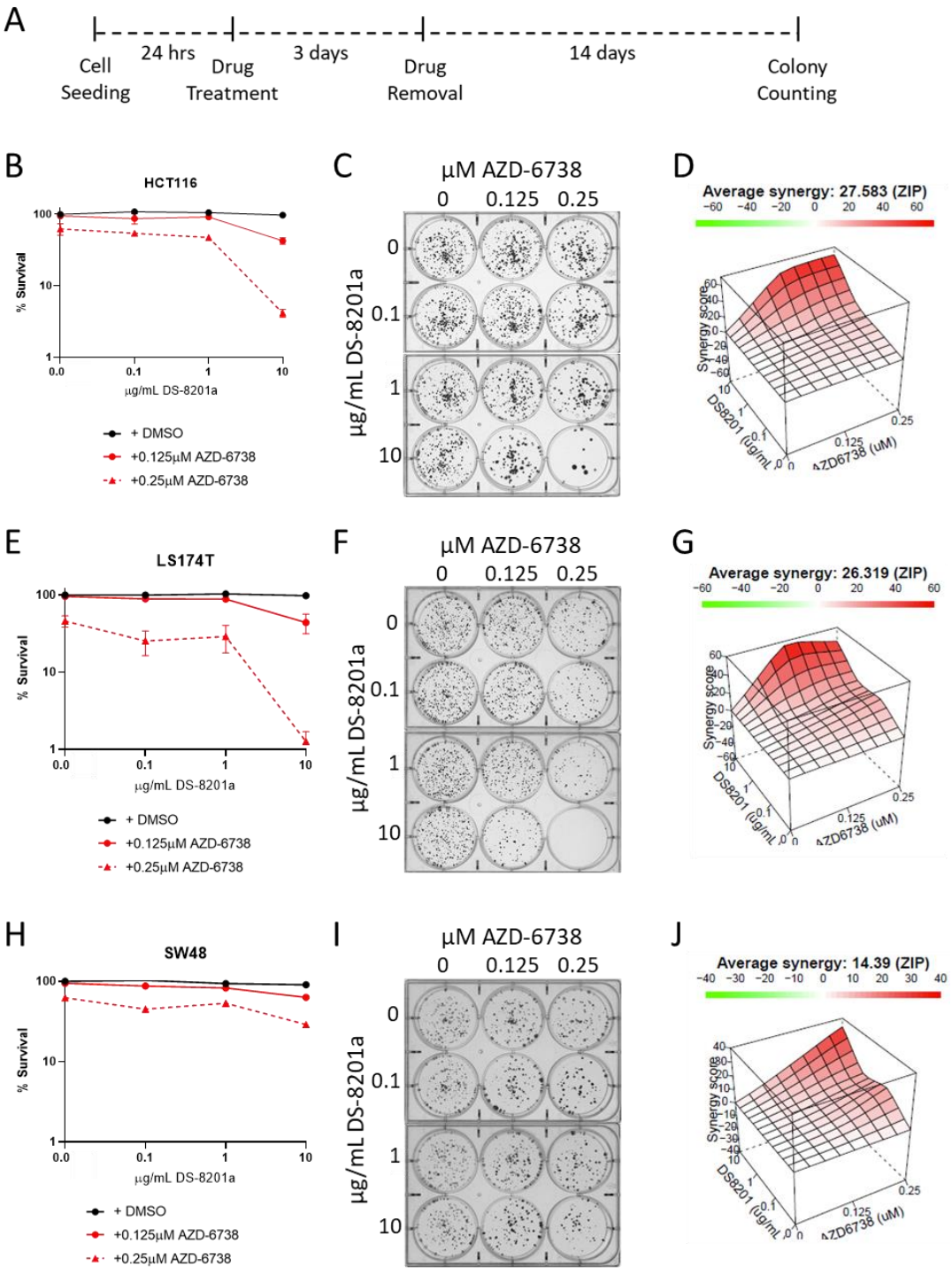

Figure 4.10. **AZD-6738 synergises with DS-8201a to reduce survival in CRC cell lines.** **A.** Scheme demonstrating the treatment and clonogenic assay schedule followed. The percentage survival following combination treatment with DS-8201a + AZD-6738 is displayed in **B.** HCT116 cells **E.** LS174T cells **H.** SW48 cells. Each datapoint is the mean of 3 biological repeats. Error bars represent +/- SEM. Representative images of clonogenic plates for **C.** HCT116 cells **F.** LS174T and **I.** SW48 cells. 3D ZIP models demonstrate the interaction between DS-8201a and AZD-6738 in **D.** HCT116 cells **G.** LS174T cells and **J.** SW48 cells.

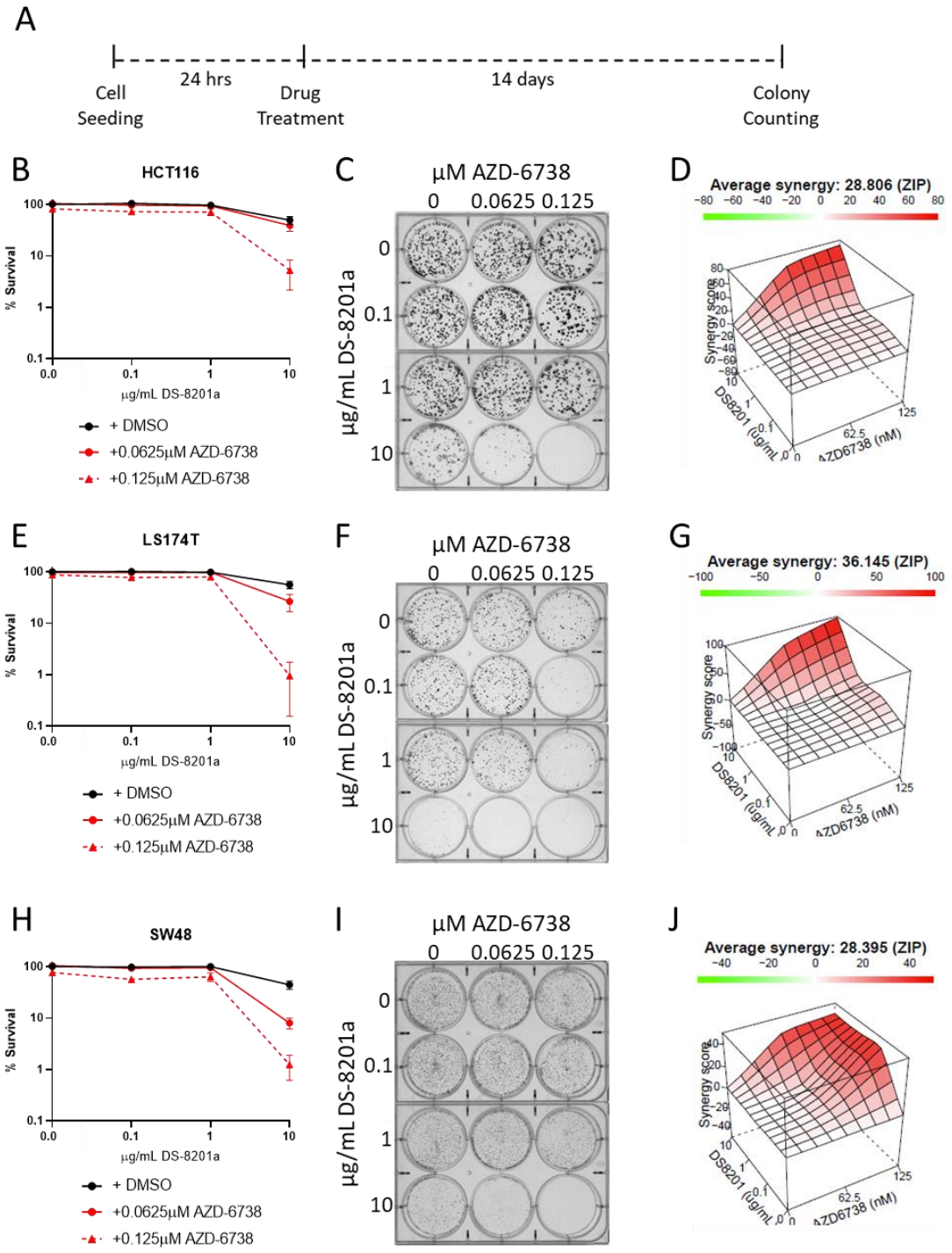

Figure 4.11. **14-day treatment with AZD-6738 + DS-8201a shows synergism.**

A. Scheme demonstrating the treatment and clonogenic assay schedule followed. The percentage survival following combination treatment with DS-8201a + AZD-6738 is displayed in **B.** HCT116 cells **E.** LS174T cells **H.** SW48 cells. Each datapoint is the mean of 3 biological repeats. Error bars represent +/- SEM. Representative images of clonogenic plates for **C.** HCT116 cells **F.** LS174T and **I.** SW48 cells. 3D ZIP models demonstrate the interaction between DS-8201a and AZD-6738 in **D.** HCT116 cells **G.** LS174T cells and **J.** SW48 cells.

4.3.4 Investigating the HER2-dependence of DS-8201a and ATR inhibition synergy

Having demonstrated that ATR inhibition can sensitise HER2-low CRC cell lines to DS-8201a therapy, confirmation of HER2-dependence was required. HER2 independent synergy would lose the cancer targeting benefit of ADC therapy. To assess the HER2-dependence of this combination treatment, synergy was investigated in HER2- MDA-MB-231 and HER2+ HCC1954 breast cancer cell lines. As with the CRC cell lines, HCC1954 and MDA-MB-231 were treated with a range of DS-8201a and AZD6738 concentrations as monotherapies and in combination for 6 days, and proliferation measured using the SRB assay. We found AZD6738 to synergise with DS-8201a in HCC1954 but not MDA-MB-231 cells, with respective average ZIP synergy scores of 14.0 (± 2.4) and 0.05 (± 0.58) (Figure 4.12). While this demonstrates synergy between the two compounds, it does not definitively show the DS-8201a or payload uptake in the CRC cell lines to be HER2 specific.

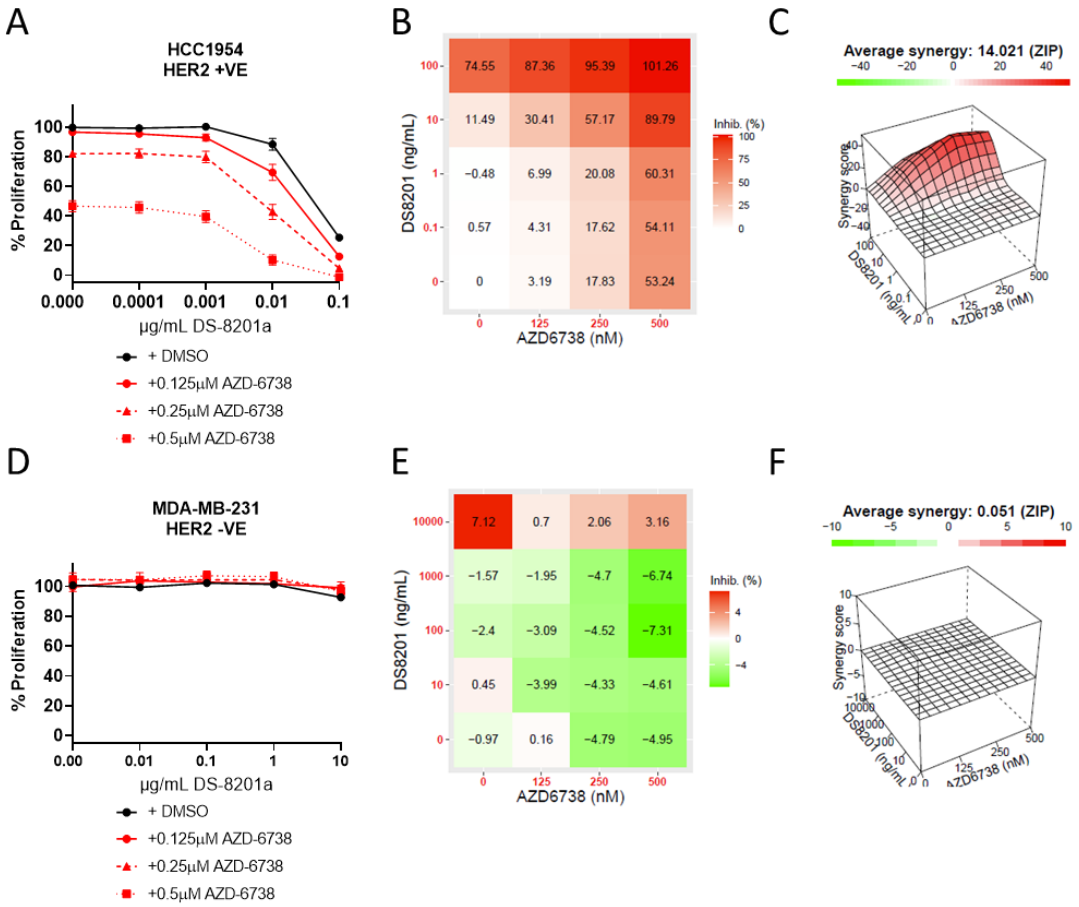

Figure 4.12. **AZD-6738 synergises with DS-8201a in HER2+ breast cancer cells but not HER2- breast cancer cells.**

Cells were treated with the indicated drugs for 6 days and the SRB assay was used to calculate proliferation rates in **A.** HCC1954 cells (HER2+) and **D.** MDA-MB-231 cells (HER2-). Each datapoint is the mean of 3 biological repeats. Error bars represent +/- SEM. The mean percentage inhibition for each drug combination is shown in a heatmap for **B.** HCC1954 cells and **E.** MDA-MB-231 cells. 3D ZIP models demonstrate the interaction between DS-8201a and AZD-6738 in **C.** HCC1954 cells and **F.** MDA-MB-231 cells.

HER2 specificity could be demonstrated using a non-targeting IgG-Dxd ADC. MAAA-9199a, is a non-targeting ADC that was developed by Daiichi Sankyo as a control for HER2 specificity. However, the properties of MAAA-9199a differ from DS-8201a, due to differences in the mAb component. The company have reported possible non-specific uptake and payload release with MAAA-9199a, causing toxicity in HER2-

settings, in a manner not observed with DS-8201a, making it a poor control ADC. To test the cytotoxicity of MAAA-9199a as a monotherapy and in combination with ATR inhibitor, HCT116, LS174T and SW48 cells were treated with a dose range of MAAA-9199a either as a monotherapy or in combination with VX-970 or AZD6738 (Figure 4.13).

As a monotherapy MAAA-9199a only reduced the proliferation of SW48 cells to 86.5% (± 8.7), and did not reduce the proliferation of HCT116 and LS174T cells. However, the addition of 0.0625μM VX-970 or 0.25μM AZD6738 caused a dramatic reduction in proliferation in all 3 cell lines. In HCT116 cells, proliferation was reduced to 28.9% (± 11.3) with the addition of VX-970 and to 20.3% (± 3.7) with the addition of AZD6738. In LS174T cells, proliferation was reduced even further to 3.2% (± 1.1) with the addition of VX-970 and to 5.9% (± 0.5) with the addition of AZD6738. The same effect was observed in SW48 cells, with proliferation reduced to 10.9% (± 2.6) with the addition of VX-970 and to 9.4% (± 2.0) with the addition of AZD6738.

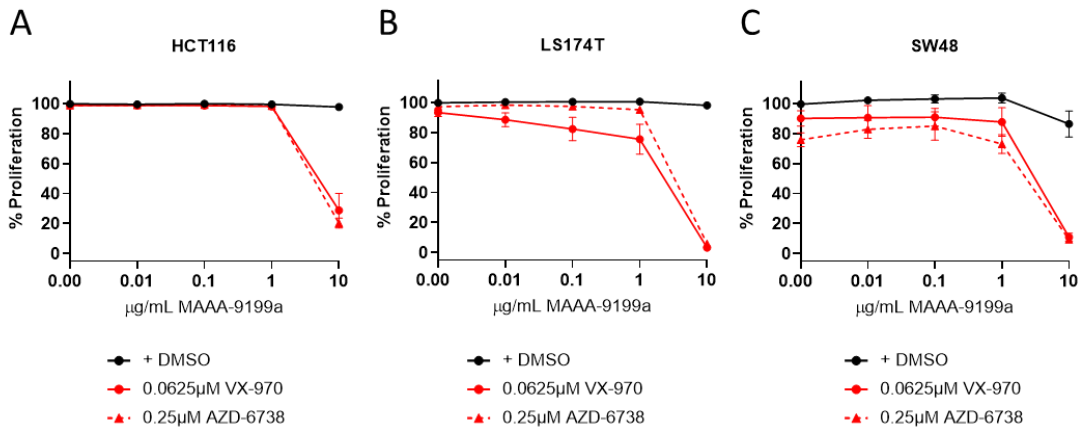

Figure 4.13**. Reduction in proliferation observed in CRC cell lines when treated with MAAA-9199a in combination with ATR inhibition.**

Cells were treated with the indicated drugs for 6 days and the SRB assay was used to calculate proliferation rates. **A.** HCT116 cells **B.** LS174T cells **C.** SW48 cells. Each datapoint is the mean of 3 biological repeats. Error bars represent +/- SEM.

The sensitisation of CRC cell lines to MAAA-9199a with the addition of an ATR inhibitor further demonstrates the potent synergy of combined TOP1 and ATR inhibition. However, as this is a non-targeting ADC, it is likely that either non-specific MAAA-9199a uptake was occurring, or that the membrane-permeable payload was being released in the media.

An additional approach to evaluate the specificity of DS-8201a toxicity, is to explore cellular HER2 expression by Western blotting. Trastuzumab, the mAb component of DS-8201a binds to HER2 causing receptor internalisation and degradation, resulting in short term loss of HER2 expression (Ben-Kasus et al. 2009). To assess whether DS-8201a internalisation was occurring via HER2, HCT116, HT29 and SW48 cell lines were treated with DS-8201a or MAAA-9199a for 48 hours and lysates analysed by Western blotting. DS-8201a but not MAAA-9199a led to a reduction in HER2, suggesting that DS-8201a is binding to HER2, causing internalisation and degradation (Figure 4.14). This suggests that the synergy observed between ATR inhibition and DS-8201a is HER2 dependent.

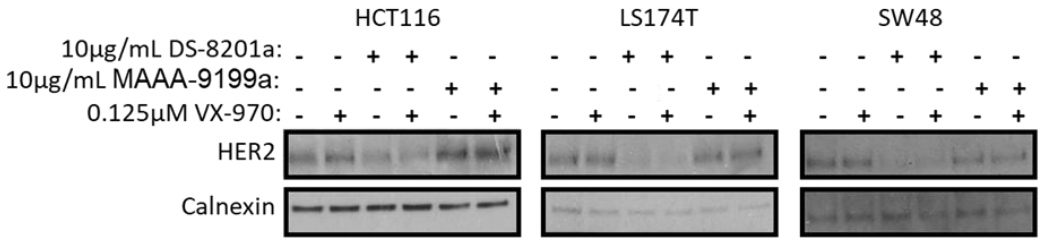

Figure 4.14. **DS-8201a and not MAAA-9199a treatment leads to a reduction in HER2.** Cells were treated with the indicated drugs for 48 hours and lysates were analysed by Western blotting. Blots are representative images of 2 biological repeats.

4.3.5 Increased p53 phosphorylation and PARP cleavage following DS-8201a and VX-970 combination therapy

Having shown DS-8201a and VX-970 to synergise in HCT116, LS174T and SW48 cells, increased DNA damage was investigated as a mechanism for increased

cytotoxicity. HCT116, LS174T and SW48 cells were treated with 10µg/mL DS-8201a or 0.125µM VX-970 as monotherapies and in combination. Lysates were collected at 24, 48 and 72 hours and analysed by Western blotting (Figure 4.15). In HCT116 cells (Figure 4.15 A), PARP cleavage could be detected at 48 hours following the combination therapy, but not in cells treated with either monotherapy. There was also increased p53 stabilisation and phosphorylation with the combination therapy, compared to either monotherapy at 24, 48 and 72 hours. No changes in pH2AX, pATR, pATM or pChk1 could be detected with either monotherapies or the combination therapy. A slight increase in DNA-PK phosphorylation occurred with 48 hours combination therapy. An increase in pChk2 was detectable at 24 hours with combination treatment, and at 48 hours with DS-8201a monotherapy and combination therapy.

In LS174T cells (Figure 4.15 B), cleaved PARP was present with VX-970 monotherapy and DS-8201a and VX-970 combination therapy, at 24, 48 and 72 hours. There was no increased PARP cleavage with the combination therapy compared to VX-970 monotherapy. Phosphorylation of H2AX, also occurred with VX-970 monotherapy and DS-8201a and VX-970 combination therapy. LS174T is a p53 null cell line, so as expected p53 was not detectable with any treatment. No change in pATR or pChk1 levels occurred with DS-8201a monotherapy or combination therapy. There was an increase in pDNA-PK with VX-970 monotherapy and DS-8201a and VX-970 combination therapy at 24, 48 and 72 hours. pATM and pChk2 were also increased with VX-970 monotherapy and DS-8201a and VX-970 combination therapy, with the highest signal at 24 hours.

In SW48 cells (Figure 4.15 C), PARP cleavage could be detected at 48 hours following the combination therapy, but not in cells treated with either monotherapy. There was also increased p53 stabilisation and phosphorylation with the combination therapy, compared to either monotherapy at 24 hours, however at 48 and 72 hours p53

phosphorylation was reduced with the combination therapy, compared to DS-8201a monotherapy. No changes in pH2AX, pATR or pChk1 could be detected with either DS-8201a monotherapy or in combination with VX-970. Phosphorylation of Chk2 could be detected with VX-970 monotherapy and in combination with DS-8201a, at 24, 48 and 72 hours, with signal being higher with combination therapy than monotherapy. No consistent changes in DNA-PK and ATM phosphorylation could be detected with either monotherapy or combination therapy across experimental repeats.

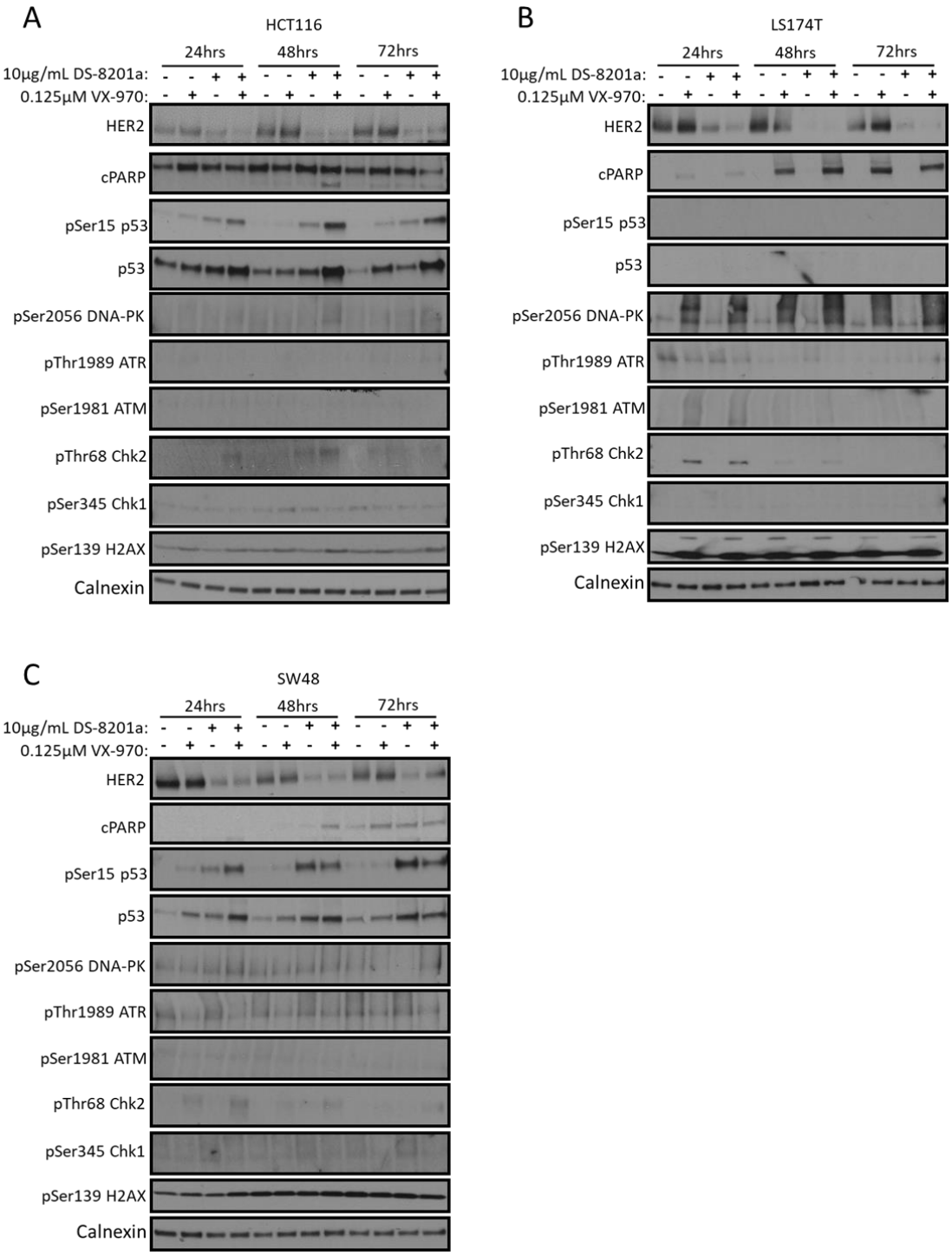

Figure 4.15**. DS-8201a and VX-970 combination treatment leads to p53 phosphorylation and PARP cleavage.**

Lysates were analysed by Western blotting for **A.** HCT116 cells **B.** LS174T cells and **C.** SW48 cells. Blots are representative images of 2 biological repeats.

4.3.6 HER2- low expressing CRC organoids show differing sensitivity to DS-8201a

Having established that DS-8201a and ATR inhibition synergise to reduce proliferation and survival in some HER2-low expressing CRC cell lines, the cytotoxicity of DS-8201a as a monotherapy and in combination with ATR inhibition was investigated in CRC PDOs. Prior to drug treatment, the HER2 expression level of PDO 021 and 027 was scored by IHC, with both PDOs being HER2 IHC1+ (Figure 4.16).

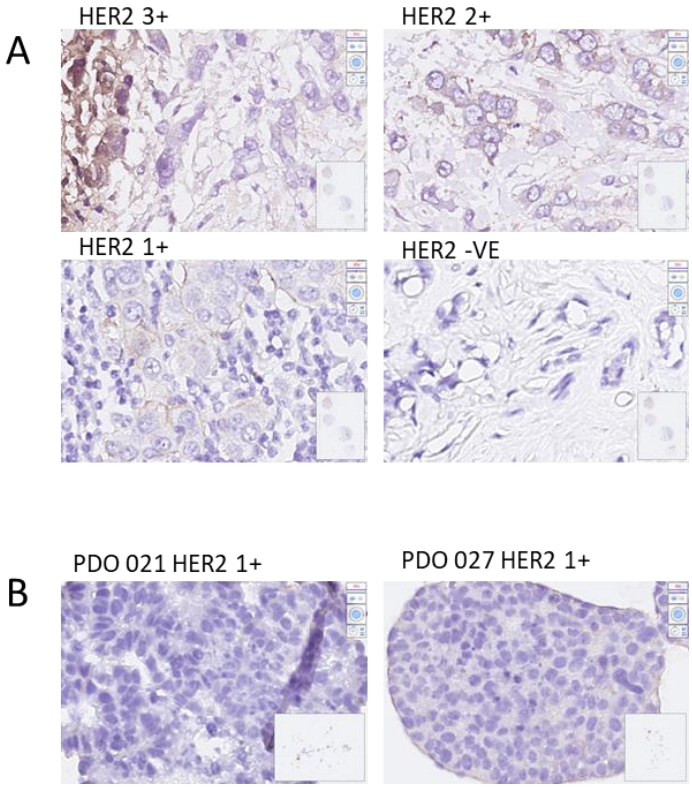

Figure 4.16. **Low levels of HER2 expression in colorectal cancer PDOs.**
A. HER2 (Brown) and H & E (Purple) IHC staining of patient tumours to act as a reference for CRC PDOs. **B.** HER2 (Brown) and H & E (Purple) IHC staining of CRC PDOs.

To assess the cytotoxicity of DS-8201a as a monotherapy in PDO 021 and 027, the organoids were treated with a dose range of DS-8201a for 72 hours. Prior to treatment, PDO 021 and PDO 027 were seeded by trypsinisation of fully developed

organoids, and left for 48 hours to allow for the division and differentiation of stem cells. Following drug removal, organoids were left to grow for a further 7 days, following which the organoids were imaged and viability measured using the 3D CellTiter-Glo assay (Figure 4.17). PDOs 021 treated with the highest dose of 10µg/mL DS-8201a grew to a similar size as untreated organoids, however an increase in dead organoid cells was observed (Figure 4.17 B). The viability of organoids was reduced to 77.6% (± 5.0) with 10µg/mL DS-8201a (Figure 4.17 C). PDO 027 grew well even with the highest dose of 10µg/mL DS-8201a, however there was also an increase in dead organoid cells (Figure 4.17 D). The viability of PDO 027 was reduced to 88.3% (± 5.1) with 10µg/mL DS-8201a (Figure 4.17 E).

As 72 hours DS-8201a treatment had a very marginal effect on the viability of the organoids, the cytotoxic effect of a longer treatment schedule was also investigated. As in the previous schedule, organoids were treated 48 hours post seeding. Organoids were treated with a dose range of DS-8201a for 7 days, after which organoids were imaged and viability was measured using the 3D CellTiter-Glo assay (Figure 4.18). With a 7-day treatment schedule, PDO 021 displayed increased sensitivity to DS-8201a monotherapy, with 1 µg/mL and 10µg/mL reducing the size and development of the organoids (Figure 4.18 B). Viability of organoids was reduced to 40.6% (± 3.3) with 10µg/mL DS-8201a treatment (Figure 4.18 C). PDOs 027 appeared smaller in size with 10µg/mL DS-8201a treatment, however viability was only reduced to 87.3% (± 3.8) (Figure 4.18 D-E).

These data show CRC PDOs, which are a more representative model of CRC than cell lines to have minimal sensitivity to DS-8201a. Particularly PDO 027 displayed almost no loss of viability with a concentration of 10µg/mL. This supports the findings in section 4.3.1, in which minimal sensitivity of HER2-low expressing CRC cell lines to DS-8201a was demonstrated, suggesting DS-8201a is unlikely to be a suitable therapeutic for patients with low-HER2 expressing mCRC.

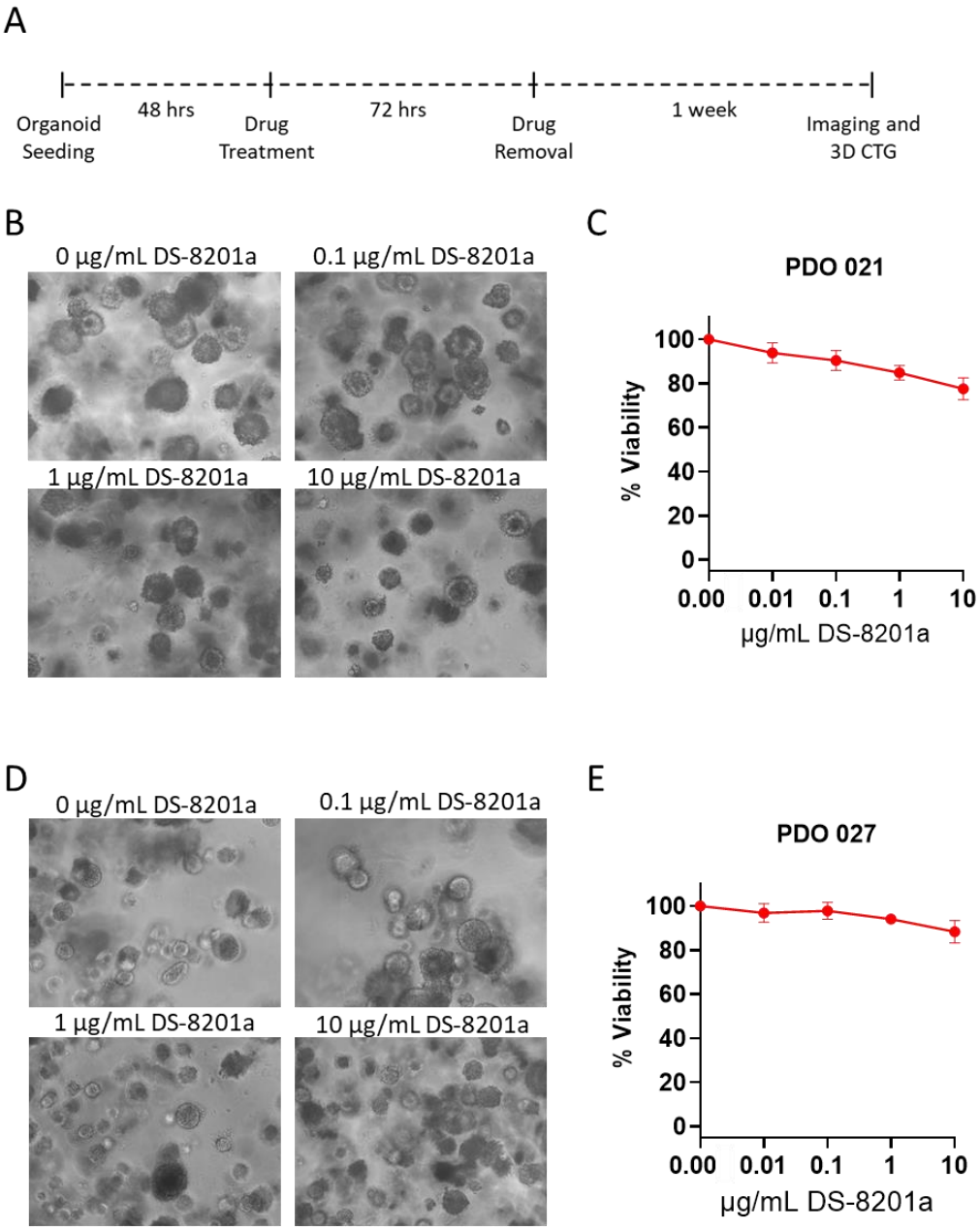

Figure 4.17. **3-day DS-8201a treatment has little effect on the viability of PDO 021 and 027.**

A. Scheme demonstrating the treatment schedule followed in B, C, D and E. **B.** Representative images of PDO 021 following treatment with DS-8201a. **D.** Representative images of PDO 027 following treatment with DS-8201a. **C.** and **E.** Organoids were treated with the indicated doses of DS-8201a and the percentage viability of PDO 021 and PDO 027 measured using the 3D CTG assay. Each datapoint is the mean of 3 biological repeats. Error bars represent +/- SEM.

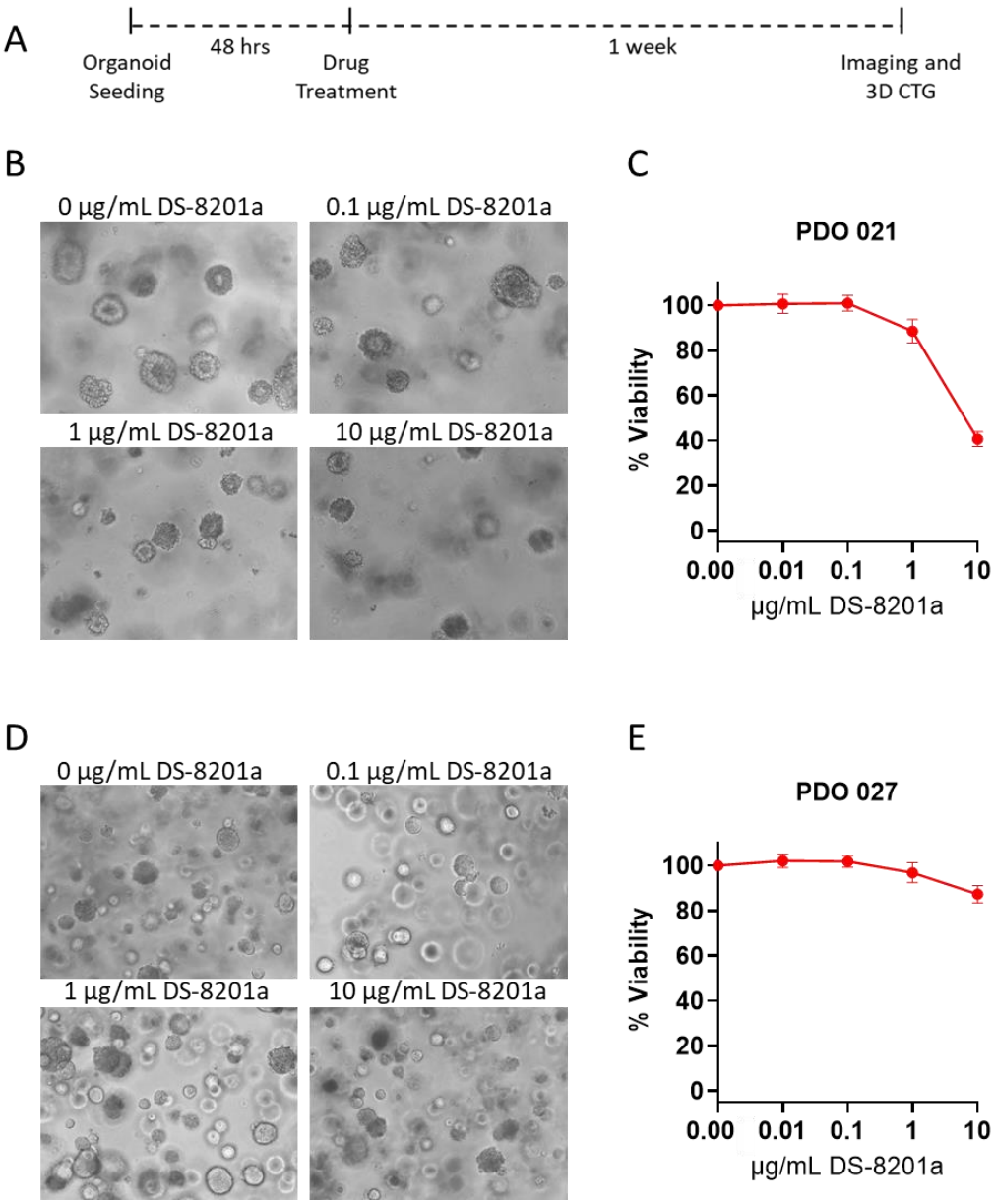

Figure 4.18. **7-day DS-8201a treatment further reduces viability of PDO 021.**
A. Scheme demonstrating the treatment schedule followed in B, C, D and E. **B.** Representative images of PDO 021 following treatment with DS-8201a. **D.** Representative images of PDO 027 following treatment with DS-8201a. **C.** and **E.** Organoids were treated with the indicated doses of DS-8201a and the percentage viability of PDO 021 and PDO 027 measured using the 3D CTG assay. Each datapoint is the mean of 3 biological repeats. Error bars represent +/- SEM

4.3.7 ATR inhibition sensitises PDOs to DS-8201a therapy

As PDO 027 showed limited sensitivity to DS-8201a, and PDO 021 only showed sensitivity to the highest dose of 10µg/mL DS-8201a, the cytotoxicity of combined DS-8201a and VX-970 treatment was explored. As with the DS-8201a monotherapy cytotoxicity experiments, two different treatment schedules were used, 3-day and 7-day. With 72-hour treatment, PDOs 021 appeared less developed with the combination of 10µg/mL DS-8201a and 0.125µM VX-970 than either monotherapy, however the organoids were viable and increasing in size, and there was no statistical difference in viability (Figure 4.19 B-C). PDOs 027 failed to grow and develop with the addition of 0.125µM VX-970 to 10µg/mL DS-8201a treatment, while the organoids grew and developed with VX-970 and DS-8201a monotherapies (Figure 4.19 D). Viability of PDO 027 was reduced to 17.1% (± 2.2) with 10µg/mL DS-8201a and 0.125µM VX-970 combination therapy compared to 81.3% (± 8.3) with 10µg/mL DS-8201a and 85.9% (± 9.2) with 0.125µM VX-970 monotherapies (Figure 4.19 E).

With a longer 7-day treatment schedule, sensitisation of PDO 021 to lower dose DS-8201a was observed. Organoids treated with 1µg/mL DS-8201a and 0.125µM VX-970 combination therapy were smaller and contained many more dead cells than organoids treated with either monotherapy (Figure 4.20 B). Viability with 1µg/mL DS-8201a and 0.125µM VX-970 combination therapy was reduced to 38.7% (± 8.0), compared to 87.3% (± 4.4) with 1µg/mL DS-8201a and 81% (± 13.5) 0.125µM VX-970 monotherapies (Figure 4.20 C). PDOs 027 failed to grow and develop with 1µg/mL DS-8201a and 0.125µM VX-970 combination therapy, but fully developed with DS-8201a and VX-970 monotherapies (Figure 4.20 D). Viability with 1µg/mL DS-8201a and 0.125µM VX-970 combination therapy was reduced to 19.8% (± 5.0), compared to 95% (± 9.4) with 1µg/mL DS-8201a and 62% (± 12.2) 0.125µM VX-970 monotherapies (Figure 4.20 E).

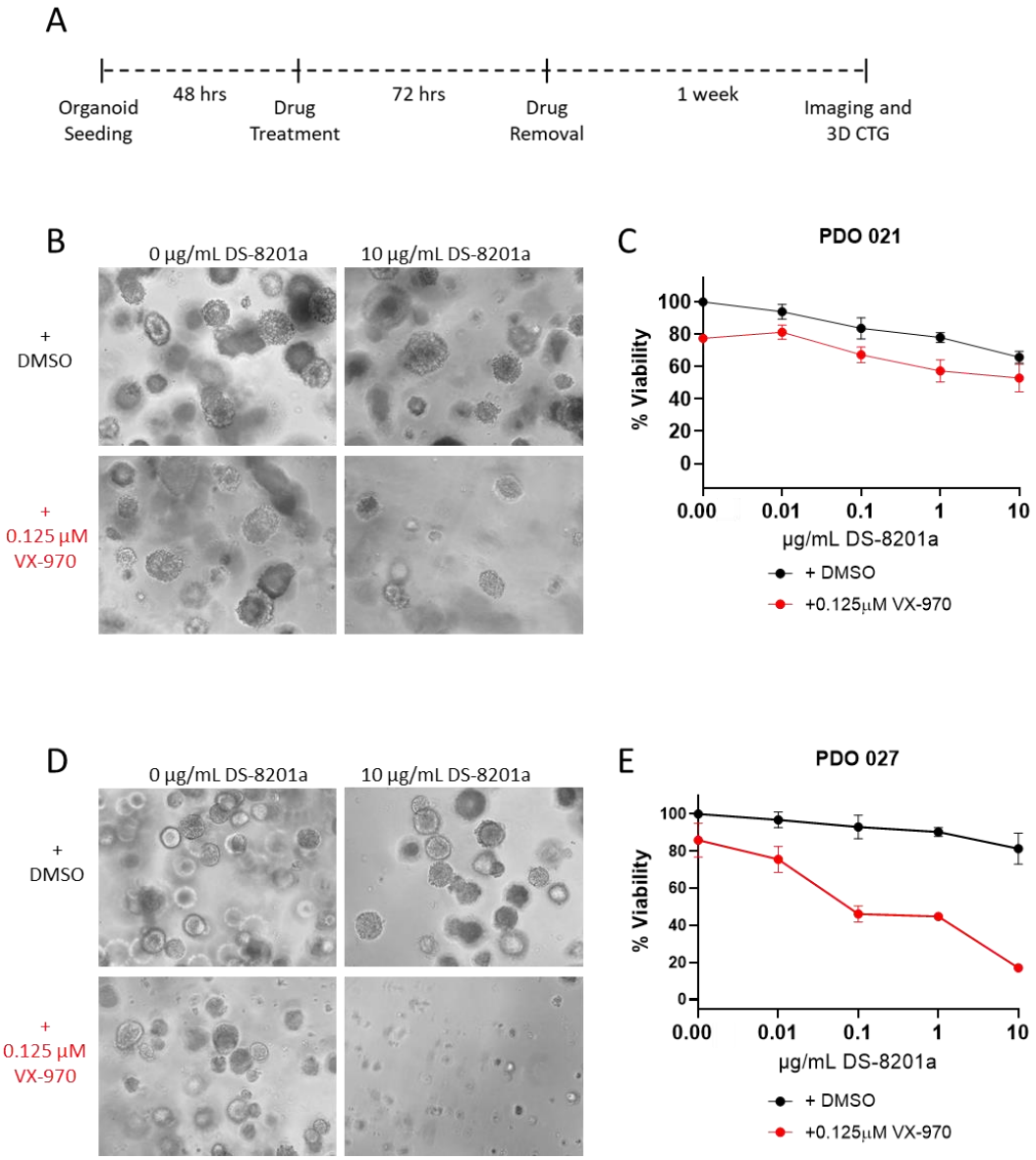

Figure 4.19. **3-Day VX-970 + DS-8201a treatment reduces developments and viability of PDOs.**

A. Scheme demonstrating the treatment schedule followed in B, C, D and E. **B.** Representative images of PDO 021 following drug treatment. **D.** Representative images of PDO 027 following drug treatment. **C.** and **E.** Organoids were treated with the indicated drugs and the percentage viability of PDO 021 and PDO 027 measured using the 3D CTG assay. Each datapoint is the mean of 3 biological repeats. Error bars represent +/- SEM.

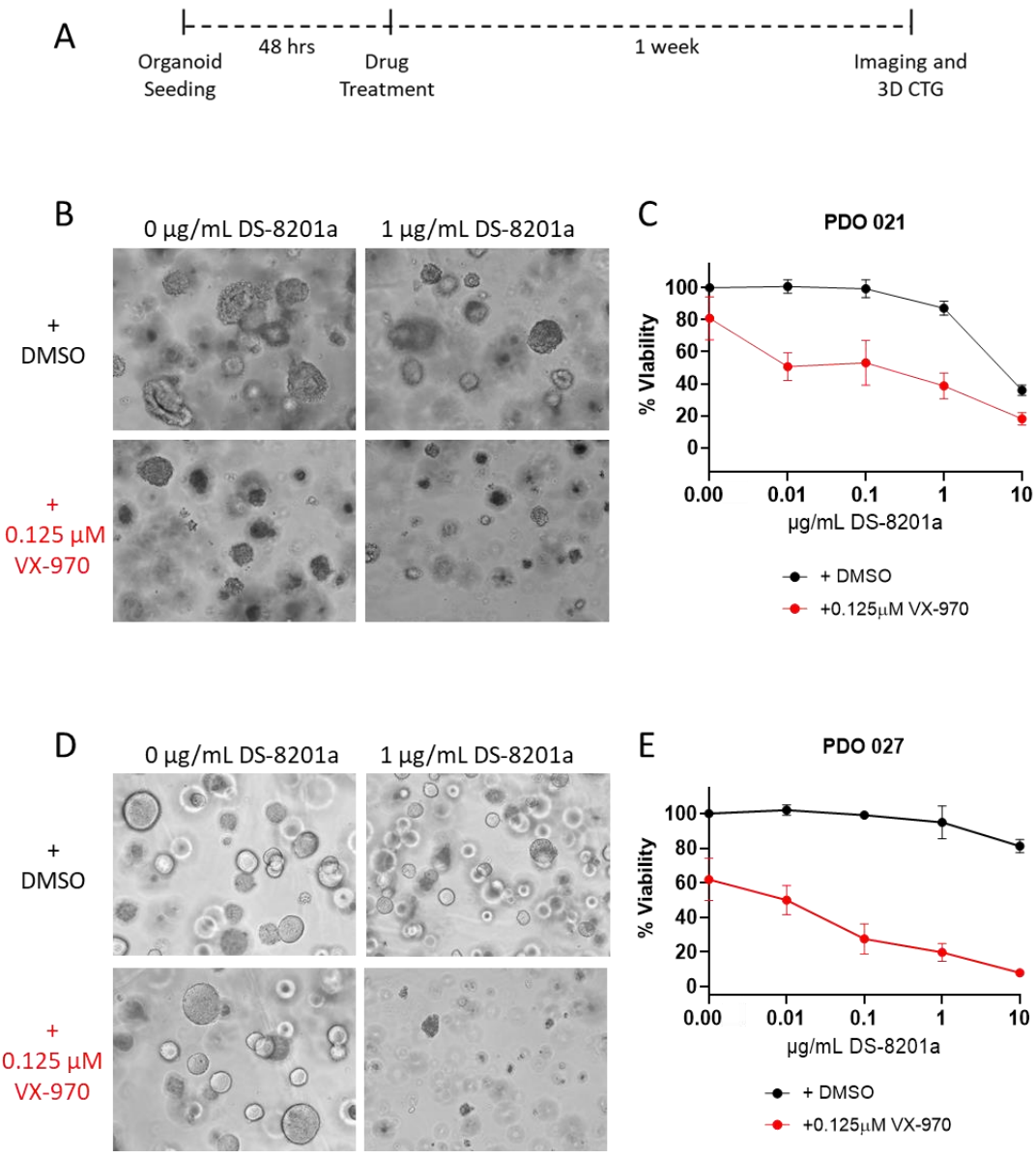

Figure 4.20. **7-Day VX-970 + DS-8201a treatment reduces viability of PDOs.**

A. Scheme demonstrating the treatment schedule followed in B, C, D and E. **B.** Representative images of PDO 021 following drug treatment. **D.** Representative images of PDO 027 following drug treatment. **C.** and **E.** Organoids were treated with the indicated drugs and the percentage viability of PDO 021 and PDO 027 measured using the 3D CTG assay. Each datapoint is the mean of 3 biological repeats. Error bars represent +/- SEM.

Sensitisation to DS-8201a by ATR inhibitor AZD6738 was also investigated, using both 3-day and 7-day treatment schedules. PDO 021 and PDO 027 were treated with dose ranges of DS-8201a and AZD6738 as monotherapies and in combination, 48 hours post seeding. In these experiments, media was replaced every 1-2 days, rather than every 2-3 days as in previous work to reduce the impact of dead cells and spent media on the viability of organoids.

With 72-hour treatment, PDOs 021 treated with DS-8201a and AZD6738 combination therapy were smaller and less developed than those treated with either monotherapy, however, they were still increasing in size (Figure 4.21 B). Viability was reduced to 66.5% (± 6.5) with 10µg/mL DS-8201a and 0.5µM AZD6738 combination therapy compared to 89.4% (±3.1) with 10µg/mL DS-8201a and 95.6% (± 4.0) with 0.5µM AZD6738 monotherapies (Figure 4.21 C-D). The average ZIP synergy score for interaction between DS-8201a and AZD6738 in PDO 021 was 13.56 (± 1.3) (Figure 4.21 E). A greater sensitisation to DS-8201a was observed with PDO 027, with organoids treated with a combination of 10µg/mL and 0.25µM AZD6738 failing to develop (Figure 4.22 B). Viability of PDOs 027 was reduced to 17.6% (± 5.2) with the combination of 10µg/mL DS-8201a and 0.5µM AZD6738 therapy, compared to 95.3% (± 3.1) with 10µg/mL DS-8201a and 59.3% (± 10.5) with 0.5µM AZD6738 monotherapies (Figure 4.22 C-D). The average ZIP synergy score for PDO 027 was 48.7 (± 1.2), demonstrating strong synergy (Figure 4.22 E).

With 7-day treatment, no sensitisation of PDO 021 to DS-8201a with the addition of AZD6738 was observed (Figure 4.23 B-D). The average ZIP synergy score for interaction between DS-8201a and AZD6738 with 7-day treatment in PDO 021 was -2.6 (± 2.6) (Figure 4.23 E). In PDO 027, synergy was observed with organoids treated with the combination failing to develop compared to those treated with either monotherapy (Figure 4.24 B). Viability with 10µg/mL DS-8201a and 0.25µM AZD6738 was reduced to 21.3% (± 1.2) compared to 93.4% (± 4.7) with 10µg/mL DS-8201a

and 89.3% (± 2.6) with 0.25μM AZD6738 monotherapies (Figure 4.24 C-D). The average ZIP synergy score was 28.0 (±1.05) (Figure 4.24 E).

Sensitisation of HER2-low expressing CRC PDOs to DS-8201 using ATR inhibition, suggests that this combination may be effective in the treatment of mCRC, despite the limited efficacy of DS-8201a monotherapy.

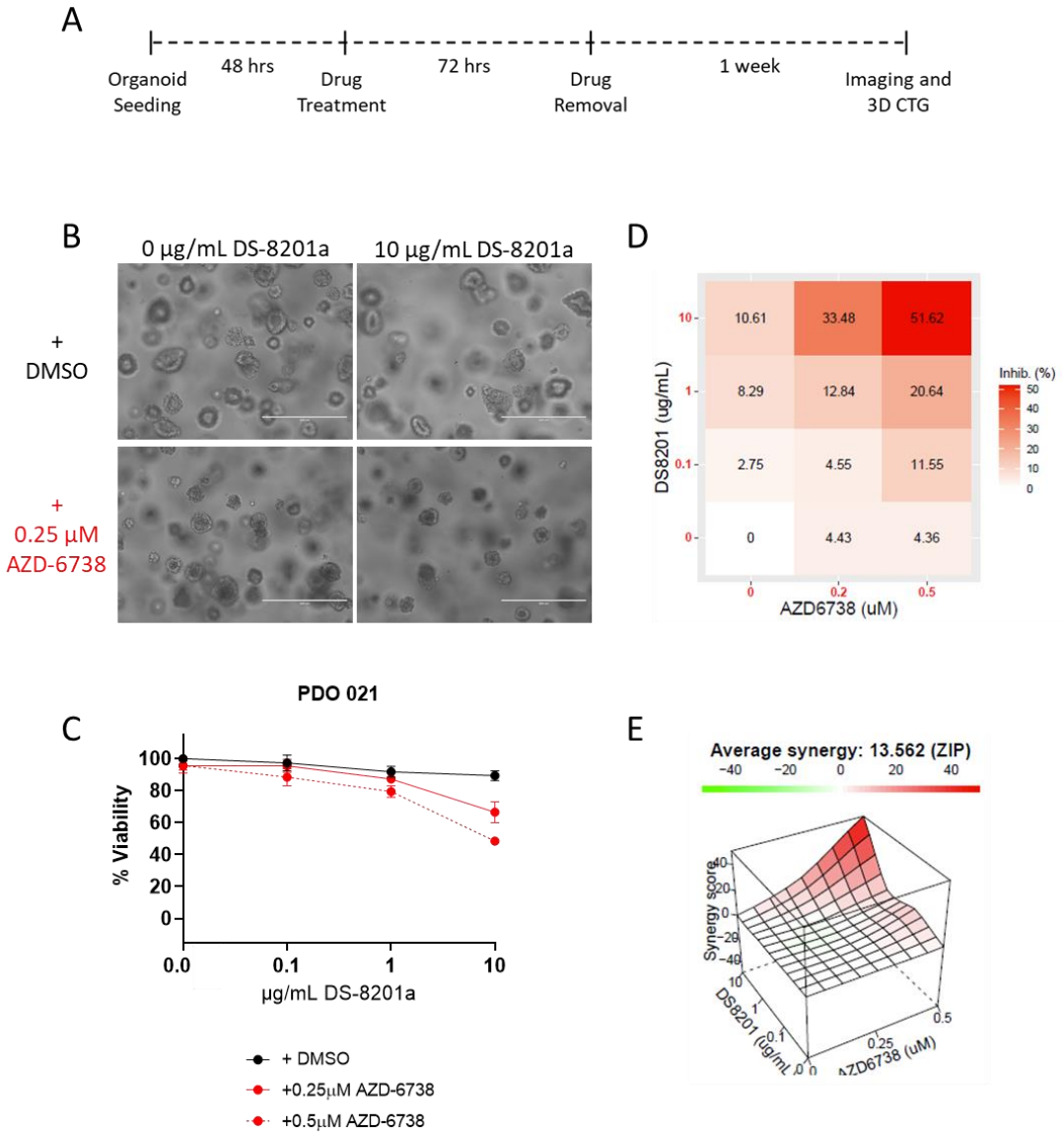

Figure 4.21. **AZD-6738 synergises with DS-8201a to reduce viability in PDO 021 following 3-day treatment.**

A. Scheme demonstrating the treatment schedule followed in B, C, D and E. **B.** Representative images of PDO 021 following drug treatment. **C.** Organoids were treated with the indicated drugs and the percentage viability of PDO 021 measured using the 3D CTG assay. Each datapoint is the mean of 3 biological repeats. Error bars represent +/- SEM. **D.** The mean percentage inhibition for each drug combination is shown in a heatmap. **E.** 3D ZIP model demonstrates the interaction between DS-8201a and AZD-6738 in PDO 021.

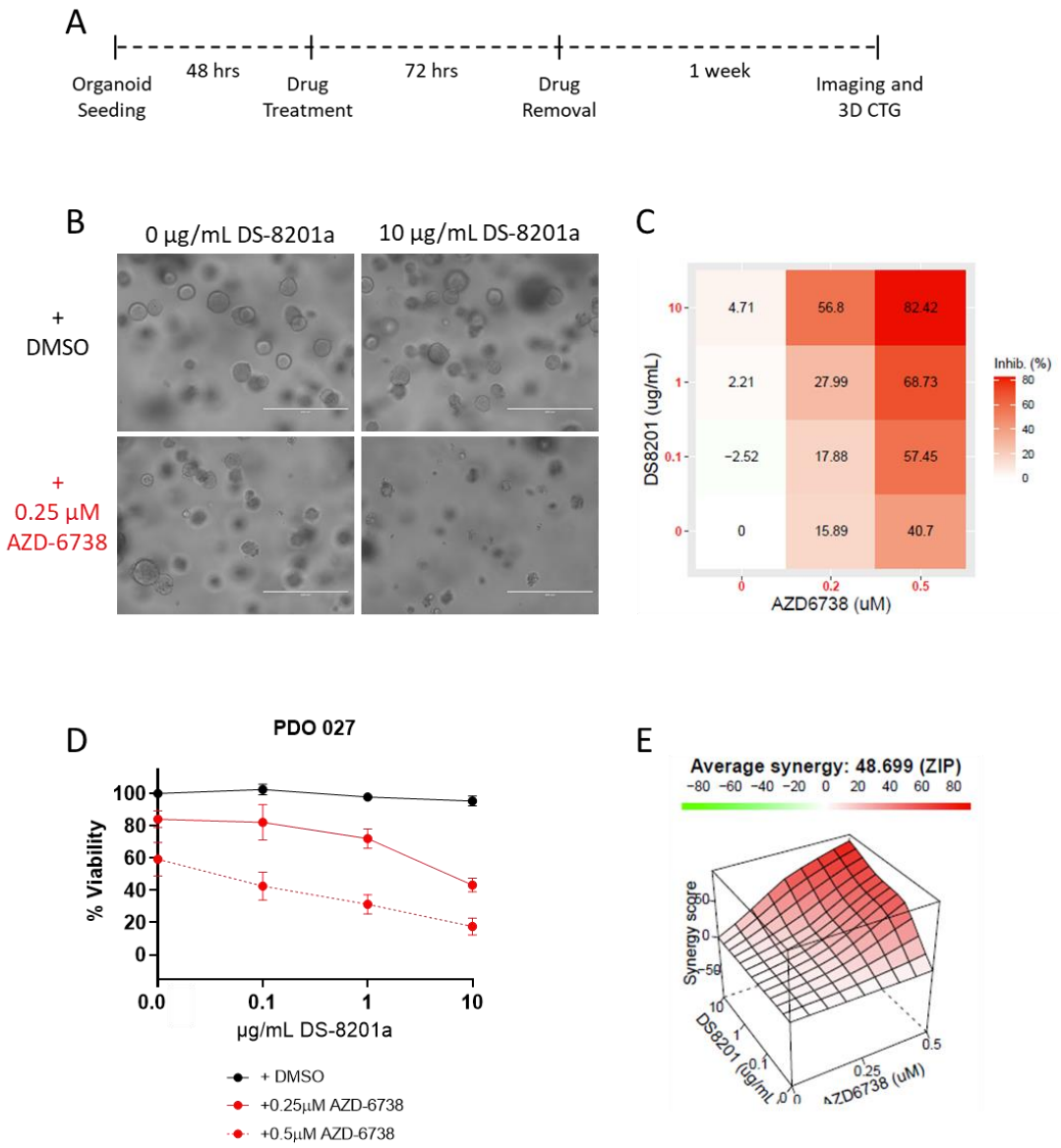

Figure 4.22. **AZD-6738 synergises with DS-8201a to reduce viability in PDO 027 following 3-day treatment.**

A. Scheme demonstrating the treatment schedule followed in B, C, D and E. **B.** Representative images of PDO 027 following drug treatment. **C.** Organoids were treated with the indicated drugs and the percentage viability of PDO 027 measured using the 3D CTG assay. Each datapoint is the mean of 3 biological repeats. Error bars represent +/- SEM. **D.** The mean percentage inhibition for each drug combination is shown in a heatmap. **E.** 3D ZIP model demonstrates the interaction between DS-8201a and AZD-6738 in PDO 027.

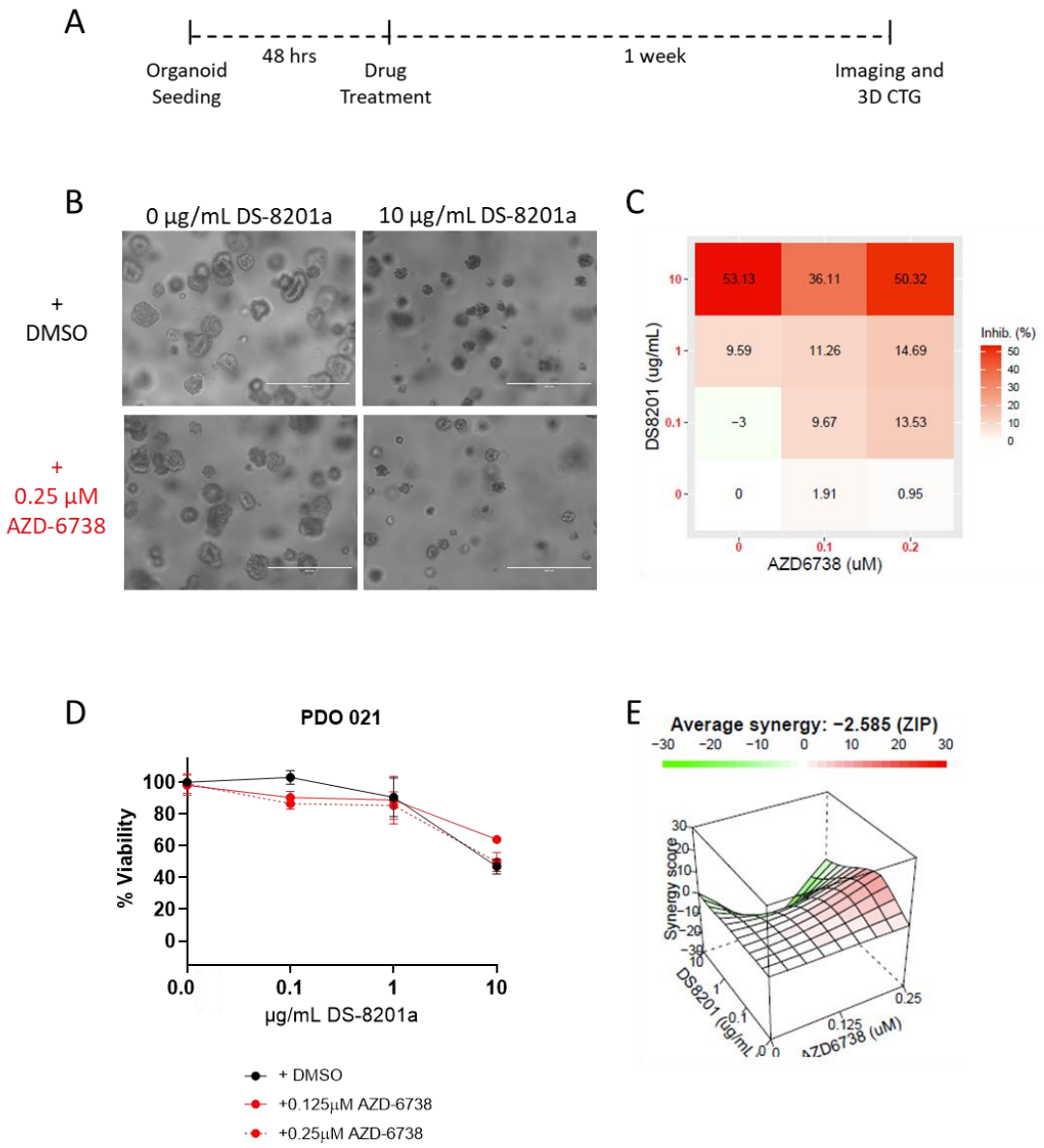

Figure 4.23. **No synergy observed between AZD-6738 and DS-8201a with 7-day treatment in PDO 021.**

A. Scheme demonstrating the treatment schedule followed in B, C, D and E. **B.** Representative images of PDO 021 following drug treatment. **C.** Organoids were treated with the indicated drugs and the percentage viability of PDO 021 measured using the 3D CTG assay. Each datapoint is the mean of 3 biological repeats. Error bars represent +/- SEM. **D.** The mean percentage inhibition for each drug combination is shown in a heatmap. **E.** 3D ZIP model demonstrates the interaction between DS-8201a and AZD-6738 in PDO 021.

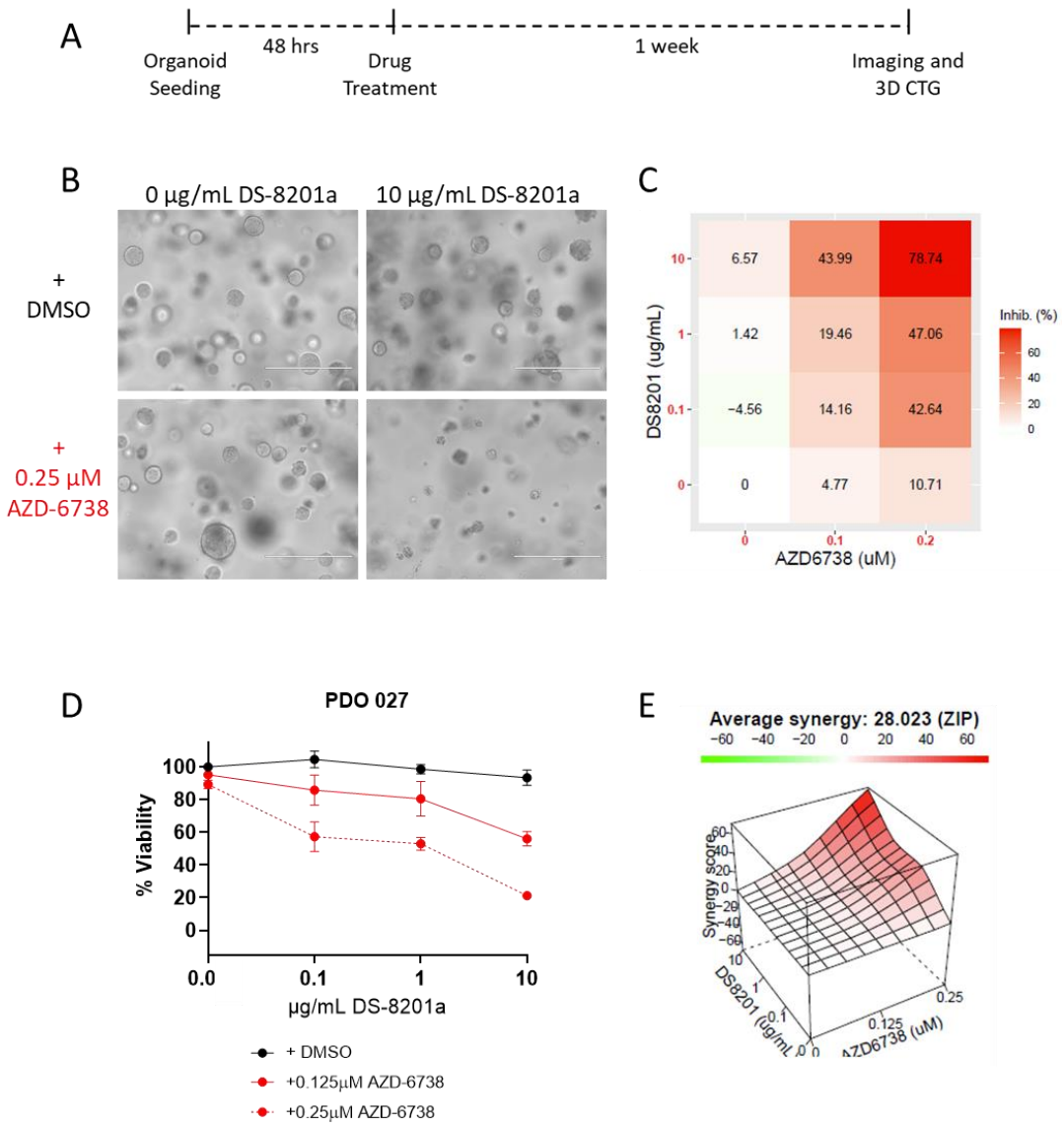

Figure 4.24. **AZD-6738 synergises with DS-8201a to reduce viability in PDO 027 with 7-day treatment.**

A. Scheme demonstrating the treatment schedule followed in B, C, D and E. **B.** Representative images of PDO 027 following drug treatment. **C.** Organoids were treated with the indicated drugs and the percentage viability of PDO 027 measured using the 3D CTG assay. Each datapoint is the mean of 3 biological repeats. Error bars represent +/- SEM. **D.** The mean percentage inhibition for each drug combination is shown in a heatmap. **E.** 3D ZIP model demonstrates the interaction between DS-8201a and AZD-6738 in PDO 027.

4.3.8 Using the CyTOF technique, increased cPARP and cCapase-3, and a reduction in pRb was detected in PDO 027 treated with DS-8201a and VX-970 combination therapy

To look at cell signalling in PDOs treated with DS-8201a monotherapy or in combination with VX-970, the CyTOF technique was used. PDOs 021 and 027 were treated on day 5 post seeding with 1µg/mL or 10µg/mL DS-8201a as a monotherapy or in combination with 0.25µM VX-970. Organoids were fixed at 24, 48 and 72 hours post treatment for CyTOF analysis. cPARP and cCaspase-3 were used as markers for apoptosis, with cells positive for both markers classed as apoptotic.

In PDO 021 there was an increase in the percentage of apoptotic cells in organoids treated with DS-8201a monotherapy at 48 and 72 hours (Figure 4.25). The effect was greatest at 72 hours, with 30.9% (± 1.5, $p<0.0001$) cPARP+/cCaspase-3+ cells with 1µg/mL DS-8201a and 37.2% (± 0.2, $p<0.0001$) cPARP+/cCaspase-3+ cells with 10µg/mL DS-8201a, compared to 5.7% (± 0.1) cPARP+/cCaspase-3+ cells in the untreated control. There was no statistical change in the percentage of cPARP+/cCaspase-3+ cells with the addition of VX-970.

In PDO 027, there was very little change in the percentage of cPARP+/cCaspase-3+ cells with DS-8201a monotherapy, with only 10µg/mL DS-8201a monotherapy at 72 hours giving a significant increase, with 20.8% (± 2.9, $p=0.03$) cPARP+/cCaspase-3+ cells compared to 10.9% (±0.06) in the untreated control (Figure 4.26). However, VX-970 as a monotherapy and in combination with DS-8201a, lead to an increase in cPARP+/cCaspase-3+ cells, with the effect being greatest with 72 hours treatment. The combination of 10µg/mL DS-8201a and 0.25µM VX-970 resulted in 52.26% (± 2.3) of cPARP+/cCaspase-3+ cells compared to 20.84% (± 2.9, $p<0.0001$) with 10µg/mL DS-8201a and 32.7% (± 2.1, $p= 0.0001$) with 0.25µM VX-970 monotherapies.

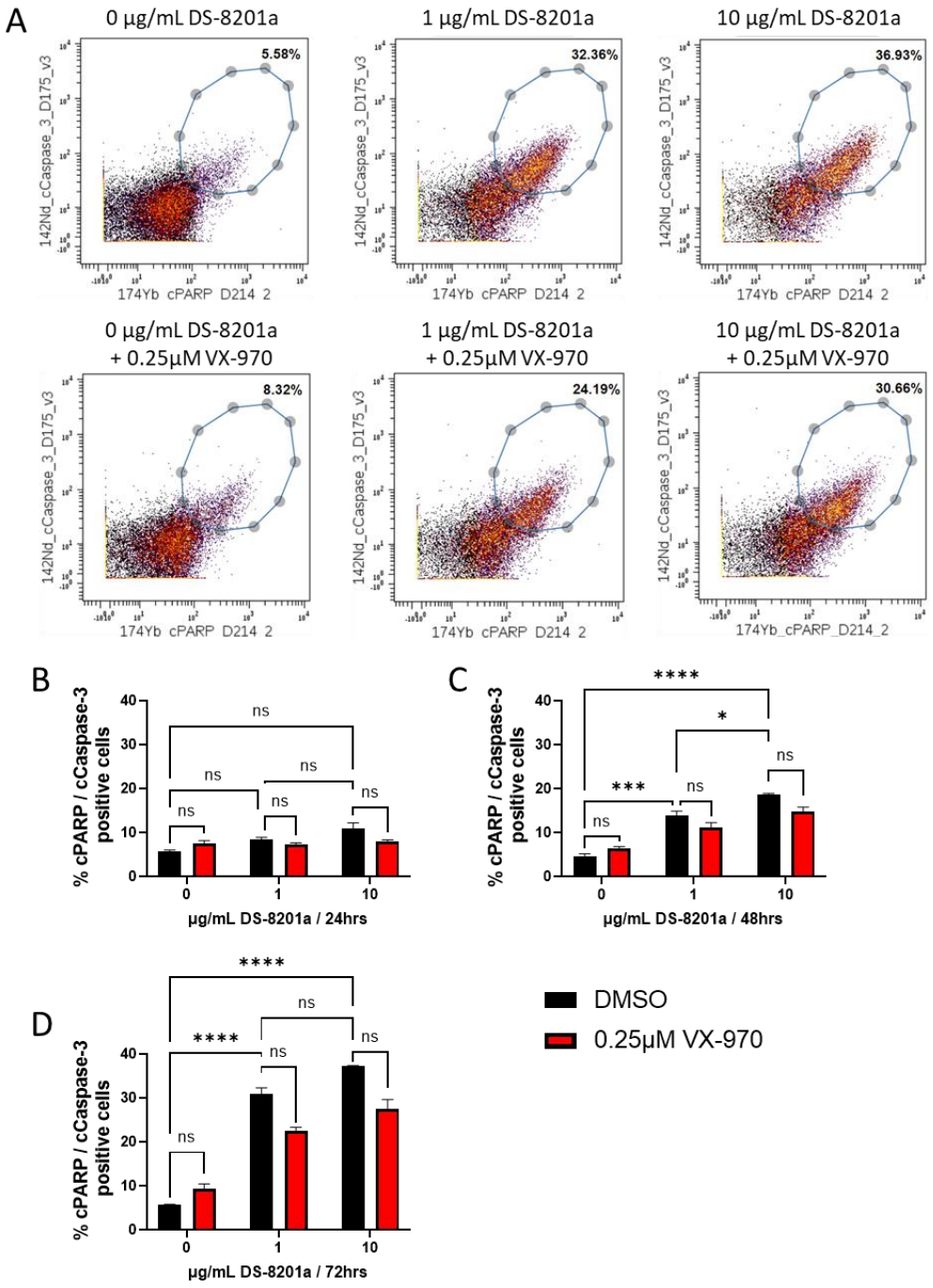

Figure 4.25. **DS-8201a monotherapy in PDO 021 leads to increased cleavage of PARP and Caspase-3.**

A. Organoids were treated for 72 hours as indicated and analysed using the CyTOF technique. Cells expressing high level of cPARP and cCaspase-3 are encircled. **B.** The percentage of cPARP and cCapase-3 positive cells at 24 hours. **C.** The percentage of cPARP and cCapase-3 positive cells at 48 hours. **D.** The percentage of cPARP and cCapase-3 positive cells at 72 hours. Plots are representative of 3 technical repeats. Statistical significance was calculated using the ANOVA test for multiple comparisons, *p* values ****<0.0001 ***<0.001 **<0.01 *<0.05.

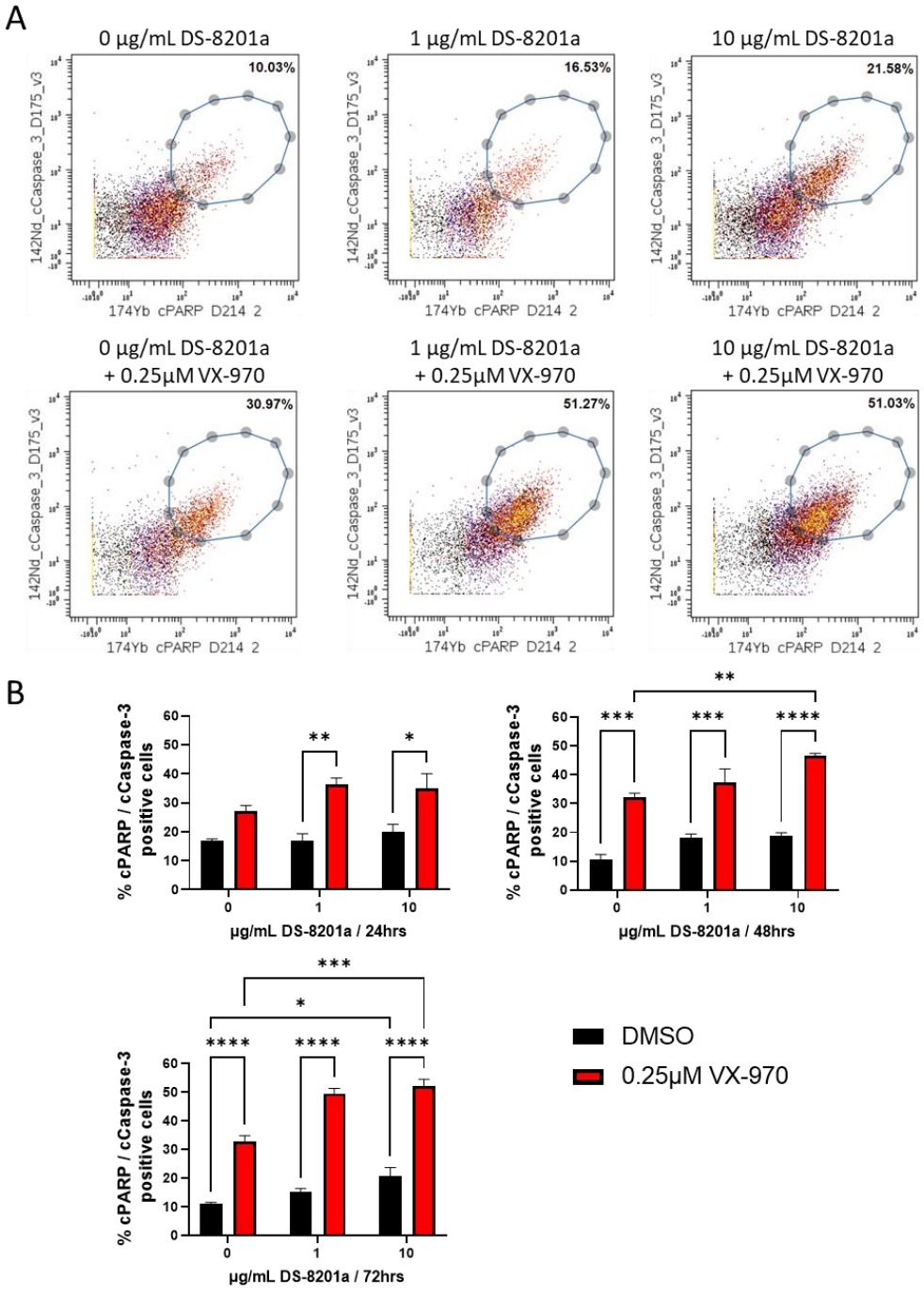

Figure 4.26. **The addition of VX-970 to DS-8201a treatment of PDO 027 results in increased cleavage of PARP and Caspase-3.**

A. Organoids were treated for 48 hours as indicated and analysed using the CyTOF technique. Cells expressing high level of cPARP and cCaspase-3 are encircled. **C.** The percentage of cPARP and cCapase-3 positive cells at 24 hours. **D.** The percentage of cPARP and cCapase-3 positive cells at 48 hours. **E.** The percentage of cPARP and cCapase-3 positive cells at 72 hours. Plots are representative of 3 technical repeats. Statistical significance was calculated using the ANOVA test for multiple comparisons, *p* values ****<0.0001 ***<0.001 **<0.01 *<0.05.

The change in viability of PDOs with DS-8201a monotherapy or in combination with VX-970 could also be visualised by uMAP analysis. In PDOs 021, plotting the uMAPs according to cell state and colouring by cPARP, showed the population of cPARP+ cells to increase with DS-8201a monotherapy, but not increase further with the addition of VX-970 (Figure 4.27 A). Furthermore, colouring the uMAPS by pRb, to show cells actively cycling, showed an increase in pRb- cells with DS-8201a monotherapy, this did not increase further with the addition of VX-970 (Figure 4.27 B). In line with the increase in cPARP+/cCaspase-3+ cells following combination therapy in PDOs 027, using uMAP analysis, there was an increase in the population of cPARP+ cells and pRb- cells in combination treated organoids, compared to those treated with either monotherapy (Figure 4.28).

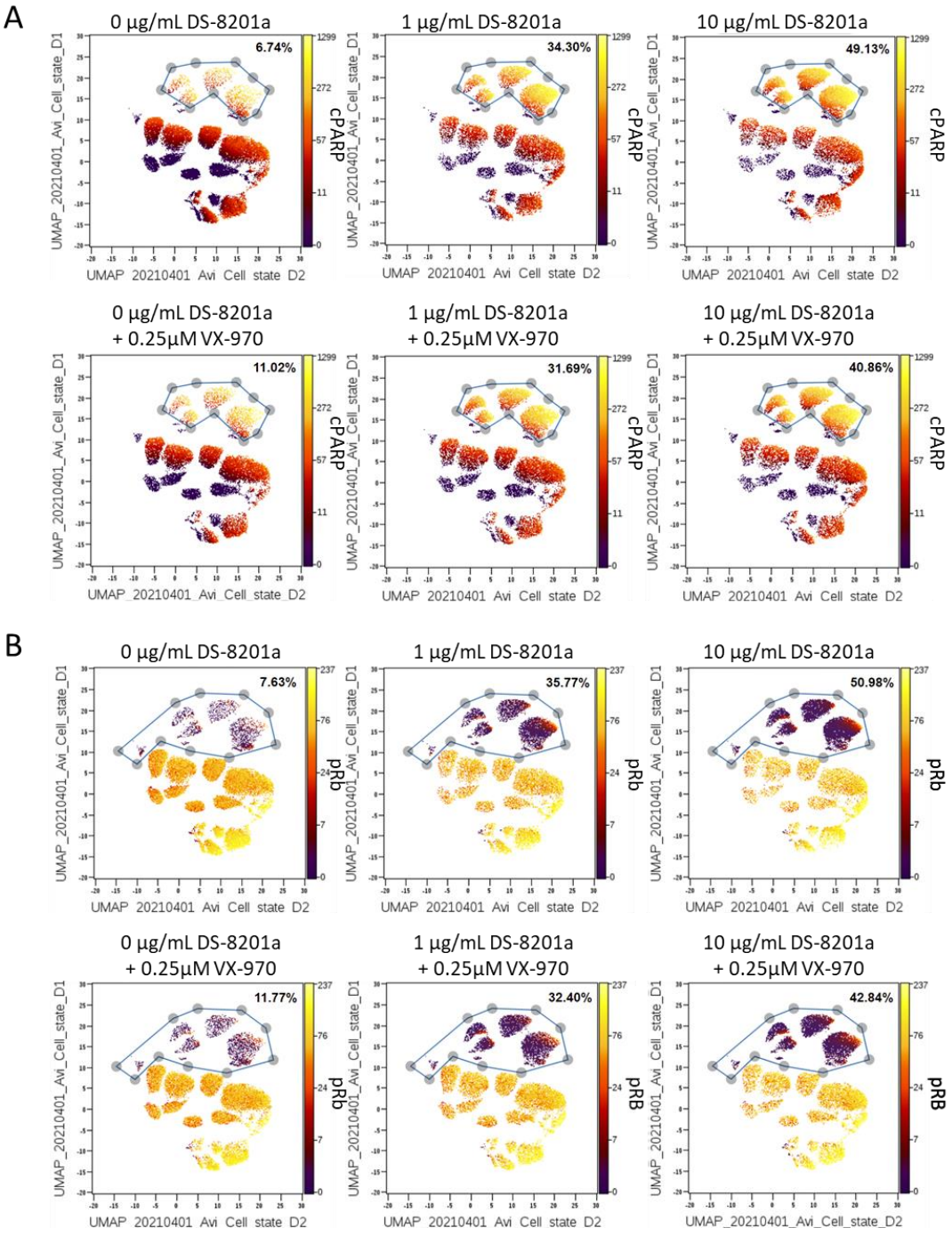

Figure 4.27. **DS-8201a monotherapy of PDO 021 increases cPARP and reduces pRb levels.**

A. Organoids were treated for 72 hours with the indicated drug combinations and analysed using the CyTOF technique. uMAPS were generated to cluster cells according to cell cycle markers and are coloured by **A.** the intensity of cPARP staining and **B.** the intensity of pRb staining. Plots are representative of 3 technical repeats.

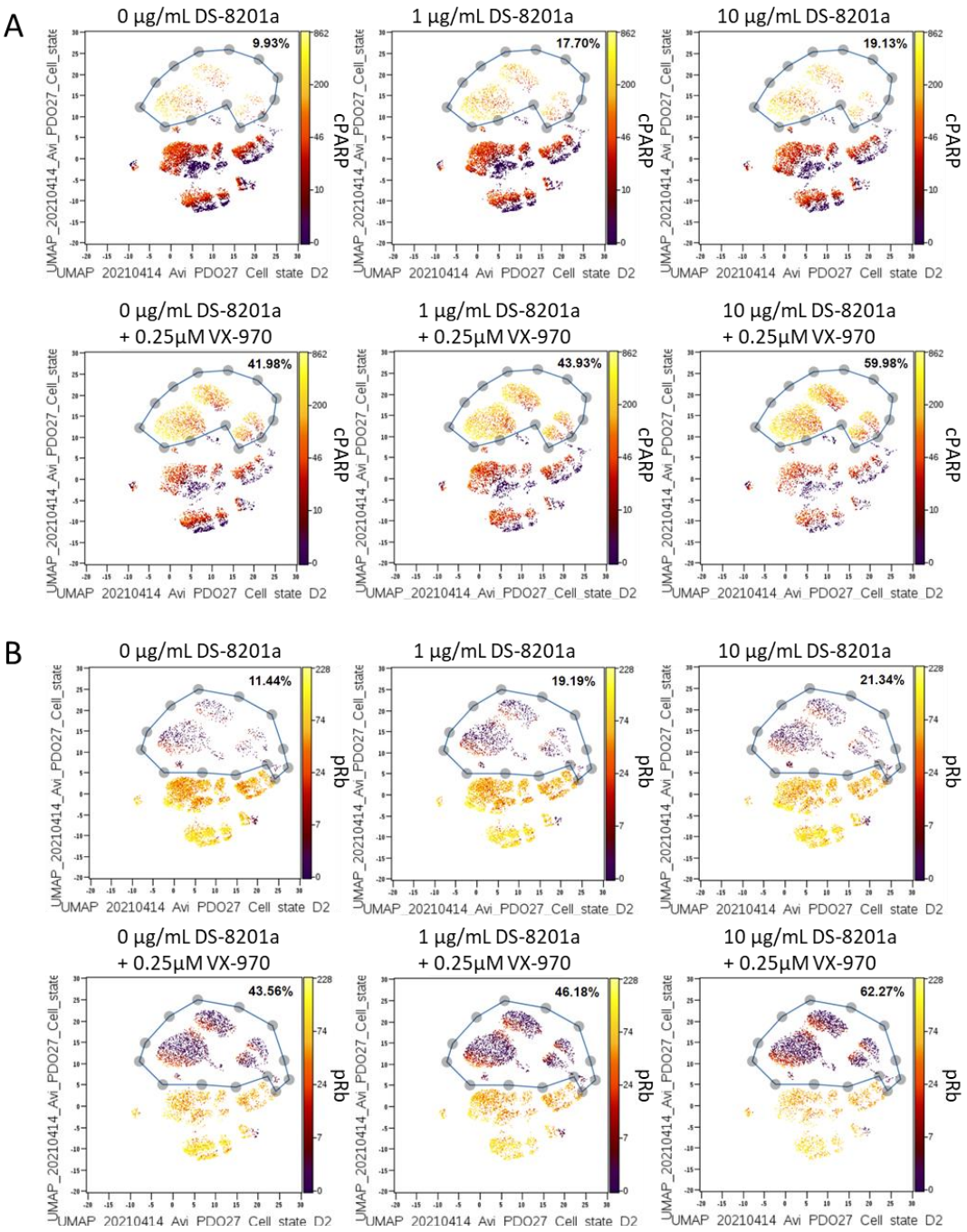

Figure 4.28. **The addition of VX-970 to DS-8201a treatment of PDO 027 increases cPARP and reduces pRb levels.**

A. Organoids were treated for 48 hours with the indicated drug combinations and analysed using the CyTOF technique. uMAPS were generated to cluster cells according to cell cycle markers and are coloured by **A.** the intensity of cPARP staining and **B.** the intensity of pRb staining. Plots are representative of 3 technical repeats.

4.3.9 VX-970 reduces DS-8201a-induced S-phase block in PDO 021

In this study we have shown ATR inhibition to enable replication fork progression in the presence of TOP1 inhibition (Figure 3.24). To assess whether DS-8201a inhibits replication fork progression, and whether VX-970 could reduce any S-phase stalling, IdU incorporation was analysed using the CyTOF technique.

In PDO 021, at 72 hours of 10µg/mL DS-8201a treatment, there was a reduction in the rate of IdU incorporation compared to the untreated controls, this could be visualised by a shift to the left of the S-phase population in IdU histograms, and a reduced IdU staining intensity of S-phase cells in uMAPs (Figure 4.29). The addition of VX-970 to 10µg/mL DS-8201a increased the rate of IdU incorporation close to that observed in untreated cells. In PDO 027, a reduction in the rate of IdU incorporation could be visualised at with DS-8201a monotherapy, however this was not as dramatic as that observed in PDO 021 (Figure 4.30 and Figure 4.31). There was no clear reversal of this reduced replication rate at 24 hours with the addition of VX-970 (Figure 4.30). At 72 hours, the percentage of S-phase cells was reduced in organoids treated with the combination treatment compared to DS-8201a monotherapy treated organoids, furthermore the replication rate was very low in the combination treated cells (Figure 4.31).

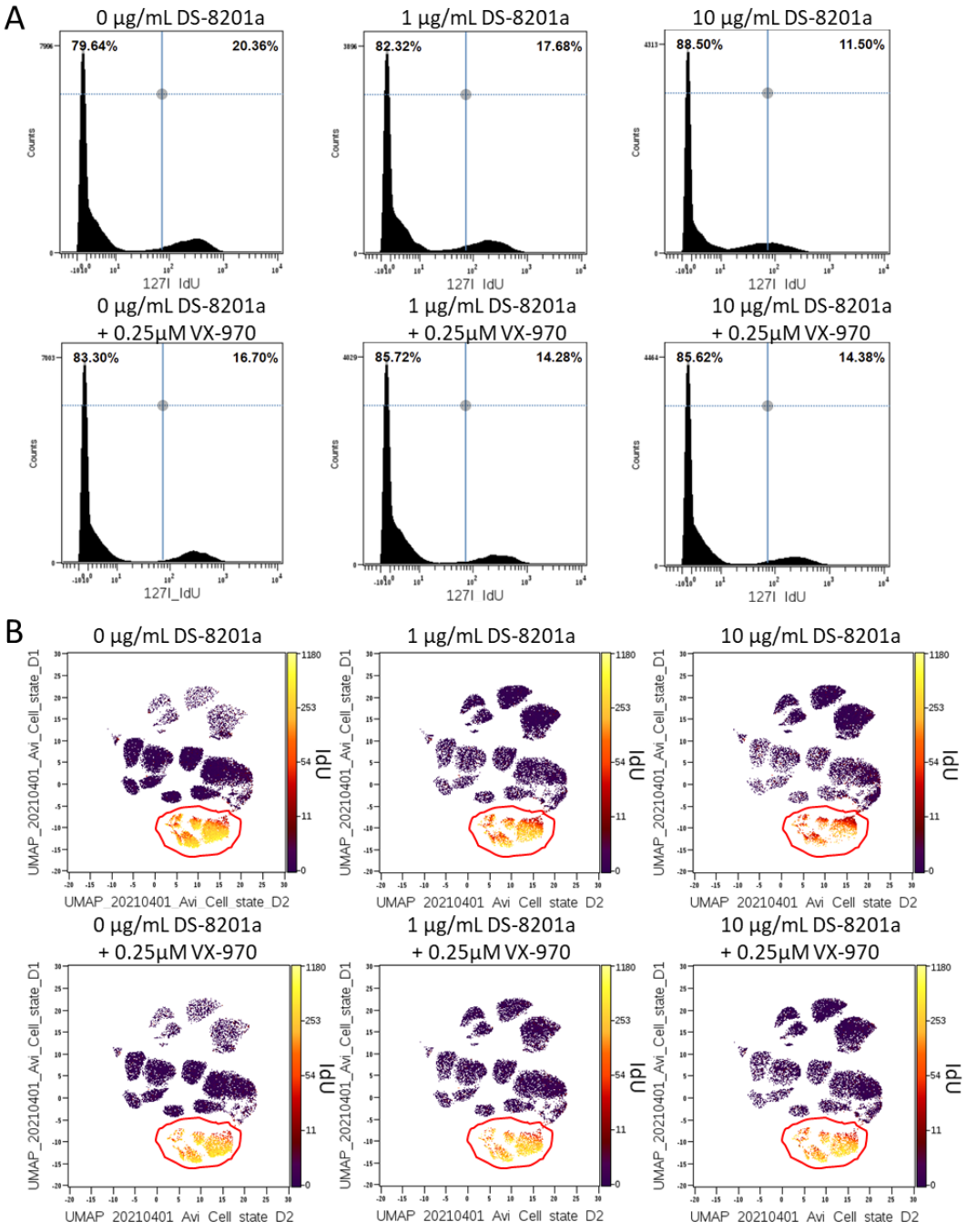

Figure 4.29. **VX-970 reduces DS-8201a induced S-phase block in PDO 021 organoids.** Organoids were treated for 72 hours with the indicated drugs and IdU incorporation measured using the CyTOF technique. **A.** IdU profiles **B.** uMAPS were generated to cluster cells according to cell cycle markers and are coloured by the intensity of IdU staining. Cells in S-phase are encircled. Plots are representative of 3 technical repeats.

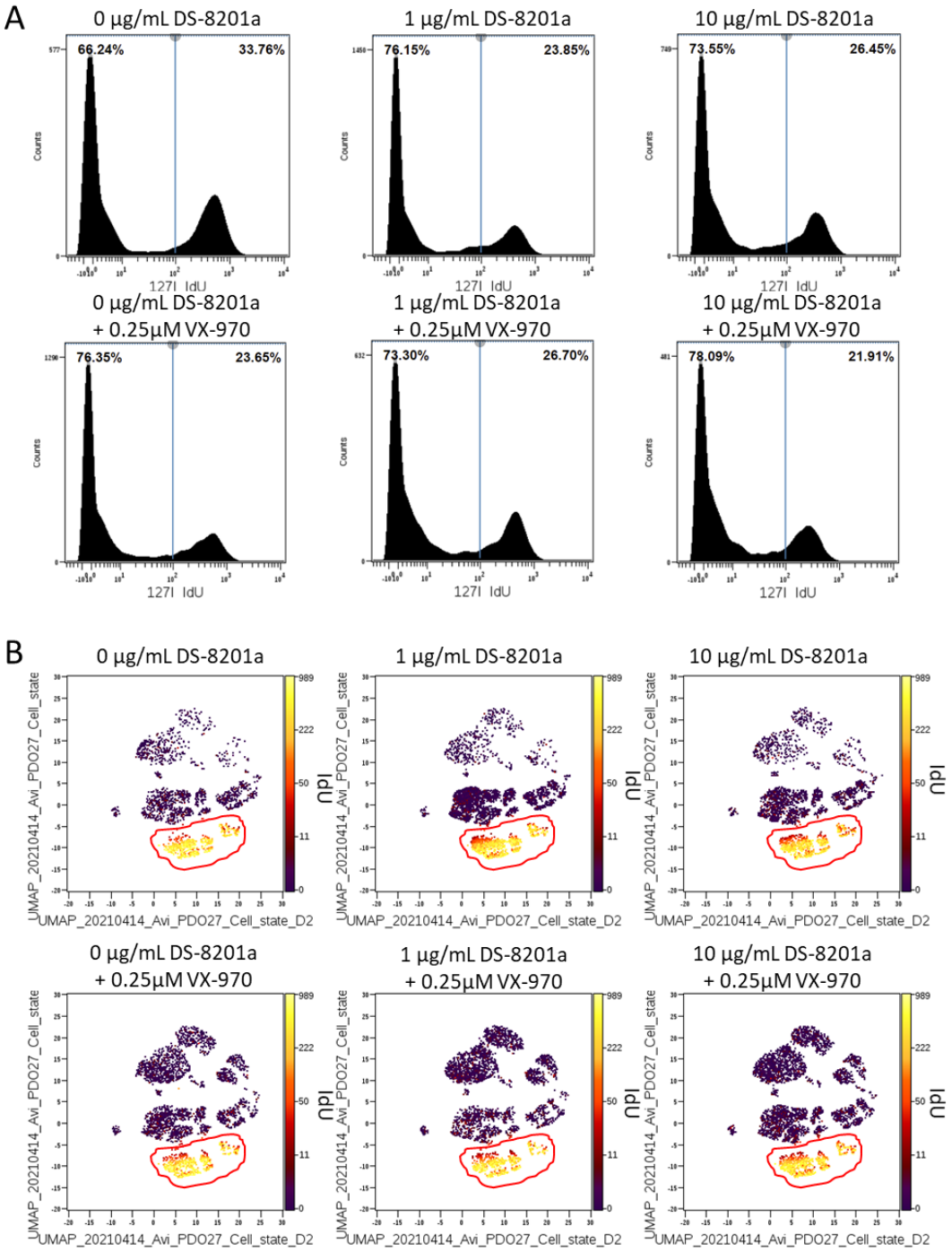

Figure 4.30. **DS-8201a reduces replication progression in PDO 027 at 24 hours.** Organoids were treated for 24 hrs with the indicated drugs and IdU incorporation measured using the CyTOF technique. **A.** IdU profiles **B.** uMAPS were generated to cluster cells according to cell cycle markers and are coloured by the intensity of IdU staining. Cells in S-phase are encircled. Images are representative of 3 technical repeats.

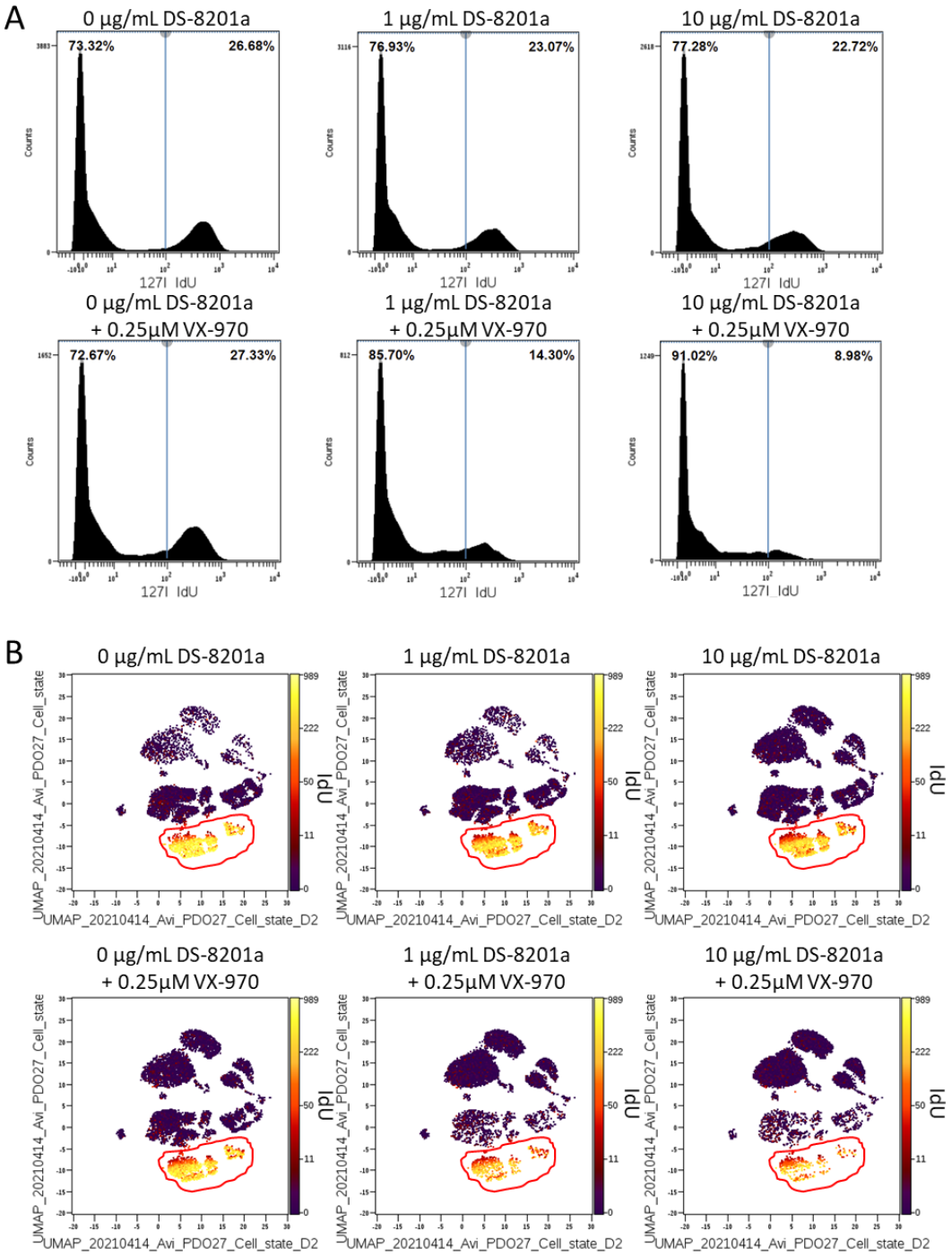

Figure 4.31. **DS-8201a-induced replication block is not reduced with VX-970 in PDO 027 at 72 hours.**

Organoids were treated for 72 hrs with the indicated drugs and IdU incorporation measured using the CyTOF technique. **A.** IdU profiles **B.** uMAPS were generated to cluster cells according to cell cycle markers and are coloured by the intensity of IdU staining. Cells in S-phase are encircled. Images are representative of 3 technical repeats.

4.3.10 DNA damage response to DS-8201a monotherapy and DS-8201a and VX-970 combination therapy

To investigate the DNA damage response in organoids following DS-8201a monotherapy and DS-8201a and VX-970 combination therapy, pH2AX, pDNA-PK and pChk1 antibodies were included in the CyTOF antibody panel. pChk1 was used as a surrogate for ATR activation, as multiple pATR antibodies failed to give a signal with the CyTOF technique using SN38 as a positive control.

In PDO 021, a small increase in the percentage of pChk1+ cells was detected at 24, 48 and 72 hours with 1µg/mL and 10µg/mL DS-8201a monotherapies (Figure 4.32). This increase was reduced with the addition of VX-970. At 48 hours, the percentage of pChk1+ cells increased from 1.2% (± 0.007) in untreated controls to 5.9% (± 0.23, p=0.015) with 1µg/mL DS-8201a and 6.9% (± 0.19, p=0.02) with 10µg/mL DS-8201a monotherapies. The addition of VX-970 to 1µg/mL DS-8201a reduced the percentage of pChk1+ cells to 1.7% (± 0.14, p=0.012), and the addition of VX-970 to 10µg/mL DS-8201a reduced the percentage of pChk1+ cells to 2.4% (± 0.16, p=0.001). A shift in pChk1 signal of the entire population with DS-8201a therapy, can be seen in a histogram plot (Figure 4.32 E). In PDO 027, a similar effect was observed, with the small increase in the percentage of pChk1+ cells detected with DS-8201a monotherapy, reduced to the level in untreated cells with the addition of VX-970 (Figure 4.33). At 48 hours, the percentage of pChk1+ cells increased from 2.1 % (± 0.03) in untreated controls to 6.3% (± 0.79, p=0.001) with 1µg/mL DS-8201a and 8.9% (± 0.73, p<0.0001) with 10µg/mL DS-8201a monotherapies. The addition of VX-970 to 1µg/mL DS-8201a reduced the percentage of pChk1+ cells to 2.2% (± 0.23, p=0.001), and the addition of VX-970 to 10µg/mL DS-8201a reduced the percentage of pChk1+ cells to 1.7% (± 0.24, p<0.0001). A shift in pChk1 signal of the entire population with DS-8201a therapy was also observed and can be seen in a histogram plot (Figure 4.33 E).

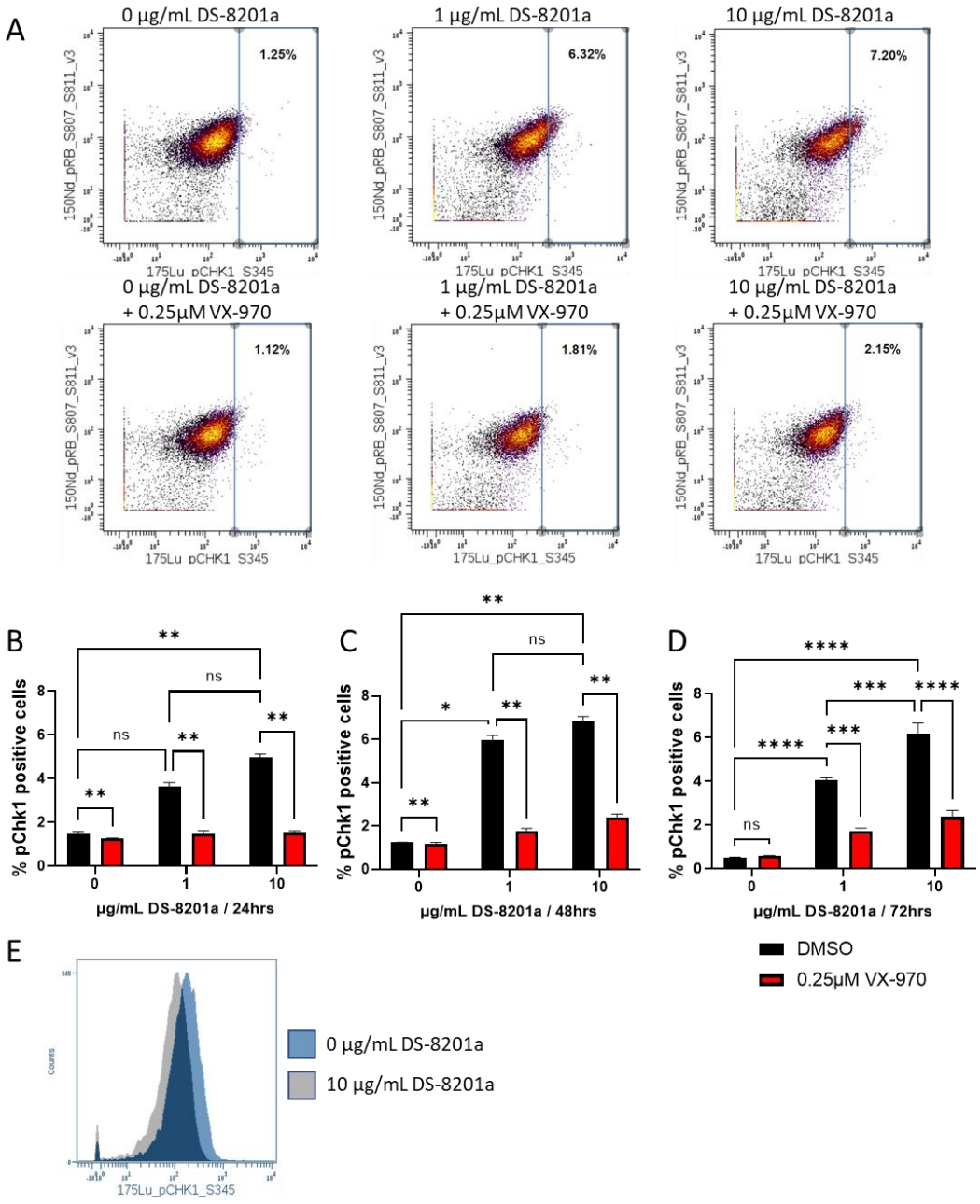

Figure 4.32. **VX-970 abrogates DS-8201a induced Chk1 phosphorylation in PDO 021.** **A.** Organoids were treated for 48 hours as indicated and analysed using the CyTOF technique. Plots are gated to show the percentage pChk1 positive cells. **B.** The percentage pChk1 positive cells at 24 hours. **C.** The percentage pChk1 positive cells at 48 hours. **D.** The percentage pChk1 positive cells at 72 hours. **E.** Histogram showing the shift in pChk1 phosphorylation with DS-8201a monotherapy at 48 hours. Plots are representative of 3 technical repeats. Statistical significance was calculated using the ANOVA test for multiple comparisons, *p* values ****<0.0001 ***<0.001 **<0.01 *<0.05.

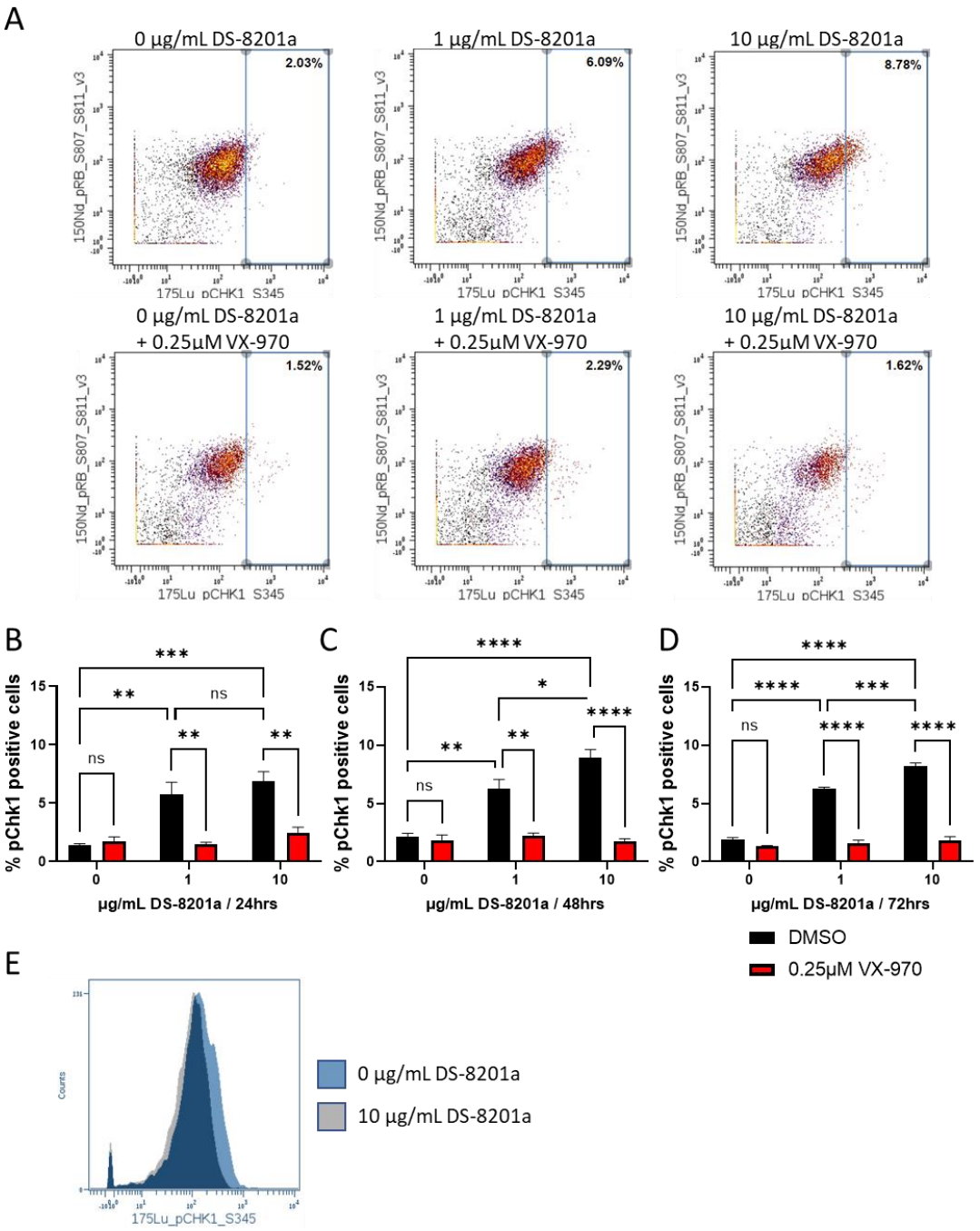

Figure 4.33. **VX-970 abrogates DS-8201a induced Chk1 phosphorylation in PDO 027.** **A.** Organoids were treated for 48 hours as indicated and analysed using the CyTOF technique. Plots are gated to show the percentage pChk1 positive cells. **B.** The percentage pChk1 positive cells at 24 hours. **C.** The percentage pChk1 positive cells at 48 hours. **D.** The percentage pChk1 positive cells at 72 hours. **E.** Histogram showing the shift in pChk1 phosphorylation with DS-8201a monotherapy at 48 hours. Plots are representative of 3 technical repeats. Statistical significance was calculated using the ANOVA test for multiple comparisons, *p* values ****<0.0001 ***<0.001 **<0. 01 *<0.05.

The percentage of pH2AX+ cells increased with DS-8201a monotherapy in PDO 021, however this was to a lesser extent than the 10nM SN38 treatment used as a positive control. The percentage of pH2AX+ cells in organoids treated with DS-8201a monotherapy increased between 24 and 48 hours and remained stable at 72 hours (Figure 4.34). At 48 hours, the percentage of pH2AX+ cells increased from 6.1% (± 0.38) in untreated organoids to 18.9% (± 0.75, $p<0.0001$) with 1µg/mL DS-8201a and 20.9% (± 0.6, $p<0.0001$) with 10µg/mL DS-8201a. The addition of VX-970 to DS-8201a monotherapy caused a reduction in the percentage of pH2AX+ cells at all time points. At 48 hours, the addition of VX-970 to 1µg/mL DS-8201a therapy reduced the percentage of pH2AX+ cells to 5.6% (± 0.8, $p<0.0001$), and the addition of VX-970 to 10µg/mL DS-8201a therapy reduced the percentage of pH2AX+ cells to 8.9% (± 0.27 $p<0.0001$).

Colouring the pH2AX dot plots by IdU signal intensity, showed that in both untreated and treated organoids, IdU+ cells had a higher pH2AX signal than IdU- cells. The change in pH2AX signal with DS-8201a monotherapy occurred via a slight shift in the pH2AX signal of S-phase cells (Figure 4.35 A). pH2AX+ cells with DS-8201a monotherapy also had increased levels of PLK compared to pH2AX- cells, further supporting an association between pH2AX signal and S-phase. Increased pH2AX signal was not associated with cPARP or cCaspase-3 signal (Figure 4.35 B).

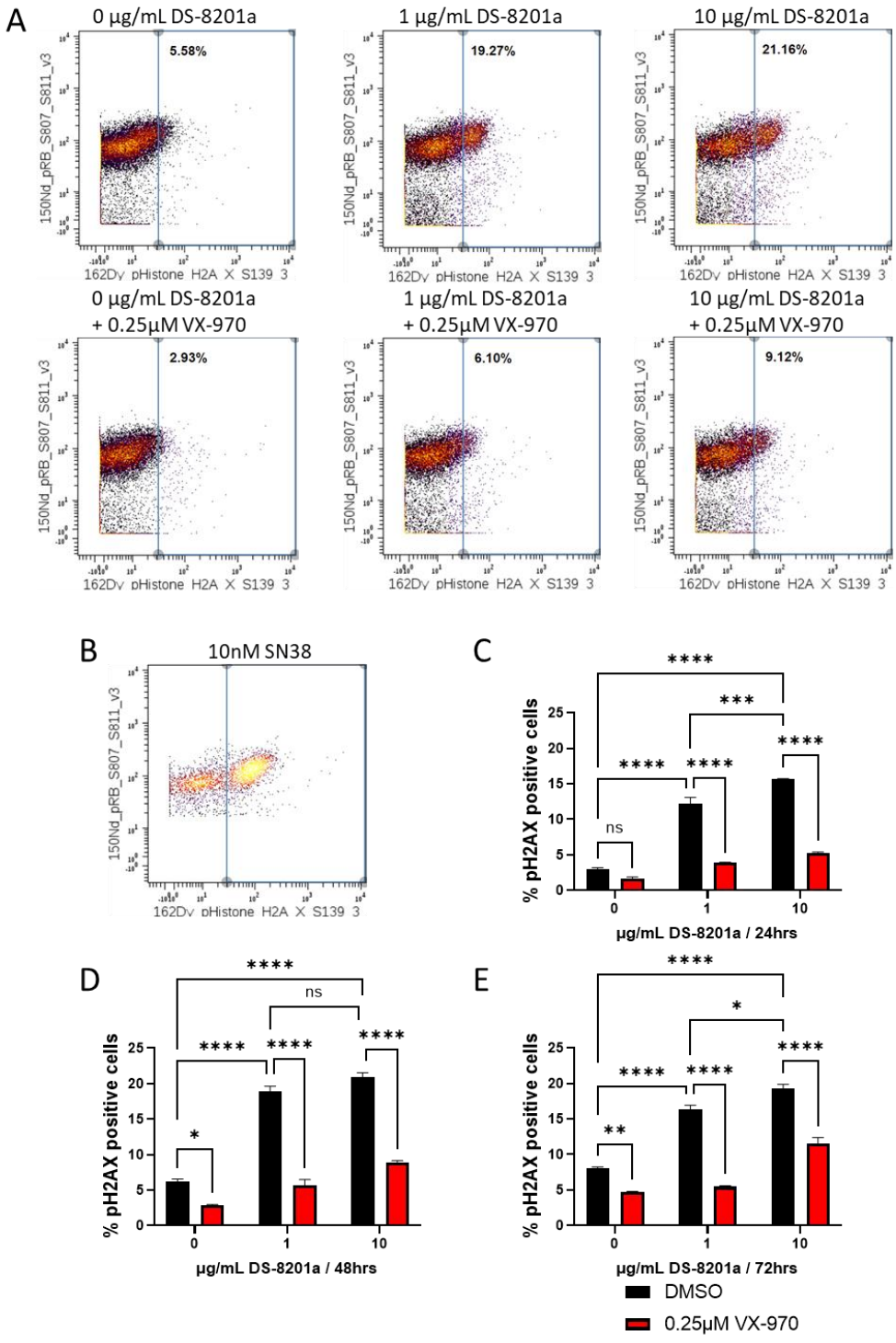

Figure 4.34. **VX-970 reduces DS-8201a induced phosphorylation of H2AX in PDO 021.** **A.** Organoids were treated for 48 hours as indicated and analysed using the CyTOF technique. Plots are gated to show the population of pH2AX positive cells. **B.** Positive control for pH2AX. **C.** The percentage of pH2AX positive cells at 24 hours. **D.** The percentage of pH2AX positive cells at 48 hours. **E.** The percentage of pH2AX positive cells at 72 hours. Plots are representative of 3 technical repeats. Statistical significance was calculated using the ANOVA test for multiple comparisons, *p* values ****<0.0001 ***<0.001 **<0.01 *<0.05.

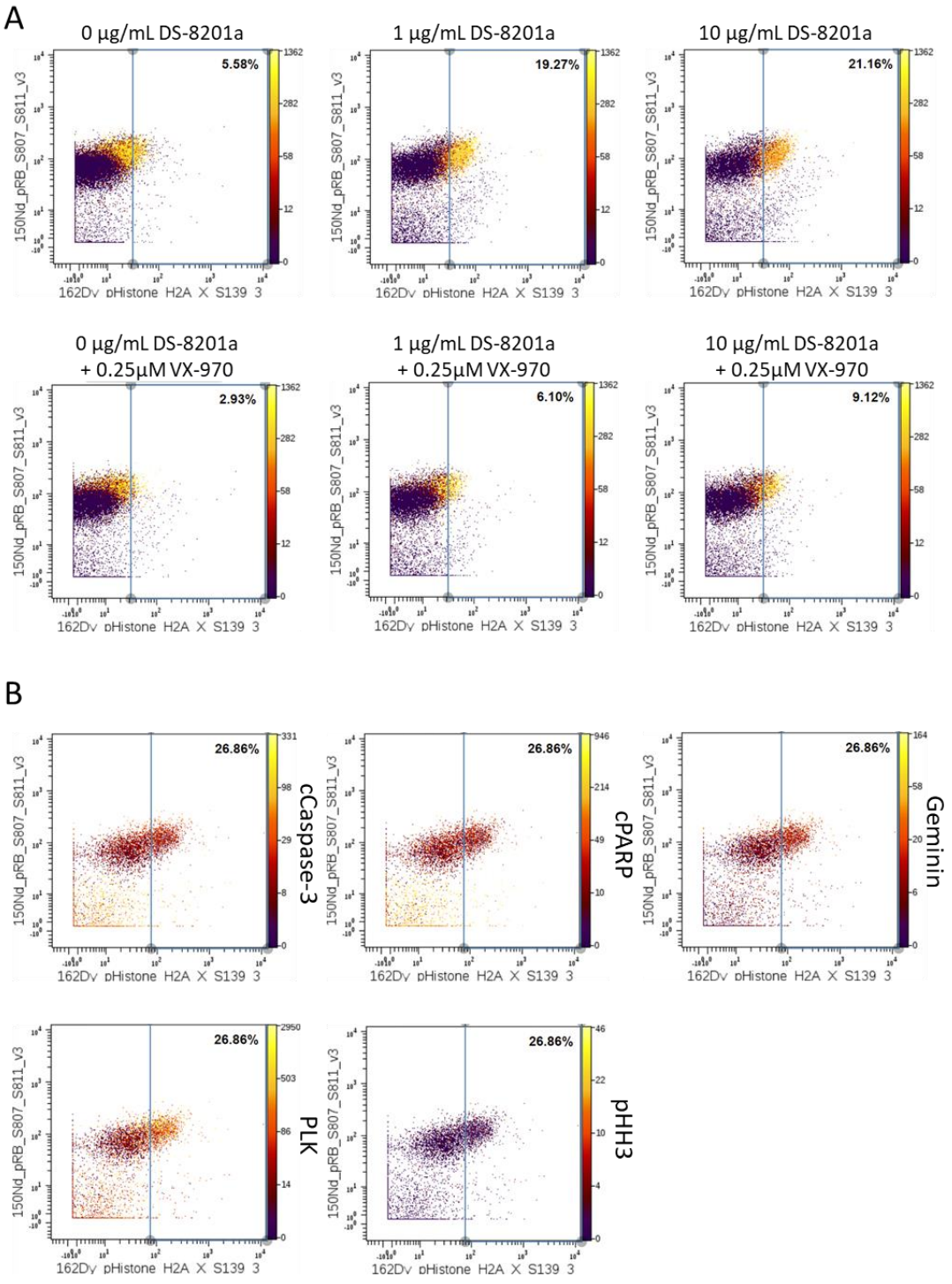

Figure 4.35. **S-phase cells from PDO 021 have increased pH2AX signal.**

A. Organoids were treated for 48 hours with the indicated drugs and analysed using the CyTOF technique. Plots show pH2AX staining, with cells in each plot are coloured according to the signal intensity of IdU. **B.** Organoids were treated for 48 hours with 10µg/mL DS-8201a. Plots show pH2AX staining, with cells in each plot are coloured according to the indicated stain.

In PDO 027, there was a distinct population of pH2AX+ cells in organoids treated with a combination of DS-8201a and VX-970 compared to organoids treated with DS-8201a monotherapy (Figure 4.36). The greatest increase in pH2AX+ cells was observed at 72 hours, with 15.4% (± 0.6) of cells treated with 10µg/mL DS-8201a and 0.25µM VX-970 combination therapy being pH2AX+, compared to 2.8% (± 0.2, $p<0.0001\%$) treated with 10µg/mL DS-8201a monotherapy. Although to a lesser extent than in PDO 021, there was a shift in the pH2AX signal in the S-phase population with DS-8201a monotherapy, however the signal was much lower than that observed with DS-8201a and VX-970 combination therapy (Figure 4.37).

There was a very low percentage of cells which were pDNA-PK positive, across all treatment groups in PDOs 021 and 027, with no treatment resulting in a greater than 2.5% pDNA-PK+ cells (Figure 4.38 and Figure 4.39). While some of the changes seen are statistically significant, these are unlikely to be of biological relevance as the changes observed were below 1%.

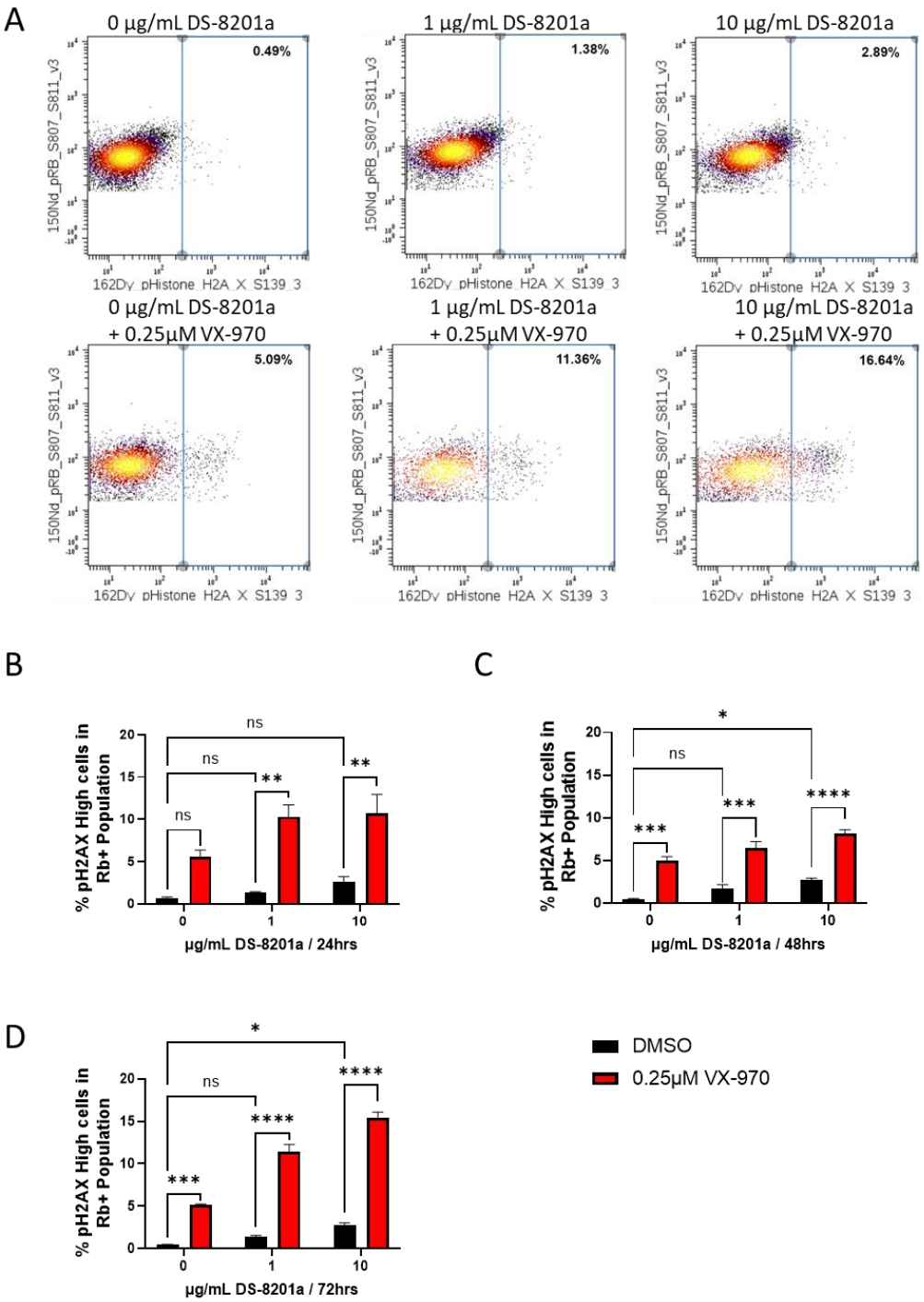

Figure 4.36. **VX-970 + DS-8201a combination treatment increases H2AX phosphorylation.**

A. Organoids were treated for 72 hours as indicated and analysed using the CyTOF technique. Plots are gated to show the population of cells with very high levels of pH2AX. **B.** The % of cells with high pH2AX at 24 hours. **C.** The % of cells with high pH2AX at 48 hours. **D.** The % of cells with high pH2AX at 72 hours. Plots are representative of 3 technical repeats. Statistical significance was calculated using the ANOVA test for multiple comparisons, *p* values ****<0.0001 ***<0.001 **<0. 01 *<0.05.

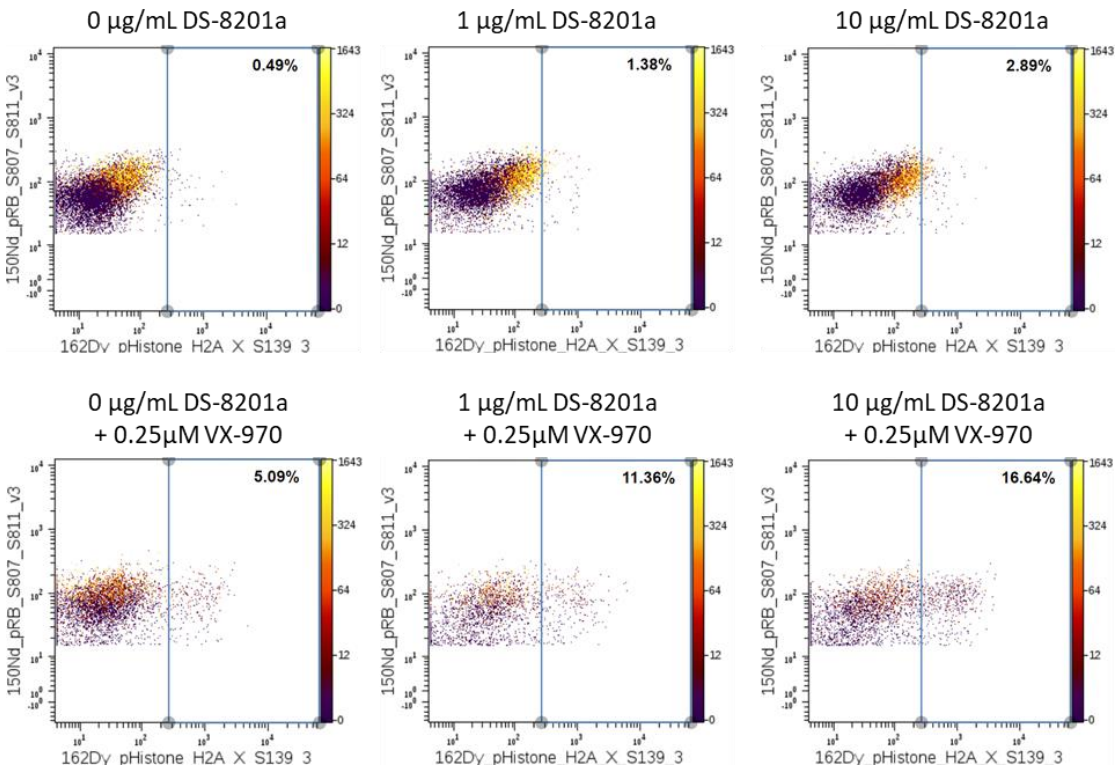

Figure 4.37. **S-phase cells from PDO 027 have increased pH2AX signal.**
Organoids were treated for 48 hours with the indicated drugs and analysed using the CyTOF technique. Plots show pH2AX staining, with cells in each plot are coloured according to the signal intensity of IdU.

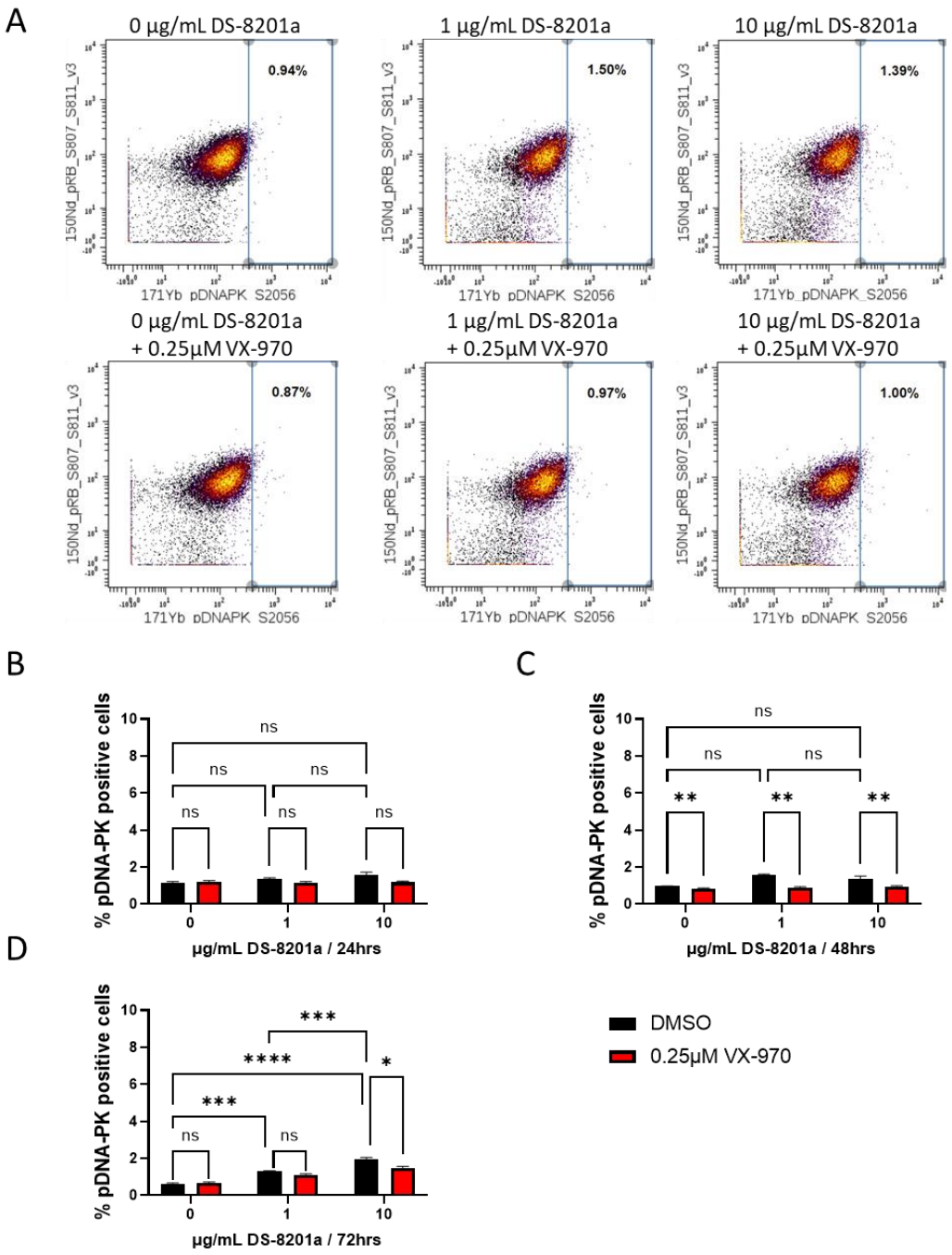

Figure 4.38. **VX-970 + DS-8201a treatment does not result in increased DNA-PK phosphorylation in PDO 021.**

A. Organoids were treated for 48 hours as indicated and analysed using the CyTOF technique. Plots are gated to show the percentage pDNA-PK positive cells. **B.** The percentage pDNA-PK positive cells at 24 hours. **C.** The % pDNA-PK positive cells at 48 hours. **D.** The percentage pDNA-PK positive cells at 72 hours. Plots are representative of 3 technical repeats. Statistical significance was calculated using the ANOVA test for multiple comparisons, *p* values ****<0.0001 ***<0.001 **<0.01 *<0.05.

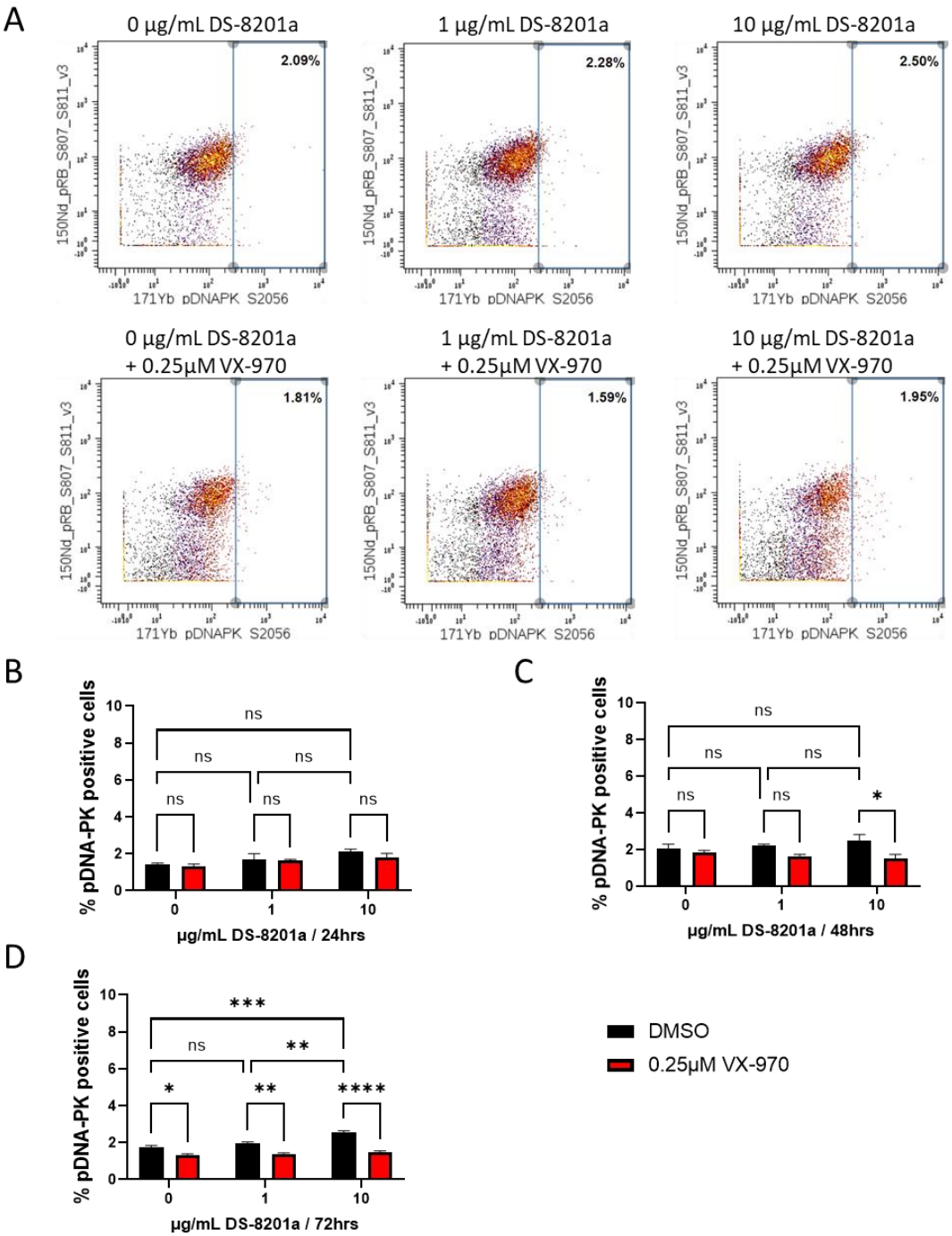

Figure 4.39. **VX-970 + DS-8201a treatment does not result in increased DNA-PK phosphorylation in PDO 027.**

A. Organoids were treated for 48 hours as indicated and analysed using the CyTOF technique. Plots are gated to show the percentage pDNA-PK positive cells. **B.** The percentage pDNA-PK positive cells at 24 hours. **C.** The percentage pDNA-PK positive cells at 48 hours. **D.** The percentage pDNA-PK positive cells at 72 hours. Plots are representative of 3 technical repeats. Statistical significance was calculated using the ANOVA test for multiple comparisons, *p* values ****<0.0001 ***<0.001 **<0. 01 *<0.05.

4.4 Discussion

4.4.1 HER2-low expressing CRC cell lines and PDOs are resistant to DS-8201a

The very high potency of the DS-8201a payload Dxd, and the high DAR of DS-8201a have been shown to reduce the level of HER2 expression required for cytotoxicity (Ogitani, Aida, et al. 2016). Indeed, preclinical and clinical studies have shown efficacy of DS-8201a in HER2-low expressing tumours (Modi, Park, et al. 2020; Ogitani, Aida, et al. 2016; Takegawa et al. 2019). However, early trial results have not shown DS-8201a efficacy in low-HER2 expressing mCRC, although very few patients within this category had been enrolled at the time of interim analysis (Siena et al. 2021). A preclinical investigation involving HER-low CRC cell lines and mouse model showed resistance to DS-8201a with only marginal reduction in cell line proliferation and no reduction in tumour growth (Takegawa et al. 2019).

In this study, a panel of CRC cell lines and 2 CRC PDOs were shown to have low-HER2 expression (Figure 4.1 and Figure 4.16). HER2 was detectable in all cell lines by Western blotting, showing that none of the cell lines were HER2-null. The findings were confirmed by IHC, with all cell lines and organoids scoring as HER2 IHC1+ (apart from HCT116, which was IHC-). These findings are consistent with those reported in a previous study, which showed very low HER2 expression levels in a panel of CRC cells including HCT116, HT29 and SW48 (Takegawa et al. 2019). In our study, SW48, was found to have slightly higher HER2 expression by Western blot than the other cell lines, again this was consistent with previous findings (Takegawa et al. 2019).

We have shown almost no growth inhibition of CRC cell lines with 10µg/mL DS-8201a monotherapy, with only SW48 showing a 25% growth inhibition (Figure 4.2). These findings are corroborated by similar findings in a panel of CRC cell lines (Takegawa et al. 2019). Slightly increased sensitivity of SW48 cells to DS-8201a in comparison

to the other cell lines was observed, this may be due to slightly higher levels of HER2 expression (Figure 4.1 A), as HER2 expression has been found to correlate with sensitivity to DS-8201a therapy (Ogitani, Aida, et al. 2016; Takegawa et al. 2019).

Analysis using the clonogenic assay following 72-hours of DS-8201a did not result in a marked reduction in survival of any of the 5 CRC cell lines (Figure 4.3). The drug exposure was increased to 2-weeks, as pharmacokinetic analysis showed DS-8201a serum concentrations above 10µg/mL at 21 days post infusion in trial patients (Yin et al. 2021). With a 2-week DS-8201a treatment schedule, there was a loss in survival in HCT116, LS174T and SW48 cell lines (Figure 4.4). Particularly, in LS174T and SW48 cells, surviving colonies were greatly reduced in size, suggesting a reduction in proliferation rate with DS-8201a exposure.

HT29 cells showed no reduction in survival, and only a small reduction in CACO2 survival was observed. CACO2 cells express high levels of the drug transporter ABCB1 (P-gp), which has been shown to lead to rapid Dxd efflux, providing an explanation for the lack of DS-8201a sensitivity (Nagai et al. 2019). HT29 cells have been shown to have a reduced sensitivity to Dxd, in comparison to HCT116 and SW48 cells, with a 10-fold greater IC_{50} (Takegawa et al. 2019). In this study, we also have shown HT29 to have increased resistance to SN38 monotherapy, compared to HCT116 and SW48 cells (Figure 3.6). As HER2 expression of HT29 cells is higher than that observed in HCT116 cells, reduced sensitivity to TOP1 inhibition, rather than reduced DS-8201a uptake is likely responsible for the reduced sensitivity to DS-8201a. A previous study has shown very rapid rates of SN38 glucuronidation in HT29 cells, with conversion of SN38 into the inactive metabolite SN38-G reducing irinotecan cytotoxicity (Cummings et al. 2002). However, as Dxd is excreted without glucuronidation, this is unlikely to be the cause of resistance to DS-8201a (Nagai et al. 2019; Okamoto et al. 2020).

As was observed with the CRC cell lines, PDO 027 was resistant to 72-hour DS-8201a monotherapy, with almost no loss in viability (Figure 4.17). Increasing the treatment duration to 7 days had very little impact on organoid survival (Figure 4.18). This was further supported by only a very small increase in cPARP and cCapase-3 in PDO 027 with DS-8201a monotherapy (Figure 4.26 and Figure 4.28). In contrast, PDO 021 was more sensitive to DS-8201a monotherapy, with an ~50% reduction in survival with 7-day treatment (Figure 4.18). This was further supported by a large increase in the percentage of cPARP and cCaspase in organoids treated with DS-8201a monotherapy (Figure 4.25 and Figure 4.27). Both PDO 021 and O27 were scored as IHC1+ (Figure 4.16), although this does not discount the possibility of differential sensitivity being as a result of HER2 expression, it makes differing sensitivity to the Dxd payload more probable. In this study, we showed PDO 021 to have greater sensitivity to SN38 than PDO 027 (Figure 3.19 and Figure 3.20), suggesting differing sensitivity to TOP1 inhibition.

4.4.2 ATR inhibition synergises with DS-8201a, reducing survival of HER2-low expressing CRC cell lines and organoids

Preclinical and clinical studies have shown a synergistic interaction between TOP1 and ATR inhibition in a range of cancer types, with ATR inhibition resulting in more severe TOP1cc induced DNA damage (Coussy et al. 2020; Huntoon et al. 2013; Jo, Murai, et al. 2021; Jo, Senatorov, et al. 2021; Josse et al. 2014; Thomas et al. 2021). In this study, we demonstrated a synergistic interaction between SN38 and VX-970 in CRC cell lines and PDOs, with increased DNA damage the identified mechanism of synergy (section 3.3).

The addition of VX-970 has been shown to sensitise CRC cell lines and organoids to very low dose SN38 (Figure 3.5 and Figure 3.6). As shown in a previous study and in this work, CRC cell lines and organoids with low HER2 expression do not accumulate

sufficient Dxd for DS-8201a to be effective as a monotherapy (Takegawa et al. 2019). The addition of ATR inhibition to DS-8201a therapy, was investigated as a means of reducing the Dxd dose required for cytotoxicity. The addition of VX-970 or AZD7638 to DS-8201a treatment caused almost a complete loss of proliferation in HCT116, HT29 and LS174T cells (Figure 4.5 and Figure 4.9). Furthermore, 3-day and 14-day clonogenic treatment schedules showed a synergistic interaction between ATR inhibitors (VX-970 or AZD6738) and DS-8201a to reduce the survival of HCT116, LS174T and SW48 cells (Figure 4.7, Figure 4.8, Figure 4.10 and Figure 4.11). An almost complete loss of surviving colonies was observed with 3-day treatment schedules in HCT116 and LS174T cells, but a longer treatment schedule of 14 days was required for the same effect in SW48 cells. These findings demonstrate sensitisation of HER2-low CRC cell lines to DS-8201a. Increased PARP cleavage also occurred in HCT116 and SW48 cells with the combination therapy, further demonstrating increased cytotoxicity (Figure 4.15).

In contrast, no/minimal sensitisation of CACO2 and HT29 cells to DS-8201a with the addition of VX-970 was observed, using proliferation or survival assays (Figure 4.6, Figure 4.7 and Figure 4.8). In CACO2 cells, it is likely that active efflux of Dxd prevents sufficient accumulation of the payload to enable a synergistic interaction. Furthermore, the transporter ABCB1, has also been reported to actively efflux VX-970 from cells (Talele et al. 2019). In this study, CACO2 showed no sensitivity to VX-970 monotherapy in proliferation and survival assays (Figure 4.6, Figure 4.7 and Figure 4.8). This suggests that VX-970 is unlikely to sensitise ABCB1 upregulated cells to DS-8201a. The lack of efficacy in HT29, is likely due to lower sensitivity to TOP1 inhibition. In this study, the addition of VX-970 did not sensitise HT29 cells to 1nM SN38, as seen with SW48 and HCT116 cells; with a higher dose of 5nM SN38 in combination with VX-970 required to cause a reduction in proliferation and survival (Figure 3.6). This suggests that there is a threshold of TOP1 inhibition required for

VX-970 to synergise with SN38 or DS-8201a, with a higher concentration required in HT29 cells than the other CRC cell lines.

ATR inhibition (VX-970 and AZD6738) synergised with DS-8201a to reduce the survival and development of PDO 027, with 3-day and 7-day treatment schedules resulting in almost a complete loss of viable organoid cells (Figure 4.19, Figure 4.20, Figure 4.22 and Figure 4.24). The synergy could also be seen in fully developed organoids using CyTOF analysis, with an increase in the percentage of cPARP+/cCaspase-3+ cells following DS-8201a combination therapy compared to either monotherapy (Figure 4.26 and Figure 4.28). The combination treatment was less effective in PDO 021, with more moderate synergy observed (Figure 4.19 and Figure 4.20, Figure 4.21 and Figure 4.23,). Furthermore, CyTOF analysis showed there was no increase in PARP cleavage in PDO 021, with the addition of VX-970 to DS-8201a treatment (Figure 4.25 and Figure 4.27). At 72 hours, loss of DS-8201a-induced replication arrest was observed with the addition of VX-970 (Figure 4.29). It is possible that with increased treatment time a lethal level of DNA damage would accumulate with the combination therapy, enabling detection of greater synergy in PDO 021.

PDO 027 has a mutation in the POLE gene, which encodes the catalytic polymerase and exonuclease subunit of polymerase-ε (Table 3.1). Mutations in POLE are associated with a very high mutational burden due to loss of function of the critical DNA-repair polymerase, which plays a role in multiple DDR pathways including NER, BER and SSB repair (Henninger and Pursell 2014; Hodel et al. 2020; Stenzinger et al. 2014). As the identified mechanism for ATR and TOP1 inhibitor synergy is increased DNA damage, a loss of POLE, could increase organoid sensitivity to the combination therapy.

4.4.3 HER2 dependence of ATR inhibition and DS-8201a synergy

The synergy observed with DS-8201a and ATR inhibition is dramatic, and strongly suggests that ATR inhibition may sensitise HER2-low CRC patients to DS-8201a. The purpose of utilising ADCs over standard chemotherapies, is the targeting of the cytotoxic agent to the cancer cells thereby widening the therapeutic window (Panowski et al. 2014; Peters and Brown 2015). Target non-specific ADC uptake can occur, with this increasing systemic toxicity and reducing the therapeutic window of the ADC (Mahalingaiah et al. 2019). HER2-dependent cytotoxicity of the combination therapy is necessary for DS-8201a targeted TOP1 inhibition to be advantageous over the non-targeted approach using Irinotecan. While a synergistic interaction between DS-8201a and AZD6738 in a HER2+ breast cancer cell, and not a HER2- breast cancer cell line, suggests HER2-dependent uptake of DS-8201a is required for the synergy, it does not definitively show HER2-dependent synergy in the CRC cell lines (Figure 4.12).

ADC studies often use a non-targeted control ADC, to show target specificity of ADC uptake and toxicity (Zammarchi et al. 2018). Daiichi Sankyo were able to provide a non-targeting-Dxd control ADC (MAAA-9199a), to assess the HER2-dependence of DS-8201a uptake in the CRC cell lines. Unfortunately, the company reported non-HER2 mediated cytotoxicity of MAAA-9199a, which does not occur with DS-8201a. The exact mechanism of this toxicity is unknown, but is likely due to non-specific ADC uptake. To act as a control ADC, a non-targeting ADC would be identical to the targeted-ADC, with only changes in the variable region of the mAb, however DS-8201a and MAAA-9199a have substantial differences in their mAb components. The mAb properties of an ADC have been reported to determine receptor dependent and receptor-independent target non-specific ADC uptake (Mahalingaiah et al. 2019). In this study we found CRC cell lines to be highly sensitive to the combination of MAAA-9199a and ATR inhibition (Figure 4.13). However, as MAAA-9199a is not a good

control for DS-8201a, this could not be used to draw conclusions about the HER2 dependance of DS-8201a uptake in the CRC cell lines.

Multiple studies have shown binding of trastuzumab (or T-DM1) to HER2 to cause HER2 internalisation and degradation (Baldassarre, Truesdell, and Craig 2017; Ben-Kasus et al. 2009; Fehling-Kaschek et al. 2019; Li et al. 2020). It can be assumed that as the mAb component of DS-8201a is the same as trastuzumab, that binding of DS-8201a to HER2 would also result in HER2 internalisation and degradation, causing a temporary reduction in HER2 expression. We found DS-8201a and not MAAA-9199a treatment to result in a reduction in cellular HER2 in HCT116, SW48 and LS174T cell lines (Figure 4.14). This demonstrates that DS-8201a is causing HER2 degradation, and strongly supports HER2-dependent uptake of DS-8201a. Loss of sensitivity to DS-8201a and ATR inhibition combination therapy with knockdown of HER2 in CRC cell lines would definitively demonstrate this.

4.4.4 Loss of ATR results in S-phase progression in the presence of SN38-induced DNA damage

Multiple studies, as well as this study have shown ATR dependent S-phase arrest with TOP1 inhibition (Figure 3.24, Figure 3.25 and section 3.4.3) (Huntoon et al. 2013; Hur et al. 2021; Josse et al. 2014; Seiler et al. 2007; Thomas et al. 2021). The mechanism by which ATR induces cell cycle arrest is covered in section 1.5.3. In PDO 021 and to a lesser extent in PDO 027, we show DS-8201a to reduce S-phase progression, with a reduction in the rate of IdU incorporation (Figure 4.29, Figure 4.30 and Figure 4.31). PDO 021 is more sensitive to DS-8201a monotherapy than PDO 027, as can be seen with the increased loss of viability, and the increase in PARP and caspase-3 cleavage (Figure 4.20 and Figure 4.25). PDO 021 is also more sensitive to SN38 monotherapy than PDO 027 (Figure 3.19 and Figure 3.20). The increased replication stalling and loss of viability with DS-8201a and SN38 monotherapy,

suggest PDO 021 is more sensitive to TOP1 inhibition than PDO 027. In PDO 021, the addition of VX-970 to DS-8201a treatment, returns the rate of IdU incorporation close to that observed in untreated organoids (Figure 4.29). This demonstrates that DS-8201a-induced S-phase arrest is ATR dependent, and would suggest that loss of this arrest would cause increased accumulation of DNA damage with cell cycle progression.

In PDO 027 it was not possible to detect a reversal in the mild DS-8201a induced replication stalling with the addition of VX-970 (Figure 4.30 and Figure 4.31). At 72 hours of combination treatment very few organoid cells are in S-phase, and the rate of IdU incorporation is reduced (Figure 4.31). In PDO 027 the combination treatment was highly cytotoxic, with an increase in apoptotic cells as early as 24 hours (Figure 4.26 and Figure 4.28). We also show increased ɣH2AX in combination treated organoids (Figure 4.36). This suggests that by 72 hours, the organoids have accumulated catastrophic DNA damage which is preventing replication progression with the combination treatment.

4.4.5 Increased DNA damage with DS-8201a and VX-970 combination therapy is the proposed mechanism of synergy

Previous studies and our work have demonstrated robust activation of ATR signalling in response to TOP1 inhibition (Figure 3.2), providing the rationale for TOP1 and ATR inhibition combination therapy (Aris and Pommier 2012; Coussy et al. 2020; Huntoon et al. 2013; Hur et al. 2021; Josse et al. 2014; Thomas et al. 2021). As Dxd is a potent TOP1 inhibitor, DS-8201a would be expected to induce ATR signalling as a result of TOP1cc-induced DNA damage and replication stress. Indeed, a study has shown phosphorylation of Chk1 to occur with 10µg/mL DS-8201a therapy in a HER2 IHC3+ breast cancer cell line (Ogitani, Aida, et al. 2016). The study also showed Chk1

phosphorylation with Dxd, demonstrating this Chk1 phosphorylation to be as a result of TOP1 inhibition.

The synergy observed between DS-8201a and ATR inhibitors, suggests a role of ATR activity in the repair of DS-8201a induced DNA damage. However, in this study, we were unable to detect ATR or Chk1 phosphorylation with 10µg/mL DS-8201a treatment of CRC cell lines by Western blotting (Figure 4.15). The CRC cell lines used in this study showed almost no sensitivity to DS-8201a monotherapy at doses of 10µg/mL, in contrast a HER2 IHC3+ breast cancer cell line displayed ~75% growth inhibition with 0.1µg/mL (Figure 4.2). It is possible that the change in ATR and Chk1 phosphorylation although biologically significant is below the threshold for detection by Western blotting. Similarly, we could only detect Chk1 phosphorylation in response to SN38 with doses higher than 10nM by Western blotting, despite lower doses being sensitive to SN38 and VX-970 combination therapy (Figure 3.8 and Figure 3.9). Using the more sensitive CyTOF technique, we were able to detect an induction of Chk1 phosphorylation in PDO 021 and 027 with DS-8201a monotherapy (Figure 4.32 and Figure 4.33). It is proposed that with a more sensitive detection method such as mass spectroscopy, pChk1 would also be detected in the CRC cell lines in response to DS-8201a, as seen with the PDOs.

Phosphorylation of Chk2, a key kinase downstream of ATM is an indicator of DNA double strand breaks, was reported to be increased with the addition of an ATR inhibitor to platinum-therapy, irradiation and TOP1 inhibition (Combès et al. 2019; Josse et al. 2014; Reaper et al. 2011; Tibbetts et al. 1999). Increased phosphorylation of Chk2 could be detected with DS-8201a and VX-970 combination therapy in HCT116 and SW48 cells in comparison to either monotherapy, suggesting increased DNA damage with the combination therapy (Figure 4.15).

DNA-PK and ATM are rapidly phosphorylated in response to double strand DNA breaks (Bakkenist and Kastan 2003; Chan et al. 2002; Chen et al. 2005). In HCT116 phosphorylation of DNA-PK could be detected in cells treated with the combination of DS-8201a and VX-970, suggesting that the combination treatment results in increased DNA damage (Figure 4.15 A). DNA-PK phosphorylation could not be detected in PDOs with the addition of VX-970 to DS-8201a (Figure 4.38 and Figure 4.39). DNA-PK phosphorylation in response to 1nM SN38 and VX-970 combination treatment was also not detectable (Figure 3.29), suggesting that higher levels of TOP1 inhibition are required for DNA-PK phosphorylation than achieved with DS-8201a. It is possible that increased treatment length would result in greater accumulation of DNA-damage and DNA-PK activation. pChk2, pATM and pDNA-PK were detectable in LS174T cells with VX-970 monotherapy and in combination with DS-8201a (Figure 4.15). LS174T is a p53 null cell line, and in this study has shown greater sensitivity to both VX-970 and AZD6738 monotherapies in comparison to the other cell lines (Figure 4.5 and Figure 4.9). Cleavage of PARP and accumulation of ɣH2AX were also observed with VX-970 monotherapy (Figure 4.15). This is consistent with previous reports that p53 null cancer models, which have greater dependance on ATR, have high levels of replication stress even in the absence of DNA damaging therapeutics (section 1.6.11) (Kwok et al. 2016; Middleton, Pollard, and Curtin 2018; Reaper et al. 2011; Toledo et al. 2011).

In this study we did not find the combination of DS-8201a and VX-970 to cause increased phosphorylation of H2AX in CRC cell lines, suggesting the absence of DNA DSBs (Figure 4.15). Furthermore, in PDO 021 a reduction in DS-8201a-induced pH2AX was observed with the addition of VX-970, suggesting a reduction in DNA damage with the combination therapy (Figure 4.34). It is well established that ATM is the key kinase involved in the phosphorylation of H2AX in response to DNA DSBs (Burma et al. 2001) (section 1.4.4). However, ATR has been implicated as the kinase

responsible for phosphorylating H2AX in the context of replication stress, prior to the formation of DNA DSBs (Sirbu et al. 2011; Ward and Chen 2001). Phosphorylation of H2AX in response to hydroxyurea and UV-exposure was found to be S-phase dependent, while irradiation induced ɣH2AX independent of cell cycle stage. ATR-KO cells had almost complete loss of ɣH2AX signal in response to hydroxyurea and UV, while ɣH2AX signal in response to irradiation was unaffected (Ward and Chen 2001). A further study also reported accumulation of ɣH2AX at stalled replication forks in response to hydroxyurea-induced replication stress. In this study ɣH2AX was found to appear prior to the formation of DNA DSBs, and was not reduced with the inhibition of DNA-PK and ATM. Caffeine the first molecule described to inhibit ATR, was found to abrogate the accumulation of ɣH2AX at stalled replication forks (Sirbu et al. 2011). Furthermore, ɣH2AX accumulation in the hours following cisplatin treatment has also been shown to be ATR dependant, with almost complete loss of ɣH2AX foci in ATR deficient cells (Pabla et al. 2008).

In this study, an increase in the ɣH2AX signal of S-phase cells in response to DS-8201a monotherapy occurred in PDO 021 and PDO 027, with this being lost with the addition of ATR inhibition (Figure 4.35 and Figure 4.37). This effect was also detectable with 1nM SN38 in PDO 021, although higher doses resulted a much greater shift of H2AX phosphorylation that is likely due to the presence of DNA DSBs (Figure 3.26). This suggests that S-phase accumulation of ɣH2AX in response to DS-8201a inhibition is ATR mediated. In PDO 027, a distinct non-S-phase dependent population of cells with comparatively higher levels of ɣH2AX staining is present, we propose this increased ɣH2AX signal is in response to DNA DSBs that occur as a result of the combination therapy (Figure 4.36).

In HCT116 cells, p53 stabilisation and phosphorylation occurred with DS-8201a and VX-970 combination therapy, and to a lesser extent with DS-8201a monotherapy. This increase in p53 stabilisation was also observed with DS-8201a and VX-970 at

24 hours in SW48 cells (Figure 4.15). This is in contrast to our findings of a reduction in SN38-induced p53 with ATR inhibition (Figure 3.4, Figure 3.8 and Figure 3.9), which has also been reported with cisplatin and UV-exposure (Reaper et al. 2011; Tibbetts et al. 1999). These findings demonstrate the complex interactions between DNA-damage repair factor, cell cycle regulators and p53. It appears that SN38, which is more potent in the CRC cell lines than DS-8201a, induces ATR dependent p53 stabilisation and phosphorylation. Robust p53 phosphorylation in response to DS-8201a and VX-970 is clearly ATR independent and may occur via ATM, as we were able to detect activation of Chk2, the kinase downstream of ATM. ATM is the principal kinase responsible for p53 phosphorylation and stabilisation in response to DNA damage (section 1.4.4) (Banin et al. 1998; Canman et al. 1998; Cheng and Chen 2010; Shieh et al. 1997). An increase in p53 phosphorylation has also been reported with the addition of VX-970 to oxaliplatin treatment in CRC cell lines (Combès et al. 2019). This finding suggests that p53 is activated following DS-8201a and VX-970 combination therapy in response to DNA damage and not via the replication stress response mediated by ATR.

4.5 Conclusions

The work in this chapter has demonstrated potent sensitisation of HER2-low expressing CRC cell lines and organoids to DS-8201a by ATR inhibition (VX-970 and AZD6738). An almost complete loss of survival in multiple cell lines and a patient derived organoid model suggest that this combination may be very effective in the treatment of CRC. Indeed, a phase I clinical trial has now been set up by Daiichi Sankyo and AstraZeneca to explore the tolerability and efficacy of combined DS-8201a and AZD6738 therapy, with a dose expansion for mCRC (NCT04704661). We were also able to show some evidence of loss of S-phase arrest and increased DNA damage with the combination therapy, suggesting a mechanism for the observed synergy.

5 ATR inhibition as a means of re-sensitising SN38 resistant CRC cells

5.1 Introduction

5.1.1 Response to irinotecan-based therapy is limited by primary and acquired resistance

The response rate for mCRC patients who receive irinotecan as part of the FOLFIRI regimen is 39-49%, demonstrating high incidence of primary resistance (Saltz et al. 2001). The response to FOLFIRI is typically short lived, with a PFS of 6.7 months (Douillard et al. 2000; Van Cutsem et al. 2014). Disease progression can occur due to primary or acquired irinotecan resistance, with either the outgrowth of a tumour cell population with primary resistance or the emergence of a newly resistant tumour cell population (Hammond, Swaika, and Mody 2016). The 5-year survival rate is low, at approximately 10%, demonstrating that most patients who do respond to treatment eventually relapse, and no longer respond to therapy (CRUK 2021).

5.1.2 Mechanisms of Irinotecan resistance

Multiple mechanisms of resistance to irinotecan therapy have been identified *in vitro*, of which some have been validated in patients. Resistance due to altered irinotecan metabolism, mutations or loss of expression of TOP1, upregulation in the repair of TOP1ccs, or pro survival signalling despite the presence of DNA damage have been reported (Hammond, Swaika, and Mody 2016; Xu and Villalona-Calero 2002).

Resistance to irinotecan can occur due to changes in expression levels of enzymes involved in irinotecan metabolism, thereby reducing the cellular concentration of the active metabolite SN38 (Xu and Villalona-Calero 2002). An example of this is the upregulation of UGT1A1, which converts SN38 into an inactive metabolite SN38-G

(Figure 1.6). Increased UGT1A1 activity has been found to lower cellular SN38 levels and increase irinotecan resistance *in vitro* (Cummings et al. 2002; Takahashi et al. 1997). The clinical significance of mutations and differential expression of enzymes involved in irinotecan metabolism has largely been studied in the context of toxicity rather than resistance. Patients with polymorphisms that increase cellular SN38 levels, have a higher incidence of treatment failure due to drug related toxicities than other patients, thereby reducing OS (Carlini et al. 2005; Rouits et al. 2004). The effect of reduced cellular SN38 on increased irinotecan resistance in patients has not been extensively studied (Hammond, Swaika, and Mody 2016).

Reduced intracellular SN38 accumulation can also be mediated by increased expression of the ATP binding cassette (ABC) efflux transporter family. Several members of the ABC family have been implicated in the resistance of irinotecan including ABCB1, ABCC2, ABCG2, ABCC1, ABCC4, ABCC3 and ABCB11 (Brangi et al. 1999; Hammond, Swaika, and Mody 2016; Matsunaga et al. 2020; Tsukamoto et al. 2019; Xu and Villalona-Calero 2002). While *in vitro,* multiple studies have shown upregulation of the ABC transporter family to cause irinotecan resistance, there have been conflicting reports on the correlation between ABC transporter expression and irinotecan response in patients (Jensen et al. 2015; Trumpi et al. 2015; Tuy et al. 2016).

Solute carrier proteins (SLCs) are a family of transmembrane proteins which play a role in cellular uptake of a wide range of substances including amino acids, glucose, cations, anions and nucleosides. Overexpression of multiple SLC transporters have been identified in wide range of cancers, driving increased tumour cell proliferation and metastasis (Alfarsi et al. 2020; Altan et al. 2018; Ban et al. 2017; Beltran et al. 2011; Cormerais et al. 2016; Fan et al. 2013; Feng et al. 2017; Hu et al. 2020; Liu, Zuo, et al. 2017; Torrents et al. 1998). The SLCO1B1 (OATP1B1) and SLCO1B3 (OATP1B3) members of the SLC family have been identified as important for cellular

uptake of SN38, with increased expression shown to increase irinotecan related toxicity. A reduction in expression or loss of function mutations in SLC1OB1 or SLCO1B3 have been reported to reduce sensitivity to cytotoxic agents, including irinotecan (Di Paolo et al. 2011; Girardi et al. 2020; Nozawa, Minami, et al. 2005; Sun, Ying, et al. 2020; Yamaguchi et al. 2008).

A link between TOP1 expression and resistance to irinotecan was initially identified in a panel of CRC and breast cancer cell lines, with resistant cell lines having reduced TOP1 expression (McLeod and Keith 1996). Furthermore, the levels of tumour TOP1 expression found to fall in CRC mouse models and patients with exposure to irinotecan (Giovanella et al. 1989; Horisberger et al. 2009). The MRC FOCUS study showed that response to irinotecan for the treatment of mCRC correlated with TOP1 expression, with patients with low TOP1 expression deriving no benefit from irinotecan therapy (Braun et al. 2008). However, this was not supported by the findings of the CAIRO study, which did not identify a statistically significant correlation between TOP1 expression and response to irinotecan (Koopman et al. 2009). Mutations in TOP1 that alter the conformation of the TOP1cc, preventing the binding of CPTs have been reported *in vitro* (Fujimori et al. 1995; Gongora et al. 2011; Li et al. 1996). Mutant TOP1 has also been reported in a tumour from a patient resistant to irinotecan therapy (Tsurutani et al. 2002).

Increased degradation of TOP1ccs and enhanced DNA damage repair prior to collision of TOP1ccs with the transcription and replication machinery reduces the toxicity of TOP1 inhibitors, and has been identified as a mechanism of resistance to irinotecan (Pommier 2006). An example of this is TDP1, an enzyme that is able to catalyse the removal of TOP1 from trapped TOP1ccs (section 1.3.5) (Das et al. 2009; Das et al. 2014; Dexheimer et al. 2008). Overexpression of TDP1 has been identified as a mechanism of resistance to TOP1 inhibitors, with a correlation between TDP1

and sensitivity to irinotecan identified in a panel of CRC cell lines (Meisenberg et al. 2015).

Increased activation of transcription factors following DNA damage that promote survival, such as nuclear factor kappa B (NFκB) have also been found to reduce sensitivity to irinotecan in cancer cell lines (Huang et al. 2000; Wang et al. 1999). In accordance with this, mCRC patients with tumours that are positive for NFκB signalling have been found to respond poorly to irinotecan in comparison to patients who are negative for NFκB signalling (Scartozzi et al. 2007).

5.1.3 ATR inhibition as a mechanism of restoring sensitivity to TOP1 inhibition

In this study, we have demonstrated ATR inhibition to sensitise CRC cell lines and PDOs to very low concentrations of SN38 (section 3.3). Several of the mechanisms of irinotecan resistance that have been identified to date result in reduced cellular SN38 accumulation (section 5.1.2). This suggest that the addition of ATR inhibition to SN38 therapy may restore sensitivity by lowering the cytotoxic dose of SN38. Indeed, two EP-SCNC patients who had previously progressed on topotecan therapy responded to topotecan and ATR inhibition in a phase II clinical trial (Thomas et al. 2021).

DS-8201a has been shown to be efficacious in CRC and gastric cancer patients that have progressed on irinotecan-based chemotherapy regimens, suggesting DS-8201a as future therapeutic in the treatment of irinotecan resistant tumours (Shitara et al. 2019; Siena et al. 2021). In this study, we have shown ATR inhibition to sensitise HER2-low expressing CRC cell lines to DS-8201a (Section 4.3). This makes the combination of DS-8201a and ATR inhibition a potential therapeutic option for patients with irinotecan resistant mCRC.

5.2 Research aim

The aim of this chapter is to generate SN38 resistant cell lines, and explore whether ATR inhibition can re-sensitise cell lines to SN38 treatment. The use of DS-8201a in combination with ATR inhibition as a means of treating SN38 resistant cells, is also investigated.

5.3 Results

5.3.1 SN38 resistant cell lines generated by pulsed drug exposure

Drug resistant cell lines are typically generated using either a continuous exposure or a pulsed exposure technique. In the continuous exposure technique, cells are continuously exposed to increasing drug concentrations until a population of resistant cells emerge. Using the pulsed approach, a lower concentration of the drug is given for a specific time period, after which the drug is removed, and cells left to recover; this cycle is repeated with increasing drug concentrations until a resistant line is generated. The pulsed approach is more clinically relevant, as it mirrors the multiple cycles of chemotherapy that typically make up a treatment regimen. The pulsed approach also leads to cell lines with stable drug resistance, that is not reversed in the absence of the drug (McDermott et al. 2014).

HT29 and SW48 cells were exposed to multiple SN38 treatment cycles, with SN38 concentration increasing from 1nM to 100nM. Each treatment cycle was 72 hours, followed by a 2-week recovery period. The clonogenic assay was used to assess the sensitivity of the resultant resistant cell lines to SN38. The SW48 cells showed the greatest resistance with 71% (± 12.6) survival with 50nM SN38, compared to 5.1% (± 1.5) survival of parental cells with a much lower dose of 5nM SN38 (Figure 5.1 B-C). The HT29 cells generated were also more resistant than the parental cell line, with 58.6% (± 9.7) survival vs 7.7% (± 1.4) with 10nM SN38 treatment (Figure 5.1 D-E).

Replication rate was a key distinguishing feature between the SW48R and SW48 parental cell lines, with SW48R cells dividing at a much slower rate. To establish the cell cycle duration in the two cell lines, SW48 and SW48R cells were seeded in 96 well plates at low density, with cells fixed on day 1 and day 6. The SRB assay was used to find the proliferation rate over the 6 days which was then used to calculate

average cell cycle duration. The average cell cycle duration in SW48R cells was 56.79 hours (± 2.8, p=0.0003) vs 22.8 hours (± 0.73) in SW48 parental cells (Figure 5.2).

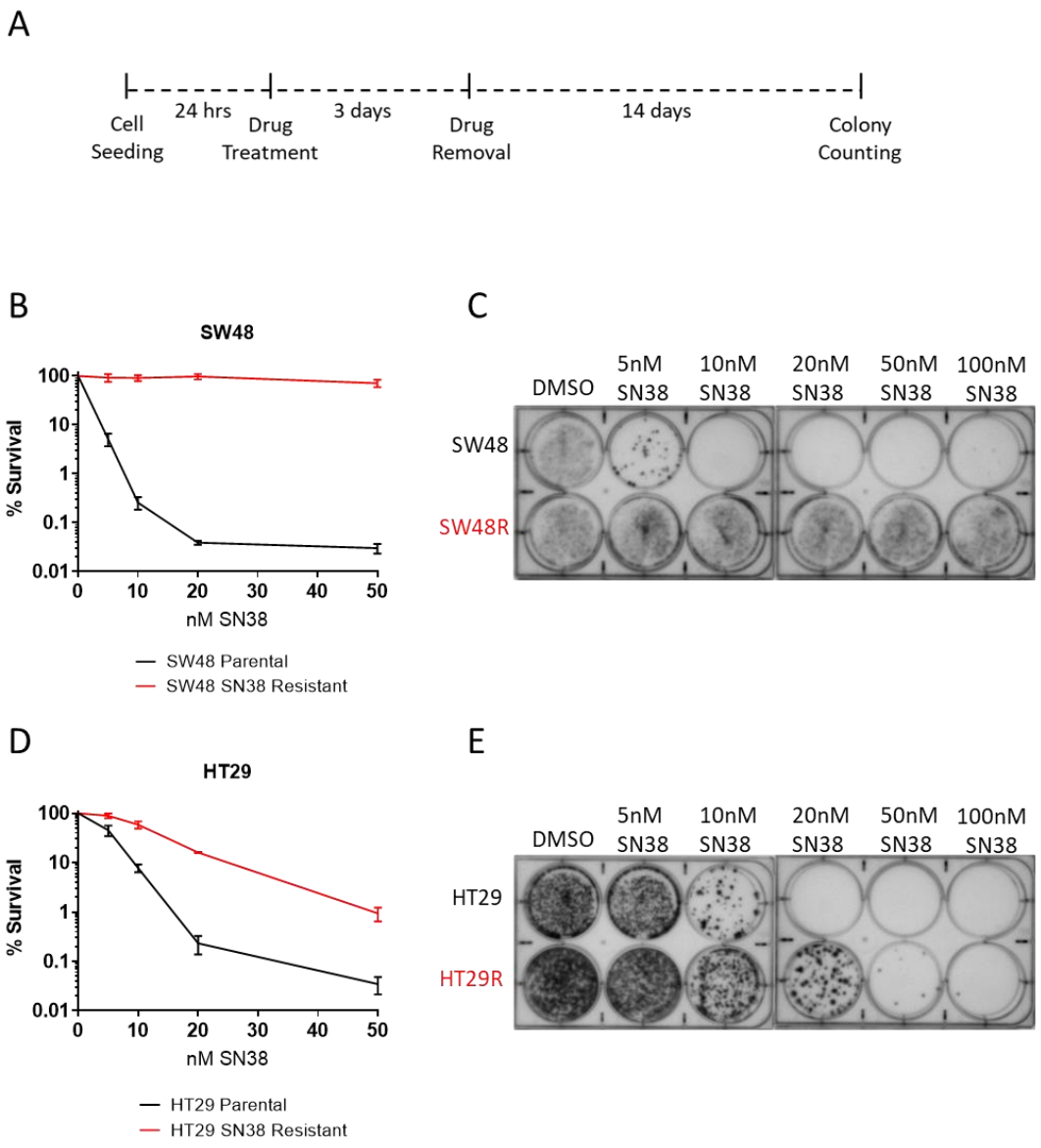

Figure 5.1. **Repeated exposure to SN38 leads to the generation of SN38 resistant cell lines.**

A. Scheme demonstrating the treatment and clonogenic assay schedule followed. **B.** The percentage survival following SN38 treatment of SW48 parental and resistant (SW48R) cell line. **D.** The percentage survival following SN38 treatment of HT29 parental and resistant (HT29R) cell line. Each datapoint is the mean of 3 biological repeats. Error bars represent +/- SEM. Representative images of clonogenic plates for **C.** SW48 parental and SW48R cells and **E.** HT29 parental and HT29R cells.

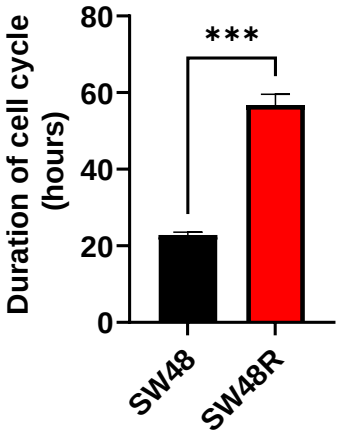

Figure 5.2. **Cell cycle duration is increased in SW48R cells.**
SW48 and SW48R cells were seeded in 96 well plates at low density, with cells fixed on day 1 and day 6. The SRB assay was used to find the proliferation rate over the 6 days, which was then used to calculate average cell cycle duration. Statistical significance was calculated using the student T-test, *p* values ****<0.0001 ***<0.001 **<0.01 *<0.05. Error bars represent +/- SEM.

5.3.2 Establishing the mechanism of resistance in HT29 and SW48 SN38 resistant cell lines

To establish the mechanism of resistance in the SW48 SN38 resistant (SW48R) and HT29 SN38 resistant (HT29R) cells, RNA-seq analysis was performed to identify changes in gene expression. Table 5.1 shows the fold changes in gene expression in HT29R cells compared to parental cells for genes previously implicated in irinotecan resistance, an adjusted (for multiple comparisons) p-value of 0.01 was set for statistical significance. In HT29R cells, a 6-fold (log_2 2.57) increase in the expression of multidrug transporter ABCC2 was observed in comparison to HT29 parental cells (p=0.0005). Additionally, there was a 1.7-fold (log_2 0.74) increase in the expression of multidrug transporter ABCG2 (p<0.0001). There was also an 8.8-fold reduction (log_2 3.13) in the expression of SLCO1B3 in HT29R cells in comparison to the parental cells (p<0.0001). There was a moderate 1.4-fold (log_2 0.53) increase in BRCA1

expression in HT29R cells (p=0.003), with no other changes in gene expression of DNA repair enzymes detected. There were also no changes in expression of enzymes involved in irinotecan metabolism that would explain reduced sensitivity.

Table 5.1. Differential gene expression for HT29R cells vs HT29 parental cells

Gene	Log_2 fold change	Adjusted p-value
Transporters		
ABCB1	-3.42	1.0
ABCC2	2.57	0.0005
ABCG2	0.74	<0.0001
ABCC1	0.212	0.567
ABCC4	-0.53	0.001
ABCC3	-0.15	0.738
ABCB11	0.7	1.0
SLCO1B1	-1.4	0.09
SLCO1B3	-3.13	<0.0001
Metabolic enzymes		
UGT1A10	-0.19	0.39
UGT1A6	-0.03	0.96
UGT1A1	-0.45	0.003
UGT1A9	0.32	1.0
CYP3A4	-1.29	1.0
CYP3A5	-0.013	0.9
Repair factors		
TDP1	-0.17	0.59
PARP1	-0.03	0.93
SPRTN	-0.2	0.55
MRE11	-0.11	0.782
MUS81	-0.63	0.047
SLX4	0.28	0.45
ATM	-0.13	0.79
DNA-PK	0.03	0.94
BRCA1	0.53	0.0003
BRCA2	-0.103	0.83
Other genes		
SLFN11	-2.58	0.28
TOP1	0.21	0.4

Table 5.2 shows the fold change in gene expression in SW48R cells compared to parental cells for genes previously implicated in irinotecan resistance. In SW48R cells, there was no significant increase in any ABC drug transporters, of which some are shown in Table 5.2. There were also no statistically significant changes in the enzymes involved in SN38 metabolism. There was a 1.5-fold increase (log_2 0.59) in the expression of TDP1, a key enzyme involved in the resolution of TOP1ccs ($p>0.0001$). There was a 2.1-fold reduction (log_2 1.08, $p>0.0001$) in the expression of TOP1, a known mechanism for TOP1 resistance.

Table 5.2. Differential gene expression for SW48R cells vs SW48 parental cells

Gene	**Log_2 fold change SW48R vs SW48 parental**	**Adjusted p-value**
Transporters		
ABCB1	2.06	1.0
ABCC2	0.4	0.78
ABCG2	0.48	0.015
ABCC1	0.35	0.129
ABCC4	-0.54	0.004
ABCC3	-0.923	0.001
ABCB11	-3.3	0.087
SLCO1B1	-1.4	0.09
SLCO1B3	-1.04	0.08
Metabolic enzymes		
UGT1A10	0	1.0
UGT1A6	0	0.97
UGT1A1	0.38	0.587
UGT1A9	0	1.0
CYP3A4	1.38	0.57
CYP3A5	-0.097	0.76
Repair factors		
TDP1	0.59	<0.0001
PARP1	0.33	0.047
SPRTN	-0.06	0.8
MRE11	-0.57	0.004
MUS81	-1.05	<0.0001

SLX4	0.71	0.0004
ATM	-0.36	0.17
DNA-PK	0.043	0.79
BRCA1	-0.16	0.306
BRCA2	-0.209	0.654
Other genes		
SLFN11	1.3	0.6
TOP1	-1.08	<0.0001

As SW48R cells have a reduced proliferation rate in comparison to the parental cell line, the expression of 46 SLC transporters which play a role in the uptake of key metabolites required for cancer cell proliferation was analysed. Multiple SLC transporters were downregulated in the SW48R cell line in comparison to the parental line (Table 5.3). SLC38A5 had a 17.1-fold reduction (Log_2 4.1, p<0.0001), SLC7A11 a 12.1-fold reduction (Log_2 3.6, p<0.0001), SLC7A5 a 4.3-fold reduction (Log_2 2.1, p<0.0001), SLC7A7 a 3.5-fold reduction (Log_2 1.8, p=0.001), SLC38A2 a 3.4-fold reduction (Log_2 1.75, p<0.0001), SLC3A2 a 2.8-fold reduction (Log_2 1.48, p<0.0001), SLCO4A1 a 2.3-fold reduction (Log_2 1.2, p<0.0001), SLC2A1 a 1.5-fold reduction (Log_2 0.62, p=0.004) and SLC29A2 a 1.5-fold reduction (Log_2 0.57, p=0.001).

Table 5.3. Statistically significant changes in SLC gene expression in SW48R cells vs SW48 parental cells

Gene	**Log_2 fold change SW48R vs SW48 parental**	**Adjusted p-value**
SLCO4A1	-1.2	<0.0001
SLC29A2	-0.57	0.001
SLC2A1	-0.62	0.004
SLC38A2	-1.75	<0.0001
SLC38A5	-4.1	<0.0001
SLC3A2	-1.48	<0.0001
SLC7A11	-3.6	<0.0001
SLC7A5	-2.12	<0.0001
SLC7A7	-1.8	0.001

To further explore the potential mechanisms of SN38 resistance in SW48R and HT29R cells, gene set enrichment analysis (GSEA) of genes in the cancer hallmark pathways was performed using the Broad Institute tools (Liberzon et al. 2011; Subramanian et al. 2005). This analysis investigates the combined changes of multiple genes which are part of the same signalling pathway, enabling identification of changes across specific cell signalling pathways. Gene expression in resistant cells was compared with parental cells and a cut off false discovery rate (FDR) q-value of 0.01 was set to identify statistically significant changes.

In SW48 cells, 5 of 50 hallmark pathways were found to be upregulated in the SW48R cells compared to the parental cells, with a normalised enrichment score (NES) >1.5. These were the unfolded protein response, MYC signalling pathway 1, MYC signalling pathway 2, TNFα signalling via NFκB and MTORC1 signalling (Figure 5.3). Two hallmark pathways, notch and apical surface signalling, were found to be downregulated in the SW48R cells, with a NES <-1.5 (Figure 5.4).

In HT29 cells, none of the 50 hallmark pathways were upregulated in the HT29R cells compared to the parental cells, with a NES >1.5 used as a cut off for pathway enrichment. Five hallmark pathways were found to be downregulated in the HT29R cells, with a NES <-1.5 (Figure 5.5). These were the interferon-α response, the interferon-ɣ response, the early oestrogen response, the late oestrogen response and the complement pathway.

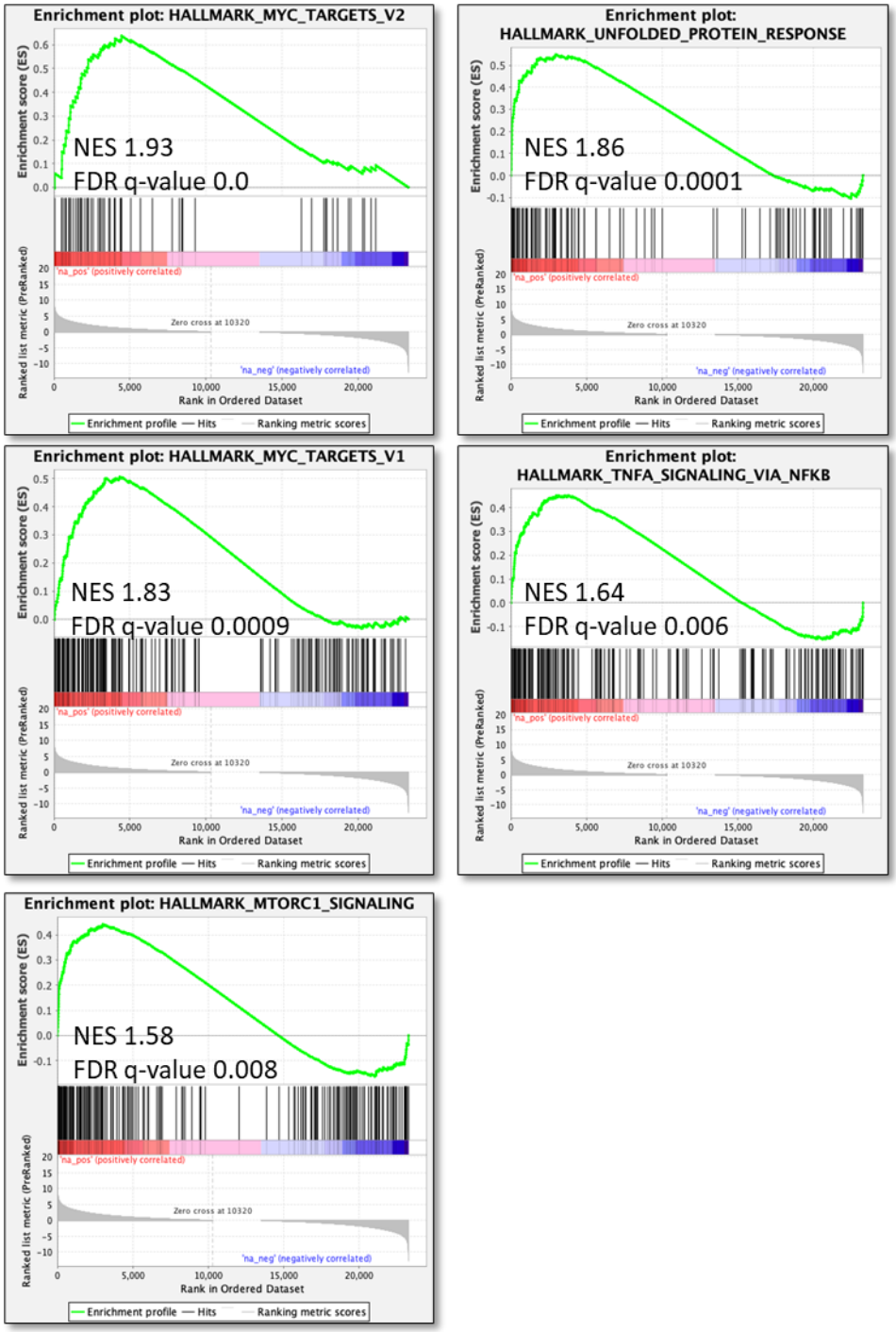

Figure 5.3. **GSEA pathway analysis of SW48R cells vs SW48 parental cells.**
MYC signalling pathway 2, The unfolded protein response, MYC signalling pathway 1, TNFα signalling via NFκB and MTORC1 signalling pathways had a NES > 1.5.

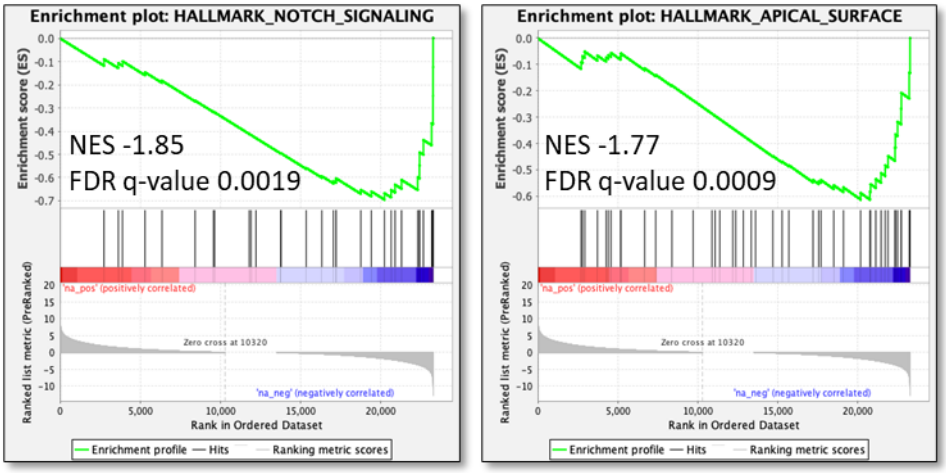

Figure 5.4. **GSEA pathway analysis of SW48R cells vs SW48 parental cells.** The notch signalling and apical surface pathways had a NES < -1.5.

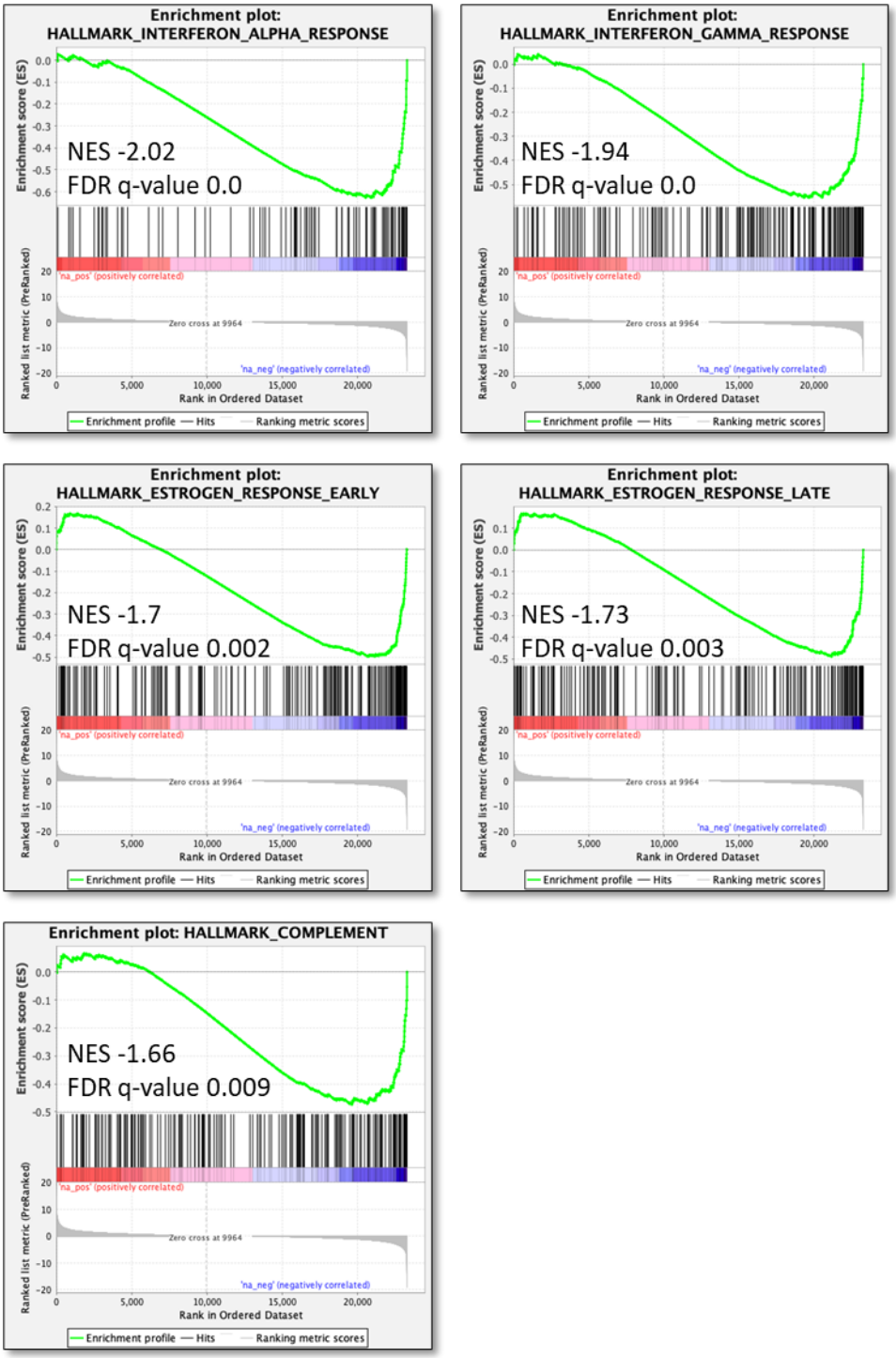

Figure 5.5. **GSEA pathway analysis of HT29R cells vs HT29 parental cells.**
The interferon-α response, the interferon-ɣ response, the early oestrogen response, the late oestrogen response and the complement pathway all had a NES < -1.5.

The RNA-seq data identified upregulation of ABCC2 and ABCG2, and downregulation of SLCO1B3 as the likely mechanisms of resistance in HT29R cells. Reduced proliferation rate due to downregulation of multiple SLCs combined with TOP1 downregulation and TDP1 upregulation are the likely causes of resistance in SW48R cells. However, it must be stressed that this technique does not explore gene mutations, and as such there may be multiple other contributing factors. Establishing the contribution of each of the identified factors to the overall resistance was beyond the scope of this study.

5.3.3 VX-970 does not re-sensitise resistant cell lines to low dose SN38

ATR inhibition is only likely to restore sensitivity to SN38, if ATR signalling is still activated in the resistant cells. To assess ATR activation in SW48R and HT29R cell lines, cells were treated with SN38 at doses ranging from 5nM to 100nM for 24 hours, and lysates analysed by Western blotting. SW48R cells showed very reduced phosphorylation of ATR in response to ≥20nM SN38 treatment, and no phosphorylation of Chk1, p53 or H2AX occurred at even 100nM SN38 (Figure 5.6 A). In HT29R cells there was similar levels of pATR in response to SN38 as observed in the parental cells (Figure 5.6 B). Chk1 phosphorylation also occurred, but pChk1 levels were reduced in comparison to the parental cells. pH2AX levels were also reduced in HT29R cells in comparison to the parental cell line, suggesting a reduction in DNA damage. An almost complete lack of ATR signalling, p53 stablisation and pH2AX accumulation in SW48R cells suggests a very marked reduction in DNA damage in response to TOP1 inhibition, making it unlikely for ATR inhibition to sensitise resistant cells to low dose SN38. However, HT29 cells still demonstrated ATR signalling and DNA damage in response to SN38, making ATR inhibition a potential mechanism for re-sensitising HT29R cells.

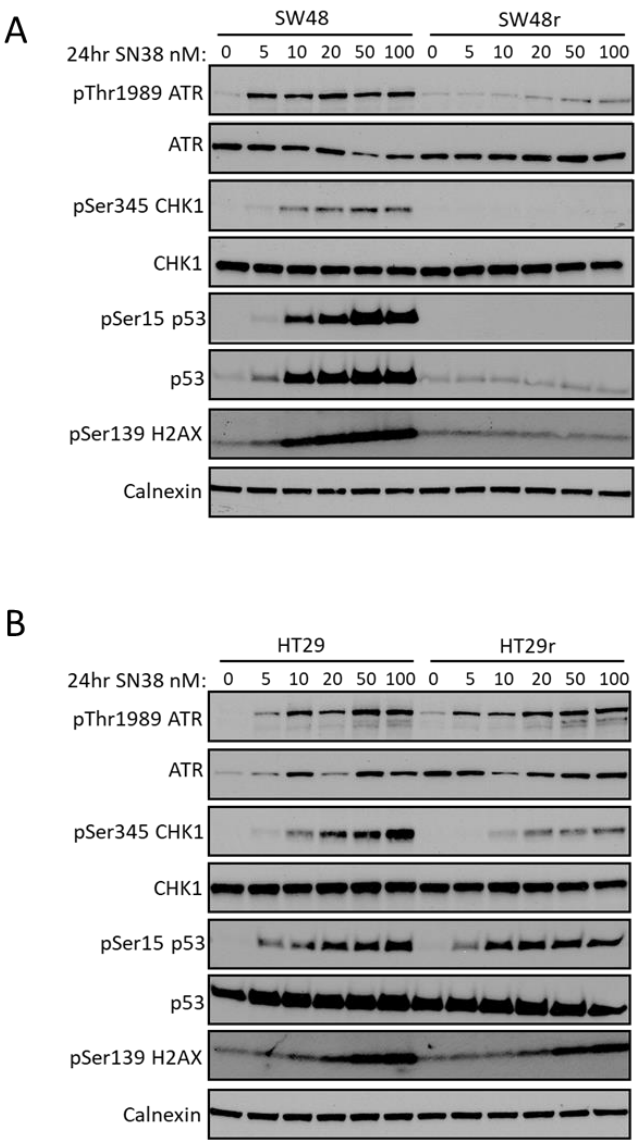

Figure 5.6. **SW48 SN38-resistant cells show almost a complete loss of ATR and DNA damage signalling.**

A. SW48 (parental) and SW48R cells were treated with the indicated doses of SN38 for 24 hours and lysates analysed by Western blotting. **B.** HT29 (parental) and HT29R cells were treated with the indicated doses of SN38 for 24 hours and lysates analysed by Western blotting. Blots are representative of 3 biological repeats.

Sensitivity of HT29R and SW48R to SN38 and VX-970 combination therapy was evaluated using the clonogenic assay (Figure 5.7). HT29R and SW48R cells showed no reduction in survival with the addition of VX-970 to SN38 treatment, with doses of up to 10nM SN38. SW48R cells retained sensitivity to the VX-970 monotherapy.

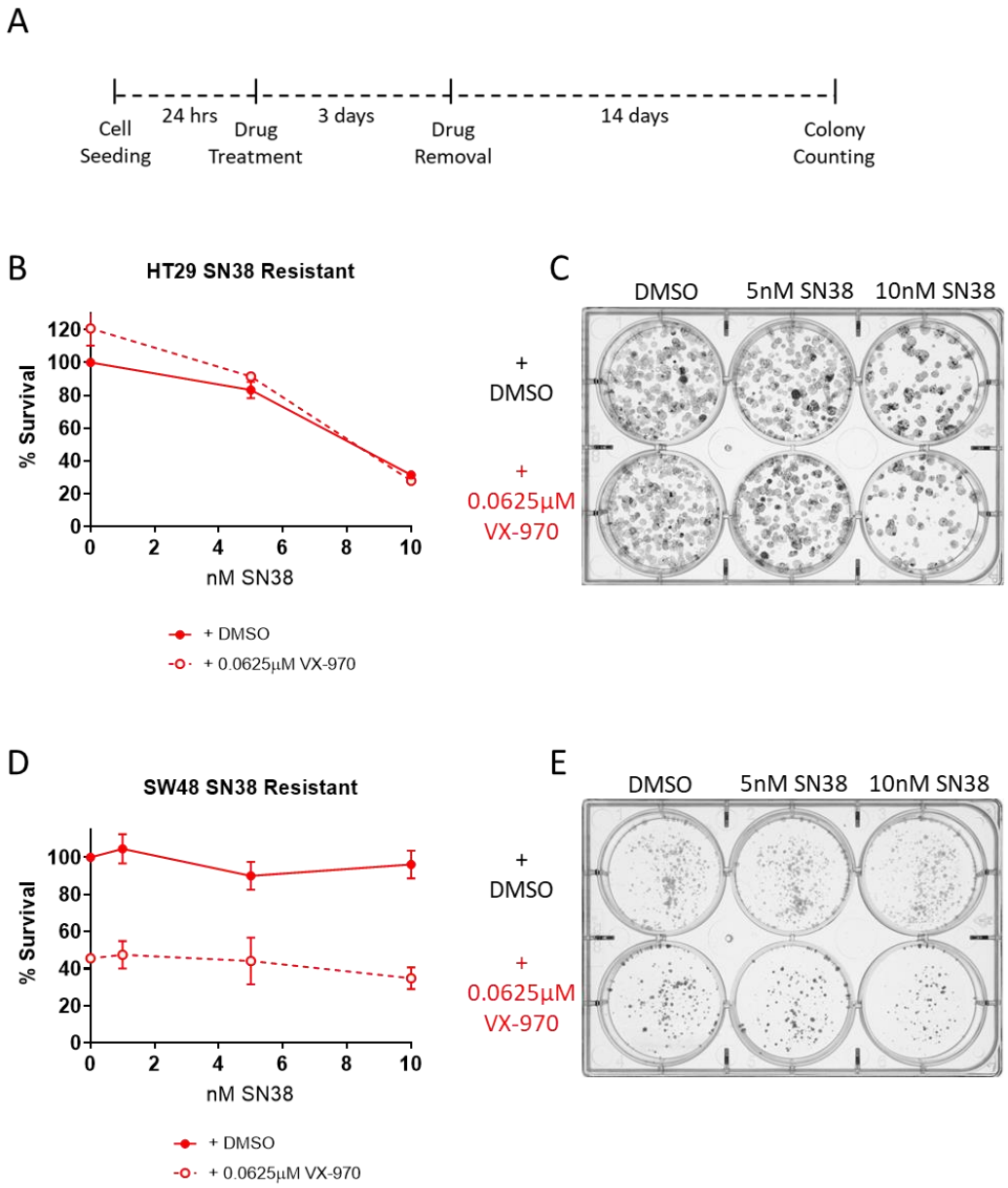

Figure 5.7. **VX-970 does not restore sensitivity to SN38 in resistant cell lines.**
A. Scheme demonstrating the treatment and clonogenic assay schedule followed. The percentage survival following combination treatment with SN38 + VX-970 is displayed in **B.** HT29R cells **D.** SW48R cells. Each datapoint is the mean of 3 biological repeats. Error bars represent +/- SEM. Representative images of clonogenic plates for **C.** HT29R cells **E.** SW48R cells.

The impact of SN38 monotherapy and in combination with VX-970 on SW48R cells was also evaluated by measuring cell proliferation using the SRB assay. SW48R cells were treated with a dose range of SN38 (1nM – 50nM) and VX-970 as monotherapies

and in combination for 6 days (Figure 5.8). An increased treatment duration was used, to compensate for the reduced proliferation rate. The combination therapy did reduce proliferation compared to SN38 and VX-970 monotherapies, with an average ZIP synergy score of 17.996 (± 2.2). Complete loss of proliferation only occurred with 50nM SN38 and 0.125µM VX-970 combination therapy, which is markedly higher than the 3nM SN38 and 0.125µM VX-970 combination therapy which caused an almost 100% growth inhibition at 3 days in SW48 parental cells (Figure 5.8 and Figure 3.5). While this does show VX-970 to sensitise SW48R cells to SN38, the dose of SN38 required to cause complete loss of proliferation may not be clinically relevant.

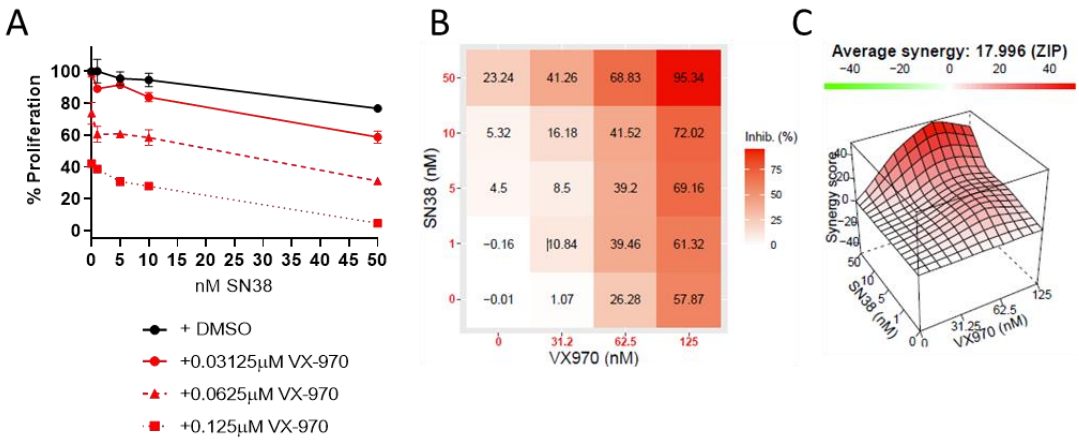

Figure 5.8. **VX-970 only synergises with SN38 to reduce proliferation at very high doses in SN38 resistant SW48 cells.**

Cells were seeded at 2,500 cells per well in 96-well plates and treated with the indicated drugs for 6 days. **A.** The SRB assay was used to calculate proliferation rates. Each datapoint is the mean of 3 biological repeats. Error bars represent +/- SEM. **B.** Heatmap showing the mean percentage inhibition for each drug combination. **C.** The 3D ZIP model demonstrates the interaction between SN38 and VX-970 at very high doses of SN38.

The scope of this investigation is limited by having only 2 resistant cell lines, with differing mechanisms of resistance. However, the survival and proliferation analysis of HT29R and SW48R cells suggest that ATR inhibition is unlikely to restore sensitivity to irinotecan in all resistant tumours.

5.3.4 SN38 resistant SW48 cells are not sensitive to DS-8201a and AZD6738 combination therapy

In this study ATR inhibition was found to sensitise the SW48 parental cell line but not the HT29 parental cell line to DS-8201a (Figure 4.5, Figure 4.6, Figure 4.7, Figure 4.8, Figure 4.9, Figure 4.10 and Figure 4.11). The clonogenic assay was used to assess whether AZD6738 could sensitise SW48R cells to DS-8201a. Cells were treated with either DS-8201a or AZD6738 as monotherapies or in combination for either 3 days or 14 days and survival measured (Figure 5.9).

SW48R cells displayed no sensitivity to DS-8201a monotherapy with either 3-day or 14-day treatment schedules. Sensitivity to AZD6738 monotherapy was observed, with survival reduced to 65.7% (± 2.0) with 3-day 0.25µM AZD6738, and to 74.4% (± 8.6) with 14-day 0.125µM AZD6738. There was no statistically significant reduction in survival with combination of DS-8201a and AZD6738 compared to AZD6738 monotherapy. With 3-day treatment, survival was reduced to 58.7% (± 4.4) with combined 0.25µM AZD6738 and 10µg/mL DS-8201a treatment compared to 65.7% (± 2.0) with 0.25µM AZD6738 monotherapy. With 2-week treatment, survival was reduced to 67.8% (± 9.7) with combined 0.125µM AZD6738 and 10µg/mL DS-8201a treatment compared to the 74.4% (± 8.6) with 0.125µM AZD6738 monotherapy. The average ZIP synergy score for DS-8201a and AZD6738 interaction was -0.63 (± 0.44) with 3-day treatment and 1.6 (± 0.48) with 14-day treatment, demonstrating lack of synergy.

Although limited clinical application can be derived from a study in a single resistant cell line, cross resistance to SN38 and DS-8201a was observed in the SW48R cell line. The lack of response to DS-8201a as a monotherapy and in combination with AZD6738 suggests that DS-8201a may not be a therapeutic option for the treatment of all irinotecan resistant tumours.

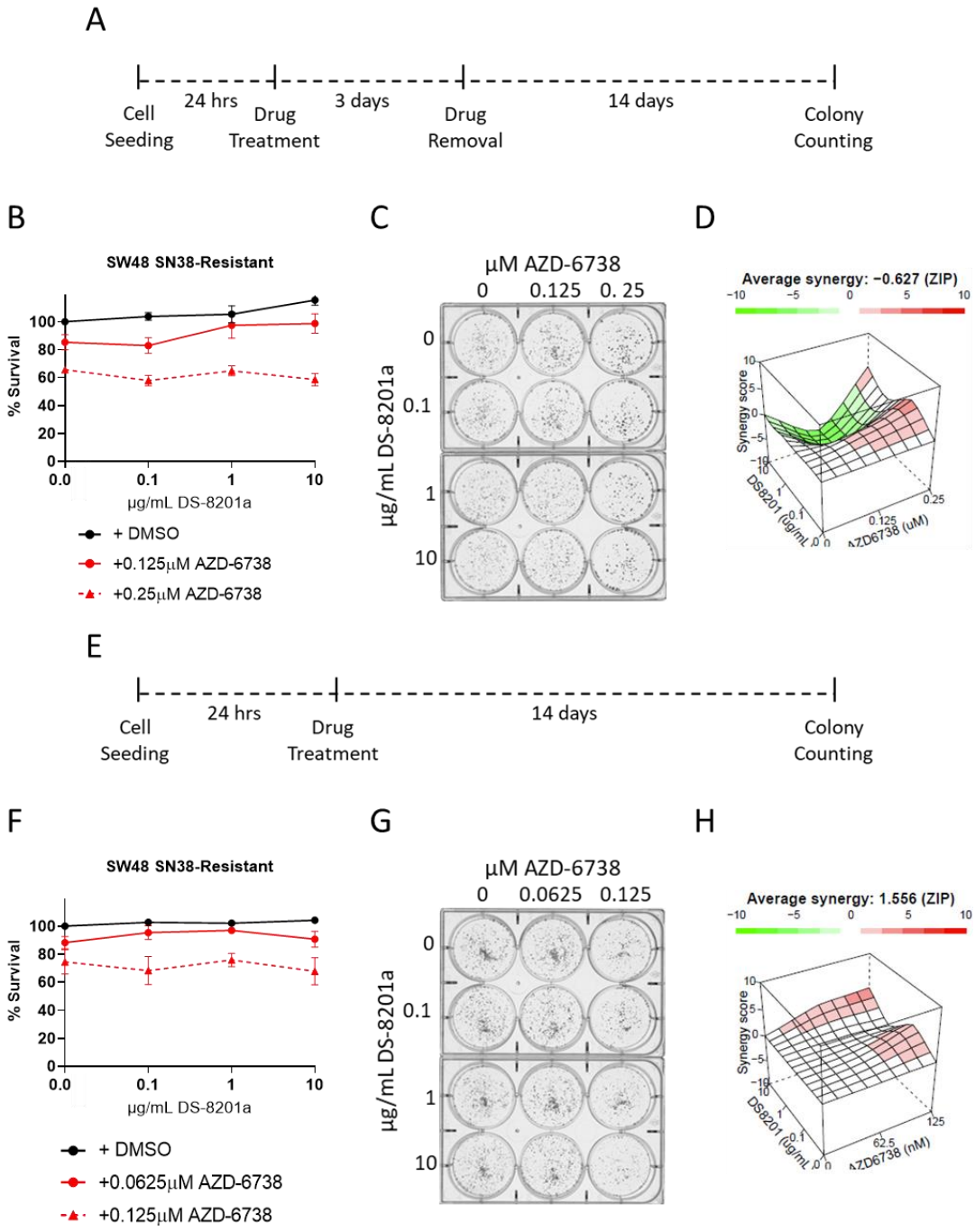

Figure 5.9. **AZD-6738 does not synergise with DS-8201a in SW48 SN38-resistant (SW48R) cells.**

A. Scheme demonstrating the treatment and clonogenic assay schedule followed in B, C and D. **E.** Scheme demonstrating the treatment and clonogenic assay schedule followed in F, G and H. **B.** and **F.** The percentage survival following combination treatment with DS-8201a + AZD-6738. Each datapoint is the mean of 3 biological repeats. Error bars represent +/- SEM. **C.** and **G.** Representative images of clonogenic plates for SW48R cells. **D.** and **H.** 3D ZIP models demonstrate the interaction between DS-8201a and AZD-6738.

5.4 Discussion

5.4.1 Reduced influx and increased efflux of SN38 the likely mechanism of SN38 resistance in HT29R cells.

In this study HT29 cells with increased resistance to SN38 were generated (Figure 5.1). The HT29R cells displayed decreased ɣH2AX accumulation in comparison to the parental cell line, suggesting reduced accumulation of genotoxic lesions (Figure 5.6). A reduction in cellular SN38 levels is a well-established mechanism for irinotecan resistance in CRC cell lines. RNA-seq analysis identified increased expression of the ABCC2 transporter and to a lesser extent the ABCG2 transporter in the HT29R cells (Table 5.1). Overexpression of the ABCC2 transporter has been reported to cause very high levels of SN38 resistance in cancer cell lines, with ABCC2 causing rapid SN38 efflux thereby preventing cytotoxicity (Brangi et al. 1999; Salphati, Plise, and Li 2009). Increased ABCG2 expression in CRC cell lines has also been reported to cause increased SN38 efflux, with resultant SN38 resistance (Candeil et al. 2004; Jensen et al. 2015; Wu et al. 2020). A study by Tuy et al., found increased ABCG2 expression in CRC tumours to be predictive of poor irinotecan treatment outcome (Tuy et al. 2016). A further study by Jensen et al., identified reduced survival in irinotecan treated CRC patients with high ABCG2 expressing tumours, although this finding was not statistically significant (Jensen et al. 2015).

In addition to HT29R cells having upregulated ABC transporters previously reported to confer resistance to SN38, a loss of SLCO1B3 expression was also identified (Table 5.1). This is likely to be contributing factor to SN38 resistance, as SN38 has been previously identified as a substrate for SLCO1B3, with the transporter causing increased SN38 cellular uptake (Yamaguchi et al. 2008). One study identified a splice variant of SLCO1B3 to be highly expressed in CRC tumours. The splice variant is truncated and does not localise to the cell membrane. Expression of the SLCO1B3

variant was found to be predictive of a poor response to irinotecan-based therapy, with reduced SN38 uptake the possible mechanism of resistance (Teft et al. 2015). A reduction in oestrogen signalling in the HT29R cells (identified using GSEA analysis Figure 5.5) supported the physiological significance of SLCO1B3 loss, as SLCO1B3 has been identified as a key transport protein involved in the uptake of oestrogen compounds (Nozawa, Suzuki, et al. 2005; Sutherland, Meeson, and Lowes 2020).

The contribution of increased ABCC2 and ABCG2 expression towards SN38 resistance in HT29R cells can be established using specific ABC transporter inhibitors. Fumitremorgin C is an inhibitor of ABCG2 (Rabindran et al. 2000), and MK-571 is an inhibitor for ABCC2 (Vezmar and Georges 2000). Rescue of resistance by SLCO1B3 gene transfection would provide an indication of the role SLCOB13 expression plays in resistance. Unfortunately, these investigations were beyond the scope of this study.

5.4.2 Reduced cell proliferation, loss of TOP1 expression and increased TDP1 activity may all contribute to SN38 resistance in SW48R cells

Multiple factors may contribute to the very high level of SN38 resistance observed in SW48R cells (Figure 5.1). The complete lack of H2AX, Chk1 and p53 phosphorylation with even high dose SN38, suggests very reduced accumulation of TOP1ccs in response to SN38 treatment (Figure 5.6). SW48R cells were found to have reduced TOP1 expression compared to parental cells (Table 5.2). A reduction in TOP1 expression was one of the first identified mechanisms of resistance to irinotecan in cancer cells (McLeod and Keith 1996). This finding has been supported by downregulation of TOP1 in patient tumours and mouse models in response to irinotecan therapy, suggesting this to be a mechanism of resistance (Giovanella et al. 1989; Horisberger et al. 2009). The findings of the MRC FOCUS study demonstrated the clinical relevance of reduced TOP1 expression, with patients with TOP1 loss

deriving no benefit from irinotecan-based therapy (Braun et al. 2008). While the differential expression of TOP1 in parental and resistant cell lines was found to be statistically significant, the biological significance remains to be explored. The functional significance of the TOP1 downregulation in SW48R cells could be assessed using a topoisomerase I assay, in which cell extracts are incubated with supercoiled DNA. The cleavage and relaxation of DNA is then measured by separation of DNA products using electrophoresis, however this was beyond the scope of this study (Nitiss et al. 2012).

SW48R cells also had a statistically significant increase in TDP1 expression (Table 5.2). TDP1 hydrolyses the tyrosyl-DNA phosphodiester bond between TOP1 and the 3' DNA end, thereby resolving trapped TOP1ccs. Overexpression of TDP1 has been identified as a mechanism of resistance to TOP1 inhibitors, with increased TDP1 expression reducing the cytotoxicity of irinotecan in a panel of CRC cell lines (Meisenberg et al. 2015). The ratio of TOP1 to TDP1 has been found to correlate with response to TOP1 inhibition in a panel of SCLC cell lines, with low TOP1 expression and high TDP1 expression driving resistance (Meisenberg et al. 2014). Furthermore, cell lines from patients with spinocerebellar ataxia with axonal neuropathy (SCAN1), which is caused by a H493R mutation in TDP1, are hypersensitive to CPT treatment. The mutant TDP1 becomes trapped in TDP1-DNA complexes, which is an intermediary complex formed in the resolution of TOP1ccs (Interthal et al. 2005). The functional significance of increased TDP1 expression in SW48R cells could be explored in future experiments by a partial knockdown of TDP1 using siRNA.

As the cytotoxicity of TOP1 inhibitors is dependent on cell cycle progression, and passage of cells through S-phase, a reduction in the proliferation causes drug resistance (Horwitz and Horwitz 1973; Hsiang et al. 1985). A reduced rate of cell cycle progression may also enable increased DNA repair, as cell cycle checkpoint inhibitors which increase the rate of cell cycle progression have been found to synergise with

TOP1 inhibitors in CRC cells (Abal et al. 2004). SW48R cells were found to have a markedly longer cell cycle than the parental cell line and this may have been a major contributor to SN38 resistance (Figure 5.2). The duration of exposure to SN38 was increased to 6-days in the SW48R proliferation assay, to allow for increased cell cycle passages (Figure 5.8). However, as the half-life of irinotecan is short, increasing SN38 exposure to sensitise cells may be clinically irrelevant (Chabot 1997).

Reduced proliferation rate in SW48R cells is likely due to the loss of expression of multiple SLC transporters (Table 5.3). SLC7A5, SLC3A2, SLC7A7 and SLC38A5 are all membrane transporters involved in the cellular uptake of amino acids (Cormerais et al. 2016; Muto et al. 2019; Nakanishi et al. 2001). Loss of SLC7A5 has been reported to reduce the proliferation rate of CRC cell lines and spheroids and cause a loss in cell viability (Cormerais et al. 2016; Muto et al. 2019). SLC3A2 dimerises with SLC7A5, and loss of expression has also been found to reduce cancer cell proliferation rate (Alfarsi et al. 2020). SLC7A7 has also been reported to dimerise with SLC3A2, and overexpression has been shown to increase proliferation rate of cancer cells and is associated with poor survival in glioblastoma patients (Fan et al. 2013; Torrents et al. 1998). SLC7A11 mediates cysteine uptake and glutamate efflux, with expression important in protecting CRC cells from oxidative stress (Ju et al. 2016; Xu et al. 2020). SLC29A2 is a nucleoside transporter with increased expression in CRC tumours (Liu, Zuo, et al. 2017). SLCO4A1 has multiple organic substrates and expression has been correlated with poor survival in CRC patients. Knockdown in SLCO4A1 in CRC cell lines has been reported to cause a loss of proliferation (Ban et al. 2017). SLC2A1 (GLUT1) is a glucose transporter that is overexpressed in CRC (Feng et al. 2017), reduced glucose uptake in SW48R cells is likely to contribute to reduced proliferation. SLC8A2 is a Na^{+}/Ca^{2+} that plays a key role in $Ca2^{+}$ homeostasis. SLC8A2 has been reported to be overexpressed in gastric cancers and

brain metastasis, but its role in the proliferation of CRC cells is not reported (Beltran et al. 2011; Hu et al. 2020).

MTORC1 and MYC among other roles, are key modulators of glucose, amino acid, nucleotide and lipid metabolism in cancer cells (Dang, Le, and Gao 2009; Kim, Cook, and Chen 2017). GSEA analysis identified upregulation of MYC and MTORC1 signalling in SW48R cells in comparison to the parental cells (Figure 5.3). This is suggestive that loss of expression of SLC transporters is having a physiological impact in the SW48R cells, leading to activation of these two signalling pathways essential for continued survival in the presence of metabolic stress.

In SW48R cells NFκB signalling was also found to be upregulated (Figure 5.3), which may play a role in promoting the survival of cells in the presence of TOP1 inhibition. Increased activation of transcription factors following DNA damage that promote survival, such as nuclear factor kappa B (NFκB) have been reported to reduce sensitivity to irinotecan in cancer cell lines (Huang et al. 2000; Wang et al. 1999). Furthermore, increased NFκB has been identified as a poor prognostic marker for response to irinotecan treatment (Scartozzi et al. 2007). However, the lack of ATR activation and DNA damage signalling observed in SW48R cells, suggests the mechanism of resistance may be upstream of NFκB signalling (Figure 5.6).

5.4.3 ATR inhibition to overcome loss of irinotecan sensitivity will likely depend on mechanism of resistance

In this study we have demonstrated ATR inhibition to sensitise HT29 and SW48 parental cells to low dose SN38, reducing the dose required for cytotoxicity (Figure 3.5 and Figure 3.6). Synergy between TOP1 and ATR inhibition has also been demonstrated in several other studies using a range of cancer models, as well as in early phase clinical trials (Huntoon et al. 2013; Hur et al. 2021; Josse et al. 2014; Thomas et al. 2018; Thomas et al. 2021). The use of ATR inhibition to overcome

resistance to TOP1 inhibition has not been previously explored, however one study has shown VX-970 to sensitise resistant CRC cells to oxaliplatin by increasing the accumulation of DNA damage (Combès et al. 2019).

The SN38 resistance in HT29R is likely due to reduced cellular SN38 accumulation, caused by reduced import by SLCO1B3 and increased export by ABCC2 and ABCG2 (Table 5.1). This suggests that ATR inhibition may be effective at sensitising the HT29R cells by reducing the cytotoxic dose of SN38. Furthermore, although at a slightly reduced level, we demonstrated robust activation of ATR signalling in the HT29R cells following SN38 treatment, showing ATR to still play a role in the cellular response to TOP1 inhibition in the HT29R cells (Figure 5.6). However, we failed to show any sensitisation of HT29R cells to SN38 with the addition of VX-970 (Figure 5.7). Although at a higher concentration than in the parental cell line, HT29R did display sensitivity to SN38, but no further reduction in survival was observed with the addition of VX-970. This strongly suggests resistance to VX-970, as the addition of VX-970 to SN38 in the parental line caused a very dramatic loss of survival (Figure 3.6). The transporter ABCB1, has been reported to actively efflux VX-970 from cells (Talele et al. 2019). It is possible that ABCC2 and ABCG2 upregulation also results in VX-970 efflux, as these transporters are implicated in resistance to a very broad spectrum of therapeutic agents (Polgar, Robey, and Bates 2008; van der Schoor et al. 2015). Cross-resistance of HT29R cells to SN38 and VX-970 would explain the lack of sensitivity to the combination therapy. This can be explored in future experiments, by assessing the ability of VX-970 to reduce ATR signalling in HT29R cells.

SW48R and SW48 cells displayed comparable sensitivity to VX-970 monotherapy, with an approximately equal loss of survival in both cell lines. No loss of survival was observed in the SW48R cells with the addition of VX-970 to even 10nM SN38 treatment, which is 10-times greater than the dose required to cause an almost

complete loss of survival in the parental cell line (Figure 3.6). The addition of VX-970 to SN38 treatment did reduce proliferation in the SW48R line, but this was at markedly higher concentrations than observed in the parental cell line (Figure 3.5 and Figure 5.8). Furthermore, the effect was observed with 6-days treatment, with only 3-day treatment required for synergy in the parental cell line. This suggests that ATR inhibition is still effective at increasing the cytotoxicity of TOP1ccs, but the dose at which SN38 is causing an accumulation of TOP1ccs, is much higher in the resistant cell line than the parental cell line. For VX-970 to restore sensitivity, the combination treatment in SW48R would be required to show the same cytotoxicity as the SN38 monotherapy in the parental line, however this was not observed. These findings show that ATR inhibition is unlikely to fully restore sensitivity in resistant CRCs that have a dramatically reduced accumulation of TOP1ccs.

5.4.4 DS-8201a as a monotherapy or in combination with ATR inhibition is ineffective in the treatment of the SN38 resistant SW48 cell line

DS-8201a has demonstrated efficacy in clinical trials in patients who have previously been treated with irinotecan (Shitara et al. 2020; Siena et al. 2021). This suggests that DS-8201a may be an effective treatment for irinotecan resistant CRC. It is however possible that patients may have discontinued irinotecan-based regimens due to cumulative toxicity, and not disease progression, thereby providing no insight into responses in patients with irinotecan resistant tumours. The differential cellular uptake of DS-8201a and irinotecan/SN38, may result in efficacy in tumours resistant to irinotecan due altered metabolic processing or poor cellular uptake. Furthermore, unlike SN38, Dxd undergoes negligible levels of metabolism prior to excretion, which may make tumours with increased UGT1A1 activity sensitive to DS-8201a over irinotecan (Okamoto et al. 2020).

In this study, we found DS-8201a to have a complete loss of cytotoxicity in SW48R cells, with no reduction in survival with even 2-week DS-8201a exposure (Figure 5.9). The mechanism of SN38 resistance in SW48R cells is proposed to be due to decreased proliferation rate, decreased TOP1 expression and increased TDP1 expression, all which are likely contributors to reducing the accumulation of trapped TOP1ccs. In the SW48 parental cells, 10µg/mL DS-8201a was found to have equivalent toxicity to about 1nM SN38 (Figure 3.5 and Figure 4.2). SW48R cells showed only a moderate loss of proliferation with 50nM SN38 (Figure 5.1), making the lack of sensitivity to 10µg/mL DS-8201a expected. The DS-8201a resistance in SW48R cells is likely affected by the minimal accumulation of Dxd due to low HER2 expression. In HER2-high expressing cancers the accumulation of high concentrations of Dxd may be sufficient to overcome SN38 resistance. Furthermore, when the mechanism of irinotecan resistance is due to reduced cellular uptake or rapid clearance, DS-8201a may be effective due to the differential mechanisms of uptake and negligible metabolic processing (Okamoto et al. 2020).

The combination of DS-8201a and AZD6738 did not cause any reduction in survival in SW48R cells in comparison to DS-8201a monotherapy (Figure 5.9). The addition of VX-970 to 10nM SN38 treatment did not reduce the survival of SW48R cells (Figure 5.7). It is therefore probable that the TOP1 inhibition achieved with 10µg/mL DS-8201a in SW48R cells, is below the threshold for any DNA damage or activation of ATR. This is supported by the lack of DNA damage and ATR signalling in SW48R cells with concentrations of up to 100nM SN38 (Figure 5.6). This suggests that ATR inhibition may not be effective in increasing the sensitivity of HER2-low CRC to DS-8201a in irinotecan resistant patients, unless the mechanism of resistance is overcome by the differential uptake and metabolism of DS-8201a (Okamoto et al. 2020).

5.5 Conclusions

The work in this chapter has demonstrated ATR inhibition to be ineffective at restoring SN38 sensitivity in two SN38 resistant cell lines. The identified mechanisms of resistance differed between the cell lines, which suggests that this finding may be of clinical significance in patients with varying mechanisms of irinotecan resistance. Cross resistance to SN38 and DS-8201a was observed in SW48R cells, suggesting that DS-8201a efficacy in irinotecan resistant tumours is likely to be dependent on the specific mechanism of resistance. Furthermore, ATR inhibition was not effective at restoring DS-8201a sensitivity in SW48R cells.

6 Final Discussion

Increased ATR expression and activation in human tumours, together with ATR-dependence for tumour development in mouse models led to the identification of ATR as an attractive target in cancer therapy (Derenzini et al. 2015; Fishler et al. 2010; Höglund et al. 2011; Kawasumi et al. 2011; López-Contreras et al. 2012; Murga et al. 2009; Tho et al. 2012; Verlinden et al. 2007). Since the development of potent ATR inhibitors with favourable pharmacokinetic properties, there has been an explosion in preclinical and clinical studies investigating ATR inhibition as a monotherapy and in combination with DNA damaging therapeutics. ATR inhibition as a monotherapy is largely being explored in the context of genetic alterations, which generate increased reliance on ATR signalling for cell cycle checkpoint activation and ATR mediated DNA damage repair (Krajewska et al. 2015; Kwok et al. 2016; Menezes et al. 2015; Middleton, Pollard, and Curtin 2018; Min et al. 2017; Mohni et al. 2015; Reaper et al. 2011; Ruiz et al. 2016; Schmitt et al. 2017; Sultana et al. 2013; Toledo et al. 2011; Williamson et al. 2016).

Treatment of cancer cells with DNA-damaging agents including TOP1 inhibitors, platinum therapies, nucleoside antimetabolites and radiation have all been shown to activate ATR signalling. Activation of ATR in the context of DNA damage and replication stress leads to cell cycle arrest and DNA-repair, limiting the cytotoxicity of therapeutics (Combès et al. 2019; Fokas et al. 2012; Josse et al. 2014; Ma and Wang 2014). Indeed, multiple preclinical studies have shown ATR inhibition to abrogate DNA-damage induce cell cycle arrest and DNA damage repair, leading to a cytotoxic accumulation of DNA damage (section 1.6.3, 1.6.4 and 1.6.7) (Combès et al. 2019; Fokas et al. 2012; Ma et al. 2017). There are multiple clinical trials evaluating the safety and efficacy of ATR inhibitors VX-970 and AZD6738 in combination with DNA-damaging therapeutics (Table 1.4 and Table 1.5).

Several pre-clinical studies have reported synergy between TOP1 (topotecan, LMP-400, CPT and belotecan) and ATR inhibition in different cancer models, including breast, ovarian, SCLC and EP-SCNC (Huntoon et al. 2013; Hur et al. 2021; Josse et al. 2014; Thomas et al. 2021). There has been limited work on the combination of TOP1 and ATR inhibition in the context of CRC, with a single study reporting synergy in two p53 deficient cell lines, and a CRC mouse model (Josse et al. 2014). Importantly, a phase I study combining topotecan and VX-970 for the treatment of advanced solid tumours reported an acceptable toxicity profile, suggesting ATR inhibition to be less cytotoxic to non-cancerous cells than tumour cells (Thomas et al. 2018). A recently published clinical study, has demonstrated VX-970 and topotecan to have efficacy in the treatment of SCLC and EP-SCNC (Thomas et al. 2021). In this thesis, the efficacy of combined ATR and TOP1 inhibition for the treatment of CRC was investigated, with synergy demonstrated in cell lines and the more translationally relevant model of PDOs.

In this study, we identified loss of cell cycle arrest and increased DNA damage as the suggested mechanism of synergy between TOP1 and ATR inhibition. In CRC cell

lines, we demonstrated increased DNA damage signalling in response to the combination therapy, with increased ɣH2AX accumulation, as well as phosphorylation of DNA-PK and ATM. Furthermore, a dramatic increase in DNA DSBs and the formation of micronuclei was also detected in response to combination therapy. Using the novel CyTOF technique, we identified that ATR inhibition abrogated SN38 induced replication fork arrest in PDOs, enabling cell cycle progression, demonstrating the role of ATR inhibition in the context of replication stress. Using a combination of CyTOF and Western blotting, phosphorylation of DNA-PK and ATM in response to combination therapy was also detected in PDOs. CyTOF analysis of combination treated PDOs, identified a population of cells with very high levels of ɣH2AX (pan-nuclear) which has previously been reported to be an indicator of catastrophic DNA damage (Ding et al. 2016; Hur et al. 2021; Meyer et al. 2013). These cells also had high levels of DNA-PK phosphorylation, implicating DNA-PK in the phosphorylation of H2AX in response to TOP1cc induced DNA damage in the absence of ATR signalling.

In recent years, the cGAS-STING pathway has been identified as a link between increased DNA damage in tumour cells and an anti-tumour immune response (Vanpouille-Box et al. 2018). In this study, the identification of cGAS-positive micronuclei with VX-970 and SN38 combination therapy indicated activation of the immunostimulatory pathway. Despite increased cGAS-positive micronuclei in combination treated cells, no production of immunostimulatory cytokines was detected. Dysfunction of the cGAS-STING pathway has been identified to occur in multiple cancer types, including CRC (Konno et al. 2018; Xia et al. 2016). In accordance with these reports, this study identified loss of cGAS and/or STING in a panel of CRC cell lines. Promoter hypermethylation of cGAS and STING genes has been identified to cause transcriptional silencing, leading to the impairment of the cGAS-STING pathway (Xia, Konno, and Barber 2016). Treatment of cells with a DNA methyltransferase (DNMT) inhibitor (decitabine), has been shown to effectively

restore the function of the cGAS-STING pathway in cancer cells (Falahat et al. 2021). Ongoing *in vitro* and *in vivo* work in the lab, is exploring whether the combination of decitabine with DNA damaging agents will result in an anti-tumour immune response via the cGAS-STING pathway. Restoration of cGAS-STING signalling combined with TOP1 and ATR inhibition may produce an anti-tumour immune response. Anti-tumour immune responses have been shown to result in durable treatment responses, with the immune elimination of persisting cancer stem cells and micro-metastasis (Waldman, Fritz, and Lenardo 2020).

Having demonstrated ATR inhibition to dramatically sensitise CRC cell lines and PDOs to SN38, the efficacy of combined ATR inhibition and DS-8201a was investigated. A previous study by Daiichi Sankyo, showed HER2-low CRC cell lines to be resistant to DS-8201a due to minimal ADC uptake and sub-cytotoxic accumulation of Dxd (Takegawa et al. 2019). These finding were validated by lack of DS-8201a efficacy in the treatment of HER2 IHC1+ and IHC2+ CRCs in a phase I clinical trial (Siena et al. 2021). In this study, we demonstrated ATR inhibition (VX-970 and AZD6738) to sensitise CRC cell lines and PDOs to DS-8201a. Sensitisation was dependent on a threshold level of Dxd accumulation and cytotoxicity, with no benefit observed in a cell line with reduced sensitivity to Dxd and an ABCB1 overexpressing cell line, that has been demonstrated to actively efflux Dxd and VX-970 (Takegawa et al. 2019; Talele et al. 2019).

We proposed the mechanism of synergy between ATR inhibition and DS-8201a, would be the same as that observed with SN38, with loss of ATR induced replication arrest and an accumulation of DNA damage. Likely due to the very minimal cytotoxicity of DS-8201a monotherapy, we were unable to detect activation of ATR signalling in CRC cell lines using Western blotting. However, using the more sensitive CyTOF technique we identified DS-8201a to induce ATR signalling in PDOs. Accumulation of ɣH2AX and phosphorylation of DNA-PK and ATM were observed in

cell lines and PDOs in response to ≥10nM SN38 and VX-970 treatment. Dxd accumulation in the HER2-low CRC cancer cell lines led to cytotoxicity equivalent to approximately 1nM SN38. Although we did show some evidence of DNA-PK and Chk2 phosphorylation in cells treated with DS-8201a combination therapy using Western blotting, a more sensitive technique such as mass spectroscopy may be a more suitable technique to detect subtle changes in DNA-damage signalling pathways.

Using the CyTOF technique, we showed a loss in DS-8201a-induced ɣH2AX signal in S-phase PDO cells with the addition of VX-970. We also showed an increase in S-phase independent ɣH2AX in response to the combination therapy in one PDO model, with this ɣH2AX accumulation being much greater than that observed in S-phase cells. This finding demonstrated the complex crosstalk between DNA-damage signalling pathways. Previous studies have shown ATR to be the primary kinase phosphorylating ɣH2AX in response to replication stress, and ATM to be the primary kinase in response to DSBs (Burma et al. 2001; Sirbu et al. 2011; Ward and Chen 2001). We propose that ATR inhibition prevents ɣH2AX accumulation at TOP1ccs, as well as preventing replication arrest. This loss of DNA-damage signalling and progression through the cell cycle results in the formation of DSBs, which results in S-phase and ATR independent ɣH2AX signal, which is likely mediated by ATM (Figure 6.1).

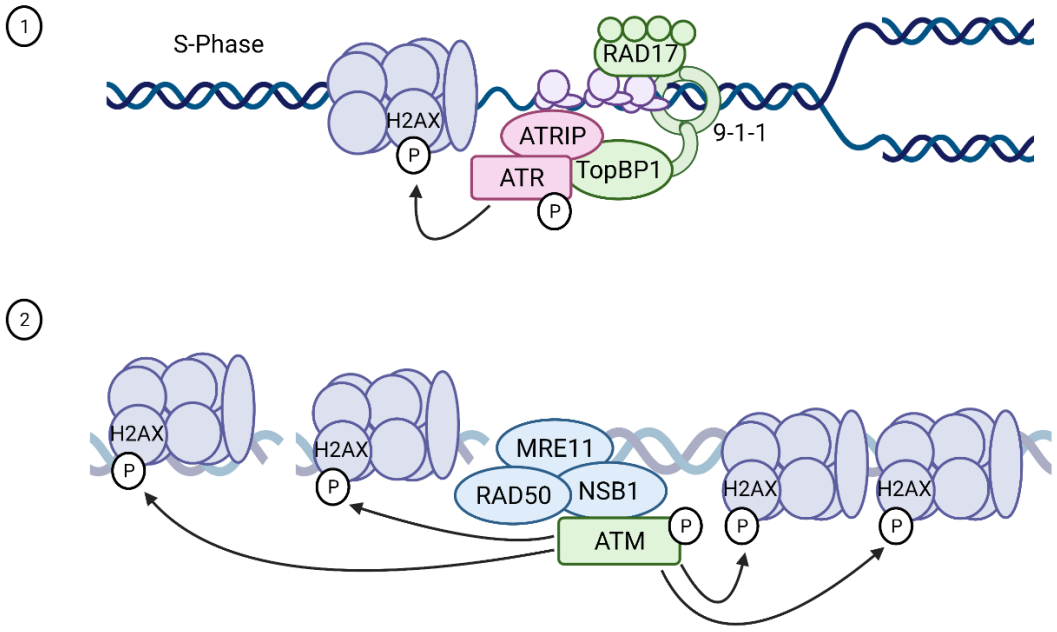

Figure 6.1. **ATR and ATM differentially phosphorylate H2AX.**
1. During S-phase in response to replication stress (such as the presence of TOP1ccs), ATR is the primary kinase phosphorylating H2AX. **2.** In the absence of ATR kinase activity, DNA-DSBs form due to unresolved replication stress, this leads to ATM dependent phosphorylation of H2AX. The amplification of pH2AX signal is greater in response to ATM signalling and is not cell cycle phase dependent. Created with Biorender.

Complex interaction between DNA-damage signalling and p53 phosphorylation and stablisation, was also shown in this study. VX-970 caused a reduction in SN38-induced p53 phosphorylation in CRC cell lines. However, increased p53 phosphorylation was observed with DS-8201a and VX-970 combination therapy compared to DS-8201a monotherapy. This suggests that the level of replication stress and subsequent DNA damage with TOP1 inhibition, may be important in determining the pathway of p53 activation. In response to SN38, which caused more potent TOP1 inhibition in the CRC cell lines, p53 activation appeared to be mediated by ATR. However, in response to DS-8201a and VX-970 combination treatment, p53 phosphorylation was ATR independent. p53 phosphorylation in this context may occur via ATM, as we were able to detect activation of Chk2, the kinase downstream of

ATM. ATM is the principal kinase responsible for p53 phosphorylation and stabilisation in response to DNA damage, which is the proposed mechanism of DS-8201a and ATR inhibitor combination therapy (Banin et al. 1998; Canman et al. 1998; Cheng and Chen 2010; Shieh et al. 1997).

Increased DNA damage in response to DS-8201a and ATR inhibition therapy, may lead to an increased anti-tumour immune response. A study using immunocompetent mouse models, has already shown DS-8201a monotherapy to have immunogenic properties. Mice bearing HER2+ positive tumours cured by DS-8201a treatment, failed to develop tumours when rechallenged with the same tumour type (even in the absence of HER2 expression). DS-8201a was found to increase tumour infiltrating DCs and CD8+ T-cells (with increased granzyme B secretion), as well as increasing IFNɣ secretion by splenocytes. Furthermore, DS-8201a was found to increase the expression of MHC-CI on tumour cells (Iwata et al. 2018). Antigen presentation to tumour infiltrating immune cells occurs via MHC-CI molecules (Shklovskaya and Rizos 2021). Increased DNA damage via combined DS-8201a and ATR inhibitor treatment may result in the accumulation of neoantigens, which in the context of increased MHC-CI mediated antigen presentation, may drive a more potent anti-tumour response. Studying the immunomodulatory properties of DS-8201a and ATR inhibitor combination treatment was not in the remit of this study, however it is an exciting research avenue which will be investigated in future studies.

In this study, the use of ATR inhibition to overcome SN38 resistance was investigated. VX-970 failed to restore sensitivity to SN38 in two resistant cell lines. Furthermore, despite clinical studies in CRC (HER2 IHC3+) and gastric cancer patients showing DS-8201a efficacy in patients previously treated with irinotecan (Shitara et al. 2020; Siena et al. 2021), no efficacy of combined ATR inhibition and DS-8201a was observed in an SN38 resistant cell line in this study. The identified mechanisms of resistance in one cell line were reduced SN38 influx and increased SN38 efflux, due

to altered expression of ABC and SLC transporters. The other cell line had reduced TOP1 expression and increased expression of TDP1 (a key enzyme for the resolution of TOP1ccs), as well as a reduced proliferation rate, likely caused by downregulation of key SLC transporters.

To further asses the clinical potential of ATR inhibition in combination with irinotecan or DS-8201a for the treatment of irinotecan resistant cancer, better models of resistance are required. The CRC PDOs which have been developed in our lab, have all been generated from tumours resected during surgery. We were not able to obtain tumours from previously treated irinotecan patients, as patients receive irinotecan post-surgery. Obtaining post-humous tumours for the development of an irinotecan resistant PDOs is a possible option for a future study. This would enable identification of biomarkers for sensitivity to DS-8201a and ATR inhibitor combination therapy in the context of irinotecan resistance.

This project was done in collaboration with Daiichi Sankyo and AstraZeneca. A phase I clinical trial has now been set up to explore the tolerability and efficacy of combined DS-8201a and AZD6738 therapy. If the findings of this trial are positive, efficacy in the CRC setting can then be explored. A trial investigating the efficacy of combined AZD6738 and irinotecan treatment for the treatment of CRC is currently being set up by AstraZeneca. Both these novel combinations are exciting new areas of therapeutic potential in the mCRC setting.

References

Abal, M., R. Bras-Goncalves, J. G. Judde, H. Fsihi, P. De Cremoux, D. Louvard, H. Magdelenat, S. Robine, and M. F. Poupon. 2004. 'Enhanced sensitivity to irinotecan by Cdk1 inhibition in the p53-deficient HT29 human colon cancer cell line', *Oncogene*, 23: 1737-44.

Abdollahpour-Alitappeh, Meghdad, Majid Lotfinia, Tohid Gharibi, Jalal Mardaneh, Behrouz Farhadihosseinabadi, Pegah Larki, Babak Faghfourian, Koushan Sineh Sepehr, Kazem Abbaszadeh-Goudarzi, Ghasem Abbaszadeh-Goudarzi, Behrooz Johari, Mohammad Reza Zali, and Nader Bagheri. 2019. 'Antibody–drug conjugates (ADCs) for cancer therapy: Strategies, challenges, and successes', *Journal of Cellular Physiology*, 234: 5628-42.

Ablasser, A., M. Goldeck, T. Cavlar, T. Deimling, G. Witte, I. Röhl, K. P. Hopfner, J. Ludwig, and V. Hornung. 2013. 'cGAS produces a 2'-5'-linked cyclic dinucleotide second messenger that activates STING', *Nature*, 498: 380-4.

Abu-Sanad, A., Y. Wang, F. Hasheminasab, J. Panasci, A. Noë, L. Rosca, D. Davidson, L. Amrein, B. Sharif-Askari, R. Aloyz, and L. Panasci. 2015. 'Simultaneous inhibition of ATR and PARP sensitizes colon cancer cell lines to irinotecan', *Front Pharmacol*, 6: 147.

Ahlskog, J. K., B. D. Larsen, K. Achanta, and C. S. Sørensen. 2016. 'ATM/ATR-mediated phosphorylation of PALB2 promotes RAD51 function', *EMBO Rep*, 17: 671-81.

Ahn, J. Y., X. Li, H. L. Davis, and C. E. Canman. 2002. 'Phosphorylation of threonine 68 promotes oligomerization and autophosphorylation of the Chk2 protein kinase via the forkhead-associated domain', *J Biol Chem*, 277: 19389-95.

Ahnesorg, P., P. Smith, and S. P. Jackson. 2006. 'XLF interacts with the XRCC4-DNA ligase IV complex to promote DNA nonhomologous end-joining', *Cell*, 124: 301-13.

Al-Subhi, N., R. Ali, T. Abdel-Fatah, P. M. Moseley, S. Y. T. Chan, A. R. Green, I. O. Ellis, E. A. Rakha, and S. Madhusudan. 2018. 'Targeting ataxia telangiectasia-mutated- and Rad3-related kinase (ATR) in PTEN-deficient breast cancers for personalized therapy', *Breast Cancer Res Treat*, 169: 277-86.

Alfarsi, L. H., R. El-Ansari, M. L. Craze, B. K. Masisi, O. J. Mohammed, I. O. Ellis, E. A. Rakha, and A. R. Green. 2020. 'Co-Expression Effect of SLC7A5/SLC3A2 to Predict Response to Endocrine Therapy in Oestrogen-Receptor-Positive Breast Cancer', *Int J Mol Sci*, 21.

Alimzhanov, Marat, Patricia Soulard, Astrid Zimmermann, Andreas Schroeder, Keyvan Tadjalli Mehr, Christiane Amendt, Geok Choo Sim, Andree Blaukat, Joern-Peter Halle, and Frank T. Zenke. 2019. 'Abstract 2269: ATR inhibitor M6620 enhances anti-tumor efficacy of the combination of the anti-PD-L1 antibody avelumab with platinum-based chemotherapy', *Cancer Res*, 79: 2269.

Altan, B., K. Kaira, A. Watanabe, N. Kubo, P. Bao, G. Dolgormaa, E. O. Bilguun, K. Araki, Y. Kanai, T. Yokobori, T. Oyama, M. Nishiyama, H. Kuwano, and K. Shirabe. 2018. 'Relationship between LAT1 expression and resistance to chemotherapy in pancreatic ductal adenocarcinoma', *Cancer Chemother Pharmacol*, 81: 141-53.

Amado, R. G., M. Wolf, M. Peeters, E. Van Cutsem, S. Siena, D. J. Freeman, T. Juan, R. Sikorski, S. Suggs, R. Radinsky, S. D. Patterson, and D. D. Chang. 2008. 'Wild-type KRAS is required for panitumumab efficacy in patients with metastatic colorectal cancer', *J Clin Oncol*, 26: 1626-34.

Ammazzalorso, F., L. M. Pirzio, M. Bignami, A. Franchitto, and P. Pichierri. 2010. 'ATR and ATM differently regulate WRN to prevent DSBs at stalled replication forks and promote replication fork recovery', *Embo j*, 29: 3156-69.

Andre, Thierry, Kai-Keen Shiu, Tae Won Kim, Benny Vittrup Jensen, Lars Henrik Jensen, Cornelis J. A. Punt, Denis Michel Smith, Rocio Garcia-Carbonero, Manuel Benavides, Peter Gibbs, Christelle De La Fouchardiere, Fernando Rivera, Elena Elez, Johanna C. Bendell, Dung T. Le, Takayuki Yoshino, Ping Yang, Mohammed Zulfiqar Husain Farooqui, Patricia Marinello, and Luis A. Diaz. 2020. 'Pembrolizumab versus chemotherapy for microsatellite instability-high/mismatch repair deficient metastatic colorectal cancer: The phase 3 KEYNOTE-177 Study', *Journal of Clinical Oncology*, 38: LBA4-LBA4.

Andreassen, P. R., A. D. D'Andrea, and T. Taniguchi. 2004. 'ATR couples FANCD2 monoubiquitination to the DNA-damage response', *Genes Dev*, 18: 1958-63.

Argilés, G., J. Tabernero, R. Labianca, D. Hochhauser, R. Salazar, T. Iveson, P. Laurent-Puig, P. Quirke, T. Yoshino, J. Taieb, E. Martinelli, and D. Arnold. 2020. 'Localised colon cancer: ESMO Clinical Practice Guidelines for diagnosis, treatment and follow-up', *Ann Oncol*, 31: 1291-305.

Aris, S. M., and Y. Pommier. 2012. 'Potentiation of the novel topoisomerase I inhibitor indenoisoquinoline LMP-400 by the cell checkpoint and Chk1-Chk2 inhibitor AZD7762', *Cancer Res*, 72: 979-89.

Arnold, M., M. S. Sierra, M. Laversanne, I. Soerjomataram, A. Jemal, and F. Bray. 2017. 'Global patterns and trends in colorectal cancer incidence and mortality', *Gut*, 66: 683-91.

Bagnardi, V., M. Rota, E. Botteri, I. Tramacere, F. Islami, V. Fedirko, L. Scotti, M. Jenab, F. Turati, E. Pasquali, C. Pelucchi, C. Galeone, R. Bellocco, E. Negri, G. Corrao, P. Boffetta, and C. La Vecchia. 2015. 'Alcohol consumption and site-specific cancer risk: a comprehensive dose-response meta-analysis', *Br J Cancer*, 112: 580-93.

Bahassi, E. M., J. L. Ovesen, A. L. Riesenberg, W. Z. Bernstein, P. E. Hasty, and P. J. Stambrook. 2008. 'The checkpoint kinases Chk1 and Chk2 regulate the functional associations between hBRCA2 and Rad51 in response to DNA damage', *Oncogene*, 27: 3977-85.

Bailey, C., J. R. M. Black, J. L. Reading, K. Litchfield, S. Turajlic, N. McGranahan, M. Jamal-Hanjani, and C. Swanton. 2021. 'Tracking Cancer Evolution through the Disease Course', *Cancer Discov*, 11: 916-32.

Bakkenist, C. J., and M. B. Kastan. 2003. 'DNA damage activates ATM through intermolecular autophosphorylation and dimer dissociation', *Nature*, 421: 499-506.

Baldassarre, T., P. Truesdell, and A. W. Craig. 2017. 'Endophilin A2 promotes HER2 internalization and sensitivity to trastuzumab-based therapy in HER2-positive breast cancers', *Breast Cancer Res*, 19: 110.

Ball, H. L., M. R. Ehrhardt, D. A. Mordes, G. G. Glick, W. J. Chazin, and D. Cortez. 2007. 'Function of a conserved checkpoint recruitment domain in ATRIP proteins', *Mol Cell Biol*, 27: 3367-77.

Ball, H. L., J. S. Myers, and D. Cortez. 2005. 'ATRIP binding to replication protein A-single-stranded DNA promotes ATR-ATRIP localization but is dispensable for Chk1 phosphorylation', *Mol Biol Cell*, 16: 2372-81.

Ban, M. J., S. H. Ji, C. K. Lee, S. B. Bae, H. J. Kim, T. S. Ahn, M. S. Lee, M. J. Baek, and D. Jeong. 2017. 'Solute carrier organic anion transporter family member 4A1 (SLCO4A1) as a prognosis marker of colorectal cancer', *J Cancer Res Clin Oncol*, 143: 1437-47.

Bang, Y. J., E. Van Cutsem, A. Feyereislova, H. C. Chung, L. Shen, A. Sawaki, F. Lordick, A. Ohtsu, Y. Omuro, T. Satoh, G. Aprile, E. Kulikov, J. Hill, M. Lehle, J. Rüschoff, and Y. K. Kang. 2010. 'Trastuzumab in combination with chemotherapy versus chemotherapy alone for treatment of HER2-positive advanced gastric or gastro-oesophageal junction cancer (ToGA): a phase 3, open-label, randomised controlled trial', *Lancet*, 376: 687-97.

Banin, S., L. Moyal, S. Shieh, Y. Taya, C. W. Anderson, L. Chessa, N. I. Smorodinsky, C. Prives, Y. Reiss, Y. Shiloh, and Y. Ziv. 1998. 'Enhanced phosphorylation of p53 by ATM in response to DNA damage', *Science*, 281: 1674-7.

Bansbach, C. E., R. Bétous, C. A. Lovejoy, G. G. Glick, and D. Cortez. 2009. 'The annealing helicase SMARCAL1 maintains genome integrity at stalled replication forks', *Genes Dev*, 23: 2405-14.

Baranello, L., D. Wojtowicz, K. Cui, B. N. Devaiah, H. J. Chung, K. Y. Chan-Salis, R. Guha, K. Wilson, X. Zhang, H. Zhang, J. Piotrowski, C. J. Thomas, D. S. Singer, B. F. Pugh, Y. Pommier, T. M. Przytycka, F. Kouzine, B. A. Lewis, K. Zhao, and D. Levens. 2016. 'RNA Polymerase II Regulates Topoisomerase 1 Activity to Favor Efficient Transcription', *Cell*, 165: 357-71.

Barlow, C., S. Hirotsune, R. Paylor, M. Liyanage, M. Eckhaus, F. Collins, Y. Shiloh, J. N. Crawley, T. Ried, D. Tagle, and A. Wynshaw-Boris. 1996. 'Atm-deficient mice: a paradigm of ataxia telangiectasia', *Cell*, 86: 159-71.

Baselga, J., J. Cortés, S. B. Kim, S. A. Im, R. Hegg, Y. H. Im, L. Roman, J. L. Pedrini, T. Pienkowski, A. Knott, E. Clark, M. C. Benyunes, G. Ross, and S. M. Swain. 2012. 'Pertuzumab plus trastuzumab plus docetaxel for metastatic breast cancer', *N Engl J Med*, 366: 109-19.

Bass, T. E., and D. Cortez. 2019. 'Quantitative phosphoproteomics reveals mitotic function of the ATR activator ETAA1', *J Cell Biol*, 218: 1235-49.

Bass, T. E., J. W. Luzwick, G. Kavanaugh, C. Carroll, H. Dungrawala, G. G. Glick, M. D. Feldkamp, R. Putney, W. J. Chazin, and D. Cortez. 2016. 'ETAA1 acts at stalled replication forks to maintain genome integrity', *Nat Cell Biol*, 18: 1185-95.

Beck, A., L. Goetsch, C. Dumontet, and N. Corvaïa. 2017. 'Strategies and challenges for the next generation of antibody-drug conjugates', *Nat Rev Drug Discov*, 16: 315-37.

Beltran, A. S., A. Russo, H. Lara, C. Fan, P. M. Lizardi, and P. Blancafort. 2011. 'Suppression of breast tumor growth and metastasis by an engineered transcription factor', *PLoS One*, 6: e24595.

Ben-Kasus, T., B. Schechter, S. Lavi, Y. Yarden, and M. Sela. 2009. 'Persistent elimination of ErbB-2/HER2-overexpressing tumors using combinations of monoclonal antibodies: relevance of receptor endocytosis', *Proc Natl Acad Sci U S A*, 106: 3294-9.

Bennouna, J., J. Sastre, D. Arnold, P. Österlund, R. Greil, E. Van Cutsem, R. von Moos, J. M. Viéitez, O. Bouché, C. Borg, C. C. Steffens, V. Alonso-Orduña, C. Schlichting, I. Reyes-Rivera, B. Bendahmane, T. André, and S. Kubicka. 2013. 'Continuation of bevacizumab after first progression in metastatic colorectal cancer (ML18147): a randomised phase 3 trial', *Lancet Oncol*, 14: 29-37.

Bentley, N. J., D. A. Holtzman, G. Flaggs, K. S. Keegan, A. DeMaggio, J. C. Ford, M. Hoekstra, and A. M. Carr. 1996. 'The Schizosaccharomyces pombe rad3 checkpoint gene', *Embo j*, 15: 6641-51.

Berniak, K., P. Rybak, T. Bernas, M. Zarębski, E. Biela, H. Zhao, Z. Darzynkiewicz, and J. W. Dobrucki. 2013. 'Relationship between DNA damage response, initiated by camptothecin or oxidative stress, and DNA replication, analyzed by quantitative 3D image analysis', *Cytometry A*, 83: 913-24.

Bétermier, M., P. Bertrand, and B. S. Lopez. 2014. 'Is non-homologous end-joining really an inherently error-prone process?', *PLoS Genet*, 10: e1004086.

Bethune, G. C., J. B. Mullen, and M. C. Chang. 2015. 'Detecting intratumoral heterogeneity in routine breast-HER2 testing: low yield of testing multiple blocks', *Ann Diagn Pathol*, 19: 385-90.

Bétous, R., A. C. Mason, R. P. Rambo, C. E. Bansbach, A. Badu-Nkansah, B. M. Sirbu, B. F. Eichman, and D. Cortez. 2012. 'SMARCAL1 catalyzes fork regression and Holliday junction migration to maintain genome stability during DNA replication', *Genes Dev*, 26: 151-62.

Beucher, A., J. Birraux, L. Tchouandong, O. Barton, A. Shibata, S. Conrad, A. A. Goodarzi, A. Krempler, P. A. Jeggo, and M. Löbrich. 2009. 'ATM and Artemis promote homologous recombination of radiation-induced DNA double-strand breaks in G2', *Embo j*, 28: 3413-27.

BLA., KADCYLA®. 2013. '"CENTER FOR DRUG EVALUATION AND RESEARCH APPLICATION NUMBER: 125427Orig1s000 MEDICAL REVIEW(S)":

'. https://www.accessdata.fda.gov/drugsatfda_docs/nda/2013/125427Orig1s000MedR.pdf.

Blackford, A. N., and S. P. Jackson. 2017. 'ATM, ATR, and DNA-PK: The Trinity at the Heart of the DNA Damage Response', *Mol Cell*, 66: 801-17.

Bokemeyer, C., I. Bondarenko, A. Makhson, J. T. Hartmann, J. Aparicio, F. de Braud, S. Donea, H. Ludwig, G. Schuch, C. Stroh, A. H. Loos, A. Zubel, and P. Koralewski. 2009. 'Fluorouracil, leucovorin, and oxaliplatin with and without cetuximab in the first-line treatment of metastatic colorectal cancer', *J Clin Oncol*, 27: 663-71.

Bolt, Jennifer, Quynh N. Vo, Wan-Ju Kim, Andrew J. McWhorter, Jessica Thomson, Michael E. Hagensee, Paul Friedlander, Kevin D. Brown, and Jill Gilbert. 2005. 'The ATM/p53 pathway is commonly targeted for inactivation in squamous cell carcinoma of the head and neck (SCCHN) by multiple molecular mechanisms', *Oral Oncology*, 41: 1013-20.

Boos, D., L. Sanchez-Pulido, M. Rappas, L. H. Pearl, A. W. Oliver, C. P. Ponting, and J. F. Diffley. 2011. 'Regulation of DNA replication through Sld3-Dpb11 interaction is conserved from yeast to humans', *Curr Biol*, 21: 1152-7.

Bosotti, R., A. Isacchi, and E. L. Sonnhammer. 2000. 'FAT: a novel domain in PIK-related kinases', *Trends Biochem Sci*, 25: 225-7.

Bowen, C., A. Stuart, J. H. Ju, J. Tuan, J. Blonder, T. P. Conrads, T. D. Veenstra, and E. P. Gelmann. 2007. 'NKX3.1 homeodomain protein binds to topoisomerase I and enhances its activity', *Cancer Res*, 67: 455-64.

Bradbury, A., S. Hall, N. Curtin, and Y. Drew. 2020. 'Targeting ATR as Cancer Therapy: A new era for synthetic lethality and synergistic combinations?', *Pharmacol Ther*, 207: 107450.

Brangi, M., T. Litman, M. Ciotti, K. Nishiyama, G. Kohlhagen, C. Takimoto, R. Robey, Y. Pommier, T. Fojo, and S. E. Bates. 1999. 'Camptothecin resistance: role of the ATP-binding cassette (ABC), mitoxantrone-resistance half-transporter (MXR), and potential for glucuronidation in MXR-expressing cells', *Cancer Res*, 59: 5938-46.

Braun, M. S., S. D. Richman, P. Quirke, C. Daly, J. W. Adlard, F. Elliott, J. H. Barrett, P. Selby, A. M. Meade, R. J. Stephens, M. K. Parmar, and M. T. Seymour. 2008. 'Predictive biomarkers of chemotherapy efficacy in colorectal cancer: results from the UK MRC FOCUS trial', *J Clin Oncol*, 26: 2690-8.

Bray, N. L., H. Pimentel, P. Melsted, and L. Pachter. 2016. 'Near-optimal probabilistic RNA-seq quantification', *Nat Biotechnol*, 34: 525-7.

Brown, E. J., and D. Baltimore. 2000. 'ATR disruption leads to chromosomal fragmentation and early embryonic lethality', *Genes Dev*, 14: 397-402.

Brown, K. F., H. Rumgay, C. Dunlop, M. Ryan, F. Quartly, A. Cox, A. Deas, L. Elliss-Brookes, A. Gavin, L. Hounsome, D. Huws, N. Ormiston-Smith, J. Shelton, C. White, and D. M. Parkin. 2018. 'The fraction of cancer attributable to modifiable risk factors in England, Wales, Scotland, Northern Ireland, and the United Kingdom in 2015', *Br J Cancer*, 118: 1130-41.

Brown, L. J., T. Meredith, J. Yu, A. Patel, B. Neal, C. Arnott, and E. Lim. 2021. 'Heart Failure Therapies for the Prevention of HER2-Monoclonal Antibody-Mediated Cardiotoxicity: A Systematic Review and Meta-Analysis of Randomized Trials', *Cancers (Basel)*, 13.

Buisson, R., J. L. Boisvert, C. H. Benes, and L. Zou. 2015. 'Distinct but Concerted Roles of ATR, DNA-PK, and Chk1 in Countering Replication Stress during S Phase', *Mol Cell*, 59: 1011-24.

Buisson, R., M. S. Lawrence, C. H. Benes, and L. Zou. 2017. 'APOBEC3A and APOBEC3B Activities Render Cancer Cells Susceptible to ATR Inhibition', *Cancer Res*, 77: 4567-78.

Buisson, R., J. Niraj, A. Rodrigue, C. K. Ho, J. Kreuzer, T. K. Foo, E. J. Hardy, G. Dellaire, W. Haas, B. Xia, J. Y. Masson, and L. Zou. 2017. 'Coupling of Homologous Recombination and the Checkpoint by ATR', *Mol Cell*, 65: 336-46.

Burdette, D. L., and R. E. Vance. 2013. 'STING and the innate immune response to nucleic acids in the cytosol', *Nat Immunol*, 14: 19-26.

Burma, S., B. P. Chen, M. Murphy, A. Kurimasa, and D. J. Chen. 2001. 'ATM phosphorylates histone H2AX in response to DNA double-strand breaks', *J Biol Chem*, 276: 42462-7.

Burn, J., J. Mathers, and D. T. Bishop. 2013. 'Genetics, inheritance and strategies for prevention in populations at high risk of colorectal cancer (CRC)', *Recent Results Cancer Res*, 191: 157-83.

Cai, Z., N. H. Chehab, and N. P. Pavletich. 2009. 'Structure and activation mechanism of the CHK2 DNA damage checkpoint kinase', *Mol Cell*, 35: 818-29.

Caldecott, K. W. 2008. 'Single-strand break repair and genetic disease', *Nat Rev Genet*, 9: 619-31.

Candeil, L., I. Gourdier, D. Peyron, N. Vezzio, V. Copois, F. Bibeau, B. Orsetti, G. L. Scheffer, M. Ychou, Q. A. Khan, Y. Pommier, B. Pau, P. Martineau, and M. Del Rio. 2004. 'ABCG2 overexpression in colon cancer cells resistant to SN38 and in irinotecan-treated metastases', *Int J Cancer*, 109: 848-54.

Canman, C. E., D. S. Lim, K. A. Cimprich, Y. Taya, K. Tamai, K. Sakaguchi, E. Appella, M. B. Kastan, and J. D. Siliciano. 1998. 'Activation of the ATM kinase by ionizing radiation and phosphorylation of p53', *Science*, 281: 1677-9.

Cardoso, F., E. Senkus, A. Costa, E. Papadopoulos, M. Aapro, F. André, N. Harbeck, B. Aguilar Lopez, C. H. Barrios, J. Bergh, L. Biganzoli, C. B. Boers-Doets, M. J. Cardoso, L. A. Carey, J. Cortés, G. Curigliano, V. Diéras, N. S. El Saghir, A. Eniu, L. Fallowfield, P. A. Francis, K. Gelmon, S. R. D. Johnston, B. Kaufman, S. Koppikar, I. E. Krop, M. Mayer, G. Nakigudde, B. V. Offersen, S. Ohno, O. Pagani, S. Paluch-Shimon, F. Penault-Llorca, A. Prat, H. S. Rugo, G. W. Sledge, D. Spence, C. Thomssen, D. A. Vorobiof, B. Xu, L. Norton, and E. P. Winer. 2018. '4th ESO-ESMO International Consensus Guidelines for Advanced Breast Cancer (ABC 4)†', *Ann Oncol*, 29: 1634-57.

Carlini, L. E., N. J. Meropol, J. Bever, M. L. Andria, T. Hill, P. Gold, A. Rogatko, H. Wang, and R. L. Blanchard. 2005. 'UGT1A7 and UGT1A9 polymorphisms predict response and toxicity in colorectal cancer patients treated with capecitabine/irinotecan', *Clin Cancer Res*, 11: 1226-36.

Castaigne, S., C. Pautas, C. Terré, E. Raffoux, D. Bordessoule, J. N. Bastie, O. Legrand, X. Thomas, P. Turlure, O. Reman, T. de Revel, L. Gastaud, N. de Gunzburg, N. Contentin, E. Henry, J. P. Marolleau, A. Aljijakli, P. Rousselot, P. Fenaux, C. Preudhomme, S. Chevret, and H. Dombret. 2012. 'Effect of gemtuzumab ozogamicin on survival of adult patients with de-novo acute myeloid leukaemia (ALFA-0701): a randomised, open-label, phase 3 study', *Lancet*, 379: 1508-16.

Ceccaldi, R., J. C. Liu, R. Amunugama, I. Hajdu, B. Primack, M. I. Petalcorin, K. W. O'Connor, P. A. Konstantinopoulos, S. J. Elledge, S. J. Boulton, T. Yusufzai, and A. D. D'Andrea. 2015. 'Homologous-recombination-deficient tumours are dependent on Polθ-mediated repair', *Nature*, 518: 258-62.

Ceccaldi, R., P. Sarangi, and A. D. D'Andrea. 2016. 'The Fanconi anaemia pathway: new players and new functions', *Nat Rev Mol Cell Biol*, 17: 337-49.

Chabot, G. G. 1997. 'Clinical pharmacokinetics of irinotecan', *Clin Pharmacokinet*, 33: 245-59.

Chan, D. W., B. P. Chen, S. Prithivirajsingh, A. Kurimasa, M. D. Story, J. Qin, and D. J. Chen. 2002. 'Autophosphorylation of the DNA-dependent protein kinase catalytic subunit is required for rejoining of DNA double-strand breaks', *Genes Dev*, 16: 2333-8.

Chaney, S. G., S. L. Campbell, E. Bassett, and Y. Wu. 2005. 'Recognition and processing of cisplatin- and oxaliplatin-DNA adducts', *Crit Rev Oncol Hematol*, 53: 3-11.

Chapman, J. R., and S. P. Jackson. 2008. 'Phospho-dependent interactions between NBS1 and MDC1 mediate chromatin retention of the MRN complex at sites of DNA damage', *EMBO Rep*, 9: 795-801.

Chari, R. V. 1998. 'Targeted delivery of chemotherapeutics: tumor-activated prodrug therapy', *Adv Drug Deliv Rev*, 31: 89-104.

Charrier, J. D., S. J. Durrant, J. M. Golec, D. P. Kay, R. M. Knegtel, S. MacCormick, M. Mortimore, M. E. O'Donnell, J. L. Pinder, P. M. Reaper, A. P. Rutherford, P. S. Wang, S. C. Young, and J. R. Pollard. 2011. 'Discovery of potent and selective inhibitors of ataxia telangiectasia mutated and Rad3 related (ATR) protein kinase as potential anticancer agents', *J Med Chem*, 54: 2320-30.

Chen, B. P., D. W. Chan, J. Kobayashi, S. Burma, A. Asaithamby, K. Morotomi-Yano, E. Botvinick, J. Qin, and D. J. Chen. 2005. 'Cell cycle dependence of DNA-dependent protein kinase phosphorylation in response to DNA double strand breaks', *J Biol Chem*, 280: 14709-15.

Chen, C. F., R. Ruiz-Vega, P. Vasudeva, F. Espitia, T. B. Krasieva, S. de Feraudy, B. J. Tromberg, S. Huang, C. P. Garner, J. Wu, D. S. Hoon, and A. K. Ganesan. 2017. 'ATR Mutations Promote the Growth of Melanoma Tumors by Modulating the Immune Microenvironment', *Cell Rep*, 18: 2331-42.

Chen, E. M., A. R. Quijano, Y. E. Seo, C. Jackson, A. D. Josowitz, S. Noorbakhsh, A. Merlettini, R. K. Sundaram, M. L. Focarete, Z. Jiang, R. S. Bindra, and W. M. Saltzman. 2018. 'Biodegradable PEG-poly(ω-pentadecalactone-co-p-dioxanone) nanoparticles for enhanced and sustained drug delivery to treat brain tumors', *Biomaterials*, 178: 193-203.

Chen, J., S. M. Harding, R. Natesan, L. Tian, J. L. Benci, W. Li, A. J. Minn, I. A. Asangani, and R. A. Greenberg. 2020. 'Cell Cycle Checkpoints Cooperate to Suppress DNA- and RNA-Associated Molecular Pattern Recognition and Anti-Tumor Immune Responses', *Cell Rep*, 32: 108080.

Chen, X., R. Zhao, G. G. Glick, and D. Cortez. 2007. 'Function of the ATR N-terminal domain revealed by an ATM/ATR chimera', *Exp Cell Res*, 313: 1667-74.

Chen, Y. H., M. J. Jones, Y. Yin, S. B. Crist, L. Colnaghi, R. J. Sims, 3rd, E. Rothenberg, P. V. Jallepalli, and T. T. Huang. 2015. 'ATR-mediated phosphorylation of FANCI regulates dormant origin firing in response to replication stress', *Mol Cell*, 58: 323-38.

Cheng, Q., and J. Chen. 2010. 'Mechanism of p53 stabilization by ATM after DNA damage', *Cell Cycle*, 9: 472-8.

Chini, C. C., and J. Chen. 2006. 'Repeated phosphopeptide motifs in human Claspin are phosphorylated by Chk1 and mediate Claspin function', *J Biol Chem*, 281: 33276-82.

Chou, D. M., B. Adamson, N. E. Dephoure, X. Tan, A. C. Nottke, K. E. Hurov, S. P. Gygi, M. P. Colaiácovo, and S. J. Elledge. 2010. 'A chromatin localization screen reveals poly (ADP ribose)-regulated recruitment of the repressive polycomb and NuRD complexes to sites of DNA damage', *Proc Natl Acad Sci U S A*, 107: 18475-80.

Ciardiello, Fortunato, Heinz-Josef Lenz, Claus-Henning Kohne, Volker Heinemann, Sabine Tejpar, Regina Esser, Frank Beier, Christopher Stroh, Klaus Duecker, and Eric Van Cutsem. 2014. 'Effect of KRAS and NRAS mutational status on first-line treatment with FOLFIRI plus cetuximab in patients with metastatic colorectal cancer (mCRC): New results from the CRYSTAL trial', *Journal of Clinical Oncology*, 32: LBA443-LBA43.

Ciccia, A., and S. J. Elledge. 2010. 'The DNA damage response: making it safe to play with knives', *Mol Cell*, 40: 179-204.

Cimprich, K. A., T. B. Shin, C. T. Keith, and S. L. Schreiber. 1996. 'cDNA cloning and gene mapping of a candidate human cell cycle checkpoint protein', *Proc Natl Acad Sci U S A*, 93: 2850-55.

Citri, A., and Y. Yarden. 2006. 'EGF-ERBB signalling: towards the systems level', *Nat Rev Mol Cell Biol*, 7: 505-16.

Civril, F., T. Deimling, C. C. de Oliveira Mann, A. Ablasser, M. Moldt, G. Witte, V. Hornung, and K. P. Hopfner. 2013. 'Structural mechanism of cytosolic DNA sensing by cGAS', *Nature*, 498: 332-7.

Clevers, H. 2016. 'Modeling Development and Disease with Organoids', *Cell*, 165: 1586-97.

Collins, N. B., J. B. Wilson, T. Bush, A. Thomashevski, K. J. Roberts, N. J. Jones, and G. M. Kupfer. 2009. 'ATR-dependent phosphorylation of FANCA on serine 1449 after DNA damage is important for FA pathway function', *Blood*, 113: 2181-90.

Colucci, G., V. Gebbia, G. Paoletti, F. Giuliani, M. Caruso, N. Gebbia, G. Cartenì, B. Agostara, G. Pezzella, L. Manzione, N. Borsellino, A. Misino, S. Romito, E. Durini, S. Cordio, M. Di Seri, M. Lopez, E. Maiello, S. Montemurro, A. Cramarossa, V. Lorusso, M. Di Bisceglie, M. Chiarenza, M. R. Valerio, T. Guida, V. Leonardi, S. Pisconti, G. Rosati, F. Carrozza, G. Nettis, M. Valdesi, G. Filippelli, S. Fortunato, S. Mancarella, and C. Brunetti. 2005. 'Phase III randomized trial of FOLFIRI versus FOLFOX4 in the treatment of advanced colorectal cancer: a multicenter study of the Gruppo Oncologico Dell'Italia Meridionale', *J Clin Oncol*, 23: 4866-75.

Combès, E., A. F. Andrade, D. Tosi, H. A. Michaud, F. Coquel, V. Garambois, D. Desigaud, M. Jarlier, A. Coquelle, P. Pasero, N. Bonnefoy, J. Moreaux, P. Martineau, M. Del Rio, R. L. Beijersbergen, N. Vezzio-Vie, and C. Gongora. 2019. 'Inhibition of Ataxia-Telangiectasia Mutated and RAD3-Related (ATR) Overcomes Oxaliplatin Resistance and Promotes Antitumor Immunity in Colorectal Cancer', *Cancer Res*, 79: 2933-46.

Cormerais, Y., S. Giuliano, R. LeFloch, B. Front, J. Durivault, E. Tambutté, P. A. Massard, L. R. de la Ballina, H. Endou, M. F. Wempe, M. Palacin, S. K. Parks, and J. Pouyssegur. 2016. 'Genetic Disruption of the Multifunctional CD98/LAT1 Complex Demonstrates the Key Role of Essential Amino Acid Transport in the Control of mTORC1 and Tumor Growth', *Cancer Res*, 76: 4481-92.

Correale, P., M. Marra, C. Remondo, C. Migali, G. Misso, F. P. Arcuri, M. T. Del Vecchio, A. Carducci, L. Loiacono, P. Tassone, A. Abbruzzese, P. Tagliaferri, and M. Caraglia. 2010. 'Cytotoxic drugs up-regulate epidermal growth factor receptor (EGFR) expression in colon cancer cells and enhance their susceptibility to EGFR-targeted antibody-dependent cell-mediated-cytotoxicity (ADCC)', *Eur J Cancer*, 46: 1703-11.

Cortez, D. 2015. 'Preventing replication fork collapse to maintain genome integrity', *DNA Repair (Amst)*, 32: 149-57.

Cortez, D., G. Glick, and S. J. Elledge. 2004. 'Minichromosome maintenance proteins are direct targets of the ATM and ATR checkpoint kinases', *Proc Natl Acad Sci U S A*, 101: 10078-83.

Cortez, D., S. Guntuku, J. Qin, and S. J. Elledge. 2001. 'ATR and ATRIP: partners in checkpoint signaling', *Science*, 294: 1713-6.

Cortez, D., Y. Wang, J. Qin, and S. J. Elledge. 1999. 'Requirement of ATM-dependent phosphorylation of brca1 in the DNA damage response to double-strand breaks', *Science*, 286: 1162-6.

Cotta-Ramusino, C., E. R. McDonald, 3rd, K. Hurov, M. E. Sowa, J. W. Harper, and S. J. Elledge. 2011. 'A DNA damage response screen identifies RHINO, a 9-1-1 and TopBP1 interacting protein required for ATR signaling', *Science*, 332: 1313-7.

Couch, F. B., C. E. Bansbach, R. Driscoll, J. W. Luzwick, G. G. Glick, R. Bétous, C. M. Carroll, S. Y. Jung, J. Qin, K. A. Cimprich, and D. Cortez. 2013. 'ATR phosphorylates SMARCAL1 to prevent replication fork collapse', *Genes Dev*, 27: 1610-23.

Coussy, Florence, Rania El-Botty, Sophie Château-Joubert, Ahmed Dahmani, Elodie Montaudon, Sophie Leboucher, Ludivine Morisset, Pierre Painsec, Laura Sourd, Léa Huguet, Fariba Nemati, Jean-Luc Servely, Thibaut Larcher, Sophie Vacher, Adrien Briaux, Cécile Reyes, Philippe La Rosa, Georges Lucotte, Tatiana Popova, Pierre

Foidart, Nor Eddine Sounni, Agnès Noel, Didier Decaudin, Laetitia Fuhrmann, Anne Salomon, Fabien Reyal, Christopher Mueller, Petra Ter Brugge, Jos Jonkers, Marie-France Poupon, Marc-Henri Stern, Ivan Bièche, Yves Pommier, and Elisabetta Marangoni. 2020. 'BRCAness, SLFN11, and RB1 loss predict response to topoisomerase I inhibitors in triple-negative breast cancers', *Science Translational Medicine*, 12: eaax2625.

Cremona, C. A., and A. Behrens. 2014. 'ATM signalling and cancer', *Oncogene*, 33: 3351-60.

CRUK. 2020. 'Bowel Cancer Risk', Accessed 03/06/2020. https://www.cancerresearchuk.org/health-professional/cancer-statistics/statistics-by-cancer-type/bowel-cancer/risk-factors#heading-Zero.

CRUK. 2021. 'Bowel cancer survival statistics', Accessed 26/07/21. https://www.cancerresearchuk.org/health-professional/cancer-statistics/statistics-by-cancer-type/bowel-cancer/survival#heading-Three.

Cummings, J., G. Boyd, B. T. Ethell, J. S. Macpherson, B. Burchell, J. F. Smyth, and D. I. Jodrell. 2002. 'Enhanced clearance of topoisomerase I inhibitors from human colon cancer cells by glucuronidation', *Biochem Pharmacol*, 63: 607-13.

Cunningham, D., I. Lang, E. Marcuello, V. Lorusso, J. Ocvirk, D. B. Shin, D. Jonker, S. Osborne, N. Andre, D. Waterkamp, and M. P. Saunders. 2013. 'Bevacizumab plus capecitabine versus capecitabine alone in elderly patients with previously untreated metastatic colorectal cancer (AVEX): an open-label, randomised phase 3 trial', *Lancet Oncol*, 14: 1077-85.

D'Angiolella, V., V. Donato, F. M. Forrester, Y. T. Jeong, C. Pellacani, Y. Kudo, A. Saraf, L. Florens, M. P. Washburn, and M. Pagano. 2012. 'Cyclin F-mediated degradation of ribonucleotide reductase M2 controls genome integrity and DNA repair', *Cell*, 149: 1023-34.

Dai, Y., and S. Grant. 2010. 'New insights into checkpoint kinase 1 in the DNA damage response signaling network', *Clin Cancer Res*, 16: 376-83.

Dang, C. V., A. Le, and P. Gao. 2009. 'MYC-induced cancer cell energy metabolism and therapeutic opportunities', *Clin Cancer Res*, 15: 6479-83.

Daniel, J. A., M. Pellegrini, J. H. Lee, T. T. Paull, L. Feigenbaum, and A. Nussenzweig. 2008. 'Multiple autophosphorylation sites are dispensable for murine ATM activation in vivo', *J Cell Biol*, 183: 777-83.

Das, B. B., S. Antony, S. Gupta, T. S. Dexheimer, C. E. Redon, S. Garfield, Y. Shiloh, and Y. Pommier. 2009. 'Optimal function of the DNA repair enzyme TDP1 requires its phosphorylation by ATM and/or DNA-PK', *Embo j*, 28: 3667-80.

Das, B. B., S. Y. Huang, J. Murai, I. Rehman, J. C. Amé, S. Sengupta, S. K. Das, P. Majumdar, H. Zhang, D. Biard, H. K. Majumder, V. Schreiber, and Y. Pommier. 2014. 'PARP1-TDP1 coupling for the repair of topoisomerase I-induced DNA damage', *Nucleic Acids Res*, 42: 4435-49.

Davies, S. L., P. S. North, A. Dart, N. D. Lakin, and I. D. Hickson. 2004. 'Phosphorylation of the Bloom's syndrome helicase and its role in recovery from S-phase arrest', *Mol Cell Biol*, 24: 1279-91.

Davies, S. L., P. S. North, and I. D. Hickson. 2007. 'Role for BLM in replication-fork restart and suppression of origin firing after replicative stress', *Nat Struct Mol Biol*, 14: 677-9.

de Goeij, B. E., D. Satijn, C. M. Freitag, R. Wubbolts, W. K. Bleeker, A. Khasanov, T. Zhu, G. Chen, D. Miao, P. H. van Berkel, and P. W. Parren. 2015. 'High turnover of tissue factor enables efficient intracellular delivery of antibody-drug conjugates', *Mol Cancer Ther*, 14: 1130-40.

de Gramont, A., A. Figer, M. Seymour, M. Homerin, A. Hmissi, J. Cassidy, C. Boni, H. Cortes-Funes, A. Cervantes, G. Freyer, D. Papamichael, N. Le Bail, C. Louvet, D. Hendler, F. de Braud, C. Wilson, F. Morvan, and A. Bonetti. 2000. 'Leucovorin and fluorouracil

with or without oxaliplatin as first-line treatment in advanced colorectal cancer', *J Clin Oncol*, 18: 2938-47.

de Klein, A., M. Muijtjens, R. van Os, Y. Verhoeven, B. Smit, A. M. Carr, A. R. Lehmann, and J. H. Hoeijmakers. 2000. 'Targeted disruption of the cell-cycle checkpoint gene ATR leads to early embryonic lethality in mice', *Curr Biol*, 10: 479-82.

De Piccoli, G., Y. Katou, T. Itoh, R. Nakato, K. Shirahige, and K. Labib. 2012. 'Replisome stability at defective DNA replication forks is independent of S phase checkpoint kinases', *Mol Cell*, 45: 696-704.

Delacroix, S., J. M. Wagner, M. Kobayashi, K. Yamamoto, and L. M. Karnitz. 2007. 'The Rad9-Hus1-Rad1 (9-1-1) clamp activates checkpoint signaling via TopBP1', *Genes Dev*, 21: 1472-7.

Demaria, O., S. Cornen, M. Daëron, Y. Morel, R. Medzhitov, and E. Vivier. 2019. 'Harnessing innate immunity in cancer therapy', *Nature*, 574: 45-56.

Derenzini, E., C. Agostinelli, E. Imbrogno, I. Iacobucci, B. Casadei, E. Brighenti, S. Righi, F. Fuligni, A. Ghelli Luserna Di Rorà, A. Ferrari, G. Martinelli, S. Pileri, and P. L. Zinzani. 2015. 'Constitutive activation of the DNA damage response pathway as a novel therapeutic target in diffuse large B-cell lymphoma', *Oncotarget*, 6: 6553-69.

Desai, S. D., L. F. Liu, D. Vazquez-Abad, and P. D'Arpa. 1997. 'Ubiquitin-dependent destruction of topoisomerase I is stimulated by the antitumor drug camptothecin', *J Biol Chem*, 272: 24159-64.

Desai, S. D., H. Zhang, A. Rodriguez-Bauman, J. M. Yang, X. Wu, M. K. Gounder, E. H. Rubin, and L. F. Liu. 2003. 'Transcription-dependent degradation of topoisomerase I-DNA covalent complexes', *Mol Cell Biol*, 23: 2341-50.

DeVita, V. T., Jr., and E. Chu. 2008. 'A history of cancer chemotherapy', *Cancer Res*, 68: 8643-53.

Dexheimer, T. S., S. Antony, C. Marchand, and Y. Pommier. 2008. 'Tyrosyl-DNA phosphodiesterase as a target for anticancer therapy', *Anticancer Agents Med Chem*, 8: 381-9.

Di Paolo, A., G. Bocci, M. Polillo, M. Del Re, T. Di Desidero, M. Lastella, and R. Danesi. 2011. 'Pharmacokinetic and pharmacogenetic predictive markers of irinotecan activity and toxicity', *Curr Drug Metab*, 12: 932-43.

Dillon, M. T., H. E. Barker, M. Pedersen, H. Hafsi, S. A. Bhide, K. L. Newbold, C. M. Nutting, M. McLaughlin, and K. J. Harrington. 2017. 'Radiosensitization by the ATR Inhibitor AZD6738 through Generation of Acentric Micronuclei', *Mol Cancer Ther*, 16: 25-34.

Dimitrova, D. S., and D. M. Gilbert. 2000. 'Temporally coordinated assembly and disassembly of replication factories in the absence of DNA synthesis', *Nat Cell Biol*, 2: 686-94.

Ding, D., Y. Zhang, J. Wang, X. Zhang, Y. Gao, L. Yin, Q. Li, J. Li, and H. Chen. 2016. 'Induction and inhibition of the pan-nuclear gamma-H2AX response in resting human peripheral blood lymphocytes after X-ray irradiation', *Cell Death Discov*, 2: 16011.

Ding, L., G. Getz, D. A. Wheeler, E. R. Mardis, M. D. McLellan, K. Cibulskis, C. Sougnez, H. Greulich, D. M. Muzny, M. B. Morgan, L. Fulton, R. S. Fulton, Q. Zhang, M. C. Wendl, M. S. Lawrence, D. E. Larson, K. Chen, D. J. Dooling, A. Sabo, A. C. Hawes, H. Shen, S. N. Jhangiani, L. R. Lewis, O. Hall, Y. Zhu, T. Mathew, Y. Ren, J. Yao, S. E. Scherer, K. Clerc, G. A. Metcalf, B. Ng, A. Milosavljevic, M. L. Gonzalez-Garay, J. R. Osborne, R. Meyer, X. Shi, Y. Tang, D. C. Koboldt, L. Lin, R. Abbott, T. L. Miner, C. Pohl, G. Fewell, C. Haipek, H. Schmidt, B. H. Dunford-Shore, A. Kraja, S. D. Crosby, C. S. Sawyer, T. Vickery, S. Sander, J. Robinson, W. Winckler, J. Baldwin, L. R. Chirieac, A. Dutt, T. Fennell, M. Hanna, B. E. Johnson, R. C. Onofrio, R. K. Thomas, G. Tonon, B. A. Weir, X. Zhao, L. Ziaugra, M. C. Zody, T. Giordano, M. B. Orringer, J. A. Roth, M. R. Spitz, Wistuba, II, B. Ozenberger, P. J. Good, A. C. Chang, D. G. Beer, M. A. Watson, M. Ladanyi, S. Broderick, A. Yoshizawa, W. D. Travis, W. Pao, M. A. Province, G. M. Weinstock, H. E. Varmus, S. B. Gabriel, E. S. Lander, R. A. Gibbs, M. Meyerson, and R.

K. Wilson. 2008. 'Somatic mutations affect key pathways in lung adenocarcinoma', *Nature*, 455: 1069-75.

Douillard, J. Y., D. Cunningham, A. D. Roth, M. Navarro, R. D. James, P. Karasek, P. Jandik, T. Iveson, J. Carmichael, M. Alakl, G. Gruia, L. Awad, and P. Rougier. 2000. 'Irinotecan combined with fluorouracil compared with fluorouracil alone as first-line treatment for metastatic colorectal cancer: a multicentre randomised trial', *The Lancet*, 355: 1041-47.

Douillard, J. Y., K. S. Oliner, S. Siena, J. Tabernero, R. Burkes, M. Barugel, Y. Humblet, G. Bodoky, D. Cunningham, J. Jassem, F. Rivera, I. Kocákova, P. Ruff, M. Błasińska-Morawiec, M. Šmakal, J. L. Canon, M. Rother, R. Williams, A. Rong, J. Wiezorek, R. Sidhu, and S. D. Patterson. 2013. 'Panitumumab-FOLFOX4 treatment and RAS mutations in colorectal cancer', *N Engl J Med*, 369: 1023-34.

Douillard, J. Y., S. Siena, J. Cassidy, J. Tabernero, R. Burkes, M. Barugel, Y. Humblet, G. Bodoky, D. Cunningham, J. Jassem, F. Rivera, I. Kocákova, P. Ruff, M. Błasińska-Morawiec, M. Šmakal, J. L. Canon, M. Rother, K. S. Oliner, M. Wolf, and J. Gansert. 2010. 'Randomized, phase III trial of panitumumab with infusional fluorouracil, leucovorin, and oxaliplatin (FOLFOX4) versus FOLFOX4 alone as first-line treatment in patients with previously untreated metastatic colorectal cancer: the PRIME study', *J Clin Oncol*, 28: 4697-705.

Drago, J. Z., S. Modi, and S. Chandarlapaty. 2021. 'Unlocking the potential of antibody-drug conjugates for cancer therapy', *Nat Rev Clin Oncol*, 18: 327-44.

Drake, P. M., and D. Rabuka. 2015. 'An emerging playbook for antibody-drug conjugates: lessons from the laboratory and clinic suggest a strategy for improving efficacy and safety', *Curr Opin Chem Biol*, 28: 174-80.

Dungrawala, H., K. L. Rose, K. P. Bhat, K. N. Mohni, G. G. Glick, F. B. Couch, and D. Cortez. 2015. 'The Replication Checkpoint Prevents Two Types of Fork Collapse without Regulating Replisome Stability', *Mol Cell*, 59: 998-1010.

Dunlop, C. R., Y. Wallez, T. I. Johnson, S. Bernaldo de Quirós Fernández, S. T. Durant, E. B. Cadogan, A. Lau, F. M. Richards, and D. I. Jodrell. 2020. 'Complete loss of ATM function augments replication catastrophe induced by ATR inhibition and gemcitabine in pancreatic cancer models', *Br J Cancer*, 123: 1424-36.

Duursma, A. M., R. Driscoll, J. E. Elias, and K. A. Cimprich. 2013. 'A role for the MRN complex in ATR activation via TOPBP1 recruitment', *Mol Cell*, 50: 116-22.

Ellison, V., and B. Stillman. 2003. 'Biochemical characterization of DNA damage checkpoint complexes: clamp loader and clamp complexes with specificity for 5' recessed DNA', *PLoS Biol*, 1: E33.

Endo, N., Y. Takeda, K. Kishida, Y. Kato, M. Saito, N. Umemoto, and T. Hara. 1987. 'Target-selective cytotoxicity of methotrexate conjugated with monoclonal anti-MM46 antibody', *Cancer Immunol Immunother*, 25: 1-6.

Eng, W. K., L. Faucette, R. K. Johnson, and R. Sternglanz. 1988. 'Evidence that DNA topoisomerase I is necessary for the cytotoxic effects of camptothecin', *Mol Pharmacol*, 34: 755-60.

Erickson, H. K., P. U. Park, W. C. Widdison, Y. V. Kovtun, L. M. Garrett, K. Hoffman, R. J. Lutz, V. S. Goldmacher, and W. A. Blättler. 2006. 'Antibody-maytansinoid conjugates are activated in targeted cancer cells by lysosomal degradation and linker-dependent intracellular processing', *Cancer Res*, 66: 4426-33.

Esashi, F., N. Christ, J. Gannon, Y. Liu, T. Hunt, M. Jasin, and S. C. West. 2005. 'CDK-dependent phosphorylation of BRCA2 as a regulatory mechanism for recombinational repair', *Nature*, 434: 598-604.

Fairbairn, D. W., P. L. Olive, and K. L. O'Neill. 1995. 'The comet assay: a comprehensive review', *Mutat Res*, 339: 37-59.

Falahat, R., A. Berglund, R. M. Putney, P. Perez-Villarroel, S. Aoyama, S. Pilon-Thomas, G. N. Barber, and J. J. Mulé. 2021. 'Epigenetic reprogramming of tumor cell-intrinsic STING function sculpts antigenicity and T cell recognition of melanoma', *Proc Natl Acad Sci U S A*, 118.

Falck, J., J. Coates, and S. P. Jackson. 2005. 'Conserved modes of recruitment of ATM, ATR and DNA-PKcs to sites of DNA damage', *Nature*, 434: 605-11.

Falck, J., N. Mailand, R. G. Syljuåsen, J. Bartek, and J. Lukas. 2001. 'The ATM-Chk2-Cdc25A checkpoint pathway guards against radioresistant DNA synthesis', *Nature*, 410: 842-7.

Falcone, A., S. Ricci, I. Brunetti, E. Pfanner, G. Allegrini, C. Barbara, L. Crinò, G. Benedetti, W. Evangelista, L. Fanchini, E. Cortesi, V. Picone, S. Vitello, S. Chiara, C. Granetto, G. Porcile, L. Fioretto, C. Orlandini, M. Andreuccetti, and G. Masi. 2007. 'Phase III trial of infusional fluorouracil, leucovorin, oxaliplatin, and irinotecan (FOLFOXIRI) compared with infusional fluorouracil, leucovorin, and irinotecan (FOLFIRI) as first-line treatment for metastatic colorectal cancer: the Gruppo Oncologico Nord Ovest', *J Clin Oncol*, 25: 1670-6.

Fan, S., D. Meng, T. Xu, Y. Chen, J. Wang, X. Li, H. Chen, D. Lu, J. Chen, and Q. Lan. 2013. 'Overexpression of SLC7A7 predicts poor progression-free and overall survival in patients with glioblastoma', *Med Oncol*, 30: 384.

Fearon, E. R. 2011. 'Molecular genetics of colorectal cancer', *Annu Rev Pathol*, 6: 479-507.

Fehling-Kaschek, M., D. B. Peckys, D. Kaschek, J. Timmer, and N. Jonge. 2019. 'Mathematical modeling of drug-induced receptor internalization in the HER2-positive SKBR3 breast cancer cell-line', *Sci Rep*, 9: 12709.

Fehrenbacher, L., R. S. Cecchini, C. E. Geyer, Jr., P. Rastogi, J. P. Costantino, J. N. Atkins, J. P. Crown, J. Polikoff, J. F. Boileau, L. Provencher, C. Stokoe, T. D. Moore, A. Robidoux, P. J. Flynn, V. F. Borges, K. S. Albain, S. M. Swain, S. Paik, E. P. Mamounas, and N. Wolmark. 2020. 'NSABP B-47/NRG Oncology Phase III Randomized Trial Comparing Adjuvant Chemotherapy With or Without Trastuzumab in High-Risk Invasive Breast Cancer Negative for HER2 by FISH and With IHC 1+ or 2', *J Clin Oncol*, 38: 444-53.

Fekairi, S., S. Scaglione, C. Chahwan, E. R. Taylor, A. Tissier, S. Coulon, M. Q. Dong, C. Ruse, J. R. Yates, 3rd, P. Russell, R. P. Fuchs, C. H. McGowan, and P. H. L. Gaillard. 2009. 'Human SLX4 is a Holliday junction resolvase subunit that binds multiple DNA repair/recombination endonucleases', *Cell*, 138: 78-89.

Feng, S., Y. Zhao, Y. Xu, S. Ning, W. Huo, M. Hou, G. Gao, J. Ji, R. Guo, and D. Xu. 2016. 'Ewing Tumor-associated Antigen 1 Interacts with Replication Protein A to Promote Restart of Stalled Replication Forks', *J Biol Chem*, 291: 21956-62.

Feng, W., G. Cui, C. W. Tang, X. L. Zhang, C. Dai, Y. Q. Xu, H. Gong, T. Xue, H. H. Guo, and Y. Bao. 2017. 'Role of glucose metabolism related gene GLUT1 in the occurrence and prognosis of colorectal cancer', *Oncotarget*, 8: 56850-57.

Feng, X., A. Tubbs, C. Zhang, M. Tang, S. Sridharan, C. Wang, D. Jiang, D. Su, H. Zhang, Z. Chen, L. Nie, Y. Xiong, M. Huang, A. Nussenzweig, and J. Chen. 2020. 'ATR inhibition potentiates ionizing radiation-induced interferon response via cytosolic nucleic acid-sensing pathways', *Embo j*, 39: e104036.

Ferguson, S. M., and P. De Camilli. 2012. 'Dynamin, a membrane-remodelling GTPase', *Nat Rev Mol Cell Biol*, 13: 75-88.

Fischel, J. L., P. Formento, J. Ciccolini, P. Rostagno, M. C. Etienne, J. Catalin, and G. Milano. 2002. 'Impact of the oxaliplatin-5 fluorouracil-folinic acid combination on respective intracellular determinants of drug activity', *Br J Cancer*, 86: 1162-68.

Fishler, T., Y. Y. Li, R. H. Wang, H. S. Kim, K. Sengupta, A. Vassilopoulos, T. Lahusen, X. Xu, M. H. Lee, Q. Liu, S. J. Elledge, T. Ried, and C. X. Deng. 2010. 'Genetic instability and mammary tumor formation in mice carrying mammary-specific disruption of Chk1 and p53', *Oncogene*, 29: 4007-17.

Fitzgerald, K. A., S. M. McWhirter, K. L. Faia, D. C. Rowe, E. Latz, D. T. Golenbock, A. J. Coyle, S. M. Liao, and T. Maniatis. 2003. 'IKKepsilon and TBK1 are essential components of the IRF3 signaling pathway', *Nat Immunol*, 4: 491-6.

Fokas, E., R. Prevo, J. R. Pollard, P. M. Reaper, P. A. Charlton, B. Cornelissen, K. A. Vallis, E. M. Hammond, M. M. Olcina, W. Gillies McKenna, R. J. Muschel, and T. B. Brunner. 2012. 'Targeting ATR in vivo using the novel inhibitor VE-822 results in selective sensitization of pancreatic tumors to radiation', *Cell Death Dis*, 3: e441.

Foote, K. M., K. Blades, A. Cronin, S. Fillery, S. S. Guichard, L. Hassall, I. Hickson, X. Jacq, P. J. Jewsbury, T. M. McGuire, J. W. Nissink, R. Odedra, K. Page, P. Perkins, A. Suleman, K. Tam, P. Thommes, R. Broadhurst, and C. Wood. 2013. 'Discovery of 4-{4-[(3R)-3-Methylmorpholin-4-yl]-6-[1-(methylsulfonyl)cyclopropyl]pyrimidin-2-yl}-1H-indole (AZ20): a potent and selective inhibitor of ATR protein kinase with monotherapy in vivo antitumor activity', *J Med Chem*, 56: 2125-38.

Foote, K. M., J. W. M. Nissink, T. McGuire, P. Turner, S. Guichard, J. W. T. Yates, A. Lau, K. Blades, D. Heathcote, R. Odedra, G. Wilkinson, Z. Wilson, C. M. Wood, and P. J. Jewsbury. 2018. 'Discovery and Characterization of AZD6738, a Potent Inhibitor of Ataxia Telangiectasia Mutated and Rad3 Related (ATR) Kinase with Application as an Anticancer Agent', *J Med Chem*, 61: 9889-907.

Fordham, S. E., H. J. Blair, C. J. Elstob, R. Plummer, Y. Drew, N. J. Curtin, O. Heidenreich, D. Pal, D. Jamieson, C. Park, J. Pollard, S. Fields, P. Milne, G. H. Jackson, H. J. Marr, T. Menne, G. L. Jones, and J. M. Allan. 2018. 'Inhibition of ATR acutely sensitizes acute myeloid leukemia cells to nucleoside analogs that target ribonucleotide reductase', *Blood Adv*, 2: 1157-69.

Forment, J. V., M. Blasius, I. Guerini, and S. P. Jackson. 2011. 'Structure-specific DNA endonuclease Mus81/Eme1 generates DNA damage caused by Chk1 inactivation', *PLoS One*, 6: e23517.

Fradet-Turcotte, A., M. D. Canny, C. Escribano-Díaz, A. Orthwein, C. C. Leung, H. Huang, M. C. Landry, J. Kitevski-LeBlanc, S. M. Noordermeer, F. Sicheri, and D. Durocher. 2013. '53BP1 is a reader of the DNA-damage-induced H2A Lys 15 ubiquitin mark', *Nature*, 499: 50-4.

Franchitto, A., and P. Pichierri. 2002. 'Bloom's syndrome protein is required for correct relocalization of RAD50/MRE11/NBS1 complex after replication fork arrest', *J Cell Biol*, 157: 19-30.

Fujimori, A., W. G. Harker, G. Kohlhagen, Y. Hoki, and Y. Pommier. 1995. 'Mutation at the catalytic site of topoisomerase I in CEM/C2, a human leukemia cell line resistant to camptothecin', *Cancer Res*, 55: 1339-46.

Galluzzi, L., L. Senovilla, I. Vitale, J. Michels, I. Martins, O. Kepp, M. Castedo, and G. Kroemer. 2012. 'Molecular mechanisms of cisplatin resistance', *Oncogene*, 31: 1869-83.

Gell, D., and S. P. Jackson. 1999. 'Mapping of protein-protein interactions within the DNA-dependent protein kinase complex', *Nucleic Acids Res*, 27: 3494-502.

Gerber, H. P., P. Sapra, F. Loganzo, and C. May. 2016. 'Combining antibody-drug conjugates and immune-mediated cancer therapy: What to expect?', *Biochem Pharmacol*, 102: 1-6.

Geyer, C. E., J. Forster, D. Lindquist, S. Chan, C. G. Romieu, T. Pienkowski, A. Jagiello-Gruszfeld, J. Crown, A. Chan, B. Kaufman, D. Skarlos, M. Campone, N. Davidson, M. Berger, C. Oliva, S. D. Rubin, S. Stein, and D. Cameron. 2006. 'Lapatinib plus capecitabine for HER2-positive advanced breast cancer', *N Engl J Med*, 355: 2733-43.

Ghosh, S., I. Marrocco, and Y. Yarden. 2020. 'Roles for receptor tyrosine kinases in tumor progression and implications for cancer treatment', *Adv Cancer Res*, 147: 1-57.

Giantonio, B. J., P. J. Catalano, N. J. Meropol, P. J. O'Dwyer, E. P. Mitchell, S. R. Alberts, M. A. Schwartz, and A. B. Benson, 3rd. 2007. 'Bevacizumab in combination with oxaliplatin, fluorouracil, and leucovorin (FOLFOX4) for previously treated metastatic colorectal

cancer: results from the Eastern Cooperative Oncology Group Study E3200', *J Clin Oncol*, 25: 1539-44.

Gilad, O., B. Y. Nabet, R. L. Ragland, D. W. Schoppy, K. D. Smith, A. C. Durham, and E. J. Brown. 2010. 'Combining ATR suppression with oncogenic Ras synergistically increases genomic instability, causing synthetic lethality or tumorigenesis in a dosage-dependent manner', *Cancer Res*, 70: 9693-702.

Gilbert, D. C., A. J. Chalmers, and S. F. El-Khamisy. 2012. 'Topoisomerase I inhibition in colorectal cancer: biomarkers and therapeutic targets', *Br J Cancer*, 106: 18-24.

Giovanella, B. C., J. S. Stehlin, M. E. Wall, M. C. Wani, A. W. Nicholas, L. F. Liu, R. Silber, and M. Potmesil. 1989. 'DNA topoisomerase I--targeted chemotherapy of human colon cancer in xenografts', *Science*, 246: 1046-8.

Girardi, E., A. César-Razquin, S. Lindinger, K. Papakostas, J. Konecka, J. Hemmerich, S. Kickinger, F. Kartnig, B. Gürtl, K. Klavins, V. Sedlyarov, A. Ingles-Prieto, G. Fiume, A. Koren, C. H. Lardeau, R. Kumaran Kandasamy, S. Kubicek, G. F. Ecker, and G. Superti-Furga. 2020. 'A widespread role for SLC transmembrane transporters in resistance to cytotoxic drugs', *Nat Chem Biol*, 16: 469-78.

Giuliani, S., C. M. Ciniselli, E. Leonardi, E. Polla, N. Decarli, C. Luchini, C. Cantaloni, F. Gasperetti, D. Cazzolli, G. Berlanda, D. Bernardi, M. Pellegrini, R. Triolo, A. Ferro, P. Verderio, and M. Barbareschi. 2016. 'In a cohort of breast cancer screened patients the proportion of HER2 positive cases is lower than that earlier reported and pathological characteristics differ between HER2 3+ and HER2 2+/Her2 amplified cases', *Virchows Arch*, 469: 45-50.

Goldenberg, D. M., T. M. Cardillo, S. V. Govindan, E. A. Rossi, and R. M. Sharkey. 2015. 'Trop-2 is a novel target for solid cancer therapy with sacituzumab govitecan (IMMU-132), an antibody-drug conjugate (ADC)', *Oncotarget*, 6: 22496-512.

Gongora, C., N. Vezzio-Vie, S. Tuduri, V. Denis, A. Causse, C. Auzanneau, G. Collod-Beroud, A. Coquelle, P. Pasero, P. Pourquier, P. Martineau, and M. Del Rio. 2011. 'New Topoisomerase I mutations are associated with resistance to camptothecin', *Mol Cancer*, 10: 64.

Gorecki, L., M. Andrs, M. Rezacova, and J. Korabecny. 2020. 'Discovery of ATR kinase inhibitor berzosertib (VX-970, M6620): Clinical candidate for cancer therapy', *Pharmacol Ther*, 210: 107518.

Grawunder, U., M. Wilm, X. Wu, P. Kulesza, T. E. Wilson, M. Mann, and M. R. Lieber. 1997. 'Activity of DNA ligase IV stimulated by complex formation with XRCC4 protein in mammalian cells', *Nature*, 388: 492-5.

Grothey, A., D. Sargent, R. M. Goldberg, and H. J. Schmoll. 2004. 'Survival of patients with advanced colorectal cancer improves with the availability of fluorouracil-leucovorin, irinotecan, and oxaliplatin in the course of treatment', *J Clin Oncol*, 22: 1209-14.

Guo, C., A. Kumagai, K. Schlacher, A. Shevchenko, A. Shevchenko, and W. G. Dunphy. 2015. 'Interaction of Chk1 with Treslin negatively regulates the initiation of chromosomal DNA replication', *Mol Cell*, 57: 492-505.

Guo, Y., W. Feng, S. M. Sy, and M. S. Huen. 2015. 'ATM-dependent Phosphorylation of the Fanconi Anemia Protein PALB2 Promotes the DNA Damage Response', *J Biol Chem*, 290: 27545-56.

Guo, Z., A. Kumagai, S. X. Wang, and W. G. Dunphy. 2000. 'Requirement for Atr in phosphorylation of Chk1 and cell cycle regulation in response to DNA replication blocks and UV-damaged DNA in Xenopus egg extracts', *Genes Dev*, 14: 2745-56.

Gurpinar, E., and K. H. Vousden. 2015. 'Hitting cancers' weak spots: vulnerabilities imposed by p53 mutation', *Trends Cell Biol*, 25: 486-95.

Haahr, P., S. Hoffmann, M. A. Tollenaere, T. Ho, L. I. Toledo, M. Mann, S. Bekker-Jensen, M. Räschle, and N. Mailand. 2016. 'Activation of the ATR kinase by the RPA-binding protein ETAA1', *Nat Cell Biol*, 18: 1196-207.

Haince, J. F., D. McDonald, A. Rodrigue, U. Déry, J. Y. Masson, M. J. Hendzel, and G. G. Poirier. 2008. 'PARP1-dependent kinetics of recruitment of MRE11 and NBS1 proteins to multiple DNA damage sites', *J Biol Chem*, 283: 1197-208.

Halazonetis, T. D., V. G. Gorgoulis, and J. Bartek. 2008. 'An oncogene-induced DNA damage model for cancer development', *Science*, 319: 1352-5.

Hall, A. B., D. Newsome, Y. Wang, D. M. Boucher, B. Eustace, Y. Gu, B. Hare, M. A. Johnson, S. Milton, C. E. Murphy, D. Takemoto, C. Tolman, M. Wood, P. Charlton, J. D. Charrier, B. Furey, J. Golec, P. M. Reaper, and J. R. Pollard. 2014. 'Potentiation of tumor responses to DNA damaging therapy by the selective ATR inhibitor VX-970', *Oncotarget*, 5: 5674-85.

Hammond, E. M., N. C. Denko, M. J. Dorie, R. T. Abraham, and A. J. Giaccia. 2002. 'Hypoxia links ATR and p53 through replication arrest', *Mol Cell Biol*, 22: 1834-43.

Hammond, William A., Abhisek Swaika, and Kabir Mody. 2016. 'Pharmacologic resistance in colorectal cancer: a review', *Therapeutic advances in medical oncology*, 8: 57-84.

Han, X., F. Mayca Pozo, J. N. Wisotsky, B. Wang, J. W. Jacobberger, and Y. Zhang. 2015. 'Phosphorylation of Minichromosome Maintenance 3 (MCM3) by Checkpoint Kinase 1 (Chk1) Negatively Regulates DNA Replication and Checkpoint Activation', *J Biol Chem*, 290: 12370-8.

Hanahan, D., and R. A. Weinberg. 2011. 'Hallmarks of cancer: the next generation', *Cell*, 144: 646-74.

Harding, S. M., J. L. Benci, J. Irianto, D. E. Discher, A. J. Minn, and R. A. Greenberg. 2017. 'Mitotic progression following DNA damage enables pattern recognition within micronuclei', *Nature*, 548: 466-70.

Hatch, E. M., A. H. Fischer, T. J. Deerinck, and M. W. Hetzer. 2013. 'Catastrophic nuclear envelope collapse in cancer cell micronuclei', *Cell*, 154: 47-60.

Hegan, D. C., Y. Lu, G. C. Stachelek, M. E. Crosby, R. S. Bindra, and P. M. Glazer. 2010. 'Inhibition of poly(ADP-ribose) polymerase down-regulates BRCA1 and RAD51 in a pathway mediated by E2F4 and p130', *Proc Natl Acad Sci U S A*, 107: 2201-6.

Hekmat-Nejad, M., Z. You, M. C. Yee, J. W. Newport, and K. A. Cimprich. 2000. 'Xenopus ATR is a replication-dependent chromatin-binding protein required for the DNA replication checkpoint', *Curr Biol*, 10: 1565-73.

Henninger, E. E., and Z. F. Pursell. 2014. 'DNA polymerase ε and its roles in genome stability', *IUBMB Life*, 66: 339-51.

Ho, G. P., S. Margossian, T. Taniguchi, and A. D. D'Andrea. 2006. 'Phosphorylation of FANCD2 on two novel sites is required for mitomycin C resistance', *Mol Cell Biol*, 26: 7005-15.

Hodel, K. P., M. J. S. Sun, N. Ungerleider, V. S. Park, L. G. Williams, D. L. Bauer, V. E. Immethun, J. Wang, Z. Suo, H. Lu, J. B. McLachlan, and Z. F. Pursell. 2020. 'POLE Mutation Spectra Are Shaped by the Mutant Allele Identity, Its Abundance, and Mismatch Repair Status', *Mol Cell*, 78: 1166-77.e6.

Hoeijmakers, J. H. 2009. 'DNA damage, aging, and cancer', *N Engl J Med*, 361: 1475-85.

Höglund, A., L. M. Nilsson, S. V. Muralidharan, L. A. Hasvold, P. Merta, M. Rudelius, V. Nikolova, U. Keller, and J. A. Nilsson. 2011. 'Therapeutic implications for the induced levels of Chk1 in Myc-expressing cancer cells', *Clin Cancer Res*, 17: 7067-79.

Hohmann, A. F., and C. R. Vakoc. 2014. 'A rationale to target the SWI/SNF complex for cancer therapy', *Trends Genet*, 30: 356-63.

Holch, J. W., I. Ricard, S. Stintzing, D. P. Modest, and V. Heinemann. 2017. 'The relevance of primary tumour location in patients with metastatic colorectal cancer: A meta-analysis of first-line clinical trials', *Eur J Cancer*, 70: 87-98.

Honeywell, R. J., V. W. Ruiz van Haperen, G. Veerman, K. Smid, and G. J. Peters. 2015. 'Inhibition of thymidylate synthase by 2',2'-difluoro-2'-deoxycytidine (Gemcitabine) and its metabolite 2',2'-difluoro-2'-deoxyuridine', *Int J Biochem Cell Biol*, 60: 73-81.

Horisberger, K., P. Erben, B. Muessle, C. Woernle, P. Stroebel, G. Kaehler, F. Wenz, A. Hochhaus, S. Post, F. Willeke, and R. D. Hofheinz. 2009. 'Topoisomerase I expression correlates to response to neoadjuvant irinotecan-based chemoradiation in rectal cancer', *Anticancer Drugs*, 20: 519-24.

Horwitz, S. B., and M. S. Horwitz. 1973. 'Effects of camptothecin on the breakage and repair of DNA during the cell cycle', *Cancer Res*, 33: 2834-6.

Houghton, J. A., D. M. Tillman, and F. G. Harwood. 1995. 'Ratio of 2'-deoxyadenosine-5'-triphosphate/thymidine-5'-triphosphate influences the commitment of human colon carcinoma cells to thymineless death', *Clin Cancer Res*, 1: 723-30.

Hsiang, Y. H., R. Hertzberg, S. Hecht, and L. F. Liu. 1985. 'Camptothecin induces protein-linked DNA breaks via mammalian DNA topoisomerase I', *J Biol Chem*, 260: 14873-8.

Hsiang, Y. H., M. G. Lihou, and L. F. Liu. 1989. 'Arrest of replication forks by drug-stabilized topoisomerase I-DNA cleavable complexes as a mechanism of cell killing by camptothecin', *Cancer Res*, 49: 5077-82.

Hu, K., W. Yu, O. E. Ajayi, L. Li, Z. Huang, Q. Rong, S. Wang, and Q. F. Wu. 2020. 'Integrated analysis of whole genome and transcriptome sequencing in a young patient with gastric cancer provides insights for precision therapy', *Oncol Lett*, 20: 115.

Huang, T. T., S. M. Wuerzberger-Davis, B. J. Seufzer, S. D. Shumway, T. Kurama, D. A. Boothman, and S. Miyamoto. 2000. 'NF-kappaB activation by camptothecin. A linkage between nuclear DNA damage and cytoplasmic signaling events', *J Biol Chem*, 275: 9501-9.

Hudson, J. J., S. C. Chiang, O. S. Wells, C. Rookyard, and S. F. El-Khamisy. 2012. 'SUMO modification of the neuroprotective protein TDP1 facilitates chromosomal single-strand break repair', *Nat Commun*, 3: 733.

Huntoon, C. J., K. S. Flatten, A. E. Wahner Hendrickson, A. M. Huehls, S. L. Sutor, S. H. Kaufmann, and L. M. Karnitz. 2013. 'ATR inhibition broadly sensitizes ovarian cancer cells to chemotherapy independent of BRCA status', *Cancer Res*, 73: 3683-91.

Hur, J., M. Ghosh, T. H. Kim, N. Park, K. Pandey, Y. B. Cho, S. D. Hong, N. B. Katuwal, M. Kang, H. J. An, and Y. W. Moon. 2021. 'Synergism of AZD6738, an ATR Inhibitor, in Combination with Belotecan, a Camptothecin Analogue, in Chemotherapy-Resistant Ovarian Cancer', *Int J Mol Sci*, 22.

Hurwitz, H., L. Fehrenbacher, W. Novotny, T. Cartwright, J. Hainsworth, W. Heim, J. Berlin, A. Baron, S. Griffing, E. Holmgren, N. Ferrara, G. Fyfe, B. Rogers, R. Ross, and F. Kabbinavar. 2004. 'Bevacizumab plus irinotecan, fluorouracil, and leucovorin for metastatic colorectal cancer', *N Engl J Med*, 350: 2335-42.

Husain, A., N. A. Begum, T. Taniguchi, H. Taniguchi, M. Kobayashi, and T. Honjo. 2016. 'Chromatin remodeller SMARCA4 recruits topoisomerase 1 and suppresses transcription-associated genomic instability', *Nat Commun*, 7: 10549.

Huxley, R. R., A. Ansary-Moghaddam, P. Clifton, S. Czernichow, C. L. Parr, and M. Woodward. 2009. 'The impact of dietary and lifestyle risk factors on risk of colorectal cancer: a quantitative overview of the epidemiological evidence', *Int J Cancer*, 125: 171-80.

Hynes, N. E., and H. A. Lane. 2005. 'ERBB receptors and cancer: the complexity of targeted inhibitors', *Nat Rev Cancer*, 5: 341-54.

Interthal, H., H. J. Chen, T. E. Kehl-Fie, J. Zotzmann, J. B. Leppard, and J. J. Champoux. 2005. 'SCAN1 mutant Tdp1 accumulates the enzyme--DNA intermediate and causes camptothecin hypersensitivity', *Embo j*, 24: 2224-33.

Ishiai, M., H. Kitao, A. Smogorzewska, J. Tomida, A. Kinomura, E. Uchida, A. Saberi, E. Kinoshita, E. Kinoshita-Kikuta, T. Koike, S. Tashiro, S. J. Elledge, and M. Takata. 2008. 'FANCI phosphorylation functions as a molecular switch to turn on the Fanconi anemia pathway', *Nat Struct Mol Biol*, 15: 1138-46.

Ishikawa, H., and G. N. Barber. 2008. 'STING is an endoplasmic reticulum adaptor that facilitates innate immune signalling', *Nature*, 455: 674-8.

Ishikawa, H., Z. Ma, and G. N. Barber. 2009. 'STING regulates intracellular DNA-mediated, type I interferon-dependent innate immunity', *Nature*, 461: 788-92.

Iwata, T. N., C. Ishii, S. Ishida, Y. Ogitani, T. Wada, and T. Agatsuma. 2018. 'A HER2-Targeting Antibody-Drug Conjugate, Trastuzumab Deruxtecan (DS-8201a), Enhances Antitumor Immunity in a Mouse Model', *Mol Cancer Ther*, 17: 1494-503.

Iwata, T. N., K. Sugihara, T. Wada, and T. Agatsuma. 2019. '[Fam-] trastuzumab deruxtecan (DS-8201a)-induced antitumor immunity is facilitated by the anti-CTLA-4 antibody in a mouse model', *PLoS One*, 14: e0222280.

Jain, N., S. W. Smith, S. Ghone, and B. Tomczuk. 2015. 'Current ADC Linker Chemistry', *Pharm Res*, 32: 3526-40.

Jaxel, C., G. Capranico, D. Kerrigan, K. W. Kohn, and Y. Pommier. 1991. 'Effect of local DNA sequence on topoisomerase I cleavage in the presence or absence of camptothecin', *J Biol Chem*, 266: 20418-23.

Jensen, N. F., J. Stenvang, M. K. Beck, B. Hanáková, K. C. Belling, K. N. Do, B. Viuff, S. B. Nygård, R. Gupta, M. H. Rasmussen, L. S. Tarpgaard, T. P. Hansen, E. Budinská, P. Pfeiffer, F. Bosman, S. Tejpar, A. Roth, M. Delorenzi, C. L. Andersen, M. U. Rømer, N. Brünner, and J. M. Moreira. 2015. 'Establishment and characterization of models of chemotherapy resistance in colorectal cancer: Towards a predictive signature of chemoresistance', *Mol Oncol*, 9: 1169-85.

Jeon, Y., E. Ko, K. Y. Lee, M. J. Ko, S. Y. Park, J. Kang, C. H. Jeon, H. Lee, and D. S. Hwang. 2011. 'TopBP1 deficiency causes an early embryonic lethality and induces cellular senescence in primary cells', *J Biol Chem*, 286: 5414-22.

Jeong, S. Y., A. Kumagai, J. Lee, and W. G. Dunphy. 2003. 'Phosphorylated claspin interacts with a phosphate-binding site in the kinase domain of Chk1 during ATR-mediated activation', *J Biol Chem*, 278: 46782-8.

Jette, N., and S. P. Lees-Miller. 2015. 'The DNA-dependent protein kinase: A multifunctional protein kinase with roles in DNA double strand break repair and mitosis', *Prog Biophys Mol Biol*, 117: 194-205.

Jette, N. R., S. Radhamani, G. Arthur, R. Ye, S. Goutam, A. Bolyos, L. F. Petersen, P. Bose, D. G. Bebb, and S. P. Lees-Miller. 2019. 'Combined poly-ADP ribose polymerase and ataxia-telangiectasia mutated/Rad3-related inhibition targets ataxia-telangiectasia mutated-deficient lung cancer cells', *Br J Cancer*, 121: 600-10.

Jiang, X., Y. Sun, S. Chen, K. Roy, and B. D. Price. 2006. 'The FATC domains of PIKK proteins are functionally equivalent and participate in the Tip60-dependent activation of DNA-PKcs and ATM', *J Biol Chem*, 281: 15741-6.

Jin, M. H., and D. Y. Oh. 2019. 'ATM in DNA repair in cancer', *Pharmacol Ther*, 203: 107391.

Jo, U., Y. Murai, S. Chakka, L. Chen, K. Cheng, J. Murai, L. K. Saha, L. M. Miller Jenkins, and Y. Pommier. 2021. 'SLFN11 promotes CDT1 degradation by CUL4 in response to replicative DNA damage, while its absence leads to synthetic lethality with ATR/CHK1 inhibitors', *Proc Natl Acad Sci U S A*, 118.

Jo, Ukhyun, Ilya S. Senatorov, Astrid Zimmermann, Liton Kumar Saha, Yasuhisa Murai, Se Hyun Kim, Vinodh N. Rajapakse, Fathi Elloumi, Nobuyuki Takahashi, Christopher W. Schultz, Anish Thomas, Frank T. Zenke, and Yves Pommier. 2021. 'Novel and highly potent ATR inhibitor M4344 kills cancer cells with replication stress and enhances the chemotherapeutic activity of widely used DNA damaging agents', *Mol Cancer Ther*: molcanther.1026.2020.

Jonker, D. J., C. J. O'Callaghan, C. S. Karapetis, J. R. Zalcberg, D. Tu, H. J. Au, S. R. Berry, M. Krahn, T. Price, R. J. Simes, N. C. Tebbutt, G. van Hazel, R. Wierzbicki, C. Langer, and M. J. Moore. 2007. 'Cetuximab for the treatment of colorectal cancer', *N Engl J Med*, 357: 2040-8.

Josse, R., S. E. Martin, R. Guha, P. Ormanoglu, T. D. Pfister, P. M. Reaper, C. S. Barnes, J. Jones, P. Charlton, J. R. Pollard, J. Morris, J. H. Doroshow, and Y. Pommier. 2014. 'ATR

inhibitors VE-821 and VX-970 sensitize cancer cells to topoisomerase i inhibitors by disabling DNA replication initiation and fork elongation responses', *Cancer Res*, 74: 6968-79.

Ju, H. Q., Y. X. Lu, D. L. Chen, T. Tian, H. Y. Mo, X. L. Wei, J. W. Liao, F. Wang, Z. L. Zeng, H. Pelicano, M. Aguilar, W. H. Jia, and R. H. Xu. 2016. 'Redox Regulation of Stem-like Cells Though the CD44v-xCT Axis in Colorectal Cancer: Mechanisms and Therapeutic Implications', *Theranostics*, 6: 1160-75.

Jungmichel, S., J. A. Clapperton, J. Lloyd, F. J. Hari, C. Spycher, L. Pavic, J. Li, L. F. Haire, M. Bonalli, D. H. Larsen, C. Lukas, J. Lukas, D. MacMillan, M. L. Nielsen, M. Stucki, and S. J. Smerdon. 2012. 'The molecular basis of ATM-dependent dimerization of the Mdc1 DNA damage checkpoint mediator', *Nucleic Acids Res*, 40: 3913-28.

Junttila, T. T., G. Li, K. Parsons, G. L. Phillips, and M. X. Sliwkowski. 2011. 'Trastuzumab-DM1 (T-DM1) retains all the mechanisms of action of trastuzumab and efficiently inhibits growth of lapatinib insensitive breast cancer', *Breast Cancer Res Treat*, 128: 347-56.

Kabbinavar, F., C. Irl, A. Zurlo, and H. Hurwitz. 2008. 'Bevacizumab improves the overall and progression-free survival of patients with metastatic colorectal cancer treated with 5-fluorouracil-based regimens irrespective of baseline risk', *Oncology*, 75: 215-23.

Karanam, K., R. Kafri, A. Loewer, and G. Lahav. 2012. 'Quantitative live cell imaging reveals a gradual shift between DNA repair mechanisms and a maximal use of HR in mid S phase', *Mol Cell*, 47: 320-9.

Karapetis, C. S., S. Khambata-Ford, D. J. Jonker, C. J. O'Callaghan, D. Tu, N. C. Tebbutt, R. J. Simes, H. Chalchal, J. D. Shapiro, S. Robitaille, T. J. Price, L. Shepherd, H. J. Au, C. Langer, M. J. Moore, and J. R. Zalcberg. 2008. 'K-ras mutations and benefit from cetuximab in advanced colorectal cancer', *N Engl J Med*, 359: 1757-65.

Karnitz, L. M., and L. Zou. 2015. 'Molecular Pathways: Targeting ATR in Cancer Therapy', *Clin Cancer Res*, 21: 4780-5.

Kato, Y., Y. Tsukada, T. Hara, and H. Hirai. 1983. 'Enhanced antitumor activity of mitomycin C conjugated with anti-alpha-fetoprotein antibody by a novel method of conjugation', *J Appl Biochem*, 5: 313-9.

Kawasumi, M., B. Lemos, J. E. Bradner, R. Thibodeau, Y. S. Kim, M. Schmidt, E. Higgins, S. W. Koo, A. Angle-Zahn, A. Chen, D. Levine, L. Nguyen, T. P. Heffernan, I. Longo, A. Mandinova, Y. P. Lu, A. H. Conney, and P. Nghiem. 2011. 'Protection from UV-induced skin carcinogenesis by genetic inhibition of the ataxia telangiectasia and Rad3-related (ATR) kinase', *Proc Natl Acad Sci U S A*, 108: 13716-21.

Keam, S. J. 2020. 'Trastuzumab Deruxtecan: First Approval', *Drugs*, 80: 501-08.

Keating, G. M. 2010. 'Panitumumab: a review of its use in metastatic colorectal cancer', *Drugs*, 70: 1059-78.

Kim, H., E. George, R. Ragland, S. Rafail, R. Zhang, C. Krepler, M. Morgan, M. Herlyn, E. Brown, and F. Simpkins. 2017. 'Targeting the ATR/CHK1 Axis with PARP Inhibition Results in Tumor Regression in BRCA-Mutant Ovarian Cancer Models', *Clin Cancer Res*, 23: 3097-108.

Kim, L. C., R. S. Cook, and J. Chen. 2017. 'mTORC1 and mTORC2 in cancer and the tumor microenvironment', *Oncogene*, 36: 2191-201.

Kim, Y., G. S. Spitz, U. Veturi, F. P. Lach, A. D. Auerbach, and A. Smogorzewska. 2013. 'Regulation of multiple DNA repair pathways by the Fanconi anemia protein SLX4', *Blood*, 121: 54-63.

Kimura, Kenjiro, Tetsuji Sawada, Midori Komatsu, Masafumi Inoue, Kazuya Muguruma, Tamahiro Nishihara, Yoshito Yamashita, Nobuya Yamada, Masaichi Ohira, and Kosei Hirakawa. 2006. 'Antitumor Effect of Trastuzumab for Pancreatic Cancer with High HER-2 Expression and Enhancement of Effect by Combined Therapy with Gemcitabine', *Clinical Cancer Research*, 12: 4925.

Kinneer, K., J. Meekin, A. C. Tiberghien, Y. T. Tai, S. Phipps, C. M. Kiefer, M. C. Rebelatto, N. Dimasi, A. Moriarty, K. P. Papadopoulos, S. Sridhar, S. J. Gregson, M. J. Wick, L. Masterson, K. C. Anderson, R. Herbst, P. W. Howard, and D. A. Tice. 2018. 'SLC46A3 as a Potential Predictive Biomarker for Antibody-Drug Conjugates Bearing Noncleavable Linked Maytansinoid and Pyrrolobenzodiazepine Warheads', *Clin Cancer Res*, 24: 6570-82.

Konno, H., S. Yamauchi, A. Berglund, R. M. Putney, J. J. Mulé, and G. N. Barber. 2018. 'Suppression of STING signaling through epigenetic silencing and missense mutation impedes DNA damage mediated cytokine production', *Oncogene*, 37: 2037-51.

Konstantinopoulos, P. A., S. C. Cheng, A. E. Wahner Hendrickson, R. T. Penson, S. T. Schumer, L. A. Doyle, E. K. Lee, E. C. Kohn, L. R. Duska, M. A. Crispens, A. B. Olawaiye, I. S. Winer, L. M. Barroilhet, S. Fu, M. T. McHale, R. J. Schilder, A. Färkkilä, D. Chowdhury, J. Curtis, R. S. Quinn, B. Bowes, A. D. D'Andrea, G. I. Shapiro, and U. A. Matulonis. 2020. 'Berzosertib plus gemcitabine versus gemcitabine alone in platinum-resistant high-grade serous ovarian cancer: a multicentre, open-label, randomised, phase 2 trial', *Lancet Oncol*, 21: 957-68.

Koopman, M., N. Knijn, S. Richman, M. Seymour, P. Quirke, H. van Tinteren, J. H. J. M. van Krieken, C. J. A. Punt, and I. D. Nagtegaal. 2009. '6003 The correlation between Topoisomerase-I (Topo1) expression and outcome of treatment with capecitabine and irinotecan in advanced colorectal cancer (ACC) patients (pts) treated in the CAIRO study of the Dutch Colorectal Cancer Group (DCCG)', *European Journal of Cancer Supplements*, 7: 321-22.

Koster, D. A., V. Croquette, C. Dekker, S. Shuman, and N. H. Dekker. 2005. 'Friction and torque govern the relaxation of DNA supercoils by eukaryotic topoisomerase IB', *Nature*, 434: 671-4.

Kovtun, Y. V., C. A. Audette, Y. Ye, H. Xie, M. F. Ruberti, S. J. Phinney, B. A. Leece, T. Chittenden, W. A. Blättler, and V. S. Goldmacher. 2006. 'Antibody-drug conjugates designed to eradicate tumors with homogeneous and heterogeneous expression of the target antigen', *Cancer Res*, 66: 3214-21.

Kovtun, Y. V., and V. S. Goldmacher. 2007. 'Cell killing by antibody-drug conjugates', *Cancer Lett*, 255: 232-40.

Krajewska, M., R. S. Fehrmann, P. M. Schoonen, S. Labib, E. G. de Vries, L. Franke, and M. A. van Vugt. 2015. 'ATR inhibition preferentially targets homologous recombination-deficient tumor cells', *Oncogene*, 34: 3474-81.

Krebs, Matthew G., Juanita Lopez, Anthony El-Khoueiry, Yung-Jue Bang, Sophie Postel-Vinay, Wassim Abida, Louise Carter, Wen Xu, Seock-Ah Im, Andrew Pierce, Paul Frewer, Alienor Berges, S. Y. Amy Cheung, Christine Stephens, Brunella Felicetti, Emma Dean, and Simon J. Hollingsworth. 2018. 'Abstract CT026: Phase I study of AZD6738, an inhibitor of ataxia telangiectasia Rad3-related (ATR), in combination with olaparib or durvalumab in patients (pts) with advanced solid cancers', *Cancer Res*, 78: CT026.

Kretzschmar, M., M. Meisterernst, and R. G. Roeder. 1993. 'Identification of human DNA topoisomerase I as a cofactor for activator-dependent transcription by RNA polymerase II', *Proc Natl Acad Sci U S A*, 90: 11508-12.

Kumagai, A., and W. G. Dunphy. 2003. 'Repeated phosphopeptide motifs in Claspin mediate the regulated binding of Chk1', *Nat Cell Biol*, 5: 161-5.

Kumagai, A., J. Lee, H. Y. Yoo, and W. G. Dunphy. 2006. 'TopBP1 activates the ATR-ATRIP complex', *Cell*, 124: 943-55.

Kumagai, A., A. Shevchenko, A. Shevchenko, and W. G. Dunphy. 2010. 'Treslin collaborates with TopBP1 in triggering the initiation of DNA replication', *Cell*, 140: 349-59.

Kumagai, A. Shevchenko, A. Shevchenko, A. Dunphy, W. G. 2011. 'Direct regulation of Treslin by cyclin-dependent kinase is essential for the onset of DNA replication', *J Cell Biol*, 193: 995-1007.

Kurmasheva, R. T., D. Kurmashev, C. P. Reynolds, M. Kang, J. Wu, P. J. Houghton, and M. A. Smith. 2018. 'Initial testing (stage 1) of M6620 (formerly VX-970), a novel ATR inhibitor, alone and combined with cisplatin and melphalan, by the Pediatric Preclinical Testing Program', *Pediatr Blood Cancer*, 65.

Kwok, M., N. Davies, A. Agathanggelou, E. Smith, C. Oldreive, E. Petermann, G. Stewart, J. Brown, A. Lau, G. Pratt, H. Parry, M. Taylor, P. Moss, P. Hillmen, and T. Stankovic. 2016. 'ATR inhibition induces synthetic lethality and overcomes chemoresistance in TP53- or ATM-defective chronic lymphocytic leukemia cells', *Blood*, 127: 582-95.

Kyrgiou, M., I. Kalliala, G. Markozannes, M. J. Gunter, E. Paraskevaidis, H. Gabra, P. Martin-Hirsch, and K. K. Tsilidis. 2017. 'Adiposity and cancer at major anatomical sites: umbrella review of the literature', *Bmj*, 356: j477.

Labianca, R., B. Nordlinger, G. D. Beretta, S. Mosconi, M. Mandalà, A. Cervantes, and D. Arnold. 2013. 'Early colon cancer: ESMO Clinical Practice Guidelines for diagnosis, treatment and follow-up', *Ann Oncol*, 24 Suppl 6: vi64-72.

Labib, Karim, José Antonio Tercero, and John F. X. Diffley. 2000. 'Uninterrupted MCM2-7 Function Required for DNA Replication Fork Progression', *Science*, 288: 1643.

Laine, J. P., P. L. Opresko, F. E. Indig, J. A. Harrigan, C. von Kobbe, and V. A. Bohr. 2003. 'Werner protein stimulates topoisomerase I DNA relaxation activity', *Cancer Res*, 63: 7136-46.

Lal, P., P. A. Salazar, C. A. Hudis, M. Ladanyi, and B. Chen. 2004. 'HER-2 testing in breast cancer using immunohistochemical analysis and fluorescence in situ hybridization: a single-institution experience of 2,279 cases and comparison of dual-color and single-color scoring', *Am J Clin Pathol*, 121: 631-6.

Lam, A. K., R. Carmichael, P. Gertraud Buettner, V. Gopalan, Y. H. Ho, and S. Siu. 2011. 'Clinicopathological significance of synchronous carcinoma in colorectal cancer', *Am J Surg*, 202: 39-44.

Lambert, J. M., and A. Berkenblit. 2018. 'Antibody-Drug Conjugates for Cancer Treatment', *Annu Rev Med*, 69: 191-207.

Lau, Alan Y., James Yates, Zena Wilson, Lucy A. Young, Adina M. Hughes, Alienor Berges, Amy Cheung, Rajesh Odedra, Elaine Brown, Mark J. Connor, and Simon Hollingsworth. 2017. 'Abstract 2494: ATR inhibitor AZD6738 as monotherapy and in combination with olaparib or chemotherapy: defining pre-clinical dose-schedules and efficacy modelling', *Cancer Res*, 77: 2494.

Le Roy, C., and J. L. Wrana. 2005. 'Clathrin- and non-clathrin-mediated endocytic regulation of cell signalling', *Nat Rev Mol Cell Biol*, 6: 112-26.

Le, T. M., S. Poddar, J. R. Capri, E. R. Abt, W. Kim, L. Wei, N. T. Uong, C. M. Cheng, D. Braas, M. Nikanjam, P. Rix, D. Merkurjev, J. Zaretsky, H. I. Kornblum, A. Ribas, H. R. Herschman, J. Whitelegge, K. F. Faull, T. R. Donahue, J. Czernin, and C. G. Radu. 2017. 'ATR inhibition facilitates targeting of leukemia dependence on convergent nucleotide biosynthetic pathways', *Nat Commun*, 8: 241.

Lecona, E., and O. Fernandez-Capetillo. 2018. 'Targeting ATR in cancer', *Nat Rev Cancer*, 18: 586-95.

Ledermann, J. A. 2019. 'Extending the scope of PARP inhibitors in ovarian cancer', *Lancet Oncol*, 20: 470-72.

Lee, A. 2021. 'Loncastuximab Tesirine: First Approval', *Drugs*.

Lee, H. E., K. U. Park, S. B. Yoo, S. K. Nam, D. J. Park, H. H. Kim, and H. S. Lee. 2013. 'Clinical significance of intratumoral HER2 heterogeneity in gastric cancer', *Eur J Cancer*, 49: 1448-57.

Lee, J., and W. G. Dunphy. 2013. 'The Mre11-Rad50-Nbs1 (MRN) complex has a specific role in the activation of Chk1 in response to stalled replication forks', *Mol Biol Cell*, 24: 1343-53.

Lee, J., A. Kumagai, and W. G. Dunphy. 2001. 'Positive regulation of Wee1 by Chk1 and 14-3-3 proteins', *Mol Biol Cell*, 12: 551-63.

Lee, J. Kumagai, A. Dunphy, W. G. 2007. 'The Rad9-Hus1-Rad1 checkpoint clamp regulates interaction of TopBP1 with ATR', *J Biol Chem*, 282: 28036-44.

Lee, J. S., K. M. Collins, A. L. Brown, C. H. Lee, and J. H. Chung. 2000. 'hCds1-mediated phosphorylation of BRCA1 regulates the DNA damage response', *Nature*, 404: 201-4.

Lee, Jeeyun, Seung Tae Kim, Simon Smith, Peter G. Mortimer, Bienvenu Loembé, Jung Hong, Iwanka Kozarewa, Andrew Pierce, and Emma Dean. 2020. 'Results from a phase I, open-label study of ceralasertib (AZD6738), a novel DNA damage repair agent, in combination with weekly paclitaxel in refractory cancer (NCT02630199)', *Journal of Clinical Oncology*, 38: 3503-03.

Lee, T. H., J. M. Park, S. H. Leem, and T. H. Kang. 2014. 'Coordinated regulation of XPA stability by ATR and HERC2 during nucleotide excision repair', *Oncogene*, 33: 19-25.

Lee, Y. C., Q. Zhou, J. Chen, and J. Yuan. 2016. 'RPA-Binding Protein ETAA1 Is an ATR Activator Involved in DNA Replication Stress Response', *Curr Biol*, 26: 3257-68.

Lemmon, M. A., J. Schlessinger, and K. M. Ferguson. 2014. 'The EGFR family: not so prototypical receptor tyrosine kinases', *Cold Spring Harb Perspect Biol*, 6: a020768.

Leonard, B. C., E. D. Lee, N. E. Bhola, H. Li, K. K. Sogaard, C. J. Bakkenist, J. R. Grandis, and D. E. Johnson. 2019. 'ATR inhibition sensitizes HPV(-) and HPV(+) head and neck squamous cell carcinoma to cisplatin', *Oral Oncol*, 95: 35-42.

Leszczynska, K. B., G. Dobrynin, R. E. Leslie, J. Ient, A. J. Boumelha, J. M. Senra, M. A. Hawkins, T. Maughan, S. Mukherjee, and E. M. Hammond. 2016. 'Preclinical testing of an Atr inhibitor demonstrates improved response to standard therapies for esophageal cancer', *Radiother Oncol*, 121: 232-38.

Li, B. T., F. Michelini, S. Misale, E. Cocco, L. Baldino, Y. Cai, S. Shifman, H. Y. Tu, M. L. Myers, C. Xu, M. Mattar, I. Khodos, M. Little, B. Qeriqi, G. Weitsman, C. J. Wilhem, A. S. Lalani, I. Diala, R. A. Freedman, N. U. Lin, D. B. Solit, M. F. Berger, P. R. Barber, T. Ng, M. Offin, J. M. Isbell, D. R. Jones, H. A. Yu, S. Thyparambil, W. L. Liao, A. Bhalkikar, F. Cecchi, D. M. Hyman, J. S. Lewis, D. J. Buonocore, A. L. Ho, V. Makker, J. S. Reis-Filho, P. Razavi, M. E. Arcila, M. G. Kris, J. T. Poirier, R. Shen, J. Tsurutani, G. A. Ulaner, E. de Stanchina, N. Rosen, C. M. Rudin, and M. Scaltriti. 2020. 'HER2-Mediated Internalization of Cytotoxic Agents in ERBB2 Amplified or Mutant Lung Cancers', *Cancer Discov*, 10: 674-87.

Li, C. C., J. C. Yang, M. C. Lu, C. L. Lee, C. Y. Peng, W. Y. Hsu, Y. H. Dai, F. R. Chang, D. Y. Zhang, W. J. Wu, and Y. C. Wu. 2016. 'ATR-Chk1 signaling inhibition as a therapeutic strategy to enhance cisplatin chemosensitivity in urothelial bladder cancer', *Oncotarget*, 7: 1947-59.

Li, S., K. R. Schmitz, P. D. Jeffrey, J. J. Wiltzius, P. Kussie, and K. M. Ferguson. 2005. 'Structural basis for inhibition of the epidermal growth factor receptor by cetuximab', *Cancer Cell*, 7: 301-11.

Li, X. G., P. Haluska, Jr., Y. H. Hsiang, A. Bharti, D. W. Kufe, and E. H. Rubin. 1996. 'Identification of topoisomerase I mutations affecting both DNA cleavage and interaction with camptothecin', *Ann N Y Acad Sci*, 803: 111-27.

Li, Z., T. Otevrel, Y. Gao, H. L. Cheng, B. Seed, T. D. Stamato, G. E. Taccioli, and F. W. Alt. 1995. 'The XRCC4 gene encodes a novel protein involved in DNA double-strand break repair and V(D)J recombination', *Cell*, 83: 1079-89.

Liberzon, A., A. Subramanian, R. Pinchback, H. Thorvaldsdóttir, P. Tamayo, and J. P. Mesirov. 2011. 'Molecular signatures database (MSigDB) 3.0', *Bioinformatics*, 27: 1739-40.

Lin, C. P., Y. Ban, Y. L. Lyu, and L. F. Liu. 2009. 'Proteasome-dependent processing of topoisomerase I-DNA adducts into DNA double strand breaks at arrested replication forks', *J Biol Chem*, 284: 28084-92.

Lindsey-Boltz, L. A., M. G. Kemp, C. Capp, and A. Sancar. 2015. 'RHINO forms a stoichiometric complex with the 9-1-1 checkpoint clamp and mediates ATR-Chk1 signaling', *Cell Cycle*, 14: 99-108.

Liu, J., S. Luo, H. Zhao, J. Liao, J. Li, C. Yang, B. Xu, D. F. Stern, X. Xu, and K. Ye. 2012. 'Structural mechanism of the phosphorylation-dependent dimerization of the MDC1 forkhead-associated domain', *Nucleic Acids Res*, 40: 3898-912.

Liu, Q., S. Guntuku, X. S. Cui, S. Matsuoka, D. Cortez, K. Tamai, G. Luo, S. Carattini-Rivera, F. DeMayo, A. Bradley, L. A. Donehower, and S. J. Elledge. 2000. 'Chk1 is an essential kinase that is regulated by Atr and required for the G(2)/M DNA damage checkpoint', *Genes Dev*, 14: 1448-59.

Liu, S., Y. Ge, T. Wang, H. Edwards, Q. Ren, Y. Jiang, C. Quan, and G. Wang. 2017. 'Inhibition of ATR potentiates the cytotoxic effect of gemcitabine on pancreatic cancer cells through enhancement of DNA damage and abrogation of ribonucleotide reductase induction by gemcitabine', *Oncol Rep*, 37: 3377-86.

Liu, S., B. Shiotani, M. Lahiri, A. Maréchal, A. Tse, C. C. Leung, J. N. Glover, X. H. Yang, and L. Zou. 2011. 'ATR autophosphorylation as a molecular switch for checkpoint activation', *Mol Cell*, 43: 192-202.

Liu, Y., T. Zuo, X. Zhu, N. Ahuja, and T. Fu. 2017. 'Differential expression of hENT1 and hENT2 in colon cancer cell lines', *Genet Mol Res*, 16.

Longley, D. B., D. P. Harkin, and P. G. Johnston. 2003. '5-fluorouracil: mechanisms of action and clinical strategies', *Nat Rev Cancer*, 3: 330-8.

López-Contreras, A. J., P. Gutierrez-Martinez, J. Specks, S. Rodrigo-Perez, and O. Fernandez-Capetillo. 2012. 'An extra allele of Chk1 limits oncogene-induced replicative stress and promotes transformation', *J Exp Med*, 209: 455-61.

Lopez-Contreras, A. J., J. Specks, J. H. Barlow, C. Ambrogio, C. Desler, S. Vikingsson, S. Rodrigo-Perez, H. Green, L. J. Rasmussen, M. Murga, A. Nussenzweig, and O. Fernandez-Capetillo. 2015. 'Increased Rrm2 gene dosage reduces fragile site breakage and prolongs survival of ATR mutant mice', *Genes Dev*, 29: 690-5.

Love, M. I., W. Huber, and S. Anders. 2014. 'Moderated estimation of fold change and dispersion for RNA-seq data with DESeq2', *Genome Biol*, 15: 550.

Luecking, Ulrich T., Julien Lefranc, Antje Wengner, Lars Wortmann, Hans Schick, Hans Briem, Gerhard Siemeister, Philip Lienau, Christoph Schatz, Benjamin Bader, Gesa Deeg, Franz von Nussbaum, Michael Brands, Dominik Mumberg, and Karl Ziegelbauer. 2017. 'Abstract 983: Identification of potent, highly selective and orally available ATR inhibitor BAY 1895344 with favorable PK properties and promising efficacy in monotherapy and combination in preclinical tumor models', *Cancer Res*, 77: 983.

Ma, J., X. Li, Y. Su, J. Zhao, D. A. Luedtke, V. Epshteyn, H. Edwards, G. Wang, Z. Wang, R. Chu, J. W. Taub, H. Lin, Y. Wang, and Y. Ge. 2017. 'Mechanisms responsible for the synergistic antileukemic interactions between ATR inhibition and cytarabine in acute myeloid leukemia cells', *Sci Rep*, 7: 41950.

Ma, J., and M. Wang. 2014. 'Interplay between DNA supercoiling and transcription elongation', *Transcription*, 5: e28636.

Macheret, M., and T. D. Halazonetis. 2015. 'DNA replication stress as a hallmark of cancer', *Annu Rev Pathol*, 10: 425-48.

Mackenzie, K. J., P. Carroll, C. A. Martin, O. Murina, A. Fluteau, D. J. Simpson, N. Olova, H. Sutcliffe, J. K. Rainger, A. Leitch, R. T. Osborn, A. P. Wheeler, M. Nowotny, N. Gilbert, T. Chandra, M. A. M. Reijns, and A. P. Jackson. 2017. 'cGAS surveillance of micronuclei links genome instability to innate immunity', *Nature*, 548: 461-65.

Mahalingaiah, P. K., R. Ciurlionis, K. R. Durbin, R. L. Yeager, B. K. Philip, B. Bawa, S. R. Mantena, B. P. Enright, M. J. Liguori, and T. R. Van Vleet. 2019. 'Potential mechanisms of target-independent uptake and toxicity of antibody-drug conjugates', *Pharmacol Ther*, 200: 110-25.

Manne, U., C. Shanmugam, V. R. Katkoori, H. L. Bumpers, and W. E. Grizzle. 2010. 'Development and progression of colorectal neoplasia', *Cancer Biomark*, 9: 235-65.

Mao, Y., M. Sun, S. D. Desai, and L. F. Liu. 2000. 'SUMO-1 conjugation to topoisomerase I: A possible repair response to topoisomerase-mediated DNA damage', *Proc Natl Acad Sci U S A*, 97: 4046-51.

Maréchal, A., and L. Zou. 2015. 'RPA-coated single-stranded DNA as a platform for post-translational modifications in the DNA damage response', *Cell Res*, 25: 9-23.

Markowitz, S. D., and M. M. Bertagnolli. 2009. 'Molecular origins of cancer: Molecular basis of colorectal cancer', *N Engl J Med*, 361: 2449-60.

Maskey, R. S., K. S. Flatten, C. J. Sieben, K. L. Peterson, D. J. Baker, H. J. Nam, M. S. Kim, T. C. Smyrk, Y. Kojima, Y. Machida, A. Santiago, J. M. van Deursen, S. H. Kaufmann, and Y. J. Machida. 2017. 'Spartan deficiency causes accumulation of Topoisomerase 1 cleavage complexes and tumorigenesis', *Nucleic Acids Res*, 45: 4564-76.

Mathe, G., L. O. Tran Ba, and J. Bernard. 1958. '[Effect on mouse leukemia 1210 of a combination by diazo-reaction of amethopterin and gamma-globulins from hamsters inoculated with such leukemia by heterografts]', *C R Hebd Seances Acad Sci*, 246: 1626-8.

Matsunaga, T., N. Okumura, H. Saito, Y. Morikawa, K. Suenami, A. Hisamatsu, S. Endo, and A. Ikari. 2020. 'Significance of aldo-keto reductase 1C3 and ATP-binding cassette transporter B1 in gain of irinotecan resistance in colon cancer cells', *Chem Biol Interact*, 332: 109295.

Matsuoka, S., M. Huang, and S. J. Elledge. 1998. 'Linkage of ATM to cell cycle regulation by the Chk2 protein kinase', *Science*, 282: 1893-7.

Mattiroli, F., J. H. Vissers, W. J. van Dijk, P. Ikpa, E. Citterio, W. Vermeulen, J. A. Marteijn, and T. K. Sixma. 2012. 'RNF168 ubiquitinates K13-15 on H2A/H2AX to drive DNA damage signaling', *Cell*, 150: 1182-95.

Maughan, T. S., R. A. Adams, C. G. Smith, A. M. Meade, M. T. Seymour, R. H. Wilson, S. Idziaszczyk, R. Harris, D. Fisher, S. L. Kenny, E. Kay, J. K. Mitchell, A. Madi, B. Jasani, M. D. James, J. Bridgewater, M. J. Kennedy, B. Claes, D. Lambrechts, R. Kaplan, and J. P. Cheadle. 2011. 'Addition of cetuximab to oxaliplatin-based first-line combination chemotherapy for treatment of advanced colorectal cancer: results of the randomised phase 3 MRC COIN trial', *Lancet*, 377: 2103-14.

McDermott, M., A. J. Eustace, S. Busschots, L. Breen, J. Crown, M. Clynes, N. O'Donovan, and B. Stordal. 2014. 'In vitro Development of Chemotherapy and Targeted Therapy Drug-Resistant Cancer Cell Lines: A Practical Guide with Case Studies', *Front Oncol*, 4: 40.

McLeod, H. L., and W. N. Keith. 1996. 'Variation in topoisomerase I gene copy number as a mechanism for intrinsic drug sensitivity', *Br J Cancer*, 74: 508-12.

Mei, C., L. Lei, L. M. Tan, X. J. Xu, B. M. He, C. Luo, J. Y. Yin, X. Li, W. Zhang, H. H. Zhou, and Z. Q. Liu. 2020. 'The role of single strand break repair pathways in cellular responses to camptothecin induced DNA damage', *Biomed Pharmacother*, 125: 109875.

Meisenberg, C., S. E. Ward, P. Schmid, and S. F. El-Khamisy. 2014. 'TDP1/TOP1 Ratio as a Promising Indicator for the Response of Small Cell Lung Cancer to Topotecan', *J Cancer Sci Ther*, 6: 258-67.

Meisenberg, Cornelia, Duncan C. Gilbert, Anthony Chalmers, Vikki Haley, Simon Gollins, Simon E. Ward, and Sherif F. El-Khamisy. 2015. 'Clinical and Cellular Roles for TDP1 and TOP1 in Modulating Colorectal Cancer Response to Irinotecan', *Mol Cancer Ther*, 14: 575.

Menezes, D. L., J. Holt, Y. Tang, J. Feng, P. Barsanti, Y. Pan, M. Ghoddusi, W. Zhang, G. Thomas, J. Holash, E. Lees, and L. Taricani. 2015. 'A synthetic lethal screen reveals enhanced sensitivity to ATR inhibitor treatment in mantle cell lymphoma with ATM loss-of-function', *Mol Cancer Res*, 13: 120-9.

Merino, A., K. R. Madden, W. S. Lane, J. J. Champoux, and D. Reinberg. 1993. 'DNA topoisomerase I is involved in both repression and activation of transcription', *Nature*, 365: 227-32.

Meyer, B., K. O. Voss, F. Tobias, B. Jakob, M. Durante, and G. Taucher-Scholz. 2013. 'Clustered DNA damage induces pan-nuclear H2AX phosphorylation mediated by ATM and DNA-PK', *Nucleic Acids Res*, 41: 6109-18.

Middleton, F. K., J. R. Pollard, and N. J. Curtin. 2018. 'The Impact of p53 Dysfunction in ATR Inhibitor Cytotoxicity and Chemo- and Radiosensitisation', *Cancers (Basel)*, 10.

Middleton, M. R., E. Dean, T. R. J. Evans, G. I. Shapiro, J. Pollard, B. S. Hendriks, M. Falk, I. Diaz-Padilla, and R. Plummer. 2021. 'Phase 1 study of the ATR inhibitor berzosertib (formerly M6620, VX-970) combined with gemcitabine ± cisplatin in patients with advanced solid tumours', *Br J Cancer*.

Min, A., S. A. Im, H. Jang, S. Kim, M. Lee, D. K. Kim, Y. Yang, H. J. Kim, K. H. Lee, J. W. Kim, T. Y. Kim, D. Y. Oh, J. Brown, A. Lau, M. J. O'Connor, and Y. J. Bang. 2017. 'AZD6738, A Novel Oral Inhibitor of ATR, Induces Synthetic Lethality with ATM Deficiency in Gastric Cancer Cells', *Mol Cancer Ther*, 16: 566-77.

Mini, E., S. Nobili, B. Caciagli, I. Landini, and T. Mazzei. 2006. 'Cellular pharmacology of gemcitabine', *Ann Oncol*, 17 Suppl 5: v7-12.

Misset, J. L., H. Bleiberg, W. Sutherland, M. Bekradda, and E. Cvitkovic. 2000. 'Oxaliplatin clinical activity: a review', *Crit Rev Oncol Hematol*, 35: 75-93.

Modi, S., H. Park, R. K. Murthy, H. Iwata, K. Tamura, J. Tsurutani, A. Moreno-Aspitia, T. Doi, Y. Sagara, C. Redfern, I. E. Krop, C. Lee, Y. Fujisaki, M. Sugihara, L. Zhang, J. Shahidi, and S. Takahashi. 2020. 'Antitumor Activity and Safety of Trastuzumab Deruxtecan in Patients With HER2-Low-Expressing Advanced Breast Cancer: Results From a Phase Ib Study', *J Clin Oncol*, 38: 1887-96.

Modi, S., C. Saura, T. Yamashita, Y. H. Park, S. B. Kim, K. Tamura, F. Andre, H. Iwata, Y. Ito, J. Tsurutani, J. Sohn, N. Denduluri, C. Perrin, K. Aogi, E. Tokunaga, S. A. Im, K. S. Lee, S. A. Hurvitz, J. Cortes, C. Lee, S. Chen, L. Zhang, J. Shahidi, A. Yver, and I. Krop. 2020. 'Trastuzumab Deruxtecan in Previously Treated HER2-Positive Breast Cancer', *N Engl J Med*, 382: 610-21.

Moeglin, E., D. Desplancq, S. Conic, M. Oulad-Abdelghani, A. Stoessel, M. Chiper, M. Vigneron, P. Didier, L. Tora, and E. Weiss. 2019. 'Uniform Widespread Nuclear Phosphorylation of Histone H2AX Is an Indicator of Lethal DNA Replication Stress', *Cancers (Basel)*, 11.

Mohni, K. N., P. S. Thompson, J. W. Luzwick, G. G. Glick, C. S. Pendleton, B. D. Lehmann, J. A. Pietenpol, and D. Cortez. 2015. 'A Synthetic Lethal Screen Identifies DNA Repair Pathways that Sensitize Cancer Cells to Combined ATR Inhibition and Cisplatin Treatments', *PLoS One*, 10: e0125482.

Mordes, D. A., G. G. Glick, R. Zhao, and D. Cortez. 2008. 'TopBP1 activates ATR through ATRIP and a PIKK regulatory domain', *Genes Dev*, 22: 1478-89.

Morgan, R. A., J. C. Yang, M. Kitano, M. E. Dudley, C. M. Laurencot, and S. A. Rosenberg. 2010. 'Case report of a serious adverse event following the administration of T cells transduced with a chimeric antigen receptor recognizing ERBB2', *Mol Ther*, 18: 843-51.

Moshous, D., I. Callebaut, R. de Chasseval, B. Corneo, M. Cavazzana-Calvo, F. Le Deist, I. Tezcan, O. Sanal, Y. Bertrand, N. Philippe, A. Fischer, and J. P. de Villartay. 2001. 'Artemis, a novel DNA double-strand break repair/V(D)J recombination protein, is mutated in human severe combined immune deficiency', *Cell*, 105: 177-86.

Müller, P., M. Kreuzaler, T. Khan, D. S. Thommen, K. Martin, K. Glatz, S. Savic, N. Harbeck, U. Nitz, O. Gluz, M. von Bergwelt-Baildon, H. Kreipe, S. Reddy, M. Christgen, and A. Zippelius. 2015. 'Trastuzumab emtansine (T-DM1) renders HER2+ breast cancer highly susceptible to CTLA-4/PD-1 blockade', *Sci Transl Med*, 7: 315ra188.

Murai, J., Y. Feng, G. K. Yu, Y. Ru, S. W. Tang, Y. Shen, and Y. Pommier. 2016. 'Resistance to PARP inhibitors by SLFN11 inactivation can be overcome by ATR inhibition', *Oncotarget*, 7: 76534-50.

Murga, M., S. Bunting, M. F. Montaña, R. Soria, F. Mulero, M. Cañamero, Y. Lee, P. J. McKinnon, A. Nussenzweig, and O. Fernandez-Capetillo. 2009. 'A mouse model of ATR-Seckel shows embryonic replicative stress and accelerated aging', *Nat Genet*, 41: 891-8.

Murga, M., S. Campaner, A. J. Lopez-Contreras, L. I. Toledo, R. Soria, M. F. Montaña, L. Artista, T. Schleker, C. Guerra, E. Garcia, M. Barbacid, M. Hidalgo, B. Amati, and O. Fernandez-Capetillo. 2011. 'Exploiting oncogene-induced replicative stress for the selective killing of Myc-driven tumors', *Nat Struct Mol Biol*, 18: 1331-35.

Muto, Y., T. Furihata, M. Kaneko, K. Higuchi, K. Okunushi, H. Morio, Y. Reien, M. Uesato, H. Matsubara, and N. Anzai. 2019. 'Different Response Profiles of Gastrointestinal Cancer Cells to an L-Type Amino Acid Transporter Inhibitor, JPH203', *Anticancer Res*, 39: 159-65.

Nagai, Y., M. Oitate, H. Shiozawa, and O. Ando. 2019. 'Comprehensive preclinical pharmacokinetic evaluations of trastuzumab deruxtecan (DS-8201a), a HER2-targeting antibody-drug conjugate, in cynomolgus monkeys', *Xenobiotica*, 49: 1086-96.

Nagel, R., A. T. Avelar, N. Aben, N. Proost, M. van de Ven, J. van der Vliet, M. Cozijnsen, H. de Vries, L. F. A. Wessels, and A. Berns. 2019. 'Inhibition of the Replication Stress Response Is a Synthetic Vulnerability in SCLC That Acts Synergistically in Combination with Cisplatin', *Mol Cancer Ther*, 18: 762-70.

Nakada, T., K. Sugihara, T. Jikoh, Y. Abe, and T. Agatsuma. 2019. 'The Latest Research and Development into the Antibody-Drug Conjugate, [fam-] Trastuzumab Deruxtecan (DS-8201a), for HER2 Cancer Therapy', *Chem Pharm Bull (Tokyo)*, 67: 173-85.

Nakanishi, T., M. Sugawara, W. Huang, R. G. Martindale, F. H. Leibach, M. E. Ganapathy, P. D. Prasad, and V. Ganapathy. 2001. 'Structure, function, and tissue expression pattern of human SN2, a subtype of the amino acid transport system N', *Biochem Biophys Res Commun*, 281: 1343-8.

Nam, E. A., R. Zhao, G. G. Glick, C. E. Bansbach, D. B. Friedman, and D. Cortez. 2011. 'Thr-1989 phosphorylation is a marker of active ataxia telangiectasia-mutated and Rad3-related (ATR) kinase', *J Biol Chem*, 286: 28707-14.

Narayan, P., C. L. Osgood, H. Singh, H. J. Chiu, T. K. Ricks, E. C. Y. Chow, J. Qiu, P. Song, J. Yu, F. Namuswe, M. Gutierrez-Lugo, S. Hou, W. F. Pierce, K. B. Goldberg, S. Tang, L. Amiri-Kordestani, M. R. Theoret, R. Pazdur, and J. A. Beaver. 2021. 'FDA Approval Summary: Fam-trastuzumab deruxtecan-nxki for the treatment of unresectable or metastatic HER2-positive breast cancer', *Clin Cancer Res*.

NICE. 2020. 'Colorectal cancer NICE guideline [NG151]', Accessed 03/06/2020. https://www.nice.org.uk/guidance/ng151/chapter/Recommendations.

NICE. 2021. 'Trastuzumab deruxtecan for treating HER2-positive unresectable or metastatic breast cancer after 2 or more anti-HER2 therapies'. https://www.nice.org.uk/guidance/ta704.

NIH. 2020. 'Cancer Stat Facts: Colorectal Cancer'.

Nikkilä, J., R. Kumar, J. Campbell, I. Brandsma, H. N. Pemberton, F. Wallberg, K. Nagy, I. Scheer, B. G. Vertessy, A. A. Serebrenik, V. Monni, R. S. Harris, S. J. Pettitt, A. Ashworth, and C. J. Lord. 2017. 'Elevated APOBEC3B expression drives a kataegic-like mutation signature and replication stress-related therapeutic vulnerabilities in p53-defective cells', *Br J Cancer*, 117: 113-23.

Nishida, H., N. Tatewaki, Y. Nakajima, T. Magara, K. M. Ko, Y. Hamamori, and T. Konishi. 2009. 'Inhibition of ATR protein kinase activity by schisandrin B in DNA damage response', *Nucleic Acids Res*, 37: 5678-89.

Nitiss, J. L. 2009a. 'DNA topoisomerase II and its growing repertoire of biological functions', *Nat Rev Cancer*, 9: 327-37.

Nitiss, J. L. 2009b. 'Targeting DNA topoisomerase II in cancer chemotherapy', *Nat Rev Cancer*, 9: 338-50.

Nitiss, J., and J. C. Wang. 1988. 'DNA topoisomerase-targeting antitumor drugs can be studied in yeast', *Proc Natl Acad Sci U S A*, 85: 7501-5.

Nozawa, T., H. Minami, S. Sugiura, A. Tsuji, and I. Tamai. 2005. 'Role of organic anion transporter OATP1B1 (OATP-C) in hepatic uptake of irinotecan and its active metabolite, 7-ethyl-10-hydroxycamptothecin: in vitro evidence and effect of single nucleotide polymorphisms', *Drug Metab Dispos*, 33: 434-9.

Nozawa, T., M. Suzuki, H. Yabuuchi, M. Irokawa, A. Tsuji, and I. Tamai. 2005. 'Suppression of cell proliferation by inhibition of estrone-3-sulfate transporter in estrogen-dependent breast cancer cells', *Pharm Res*, 22: 1634-41.

O'Driscoll, M., V. L. Ruiz-Perez, C. G. Woods, P. A. Jeggo, and J. A. Goodship. 2003. 'A splicing mutation affecting expression of ataxia-telangiectasia and Rad3-related protein (ATR) results in Seckel syndrome', *Nat Genet*, 33: 497-501.

O'Sullivan Coyne, Geraldine Helen, Khanh Tu Do, Shivaani Kummar, Naoko Takebe, Mary Flanagan Quinn, Sarina Anne Piha-Paul, Ashley Bruns, Lamin Juwara, Elad Sharon, Richard Piekarz, Howard Streicher, Larry Rubinstein, Deborah Wilsker, Robert J. Kinders, Ralph E. Parchment, Elliot B. Levy, Austin Doyle, James H. Doroshow, and Alice P. Chen. 2018. 'Phase I trial of the triplet M6620 (formerly VX970) + veliparib + cisplatin in patients with advanced solid tumors', *Journal of Clinical Oncology*, 36: 2549-49.

Ochi, T., A. N. Blackford, J. Coates, S. Jhujh, S. Mehmood, N. Tamura, J. Travers, Q. Wu, V. M. Draviam, C. V. Robinson, T. L. Blundell, and S. P. Jackson. 2015. 'DNA repair. PAXX, a paralog of XRCC4 and XLF, interacts with Ku to promote DNA double-strand break repair', *Science*, 347: 185-88.

Ogitani, Y., T. Aida, K. Hagihara, J. Yamaguchi, C. Ishii, N. Harada, M. Soma, H. Okamoto, M. Oitate, S. Arakawa, T. Hirai, R. Atsumi, T. Nakada, I. Hayakawa, Y. Abe, and T. Agatsuma. 2016. 'DS-8201a, A Novel HER2-Targeting ADC with a Novel DNA Topoisomerase I Inhibitor, Demonstrates a Promising Antitumor Efficacy with Differentiation from T-DM1', *Clin Cancer Res*, 22: 5097-108.

Ogitani, Y., K. Hagihara, M. Oitate, H. Naito, and T. Agatsuma. 2016. 'Bystander killing effect of DS-8201a, a novel anti-human epidermal growth factor receptor 2 antibody-drug conjugate, in tumors with human epidermal growth factor receptor 2 heterogeneity', *Cancer Sci*, 107: 1039-46.

Okamoto, H., M. Oitate, K. Hagihara, H. Shiozawa, Y. Furuta, Y. Ogitani, and H. Kuga. 2020. 'Pharmacokinetics of trastuzumab deruxtecan (T-DXd), a novel anti-HER2 antibody-drug conjugate, in HER2-positive tumour-bearing mice', *Xenobiotica*, 50: 1242-50.

Olive, P. L. 2002. 'The comet assay. An overview of techniques', *Methods Mol Biol*, 203: 179-94.

Oroudjev, E., M. Lopus, L. Wilson, C. Audette, C. Provenzano, H. Erickson, Y. Kovtun, R. Chari, and M. A. Jordan. 2010. 'Maytansinoid-antibody conjugates induce mitotic arrest by suppressing microtubule dynamic instability', *Mol Cancer Ther*, 9: 2700-13.

Pabla, N., S. Huang, Q. S. Mi, R. Daniel, and Z. Dong. 2008. 'ATR-Chk2 signaling in p53 activation and DNA damage response during cisplatin-induced apoptosis', *J Biol Chem*, 283: 6572-83.

Panowski, S., S. Bhakta, H. Raab, P. Polakis, and J. R. Junutula. 2014. 'Site-specific antibody drug conjugates for cancer therapy', *MAbs*, 6: 34-45.

Parker, B. S., J. Rautela, and P. J. Hertzog. 2016. 'Antitumour actions of interferons: implications for cancer therapy', *Nat Rev Cancer*, 16: 131-44.

Parsels, L. A., J. D. Parsels, D. M. Tanska, J. Maybaum, T. S. Lawrence, and M. A. Morgan. 2018. 'The contribution of DNA replication stress marked by high-intensity, pan-nuclear γH2AX staining to chemosensitization by CHK1 and WEE1 inhibitors', *Cell Cycle*, 17: 1076-86.

Peasland, A., L. Z. Wang, E. Rowling, S. Kyle, T. Chen, A. Hopkins, W. A. Cliby, J. Sarkaria, G. Beale, R. J. Edmondson, and N. J. Curtin. 2011. 'Identification and evaluation of a potent novel ATR inhibitor, NU6027, in breast and ovarian cancer cell lines', *Br J Cancer*, 105: 372-81.

Peeters, M., T. J. Price, A. Cervantes, A. F. Sobrero, M. Ducreux, Y. Hotko, T. André, E. Chan, F. Lordick, C. J. Punt, A. H. Strickland, G. Wilson, T. E. Ciuleanu, L. Roman, E. Van Cutsem, V. Tzekova, S. Collins, K. S. Oliner, A. Rong, and J. Gansert. 2010. 'Randomized phase III study of panitumumab with fluorouracil, leucovorin, and irinotecan (FOLFIRI) compared with FOLFIRI alone as second-line treatment in patients with metastatic colorectal cancer', *J Clin Oncol*, 28: 4706-13.

Pellegrini, M., A. Celeste, S. Difilippantonio, R. Guo, W. Wang, L. Feigenbaum, and A. Nussenzweig. 2006. 'Autophosphorylation at serine 1987 is dispensable for murine Atm activation in vivo', *Nature*, 443: 222-5.

Peng, C. Y., P. R. Graves, R. S. Thoma, Z. Wu, A. S. Shaw, and H. Piwnica-Worms. 1997. 'Mitotic and G2 checkpoint control: regulation of 14-3-3 protein binding by phosphorylation of Cdc25C on serine-216', *Science*, 277: 1501-5.

Pentheroudakis, G., and C. Twelves. 2002. 'The rational development of capecitabine from the laboratory to the clinic', *Anticancer Res*, 22: 3589-96.

Perry, J., and N. Kleckner. 2003. 'The ATRs, ATMs, and TORs are giant HEAT repeat proteins', *Cell*, 112: 151-5.

Peters, C., and S. Brown. 2015. 'Antibody-drug conjugates as novel anti-cancer chemotherapeutics', *Biosci Rep*, 35.

Petersdorf, S. H., K. J. Kopecky, M. Slovak, C. Willman, T. Nevill, J. Brandwein, R. A. Larson, H. P. Erba, P. J. Stiff, R. K. Stuart, R. B. Walter, M. S. Tallman, L. Stenke, and F. R. Appelbaum. 2013. 'A phase 3 study of gemtuzumab ozogamicin during induction and postconsolidation therapy in younger patients with acute myeloid leukemia', *Blood*, 121: 4854-60.

Pfister, S. X., E. Markkanen, Y. Jiang, S. Sarkar, M. Woodcock, G. Orlando, I. Mavrommati, C. C. Pai, L. P. Zalmas, N. Drobnitzky, G. L. Dianov, C. Verrill, V. M. Macaulay, S. Ying, N. B. La Thangue, V. D'Angiolella, A. J. Ryan, and T. C. Humphrey. 2015. 'Inhibiting WEE1 Selectively Kills Histone H3K36me3-Deficient Cancers by dNTP Starvation', *Cancer Cell*, 28: 557-68.

Phan, L. M., and A. H. Rezaeian. 2021. 'ATM: Main Features, Signaling Pathways, and Its Diverse Roles in DNA Damage Response, Tumor Suppression, and Cancer Development', *Genes (Basel)*, 12.

Pichierri, P., F. Rosselli, and A. Franchitto. 2003. 'Werner's syndrome protein is phosphorylated in an ATR/ATM-dependent manner following replication arrest and DNA damage induced during the S phase of the cell cycle', *Oncogene*, 22: 1491-500.

Pimm, M. V., M. A. Paul, Y. Ogumuyiwa, and R. W. Baldwin. 1988. 'Biodistribution and tumour localisation of a daunomycin-monoclonal antibody conjugate in nude mice with human tumour xenografts', *Cancer Immunol Immunother*, 27: 267-71.

Pires, I. M., M. M. Olcina, S. Anbalagan, J. R. Pollard, P. M. Reaper, P. A. Charlton, W. G. McKenna, and E. M. Hammond. 2012. 'Targeting radiation-resistant hypoxic tumour cells through ATR inhibition', *Br J Cancer*, 107: 291-9.

Plummer, Elizabeth Ruth, Natalie Cook, Hendrik-Tobias Arkenau, Jason M. Melear, Charles H. Redfern, Alexander I. Spira, Ki Y. Chung, Geoffrey Shapiro, Tufia C. Haddad, Suresh S. Ramalingam, Robert Wesolowski, Thomas Goddemeier, Martin H. Falk, and Emma Dean. 2018. 'Dose expansion cohort of a phase I trial of M6620 (formerly VX-970), a

first-in-class ATR inhibitor, combined with gemcitabine (Gem) in patients (pts) with advanced non-small cell lung cancer (NSCLC)', *Journal of Clinical Oncology*, 36: e21048-e48.

Polgar, O., R. W. Robey, and S. E. Bates. 2008. 'ABCG2: structure, function and role in drug response', *Expert Opin Drug Metab Toxicol*, 4: 1-15.

Pommier, Y. 2006. 'Topoisomerase I inhibitors: camptothecins and beyond', *Nat Rev Cancer*, 6: 789-802.

Pommier, Y., Y. Sun, S. N. Huang, and J. L. Nitiss. 2016. 'Roles of eukaryotic topoisomerases in transcription, replication and genomic stability', *Nat Rev Mol Cell Biol*, 17: 703-21.

Pondé, N., P. Aftimos, and M. Piccart. 2019. 'Antibody-Drug Conjugates in Breast Cancer: a Comprehensive Review', *Curr Treat Options Oncol*, 20: 37.

Press, M. F., C. Cordon-Cardo, and D. J. Slamon. 1990. 'Expression of the HER-2/neu proto-oncogene in normal human adult and fetal tissues', *Oncogene*, 5: 953-62.

Prevo, R., E. Fokas, P. M. Reaper, P. A. Charlton, J. R. Pollard, W. G. McKenna, R. J. Muschel, and T. B. Brunner. 2012. 'The novel ATR inhibitor VE-821 increases sensitivity of pancreatic cancer cells to radiation and chemotherapy', *Cancer Biol Ther*, 13: 1072-81.

Price, T. J., M. Peeters, T. W. Kim, J. Li, S. Cascinu, P. Ruff, A. S. Suresh, A. Thomas, S. Tjulandin, K. Zhang, S. Murugappan, and R. Sidhu. 2014. 'Panitumumab versus cetuximab in patients with chemotherapy-refractory wild-type KRAS exon 2 metastatic colorectal cancer (ASPECCT): a randomised, multicentre, open-label, non-inferiority phase 3 study', *Lancet Oncol*, 15: 569-79.

Qin, X., J. Sufi, P. Vlckova, P. Kyriakidou, S. E. Acton, V. S. W. Li, M. Nitz, and C. J. Tape. 2020. 'Cell-type-specific signaling networks in heterocellular organoids', *Nat Methods*, 17: 335-42.

Rabik, C. A., and M. E. Dolan. 2007. 'Molecular mechanisms of resistance and toxicity associated with platinating agents', *Cancer Treat Rev*, 33: 9-23.

Rabindran, S. K., D. D. Ross, L. A. Doyle, W. Yang, and L. M. Greenberger. 2000. 'Fumitremorgin C reverses multidrug resistance in cells transfected with the breast cancer resistance protein', *Cancer Res*, 60: 47-50.

Ragland, R. L., S. Patel, R. S. Rivard, K. Smith, A. A. Peters, A. K. Bielinsky, and E. J. Brown. 2013. 'RNF4 and PLK1 are required for replication fork collapse in ATR-deficient cells', *Genes Dev*, 27: 2259-73.

Raymond, E., S. Faivre, S. Chaney, J. Woynarowski, and E. Cvitkovic. 2002. 'Cellular and molecular pharmacology of oxaliplatin', *Mol Cancer Ther*, 1: 227-35.

Reaper, P. M., M. R. Griffiths, J. M. Long, J. D. Charrier, S. Maccormick, P. A. Charlton, J. M. Golec, and J. R. Pollard. 2011. 'Selective killing of ATM- or p53-deficient cancer cells through inhibition of ATR', *Nat Chem Biol*, 7: 428-30.

Redman, J. M., E. M. Hill, D. AlDeghaither, and L. M. Weiner. 2015. 'Mechanisms of action of therapeutic antibodies for cancer', *Mol Immunol*, 67: 28-45.

Rehman, I., S. M. Basu, S. K. Das, S. Bhattacharjee, A. Ghosh, Y. Pommier, and B. B. Das. 2018. 'PRMT5-mediated arginine methylation of TDP1 for the repair of topoisomerase I covalent complexes', *Nucleic Acids Res*, 46: 5601-17.

Ricart, A. D. 2011. 'Antibody-drug conjugates of calicheamicin derivative: gemtuzumab ozogamicin and inotuzumab ozogamicin', *Clin Cancer Res*, 17: 6417-27.

Rios-Doria, J., J. Harper, R. Rothstein, L. Wetzel, J. Chesebrough, A. Marrero, C. Chen, P. Strout, K. Mulgrew, K. McGlinchey, R. Fleming, B. Bezabeh, J. Meekin, D. Stewart, M. Kennedy, P. Martin, A. Buchanan, N. Dimasi, E. Michelotti, and R. Hollingsworth. 2017. 'Antibody-Drug Conjugates Bearing Pyrrolobenzodiazepine or Tubulysin Payloads Are Immunomodulatory and Synergize with Multiple Immunotherapies', *Cancer Res*, 77: 2686-98.

Ritchie, M., L. Tchistiakova, and N. Scott. 2013. 'Implications of receptor-mediated endocytosis and intracellular trafficking dynamics in the development of antibody drug conjugates', *MAbs*, 5: 13-21.

Rogakou, E. P., D. R. Pilch, A. H. Orr, V. S. Ivanova, and W. M. Bonner. 1998. 'DNA double-stranded breaks induce histone H2AX phosphorylation on serine 139', *J Biol Chem*, 273: 5858-68.

Roos, W. P., A. D. Thomas, and B. Kaina. 2016. 'DNA damage and the balance between survival and death in cancer biology', *Nat Rev Cancer*, 16: 20-33.

Ross, J. S., M. Fakih, S. M. Ali, J. A. Elvin, A. B. Schrock, J. Suh, J. A. Vergilio, S. Ramkissoon, E. Severson, S. Daniel, D. Fabrizio, G. Frampton, J. Sun, V. A. Miller, P. J. Stephens, and L. M. Gay. 2018. 'Targeting HER2 in colorectal cancer: The landscape of amplification and short variant mutations in ERBB2 and ERBB3', *Cancer*, 124: 1358-73.

Rouits, E., M. Boisdron-Celle, A. Dumont, O. Guérin, A. Morel, and E. Gamelin. 2004. 'Relevance of different UGT1A1 polymorphisms in irinotecan-induced toxicity: a molecular and clinical study of 75 patients', *Clin Cancer Res*, 10: 5151-9.

Rowland, A. J., G. A. Pietersz, and I. F. McKenzie. 1993. 'Preclinical investigation of the antitumour effects of anti-CD19-idarubicin immunoconjugates', *Cancer Immunol Immunother*, 37: 195-202.

Ruiz, S., C. Mayor-Ruiz, V. Lafarga, M. Murga, M. Vega-Sendino, S. Ortega, and O. Fernandez-Capetillo. 2016. 'A Genome-wide CRISPR Screen Identifies CDC25A as a Determinant of Sensitivity to ATR Inhibitors', *Mol Cell*, 62: 307-13.

Ruzankina, Y., D. W. Schoppy, A. Asare, C. E. Clark, R. H. Vonderheide, and E. J. Brown. 2009. 'Tissue regenerative delays and synthetic lethality in adult mice after combined deletion of Atr and Trp53', *Nat Genet*, 41: 1144-9.

Sabini, E., S. Hazra, S. Ort, M. Konrad, and A. Lavie. 2008. 'Structural basis for substrate promiscuity of dCK', *J Mol Biol*, 378: 607-21.

Sacho, E. J., and N. Maizels. 2011. 'DNA repair factor MRE11/RAD50 cleaves 3'-phosphotyrosyl bonds and resects DNA to repair damage caused by topoisomerase 1 poisons', *J Biol Chem*, 286: 44945-51.

Salceda, J., X. Fernández, and J. Roca. 2006. 'Topoisomerase II, not topoisomerase I, is the proficient relaxase of nucleosomal DNA', *Embo j*, 25: 2575-83.

Saldivar, J. C., S. Hamperl, M. J. Bocek, M. Chung, T. E. Bass, F. Cisneros-Soberanis, K. Samejima, L. Xie, J. R. Paulson, W. C. Earnshaw, D. Cortez, T. Meyer, and K. A. Cimprich. 2018. 'An intrinsic S/G(2) checkpoint enforced by ATR', *Science*, 361: 806-10.

Salphati, L., E. G. Plise, and G. Li. 2009. 'Expression and activity of the efflux transporters ABCB1, ABCC2 and ABCG2 in the human colorectal carcinoma cell line LS513', *Eur J Pharm Sci*, 37: 463-8.

Saltz, L. B., S. Clarke, E. Díaz-Rubio, W. Scheithauer, A. Figer, R. Wong, S. Koski, M. Lichinitser, T. S. Yang, F. Rivera, F. Couture, F. Sirzén, and J. Cassidy. 2008. 'Bevacizumab in combination with oxaliplatin-based chemotherapy as first-line therapy in metastatic colorectal cancer: a randomized phase III study', *J Clin Oncol*, 26: 2013-9.

Saltz, L. B., J. Y. Douillard, N. Pirotta, M. Alakl, G. Gruia, L. Awad, G. L. Elfring, P. K. Locker, and L. L. Miller. 2001. 'Irinotecan plus fluorouracil/leucovorin for metastatic colorectal cancer: a new survival standard', *Oncologist*, 6: 81-91.

Sanchez, Y., C. Wong, R. S. Thoma, R. Richman, Z. Wu, H. Piwnica-Worms, and S. J. Elledge. 1997. 'Conservation of the Chk1 checkpoint pathway in mammals: linkage of DNA damage to Cdk regulation through Cdc25', *Science*, 277: 1497-501.

Sansam, C. L., N. M. Cruz, P. S. Danielian, A. Amsterdam, M. L. Lau, N. Hopkins, and J. A. Lees. 2010. 'A vertebrate gene, ticrr, is an essential checkpoint and replication regulator', *Genes Dev*, 24: 183-94.

Santi, D. V., C. S. McHenry, and H. Sommer. 1974. 'Mechanism of interaction of thymidylate synthetase with 5-fluorodeoxyuridylate', *Biochemistry*, 13: 471-81.

Sarkaria, J. N., E. C. Busby, R. S. Tibbetts, P. Roos, Y. Taya, L. M. Karnitz, and R. T. Abraham. 1999. 'Inhibition of ATM and ATR kinase activities by the radiosensitizing agent, caffeine', *Cancer Res*, 59: 4375-82.

Sarmento, L. M., V. Póvoa, R. Nascimento, G. Real, I. Antunes, L. R. Martins, C. Moita, P. M. Alves, M. Abecasis, L. F. Moita, R. M. Parkhouse, J. P. Meijerink, and J. T. Barata. 2015. 'CHK1 overexpression in T-cell acute lymphoblastic leukemia is essential for proliferation and survival by preventing excessive replication stress', *Oncogene*, 34: 2978-90.

Sartori, A. A., C. Lukas, J. Coates, M. Mistrik, S. Fu, J. Bartek, R. Baer, J. Lukas, and S. P. Jackson. 2007. 'Human CtIP promotes DNA end resection', *Nature*, 450: 509-14.

Scartozzi, M., I. Bearzi, C. Pierantoni, A. Mandolesi, F. Loupakis, A. Zaniboni, V. Catalano, A. Quadri, F. Zorzi, R. Berardi, T. Biscotti, R. Labianca, A. Falcone, and S. Cascinu. 2007. 'Nuclear factor-kB tumor expression predicts response and survival in irinotecan-refractory metastatic colorectal cancer treated with cetuximab-irinotecan therapy', *J Clin Oncol*, 25: 3930-5.

Schalper, K. A., S. Kumar, P. Hui, D. L. Rimm, and P. Gershkovich. 2014. 'A retrospective population-based comparison of HER2 immunohistochemistry and fluorescence in situ hybridization in breast carcinomas: impact of 2007 American Society of Clinical Oncology/College of American Pathologists criteria', *Arch Pathol Lab Med*, 138: 213-9.

Schmitt, A., G. Knittel, D. Welcker, T. P. Yang, J. George, M. Nowak, U. Leeser, R. Büttner, S. Perner, M. Peifer, and H. C. Reinhardt. 2017. 'ATM Deficiency Is Associated with Sensitivity to PARP1- and ATR Inhibitors in Lung Adenocarcinoma', *Cancer Res*, 77: 3040-56.

Schoonen, P. M., Y. P. Kok, E. Wierenga, B. Bakker, F. Foijer, D. C. J. Spierings, and Matm van Vugt. 2019. 'Premature mitotic entry induced by ATR inhibition potentiates olaparib inhibition-mediated genomic instability, inflammatory signaling, and cytotoxicity in BRCA2-deficient cancer cells', *Mol Oncol*, 13: 2422-40.

Schoppy, D. W., R. L. Ragland, O. Gilad, N. Shastri, A. A. Peters, M. Murga, O. Fernandez-Capetillo, J. A. Diehl, and E. J. Brown. 2012. 'Oncogenic stress sensitizes murine cancers to hypomorphic suppression of ATR', *J Clin Invest*, 122: 241-52.

Schulze, J., A. J. Lopez-Contreras, Ö Uluçkan, O. Graña-Castro, O. Fernandez-Capetillo, and E. F. Wagner. 2014. 'Fos-dependent induction of Chk1 protects osteoblasts from replication stress', *Cell Cycle*, 13: 1980-6.

Schuurman, J., and P. W. Parren. 2016. 'Editorial overview: Special section: New concepts in antibody therapeutics: What's in store for antibody therapy?', *Curr Opin Immunol*, 40: vii-xiii.

Scripture, C. D., and W. D. Figg. 2006. 'Drug interactions in cancer therapy', *Nat Rev Cancer*, 6: 546-58.

Seiler, J. A., C. Conti, A. Syed, M. I. Aladjem, and Y. Pommier. 2007. 'The intra-S-phase checkpoint affects both DNA replication initiation and elongation: single-cell and -DNA fiber analyses', *Mol Cell Biol*, 27: 5806-18.

Seinsoth, S., H. Uhlmann-Schiffler, and H. Stahl. 2003. 'Bidirectional DNA unwinding by a ternary complex of T antigen, nucleolin and topoisomerase I', *EMBO Rep*, 4: 263-8.

Seymour, M. T., S. R. Brown, G. Middleton, T. Maughan, S. Richman, S. Gwyther, C. Lowe, J. F. Seligmann, J. Wadsley, N. Maisey, I. Chau, M. Hill, L. Dawson, S. Falk, A. O'Callaghan, K. Benstead, P. Chambers, A. Oliver, H. Marshall, V. Napp, and P. Quirke. 2013. 'Panitumumab and irinotecan versus irinotecan alone for patients with KRAS wild-type, fluorouracil-resistant advanced colorectal cancer (PICCOLO): a prospectively stratified randomised trial', *Lancet Oncol*, 14: 749-59.

Shanbhag, N. M., I. U. Rafalska-Metcalf, C. Balane-Bolivar, S. M. Janicki, and R. A. Greenberg. 2010. 'ATM-dependent chromatin changes silence transcription in cis to DNA double-strand breaks', *Cell*, 141: 970-81.

Shapiro, G. I., R. Wesolowski, C. Devoe, S. Lord, J. Pollard, B. S. Hendriks, M. Falk, I. Diaz-Padilla, R. Plummer, and T. A. Yap. 2021. 'Phase 1 study of the ATR inhibitor berzosertib in combination with cisplatin in patients with advanced solid tumours', *Br J Cancer*.

Sheng, H., Y. Huang, Y. Xiao, Z. Zhu, M. Shen, P. Zhou, Z. Guo, J. Wang, H. Wang, W. Dai, W. Zhang, J. Sun, and C. Cao. 2020. 'ATR inhibitor AZD6738 enhances the antitumor activity of radiotherapy and immune checkpoint inhibitors by potentiating the tumor immune microenvironment in hepatocellular carcinoma', *J Immunother Cancer*, 8.

Shi, Q., L. Y. Shen, B. Dong, H. Fu, X. Z. Kang, Y. B. Yang, L. Dai, W. P. Yan, H. C. Xiong, Z. Liang, and K. N. Chen. 2018. 'The identification of the ATR inhibitor VE-822 as a therapeutic strategy for enhancing cisplatin chemosensitivity in esophageal squamous cell carcinoma', *Cancer Lett*, 432: 56-68.

Shieh, S. Y., M. Ikeda, Y. Taya, and C. Prives. 1997. 'DNA damage-induced phosphorylation of p53 alleviates inhibition by MDM2', *Cell*, 91: 325-34.

Shigechi, T., J. Tomida, K. Sato, M. Kobayashi, J. K. Eykelenboom, F. Pessina, Y. Zhang, E. Uchida, M. Ishiai, N. F. Lowndes, K. Yamamoto, H. Kurumizaka, Y. Maehara, and M. Takata. 2012. 'ATR-ATRIP kinase complex triggers activation of the Fanconi anemia DNA repair pathway', *Cancer Res*, 72: 1149-56.

Shiloh, Y., and Y. Ziv. 2013. 'The ATM protein kinase: regulating the cellular response to genotoxic stress, and more', *Nat Rev Mol Cell Biol*, 14: 197-210.

Shitara, K., Y. J. Bang, S. Iwasa, N. Sugimoto, M. H. Ryu, D. Sakai, H. C. Chung, H. Kawakami, H. Yabusaki, J. Lee, K. Saito, Y. Kawaguchi, T. Kamio, A. Kojima, M. Sugihara, and K. Yamaguchi. 2020. 'Trastuzumab Deruxtecan in Previously Treated HER2-Positive Gastric Cancer', *N Engl J Med*, 382: 2419-30.

Shitara, K., H. Iwata, S. Takahashi, K. Tamura, H. Park, S. Modi, J. Tsurutani, S. Kadowaki, K. Yamaguchi, S. Iwasa, K. Saito, Y. Fujisaki, M. Sugihara, J. Shahidi, and T. Doi. 2019. 'Trastuzumab deruxtecan (DS-8201a) in patients with advanced HER2-positive gastric cancer: a dose-expansion, phase 1 study', *Lancet Oncol*, 20: 827-36.

Shklovskaya, E., and H. Rizos. 2021. 'MHC Class I Deficiency in Solid Tumors and Therapeutic Strategies to Overcome It', *Int J Mol Sci*, 22.

Shykind, B. M., J. Kim, L. Stewart, J. J. Champoux, and P. A. Sharp. 1997. 'Topoisomerase I enhances TFIID-TFIIA complex assembly during activation of transcription', *Genes Dev*, 11: 397-407.

Siegel, R. L., L. A. Torre, I. Soerjomataram, R. B. Hayes, F. Bray, T. K. Weber, and A. Jemal. 2019. 'Global patterns and trends in colorectal cancer incidence in young adults', *Gut*, 68: 2179-85.

Siena, S., M. Di Bartolomeo, K. Raghav, T. Masuishi, F. Loupakis, H. Kawakami, K. Yamaguchi, T. Nishina, M. Fakih, E. Elez, J. Rodriguez, F. Ciardiello, Y. Komatsu, T. Esaki, K. Chung, Z. Wainberg, A. Sartore-Bianchi, K. Saxena, E. Yamamoto, E. Bako, Y. Okuda, J. Shahidi, A. Grothey, and T. Yoshino. 2021. 'Trastuzumab deruxtecan (DS-8201) in patients with HER2-expressing metastatic colorectal cancer (DESTINY-CRC01): a multicentre, open-label, phase 2 trial', *Lancet Oncol*, 22: 779-89.

Siena, S., A. Sartore-Bianchi, S. Marsoni, H. I. Hurwitz, S. J. McCall, F. Penault-Llorca, S. Srock, A. Bardelli, and L. Trusolino. 2018. 'Targeting the human epidermal growth factor receptor 2 (HER2) oncogene in colorectal cancer', *Ann Oncol*, 29: 1108-19.

Sievers, E. L., and M. Linenberger. 2001. 'Mylotarg: antibody-targeted chemotherapy comes of age', *Curr Opin Oncol*, 13: 522-7.

Sievers, E. L., and P. D. Senter. 2013. 'Antibody-drug conjugates in cancer therapy', *Annu Rev Med*, 64: 15-29.

Singh, T. R., A. M. Ali, M. Paramasivam, A. Pradhan, K. Wahengbam, M. M. Seidman, and A. R. Meetei. 2013. 'ATR-dependent phosphorylation of FANCM at serine 1045 is essential for FANCM functions', *Cancer Res*, 73: 4300-10.

Singleton, B. K., M. I. Torres-Arzayus, S. T. Rottinghaus, G. E. Taccioli, and P. A. Jeggo. 1999. 'The C terminus of Ku80 activates the DNA-dependent protein kinase catalytic subunit', *Mol Cell Biol*, 19: 3267-77.

Sirbu, B. M., F. B. Couch, J. T. Feigerle, S. Bhaskara, S. W. Hiebert, and D. Cortez. 2011. 'Analysis of protein dynamics at active, stalled, and collapsed replication forks', *Genes Dev*, 25: 1320-7.

Slamon, D. J., B. Leyland-Jones, S. Shak, H. Fuchs, V. Paton, A. Bajamonde, T. Fleming, W. Eiermann, J. Wolter, M. Pegram, J. Baselga, and L. Norton. 2001. 'Use of chemotherapy plus a monoclonal antibody against HER2 for metastatic breast cancer that overexpresses HER2', *N Engl J Med*, 344: 783-92.

Smith, G., F. A. Carey, J. Beattie, M. J. Wilkie, T. J. Lightfoot, J. Coxhead, R. C. Garner, R. J. Steele, and C. R. Wolf. 2002. 'Mutations in APC, Kirsten-ras, and p53--alternative genetic pathways to colorectal cancer', *Proc Natl Acad Sci U S A*, 99: 9433-8.

Smits, V. A., and D. A. Gillespie. 2015. 'DNA damage control: regulation and functions of checkpoint kinase 1', *Febs j*, 282: 3681-92.

Smits, V. A., P. M. Reaper, and S. P. Jackson. 2006. 'Rapid PIKK-dependent release of Chk1 from chromatin promotes the DNA-damage checkpoint response', *Curr Biol*, 16: 150-9.

Smogorzewska, A., S. Matsuoka, P. Vinciguerra, E. R. McDonald, 3rd, K. E. Hurov, J. Luo, B. A. Ballif, S. P. Gygi, K. Hofmann, A. D. D'Andrea, and S. J. Elledge. 2007. 'Identification of the FANCI protein, a monoubiquitinated FANCD2 paralog required for DNA repair', *Cell*, 129: 289-301.

Smyth, M. J., G. A. Pietersz, and I. F. McKenzie. 1987. 'Selective enhancement of antitumor activity of N-acetyl melphalan upon conjugation to monoclonal antibodies', *Cancer Res*, 47: 62-9.

Sommer, H., and D. V. Santi. 1974. 'Purification and amino acid analysis of an active site peptide from thymidylate synthetase containing covalently bound 5-fluoro-2'-deoxyuridylate and methylenetetrahydrofolate', *Biochem Biophys Res Commun*, 57: 689-95.

Sørensen, C. S., L. T. Hansen, J. Dziegielewski, R. G. Syljuåsen, C. Lundin, J. Bartek, and T. Helleday. 2005. 'The cell-cycle checkpoint kinase Chk1 is required for mammalian homologous recombination repair', *Nat Cell Biol*, 7: 195-201.

Sørensen, C. S., R. G. Syljuåsen, J. Falck, T. Schroeder, L. Rönnstrand, K. K. Khanna, B. B. Zhou, J. Bartek, and J. Lukas. 2003. 'Chk1 regulates the S phase checkpoint by coupling the physiological turnover and ionizing radiation-induced accelerated proteolysis of Cdc25A', *Cancer Cell*, 3: 247-58.

Souglakos, J., N. Androulakis, K. Syrigos, A. Polyzos, N. Ziras, A. Athanasiadis, S. Kakolyris, S. Tsousis, Ch Kouroussis, L. Vamvakas, A. Kalykaki, G. Samonis, D. Mavroudis, and V. Georgoulias. 2006. 'FOLFOXIRI (folinic acid, 5-fluorouracil, oxaliplatin and irinotecan) vs FOLFIRI (folinic acid, 5-fluorouracil and irinotecan) as first-line treatment in metastatic colorectal cancer (MCC): a multicentre randomised phase III trial from the Hellenic Oncology Research Group (HORG)', *Br J Cancer*, 94: 798-805.

Spearman, M. E., R. M. Goodwin, L. D. Apelgren, and T. F. Bumol. 1987. 'Disposition of the monoclonal antibody-vinca alkaloid conjugate KS1/4-DAVLB (LY256787) and free 4-desacetylvinblastine in tumor-bearing nude mice', *J Pharmacol Exp Ther*, 241: 695-703.

Spruck, C. H., K. A. Won, and S. I. Reed. 1999. 'Deregulated cyclin E induces chromosome instability', *Nature*, 401: 297-300.

Stenmark, H. 2009. 'Rab GTPases as coordinators of vesicle traffic', *Nat Rev Mol Cell Biol*, 10: 513-25.

Stenzinger, A., N. Pfarr, V. Endris, R. Penzel, L. Jansen, T. Wolf, E. Herpel, A. Warth, F. Klauschen, M. Kloor, W. Roth, H. Bläker, J. Chang-Claude, H. Brenner, M. Hoffmeister, and W. Weichert. 2014. 'Mutations in POLE and survival of colorectal cancer patients--link to disease stage and treatment', *Cancer Med*, 3: 1527-38.

Stewart, L., M. R. Redinbo, X. Qiu, W. G. Hol, and J. J. Champoux. 1998. 'A model for the mechanism of human topoisomerase I', *Science*, 279: 1534-41.

Stolz, Ailine, Norman Ertych, and Holger Bastians. 2011. 'Tumor Suppressor CHK2: Regulator of DNA Damage Response and Mediator of Chromosomal Stability', *Clinical Cancer Research*, 17: 401.

Strebhardt, K., and A. Ullrich. 2008. 'Paul Ehrlich's magic bullet concept: 100 years of progress', *Nat Rev Cancer*, 8: 473-80.

Subramanian, A., P. Tamayo, V. K. Mootha, S. Mukherjee, B. L. Ebert, M. A. Gillette, A. Paulovich, S. L. Pomeroy, T. R. Golub, E. S. Lander, and J. P. Mesirov. 2005. 'Gene set enrichment analysis: a knowledge-based approach for interpreting genome-wide expression profiles', *Proc Natl Acad Sci U S A*, 102: 15545-50.

Sufi J., Qin X., Cardoso Rodriguez F., Bu Y., Vlckova P., Ramos Zapatero M., Nitz M., and Tape C.J. In press. 'Multiplexed Single-Cell Analysis of Organoid Signalling Networks', *Nature Protocols*.

Sultana, R., T. Abdel-Fatah, C. Perry, P. Moseley, N. Albarakti, V. Mohan, C. Seedhouse, S. Chan, and S. Madhusudan. 2013. 'Ataxia telangiectasia mutated and Rad3 related (ATR) protein kinase inhibition is synthetically lethal in XRCC1 deficient ovarian cancer cells', *PLoS One*, 8: e57098.

Sun, L., J. Wu, F. Du, X. Chen, and Z. J. Chen. 2013. 'Cyclic GMP-AMP synthase is a cytosolic DNA sensor that activates the type I interferon pathway', *Science*, 339: 786-91.

Sun, R., Y. Ying, Z. Tang, T. Liu, F. Shi, H. Li, T. Guo, S. Huang, and R. Lai. 2020. 'The Emerging Role of the SLCO1B3 Protein in Cancer Resistance', *Protein Pept Lett*, 27: 17-29.

Sun, Y., X. Jiang, S. Chen, N. Fernandes, and B. D. Price. 2005. 'A role for the Tip60 histone acetyltransferase in the acetylation and activation of ATM', *Proc Natl Acad Sci U S A*, 102: 13182-7.

Sun, Y., X. Jiang, Y. Xu, M. K. Ayrapetov, L. A. Moreau, J. R. Whetstine, and B. D. Price. 2009. 'Histone H3 methylation links DNA damage detection to activation of the tumour suppressor Tip60', *Nat Cell Biol*, 11: 1376-82.

Sun, Y., S. Saha, W. Wang, L. K. Saha, S. N. Huang, and Y. Pommier. 2020. 'Excision repair of topoisomerase DNA-protein crosslinks (TOP-DPC)', *DNA Repair (Amst)*, 89: 102837.

Sun, Y., Y. Xu, K. Roy, and B. D. Price. 2007. 'DNA damage-induced acetylation of lysine 3016 of ATM activates ATM kinase activity', *Mol Cell Biol*, 27: 8502-9.

Sundar, R., J. Brown, A. Ingles Russo, and T. A. Yap. 2017. 'Targeting ATR in cancer medicine', *Curr Probl Cancer*, 41: 302-15.

Sutherland, M. S., R. J. Sanderson, K. A. Gordon, J. Andreyka, C. G. Cerveny, C. Yu, T. S. Lewis, D. L. Meyer, R. F. Zabinski, S. O. Doronina, P. D. Senter, C. L. Law, and A. F. Wahl. 2006. 'Lysosomal trafficking and cysteine protease metabolism confer target-specific cytotoxicity by peptide-linked anti-CD30-auristatin conjugates', *J Biol Chem*, 281: 10540-7.

Sutherland, R., A. Meeson, and S. Lowes. 2020. 'Solute transporters and malignancy: establishing the role of uptake transporters in breast cancer and breast cancer metastasis', *Cancer Metastasis Rev*, 39: 919-32.

Suzuki, M., S. Yagishita, K. Sugihara, Y. Ogitani, T. Nishikawa, M. Ohuchi, T. Teishikata, T. Jikoh, Y. Yatabe, K. Yonemori, K. Tamura, K. Hasegawa, and A. Hamada. 2021. 'Visualization of Intratumor Pharmacokinetics of [fam-] Trastuzumab Deruxtecan (DS-8201a) in

HER2 Heterogeneous Model Using Phosphor-integrated Dots Imaging Analysis', *Clin Cancer Res*.

Svendsen, J. M., A. Smogorzewska, M. E. Sowa, B. C. O'Connell, S. P. Gygi, S. J. Elledge, and J. W. Harper. 2009. 'Mammalian BTBD12/SLX4 assembles a Holliday junction resolvase and is required for DNA repair', *Cell*, 138: 63-77.

Tabernero, J., T. Yoshino, A. L. Cohn, R. Obermannova, G. Bodoky, R. Garcia-Carbonero, T. E. Ciuleanu, D. C. Portnoy, E. Van Cutsem, A. Grothey, J. Prausová, P. Garcia-Alfonso, K. Yamazaki, P. R. Clingan, S. Lonardi, T. W. Kim, L. Simms, S. C. Chang, and F. Nasroulah. 2015. 'Ramucirumab versus placebo in combination with second-line FOLFIRI in patients with metastatic colorectal carcinoma that progressed during or after first-line therapy with bevacizumab, oxaliplatin, and a fluoropyrimidine (RAISE): a randomised, double-blind, multicentre, phase 3 study', *Lancet Oncol*, 16: 499-508.

Takahashi, T., Y. Fujiwara, M. Yamakido, O. Katoh, H. Watanabe, and P. I. Mackenzie. 1997. 'The role of glucuronidation in 7-ethyl-10-hydroxycamptothecin resistance in vitro', *Jpn J Cancer Res*, 88: 1211-7.

Takai, H., K. Tominaga, N. Motoyama, Y. A. Minamishima, H. Nagahama, T. Tsukiyama, K. Ikeda, K. Nakayama, M. Nakanishi, and K. Nakayama. 2000. 'Aberrant cell cycle checkpoint function and early embryonic death in Chk1(-/-) mice', *Genes Dev*, 14: 1439-47.

Takegawa, N., Y. Nonagase, K. Yonesaka, K. Sakai, O. Maenishi, Y. Ogitani, T. Tamura, K. Nishio, K. Nakagawa, and J. Tsurutani. 2017. 'DS-8201a, a new HER2-targeting antibody-drug conjugate incorporating a novel DNA topoisomerase I inhibitor, overcomes HER2-positive gastric cancer T-DM1 resistance', *Int J Cancer*, 141: 1682-89.

Takegawa, N., J. Tsurutani, H. Kawakami, K. Yonesaka, R. Kato, K. Haratani, H. Hayashi, M. Takeda, Y. Nonagase, O. Maenishi, and K. Nakagawa. 2019. '[fam-] trastuzumab deruxtecan, antitumor activity is dependent on HER2 expression level rather than on HER2 amplification', *Int J Cancer*, 145: 3414-24.

Takizawa, C. G., and D. O. Morgan. 2000. 'Control of mitosis by changes in the subcellular location of cyclin-B1-Cdk1 and Cdc25C', *Curr Opin Cell Biol*, 12: 658-65.

Talele, Surabhi, Afroz Mohammad, Minjee Kim, Danielle Burgenske, Ann C. Mladek Tuma, Jann N. Sarkaria, and William F. Elmquist. 2019. 'Abstract 4858: CNS delivery of VX-970: A selective ATR inhibitor for radiosensitization in GBM', *Cancer Res*, 79: 4858.

Tamura, K., J. Tsurutani, S. Takahashi, H. Iwata, I. E. Krop, C. Redfern, Y. Sagara, T. Doi, H. Park, R. K. Murthy, R. A. Redman, T. Jikoh, C. Lee, M. Sugihara, J. Shahidi, A. Yver, and S. Modi. 2019. 'Trastuzumab deruxtecan (DS-8201a) in patients with advanced HER2-positive breast cancer previously treated with trastuzumab emtansine: a dose-expansion, phase 1 study', *Lancet Oncol*, 20: 816-26.

Tanaka, A., S. Weinel, N. Nagy, M. O'Driscoll, J. E. Lai-Cheong, C. L. Kulp-Shorten, A. Knable, G. Carpenter, S. A. Fisher, M. Hiragun, Y. Yanase, M. Hide, J. Callen, and J. A. McGrath. 2012. 'Germline mutation in ATR in autosomal- dominant oropharyngeal cancer syndrome', *Am J Hum Genet*, 90: 511-7.

Tanaka, S., and H. Araki. 2013. 'Helicase activation and establishment of replication forks at chromosomal origins of replication', *Cold Spring Harb Perspect Biol*, 5: a010371.

Tanaka, Y., and Z. J. Chen. 2012. 'STING specifies IRF3 phosphorylation by TBK1 in the cytosolic DNA signaling pathway', *Sci Signal*, 5: ra20.

Tebbutt, Niall C., Kate Wilson, Val J. Gebski, Michelle M. Cummins, Diana Zannino, Guy A. van Hazel, Bridget Robinson, Adam Broad, Vinod Ganju, Stephen P. Ackland, Garry Forgeson, David Cunningham, Mark P. Saunders, Martin R. Stockler, YuJo Chua, John R. Zalcberg, R. John Simes, and Timothy J. Price. 2010. 'Capecitabine, Bevacizumab, and Mitomycin in First-Line Treatment of Metastatic Colorectal Cancer: Results of

the Australasian Gastrointestinal Trials Group Randomized Phase III MAX Study', *Journal of Clinical Oncology*, 28: 3191-98.

Teft, W. A., S. Welch, J. Lenehan, J. Parfitt, Y. H. Choi, E. Winquist, and R. B. Kim. 2015. 'OATP1B1 and tumour OATP1B3 modulate exposure, toxicity, and survival after irinotecan-based chemotherapy', *Br J Cancer*, 112: 857-65.

Tejpar, Sabine, Heinz-Josef Lenz, Claus-Henning Köhne, Volker Heinemann, Fortunato Ciardiello, Regina Esser, Frank Beier, Christopher Stroh, Klaus Duecker, and Carsten Bokemeyer. 2014. 'Effect of KRAS and NRAS mutations on treatment outcomes in patients with metastatic colorectal cancer (mCRC) treated first-line with cetuximab plus FOLFOX4: New results from the OPUS study', *Journal of Clinical Oncology*, 32: LBA444-LBA44.

Telli, M. L., S. Lord, E. Dean, V. Abramson, H. T. Arkenau, C. Murias, C. Becerra, R. Tang, M. S. Penney, J. Pollard, G. Conboy, S. Z. Fields, G. Shapiro, and S. M. Tolaney. 2018. 'Abstract OT2-07-07: ATR inhibitor M6620 (formerly VX-970) with cisplatin in metastatic triple-negative breast cancer: Preliminary results from a phase 1 dose expansion cohort (NCT02157792)', *Cancer Res*, 78: OT2-07-07.

Thirion, P., S. Michiels, J. P. Pignon, M. Buyse, A. C. Braud, R. W. Carlson, M. O'Connell, P. Sargent, and P. Piedbois. 2004. 'Modulation of fluorouracil by leucovorin in patients with advanced colorectal cancer: an updated meta-analysis', *J Clin Oncol*, 22: 3766-75.

Tho, L. M., S. Libertini, R. Rampling, O. Sansom, and D. A. Gillespie. 2012. 'Chk1 is essential for chemical carcinogen-induced mouse skin tumorigenesis', *Oncogene*, 31: 1366-75.

Thomas, A., and Y. Pommier. 2019. 'Targeting Topoisomerase I in the Era of Precision Medicine', *Clin Cancer Res*, 25: 6581-89.

Thomas, A., C. E. Redon, L. Sciuto, E. Padiernos, J. Ji, M. J. Lee, A. Yuno, S. Lee, Y. Zhang, L. Tran, W. Yutzy, A. Rajan, U. Guha, H. Chen, R. Hassan, C. C. Alewine, E. Szabo, S. E. Bates, R. J. Kinders, S. M. Steinberg, J. H. Doroshow, M. I. Aladjem, J. B. Trepel, and Y. Pommier. 2018. 'Phase I Study of ATR Inhibitor M6620 in Combination With Topotecan in Patients With Advanced Solid Tumors', *J Clin Oncol*, 36: 1594-602.

Thomas, A., N. Takahashi, V. N. Rajapakse, X. Zhang, Y. Sun, M. Ceribelli, K. M. Wilson, Y. Zhang, E. Beck, L. Sciuto, S. Nichols, B. Elenbaas, J. Puc, H. Dahmen, A. Zimmermann, J. Varonin, C. W. Schultz, S. Kim, H. Shimellis, P. Desai, C. Klumpp-Thomas, L. Chen, J. Travers, C. McKnight, S. Michael, Z. Itkin, S. Lee, A. Yuno, M. J. Lee, C. E. Redon, J. D. Kindrick, C. J. Peer, J. S. Wei, M. I. Aladjem, W. D. Figg, S. M. Steinberg, J. B. Trepel, F. T. Zenke, Y. Pommier, J. Khan, and C. J. Thomas. 2021. 'Therapeutic targeting of ATR yields durable regressions in small cell lung cancers with high replication stress', *Cancer Cell*, 39: 566-79.e7.

Thorslund, T., A. Ripplinger, S. Hoffmann, T. Wild, M. Uckelmann, B. Villumsen, T. Narita, T. K. Sixma, C. Choudhary, S. Bekker-Jensen, and N. Mailand. 2015. 'Histone H1 couples initiation and amplification of ubiquitin signalling after DNA damage', *Nature*, 527: 389-93.

Thuss-Patience, P. C., M. A. Shah, A. Ohtsu, E. Van Cutsem, J. A. Ajani, H. Castro, W. Mansoor, H. C. Chung, G. Bodoky, K. Shitara, G. D. L. Phillips, T. van der Horst, M. L. Harle-Yge, B. L. Althaus, and Y. K. Kang. 2017. 'Trastuzumab emtansine versus taxane use for previously treated HER2-positive locally advanced or metastatic gastric or gastro-oesophageal junction adenocarcinoma (GATSBY): an international randomised, open-label, adaptive, phase 2/3 study', *Lancet Oncol*, 18: 640-53.

Tibbetts, R. S., K. M. Brumbaugh, J. M. Williams, J. N. Sarkaria, W. A. Cliby, S. Y. Shieh, Y. Taya, C. Prives, and R. T. Abraham. 1999. 'A role for ATR in the DNA damage-induced phosphorylation of p53', *Genes Dev*, 13: 152-7.

Tibbetts, R. S., D. Cortez, K. M. Brumbaugh, R. Scully, D. Livingston, S. J. Elledge, and R. T. Abraham. 2000. 'Functional interactions between BRCA1 and the checkpoint kinase ATR during genotoxic stress', *Genes Dev*, 14: 2989-3002.

Toledo, L. I., M. Altmeyer, M. B. Rask, C. Lukas, D. H. Larsen, L. K. Povlsen, S. Bekker-Jensen, N. Mailand, J. Bartek, and J. Lukas. 2013. 'ATR prohibits replication catastrophe by preventing global exhaustion of RPA', *Cell*, 155: 1088-103.

Toledo, L. I., M. Murga, R. Zur, R. Soria, A. Rodriguez, S. Martinez, J. Oyarzabal, J. Pastor, J. R. Bischoff, and O. Fernandez-Capetillo. 2011. 'A cell-based screen identifies ATR inhibitors with synthetic lethal properties for cancer-associated mutations', *Nat Struct Mol Biol*, 18: 721-7.

Torrents, D., R. Estévez, M. Pineda, E. Fernández, J. Lloberas, Y. B. Shi, A. Zorzano, and M. Palacín. 1998. 'Identification and characterization of a membrane protein (y+L amino acid transporter-1) that associates with 4F2hc to encode the amino acid transport activity y+L. A candidate gene for lysinuric protein intolerance', *J Biol Chem*, 273: 32437-45.

Tournigand, C., T. André, E. Achille, G. Lledo, M. Flesh, D. Mery-Mignard, E. Quinaux, C. Couteau, M. Buyse, G. Ganem, B. Landi, P. Colin, C. Louvet, and A. de Gramont. 2004. 'FOLFIRI followed by FOLFOX6 or the reverse sequence in advanced colorectal cancer: a randomized GERCOR study', *J Clin Oncol*, 22: 229-37.

Trenz, K., E. Smith, S. Smith, and V. Costanzo. 2006. 'ATM and ATR promote Mre11 dependent restart of collapsed replication forks and prevent accumulation of DNA breaks', *Embo j*, 25: 1764-74.

Tripathi, V., S. Kaur, and S. Sengupta. 2008. 'Phosphorylation-dependent interactions of BLM and 53BP1 are required for their anti-recombinogenic roles during homologous recombination', *Carcinogenesis*, 29: 52-61.

Trumpi, K., B. L. Emmink, A. M. Prins, M. G. van Oijen, P. J. van Diest, C. J. Punt, M. Koopman, O. Kranenburg, and I. H. Rinkes. 2015. 'ABC-Transporter Expression Does Not Correlate with Response to Irinotecan in Patients with Metastatic Colorectal Cancer', *J Cancer*, 6: 1079-86.

Tsuchikama, K., and Z. An. 2018. 'Antibody-drug conjugates: recent advances in conjugation and linker chemistries', *Protein Cell*, 9: 33-46.

Tsukamoto, M., M. Yamashita, T. Nishi, and H. Nakagawa. 2019. 'A Human ABC Transporter ABCC4 Gene SNP (rs11568658, 559 G > T, G187W) Reduces ABCC4-Dependent Drug Resistance', *Cells*, 8.

Tsurutani, J., T. Nitta, T. Hirashima, T. Komiya, H. Uejima, H. Tada, N. Syunichi, A. Tohda, M. Fukuoka, and K. Nakagawa. 2002. 'Point mutations in the topoisomerase I gene in patients with non-small cell lung cancer treated with irinotecan', *Lung Cancer*, 35: 299-304.

Tu, X., M. M. Kahila, Q. Zhou, J. Yu, K. R. Kalari, L. Wang, W. S. Harmsen, J. Yuan, J. C. Boughey, M. P. Goetz, J. N. Sarkaria, Z. Lou, and R. W. Mutter. 2018. 'ATR Inhibition Is a Promising Radiosensitizing Strategy for Triple-Negative Breast Cancer', *Mol Cancer Ther*, 17: 2462-72.

Tuduri, S., L. Crabbé, C. Conti, H. Tourrière, H. Holtgreve-Grez, A. Jauch, V. Pantesco, J. De Vos, A. Thomas, C. Theillet, Y. Pommier, J. Tazi, A. Coquelle, and P. Pasero. 2009. 'Topoisomerase I suppresses genomic instability by preventing interference between replication and transcription', *Nat Cell Biol*, 11: 1315-24.

Tuy, H. D., H. Shiomi, K. I. Mukaisho, S. Naka, T. Shimizu, H. Sonoda, E. Mekata, Y. Endo, Y. Kurumi, H. Sugihara, M. Tani, and T. Tani. 2016. 'ABCG2 expression in colorectal adenocarcinomas may predict resistance to irinotecan', *Oncol Lett*, 12: 2752-60.

Tveit, K. M., T. Guren, B. Glimelius, P. Pfeiffer, H. Sorbye, S. Pyrhonen, F. Sigurdsson, E. Kure, T. Ikdahl, E. Skovlund, T. Fokstuen, F. Hansen, E. Hofsli, E. Birkemeyer, A. Johnsson, H. Starkhammar, M. K. Yilmaz, N. Keldsen, A. B. Erdal, O. Dajani, O. Dahl, and T.

Christoffersen. 2012. 'Phase III trial of cetuximab with continuous or intermittent fluorouracil, leucovorin, and oxaliplatin (Nordic FLOX) versus FLOX alone in first-line treatment of metastatic colorectal cancer: the NORDIC-VII study', *J Clin Oncol*, 30: 1755-62.

Van Cutsem, E., A. Cervantes, B. Nordlinger, and D. Arnold. 2014. 'Metastatic colorectal cancer: ESMO Clinical Practice Guidelines for diagnosis, treatment and follow-up', *Ann Oncol*, 25 Suppl 3: iii1-9.

Van Cutsem, E., C. H. Köhne, E. Hitre, J. Zaluski, C. R. Chang Chien, A. Makhson, G. D'Haens, T. Pintér, R. Lim, G. Bodoky, J. K. Roh, G. Folprecht, P. Ruff, C. Stroh, S. Tejpar, M. Schlichting, J. Nippgen, and P. Rougier. 2009. 'Cetuximab and chemotherapy as initial treatment for metastatic colorectal cancer', *N Engl J Med*, 360: 1408-17.

Van Cutsem, E., C. H. Köhne, I. Láng, G. Folprecht, M. P. Nowacki, S. Cascinu, I. Shchepotin, J. Maurel, D. Cunningham, S. Tejpar, M. Schlichting, A. Zubel, I. Celik, P. Rougier, and F. Ciardiello. 2011. 'Cetuximab plus irinotecan, fluorouracil, and leucovorin as first-line treatment for metastatic colorectal cancer: updated analysis of overall survival according to tumor KRAS and BRAF mutation status', *J Clin Oncol*, 29: 2011-9.

Van Cutsem, E., M. Peeters, S. Siena, Y. Humblet, A. Hendlisz, B. Neyns, J. L. Canon, J. L. Van Laethem, J. Maurel, G. Richardson, M. Wolf, and R. G. Amado. 2007. 'Open-label phase III trial of panitumumab plus best supportive care compared with best supportive care alone in patients with chemotherapy-refractory metastatic colorectal cancer', *J Clin Oncol*, 25: 1658-64.

van der Geest, L. G., J. Lam-Boer, M. Koopman, C. Verhoef, M. A. Elferink, and J. H. de Wilt. 2015. 'Nationwide trends in incidence, treatment and survival of colorectal cancer patients with synchronous metastases', *Clin Exp Metastasis*, 32: 457-65.

van der Schoor, L. W., H. J. Verkade, F. Kuipers, and J. W. Jonker. 2015. 'New insights in the biology of ABC transporters ABCC2 and ABCC3: impact on drug disposition', *Expert Opin Drug Metab Toxicol*, 11: 273-93.

Vanpouille-Box, C., S. Demaria, S. C. Formenti, and L. Galluzzi. 2018. 'Cytosolic DNA Sensing in Organismal Tumor Control', *Cancer Cell*, 34: 361-78.

Vávrová, J., L. Zárybnická, E. Lukášová, M. Řezáčová, E. Novotná, Z. Sinkorová, A. Tichý, J. Pejchal, and K. Durišová. 2013. 'Inhibition of ATR kinase with the selective inhibitor VE-821 results in radiosensitization of cells of promyelocytic leukaemia (HL-60)', *Radiat Environ Biophys*, 52: 471-9.

Vaz, B., M. Popovic, J. A. Newman, J. Fielden, H. Aitkenhead, S. Halder, A. N. Singh, I. Vendrell, R. Fischer, I. Torrecilla, N. Drobnitzky, R. Freire, D. J. Amor, P. J. Lockhart, B. M. Kessler, G. W. McKenna, O. Gileadi, and K. Ramadan. 2016. 'Metalloprotease SPRTN/DVC1 Orchestrates Replication-Coupled DNA-Protein Crosslink Repair', *Mol Cell*, 64: 704-19.

Vendetti, F. P., A. Lau, S. Schamus, T. P. Conrads, M. J. O'Connor, and C. J. Bakkenist. 2015. 'The orally active and bioavailable ATR kinase inhibitor AZD6738 potentiates the anti-tumor effects of cisplatin to resolve ATM-deficient non-small cell lung cancer in vivo', *Oncotarget*, 6: 44289-305.

Verlinden, L., I. Vanden Bempt, G. Eelen, M. Drijkoningen, I. Verlinden, K. Marchal, C. De Wolf-Peeters, M. R. Christiaens, L. Michiels, R. Bouillon, and A. Verstuyf. 2007. 'The E2F-regulated gene Chk1 is highly expressed in triple-negative estrogen receptor /progesterone receptor /HER-2 breast carcinomas', *Cancer Res*, 67: 6574-81.

Verma, S., D. Miles, L. Gianni, I. E. Krop, M. Welslau, J. Baselga, M. Pegram, D. Y. Oh, V. Diéras, E. Guardino, L. Fang, M. W. Lu, S. Olsen, and K. Blackwell. 2012. 'Trastuzumab emtansine for HER2-positive advanced breast cancer', *N Engl J Med*, 367: 1783-91.

Vezmar, M., and E. Georges. 2000. 'Reversal of MRP-mediated doxorubicin resistance with quinoline-based drugs', *Biochem Pharmacol*, 59: 1245-52.

Vincenzi, B., G. Schiavon, M. Silletta, D. Santini, and G. Tonini. 2008. 'The biological properties of cetuximab', *Crit Rev Oncol Hematol*, 68: 93-106.

Vogelstein, B., N. Papadopoulos, V. E. Velculescu, S. Zhou, L. A. Diaz, Jr., and K. W. Kinzler. 2013. 'Cancer genome landscapes', *Science*, 339: 1546-58.

von Minckwitz, G., C. S. Huang, M. S. Mano, S. Loibl, E. P. Mamounas, M. Untch, N. Wolmark, P. Rastogi, A. Schneeweiss, A. Redondo, H. H. Fischer, W. Jacot, A. K. Conlin, C. Arce-Salinas, I. L. Wapnir, C. Jackisch, M. P. DiGiovanna, P. A. Fasching, J. P. Crown, P. Wülfing, Z. Shao, E. Rota Caremoli, H. Wu, L. H. Lam, D. Tesarowski, M. Smitt, H. Douthwaite, S. M. Singel, and C. E. Geyer, Jr. 2019. 'Trastuzumab Emtansine for Residual Invasive HER2-Positive Breast Cancer', *N Engl J Med*, 380: 617-28.

Vos, S. M., E. M. Tretter, B. H. Schmidt, and J. M. Berger. 2011. 'All tangled up: how cells direct, manage and exploit topoisomerase function', *Nat Rev Mol Cell Biol*, 12: 827-41.

Waight, A. B., K. Bargsten, S. Doronina, M. O. Steinmetz, D. Sussman, and A. E. Prota. 2016. 'Structural Basis of Microtubule Destabilization by Potent Auristatin Anti-Mitotics', *PLoS One*, 11: e0160890.

Waldman, A. D., J. M. Fritz, and M. J. Lenardo. 2020. 'A guide to cancer immunotherapy: from T cell basic science to clinical practice', *Nat Rev Immunol*, 20: 651-68.

Wall, M. E., and M. C. Wani. 1995. 'Camptothecin and taxol: discovery to clinic--thirteenth Bruce F. Cain Memorial Award Lecture', *Cancer Res*, 55: 753-60.

Wallez, Y., C. R. Dunlop, T. I. Johnson, S. B. Koh, C. Fornari, J. W. T. Yates, S. Bernaldo de Quirós Fernández, A. Lau, F. M. Richards, and D. I. Jodrell. 2018. 'The ATR Inhibitor AZD6738 Synergizes with Gemcitabine In Vitro and In Vivo to Induce Pancreatic Ductal Adenocarcinoma Regression', *Mol Cancer Ther*, 17: 1670-82.

Wang, C. Y., J. C. Cusack, Jr., R. Liu, and A. S. Baldwin, Jr. 1999. 'Control of inducible chemoresistance: enhanced anti-tumor therapy through increased apoptosis by inhibition of NF-kappaB', *Nat Med*, 5: 412-7.

Wang, H., S. Li, H. Zhang, Y. Wang, S. Hao, and X. Wu. 2018. 'BLM prevents instability of structure-forming DNA sequences at common fragile sites', *PLoS Genet*, 14: e1007816.

Wang, H., L. Z. Shi, C. C. Wong, X. Han, P. Y. Hwang, L. N. Truong, Q. Zhu, Z. Shao, D. J. Chen, M. W. Berns, J. R. Yates, 3rd, L. Chen, and X. Wu. 2013. 'The interaction of CtIP and Nbs1 connects CDK and ATM to regulate HR-mediated double-strand break repair', *PLoS Genet*, 9: e1003277.

Wang, J. C. 2002. 'Cellular roles of DNA topoisomerases: a molecular perspective', *Nat Rev Mol Cell Biol*, 3: 430-40.

Ward, I. M., and J. Chen. 2001. 'Histone H2AX is phosphorylated in an ATR-dependent manner in response to replicational stress', *J Biol Chem*, 276: 47759-62.

Watson, J. D., and F. H. Crick. 1953. 'Genetical implications of the structure of deoxyribonucleic acid', *Nature*, 171: 964-7.

WCRF, International. 2018. 'Global cancer statistics for the most common cancers

'. https://www.wcrf.org/dietandcancer/cancer-trends/worldwide-cancer-data.

Weber, A. M., and A. J. Ryan. 2015. 'ATM and ATR as therapeutic targets in cancer', *Pharmacol Ther*, 149: 124-38.

Wengner, A. M., G. Siemeister, U. Lücking, J. Lefranc, L. Wortmann, P. Lienau, B. Bader, U. Bömer, D. Moosmayer, U. Eberspächer, S. Golfier, C. A. Schatz, S. J. Baumgart, B. Haendler, P. Lejeune, A. Schlicker, F. von Nussbaum, M. Brands, K. Ziegelbauer, and D. Mumberg. 2020. 'The Novel ATR Inhibitor BAY 1895344 Is Efficacious as Monotherapy and Combined with DNA Damage-Inducing or Repair-Compromising Therapies in Preclinical Cancer Models', *Mol Cancer Ther*, 19: 26-38.

Wengner, Antje Margret, Gerhard Siemeister, Ulrich Luecking, Julien Lefranc, Philip Lienau, Gesa Deeg, Eleni Lagkadinou, Li Liu, Sven Golfier, Christoph Schatz, Arne Scholz, Franz von Nussbaum, Michael Brands, Dominik Mumberg, and Karl Ziegelbauer. 2017. 'Abstract 836: ATR inhibitor BAY 1895344 shows potent anti-tumor efficacy in monotherapy and strong combination potential with the targeted alpha therapy Radium-223 dichloride in preclinical tumor models', *Cancer Res*, 77: 836.

Wengner, Antje Margret, Gerhard Siemeister, Ulrich Luecking, Julien Lefranc, Kirstin Meyer, Eleni Lagkadinou, Bernard Haendler, Pascale Lejeune, and Dominik Mumberg. 2018. 'Abstract 321: Synergistic activity of the ATR inhibitor BAY 1895344 in combination with DNA damage inducing and DNA repair compromising therapies in preclinical tumor models', *Cancer Res*, 78: 321.

WHO. 2021. 'Colorectal cancer', Accessed 05/07/2021. https://gco.iarc.fr/today/data/factsheets/cancers/10_8_9-Colorectum-fact-sheet.pdf.

Williamson, C. T., R. Miller, H. N. Pemberton, S. E. Jones, J. Campbell, A. Konde, N. Badham, R. Rafiq, R. Brough, A. Gulati, C. J. Ryan, J. Francis, P. B. Vermulen, A. R. Reynolds, P. M. Reaper, J. R. Pollard, A. Ashworth, and C. J. Lord. 2016. 'ATR inhibitors as a synthetic lethal therapy for tumours deficient in ARID1A', *Nat Commun*, 7: 13837.

Wilson, J. B., K. Yamamoto, A. S. Marriott, S. Hussain, P. Sung, M. E. Hoatlin, C. G. Mathew, M. Takata, L. H. Thompson, G. M. Kupfer, and N. J. Jones. 2008. 'FANCG promotes formation of a newly identified protein complex containing BRCA2, FANCD2 and XRCC3', *Oncogene*, 27: 3641-52.

Wong, S. F. 2005. 'Cetuximab: an epidermal growth factor receptor monoclonal antibody for the treatment of colorectal cancer', *Clin Ther*, 27: 684-94.

Wu, J., L. Sun, X. Chen, F. Du, H. Shi, C. Chen, and Z. J. Chen. 2013. 'Cyclic GMP-AMP is an endogenous second messenger in innate immune signaling by cytosolic DNA', *Science*, 339: 826-30.

Wu, X., S. M. Shell, Y. Liu, and Y. Zou. 2007. 'ATR-dependent checkpoint modulates XPA nuclear import in response to UV irradiation', *Oncogene*, 26: 757-64.

Wu, X., S. M. Shell, Z. Yang, and Y. Zou. 2006. 'Phosphorylation of nucleotide excision repair factor xeroderma pigmentosum group A by ataxia telangiectasia mutated and Rad3-related-dependent checkpoint pathway promotes cell survival in response to UV irradiation', *Cancer Res*, 66: 2997-3005.

Wu, Z. X., Y. Yang, L. Zeng, H. Patel, L. Bo, L. Lin, and Z. S. Chen. 2020. 'Establishment and Characterization of an Irinotecan-Resistant Human Colon Cancer Cell Line', *Front Oncol*, 10: 624954.

Xia, T., H. Konno, J. Ahn, and G. N. Barber. 2016. 'Deregulation of STING Signaling in Colorectal Carcinoma Constrains DNA Damage Responses and Correlates With Tumorigenesis', *Cell Rep*, 14: 282-97.

Xia, T., H. Konno, and G. N. Barber. 2016. 'Recurrent Loss of STING Signaling in Melanoma Correlates with Susceptibility to Viral Oncolysis', *Cancer Res*, 76: 6747-59.

Xu, X., L. M. Tsvetkov, and D. F. Stern. 2002. 'Chk2 activation and phosphorylation-dependent oligomerization', *Mol Cell Biol*, 22: 4419-32.

Xu, X., X. Zhang, C. Wei, D. Zheng, X. Lu, Y. Yang, A. Luo, K. Zhang, X. Duan, and Y. Wang. 2020. 'Targeting SLC7A11 specifically suppresses the progression of colorectal cancer stem cells via inducing ferroptosis', *Eur J Pharm Sci*, 152: 105450.

Xu, Y., and M. A. Villalona-Calero. 2002. 'Irinotecan: mechanisms of tumor resistance and novel strategies for modulating its activity', *Ann Oncol*, 13: 1841-51.

Yadav, B., K. Wennerberg, T. Aittokallio, and J. Tang. 2015. 'Searching for Drug Synergy in Complex Dose-Response Landscapes Using an Interaction Potency Model', *Comput Struct Biotechnol J*, 13: 504-13.

Yamaguchi, H., M. Kobayashi, M. Okada, T. Takeuchi, M. Unno, T. Abe, J. Goto, T. Hishinuma, and N. Mano. 2008. 'Rapid screening of antineoplastic candidates for the human organic anion transporter OATP1B3 substrates using fluorescent probes', *Cancer Lett*, 260: 163-9.

Yan, M., B. A. Parker, R. Schwab, and R. Kurzrock. 2014. 'HER2 aberrations in cancer: implications for therapy', *Cancer Treat Rev*, 40: 770-80.

Yan, M., M. Schwaederle, D. Arguello, S. Z. Millis, Z. Gatalica, and R. Kurzrock. 2015. 'HER2 expression status in diverse cancers: review of results from 37,992 patients', *Cancer Metastasis Rev*, 34: 157-64.

Yap, T. A., M. G. Krebs, S. Postel-Vinay, Y. J. Bang, A. El-Khoueiry, W. Abida, K. Harrington, R. Sundar, L. Carter, E. Castanon-Alvarez, S. A. Im, A. Berges, M. Khan, C. Stephens, G. Ross, and J. C. Soria. 2016. '1LBA - Phase I modular study of AZD6738, a novel oral, potent and selective ataxia telangiectasia Rad3-related (ATR) inhibitor in combination (combo) with carboplatin, olaparib or durvalumab in patients (pts) with advanced cancers', *European Journal of Cancer*, 69: S2.

Yap, T. A., B. O'Carrigan, M. S. Penney, J. S. Lim, J. S. Brown, M. J. de Miguel Luken, N. Tunariu, R. Perez-Lopez, D. N. Rodrigues, R. Riisnaes, I. Figueiredo, S. Carreira, B. Hare, K. McDermott, S. Khalique, C. T. Williamson, R. Natrajan, S. J. Pettitt, C. J. Lord, U. Banerji, J. Pollard, J. Lopez, and J. S. de Bono. 2020. 'Phase I Trial of First-in-Class ATR Inhibitor M6620 (VX-970) as Monotherapy or in Combination With Carboplatin in Patients With Advanced Solid Tumors', *J Clin Oncol*, 38: 3195-204.

Yap, Timothy A., Maria J. de Miguel Luken, Brent Carrigan, Desam Roda, Dionysis Papadatos-Pastos, David Lorente, Nina Tunariu, Raquel Perez Lopez, Sasha Gayle, Ruth Riisnaes, Ines Figueiredo, Susana Miranda, Suzanne Carreira, Fang Yang, Sharon Karan, Marina Penney, John Pollard, L. Rhoda Molife, Udai Banerji, Mohammed Asmal, Scott Z. Fields, and Johann S. de Bono. 2015. 'Abstract PR14: Phase I trial of first-in-class ataxia telangiectasia-mutated and Rad3-related (ATR) inhibitor VX-970 as monotherapy (mono) or in combination with carboplatin (CP) in advanced cancer patients (pts) with preliminary evidence of target modulation and antitumor activity', *Mol Cancer Ther*, 14: PR14.

Yarden, Y., and M. X. Sliwkowski. 2001. 'Untangling the ErbB signalling network', *Nat Rev Mol Cell Biol*, 2: 127-37.

Yazinski, S. A., V. Comaills, R. Buisson, M. M. Genois, H. D. Nguyen, C. K. Ho, T. Todorova Kwan, R. Morris, S. Lauffer, A. Nussenzweig, S. Ramaswamy, C. H. Benes, D. A. Haber, S. Maheswaran, M. J. Birrer, and L. Zou. 2017. 'ATR inhibition disrupts rewired homologous recombination and fork protection pathways in PARP inhibitor-resistant BRCA-deficient cancer cells', *Genes Dev*, 31: 318-32.

Yin, O., Y. Xiong, S. Endo, K. Yoshihara, T. Garimella, M. AbuTarif, R. Wada, and F. LaCreta. 2021. 'Population Pharmacokinetics of Trastuzumab Deruxtecan in Patients With HER2-Positive Breast Cancer and Other Solid Tumors', *Clin Pharmacol Ther*, 109: 1314-25.

Yoo, H. Y., A. Shevchenko, A. Shevchenko, and W. G. Dunphy. 2004. 'Mcm2 is a direct substrate of ATM and ATR during DNA damage and DNA replication checkpoint responses', *J Biol Chem*, 279: 53353-64.

Yoshioka, A., S. Tanaka, O. Hiraoka, Y. Koyama, Y. Hirota, D. Ayusawa, T. Seno, C. Garrett, and Y. Wataya. 1987. 'Deoxyribonucleoside triphosphate imbalance. 5-Fluorodeoxyuridine-induced DNA double strand breaks in mouse FM3A cells and the mechanism of cell death', *J Biol Chem*, 262: 8235-41.

Yu, J., Y. Song, and W. Tian. 2020. 'How to select IgG subclasses in developing anti-tumor therapeutic antibodies', *J Hematol Oncol*, 13: 45.

Zammarchi, F., S. Corbett, L. Adams, P. C. Tyrer, K. Kiakos, N. Janghra, T. Marafioti, C. E. Britten, C. E. G. Havenith, S. Chivers, F. D'Hooge, D. G. Williams, A. Tiberghien, P. W.

Howard, J. A. Hartley, and P. H. van Berkel. 2018. 'ADCT-402, a PBD dimer-containing antibody drug conjugate targeting CD19-expressing malignancies', *Blood*, 131: 1094-105.

Zannini, L., D. Delia, and G. Buscemi. 2014. 'CHK2 kinase in the DNA damage response and beyond', *J Mol Cell Biol*, 6: 442-57.

Zeng, Y., K. C. Forbes, Z. Wu, S. Moreno, H. Piwnica-Worms, and T. Enoch. 1998. 'Replication checkpoint requires phosphorylation of the phosphatase Cdc25 by Cds1 or Chk1', *Nature*, 395: 507-10.

Zenke, Frank T., Astrid Zimmermann, Heike Dahmen, Brian Elenbaas, John Pollard, Philip Reaper, S. Bagrodia, M. E. Spilker, C. Amendt, and Andree Blaukat. 2019. 'Abstract 369: Antitumor activity of M4344, a potent and selective ATR inhibitor, in monotherapy and combination therapy', *Cancer Res*, 79: 369.

Zhang, Y. W., T. L. Jones, S. E. Martin, N. J. Caplen, and Y. Pommier. 2009. 'Implication of checkpoint kinase-dependent up-regulation of ribonucleotide reductase R2 in DNA damage response', *J Biol Chem*, 284: 18085-95.

Zhang, Y. W., M. Regairaz, J. A. Seiler, K. K. Agama, J. H. Doroshow, and Y. Pommier. 2011. 'Poly(ADP-ribose) polymerase and XPF-ERCC1 participate in distinct pathways for the repair of topoisomerase I-induced DNA damage in mammalian cells', *Nucleic Acids Res*, 39: 3607-20.

Zhao, H., and H. Piwnica-Worms. 2001. 'ATR-mediated checkpoint pathways regulate phosphorylation and activation of human Chk1', *Mol Cell Biol*, 21: 4129-39.

Zheng, F., Y. Zhang, S. Chen, X. Weng, Y. Rao, and H. Fang. 2020. 'Mechanism and current progress of Poly ADP-ribose polymerase (PARP) inhibitors in the treatment of ovarian cancer', *Biomed Pharmacother*, 123: 109661.

Zheng, S. Tang, J. 2021. 'ZIP: Calculate Delta Synergy Score Based on ZIP Model'. https://rdrr.io/bioc/synergyfinder/man/ZIP.html#heading-5.

Zhou, Z. W., C. Liu, T. L. Li, C. Bruhn, A. Krueger, W. Min, Z. Q. Wang, and A. M. Carr. 2013. 'An essential function for the ATR-activation-domain (AAD) of TopBP1 in mouse development and cellular senescence', *PLoS Genet*, 9: e1003702.

Zitvogel, L., L. Galluzzi, O. Kepp, M. J. Smyth, and G. Kroemer. 2015. 'Type I interferons in anticancer immunity', *Nat Rev Immunol*, 15: 405-14.

Zou, L., D. Cortez, and S. J. Elledge. 2002. 'Regulation of ATR substrate selection by Rad17-dependent loading of Rad9 complexes onto chromatin', *Genes Dev*, 16: 198-208.

Zou, L., and S. J. Elledge. 2003. 'Sensing DNA damage through ATRIP recognition of RPA-ssDNA complexes', *Science*, 300: 1542-8.

Zou, L., D. Liu, and S. J. Elledge. 2003. 'Replication protein A-mediated recruitment and activation of Rad17 complexes', *Proc Natl Acad Sci U S A*, 100: 13827-32.

Appendix

EMD Plots from SN38 and VX-970 combination therapy

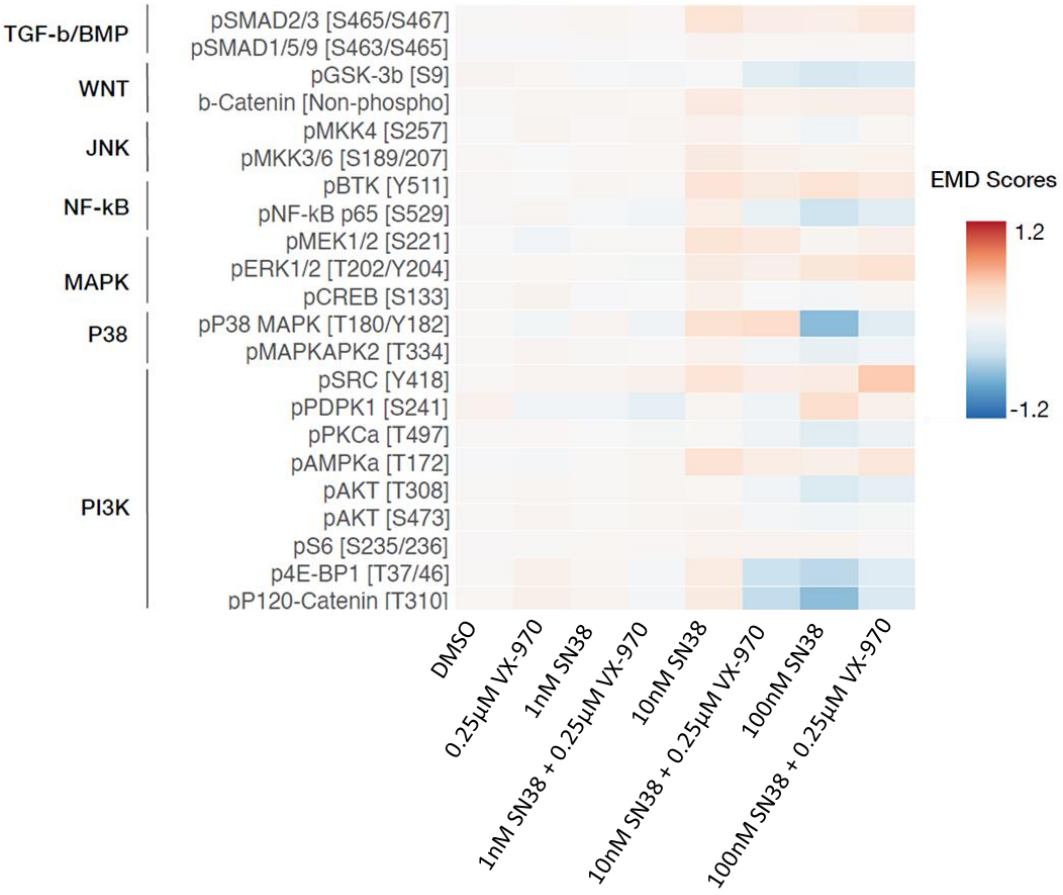

Figure Appendix 1. **CyTOF EMD plot following 24 hours treatment of PDO 021 with SN38 +/- VX-970.**

EMD plot showing the average signal intensity of organoid cells stained with a panel of antibodies using the CyTOF technique. Signal intensities are representative of 3 technical repeats.

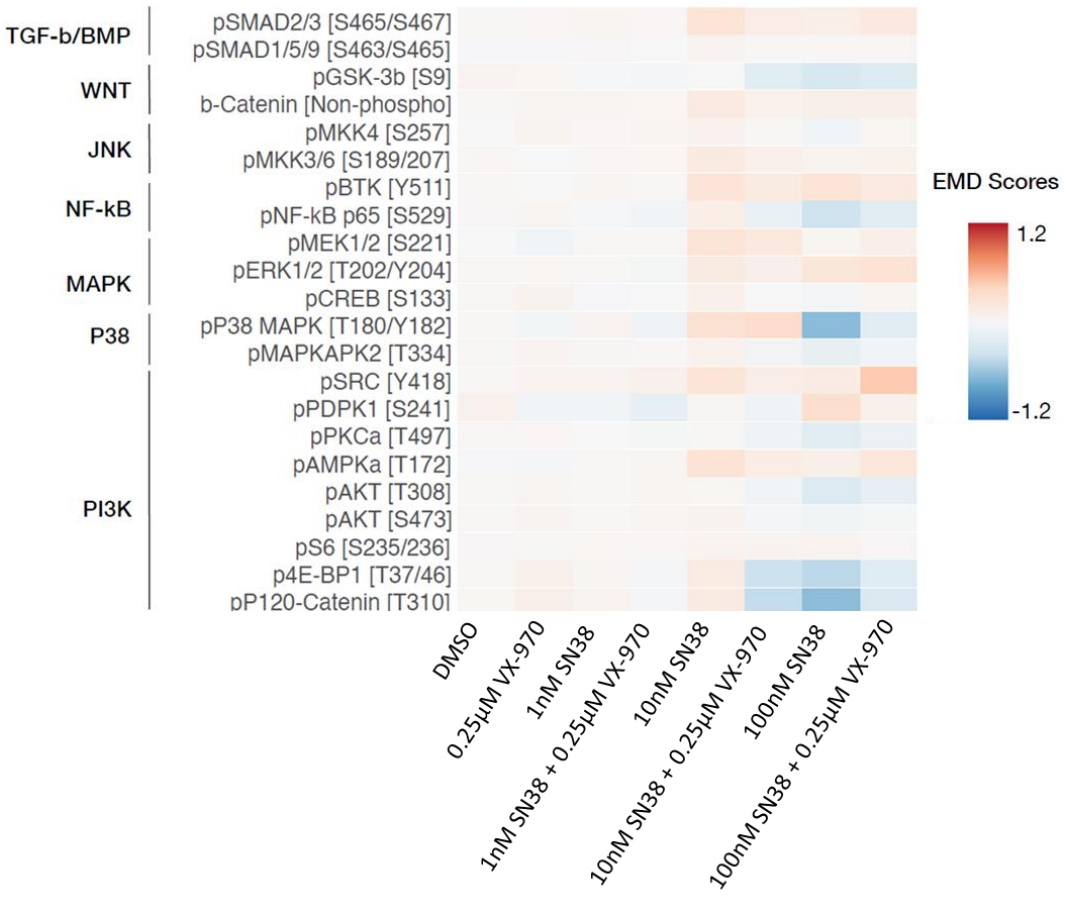

Figure Appendix 2. **CyTOF EMD plot following 48 hours treatment of PDO 021 with SN38 +/- VX-970.**

EMD plot showing the average signal intensity of organoid cells stained with a panel of antibodies using the CyTOF technique. Signal intensities are representative of 3 technical repeats.

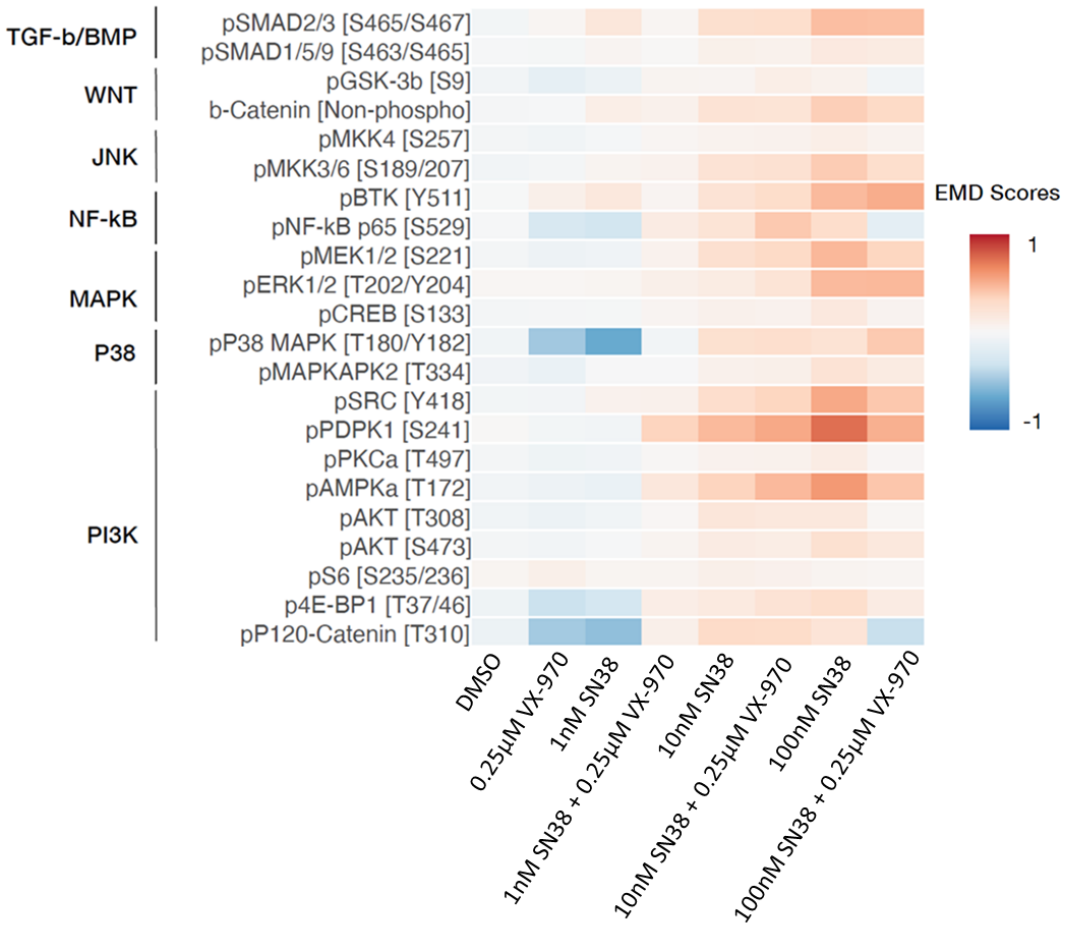

Figure Appendix 3. **CyTOF EMD plot following 72 hours treatment of PDO 021 with SN38 +/- VX-970.**

EMD plot showing the average signal intensity of organoid cells stained with a panel of antibodies using the CyTOF technique. Signal intensities are representative of 3 technical repeats.

EMD Plots from DS-8201a and VX-970 combination therapy

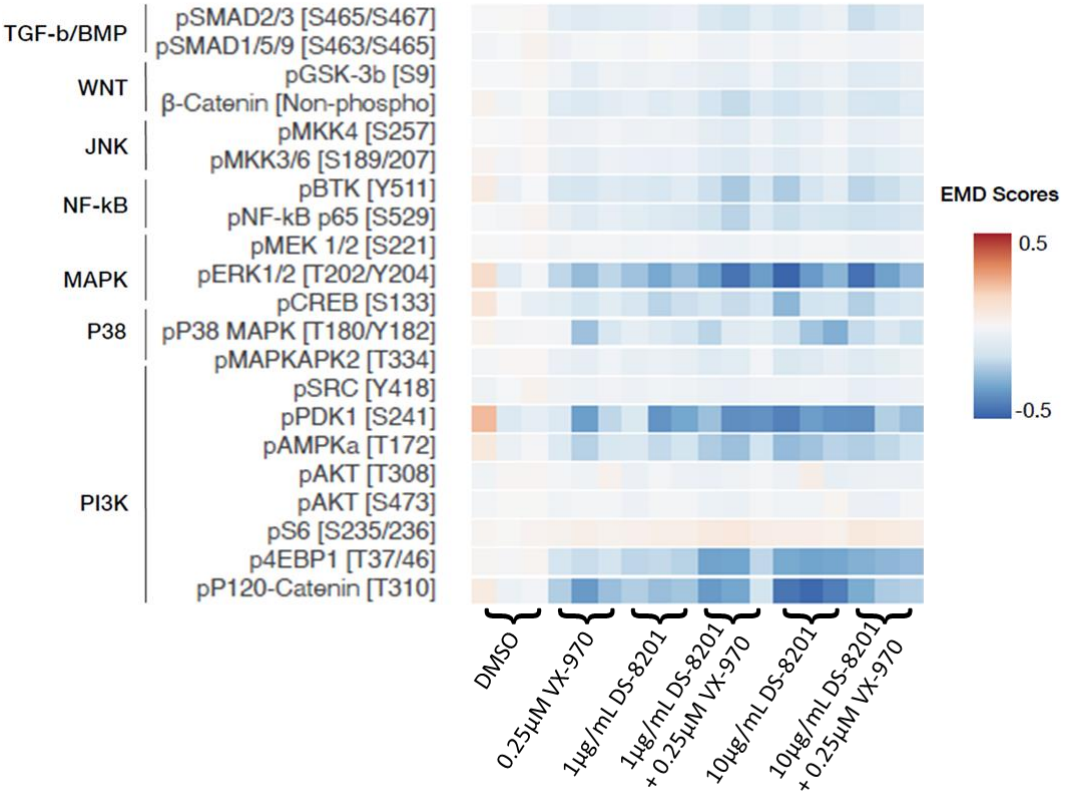

Figure Appendix 4. **CyTOF EMD plot following 24 hours treatment of PDO 021 with DS-8201 +/- VX-970.**

EMD plot showing the average signal intensity of organoid cells stained with a panel of antibodies using the CyTOF technique. Signal intensities are shown for each experimental repeat.

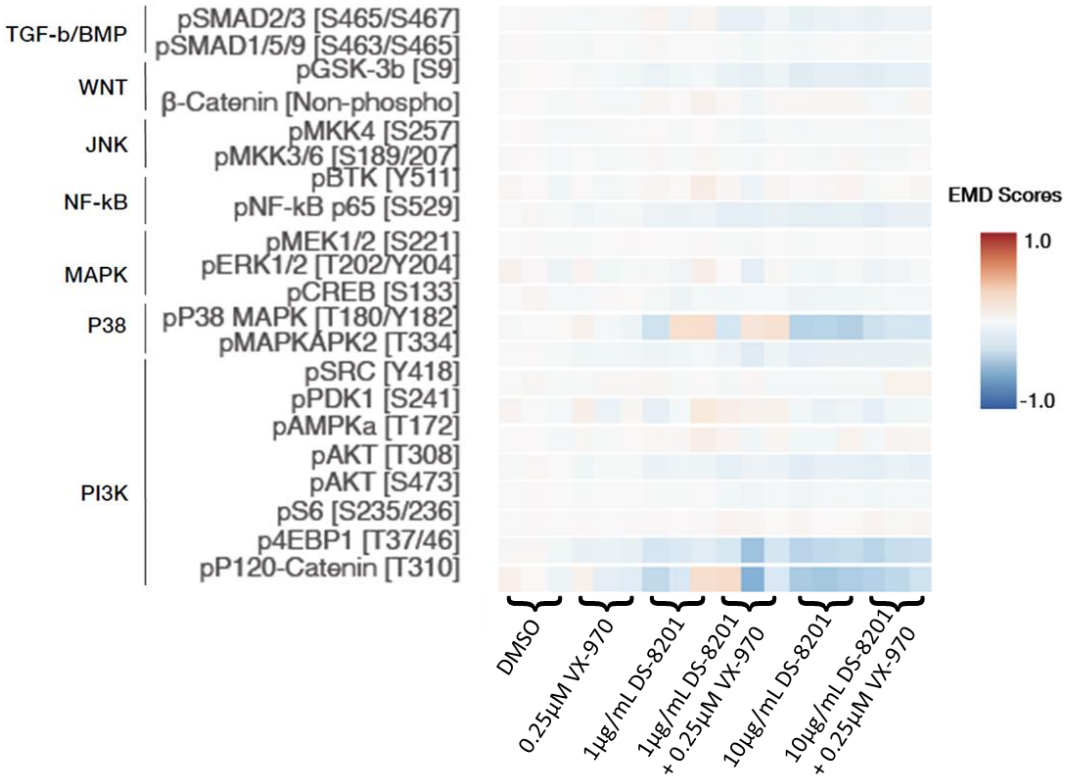

Figure Appendix 5. **CyTOF EMD plot following 48 hours treatment of PDO 021 with DS-8201 +/- VX-970.**

EMD plot showing the average signal intensity of organoid cells stained with a panel of antibodies using the CyTOF technique. Signal intensities are shown for each experimental repeat.

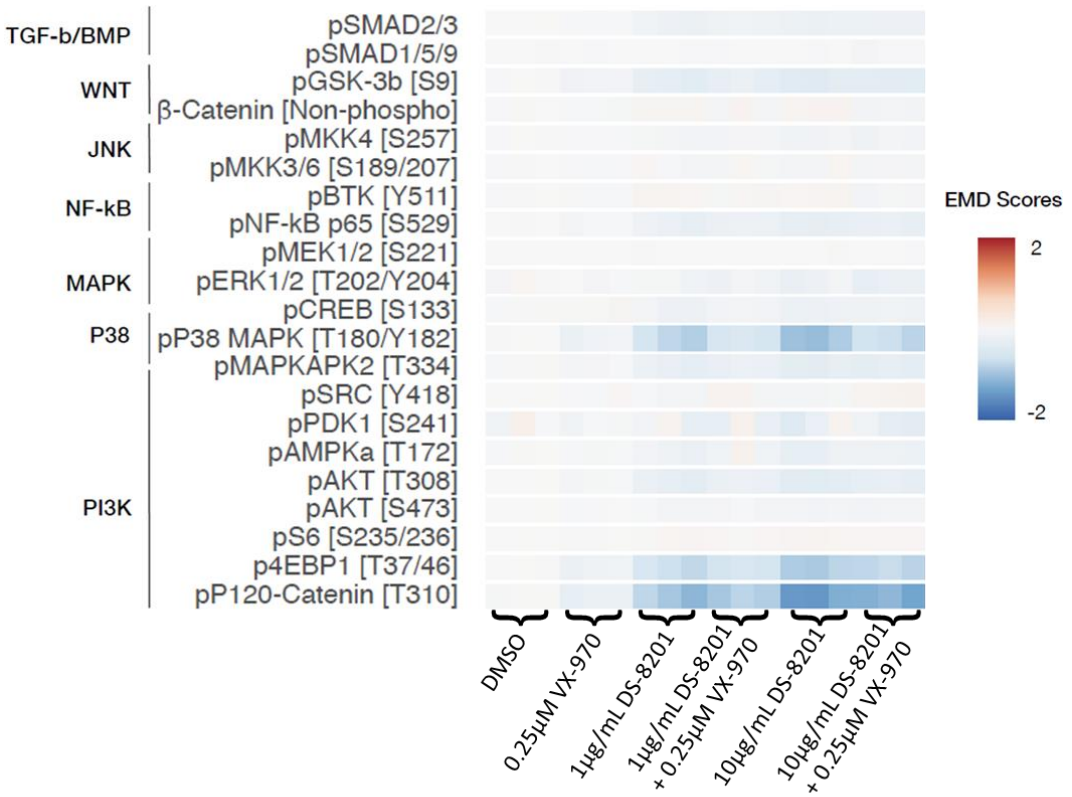

Figure Appendix 6. **CyTOF EMD plot following 72 hours treatment of PDO 021 with DS-8201 +/- VX-970.**

EMD plot showing the average signal intensity of organoid cells stained with a panel of antibodies using the CyTOF technique. Signal intensities are shown for each experimental repeat.

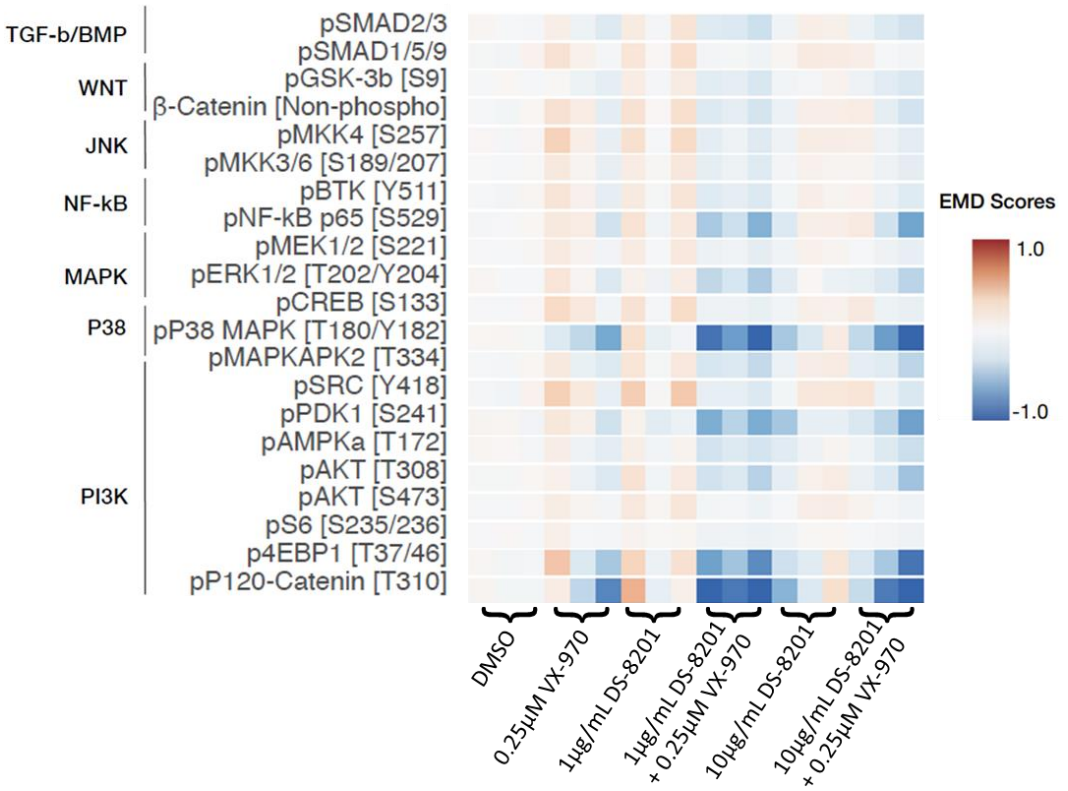

Figure Appendix 7. **CyTOF EMD plot following 24 hours treatment of PDO 027 with DS-8201 +/- VX-970.**

EMD plot showing the average signal intensity of organoid cells stained with a panel of antibodies using the CyTOF technique. Signal intensities are shown for each experimental repeat.

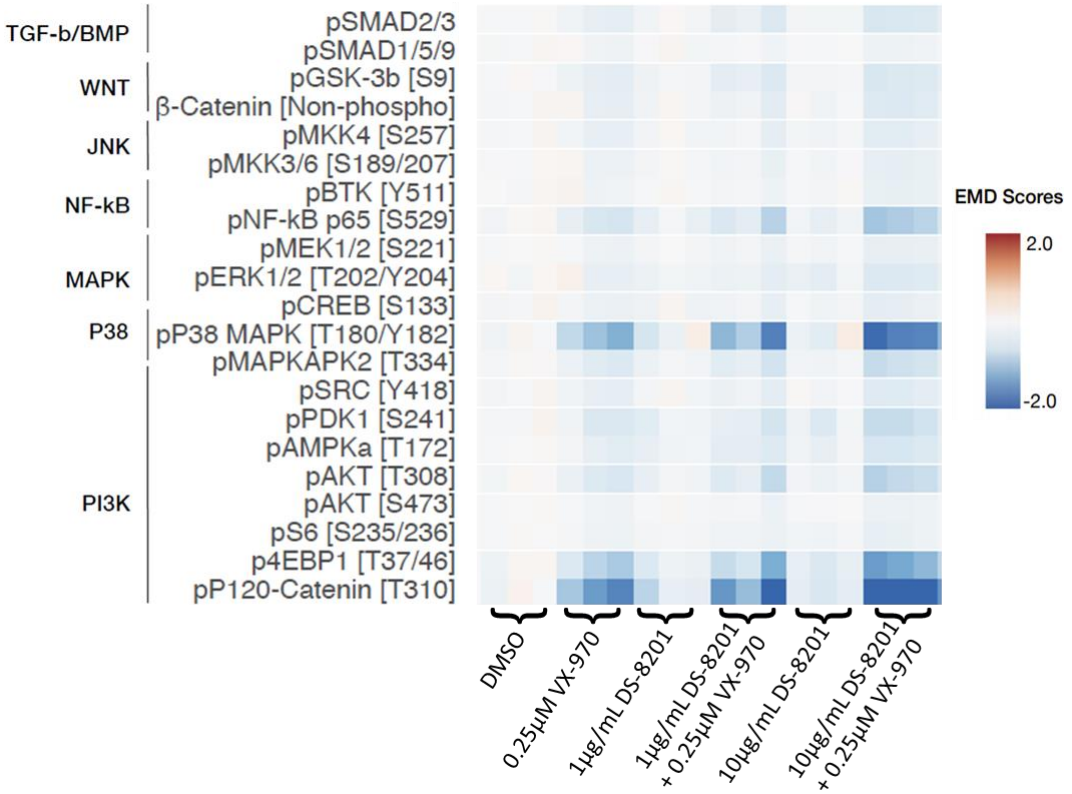

Figure Appendix 8. **CyTOF EMD plot following 48 hours treatment of PDO 027 with DS-8201 +/- VX-970.**

EMD plot showing the average signal intensity of organoid cells stained with a panel of antibodies using the CyTOF technique. Signal intensities are shown for each experimental repeat.

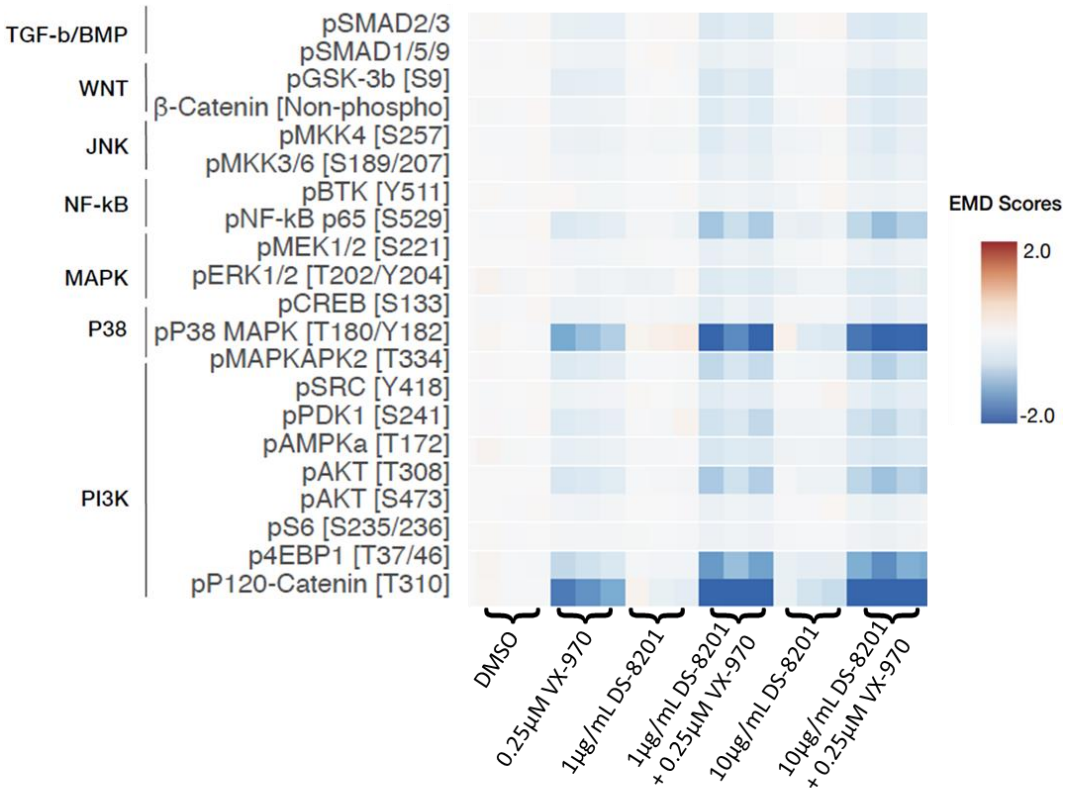

Figure Appendix 9. **CyTOF EMD plot following 72 hours treatment of PDO 027 with DS-8201 +/- VX-970.**

EMD plot showing the average signal intensity of organoid cells stained with a panel of antibodies using the CyTOF technique. Signal intensities are shown for each experimental repeat.